

Universitat de Lleida

Organització molecular dels aferents sinàptics de tipus C i la seva implicació en la patologia degenerativa de la neurona motora

Sara Salvany Montserrat

<http://hdl.handle.net/10803/674022>

ADVERTIMENT. L'accés als continguts d'aquesta tesi doctoral i la seva utilització ha de respectar els drets de la persona autora. Pot ser utilitzada per a consulta o estudi personal, així com en activitats o materials d'investigació i docència en els termes establerts a l'art. 32 del Text Refós de la Llei de Propietat Intel·lectual (RDL 1/1996). Per altres utilitzacions es requereix l'autorització prèvia i expressa de la persona autora. En qualsevol cas, en la utilització dels seus continguts caldrà indicar de forma clara el nom i cognoms de la persona autora i el títol de la tesi doctoral. No s'autoritza la seva reproducció o altres formes d'explotació efectuades amb finalitats de lucre ni la seva comunicació pública des d'un lloc aliè al servei TDX. Tampoc s'autoritza la presentació del seu contingut en una finestra o marc aliè a TDX (framing). Aquesta reserva de drets afecta tant als continguts de la tesi com als seus resums i índexs.

ADVERTENCIA. El acceso a los contenidos de esta tesis doctoral y su utilización debe respetar los derechos de la persona autora. Puede ser utilizada para consulta o estudio personal, así como en actividades o materiales de investigación y docencia en los términos establecidos en el art. 32 del Texto Refundido de la Ley de Propiedad Intelectual (RDL 1/1996). Para otros usos se requiere la autorización previa y expresa de la persona autora. En cualquier caso, en la utilización de sus contenidos se deberá indicar de forma clara el nombre y apellidos de la persona autora y el título de la tesis doctoral. No se autoriza su reproducción u otras formas de explotación efectuadas con fines lucrativos ni su comunicación pública desde un sitio ajeno al servicio TDR. Tampoco se autoriza la presentación de su contenido en una ventana o marco ajeno a TDR (framing). Esta reserva de derechos afecta tanto al contenido de la tesis como a sus resúmenes e índices.

WARNING. Access to the contents of this doctoral thesis and its use must respect the rights of the author. It can be used for reference or private study, as well as research and learning activities or materials in the terms established by the 32nd article of the Spanish Consolidated Copyright Act (RDL 1/1996). Express and previous authorization of the author is required for any other uses. In any case, when using its content, full name of the author and title of the thesis must be clearly indicated. Reproduction or other forms of for profit use or public communication from outside TDX service is not allowed. Presentation of its content in a window or frame external to TDX (framing) is not authorized either. These rights affect both the content of the thesis and its abstracts and indexes.



Organització molecular dels aferents sinàptics de tipus C i la seva implicació en la patologia degenerativa de la neurona motora

Sara Salvany Montserrat

2021



Universitat de Lleida

TESI DOCTORAL

Organització molecular dels aferents sinàptics de tipus C i la seva implicació en la patologia degenerativa de la neurona motora

Sara Salvany Montserrat

2021

Departament de Medicina Experimental

Memòria per optar al grau de Doctor per la Universitat de Lleida
Programa de Doctorat en Salut

Directors de Tesi

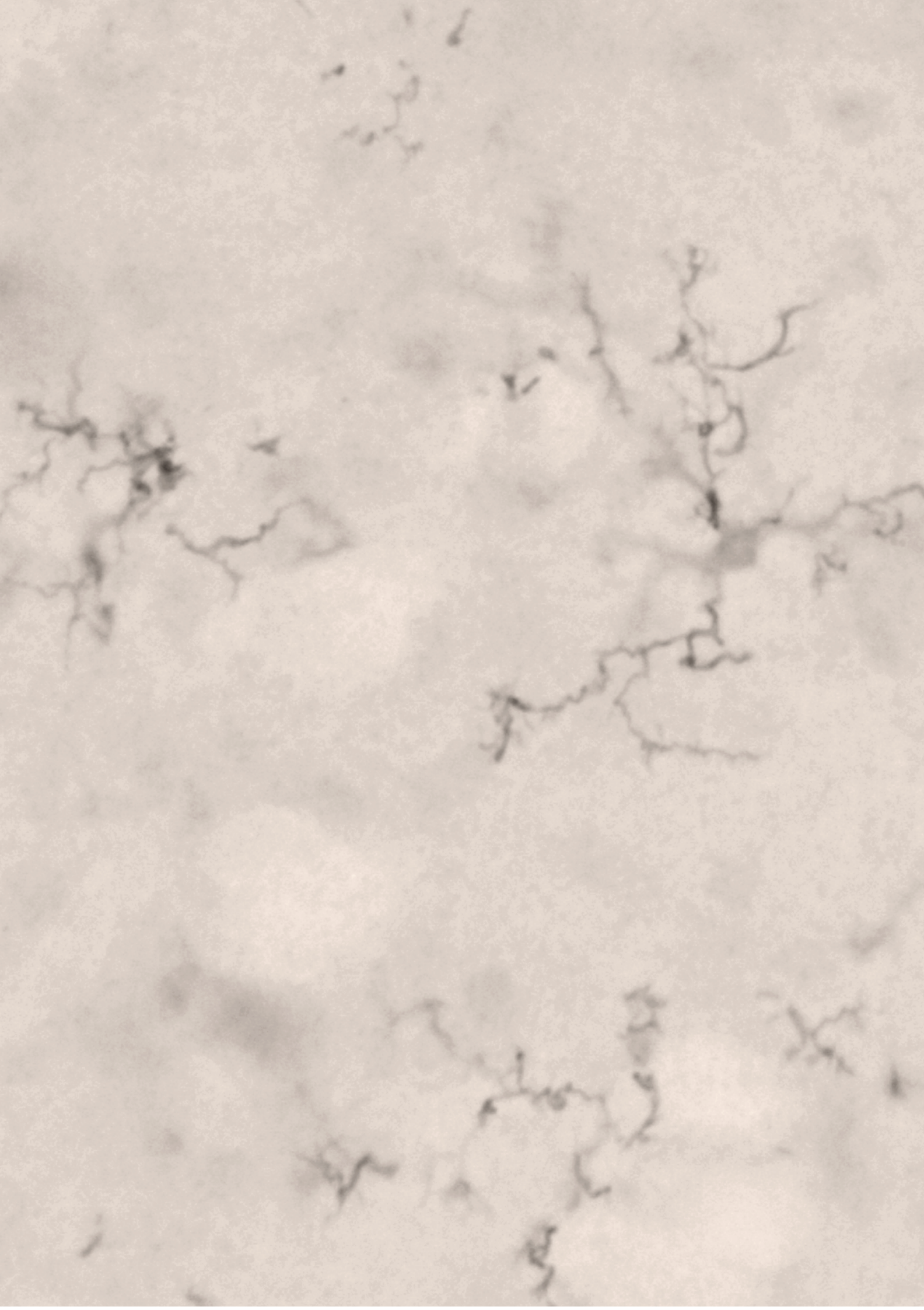
Dr. Josep E. Esquerda Colell
Dra. Anna Casanovas Llorens

Tutor

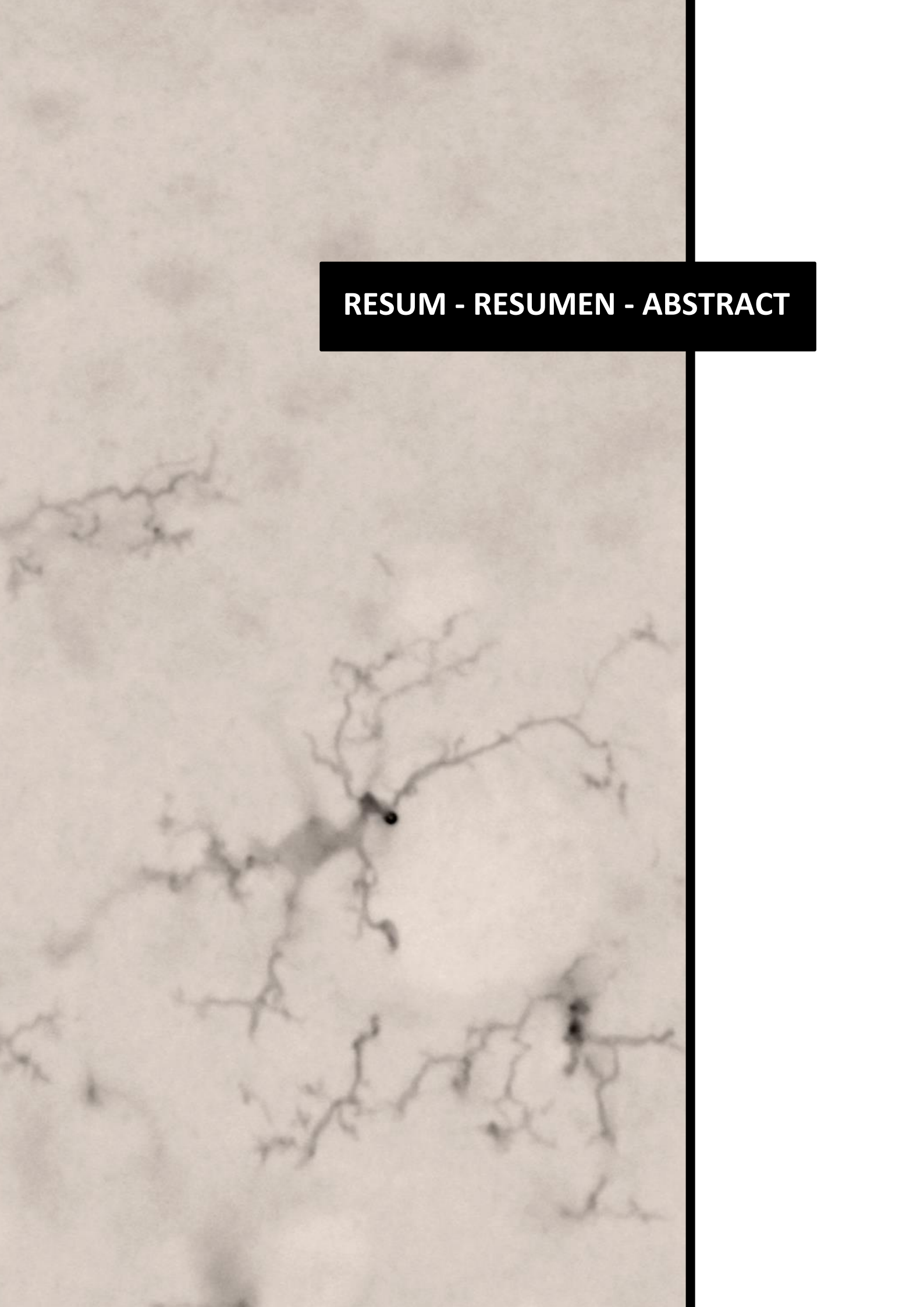
Dr. Josep E. Esquerda Colell

El present treball ha estat finançat per les següents entitats públiques i privades:

- Ajuts per a personal predoctoral de la Universitat de Lleida en formació i ajuts Jade Plus per a l'any 2016 – 2017
- Ajuts per a la *Formación de Profesorado Universitario* (FPU) del *Ministerio de Educación, Cultura y Deporte* per a l'any 2017 – 2020
- Ajuts 2020 de Promoció de la Recerca en Salut-8^a edició” de l'IRBLleida/Diputació de Lleida per a l'any 2021
- *Ministerio de Economía y Competitividad* cofinançat pel *Fondo Europeo de Desarrollo regional* (SAF2015–70801-R)
- *Ministerio de Ciencia, Innovación y Universidades* cofinançat pel *Fondo Europeo de Desarrollo regional* (FEDER; RTI2018-099278-B100)
- Jack Van den Hock a la Investigació de l'ELA – Fundació Miquel Valls.



RESUM - RESUMEN - ABSTRACT



RESUM

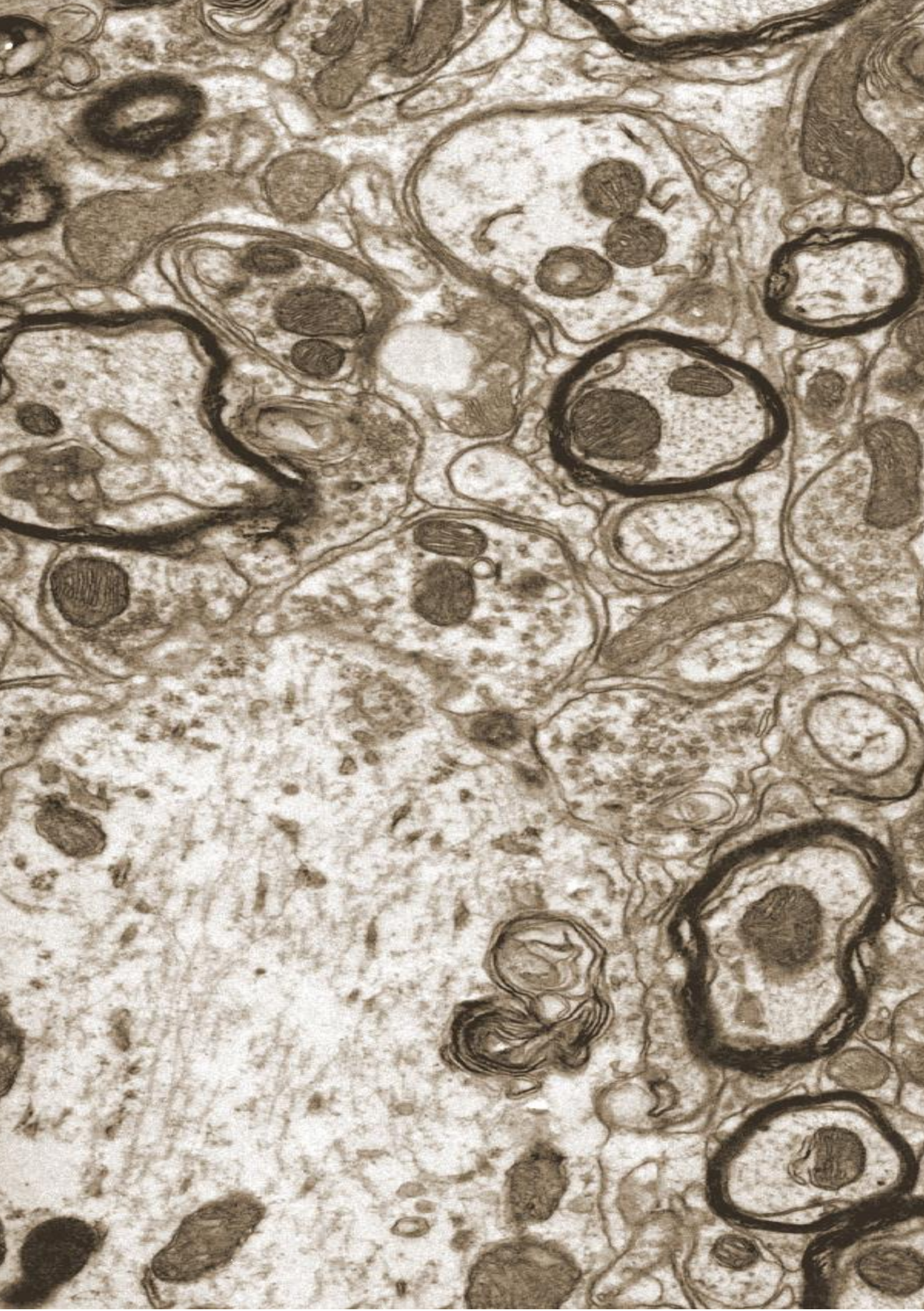
L'esclerosi lateral amiotòrfica (ELA) és una malaltia que cursa amb degeneració i pèrdua de les motoneurones (MNs), determinant una paràlisi muscular progressiva i de pronòstic fatal. L'acumulació de la proteïna superòxid dismutasa 1 mal plegada (mfSOD1) en les MNs és el factor intrínsec distintiu de la patologia en el model murí per l'estudi de l'ELA SOD1^{G93A} que reproduceix una forma familiar de la ELA humana. No obstant, factors extrínsecos a les MNs tals com l'activitat elèctrica mitjançada per les aferències sinàptiques, així com l'entorn cel·lular determinat per les cèl·lules glials, també són molt rellevants en la fisiopatologia de l'ELA. Entre les aferències, els botons C (BC) són uns importants reguladors colinèrgics de l'excitabilitat de les MNs. Aquests es caracteritzen per tenir una cisterna subsinàptica (SSC) adjacent a la membrana postsinàptica, on s'hi ha descrit un complex macromolecular específic format per diferents proteïnes, entre elles, la neuregulina-1 (NRG1). Tot i que s'han descrit alteracions en els BC en l'ELA, la funció de la NRG1 en la fisiologia i la patologia de la MN es completament desconeguda. L'objectiu del present treball ha estat caracteritzar millor l'arquitectura molecular del BC i analitzar les seves alteracions així com la implicació en la regulació de la resposta microglial al voltant de les MNs danyades. Per a aquesta finalitat, hem analitzat la localització i distribució de diverses proteïnes dins dels subcompartiments sinàptics del BC i la seva relació amb la glia mitjançant microscòpia confocal i electrònica en diferents models animals. Els resultats demostren que, en la SSC, la NRG1 està situada en microdominis molt específics i no solapats amb altres proteïnes, mentre que el seu receptor, els ErbB2/4, estan presents en el compartiment presinàptic adjacent. D'altra banda, també s'ha evidenciat que les diferents isoformes de NRG1 regulen funcions diferents en el BC específicament a nivell pre- o postsinàptic. Les aferències de tipus C es desorganitzen en presència d'estressos aguts, tals com la lesió del nervi perifèric, on aquesta pèrdua de BCs es produeix en conjunció a un augment del reclutament de cèl·lules microglials. A més, la micròglia, està involucrada en l'eliminació del detritus de terminals sinàptics prèviament desintegrats per la via necroptòtica activada després de l'axotomia. En el model murí SOD1^{G93A}, hem definit 3 fenotips de MNs d'acord a l'expressió de mfSOD1 i a la degeneració vacuolar. Hem caracteritzat aquesta vacuolització utilitzant marcadors mitocondrials i de vesícules extracel·lulars així com la seva relació amb els canvis en les aferències sinàptiques i l'activació microglial. En conjunt, els nostres resultats aporten noves dades sobre l'organització dels BC i dels canvis que tenen lloc tant en lesions agudes en les MNs com en l'ELA. També aportem noves dades sobre la citopatologia relacionada amb l'expressió de mfSOD1 durant les fases inicials de la degeneració de les MNs en l'ELA.

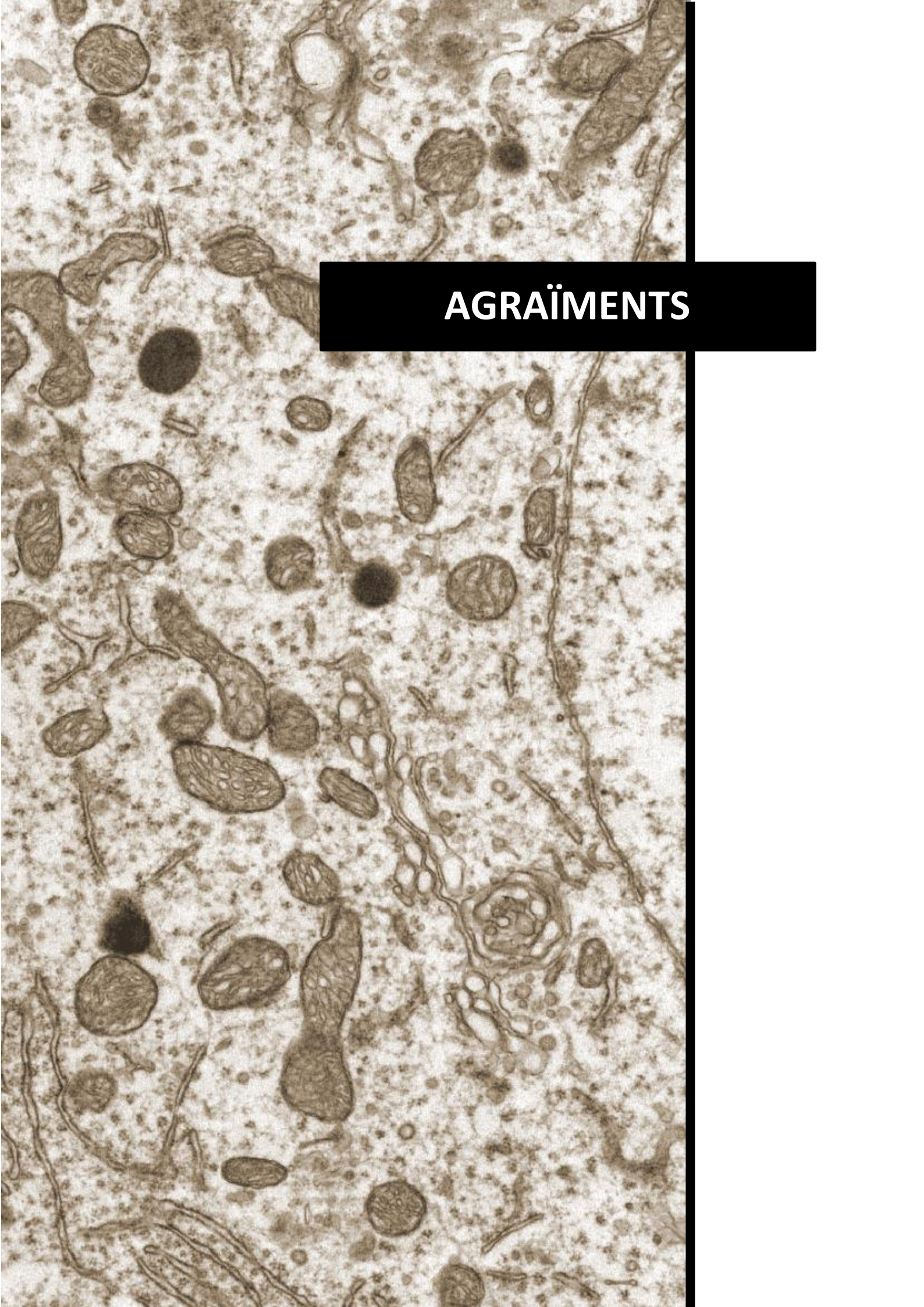
RESUMEN

La esclerosis lateral amiotrófica (ELA) es una enfermedad que cursa con degeneración y pérdida de las motoneuronas (MNs), determinando una parálisis muscular progresiva y de pronóstico fatal. La acumulación de la proteína superóxido dismutasa 1 mal plegada (mfSOD1) en las MNs es el factor intrínseco distintivo de la patología en el modelo murino para el estudio de la ELA SOD1^{G93A}, el cual reproduce una forma familiar de la ELA humana. No obstante, factores extrínsecos a las MNs como la actividad eléctrica mediada por las aferencias sinápticas, así como el entorno celular determinado por las células gliales, también son muy relevantes en la fisiopatología de la ELA. Entre las aferencias, los botones C (BC) son unos importantes reguladores colinérgicos de la excitabilidad de las MNs. Estos se caracterizan por tener una cisterna subsináptica (SSC) adyacente a la membrana postsináptica, donde se ha descrito un complejo macromolecular específico formado por distintas proteínas, entre ellas, la neuregulina-1 (NRG1). Aunque se han descrito alteraciones en los BC en la ELA, la función de la NRG1 en la fisiología y la patología de la MN es completamente desconocida. El objetivo del presente trabajo ha sido caracterizar mejor la arquitectura molecular del BC y analizar sus alteraciones, así como su implicación en la regulación de la respuesta microglial alrededor de las MNs dañadas. Para esta finalidad, hemos analizado la localización y distribución de varias proteínas de los subcompartimentos sinápticos de los BC y su relación con la glía mediante microscopía confocal y electrónica en distintos modelos animales. Los resultados demuestran que, en la SSC, la NRG1 está ubicada en microdominios muy específicos y no solapados con otras proteínas, mientras que su receptor, los ErbB2/4, están presentes en el compartimento presináptico adyacente. Por otro lado, también se ha evidenciado que las distintas isoformas de NRG1 regulan funciones diferentes en los BC específicamente a nivel pre- o postsináptico. Las aferencias de tipo C se desorganizan en presencia de un estrés agudo como es la lesión del nervio periférico, donde ésta pérdida de BCs se produce junto a un aumento del reclutamiento de células microgliales. Además, la microglía, está involucrada en la eliminación de los detritus de los terminales sinápticos previamente desintegrados por la vía necrotótica activada después de la axotomía. En el modelo murino SOD1^{G93A}, hemos definido 3 fenotipos de MNs de acuerdo a la expresión de mfSOD1 y a la degeneración vacuolar. Hemos caracterizado la vacuolización mediante marcadores mitocondriales y de vesículas extracelulares, así como su relación con los cambios con las aferencias sinápticas y la activación microglial. En conjunto, nuestros resultados aportan nuevos datos sobre la organización de los BC y de los cambios que tienen lugar tan en lesiones agudas en las MNs como en la ELA. También aportamos nuevos datos sobre la citopatología relacionada con la expresión de mfSOD1 durante las fases iniciales de la degeneración de las MNs en la ELA.

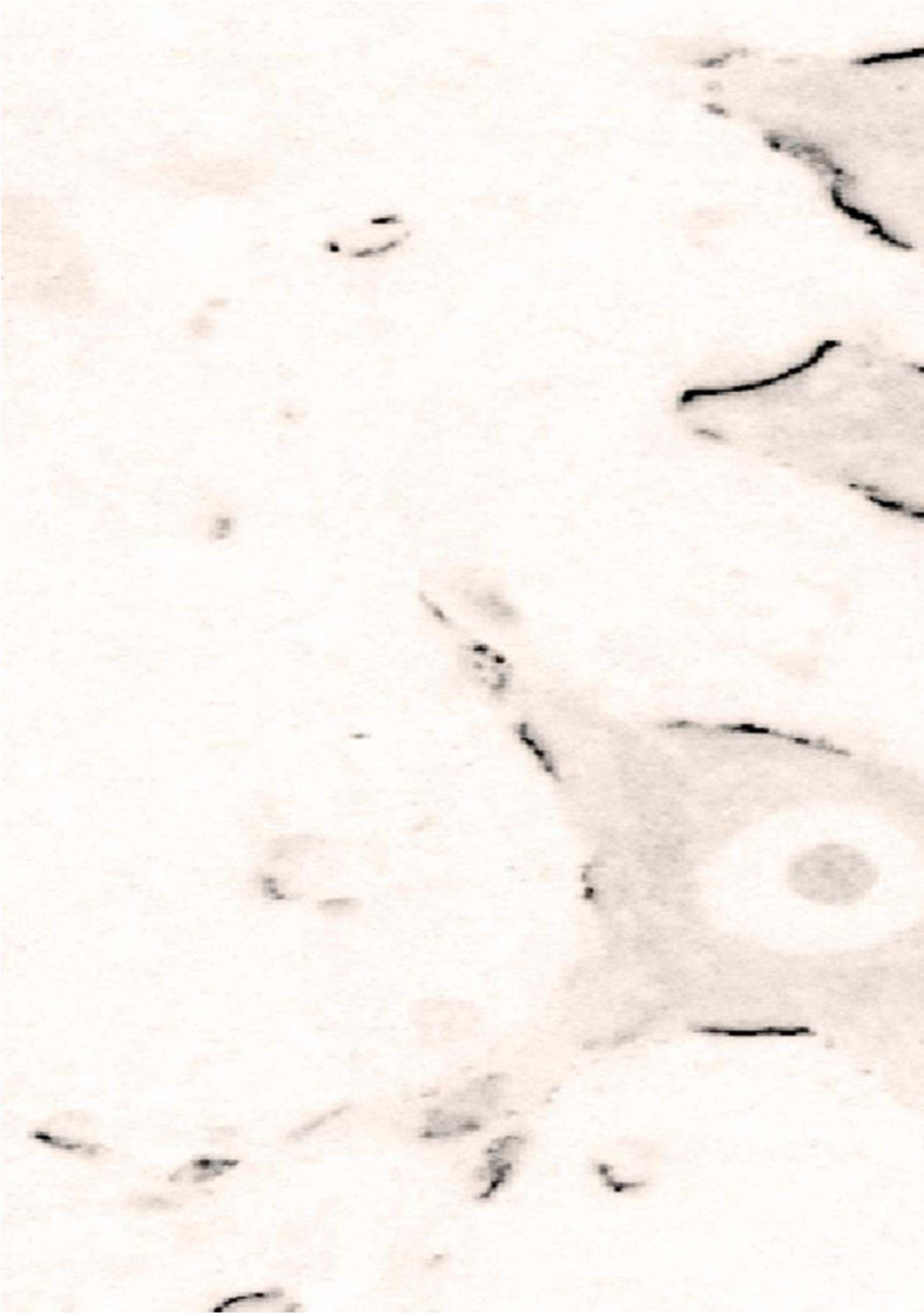
ABSTRACT

Amyotrophic lateral sclerosis (ALS) is a fatal disease characterised by the degeneration and loss of motor neurons (MNs) determining a progressive muscle paralysis. A distinctive intrinsic factor in the ALS mice model SOD1^{G93A} is the accumulation of superoxide dismutase protein in a misfolded form (mfSOD1), reproducing a familiar form of human ALS. However, extrinsic factors such as electric activity mediated by synaptic afferents, along with glial cellular environment, are crucial in ALS physiopathology. Among the afferents, C-boutons (BC) are very important cholinergic regulators of MN excitability. A distinctive feature of BC is the presence of an endoplasmic reticulum-related subsynaptic cistern (SSC) close to the postsynaptic membrane. At this site, a specific macromolecular complex formed by a variety of proteins, including neuregulin-1 (NRG1), has been described. Although some alterations in BC have been described in ALS, the role of NRG1 in BC signalling in normal or altered MNs is not known. The main objective of the present work is to characterise the molecular architecture of BC and to investigate how is altered in injured MNs; also the BC-derived signalling in the regulation of the neuroinflammatory response that takes place at the vicinity of damaged MNs was analysed. To this aim, we applied confocal and electron microscopy in different animal models, and we have determined the localisation of a variety of proteins in relation to the distinct BC synaptic subcompartments and its relation with glial cells. Our results showed that NRG1 is specifically concentrated at the SSC forming non-overlapping microdomains with other SSC proteins. By contrast, its receptors ErbB2/4 are identified in the adjacent presynaptic compartment. Furthermore, we have also found that different NRG1 isoforms are involved in the regulation of BC morphogenesis acting differentially on its pre- or postsynaptic components. BCs is disorganised in response to acute stressors, such as a peripheral nerve injury. In this situation, the loss of BCs is produced in conjunction of local recruitment of microglial cells. We also described how microglia is involved in the elimination of degenerating synaptic terminal, which were previously disrupted by a mechanism involving necroptotic pathway that was activated after axotomy. In SOD1^{G93A} mice model, we have defined 3 MN phenotypes according to the expression of mfSOD1 and vacuolar degeneration at the early presymptomatic stages of the disease. Vacuolar degeneration was characterised using mitochondrial and extracellular vesicle markers and its relationship with changes in afferent synapses and microglial cell activation. As a whole, our results provide new data on molecular organisation of the BC and the changes that takes place both, in acutely injured MNs and also during ALS. Furthermore, we provide new data regarding the cytopathology of mfSOD1 expression during early phases of MN degeneration in ALS.





AGRAÏMENTS



ÍNDEX

ABREVIATURES

I

INTRODUCCIÓ

1

PART 1. L'Esclerosi Lateral Amiotròfica

2

1.1	El sistema nerviós en humans	2
1.2.	Descobriment de l'Esclerosi Lateral Amiotròfica	2
1.3.	Símptomes clínics de les formes clàssiques d'Esclerosi Lateral Amiotròfica	3
1.4.	Epidemiologia	4
1.5.	Diagnòstic i tractament	5
1.6.	Contribució dels gens en l'Esclerosi Lateral Amiotròfica	6
1.6.1.	Superòxid dismutasa	7
1.6.2.	Chromosome 9 open reading frame	11
1.6.3.	Tar DNA Binding Protein	12
1.6.4.	Fused in sarcoma/translocated in liposarcoma	14

PART 2. Mecanismes patogènics en l'Esclerosi Lateral Amiotròfica

16

2.1	Estrès oxidatiu	17
2.2.	Disfunció mitocondrial	19
2.3.	Excitotoxicitat	20
2.4.	Alteració de l'homeòstasi proteica	21
2.5.	Estrès de reticle endoplasmàtic	22
2.6.	Alteracions en la transcripció i processament de l'ARN	23
2.7.	Alteracions del transport axonal	23
2.8.	Resposta glial i neuroinflamació	25
2.8.1.	Micròglia	25
2.8.2.	Astròglia	30
2.8.3.	Interacció micròglia-astròglia	31
2.8.4.	Oligodendròglia	32

PART 3. Sinapsis i comunicació sinàptica entre les neurones

34

3.1.	Citoarquitectura de la medul·la espinal	34
3.2.	Propietats funcionals de les MNs	35
3.3	. Sinapsis i comunicació sinàptica entre les neurones	38
3.4.	El botó C	39

3.4.1	Neuregulina-1	41
3.5.	Interrelació micròglia-sinapsis	43
HIPÒTESIS I OBJECTIUS		50
MATERIALS I MÈTODES		56
1.	Models animals	58
2.	Procediments quirúrgics i farmacològics <i>in vivo</i>	59
3.	Estimulació elèctrica	62
4.	Preparació de les mostres i anàlisis histològic	62
5.	Immunohistoquímica de fluorescència i captura d'imatges	63
6.	Microscòpia electrònica	68
7.	Cultius de medul·la espinal	70
8.	Slices <i>in vitro</i>	70
9.	Western Blot	71
10.	Anàlisi estadístic	72
RESULTATS		74
Article I. Neuregulin 1- ErbB module in C-bouton synapses on somatic motor neurons: molecular compartmentation and response to peripheral nerve injury		76
Article II. Localization and dynamic changes of neuregulin-1 at C-type synaptic boutons in association with motor neuron injury and repair		102
Article III. Microglial recruitment and mechanisms involved in the disruption of afferent synaptic terminals on spinal cord motor neurons after acute peripheral nerve injury		132
Article IV. Accumulation of misfolded SOD1 outlines distinct patterns of motor neuron pathology and death during disease progression in SOD1G93A mouse model of amyotrophic lateral sclerosis		168
DISCUSSIÓ		220
1.	Caracterització molecular i estructural dels terminals de tipus C	222
2.	Mòdul NRG1/ErbB	224

3.	Resposta del BC a diferents paradigmes de dany experimental en les MNs	225
4.	Degeneració de les MNs en el model SOD1 G93A-f	231

CONCLUSIONS	240
--------------------	------------

REFERENCES	246
-------------------	------------

ADDENDA	284
----------------	------------

ÍNDEX DE FIGURES

Figura 1. Representació esquemàtica del fascicle corticoespinal	3
Figura 2. Diagrama de les mutacions descrites en la proteïna SOD1 humana	8
Figura 3. Possibles mecanismes neurotòxics a conseqüència de l'agregació de la mfSOD1	9
Figura 4. Representació esquemàtica de les diferents fases de la progressió de l'ELA en el ratolí SOD1 G93A	10
Figura 5. Representació dels mecanismes patològics en els que està involucrat C9orf72	12
Figura 6. Esquema de la neurotoxicitat mediada per TDP-43	13
Figura 7. Principals hipòtesis sobre els mecanismes fisiopatològics contribuents a la degeneració de les MNs en l'ELA	
	17
Figura 8. Esquema de la remodelació morfològica de la micròglia	27
Figura 9. Esquema de la polarització M1/M2	28
Figura 10. Esquema de l'organització de les agrupacions de MNs en una secció transversal de medul·la espinal lumbar	
	35
Figura 11. Representació esquemàtica d'un potencial d'acció	36
Figura 12. Esquema de les fibres musculars en una secció longitudinal	37
Figura 13. Esquema gràfic on es representa l'organització molecular dels BC	40
Figura 14. Immunolocalització de la NRG1 en els BC de MNs espinals	40
Figura 15. Estructura proteica de les isoformes I i III de la NRG1	42
Figura 16. Isoformes de NRG1 i tipus de senyalització que desencadenen	43
Figura 17. Representació gràfica de la via necroptòtica	46
Figura 18. Model hipotètic de la comunicació entre el mitocondri i el RE en la paraptosi	47

Figura 19. Esquema de la pauta farmacològica seguida pels tractaments amb l'agonista Oxotremorina i l'antagonista Metocatrina dels receptors M2 muscarítics	60
Figura 20. Esquema de la pauta farmacològica seguida amb els fàrmacs Tunicamicina i Salubrinal (inductor i inhibidor de l'estrés de reticle respectivament)	61
Figura 21. Esquema de la pauta farmacològica seguida amb l'inhibidor del CSF-1 anomenat PLX5622 per tal d'inhibir la proliferació microglial	61
Figura 22. Esquema de la possible distribució d'algunes de les proteïnes específicament concentrades als BC	222
Figura 23. Esquema dels possibles mecanismes de comunicació transinàptica que farien possible el contacte NRG1-ErbB la senyalització via exosomal o la interacció juxtacrina	225
Figura 24. Representació esquemàtica del possible rol primari de la micròglia en la deafferentació sinàptica postaxotomia	228
Figura 25. Representació esquemàtica del possible rol tardà de la micròglia en la deafferentació sinàptica postaxotomia	229
Figura 26. Representació esquemàtica de les dos funcions que poden derivar de l'activació del p-MLKL	231
Figura 27. Esquema representatiu de l'evolució de les MNs durant el curs de l'ELA segons els fenotips definits	236

ÍNDEX DE TAULES

Taula 1. Llista de gens implicats en la patogènesi de l'ELA, d'acord amb la base de dades de l'Herència Mendelianiana en línia en l'home (Online Mendelian Inheritance in Man (OMIM))

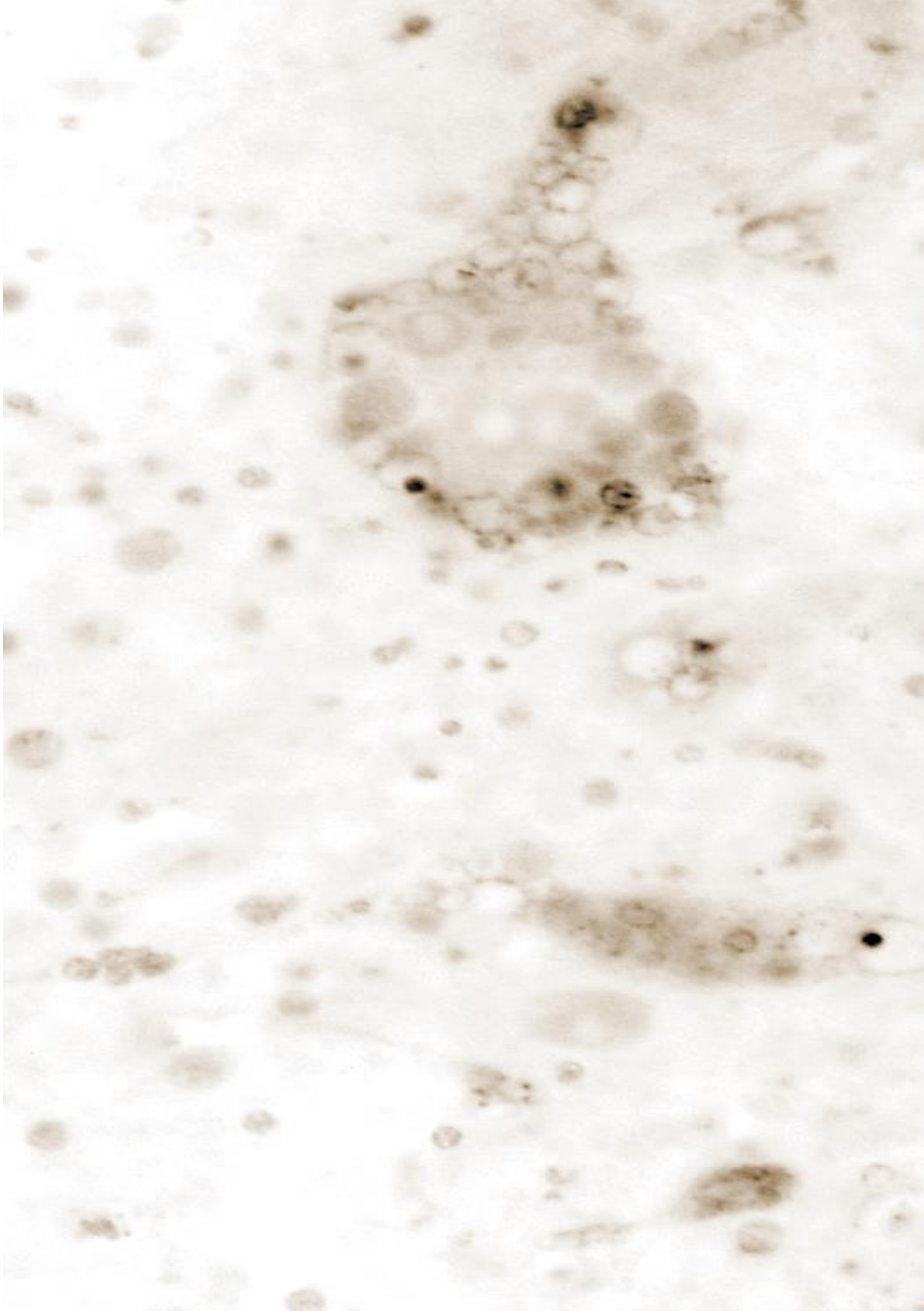
7

Taula 2. Anticossos utilitzats per immunohistoquímica de fluorescència

65

Taula 3. Anticossos utilitzats per l'immunomarcatge ultraestructural abans de la inclusió en la reina

	69
Taula 4. Anticossos utilitzats per l'immunomarcatge ultraestructural després de la inclusió en la reïna	
	69
Taula 5. Anticossos utilitzats per WB	72



ABREVIATURES

A**ACSF**

Artificial Cerebrospinal Fluid
Líquid cefalorraquídai artificial

ADN

Àcid Desoxiribonucleic

ADP

Adenosine Diphosphate
Difosfat d'adenosina

AHP

After Hyperpolarization Peak
Període posthiperpolarització

ARN

Àcid Ribonucleic

ATP

Adenosine Triphosphate
Trifosfat d'adenosina

B**BACE-1**

β-site Amyloid precursor protein-Cleaving Enzyme1
Enzim de trencament de proteïnes precursor amiloide del lloc β 1

BC

Botó C

BSA

Bovin Serum Albumin
Albúmina sèrica de boví

C**C9ORF72**

Chromosome 9 open reading frame 72

CSF-1

Colony Stimulating Factor-1
Factor estimulant de la colònia-1

CTB

Cholera Toxin B
Toxina colèrica B

E**EAAT**

Excitatory Amino Acid Transporter
Transportadors específics de glutamat

EGF-like

Epidermal Growth Factor-like
Factor de creixement epidèrmic

ELA

Esclerosi Lateral Amiotròfica

F**FF**

Fast-twitch Fatigable
Fatigables i de contracció ràpida

FFR

Fast-twitch Fatigue-Resistant
Resistents a la fatiga i de contracció ràpida

FUS

Fused in sarcoma/translocated in liposarcoma

G**GABA**

γ-Aminobutyric acid
Àcid γ -aminobutíric

GFAP

Glial Fibrilar Acid Protein
Proteïna àcida fibril·lar glial

GFP

Green Fluorescent Protein
Proteïna verda fluorescent

H**HA-NRG1^{FL}**

Sobreexpressor de NRG1 tipus III conjugada a la proteïna hemaglutinina

HA-NRG1^{GIEF}

Sobreexpressor de la variant processada per la proteasa BACE1 de la NRG1 tipus III

I**Iba-1**

Ionized calcium Binding Adaptor molecule 1

Molècula adaptadora d'unió de calci ionitzat-1

Ig-like

Immunoglobulin-like
Semblant a immunoglobulines

IL

Interleucina

K**KO**

Knock-Out
Genèticament deficients

Kv2.1

Potassium channel, Voltage dependent 2.1

Canal de potassi voltagte dependent 2.1

M**MBP**

Myelin Basic Protein
Proteïna bàsica de la mielina

MCT1

Monocarboxylate Transporter 1
Transportador de monocarboxilats

mfSOD1	P	SNP
<i>Misfolded SOD1</i>		Sistema Nerviós Perifèric
Mal plegament de la proteïna SOD1	p	
	Postnatal	SOD1
MLKL	PB	Superòxid Dismutasa-1
<i>Mixed Lineage Kinase domain-Like</i>	<i>Phosphate Buffer</i>	
Proteïna efectora de llinatge cinasa mixta semblant a un domini	Tampó fosfat	SR1
		<i>Sigma Receptor-1</i>
MMP-9	PBS	Receptor sigma-1
<i>Matrix Metallopeptidase-9</i>	<i>Phosphate-Buffered Saline</i>	
Matriu metalopeptidasa-9	Tampó fosfat salí	SSC
		<i>Subsynaptic Cistern</i>
MN	PCR	cisterna subsinàptica
Motoneurones	<i>Polymerase Chain Reaction</i>	
	Reacció en Cadena de la Polimerasa	T
N		
NGF	PFA	TBST
<i>Nerve Growth Factor</i>	Paraformaldehid	Tampó Tris Salí
Factor de creixement neural		
NGS	R	TDP-43
<i>Normal Goat Serum</i>		<i>Tar DNA binding protein-43</i>
Sèrum de cabra	RE	
	Reticle Endoplasmàtic	TG
NHS	RIPA	Transgènic
<i>Normal Horse Serum</i>	<i>Radioimmunoprecipitation Assay buffer</i>	TLR
Sèrum de cavall	Tampó de lisis de radioimmunoprecipitació	<i>Toll-Like Receptors</i>
NO		Receptors <i>toll-like</i>
<i>Nitric oxide</i>	ROS	TNF-α
Òxid nítric	<i>Reactive Oxigen Species</i>	<i>Tumoral Necrosis Factor-α</i>
	Espècies Reactives d'Oxigen	Factor de necrosis tumoral α
NRG1^{type I}		U
Sobreexpressors de la isoforma I de NRG1		
NRG1	S	UPR
Neuregulina-1	SDS	<i>Unfolded Protein Response</i>
	<i>Sodium Dodecyl Sulfate</i>	Resposta a proteïnes mal plegades
	Dodecilsulfat Sòdnic	
O		V
OMIM	SFR	VAChT
<i>Online Mendelian Inheritance in Man</i>	<i>Slow-twitch Fatigue-Resistant</i>	<i>Vesicular Acetyl Choline Transporter</i>
Herència Mendeliana en línia en l'home	Resistents a la fatiga i de contracció lenta	Transportador vesicular de l'acetilcolina
	SNC	
	Sistema Nerviós Central	

VDAC1

Voltage Dependent Anion Channel

1

Canal aniónic voltatge dependent

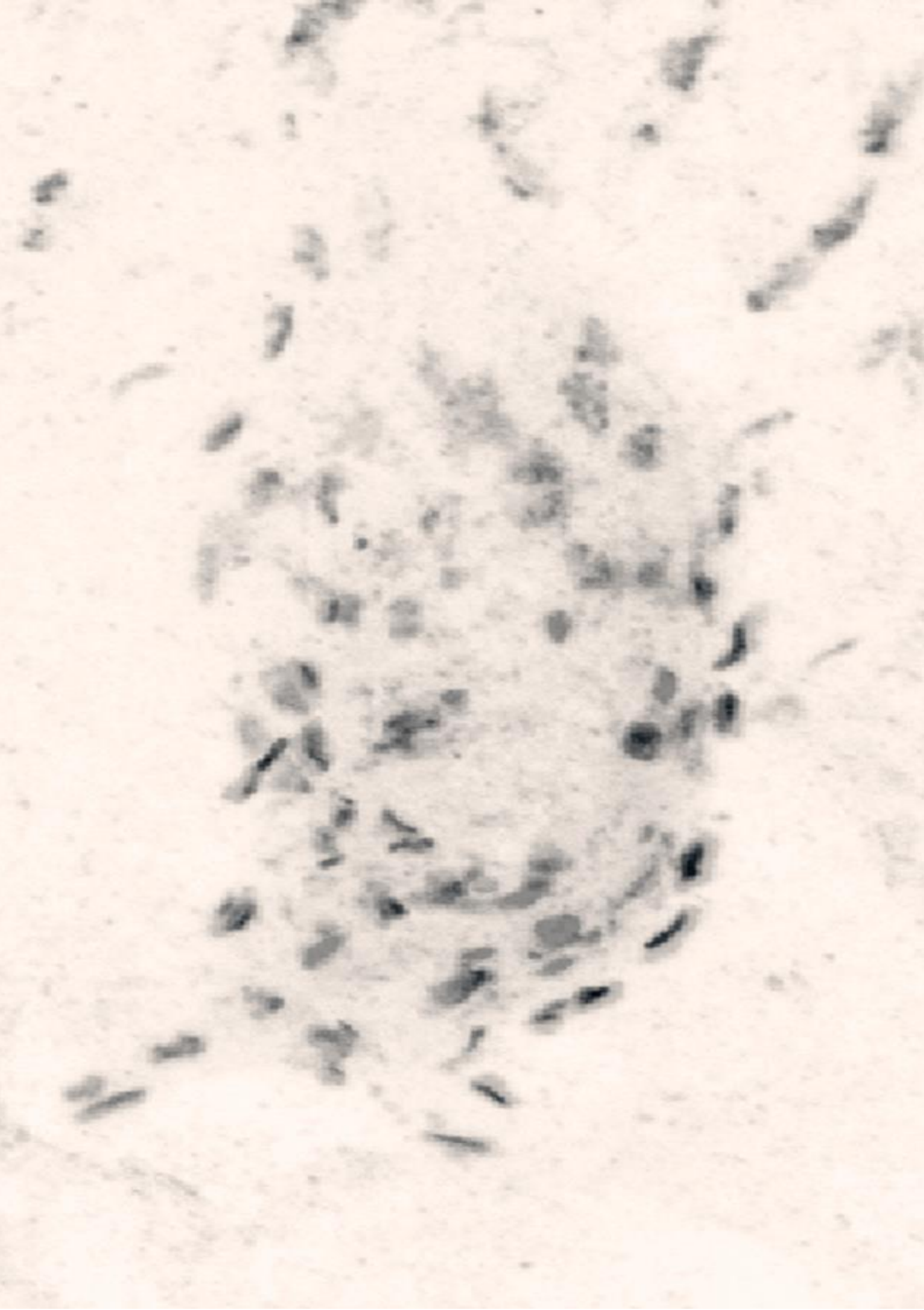
W**WB**

Western Blot

WT

Wild-Type

Salvatge



INTRODUCCIÓ

1

L'Esclerosi Lateral Amiotròfica

1.1 El sistema nerviós en humans

El sistema nerviós és una de les estructures més complexes i altament organitzades del cos humà. La seva funció essencial és integrar, analitzar i respondre de manera adequada als estímuls interns i externs que rebem constantment.

Des del punt de vista anatòmic, el sistema nerviós està dividit en el sistema nerviós central (SNC), format per l'encèfal i la medul·la espinal; i el sistema nerviós perifèric (SNP), format pels nervis cranials i els nervis espinals, els quals condueixen impulsos des del SNC (nervis eferents o motors) i cap al SNC (nervis aferents o sensitius) (Ross & Pawlina, 2015). També formen part del SNC els ganglis simpàtics, parasimpàtics i sensorials així com els plexes mientèrics i estructures receptors sensorials.

Les neurones són la unitat estructural i funcional del sistema nerviós. Les motoneurones (MNs) són una població específica de neurones localitzades en el SNC que s'encarreguen de controlar els moviments motors voluntaris de l'organisme. Citològicament es caracteritzen, a grans trets, per tenir un cos cel·lular o soma gran i en forma estrellada, amb un gran nucli esfèric i abundants grumolls de Nissl dins del citoplasma (Ross & Pawlina, 2015). Les MNs degeneren selectivament en determinats processos patològics, com és el cas de l'Esclerosi Lateral Amiotròfica (ELA).

1.2. Descobriment de l'Esclerosi Lateral Amiotròfica

L'ELA va ser caracteritzada pel neuròleg francès *Jean-Martin Charcot* l'any 1869, qui va establir per primera vegada la relació entre els símptomes clínics i les alteracions neuropatològiques subjacentes a l'evolució d'aquesta malaltia. Va ser el *Charcot* qui va introduir el terme ELA per referir-se a la malaltia, tot i que de vegades també s'anomena “Malaltia de *Charcot*”. En canvi, als Estats Units, es

coneix com a “Malaltia de *Lou Gehring*”, en memòria del famós jugador de beisbol que va morir als 38 anys a conseqüència de l’ELA.

El nom ELA fa referència a les troballes anatopatològiques on s’observa desmielinització i esclerosi en el cordó lateral de la medul·la espinal corresponent a la via corticospinal o piramidal. El terme esclerosis es refereix a l’ “enduriment patològic d’un teixit o òrgan degut a la hiperplàsia de les cèl·lules de teixit conjuntiu que formen la seva estructura”, que en aquest cas, fa referència al procés de gliosi cicatricial que substitueix a les MNs degenerades. Lateral identifica el tracte piramidal en el cordó lateral de la medul·la espinal. Finalment, el terme “amiotròfica” prové del grec on “*a-*” significa “no”, “*-mio-*” fa referència al múscul i “*-tròfia*”, forma sufixada del mot “*trophé*”, que significa alimentació. Llavors, amiotròfia significa “múscul sense nutrició” el qual descriu la desnervació i debilitat muscular que s’observa en aquesta malaltia (Hulisz, 2018; Rowland & Shneider, 2001; Taylor *et al.*, 2016).

1.3. Símptomes clínics de les formes clàssiques d’Esclerosis Lateral Amiotròfica

En l’ELA s’afecta la primera neurona (MN superior) situada en l’àrea 4-γ de Brodmann en l’escorça motora del lòbul frontal. Aquesta, projecta el seu axó directament a una segona neurona (MN inferior), situada a la banya ventral de la medul·la espinal o en els nuclis motors del parells cranials del tronc de l’encèfal. Finalment, la MN inferior projecta el seu axó fora del SNC fins a establir una connexió sinàptica amb els músculs esquelètics corresponents, controlant així la seva capacitat contràctil, i en definitiva, els moviments voluntaris (Fig. 1).

En l’ELA es produeix un desacoblament selectiu de les MNs corticals de la seva

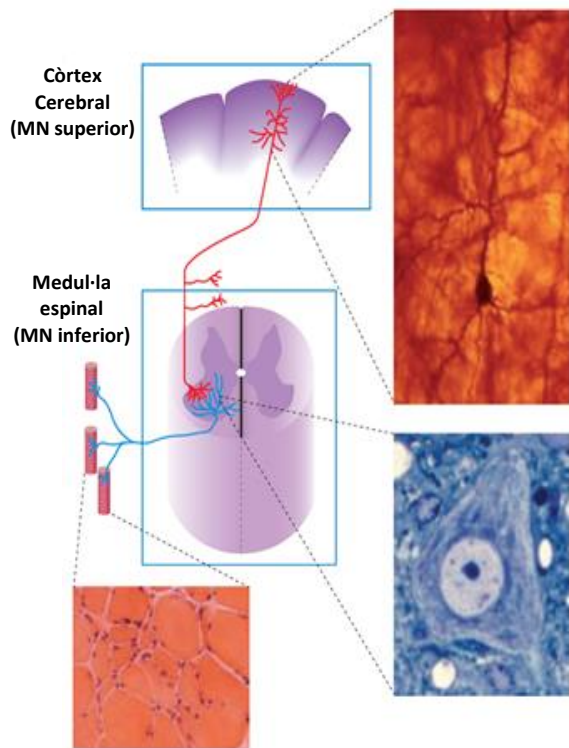


Figura 1 | Representació esquemàtica del fascicle corticospinal. Esquema de la via motora voluntària directa, des del seu origen en el còrtex motor (MN superior), connectant amb la medul·la espinal (MN inferior), fins a establir connexió amb les fibres musculars esquelètiques. Cada estació neuronal va acompanyada de la imatge histològica corresponent. Adaptat de JE. Esquerda, 2006.

diana, la segona neurona, i alhora, aquestes també es disconnecten de la seva diana muscular. La degeneració progressiva de les MNs dóna lloc a l'aparició dels primers símptomes de la malaltia, els quals depenen de la localització de les MNs en procés de degeneració més avançat. En la majoria dels pacients (70%) els primers símptomes acostumen a ser hiperreflexia i debilitat muscular gradual d'inici asimètric i distal (normalment en les extremitats), que poc a poc es va fent bilateral per afectació de les MNs espinals. Aproximadament en un 25% dels pacients, el símptoma inicial consisteix en problemes en la parla o dificultat per deglutir, la qual cosa indica que la població de MNs més afectades són les localitzades a la zona bulbar (Kiernan *et al.*, 2011).

En etapes més avançades, l'ELA es manifesta per fasciculacions i, secundàriament a la denervació causada per la degeneració, es produeix atròfia muscular (per afectació de la MN inferior) i hiperreflexia i espasticitat (signe d'afectació de la MN superior). S'instaura una paràlisi muscular progressiva que conduceix a la mort del pacient entre els 3 i 5 anys des de l'inici dels símptomes, generalment degut a un fracàs respiratori. Excepcionalment, es poden observar supervivències majors, sobre tot si s'ofereixen dispositius de ventilació artificial. En general, es mantenen inalterades les funcions no vinculades a l'activitat motora, com són les funcions cognitives i sensitives les quals estan preservades.

Tot i que són molt menys freqüents, també hi ha altres possibles presentacions clíniques de l'ELA, com són la insuficiència respiratòria, pèrdua de pes, astènia sense causa aparent, rampes i fasciculacions sense debilitat muscular, espasticitat en cames, labilitat emocional o deteriorament cognitiu.

Cal dir que algunes MN són resistents a l'ELA, és a dir, que no degeneren i que per tant, hi ha algunes funcions motores que no s'affecten. La majoria dels pacients tenen poca o nul·la afectació de la musculatura extraocular i mantenen també el control dels esfínters que controlen la defecació i la micció, tot i que poden desenvolupar problemes d'incontinència a conseqüència de la debilitat de la musculatura abdominal.

1.4. Epidemiologia

Epidemiològicament, l'ELA té una incidència d'aproximadament 1-2 nous casos per any per cada 100.000 habitants (es diagnostiquen 3 nous casos cada dia a Espanya), i una prevalença de 3-5 afectats per cada 100.000 habitants, sent més prevalent en el sexe masculí (1.5:1) (Kiernan *et al.*, 2011). Segons dades de la *Sociedad Española de Neurología*, el número total de pacients amb ELA a

Espanya és d'aproximadament d'uns 3.000 casos, cosa que posa de manifest l'elevada i ràpida mortalitat d'aquesta malaltia neurodegenerativa. L'ELA és una malaltia de l'adult, ja que sol debutar clínicament entre els 40 – 70 anys, trobant-se la incidència més alta entre els 50-60 anys (60% del total d'afectats). És inhabitual en gent de < 30 anys i també és excepcional que gent de > 70 anys debuti amb ELA. L'esperança de vida és d'aproximadament 3 anys, encara que un 20% dels pacients viuen > 5 anys i un 10%, >10 anys (Hulisz, 2018).

1.5. Diagnòstic i tractament

Pel que fa al diagnòstic de l'ELA, al 1990 es van establir les directrius a seguir en un document consens anomenat *Criterios del Escorial*, les quals s'han anat revisant i actualitzat periòdicament. El diagnòstic d'ELA és el que s'anomena “d'exclusió” ja que abans de fer el diagnòstic definitiu s'han d'anar descartant patologies que cursen amb una clínica similar. La diagnosi està fonamentada en criteris clínics i tests electrofisiològics, principalment electromiogrames, ja que actualment no es disposa de biomarcadors que confirmen objectivament el diagnòstic en les etapes inicials. Degut a això i a que la manifestació clínica de l'ELA pot ser diversa, el diagnòstic definitiu pot allargar-se més enllà d'un any.

Els criteris diagnòstics del *Escorial* requereixen que primer hi hagi un quadre clínic compatible amb l'ELA que vagi progressant a diferents regions medul·lars. Són necessàries també proves complementàries, com proves d'imatge o biòpsies per descartar altres processos que puguin afectar la via piramidal (tumors de l'àrea frontal i motora,...). Una vegada complerts aquestes dos condicions, a trets generals, es parla de 4 categories: sospita d'ELA, possible ELA, probable ELA i ELA definitiva, segons el grau de certesa del diagnòstic tenint en compte tota la informació clínica disponible (Brooks, 1994).

Actualment no es disposa de cap fàrmac capaç de curar o modificar el curs natural de l'ELA. Només el *Riluzole* (agent antiglutamatèrgic) (Doble, 1996) i l'*Edaravone* (agent antioxidant) (Jeffrey D. Rothstein, 2017) són els únics dos fàrmacs aprovats pel tractament de l'ELA, amb efectes terapèutics molt modestos i inclús controvertits, els quals tot i que no reverteixen el dany causat en la malaltia, poden alentir una mica la progressió, cosa que es tradueix en una moderada millora en la supervivència dels pacients (3 – 6 mesos).

Per tant, l'única teràpia per als pacients d'ELA és una aproximació multidisciplinar destinada a les cures paliatives, per tal de prevenir complicacions i incrementar la qualitat de vida dels pacients, sobretot en les fases de major afectació.

1.6. Contribució dels gens en l'Esclerosi Lateral Amiotròfica

Tot i la semblança a nivell de progressió i manifestació clínica, en l'ELA, es distingeixen dos formes: l'ELA esporàdica (90% dels casos), on la causa és desconeguda i no s'observa herència familiar; i l'ELA familiar (10% dels casos), on es coneix l'origen genètic de la malaltia i s'hi associa una herència familiar, normalment dominant i amb una alta penetrància.

Tot i que en els casos esporàdics no es conegui la causa, aquesta pot estar en mutacions genètiques, però que aquestes mutacions hagin sorgit *de novo* en un individu, i que per tant, no passin a la descendència. Aquestes alteracions genètiques poden contribuir a l'etiològia directament o només donar susceptibilitat a l'individu per patir ELA, el qual necessitaria de factors ambientals per acabar desenvolupant la malaltia. Alguns factors de risc que s'han relacionat amb l'ELA són professions relacionades amb metalls pesats, esportistes d'elit, pesticides, químics, entre d'altres, tot i que no hi ha una relació clara que provi la causalitat (Hulisz, 2018).

Encara que les formes familiars d'ELA són molt menys freqüents que les formes esporàdiques, han tingut un paper central per entendre els mecanismes patogènics de l'ELA ja que han permès descobrir mutacions causants de la malaltia en famílies, traslladar-les a models animals i estudiar en aquests quins efectes tenen.

L'any 1993 es va descriure per primera vegada que mutacions en el gen que codifica per la proteïna Superòxid Dismutasa-1 citosòlica (SOD1) era la causa d'un tipus d'ELA familiar (Rosen *et al.*, 1993). Des de llavors, s'han descrit diverses mutacions en diferents gens associats inequívocament en a la patogènesi de l'ELA (Su *et al.*, 2014) (Taula 1.). De tots, els 4 que més freqüentment es troben mutats, tant en formes esporàdiques com familiars són: *Chromosome 9 open reading frame 72* (*C9orf72*), *Sod1*, *Tar DNA binding protein* (*Tardbp*) i *Fused in sarcoma/translocated in liposarcoma* (*Fus*) (Y. Hayashi *et al.*, 2016).

Gene/Locus	Location	Phenotype	Inheritance
<i>TARDBP</i>	1p36.22	ALS/FTD	AD
<i>ALS2</i>	2q33.1	ALS, juvenile	AR
<i>ERBB4</i>	2q34	ALS	AD
<i>TUBA4A</i>	2q35	ALS/FTD	AD
<i>CHMP2B</i>	3p11.2	ALS	AD
<i>MATR3</i>	5q31.2	ALS	AD
<i>SQSTM1</i>	5q35.3	ALS/FTD	AD
<i>FIG4</i>	6q21	ALS	AD
<i>C9orf72</i>	9p21.2	ALS/FTD	AD
<i>SIGMAR1</i>	9p13.3	ALS, juvenile	AR
<i>VCP</i>	9p13.3	ALS/FTD	
<i>SETX</i>	9q34.13	ALS, juvenile	AD
<i>OPTN</i>	10p13	ALS	
<i>ANXA11</i>	10q22.3	ALS	AD
<i>HNRNPA1</i>	12q13.13	ALS	AD
<i>TBK1</i>	12q14.2	ALS/FTD	AD
<i>ANG</i>	14q11.2	ALS	
<i>SPG11</i>	15q21.1	ALS, juvenile	AR
<i>FUS</i>	16p11.2	ALS/FTD	
<i>PFN1</i>	17p13.2	ALS	
<i>ALS3</i>	18q21	ALS	AD
<i>ALS7</i>	20p13	ALS	
<i>VAPB</i>	20q13.32	ALS	AD
<i>SOD1</i>	21q22.11	ALS	AD, AR
<i>CHCHD10</i>	22q11.23	ALS/FTD	AD
<i>UBQLN2</i>	Xp11.21	ALS/FTD	XLD

Taula 1. Llista de gens implicats en la patogènesi de l'ELA, d'acord amb la base de dades de l'Herència Mendeliana en línia en l'home (*Online Mendelian Inheritance in Man (OMIM)*) . ALS: ELA; FTD: demència frontotemporal; AD: herència autosòmica dominant; AR: herència autosòmica recessiva; XLD: herència lligada al cromosoma X. Adaptat de Ferrara et al., 2018.

1.6.1 Superòxid dismutasa 1

La proteïna SOD1 és un enzim que en condicions fisiològiques protegeix les cèl·lules de les espècies reactives d'oxigen mitjançant la dismutació de l'anió superòxid en oxigen i peròxid d'hidrogen. La SOD1 s'expressa ubliquament en les cèl·lules dels organismes i es localitza en molts compartiments cel·lulars, incloent el citoplasma, el nucli, l'espai mitocondrial intermembrana, els lisosomes i els peroxisomes.

Els estudis genètics van començar amb la identificació d'onze mutacions sense sentit en el gen *Sod1* en 13 famílies diferents (Rosen et al., 1993). Actualment, s'han descrit en pacients d'ELA més de 150 mutacions en aquest gen distribuïdes en totes les regions dels 153 aminoàcids del polipèptid de la SOD1 (Fig. 2). Les mutacions en aquest gen representen aproximadament un 20% de les formes familiars d'ELA, essent de transmissió autosòmica dominant, i constituint un 1% de les formes esporàdiques (G. Kim et al., 2020; Zou et al., 2017).

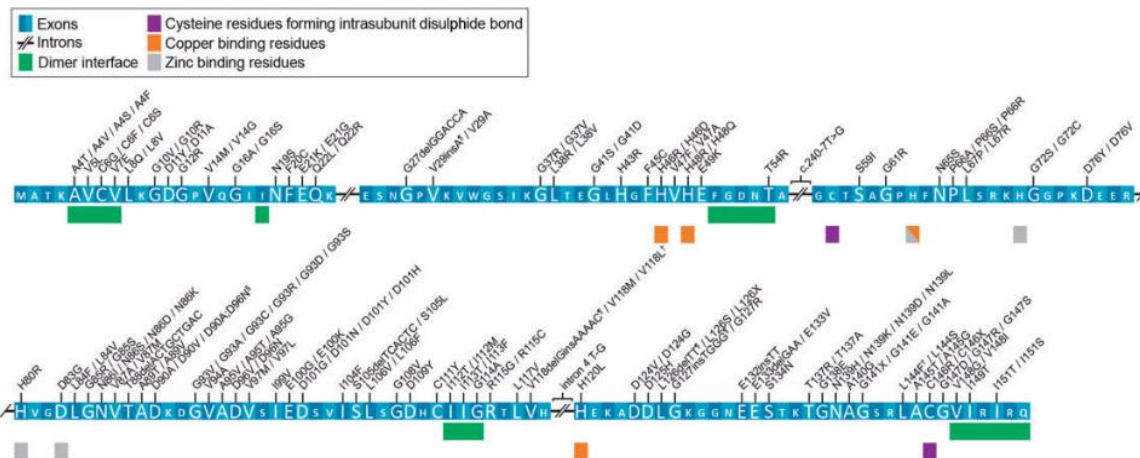


Figura 2 | Diagrama de les mutacions descrites en la proteïna SOD1 humana. S'observa tota la seqüència d'aminoàcids de la proteïna SOD1 amb les 155 mutacions descrites en pacients amb ELA. Extret de Saccon *et al.*, 2013.

No totes les mutacions en la SOD1 causen la mateixa clínica, per exemple, la mutació SOD1^{D90A} en homozigosi (és d'herència recessiva) causa una clínica moderada, amb una supervivència mitja de més de 10 anys; en canvi, la mutació SOD1^{A4V} és dominant i causa una ELA ràpidament progressiva (Hulisz, 2018; Su *et al.*, 2014).

Tot i les múltiples alteracions genètiques associades a la SOD1, la patologia no correlaciona amb una disminució de l'activitat enzimàtica d'aquesta proteïna. La SOD1 mutada és neurotòxica degut a un guany de funció causant el mal plegament de la proteïna (*misfolded SOD1* (mfSOD1)) i implicant una acumulació i agregació d'aquesta. Aquests agregats poden interferir en la funció d'altres proteïnes cel·lulars, interferir en el normal funcionament del sistema ubiquítina-proteasoma i, fins i tot, causar disfuncions en diferents orgànuls com els mitocondris o el reticle endoplasmàtic (Fig. 3) (Morgan & Orrell, 2016).

Tot i la presència de SOD1 en el citosol de totes les cèl·lules, la vida mitjana d'aquesta és major en les MNs. Sembla ser que el dany oxidatiu, el qual s'acumula amb el temps afectant especialment cèl·lules postmitòtiques com són les neurones, induceix preferentment el mal plegament de la SOD1 mutada, cosa que explicaria parcialment la selectiva vulnerabilitat de les MNs a l'ELA en presència de la SOD1 mutada (Su *et al.*, 2014).

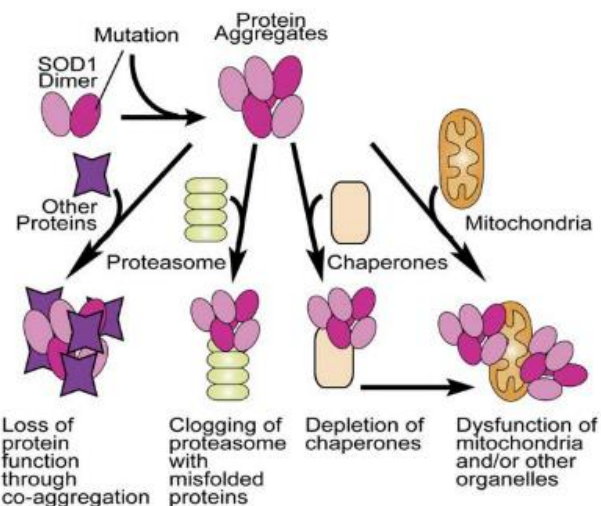


Figura 3 | Possibles mecanismes neurotòxics a conseqüència de l'agregació de la mfSOD1. Els agregats de mfSOD1 poden estar induint l'agregació de components citoplasmàtics essencials; saturant el proteasoma i per tant, afectant la degradació proteica; col·lapsant les xaperones alterant així el correcte plegament de les proteïnes; i danyant els mitocondris. Extret de Boillée et al., 2006.

Després del descobriment de la mutació de l'enzim SOD1, el gen mutat de la *Sod1* humana es va inserir en un ratolí, generant un model animal transgènic que reproduïa el fenotip de l'ELA humana *in vivo*, obrint així la possibilitat d'investigar els mecanismes etiopatogènics subjacents a la malaltia (Gurney et al., 1994; Ripps et al., 1995). Des de llavors, el model animal més utilitzat en la recerca preclínica en el context d'ELA és el ratolí amb la mutació SOD1^{G93A} (Gois et al., 2020). Aquest ratolí transgènic sobreexpressa una variant mutada del gen humà per la SOD1 sota el control del promotor humà *Sod1*. L'agressivitat de la malaltia depèn del nivell de sobreexpressió del transgèn, ja que en funció del nombre de copies variarà la precocitat del debut simptomatològic així com la velocitat de progressió (Thomas Philips & Rothstein, 2015). Així doncs, el model de ratolí SOD1^{G93A} reproduceix bastant fidelment els símptomes clínics de la malaltia (Boillée et al., 2006; Kanning et al., 2010).

En aquesta tesi, s'utilitzen ratolins que expressen altos nivells de l'enzim SOD1^{G93A} humà el qual causa una ràpida progressió de la malaltia, sent la vida màxima d'aquests animals 120 ± 9 dies. Els primers 30 dies postnatals (p30) són clínicament asimptomàtics, però ja en aquesta fase es poden detectar algun canvis fisiopatològics en les MNs. Des de p30 fins a p60, els animals comencen a desenvolupar símptomes conductuals lleugers sense clínica evident, corresponents al període presimptomàtic.

Entre p60 i p90 es manifesten els símptomes clínics característics (tremor, rigidesa,...). Finalment, entre p90 i p120, els ratolins entren en la fase terminal, on hi ha una pèrdua massiva de MNs, els símptomes clínics tals com espasticitat i paràlisi es fan més evidents i progressen ràpidament fins a

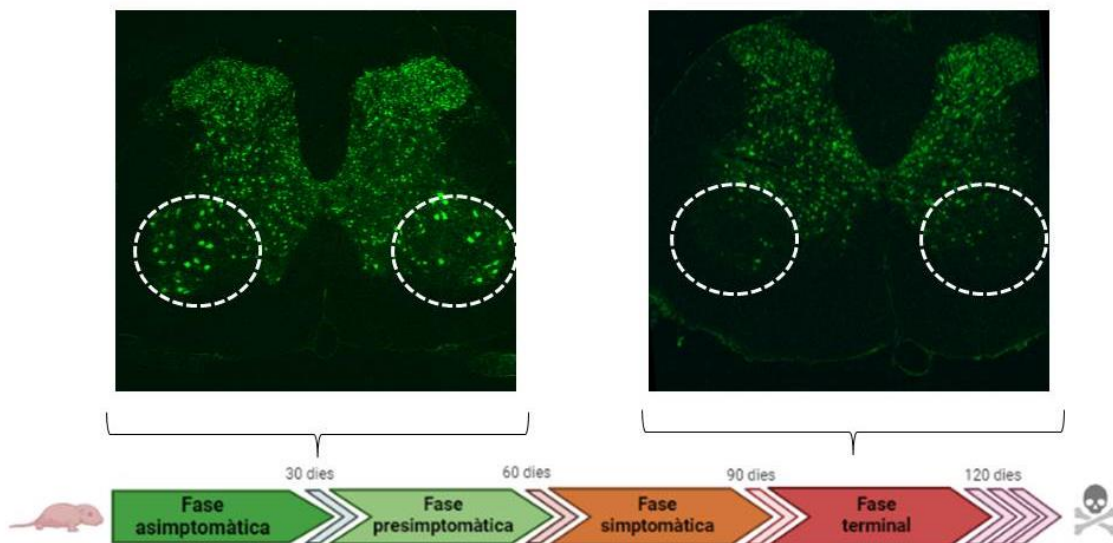


Figura 4 | Representació esquemàtica de les diferents fases de la progressió de l'ELA en el ratolí SOD1^{G93A}. Fins a p30 no presenten cap síntoma clínic; de p30 a p60 no tenen clínica evident però ja s'observen canvis a nivell cel·lular; de p60 a p90 debuta la clínica de l'ELA progressant ràpidament fins que als 3 mesos d'edat es produeix la mort de l'animal. Les imatges mostren una secció transversal de medul·la espinal on s'ha immunomarcat les neurones (verd) i on en la banya ventral de la medul·la espinal (cercles amb línia discontinua) es pot observar la pèrdua massiva de MNs. Creat amb Biorender.

causar la mort de l'animal (Mancuso *et al.*, 2012; B. Turner & Talbot, 2008) (Fig. 4).

No obstant, existeixen altres ratolins transgènics que tenen deleccions, insercions, altres mutacions puntuals o mutacions que provoquen una proteïna truncada de la SOD1 que també reproduueixen el fenotip de l'ELA humana.

També hi ha altres models animals amb mutacions en el gen per la SOD1 que s'utilitzen per estudiar l'ELA com són les rates, amb la mutació SOD1^{G93A} o SOD1^{H46R} (Howland *et al.*, 2002; M. Nagai *et al.*, 2001; Sanagi *et al.*, 2010); el peix zebra (*Danio rerio*), amb la mutació SOD1^{T70I} o SOD1^{G93R} (Benedetti *et al.*, 2016; Da Costa *et al.*, 2013; Powers *et al.*, 2017; Ramesh *et al.*, 2010); les mosques (*Drosophila melanogaster*) en la que s'insereix el gen humà per la SOD1 amb mutacions puntuals (Watson *et al.*, 2008), o fins i tot el nemàtode (*Caenorhabditis elegans*) (Cornaglia *et al.*, 2016; J. Li *et al.*, 2013, 2014; Oeda *et al.*, 2001) o el llevat (*Saccharomyces cerevisiae*) (Bastow *et al.*, 2016; Gois *et al.*, 2020; Martins & English, 2014).

Tots aquests models reproduueixen certs aspectes de l'ELA, però no totes les característiques que s'han descrit en pacients. Tot i això, han servit per millorar el coneixement sobre els aspectes bàsics de la fisiopatologia d'aquesta malaltia.

1.6.2. Chromosome 9 open reading frame 72

Fisiològicament el gen *C9orf72* codifica per la proteïna “*Guanine nucleotide Exchange C9orf72*” (*C9ORF72*) la qual, tot i que la seva funció no es coneix completament, sembla estar involucrada en la regulació de l'autofàgia. Aquest gen s'expressa en diversos òrgans i teixits cel·lulars, tals com el SNC, els limfòcits, la medul·la óssia i la melsa.

En l'intró 1 del gen s'hi localitza l'hexanucleòtid GGGGCC, el qual en individus sans pot estar repetit de 2 a 25 vegades. En pacients d'ELA aquesta seqüència pot estar repetida de centenars a milers de cops, donant lloc a ARN missatgers (ARNm) i proteïnes disfuncionals (DeJesus-Hernandez *et al.*, 2011; Renton *et al.*, 2011). Actualment, l'expansió d'aquest hexanucleòtid és la causa genètica coneguda més freqüent d'ELA (25-40% de casos familiars), d'herència autosòmica dominant i associada a demència frontotemporal. També representa un 5-7% dels casos esporàdics de pacients amb ancestres europeus (Hulisz, 2018; G. Kim *et al.*, 2020; Zou *et al.*, 2017).

Aquesta expansió induceix neurodegeneració via un guany de funció tòxica del ARN i/o de la proteïna. L'ARNm transcrit segresta proteïnes d'unió a ARN (*RNA binding proteins*), disminuint la quantitat d'aquestes proteïnes en la cèl·lula i alterant així el metabolisme de l'ARN.

Una característica d'aquesta expansió és que pot promoure la traducció no iniciada per ATG de l'hexanucleòtid en 6 sentits diferents, la qual cosa produeix repetitions de 5 dipèptids diferents extremadament hidrofòbics que s'agreguen i que s'han localitzat acumulats en regions afectades per l'ELA (Fig. 5). També s'han de tenir en compte les alteracions epigenètiques d'aquest gen, ja que la hipermetilació de les citocines de l'hexanucleòtid es correlaciona amb supervivències més curtes. Això fa que es proposi aquesta alteració epigenètica com un possible marcador de mal pronòstic per l'ELA (Morgan & Orrell, 2016; Su *et al.*, 2014).

En relació als models animals generats, presenten la inserció d'un número de repetitions variables (entre 100 – 1000) com a mínim de l'hexanucleòtid GGGGCC. El principal model és el ratolí. Malgrat s'han generat diferents ratolins amb alteracions motores lleus i que no desenvolupaven paràlisi motora, Liu *et al.*, (2016), ha caracteritzat un model de ratolí que desenvolupa les característiques d'ELA *C9orf72*. Aquest ratolí reproduceix trets neuropatològics com alteracions en la unió

neuromuscular, pèrdua de MNs, reducció de la mida dels axons, inclusions citoplasmàtiques, degeneració en l'hipocamp així com paràlisi motora i disminució de la supervivència.

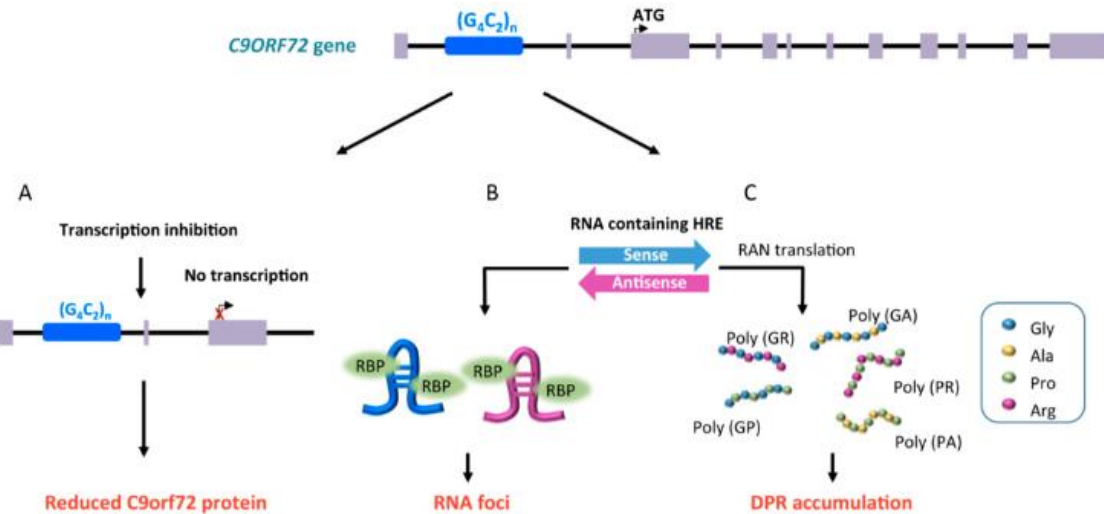


Figura 5 | Representació dels mecanismes patològics en els que està involucrat C9orf72. L'expansió es pot transcriure bidireccionalment, causant la producció de seqüències curtes de ARN les quals poden segrerar les proteïnes d'unió al ARN i alterar la seva homeòstasis; o traduir-se i causar la producció de pèptids tòxics per les cèl·lules. Adaptat de Cappella et al., 2019.

1.6.3. Tar DNA Binding Protein 43

Tar DNA binding protein 43 (TDP-43) és la proteïna codificada pel gen *Tardbp*. És una proteïna que s'uneix tant al ARN com al àcid desoxiribonucleic (ADN), per la qual cosa la seva localització habitual és en el nucli. La seva funció és regular diversos passos del metabolisme de l'ARN, tals com l'*splicing*, el transport i la traducció, així com modular la biogènesis de microARNs. En el ratolí, TDP-43 s'ha vist que interacciona amb l'ARN missatger de més de 6000 gens, on s'uneix preferentment en seqüències riques en UG les quals es localitzen en els introns, en regions no codificant d'ARN i regions intergèniques.

En l'ELA, la proteïna TDP-43 es deslocalitza del nucli i es situa en el citoplasma, on es troba hiperfosforil·lada i formant agregats en un 97% de pacients d'ELA (Sreedharan et al., 2008). Tot i l'associació del TDP-43 amb l'ELA, en pocs casos la mutació d'aquesta és l'etiologia principal de la malaltia, ja que només s'ha descrit en un 2-5% de les formes familiars amb herència autosòmica dominant, i en menys d'1% en casos rars de les formes esporàdiques (Lagier-Tourenne & Cleveland,

2009; Zou *et al.*, 2017), indicant que TDP-43 pot estar implicada en el mecanisme patogènic de la malaltia (G. Kim *et al.*, 2020).

Es parla que TDP-43 mutada pot tenir una funció tòxica tant per guany de funció com per pèrdua de funció. El guany, és degut a la localització citoplasmàtica, on induceix neurotoxicitat mitjançant la disruptió dels grànuls citoplasmàtics, els quals s'agreguen i formen les inclusions citoplasmàtiques de proteïnes ubiquitinitzades descrites en l'ELA (Fig. 6). La pèrdua de funció és conseqüència de la deslocalització nuclear, ja que deixa de regular el metabolisme de l'ARN nuclear (Morgan & Orrell,

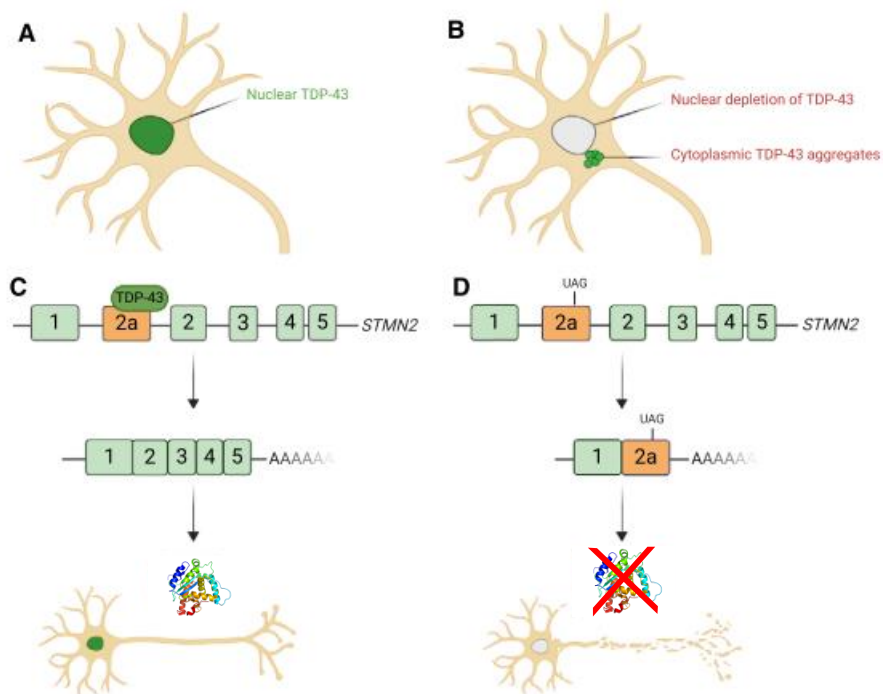


Figura 6 | Esquema de la neurotoxicitat mediada per TDP-43. En condicions fisiològiques, TDP-43 es localitza essencialment en el nucli, on regula el metabolisme de molts ARNm. En l'ELA, es deslocalitza del nucli, alterant així d'expressió de les proteïnes que modula i causant agregats en el citoplasma. Extret de Kim *et al.*, 2020.

2016; Su *et al.*, 2014) i s'altera l'expressió de totes les proteïnes que regula (G. Kim *et al.*, 2020).

Les mutacions en el gen *Tardbp* es concentren en el domini C-terminal de la proteïna per la que codifiquen. Algunes d'aquestes mutacions s'han traslladat a models animals tals com el primat *Macaca fascicularis* (Uchida *et al.*, 2012), en ratolí (Alfieri *et al.*, 2016; P. Wang *et al.*, 2017), en rates (Dayton *et al.*, 2013; Huang *et al.*, 2012; Tong *et al.*, 2013), en el peix zebra (Kabashi *et al.*, 2011; Vaccaro *et al.*, 2013) i en mosques (J.-C. Chang *et al.*, 2014).

Aquests animals transgènics tenen un número variable de copies del gen *Tardbp* mutat. La patologia i el fenotip d'aquests models depèn del número de copies del transgèn, del promotor genètic, el fons genètic de l'animal i de la pròpia mutació. Algunes de les mutacions en TDP-43 que s'han introduït en ratolins són TDP-43^{A315T}, TDP-43^{M337V}, TDP-43^{Q331K}, TDP-43^{G348C}, totes elles causen fenotip motor (Thomas Philips & Rothstein, 2015).

Tots aquests models reproduueixen certes característiques típiques de l'ELA com són la debilitat muscular progressiva, els dèficits motors, la pèrdua neuronal, les fasciculacions,... però cap recrea el fenotip complet (Gois *et al.*, 2020).

1.6.4. Fused in sarcoma/translocated in liposarcoma

En condicions fisiològiques, la proteïna *Fused in sarcoma/translocated in liposarcoma* (FUS) també és una proteïna que s'uneix a l'ADN/ARN, per tant, també es localitza en el nucli i està involucrada en la reparació de l'ADN després del dany així com en diversos aspectes del metabolisme de l'ARN (transcripció, *splicing*, transport, estabilitat i biogènesis de microARNs) regulant més de 5500 ARNm.

Les mutacions en FUS poden ser causa de formes d'ELA (Kwiatkowski *et al.*, 2009), ja que s'han descrit més de 50 mutacions diferents en aquest gen en pacients d'ELA, de les quals moltes causen una deslocalització de FUS del nucli cap a citoplasma.

Aquesta proteïna mutada s'ha observat en aproximadament un 4% de pacients amb ELA familiar, típicament amb una herència autosòmica dominant, i en menys d'1% en pacients aparentment amb ELA esporàdica (Lagier-Tourenne & Cleveland, 2009; Zou *et al.*, 2017).

La patogènesi de FUS en l'ELA és similar al que succeeix amb el TDP-43. S'hi associa un guany de funció degut a la formació d'agregats en el citoplasma on també altera els grànuls d'estrés citoplasmàtic; i una pèrdua de funció resultat de la localització anòmala en el citoplasma, que comporta la pèrdua de les seves funcions nuclears, on deixa de regular aproximadament 640 ARNm i l'*splicing* de 300 ARNm més (Vance *et al.*, 2009). Tot i que FUS i TDP-43 semblen tenir un comportament similar, exerceixen les seves funcions, tant fisiològiques com alterades, per vies neurotòxiques diferents (G. Kim *et al.*, 2020; Morgan & Orrell, 2016; Su *et al.*, 2014).

En referència als models animals, els rosegadors són els més utilitzats, tot i que també existeixen models en peixos, mosques i nematodes. Es caracteritzen per reproduir aspectes com alteracions motores progressives, degeneració axonal, pèrdua de neurones i finalment paràlisis muscular.

2

Mecanismes patogènics en l'Esclerosi Lateral Amiotròfica

L'etiopatogènia subjacent a l'ELA no es coneix, però tal com succeeix en altres malalties neurodegeneratives, sembla que pot tenir un origen multifactorial, on hi estarien involucrats diversos mecanismes cel·lulars no excloents entre ells (Kiernan *et al.*, 2011; Mancuso & Navarro, 2015).

Les alteracions en els gens que en les últimes dècades s'han associat a l'ELA, es poden agrupar vagament segons la funció que desenvolupen: aquells que alteren la proteostasis i el control de qualitat de les proteïnes; aquells que pertorben aspectes de l'ARN tals com l'estabilitat, la funció i el metabolisme; i en aquells que modifiquen la dinàmica del citoesquelet entre l'axó de la motoneurona i el terminal distal (Morgan & Orrell, 2016). La convergència de les diferents alteracions genètiques relacionades amb l'ELA en aquests processos cel·lulars, suggereix possibles mecanismes etiopatogènics de la malaltia, que inclús podrien estar interaccionant entre ells per acabar provocant el fenotip de la malaltia.

Encara que l'ELA esporàdica es presenta com una malaltia sense un historial amb component genètic clar, a part de la presència d'agregats proteïcs que contenen TDP-43 i FUS en un 1% dels casos (tal i com s'ha esmentat anteriorment), els avenços tecnològics sobre la seqüenciació de l'ADN han revelat que d'un 1-3% dels casos esporàdics d'ELA presenten mutacions de SOD1 (Gamez *et al.*, 2006) i en un 5% o més són causades per expansions intròniques de C9orf72 (Cooper-Knock *et al.*, 2012). A més, un estudi indica que la SOD1 no mutada o salvatge (*wild-type* (WT)) pateix modificacions posttraduccionals que resulten neurotòxiques per les MNs (Bosco *et al.*, 2010). Aquests resultats

posen de manifest que les formes familiars d'ELA comparteixen mecanismes etiopatogènics comuns amb les formes esporàdiques, on la SOD1 juga un paper central.

En base als processos cel·lulars alterats, s'han proposat diverses hipòtesis per intentar elucidar la causa patogènica primària de l'ELA (Fig. 7): l'estrés oxidatiu, l'excitotoxicitat, la disfunció

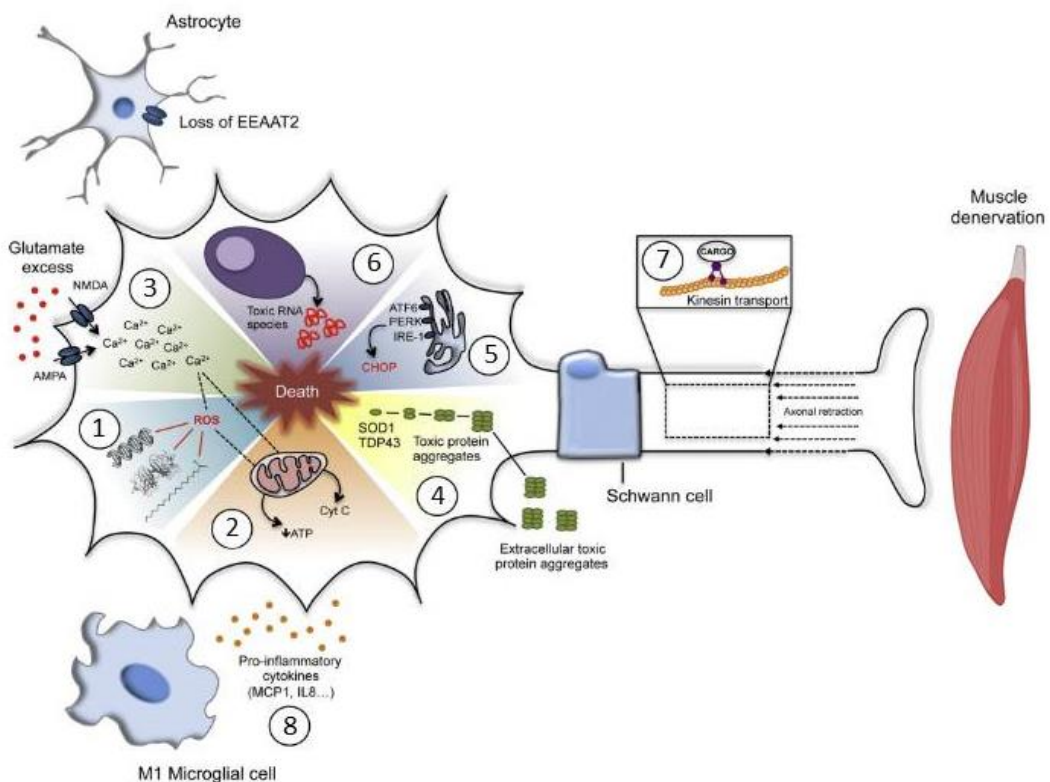


Figura 7 | Principals hipòtesis sobre els mecanismes fisiopatològics contribuents a la degeneració de les MNs en l'ELA. (1) Estrès oxidatiu, (2) disfunció mitocondrial, (3) excitotoxicitat, (4) alteració de l'homeòstasi proteica, (5) estrès de reticle endoplasmàtic, (6) alteracions en la transcripció i processament de l'ARN, (7) alteracions axonals i (8) neuroinflamació. Adaptat de *Mancuso and Navarro, 2015*.

mitocondrial, l'alteració en l'homeòstasi proteica, l'estrés de reticle endoplasmàtic, les alteracions en la transcripció i processament de l'ARN, alteracions axonals i la neuroinflamació (Ferraiuolo *et al.*, 2011).

2.1. Estrès oxidatiu

En organismes vius i sota condicions aeròbiques, més del 90% d'oxigen que es consumeix s'acaba reduint a aigua en la cadena transportadora d'electrons localitzada en la membrana interna mitocondrial, la funció principal de la qual és produir energia. El subproducte final de la cadena

transportadora d'electrons és l'anió superòxid (O_2^-), compost tòxic que mitjançant successives reaccions de reducció-oxidació, s'acaba transformant en aigua. En el procés de detoxificació, es poden produir diverses espècies reactives d'oxigen (*Reactive Oxigen Species (ROS)*), les quals són químicament inestables i reaccionen amb molta facilitat amb els diferents components cel·lulars, oxidant-los i, moltes vegades, causant-los-hi disfuncionalitat. Per evitar aquest dany oxidatiu, les cèl·lules tenen sistemes antioxidants destinats a eliminar els ROS abans que aquests reaccionin.

La producció i l'eliminació de ROS ha d'estar en equilibri, ja que del contrari, es pot produir una acumulació de ROS donant com a resultat estrès oxidatiu en les cèl·lules (Lushchak, 2014). Les cèl·lules amb cicle mitòtic actiu, poden utilitzar les divisions cel·lulars per diluir l'estrès oxidatiu i fer-hi front més eficientment, procés que no es pot donar en les neurones, cosa que explicaria que aquestes siguin més propenses a degenerar (Ferraiuolo *et al.*, 2011).

Entre els agents antioxidants trobem la SOD1, la qual catalitza la dismutació de l'anió superòxid en oxigen i peròxid d'hidrogen. És per això, que quan es va identificar que les mutacions de SOD1 estaven associades a formes familiars d'ELA, es va suggerir que era deguda a una pèrdua de l'activitat enzimàtica de l'enzim SOD1 (Morgan & Orrell, 2016). Posteriorment es va demostrar que la mort selectiva de les MNs estava relacionada amb un guany de funció tòxica per l'acumulació de mfSOD1, més que en la pèrdua de la seva funció antioxidant, ja que la delecio de la SOD1 en ratolins no desencadenava la degeneració de MNs (Reaume *et al.*, 1996), evidenciant així la independència de l'activitat enzimàtica de la SOD1 en relació al fenotip ELA.

No obstant, l'anàlisi de mostres biològiques tant de pacients amb ELA esporàdica com familiar, presenten concentracions elevades de marcadors de dany oxidatiu (Mitsumoto *et al.*, 2008; Simpson *et al.*, 2004; R. G. Smith *et al.*, 1998). Alhora, també s'ha demostrat la presència de dany oxidatiu en proteïnes (Shaw *et al.*, 1995), lípids (Simpson *et al.*, 2004) i ADN (Bogdanov *et al.*, 2000) en teixit *postmortem* de pacients d'ELA (Mancuso & Navarro, 2015).

En base a aquestes observacions, i després de múltiples assajos clínics amb molècules antioxidants (Barber *et al.*, 2006), l'Agència Americana del medicament (*Food and Drug Administration (FDA)*) va aprovar l'any 2017 el fàrmac *Edavarone* per al tractament de l'ELA. Aquesta molècula antioxidant s'ha descrit que elimina la peroxidació de lípids i els radicals hidroxils. Clínicament, actua alentint la progressió de la malaltia (Jeffrey D. Rothstein, 2017).

Múltiples estudis han demostrat que l'estrès oxidatiu exacerba altres processos fisiopatològics com són l'excitotoxicitat, el dany mitocondrial, l'agregació de proteïnes, entre d'altres, cosa que en conjunt, contribueix a danyar les MNs (Barber *et al.*, 2006) (Ferraiuolo *et al.*, 2011). Així doncs, tot i

que l'estrés oxidatiu no sembla ser la causa primària de l'ELA, pot ser un mecanisme secundari que contribueixi a empitjorar totes les altres alteracions cel·lulars reportades en l'ELA.

2.2. Disfunció mitocondrial

Els mitocondris són orgànuls cel·lulars que intervenen en processos essencials, com són el metabolisme energètic, l'homeòstasi del calci, la biosíntesi de lípids i l'apoptosi. És per això, que quan es produueixen alteracions en els mitocondris, sobretot en cèl·lules tant exigents metabòlicament com són les neurones, les conseqüències poden ser molt perjudicials. En l'ELA, s'han descrit alteracions en l'estructura, en la dinàmica, la bioenergètica i en el tamponament del calci (Ferraiuolo *et al.*, 2011; E. F. Smith *et al.*, 2017).

Un dels primers canvis histopatològics que s'observen en les MNs, tant de pacients d'ELA com en models animals amb la proteïna SOD1 mutada, és una estructura mitocondrial alterada amb un aspecte inflat i vacuolitzat (Kong & Xu, 1998; Sasaki & Iwata, 2007). En models *in vivo*, s'observen agregats de proteïnes mal plegades en vacuoles situades en l'espai intermembranós mitocondrial, les quals poden arribar a tenir grans dimensions i que provoquen disfuncionalitat en l'orgànul. Aquestes alteracions estructurals s'observen inclús abans del debut simptomàtic, cosa que suggereix que aquest fenomen pot ser un esdeveniment primerenc en la fisiopatologia de l'ELA (Wong *et al.*, 1995).

També s'ha descrit que es produueix una disminució de la taxa de respiració mitocondrial (Mattiazzi *et al.*, 2002; Wiedemann *et al.*, 2002), fet que s'associa a un augment de la producció de ROS. S'ha descrit que formes mfSOD1 s'uneixen al canal aniónic voltatge dependent (VDAC1) que es troba en la membrana externa del mitocondri. La unió de SOD1 al canal, bloqueja el flux de metabòlits, tant d'entrada com de sortida, la qual cosa condueix a una menor producció energètica i excés d'estrés oxidatiu (Israelson *et al.*, 2010). Aquest excés de ROS, afecta de forma important els mitocondris, especialment a l'ADN mitocondrial, cosa que també condueix a alterar la funcionalitat mitocondrial (Cui *et al.*, 2012).

En referència a l'homeòstasi del calci, hi ha estudis que demostren una pèrdua significativa de la capacitat de tamponament d'aquest catió per part dels mitocondris en models de mSOD1 (Damiano *et al.*, 2006). Secundàriament, aquest fenomen, incrementa la susceptibilitat de la neurona a l'excitotoxicitat mediada per glutamat (Parone *et al.*, 2013).

Finalment, els mitocondris són orgànuls molt dinàmics els quals es fissionen o fusionen en funció dels requeriments energètics puntuals de la cèl·lula. La fusió permet als mitocondrials compartir

metabòlits, ADN i proteïnes. La fissió facilita la motilitat i permet l'aïllament de parts danyades i a la seva eliminació per mitofàgia (Chan, 2012). Hi ha evidències d'alteracions en la dinàmica de fissió/fusió mitocondrial en l'ELA (E. F. Smith *et al.*, 2017).

2.3. Excitotoxicitat

El glutamat és el principal neurotransmissor amb propietats excitadores del SNC. Durant la neurotransmissió glutamatèrgica, el glutamat és alliberat per la neurona presinàptica i s'uneix als seus receptors presents en la membrana de la neurona postsinàptica. Funcionalment, el subtipus de receptors per glutamat AMPA són els més importants per modular ràpidament la transmissió excitadora. Aquest està constituït per tetràmers formats per una associació variable de 4 subunitats (GluR1-4) i és permeable al calci en graus variables. La permeabilitat, està determinada per la absència/presència de la subunitat GluR2 en el tetràmer: si aquest està present el receptor té una baixa permeabilitat en comparació amb els que no el tenen. La impermeabilitat al calci dels receptors AMPA-GluR2 es deu a la introducció d'una arginina en la posició 586 de la subunitat GluR2 enlloc de la glutamina mitjançant modificacions posttranspcionals (Kawahara *et al.*, 2004).

L'absència de la subunitat GluR2 en MNs espinals d'humans, proporciona un possible mecanisme pel qual les alteracions de la neurotransmissió del glutamat en l'ELA afecten de manera selectiva a aquest grup cel·lular (Williams *et al.*, 1997). A més, les MNs tenen una capacitat limitada per tamponar els increments intracel·lulars de calci, ja que expressen baixos nivells de proteïnes tamponadores d'aquest catió, cosa que les fa més propenses a l'excitotoxicitat (Van Den Bosch *et al.*, 2006).

L'activació d'aquests receptors de glutamat provoca un influx d'ions sodi i calci cap a l'interior de les cèl·lules, causant una despolarització que donarà lloc al potencial d'acció. L'acció del glutamat sobre els receptors és ràpida i transitòria. La senyal excitadora s'acaba degut a l'eliminació del glutamat de la fenedura sinàptica per part dels transportadors específics de glutamat (*excitatory amino acid transporter*, EAAT) presents en neurones i astròcits (Foran & Trotti, 2009). D'aquests, el més afí i abundant és el EAAT2 o GLT-1, que s'expressa prominentment en els astròcits del SNC (Van Den Bosch *et al.*, 2006).

L'excessiva activació dels receptors de glutamat causa dany neuronal, fenomen conegut com excitotoxicitat (Olney, 1989). Elevacions agudes de l'activitat glutamatèrgica es creu que induceixen dany neuronal; elevacions moderades però cròniques s'han associat a malalties neurodegeneratives (Van Den Bosch *et al.*, 2006).

Aquest augment de l'activitat dels receptors provoca un influx de calci cap a l'interior de les cèl·lules, cosa que altera l'homeòstasi del calci intracel·lular. Aquest excedent de calci, pot resultar en l'activació de moltsenzims com lipases, fosfolipases, proteases, endonucleases, fosfatases de proteïnes, entre d'altres. A més, la disfunció mitocondrial degut a l'augment de calci en el mitocondri i la subseqüent formació de ROS, també poden contribuir a la mort cel·lular excitotòxica (Ferraiuolo *et al.*, 2011; Kiernan *et al.*, 2011).

L'excitotoxicitat pot ser deguda a un increment en el glutamat de l'espai extracel·lular o un increment en la sensibilitat de la neurona postsinàptica al glutamat. L'increment extracel·lular, pot ser resultat de la disruptió de la membrana presinàptica o de la manca de la recaptació del glutamat en la fenedura sinàptica. S'han detectat dèficits en el transport de glutamat a partir de sinaptosomes aïllats en el còrtex motor i en medul·les espinals de pacients amb ELA (Jeffrey D. Rothstein *et al.*, 1992). Aquest dèficit s'ha atribuït a la pèrdua selectiva del transportador astrocitari EAAT2. El mecanisme pel qual es produeix la pèrdua de EAAT2 ha sigut objecte d'intensa recerca, però no hi ha una associació clara entre mutació i malaltia (Van Den Bosch *et al.*, 2006).

Les principals evidències que donen suport a l'excitotoxicitat com a mecanisme implicat en la fisiopatologia de l'ELA, per una banda, és que s'ha descrit l'elevació de 3 vegades els nivells de glutamat en el líquidcefalorraquídi de pacients amb ELA (T. L. Perry *et al.*, 1990). D'altra banda, la única estratègia que actualment s'utilitza per alentir la progressió de la malaltia és el *Riluzole*, el mecanisme d'acció del qual passa per inhibir l'alliberació presinàptica de glutamat, entre altres (Ludolph & Jesse, 2009; Mancuso & Navarro, 2015). Tot i això, no hi ha evidències clares de que sigui el mecanisme primari de la malaltia (Ferraiuolo *et al.*, 2011).

2.4 Alteració de l'homeòstasi proteica

En condicions fisiològiques hi ha d'haver un equilibri entre la producció i la degradació de proteïnes en les cèl·lules per tal de mantenir l'homeòstasi proteica, la qual és essencial pel funcionament i supervivència cel·lular. Per a que les proteïnes siguin funcionals després de sintetitzar-se, es necessita que adquireixin una estructura tridimensional específica. Les cèl·lules tenen mecanismes de control de qualitat de les proteïnes, per tal de detectar i reparar proteïnes que no s'han plegat correctament i evitar que s'agreguin (Braakman & Bulleid, 2011). En el cas que no s'aconsegueixi corregir les proteïnes defectuoses, aquestes es degraden via el sistema ubiquitina-proteasoma (Ciechanover & Brundin, 2003; Ciechanover & Kwon, 2015) o per la via autofàgia-lisosomal (Mizushima & Komatsu, 2011).

En diverses malalties neurodegeneratives l'homeòstasi proteica es desequilibra degut a un fracàs en la reparació o degradació de proteïnes mal plegades, les quals s'acumulen formant agregats potencialment tòxics en diferents regions del SNC (Ruegsegger & Saxena, 2016).

Els agregats proteics tant dins les MNs com en la glia circumdant, són una característica present en l'ELA (Nishihira *et al.*, 2008; Piao *et al.*, 2006; H. Zhang *et al.*, 2008). En la gran majoria de les formes esporàdiques i familiars d'ELA es troben inclusions proteïques de TDP-43 (Arai *et al.*, 2006; Neumann *et al.*, 2006), excepte en els pacients amb mutacions en la SOD1 o en FUS, els quals presenten agregats d'aquestes proteïnes respectivament (Kwiatkowski *et al.*, 2009; Mackenzie *et al.*, 2007; Vance *et al.*, 2009; M. Watanabe *et al.*, 2001).

Per la seva banda, la mfSOD1 no només sembla escapar del procés normal de degradació via proteasoma, sinó que també té efectes tòxics en la pròpia maquinària de degradació (S. Chen *et al.*, 2012; Cheroni *et al.*, 2009; Robberecht & Philips, 2013). Al seu torn, l'activitat proteasomal reduïda promou l'acumulació de SOD1 mutada en forma d'agregats (Crippa *et al.*, 2010).

Altres inclusions associades a l'ELA són els cossos de Bunina, els quals estan formats per cistatina C i transferrina (Okamoto *et al.*, 1993). Aquests agregats, tot i trobar-se en aproximadament el 86% de pacients amb formes esporàdiques, no està clar quin paper tenen en la fisiopatologia.

La presència d'inclusions en les MNs de gairebé tots els pacients d'ELA, així com en tots els models animals, suggereix que el col·lapse de la proteostasi pot contribuir en l'etiologia de l'ELA. És per això, que influir en els diferents processos involucrats en l'homeòstasi proteica s'ha proposat com a possible diana terapèutica. No obstant, també es postula l'agregació proteica com un mecanisme defensiu de les cèl·lules, concentrant i aïllant proteïnes tòxiques per tal d'evitar que causin dany als altres components cel·lulars i facilitar així l'eliminació d'aquestes (Webster *et al.*, 2017).

2.5. Estrès de reticle endoplasmàtic

El reticle endoplasmàtic (RE) és l'estructura membranosa on es sintetitzen les proteïnes. El RE té un paper fonamental en la maduració i en el control de qualitat de les proteïnes i només permet l'exportació d'aquelles que estan plegades i modificades correctament (Braakman & Bulleid, 2011).

Són les xaperones residents en el RE les que reconeixen l'acumulació de proteïnes mal plegades i activen la resposta corresponent a proteïnes mal plegades (*unfolded protein response (UPR)*), la qual para la traducció de proteïnes en el reticle i activa els mecanismes de degradació. Tot i que aquests

mecanismes es consideren protectors en el seu inici, una activació prolongada de la UPR condueix a la mort de les cèl·lules (Kaufman, 2002). Les proteïnes associades a la UPR s'han vist incrementades en pacients d'ELA esporàdica (Atkin *et al.*, 2008) i en models animals de mfSOD1 (Saxena *et al.*, 2009).

En els últims anys, s'han descrit evidències de disfunció entre la senyalització de RE i el mitocondri, com un nou mecanisme que pot estar involucrat en la mort de les MNs (Mancuso & Navarro, 2015). En aquesta alteració hi podria estar implicada la xaperona Sigma receptor-1 (SR1), la qual es relaciona en els contactes RE-mitocondri així com en la cisterna subsinàptica de les sinapsis colinèrgiques (Mavlyutov *et al.*, 2012). La seva alteració afecta la senyalització intracel·lular de calci, altera el transport mitocondrial i induceix estrès de reticle (Bernard-Marissal *et al.*, 2015). La proteïna SR1 s'ha vist alterada en formes adults i juvenils d'ELA (Al-Saif *et al.*, 2011; Luty *et al.*, 2010).

2.6. Alteracions en la transcripció i processament de l'ARN

L'expressió gènica és un procés altament regulat per mecanismes cel·lulars complexos a través dels quals es genera, s'emmagatzema, madura, es transporta i es tradueix l'ARN.

La identificació de mutacions en la proteïna TDP-43 en formes familiars i esporàdiques d'ELA, així com la seva deslocalització del nucli al citoplasma, on és la principal component de les inclusions proteïques ubiquitinitzades (Neumann *et al.*, 2006), va suggerir que les alteracions en el metabolisme de l'ARN podrien ser un mecanisme fisiopatològic subjacent a la malaltia. Aquesta hipòtesis va ser reforçada al també trobar-se deslocalitzada al citoplasma la proteïna FUS, una altra proteïna d'unió al ADN/ARN.

A part de les mutacions directes en aquestes proteïnes, també hi ha evidències que suggereixen que l'oxidació de l'ARN també contribueix a danyar les MNs en l'ELA, ja que s'han detectat ARNs oxidats en pacients i en el model animal de mfSOD1 (Y. Chang *et al.*, 2008). També s'ha descrit certa repressió transcripcional en el model animal de mfSOD1 (Ferraiuolo *et al.*, 2007; Kirby *et al.*, 2005).

2.7. Alteracions del transport axonal

Les MNs són unes cèl·lules altament polaritzades amb axons molt llargs, que en el seu extrem més distal fan sinapsis amb el múscul (unió neuromuscular). Degut a la longitud d'aquests axons, es

requereix de mecanismes per transportar components essencials (proteïnes, vesícules, orgànuls,...) a l'extrem de l'axó, per tal de que aquest continuï sent funcional. La principal maquinària utilitzada pel transport axonal bidireccional es produeix mitjançant les cinesines, responsables del transport anterògrad, i les dineïnes, involucrades en el transport retrògrad (Ferraiuolo *et al.*, 2011).

L'ELA s'està redefinint com una axonopatia distal, en la que molts canvis moleculars que influencien la degeneració de les MNs succeeixen distalment en l'axó o en la unió neuromuscular en estadis molt inicials de la malaltia, inclús abans del debut clínic. En els últims anys, la hipòtesi anomenada *dying-back* ha guanyat importància en el context fisiopatològic de l'ELA, ja que hi ha evidències que la suporten tant en models animals com en pacients (Fischer *et al.*, 2004).

D'acord amb aquesta hipòtesi, els canvis funcionals i patològics en els segments més distals dels axons motors i els terminals nerviosos apareixen en primer lloc i progressen proximalment cap al soma de les MNs, provocant secundàriament la degeneració d'aquests i conseqüentment, l'aparició dels símptomes clínics (Moloney *et al.*, 2014). Aquesta teoria manté també que la malaltia començaria degut a una lesió subletal en el soma de les MNs, cosa que es manifestaria en la part més vulnerable de la MN, l'axó. Això causaria l'alteració en el transport axonal i conseqüentment la disminució de l'aportació de components essencials a l'extrem distal de l'axó, provocant els canvis funcionals i patològics. Això concordaria amb les anomalies en el tràfic d'orgànuls descrit en els axons de pacients d'ELA (Breuer *et al.*, 1987).

Estudis morfològics del curs temporal en el model de ratolí SOD1, han demostrat que es produeix desnervació muscular i una pèrdua important d'axons motors abans de la degeneració de cossos de MNs, cosa que suporta la hipòtesi del *dying-back* en l'ELA (Fischer *et al.*, 2004).

D'altra banda, la teoria del *dying-back* pot integrar les altres teories: el cùmul de complexes insolubles de mfSOD1 (Johnston *et al.*, 2000) o la toxicitat crònica provocada pel glutamat (J. D. Rothstein *et al.*, 1993), poden ser els responsables de l'insuficient manteniment de la porció distal dels axons, provocant una degeneració inicial distal però mantenint el cos cel·lular intacte. A més, el transport axonal és un mecanisme altament dependent d'energia, per tant, una funció mitocondrial danyada pot portar a un transport defectuós degut a aquesta falta d'energia. Tanmateix, tampoc es transporten mitocondris cap als terminals, quedant aquests en un dèficit metabòlic important i contribuint a la degeneració (De Vos *et al.*, 2007; K. E. Miller & Sheetz, 2004).

També s'ha descrit l'acumulació de neurofilaments hiperfosforilats en el citoplasma, en les dendrites proximals i en els axons de llarg calibre de les MNs espinals, tant en el ratolí SOD1 (B. Zhang *et al.*,

1997), provocant un transport axonal anterògrad defectuós (Griffin & Watson, 1988), com en les formes esporàdiques i familiars en pacients d'ELA (Hirano *et al.*, 1984; Julien, 1997).

En base a la teoria del *dying back*, en la present tesis, hem utilitzat el model quirúrgic d'axotomia en rosejadors, en el qual, mitjançant la interrupció del nervi ciàtic, es reproduceix de forma aguda aquesta afectació distal suposadament inicial de l'ELA. Aquest model permet també simular alguns dels processos patològics de l'ELA, com podria ser la neuroinflamació i deafferentació associada a la medul·la espinal. Clàssicament, s'ha utilitzat el model d'axotomia per estudiar processos de regeneració en el nervi (Leibinger *et al.*, 2016; Savastano *et al.*, 2014); per investigar el dolor neuropàtic (Calvo & Bennett, 2012); o el fenomen de neuroinflamació, procés interessant d'estudiar en el context de l'ELA mitjançant aquest model, ja que hi ha evidències que relacionen la resposta inflamatòria i l'ELA (Puentes *et al.*, 2016).

2.8. Resposta glial i neuroinflamació

Tot i que generalment està acceptat que la causa primària de l'ELA es dóna en les MNs, diferents tipus cel·lulars no neuronals tenen un paper fonamental en la patogènesis i progressió de la malaltia (Beers & Appel, 2019; Morgan & Orrell, 2016; T. Philips & Rothstein, 2014). Corroboren aquesta teoria estudis en els que es limitava l'expressió de mfsOD1 a les cèl·lules neuronals i això no causava un fenotip motor suficient com per explicar l'espectre patològic sencer de l'ELA (Clement *et al.*, 2003; Pramatarova *et al.*, 2001; Yamanaka *et al.*, 2008).

La neurodegeneració desencadena una resposta inflamatòria, la qual alhora, contribueix al procés de neurodegeneració, establint-se d'aquesta manera un cercle viciós (B. E. Clarke & Patani, 2020; Geloso *et al.*, 2017; Gupta *et al.*, 2011; Tateishi *et al.*, 2010). S'ha descrit la presència de neuroinflamació tant en casos esporàdics com familiars així com en models animals transgènics de la malaltia (Engelhardt & Appel, 1990; Hall *et al.*, 1998; Henkel *et al.*, 2004, 2006; Mantovani *et al.*, 2009; Schiffer *et al.*, 1996).

La neuroinflamació inclou l'activació de la micròglia i l'astròglia.

2.8.1. Micròglia

La micròglia són les cèl·lules glials de dimensions més petites, constitueixen aproximadament un 5% del total de cèl·lules glials i es defineixen com els macròfags residents del SNC tenint capacitat migratòria i fagocítica, representant així la defensa immunitària innata en el SNC.

A diferència dels altres components del SNC, els quals tenen el seu origen embrionari en el neuroectoderm, la micròglia té origen en el mesoderme. Durant el desenvolupament, precursores mieloides migren fins al SNC abans de que es formi la barrera hematoencefàlica o apareguin les altres cèl·lules glials, i es diferencien donant lloc a la micròglia. Això implica que aquesta població glial es manté estable per autorenovació de la colònia establerta (proliferació local), i que no hi ha substitució per macròfags circulants.

En un context prenatal on s'estan generant les neurones i sense altres components cel·lulars, la micròglia ja desenvolupa funcions fonamentals com donar suport en el procés de neurogènesis, participa en la mort cel·lular programada i en l'eliminació fisiològica de sinapsis i està involucrada en l'establiment i remodelat dels circuits neuronals, totes elles, funcions que continuarà desenvolupant en etapes perinatales i fases inicials postnatals, entre d'altres.

En condicions fisiològiques durant l'edat adulta, la micròglia interacciona amb gairebé tots els components del SNC. Està implicada en processos com la remodelació i modulació sinàptica, ja que en monitoritza i regula la seva activitat constantment mitjançant l'elongació o retracció dels seu lamel·lipodis ramificats. Estudis recents han descrit característiques regió-específiques i edat-específiques de la micròglia (Q. Li & Barres, 2018).

La morfologia de la micròglia varia en funció del context en el que aquesta es trobi. Típicament, la micròglia madura en estat fisiològic es caracteritza per tenir un nucli ovoïdal i petit del qual emergeixen radialment lamel·lipodis o branques primàries poc ramificades. Aquesta micròglia en estat basal, pot esdevenir micròglia reactiva en resposta a diversos estímuls externs (patològics o no) com poden ser la secreció de citocines, quimiocines, inclús factors tròfics i altres molècules com el trifosfat d'adenosina (*adenosine triphosphate*, ATP). Aquest estat reactiu, comporta una reestructuració morfològica que es caracteritza principalment per l'augment de les ramificacions dels lamel·lipodis. Aquesta micròglia hiperamificada té l'habilitat de reorientar-se en resposta a canvis en l'activitat neuronal (Nimmerjahn *et al.*, 2005) o al dany tissular, i estén les branques per migrar ràpidament cap al lloc alterat o danyat (Fig. 8).

La micròglia reactiva en condicions patològiques, encara pot convertir-se en micròglia fagocítica, altrament coneguda com a micròglia ameboide, en la qual s'observa un gran nucli rodó amb escasses branques poc ramificades i curtes (Beynon & Walker, 2012; Ransohoff, 2016).

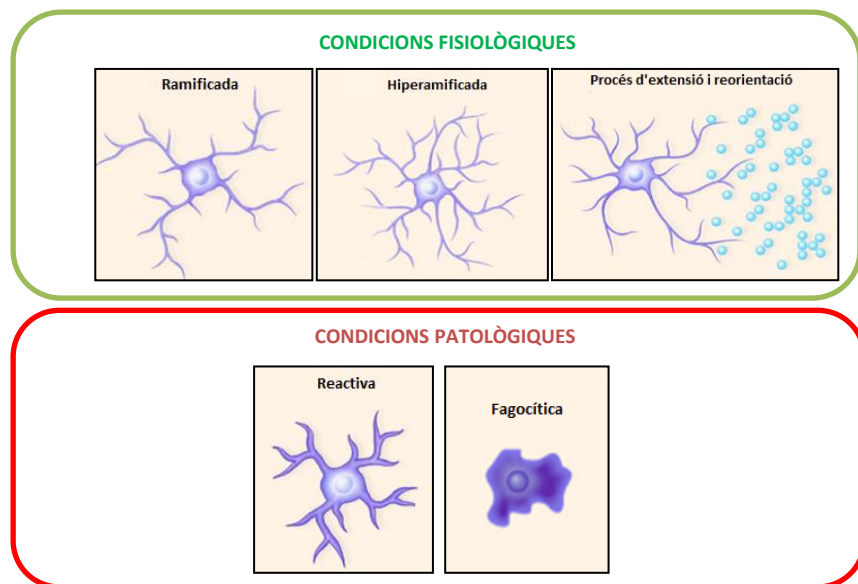


Figura 8 | Esquema de la remodelació morfològica de la micròglia. La micròglia en condicions fisiològiques i en resposta a determinats estímuls, pot hiperamificar-se i estendre les seves branques per reorientar-se i migrar cap on s'hagi produït una alteració. En condicions patològiques, la micròglia reactiva pot esdevenir micròglia fagocítica. Adaptat de Beynon & Walker, 2012.

D'altra banda i tret del camp dels macròfags, es poden postular dos tipus d'estats d'activació funcional de la micròglia: el fenotip M1, com un estat proinflamatatori; i el fenotip M2, com un estat antiinflamatatori o relacionat amb la reparació. Que la micròglia tingui un fenotip o l'altre, depèn de l'entorn o els factors que n'estimulen l'activació, els quals poden promoure "l'activació clàssica" o "l'activació alternativa". Ambdós processos pro i antiinflamatatori podrien estar significativament influenciats pels limfòcits T (Appel *et al.*, 2011; Chiu *et al.*, 2008).

L'activació clàssica s'associa amb la inducció de micròglia M1 degut a la producció de citocines proinflamatòries com el factor de necrosis tumoral α (*tumoral necrosis factor- α* , TNF- α), la interleucina-1 β (IL-1 β), l'òxid nítric (*nitric oxide*, NO) i ROS. Aquesta resposta és essencial per defensar el sistema de possibles patògens així com de l'aparició de cèl·lules potencialment tumorals, però alhora, pot causar danys colaterals com és la neurotoxicitat (Fig. 9).

L'activació alternativa de la micròglia, la qual promou el fenotip M2, s'inicia mitjançant l'IL-4 o l'IL-13, les quals promouen l'expressió de gens associats a funcions antiinflamatòries, a factors neurotròfics i a l'eliminació d'agregats tòxics de proteïnes i detritus cel·lulars del SNC, per tal de prevenir el dany neuronal i promoure la supervivència (Fig. 9).

Aquests dos fenotips microglials no s'han d'entendre com fenòmens aïllats l'un de l'altre, sinó que interaccionen entre ells: quan s'activa la micròglia M1, paral·lelament, també s'activa micròglia M2 amb l'objectiu d'antagonitzar la resposta proinflamatòria per tal de tornar a la homeostàsia. És en funció de quin sigui l'estímul majoritari en cada context el que determinarà l'abundància de cada un dels fenotips. A més, la micròglia pot transitar entre un fenotip i l'altre en funció del context, cosa que explicaria que en els estadis terminals de malalties neurodegeneratives on s'ha descrit dany neuronal, agents neurotòxics, agregats proteïcs,... un alt percentatge de micròglia presenti fenotip M1 (Y. Tang & Le, 2016) (Fig. 9).

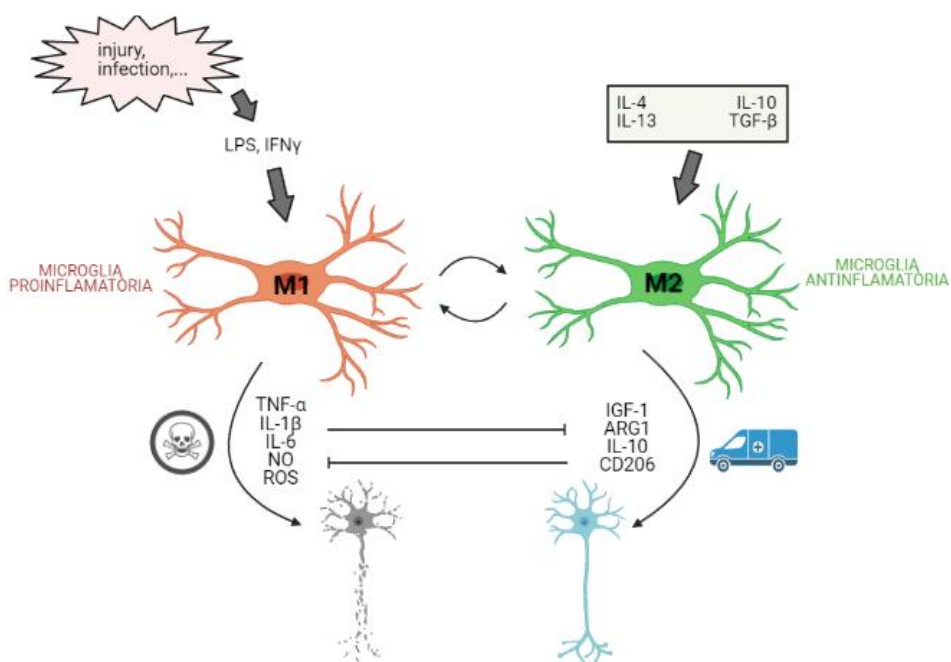


Figura 9 | Esquema de la polarització M1/M2. La micròglia amb fenotip M1 produeix citocines que provoquen un augment de la inflamació i per tant, indueixen més micròglia M1 contribuint així a la mort neuronal. La micròglia amb fenotip M2, promou la reparació de teixits, afavoreix la supervivència neuronal i allibera factors neuroprotectors. Basat en Tang & Le, 2016; Geloso et al, 2017 i creat a Biorender.

Pel que fa a les tècniques histològiques per l'observació de la micròglia en ratolins, el que més s'utilitza avui en dia és el marcatge mitjançant anticossos específics contra proteïnes específiques de la microglia, com és la molècula adaptadora d'unió de calci ionitzat-1 (*ionized calcium binding adaptor molecule 1*, Iba-1). També existeixen anticossos més o menys específics de micròglia M1, com el MAC-2 (o galectina-3) CD86, CD16 i CD32; i de micròglia M2, com el CD206 i l'arginina-1 (Kigerl et al., 2009). A banda, i d'especial interès en aquesta tesi, l'anticòs anti-CD68 marca els lisosomes de la micròglia, associant-se a l'estat fagocític d'aquesta.

A part de l'immunomarcatge per estudiar la micròglia, en els últims anys, s'han generat animals transgènics en els que per visualitzar-la, aquesta expressa la proteïna verda fluorescent (*Green Fluorescent Protein, GFP*) sota un promotor específic d'aquest tipus cel·lular, com pot ser el promotor del gen Iba-1 (Hirasawa *et al.*, 2005). A més, molt recentment, han sorgit estudis en els que mitjançant la microscòpia multifotó, s'estudia *in vivo* el comportament de la micròglia en diferents condicions, obtenint imatges d'alta resolució d'una única cèl·lula microglial (Hierro-Bujalance *et al.*, 2018).

En relació a l'ELA, hi ha estudis que descriuen activació microglial tant en el còrtex motor (Corcia *et al.*, 2012; Dols-Icardo *et al.*, 2020; M. Turner *et al.*, 2004) com en la medul·la espinal en casos esporàdics (Brettschneider *et al.*, 2012; D'Erchia *et al.*, 2017). Tot i que en estudis inicials es suggeria que la micròglia només era important en fases finals de la malaltia (Boillée *et al.*, 2006), recentment, s'ha vist reactivitat microglial i canvis en l'expressió de certs gens en la micròglia abans de que es produixin canvis en les MNs (Maniatis *et al.*, 2019) o del debut clínic de la malaltia (Brites & Vaz, 2014; Y. Tang & Le, 2016).

S'ha vist que en models *in vivo*, la micròglia resident incrementa en nombre durant la progressió de la malaltia, i els seus estats d'activació representen un continu entre el fenotip tòxic M1 i el neuroprotector M2 (Liao *et al.*, 2012). En etapes asimptomàtiques s'ha descrit en la micròglia un perfil neuroprotector (Gravel *et al.*, 2016), perfil que es manté en el debut simptomàtic inicial. No obstant, en els animals terminals, la majoria de la micròglia és M1 (Beers *et al.*, 2011). Això s'ha corroborat amb experiments en els que es co-cultivava motoneurones sanes amb micròglia aïllada d'animals amb mfSOD1 a diferents etapes de la malaltia, es va veure que la micròglia de períodes inicials expressava característiques neuroprotectores, mentre que si s'aïllava de fases terminals, presentava propietats tòxiques i induïa la mort de les MNs (Liao *et al.*, 2012).

Diversos estudis han suggerit que aquest canvi cap al fenotip tòxic pot ser degut a l'aparició i acumulació progressiva de proteïnes mutades (Beers *et al.*, 2006; Liao *et al.*, 2012). Experiments *in vitro* recolzen aquesta hipòtesis, ja que l'addició extracel·lular de la proteïna mfSOD1 induceix canvis morfològics i funcionals en cultius de micròglia a través dels receptors *toll-like* (*Toll-Like Receptors, TLR*). Això provoca que aquesta micròglia alliberi més citocines proinflamatòries i radicals lliures, convertint-la així en neurotòxica ja que acaba danyant les pròpies MNs (W. Zhao *et al.*, 2010). Això no obstant, més que una transició del fenotip M2 al M1, es creu que durant la progressió de l'ELA coexisten els dos fenotips, predominant més un que l'altre en les diferents fases (Chiu *et al.*, 2008).

D'altra banda i en relació a l'ELA causada per mfSOD1, s'ha vist que l'expressió d'aquesta proteïna només en la micròglia no és suficient per causar degeneració de les MNs, descartant que sigui la única causa patogènica. Pel contrari, quan s'elimina la mfSOD1 de la micròglia, el debut de la malaltia no s'altera, però retarda la progressió de la malaltia significativament (Boillée *et al.*, 2006).

Tots aquests estudis posen de manifest la rellevància de la micròglia en la patogènesis de l'ELA. És per això que s'han dut a terme múltiples estratègies terapèutiques, tant farmacològiques com genètiques, per intentar modular la reactivitat i la funció de la micròglia, en un intent de millorar la simptomatologia en animals models de diferents malalties neurodegeneratives. Els resultats demostren que la modulació de vies específiques de la micròglia pot millorar parcialment la neurodegeneració. No obstant, cada vegada hi ha més evidències que suggereixen que l'estrategia terapèutica que tindrà èxit serà aquella que interfereixi en diferents vies en diferents tipus cel·lulars (Geloso *et al.*, 2017).

2.8.2. Astròglia

Els astròcits són les cèl·lules glials més abundants del SNC, constituint aproximadament un 30% del total. Morfològicament es caracteritzen per tenir abundants evaginacions citoplasmàtiques o branques que s'originen del cos cel·lular, les quals són curtes i ramificades. Les branques primàries es divideixen profusament en branques secundàries, terciàries i, finalment, apareixen els peus terminals dels astròcits. Aquests peus són característics d'aquest tipus cel·lular i estan en contacte físic amb els vasos sanguinis, contribuint així a l'establiment de la barrera hematoencefàlica. A través dels peus perivasculars, els astròcits duen a terme funcions importants en el moviment de metabòlits i productes de rebuig des de les neurones i cap a elles. Alternativament, els peus dels astròcits poden cobrir fins a milers de sinapsis.

Els astròcits tenen feixos prominents de filaments intermedis formats per la proteïna àcida fibril·lar glial (*glial fibrilar acid protein (GFAP)*), la qual es pot immunomarcar específicament per identificar aquest tipus cel·lular (Ross & Pawlina, 2015).

Inicialment, es pensava que la funció dels astròcits es limitava a mantenir la homeòstasis iònica en el SNC i proveir suport estructural. Ara es sap que no només donen suport físic a les neurones, sinó també metabòlic.

Recentment s'ha descrit que els astròcits regulen moltes funcions neuronals. Una d'elles és el suport neurotròfic, ja que a través de l'alliberació de factors tròfics, molts d'ells encara desconeguts, promouen la supervivència neuronal. També intervenen en la sinaptogènesi, la regulació iònica

extracel·lular, la recaptació de neurotransmissors i en la maduració i manteniment de les sinapsis, ja que secreteuen varíes molècules per tal de modular tant el compartiment presinàptic com el postsinàptic. Contràriament, també participen en l'eliminació activa de sinapsis quan es requereix. Una altra funció clàssicament associada als astròcits és la de formar una barrera per confinar els neurotransmissors a una sinapsis concreta, evitant d'aquesta manera que difonguin i puguin acabar afectant l'activitat de les neurones circumdants. També eliminén l'excés de neurotransmissors per pinocitosi (Zhou *et al.*, 2019).

Una característica particular dels astròcits és la seva comunicació interna, ja que el seu citoplasma està connectat mitjançant unions comunicants (*gap junctions*). D'aquesta manera, es propaguen entre astròcits ones lentes (desenes de segons) de calci espontàniament en tot el SNC a mode de senyalització. Aquesta senyalització entre astròcits és útil, per exemple, per regular el flux sanguini en el SNC ja que, segons les necessitats energètiques puntuals de les neurones d'una regió, es provoca que molts astròcits alliberin de forma coordinada prostanoïdes, àcid araquidònic, i altres molècules vasoactives per tal d'ajustar el torrent sanguini (S. Liddelow & Barres, 2015).

La disfunció astrocitària, anomenada “astrogliosis reactiva”, és una resposta comú a totes les lesions o malalties del SNC. Mitjançant estudis de perfils genètics, s'ha evidenciat que hi ha almenys dos tipus d'astròcits reactius. Així doncs, en funció de quin sigui l'estímul que induceixi la lesió en el SNC, trobem els astròcits A1 i A2 (homòlogament a la terminologia M1 i M2 de la micròglia).

Els astròcits amb fenotip A1 activen l'expressió de gens relacionats amb la neuroinflamació descrits com a neurotóxics i per tant, es postula com un fenotip perjudicial (S. A. Liddelow *et al.*, 2017; S. Liddelow & Barres, 2015). En canvi, en l'astrocitosis reactiva A2, s'indueix l'expressió de gens de factors neurotròfics, els quals promouen la supervivència, el creixement neuronal i la reparació sinàptica. Conseqüentment, els astròcits A2 es postulen com a protectors (S. A. Liddelow *et al.*, 2017).

En l'ELA, la disfunció dels astròcits semblen tenir dos rols interconnectats (Makiko Nagai *et al.*, 2007; Yamanaka *et al.*, 2008): per una banda contribueixen a la toxicitat de les MNs mitjançant la secreció de factors neurotóxics (fenotip A1); per altra banda, perden les seves funcions i degeneren, privant les neurones de suport tròfic, cosa que conduceix a accelerar la degeneració neuronal (Serio & Patani, 2018; Valori *et al.*, 2014).

La introducció d'astròcits, els quals expressen mfsOD1, en medul·les espinals d'animals sans o en co-cultius de MNs *in vitro* provoca en ambdós casos neurodegeneració de les MNs (Di Giorgio *et al.*, 2008; Ferraiuolo *et al.*, 2011; Haidet-Phillips *et al.*, 2011; Marchetto *et al.*, 2008; Makiko Nagai *et al.*,

2007; Phatnani *et al.*, 2013) i, en els animals, símptomes d'ELA (Papadeas *et al.*, 2011). Contràriament, astròcits sans o amb una baixa expressió de mfSOD1 introduïts en el SNC de models animals d'ELA, alenteixen la malaltia i allarguen la supervivència (Lepore *et al.*, 2008; Yamanaka *et al.*, 2008). Aquests experiments demostren l'alliberació de factors neurotòxics perjudicials per les MNs per part d'astròcits alterats amb mfSOD1 (Hensley *et al.*, 2006).

Aquestes observacions suggereixen que les interaccions entre astròcits i MNs són dinàmiques i poden estar alterades a diferents nivells durant la progressió de la malaltia d'ELA.

2.8.3. Interacció micròglia-astròglia

En els últims anys han sorgit evidències que demostren una comunicació bidireccional entre la micròglia i els astròcits (Jha *et al.*, 2016; S. A. Liddelow *et al.*, 2017; Vainchtein *et al.*, 2018). Aquesta comunicació es du a terme mitjançant l'alliberació de varíes molècules (Jha *et al.*, 2019), incloent citocines, quimiocines, ATP i factors de creixement. Inclús s'ha descrit que la micròglia pot alliberar mitocondris fragmentats capaços d'induir la resposta A1 (Joshi *et al.*, 2019).

Aquesta comunicació s'ha comprovat en el model de ratolí mfSOD1 ja que quan es redueix la proliferació microglial en el model mfSOD1, disminueix l'activació dels astròcits (Gowing *et al.*, 2008). De la mateixa manera, la supressió de la mfSOD1 en els astròcits, resulta en una disminució de l'activació microglial (Yamanaka *et al.*, 2008).

S'han dut a terme múltiples estratègies terapèutiques, tant farmacològiques com genètiques, per intentar modular la reactivitat i la funció de la glial, en un intent per millorar la simptomatologia motora. Els resultats demostren que la modulació de vies específiques pot millorar localment la neurodegeneració. No obstant, cada vegada hi ha més evidències que suggereixen que l'estratègia terapèutica que tindrà èxit serà aquella que interfereix en diferents vies de diversos tipus cel·lulars (Geloso *et al.*, 2017).

2.8.4. Oligodendròglia

L'oligodendròglia o oligodendròcits és caracteritzat per tenir cossos cel·lulars petits amb un gran nucli el qual conté grans quantitats de cromatina.

La funció principal i clàssicament descrita dels oligodendròcits és embolcallar i aïllar els axons mitjançant formació de les beines de mielina en el SNC. No obstant, deixen petits segments sense ocupar, els nodes de Ranvier, promovent així la conducció elèctrica saltatòria característica del SNC. A diferència dels seus anàlegs en el SNP, les cèl·lules de Schwann, un oligodendròcit pot produir mielina a segments de múltiples axons. Diversos estudis han descrit que la deposició de mielina no és estàtica, és molt més dinàmica del que inicialment es creia, amb canvis adaptatius deguts a l'activitat neuronal (Philips & Rothstein, 2017).

La mielina està formada per lípids en un 70-80%, amb poques proteïnes entre les diferents capes. La més característica de les quals és la proteïna Bàsica de la Mielina (*Myelin Basic Protein (MBP)*). Per tant, s'utilitzen anticossos contra aquesta proteïna per visualitzar els oligodendròcits immunohistoquímicament.

Tot i que la formació de la mielina és la funció principal dels oligodendròcits, actualment es sap que no és la única. Dades recents indiquen que els oligodendròcits són essencials per proveir suport metabòlic ràpid a demanda de les neurones, ja que tenen la capacitat de transferir metabòlits energètics com el lactat a l'espai periaxonal mitjançant els transportador de monocarboxilats 1 (*Monocarboxylate transporter 1 (MCT1)*) (Lee *et al.*, 2012; Philips & Rothstein, 2017; Simons & Nave, 2016).

En relació a l'ELA, s'han descrit canvis degeneratius en els oligodendròcits tant en pacients humans com en models animals per la malaltia, tals com una reducció selectiva del transportador MCT1 (Kang *et al.*, 2013; Lee *et al.*, 2012; Philips *et al.*, 2013). En el model de ratolí *SOD1^{G93A}*, els canvis morfològics degeneratius en els oligodendròcits esdevenen aparents inclús abans del debut de l'ELA i incrementen durant la progressió de la malaltia fins que finalment moren (Kang *et al.*, 2013; Philips *et al.*, 2013). Aquesta pèrdua d'oligodendròcits s'intenta compensar amb un increment en la proliferació i diferenciació de cèl·lules precursores. No obstant, aquests oligodendròcits nous són disfuncionals: a nivell molecular, tenen reduïda l'expressió de MBP i MCT1, aquest últim, crític per la supervivència dels axons; i a nivell funcional, són incapços de mielinitzar i de donar suport tròfic als axons, essent el resultat final la desmielinització dels axons (Kang *et al.*, 2013; Philips *et al.*, 2013).

In vitro, s'ha constatat que si en l'animal *SOD1^{G37R}* s'elimina la mutació només en els oligodendròcits, dóna com a resultat un retràs significatiu del debut simptomatològic en i s'incrementa la supervivència de l'animal (Kang *et al.*, 2013). D'altra banda, també s'ha descrit que els oligodendròcits provinents de mostres d'ELA són tòxics per MNs WT ja que n'indueixen la mort per diferents mecanismes inclús abans de que els oligodendròcits mostrin signes de degeneració

(Ferraiuolo *et al.*, 2016). Aquests estudis denoten el rellevant paper dels oligodendròcits en la fisiopatologia de l'ELA (Traiffort *et al.*, 2021).

3

Sinapsis i comunicació sinàptica entre les neurones

3.1. Citoarquitectura de la medul·la espinal

En la medul·la espinal les neurones estan agrupades en diferents nuclis. Aquests nuclis es descriuen segons unes zones delimitades que reben el nom de làmines de Rexed (Rexed, 1957) (Fig. 10). En la banya dorsal, les neurones sensitivas es distribueixen en làmines horizontals (làmines I-IV) on les làmines V-VI, no tenen cap nucli específic. En la làmina VII, es troben nuclis en els segments medul·lars toràcics, els quals formen la columna intermedio lateral i intermedio medial amb neurones viscerals i el nucli dorsalis (columna de Clarke), el qual correspon al nucli de la propiocepció inconscient. En la làmina VIII hi ha neurones grans, mentre que les MNs es troben ubicades en la làmina IX de la banya ventral agrupades en formacions esfèriques. La làmina X està ocupada per neurones al voltant del conducte ependimari.

Les MNs es disposen al llarg de tota la medul·la espinal format columnes motores. Aquestes, són molt abundants en les intumescències cervical i lumbar, corresponent als segments medul·lars destinats a la innervació de les extremitats superiors i inferiors respectivament.

En una secció transversal de medul·la espinal lumbar, quan s'observa la substància gris de la banya ventral, concretament la làmina IX de Rexed, es distingeixen bàsicament tres agrupacions de MNs clarament diferenciades espacialment: (i) una agrupació motora medial, les quals innerven músculs situats a la regió dorsal del cos; (ii) una agrupació motora anterior, que projecta a músculs de la part ventral del cos; (iii) una agrupació motora lateral o anterolateral, la qual innerva músculs de les extremitats (Kanning *et al.*, 2010) (Fig. 10).

Cadascuna de les agrupacions motores conté tots els tipus de MNs (α -MN, β -MN i γ -MN).

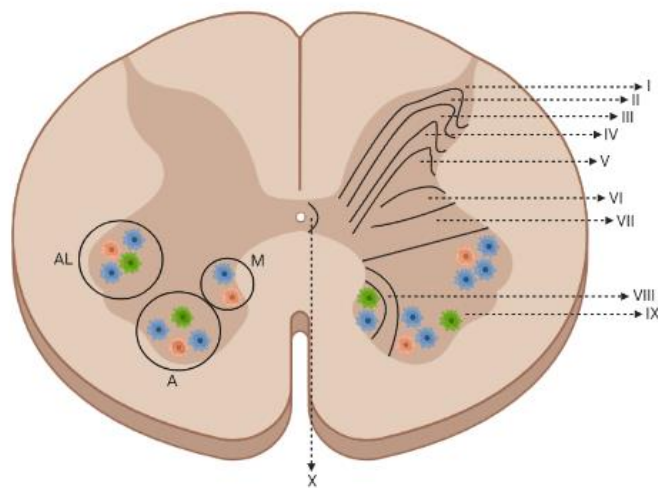


Figura 10 | Esquema de l'organització de les agrupacions de MNs en una secció transversal de medul·la espinal lumbar. A l'hemimedul·la de l'esquerra, es distingeixen les diferents agrupacions de MNs en la banya anterior: agrupació anterolateral (AL), agrupació anterior (A) i agrupació medial (M). En cada agrupació s'hi troben els 3 tipus de MN: α -MN (blau), γ -MN (taronja) i β -MN (verd). A l'hemimedul·la de la dreta, s'observen la distribució de les làmines de Rexed. Creat amb Biorender.

3.2. Propietats funcionals de les MNs

Les MNs regulen l'activitat muscular mitjançant la descàrrega de potencials d'acció que, a la vegada, depenen de la seva excitabilitat. Quan aquestes neurones reben un estímul d'una intensitat llindar, es desencadena un potencial d'acció, és a dir, es produeix una entrada massiva de ions sodi a favor de gradient en la cèl·lula, cosa que provoca una despolarització. Aquest canvi elèctric va seguit d'una repolarització i hiperpolarització transitòria, degut a la sortida dels ions potassi intracel·lulars, amb els quals s'intenta compensar el canvi de potencial. Durant el període de posthiperpolarització (*after hyperpolarization peak, AHP*), la neurona és menys excitable, i, en conseqüència, la duració d'aquesta fase limitant determinarà l'excitabilitat de la cèl·lula nerviosa i, per tant, la freqüència en què s'inicia cada potencial d'acció. Al final, el potencial de la cèl·lula torna a l'estat basal (Fig. 11). Aquest cicle d'activitat elèctrica, es va propagant per la neurona fins al terminal axonal, on hi provoca l'alliberament d'acetilcolina en la sinapsi neuromuscular per tal de que el múscul es contregui i es produueixi així el moviment. Així doncs, l'excitabilitat és la facilitat amb què una neurona dispara potencials d'acció i transmet aquest canvi a través del seu axó.

Les MNs innerven exclusivament músculs esquelètics, els quals són els responsables de la postura i del moviment. Cada MN innerva varíes fibres musculars del mateix tipus. Segons el tipus de fibra muscular que innerven, les MNs es poden classificar en alfa (α), beta (β) i gamma (γ) (Fig. 12) (Kanning K. et al., 2010; Stifani, 2014).

Les α -MNs són el tipus de MNs més abundants i és caracteritzan per ser les més grans. Innerven les fibres musculars extrafusals, encarregades de generar la força muscular sent, per tant, les responsables pròpiament de la contracció muscular. Alhora, les α -MN es poden subclassificar segons les propietats contràctils de les fibres extrafusals que innerven: (i) α -MNs fatigables i de contracció ràpida (*fast-twitch fatigable* (FF)), es caracteritzen per tenir un període d'AHP més curt i innerven fibres musculars de contracció ràpida (músculs fàsics) sensibles a la fatiga (ii) α -MNs resistentes a la fatiga i de contracció ràpida (*fast-twitch fatigue-resistant* (FFR)), connecten amb fibres de contracció ràpida resistentes a la fatiga; (iii) α -MNs resistentes a la fatiga i de contracció lenta (*slow-twitch fatigue-resistant* (SFR)), es caracteritzen per tenir un període d'AHP més perllongat i innerven fibres de contracció lenta (músculs tònics) i resistentes a la fatiga (E. Burke; 1973).

Les β -MNs són les menys abundants, i en conseqüència són les que estan menys caracteritzades. Innerven tant fibres musculars extrafusals com intrafusals.

Les γ -MNs innerven les fibres musculars intrafusals, que es caracteritzen per respondre a la informació proprioceptiva referent a la posició i a l'estat d'extensió del múscul. Per tant, aquestes MNs no participen pròpiament en la generació de la força muscular, si no que la modulen.

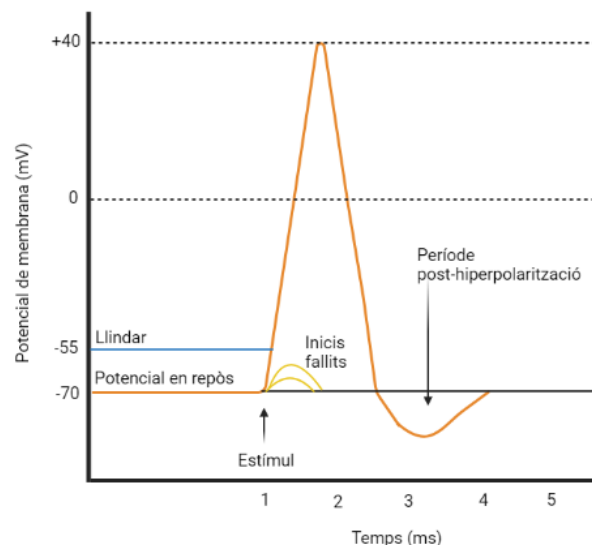


Figura 11 | Representació esquemàtica d'un potencial d'acció. Adaptat de *Brain Electricity and the Mind*, Jon Lieff i creat amb Biorender.

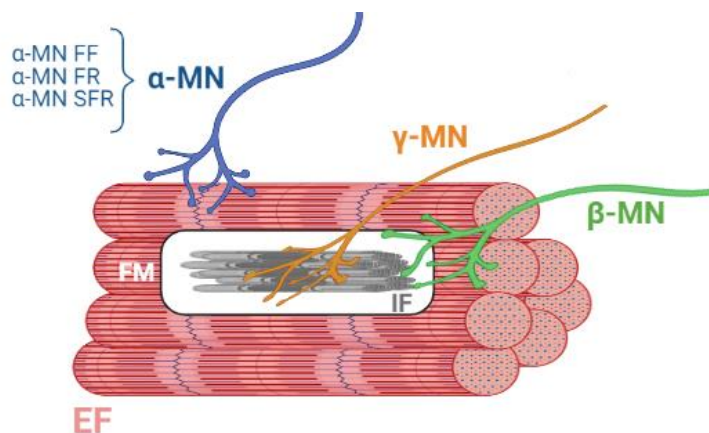


Figura 12 | Esquema de les fibres musculars en una secció longitudinal. α -MN (blau) innerven les fibres musculars extrafusals (EF, vermell); mentre que les γ -MN (taronja) fan connexió amb les fibres musculars intrafusals (IF, gris) en el fusos musculars (FM). En canvi, les β -MN (verd) innerven tant les fibres extrafusals com les intrafusals. Basat en Stifani, et al. 2014.

Molts estudis en els últims anys s'han centrat en analitzar l'excitabilitat dels subtipus d' α -MNs relacionant-ho amb la diferent vulnerabilitat que presenten a la malaltia de l'ELA. Aquesta línia experimental es basa en l'evidència que no totes les MNs s'affecten de la mateixa manera en aquesta malaltia. En el ratolí $SOD1^{G93A}$, les α -MN FF són més susceptibles a la lesió axonal i es desnerven més aviat durant el transcurs de la malaltia en comparació amb les α -MN FFR i α -MN SFR, tot i que les α -MN FFR també degeneren ràpidament poc després de les α -MN FF. Contràriament, les α -MN SFR resten ben preservades fins a etapes ben avançades de la malaltia (Kanning et al., 2010).

Davant d'aquesta situació, tant les α -MN FFR en un inici com les α -MN SFR, activen el procés d'*sprouting* (Duchen & Tonge, 1973; Schaefer et al., 2005), mitjançant el qual reactiven el creixement de la porció distal de l'axó per tal d'estendre'l a noves localitzacions i així poder reinnervar les zones musculars on abans contactaven les α -MN FF (Kanning et al., 2010; Saxena et al., 2009, 2013). Això pot suggerir que les manifestacions simptomàtiques, començarien a aparèixer en el moment que els mecanismes de compensació per part de les α -MN SFR fracassin.

Aquesta diferent vulnerabilitat dels subtipus d' α -MNs és una característica comú en totes les formes d'ELA (Kanning et al., 2010). Això implica que en determinats moments de la malaltia, coexisten, en la banya ventral de la medul·la espinal, una proporció variable de MNs en degeneració, MNs resistent i probablement algunes amb mecanismes de regeneració actius. Tots aquests estats morfopatològics diferents de les MNs individuals pot ser heterogeni i dissociat del curs temporal de la malaltia: en etapes inicials de l'ELA hi poden haver MNs severament alterades i degenerants tot i

que en baixa proporció, i al contrari, algunes MNs sanes o resistentes poden estar presents en etapes terminals.

Una millor caracterització de com es produeixen els canvis patològics espacials i temporals ajudaria a dissenyar i avaluar els efectes dels potencials agents terapèutics en assajos preclínics en el model per l'ELA SOD1^{G93A}.

3.3. Sinapsis i comunicació sinàptica entre les neurones

El sistema de senyalització entre neurones consta d'un conjunt molt ampli de diferents molècules senyalitzadores i neurotransmissors. Aquests inclouen el glutamat, la glicina, l'àcid γ-aminobutíric (GABA), l'acetilcolina, la serotonina, la norepinefrina, neuropèptids i altres (Rekling *et al.*, 2000). Els neurotransmissors són alliberats pel terminal presinàptic d'una primera neurona, i actuen unint-se específicament al seu receptor ionotrópic o metabotròpic localitzat en la membrana plasmàtica, també anomenada postsinàptica, d'una segona neurona.

Al seu torn, l'excitabilitat de la MN està regulada per les propietats biofísiques intrínseqües i també pel conjunt d'aferències sinàptiques o inputs sinàptics que aquesta rep, essencialment a través de molècules neurotransmissores. Tots aquests estímuls, alguns excitadors i d'altres inhibidors, són integrats per la cèl·lula per tal que aquesta pugui generar una resposta apropiada en conseqüència. Aquestes molècules encarregades de transmetre les senyals entre MNs, poden tenir diferent naturalesa i actuar sobre diferents tipus de receptors situats en la superfície de les MNs.

Utilitzant la microscòpia electrònica s'ha pogut descriure la gran diversitat estructural dels diferents tipus de sinapsis de les MNs. En base a la morfologia esfèrica o aplanada de les vesícules sinàptiques i en la prominència de les densificacions pre- i postsinàptiques (simètriques o asimètriques) s'han definit diferents tipus de sinapsis: els botons F, els botons S, els botons P i els botons C (Bernstein & Bernstein, 1976; Bodian, 1970; Conradi & Skoglund, 1969).

Les sinapsis de tipus F (*flattened*) es caracteritzen per tenir vesícules aplanades, amb una densificació postsinàptica poc prominent i molt semblant a la presinàptica, sent així una sinapsi simètrica de caràcter inhibitori, en la que els neurotransmissors principals són el GABA o la glicina. Els botons S (*spherical*) es descriuen amb vesícules rodones, densificacions postsinàptiques prominentes, les quals la converteixen aquest tipus de sinapsis en asimètrica. El neurotransmissor principal és el glutamat, per tant, tenen un caràcter excitador. Les sinapsis de tipus P es particularitzen per tenir vesícules

grosses amb un nucli dens (*dense core*). En aquest cas, les molècules senyalitzadores són neuropèptids, essent per tant, sinapsis peptidèrgiques.

La majoria de les sinapsis que reben les MN són de tipus F i S (Destombes *et al.*, 1992; Murphy *et al.*, 1996; Örnung *et al.*, 1996).

Un quart tipus de sinapsis particularment destacable a les MNs, es correspon als aferents de tipus C o botó C (BC), el qual es va identificar morfològicament fa més de 40 anys (Conradi & Skoglund, 1969). Recentment aquesta sinapsis de tipus C ha tornat a cobrar molt interès (Witts *et al.*, 2014).

3.4. El botó C

Els BC són uns terminals sinàptics amb vesícules grosses i rodones de tipus colinèrgic. Són sinapsis inusualment grans (3-5 μm de longitud) úniques i característiques de les α -MN. Recentment i llargament buscat, s'ha descrit que l'origen d'aquest aferent presinàptic prové d'un grup d'interneurones colinèrgiques localitzades rodejant el conducte ependimari (làmina X de Rexed), les quals mitjançant l'alliberament del neurotransmissor acetilcolina regulen l'excitabilitat de les α -MN, i en última instància, contribueixen a la modulació del comportament motor (Frank, 2009; Zagoraiou *et al.*, 2009). Els BC són particularment importants degut a la seva capacitat de modular el potencial d'acció després de la hiperpolarització via regulació dels canals de potassi (Miles *et al.*, 2007). Degut doncs, a les propietats intrínseqües i extrínseqües d'aquestes sinapsis, els BC són els que modulen majoritàriament l'excitabilitat de les α -MN.

En el compartiment presinàptic s'hi troba una gran densitat de vesícules rodones o lleugerament aplanades i d'aspecte poc electrodens. A la regió postsinàptica, el BC presenta una estructura única derivada del RE rugós, situada a uns 10-20 nm de la membrana postsinàptica de la MN, anomenada cisterna subsinàptica (*subsynaptic cistern (SSC)*).

Després de conèixer el fenotip colinèrgic dels BC amb la presència del transportador vesicular de l'acetilcolina (*vesicular acetyl choline transporter (VACHT)*) en el compartiment presinàptic, i la seva associació amb els receptors muscarítics M2 situats en la regió postsinàptica (Hellström *et al.*, 2003), s'han descrit diverses molècules associades als BC. Algunes, es localitzen en la SSC, com són el canal de potassi voltatge dependent Kv2.1 (Muennich & Fyffe, 2004), els canals de potassi activats per calci SK (Deardorff *et al.*, 2013) i el SR1 (Mavlyutov *et al.*, 2010, 2012) (Fig. 13).

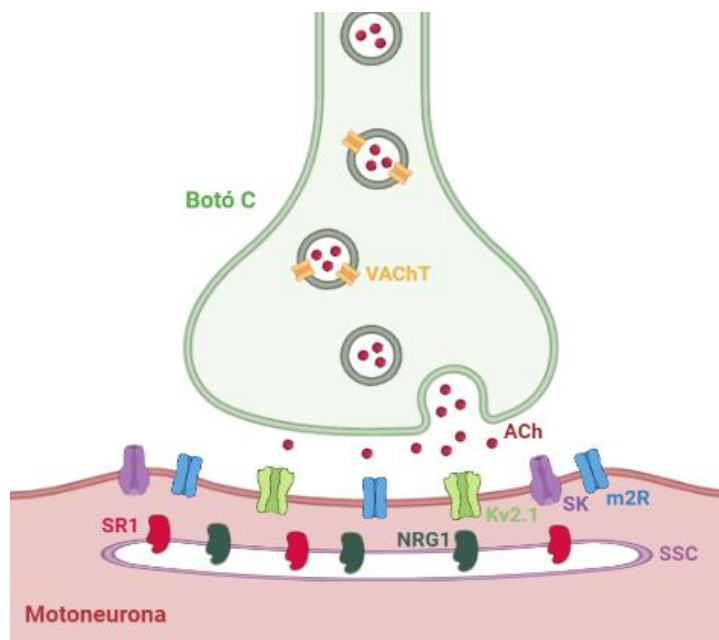


Figura 13 | Esquema gràfic on es representa l'organització molecular dels BC. En el terminal presinàptic (verd) es localitza el VACHT (groc). En l'espai intersinàptic s'hi situa l'acetilcolina (ACh). En el component postsinàptic (vermell), a nivell de la membrana de la MN s'hi troba el receptor muscarínic m₂ (m₂R), els canals SK (lila) i el canal Kv2.1 (verd). En la SSC, s'hi observa el SR1 i la NRG1. Creat amb el Biorender.

En estudis previs del grup de Patologia Neuromuscular Experimental de l'IRB Lleida en el qual s'ha dut a terme la present tesi, es va descriure l'associació de la proteïna Neuregulina-1 (NRG1) en els BC, concretament en el component postsinàptic associada a la SSC (Fig. 14) (Gallart-Palau *et al.*, 2014).

A nivell presinàptic s'hi ha va relacionar el receptors tirosina-cinasa ErbB2 i ErbB4 (Gallart-Palau *et al.*, 2014), suggerint una possible senyalització retrògrada NRG1-ErbB2/4 en aquest tipus de sinapsis.

Tanmateix, es desconeix l'existència d'una possible relació estructural o funcional entre tots aquests components.

Un aspecte interessant dels BC és la seva presència en la majoria de nuclis motors cranials, on les MNs manifesten el

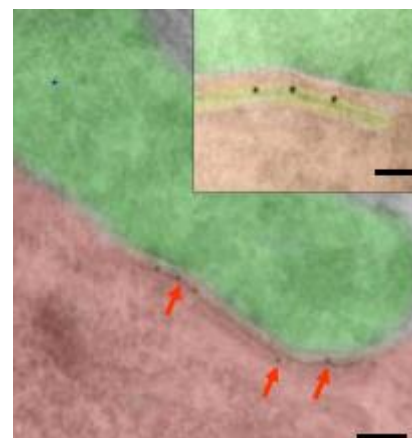


Figura 14 | Immunolocalització de la NRG1 en els BC de MNs espinals. El terminal presinàptic (verd) es contraposa a la regió postsinàptica (vermell). La NRG1 (fletxes) es localitza en el compartiment postsinàptic del BC. Concretament, en la fotografia superior on es mostra una ampliació del BC, s'observa la NRG1 (partícules d'*immunogold* de 12 nm) en la SSC (groc). Extret de Gallart-Palau *et al.* 2014.

mateix patró de NRG1 que l'observat en les MNs espinals. Contràriament, les MNs dels nuclis oculomotorius, els quals són resistentes a l'ELA, no tenen BC ni NRG1 associada a la SSC (Gallart-Palau *et al.*, 2014; Hellström *et al.*, 2003).

Els BC són estructures poc investigades tot i que s'ha demostrat que pateixen canvis plàstics en MNs danyades després de la lesió de la medul·la espinal (Novikov *et al.*, 2000) o també en l'ELA (Gallart-Palau *et al.*, 2014; Pullen & Athanasiou, 2009; Song *et al.*, 2012). També manca conèixer com determinades mutacions, descrites molt recentment en algunes d'aquestes molècules com en el SR1 (Al-Saif *et al.*, 2011) o en els receptors ErbB4 (Takahashi *et al.*, 2013), poden ser causants de formes esporàdiques o familiars d'ELA.

3.4.1. Neuregulina-1

Les neuregulines (NRG) són una família de proteïnes pleiotòpiques implicades en la senyalització cèl·lula-cèl·lula, lligands dels receptors tirosina-cinasa de la família ErbB.

La família de les NRGs inclou 4 gens: NRG1, NRG2, NRG3 i NRG4 (Falls, 2003). Pràcticament es desconeixen les funcions biològiques de les proteïnes NRG2, 3 i 4. En canvi, s'ha descrit que la NRG1 és essencial en el desenvolupament del sistema nerviós (Buonanno & Fischbach, 2001; Mei & Nave, 2014) i en la morfogènesis cardíaca (Pentassuglia & Sawyer, 2009), entre altres processos, fent-la una proteïna de vital importància per a la supervivència i, per tant, impossibilitant la creació d'animals transgènics deficientes (*knock-out (KO)*) (Falls, 2003).

La senyalització per NRG necessita que aquesta proteïna s'uneixi al domini extracel·lular dels receptors tirosina quinasa ErbB3 o ErbB4, la qual cosa activa l'homodimerització d'aquests receptors o l'heterodimerització amb la subunitat ErbB2. A partir d'aquí, s'activa la senyalització intracel·lular per donar lloc a respostes cel·lulars tals com l'estimulació o inhibició de la proliferació, l'apoptosis, la migració, la diferenciació i l'adhesió (Yarden & Sliwkowski, 2001).

Només un 0.3% de tot el gen codificant per la NRG1 es tradueix a proteïna, cosa que implica que en la seqüència gènica hi hagi múltiples promotores i diverses regions d'*splicing* alternatiu, fent que hi hagi més de 15 isoformes de NRG1 codificades a partir d'un únic gen (Buonanno & Fischbach, 2001; Kao *et al.*, 2010).

Estructuralment, totes les isoformes de NRG contenen el domini semblant al factor de creixement epidèrmic (*epidermal growth factor-like (EGF-like)*), amb el qual activen els receptors ErbB

(Buonanno & Fischbach, 2001), així com un domini transmembrana. En el SNC, les formes més abundants de NRG1 són la tipus I i la tipus III, les quals s'han detectat en MNs, en neurones dels ganglis raquidis i en la glia. Aquestes dues isoformes es diferencien en que la NRG1 de tipus I té un domini anomenat semblant a immunoglobulines (*Immunoglobulin-like* (Ig-like)), mentre que la isoforma de tipus III, es caracteritza per tenir un domini ric en cisteïnes (*cysteine rich domain* (CRD))



Figura 15 | Estructura proteica de les isoformes I i III de la NRG1. Totes les NRG1 contenen un domini EGF-like necessari per unir-se als receptors ErbB i almenys 1 domini transmembrana (TM). A més, la isoforma I té el domini Ig, característic d'aquest subtípus. D'altra banda, en la NRG1 tipus III es descriu el domini CRD, la segona regió transmembrana d'aquesta isoforma. Adaptat de Chen *et al.* 2008.

(Fig. 15).

Les diferents isoformes de NRG1 amb les seves variants estructurals, suggereixen que actuen mitjançant tipus de senyalització diferents. La NRG1 tipus I sembla actuar principalment per via paracrina. El fet que aquesta proteïna tingui un únic domini transmembrana implica que quan es produeix el processament proteolític en el domini extracel·lular per part de varies proteases com l'enzim de trencament de proteïnes precursor amiloide del lloc β -1 (*β -site amyloid precursor protein-cleaving enzyme1* (BACE-1)), s'allibera el domini EGF-like, resultant en la senyalització paracrina (Falls, 2003). D'altra banda, la NRG1 tipus III al tenir el domini CRD el qual serveix de segon domini transmembrana (Wolpowitz *et al.*, 2000), quan es produeix la proteòlisis, en aquest cas el domini EGF-like es manté ancorat a la membrana cel·lular, apuntant a una senyalització juxtacrina (Willem, 2016) (Fig. 16). No obstant, es desconeixen les funcions específiques de les diferents isoformes de NRG1 en els BC.

Entre les diferents funcions que se li atribueixen en el SNC, la NRG1 està involucrada en les interaccions glia-axó (mielinització), el desenvolupament de les plaques motores, la migració neuronal, la sinaptogènesi i la plasticitat en el SNC (Buonanno & Fischbach, 2001; Falls, 2003; Kerber *et al.*, 2003; Mei & Nave, 2014; Stassart *et al.*, 2013). Diversos membres d'aquesta família s'han relacionat amb desordres psiquiàtrics com l'esquizofrènia, el trastorn bipolar o la depressió (Karl, 2013).

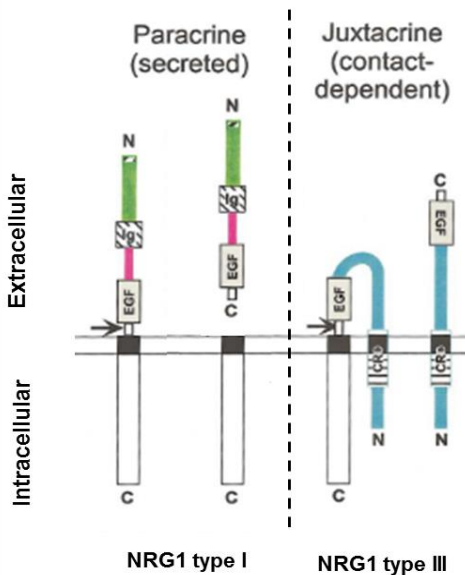


Figura 16 | Isoformes de NRG1 i tipus de senyalització que desencadenen. La isoforma I consta d'un únic pas transmembrana; en canvi, la isoforma 3 travessa dos vegades la membrana cel·lular. La fletxa indica el punt de proteòlisi de varies proteases (BACE1,...). Després del processament, la isoforma 1 allibera el fragment extracel·lular (que conté el domini EGF-like) per dur a terme una senyalització paracrínia. La isoforma III, es manté unida a la membrana després de la proteòlisis però exposant el domini EGF-like, desencadenant així la senyalització juxtaocrínia. Adaptat de Falls, 2003.

3.5. Interrelació micròglia-sinapsis

La degeneració de les MNs en models de ratolí per la mutació de SOD1 s'ha descrit com un procés dependent d'altres cèl·lules no neuronals a part de les pròpies MNs (Boillée *et al.*, 2006; Clement *et al.*, 2003). Per aquesta raó, a l'hora d'estudiar els fenòmens que van succeirent durant la vida del ratolí transgènic, no només s'ha de prestar atenció a les MNs, sinó també al seu entorn, el neuròpil. Aquest, inclou les aferències que reben les MNs, els astròcits, la micròglia i com aquests es relacionen entre ells, posant en el centre de les interrelacions les MNs.

Acompanyant la degeneració de les MNs s'observa una important resposta microglial, la qual augmenta progressivament a mesura que es desenvolupa la paràlisi motora en el ratolí (Kawamata *et al.*, 1992). Una forma d'entendre la resposta inflamatòria progressiva i crònica que es produeix en els animals SOD1^{G93A}, és mitjançant el model d'axotomia. Amb aquest tipus de lesió es reproduceix el fenomen neuroinflamatori al voltant de les MNs axotomitzades de forma aguda (Blinzinger & Kreutzberg, 1968; Moran & Graeber, 2004; V. H. Perry & O'Connor, 2010). Aplicada com a model

experimental, podem considerar que l'axotomia reproduceix de forma induïda el dany axonal inicial que es postula com a desencadenant de la malaltia d'acord amb la hipòtesis del *dying-back* (Moloney *et al.*, 2014). Tot l'anterior suggereix que la resposta reactiva que s'observa en les MNs axotomitzades pot compartir alguns mecanismes comuns amb l'ELA.

Paral·lelament a la microgliosis, tant en el model SOD1^{G93A} com en el d'axotomia, es produeix una important pèrdua d'aferents sinàptics en les MNs degenerades, en la qual la micròglia hi podria estar implicada (Aldskogius, 2011; Brännström & Kellerth, 1998; Fischer *et al.*, 2004; V. H. Perry & O'Connor, 2010; Sumner, 1975; Sumner & Sutherland, 1973). Blinzing i Kreutzberg suggerien l'any 1968 que la pèrdua dels terminals sinàptics en les MNs axotomitzades es produeix mitjançant el reclutament perineuronal de micròglia i introduïen el concepte de *stripping* sinàptic. En aquest estudi (Blinzinger & Kreutzberg, 1968) els autors sostenen que l'eliminació d'aferents sinàptics que contacten les MNs lesionades és produeix per la intervenció de la micròglia, suggerint que les cèl·lules microglials introduceixen pseudòpodes en les fenedures sinàptiques desprendent físicament els terminals de la membrana de la MN o de les dendrites, però sense que terminals presentessin signes de degeneració ni que hi haguessin indicis de fagocitosis per part de la micròglia. Així doncs, el concepte d'*stripping*, que s'ha mantingut vigent fins el moment, s'ha considerat que promou la supervivència i la recuperació funcional de les MNs danyades i, per tant, la micròglia estaria actuant d'una manera protectora. Aquesta teoria es va fer extensiva a la deafferentació que es produeix en altres tipus de neurones secundari a diferents tipus de lesions (Kettenmann *et al.*, 2013).

Estudis posteriors han evidenciat que la degeneració de les sinapsis és una de les característiques patològiques inicials en diverses malalties neurodegeneratives cròniques, produint-se abans que la pròpia pèrdua dels cossos neuronals (Fischer *et al.*, 2004; Geracitano *et al.*, 2003; V. H. Perry & O'Connor, 2010). Aquests terminals degenerants es reconeixen a nivell ultraestructural per tenir un citoplasma electrodens, orgànuls foscos i pèrdua de la definició de les vesícules sinàptiques (Adalbert *et al.*, 2009; Šišková *et al.*, 2009).

En els últims anys, s'ha descrit que en etapes inicials postnatals es produeix una eliminació de l'excés de connexions sinàptiques, procés conegut com *synaptic pruning*, en el que la micròglia hi participa de forma activa. Aquesta, elimina les sinapsis prèviament marcades amb factors del sistema del complement, com el C1q o el C3 mitjançant la fagocitosis (Stevens *et al.*, 2007). En altres condicions patològiques, tals com el glaucoma o l'Alzheimer, on també es produeix una pèrdua sinàptica, la micròglia també participa en el procés d'eliminació/remodelació de les sinapsis també amb la participació del sistema del complement (Cullheim & Thams, 2007; Hong *et al.*, 2016; Paolicelli *et al.*,

2011; Schafer *et al.*, 2012; Sipe *et al.*, 2016; Tremblay *et al.*, 2010). No obstant això, no es coneix exactament el mecanisme pel qual la micròglia ingereix i destrueix els terminals sinàptics.

Alguns autors han suggerit que aquesta poda sinàptica per part de la micròglia es dóna per un procés de fagocitosi parcial i selectiva de petits fragments d'estructures sinàptiques, un procés anàleg a l'anomenada trogocitosi en el sistema immunològic. Així doncs, la micròglia, enlloc de fagocitar grans estructures com el terminal sinàptic sencer (*bulk phagocytosis*), estaria digerint petites estructures provinents dels terminals degenerants, com per exemple, a través de la formació d'exosomes (Dopfer *et al.*, 2011).

Que hi hagi trogocitosi implica que els terminals sinàptics s'han de fragmentar en trossos de menors dimensions per a que la micròglia els pugui englobar, engolir i digerir. Un possible mecanisme pel qual es podria estar fragmentant el terminal presinàptic és mitjançant la necroptosi, un mecanisme de mort cel·lular necròtica programada (Vandenabeele *et al.*, 2017), mediada per les proteïnes RIPK1/3 i executada mitjançant fosforilació de la proteïna efectora de llinatge cinasa mixta semblant a un domini (*mixed lineage kinase domain-like* (MLKL)), la qual media la formació de porus a les membranes plasmàtiques (Fig. 17), en aquest cas, de neurones (Cho *et al.*, 2009; He *et al.*, 2009; Sun *et al.*, 2012). A més, l'activació de la via necroptòtica es creu que promou la inflamació (Christofferson *et al.*, 2014; Ito *et al.*, 2016), en aquest cas, de la micròglia. En estudis recents s'ha relacionat aquesta via de mort cel·lular programada a malalties neurodegeneratives com l'Alzheimer, a dany neuronal associat a lesions en la medul·la espinal, inclús a la degeneració axonal associada a l'ELA (Jiao *et al.*, 2020; Ofengeim *et al.*, 2017).

Tot i les evidències que assenyalen l'eliminació dels inputs sinàptics en les MNs axotomitzades i la seva associació amb l'activació de cèl·lules microglials, el mecanisme pel qual els terminals sinàptics desapareixen de la superfície de MNs danyades necessita ser reexaminat en profunditat.

Hi ha estudis que suggereixen que la degeneració sinàptica prèvia disfunció, va seguida de la mort neuronal (V. H. Perry & O'Connor, 2010). La mort cel·lular es va dividir inicialment en dos tipus: necrosi i apoptosis. La necrosi es considera un tipus de mort passiva i accidental (Fink & Cookson, 2005). L'apoptosi en canvi, es considera un procés que succeeix de forma programada on la cèl·lula hi participa activament mitjançant l'expressió de proteïnes i que no comporta l'alliberament del contingut citoplasmàtic a l'espai extracel·lular (Fink & Cookson, 2005).

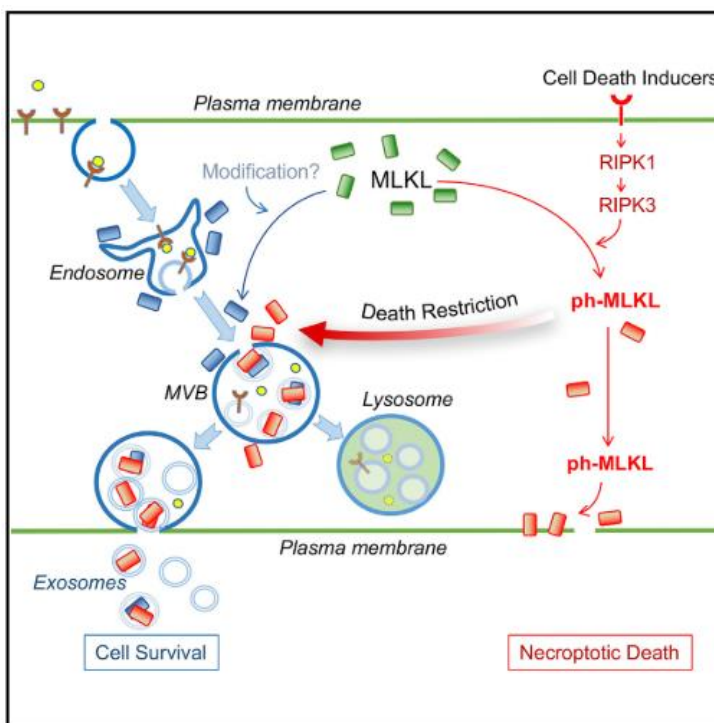


Figura 17 | Representació gràfica de la via necroptòtica. Les proteïnes RIPK1/3 promouen la fosforilació de la proteïna efectora p-MLKL, la qual promou la formació de porus a la membrana plasmàtica que conueixen a la mort per necroptosi. Extret de Yoon *et al.*, 2017.

En els últims anys s'han descrit varíes formes més de mort cel·lular programada, com seria la necroptosi o la paraptosi (Cabon *et al.*, 2013). Cada vegada hi ha més investigacions centrades en els mecanismes de mort cel·lular programada que succeeixen en el SNC durant el desenvolupament, les malalties neurodegeneratives, els trastorns psiquiàtrics i durant diferents tipus de lesions en el SNC (Shi *et al.*, 2021). La paraptosi és un tipus de mort cel·lular programada no apoptòtica que es caracteritza per la dilatació del RE i/o dels mitocondris resultant en la vacuolització citoplasmàtica en un procés independent de caspases (Sperandio *et al.*, 2000). És un concepte aplicat i utilitzat en el context del càncer que no s'ha desenvolupat en malalties neurodegeneratives. Es té molt poc coneixement sobre les bases moleculars de la paraptosi, però les pertorbacions en la proteostasi cel·lular, normalment relacionades amb la presència de proteïnes defectuoses en el RE, i l'alteració de l'homeòstasi iònica, sobretot del calci, semblen contribuir de forma crítica en el procés (Fontana *et al.*, 2020; D. Lee *et al.*, 2016). En particular, un influx de calci procedent del RE cap a l'interior del mitocondri, pot induir la dilatació d'aquests durant la paraptosi, mentre que l'acumulació de proteïnes malplegades en el lumen del RE es creu que exerceix una força osmòtica suficient com per

promoure l'entrada d'aigua en aquest i causar la seva distensió. En el procés, el calci alliberat del RE pot contribuir alhora a agreujar l'estrés de reticle i la dilatació d'aquest (Fig. 18) (E. Kim *et al.*, 2021).

Alguns estudis recents suggereixen que es podria produir mort neuronal mediada per la paraptosi en etapes inicials de malalties neurodegeneratives, com l'Alzheimer (Jia *et al.*, 2015; Pehar *et al.*, 2010), així com en la retina després d'una isquèmia i reperfusió en el model de rata (Wei *et al.*, 2015).

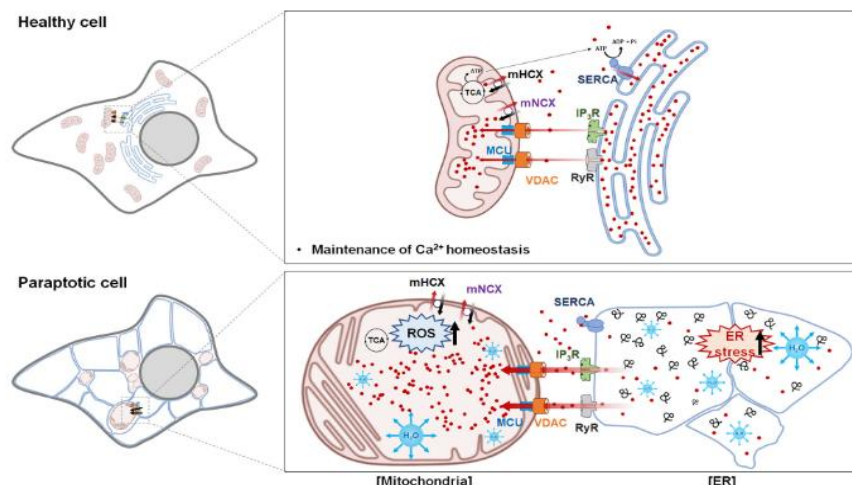
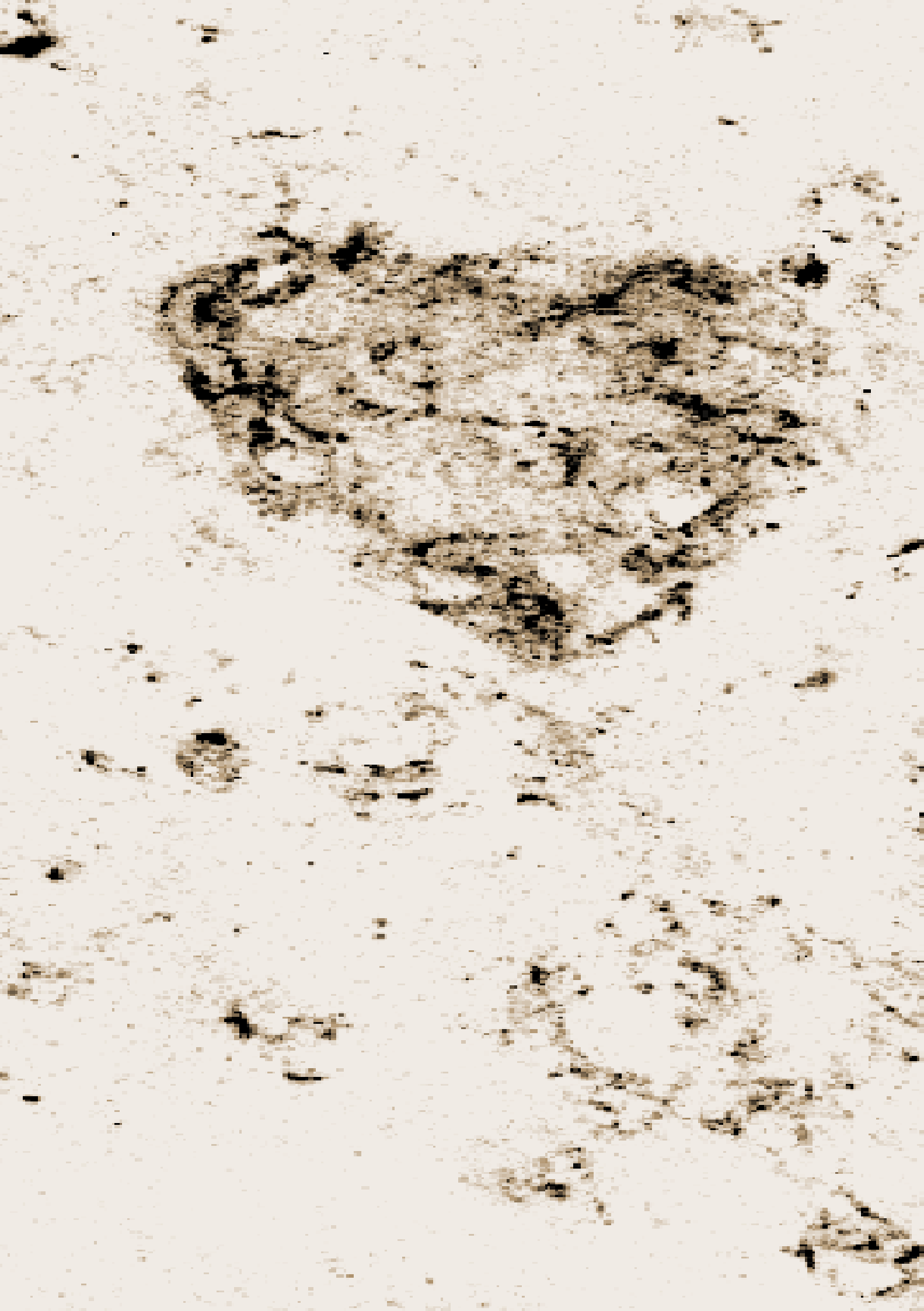
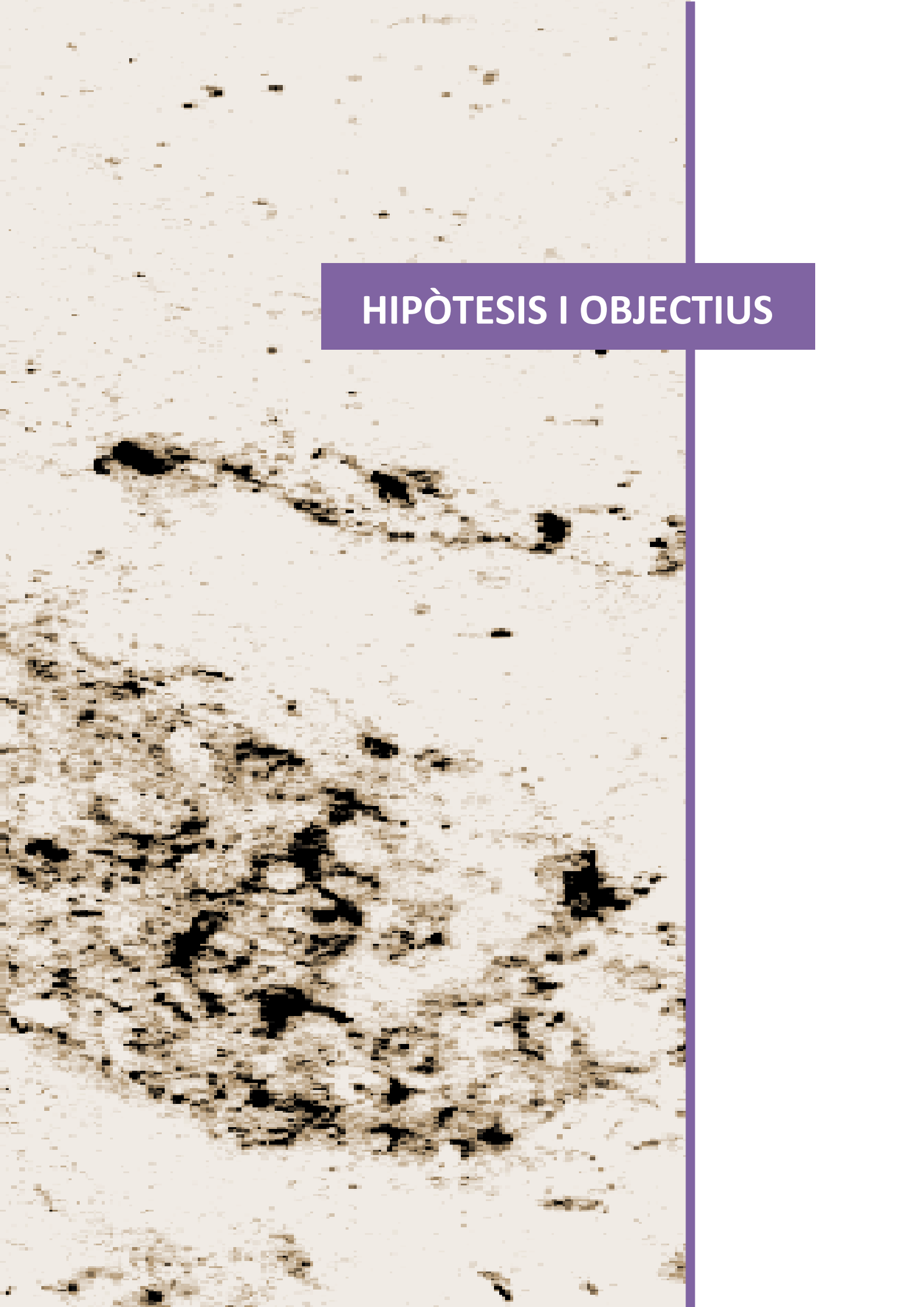


Figura 18 | Model hipotètic de la comunicació entre el mitocondri i el RE en la paraptosi. El calci alliberat pel RE s'incorpora en els mitocondris, provocant una sobrecàrrega en aquest. Aquesta situació de forma mantinguda en el temps, provoca un influx d'aigua dins del mitocondri causant la seva dilatació. D'altra banda, l'acumulació de proteïnes mal plegades en el RE causa un desequilibri osmòtic que es compensa amb l'entrada d'aigua en aquest i la conseqüent distensió del RE. Aquests fenòmens causa un dany estructural irreversible així com defectes funcionals en aquests dos orgànuls, conduint a la mort de la cèl·lula. Adaptat de Kim *et al.*, 2021.



HIPÒTESIS I OBJECTIUS



Com s'ha comentat en la introducció, els BC són els reguladors més importants de l'excitabilitat de les α-MNs. No només s'ha descrit que aquests pateixen canvis plàstics durant el curs de l'ELA, sinó que s'han caracteritzat mutacions en proteïnes relacionades amb els BC causants de formes esporàdiques o familiars d'ELA, suggerint una especial rellevància d'aquestes aferències en relació a aquesta malaltia neurodegenerativa. Tot i això, aquests terminals colinèrgics estan poc estudiats, desconeixent-se la seva estructura molecular així com la funció de les proteïnes singulars, tals com la NRG1, que l'integren.

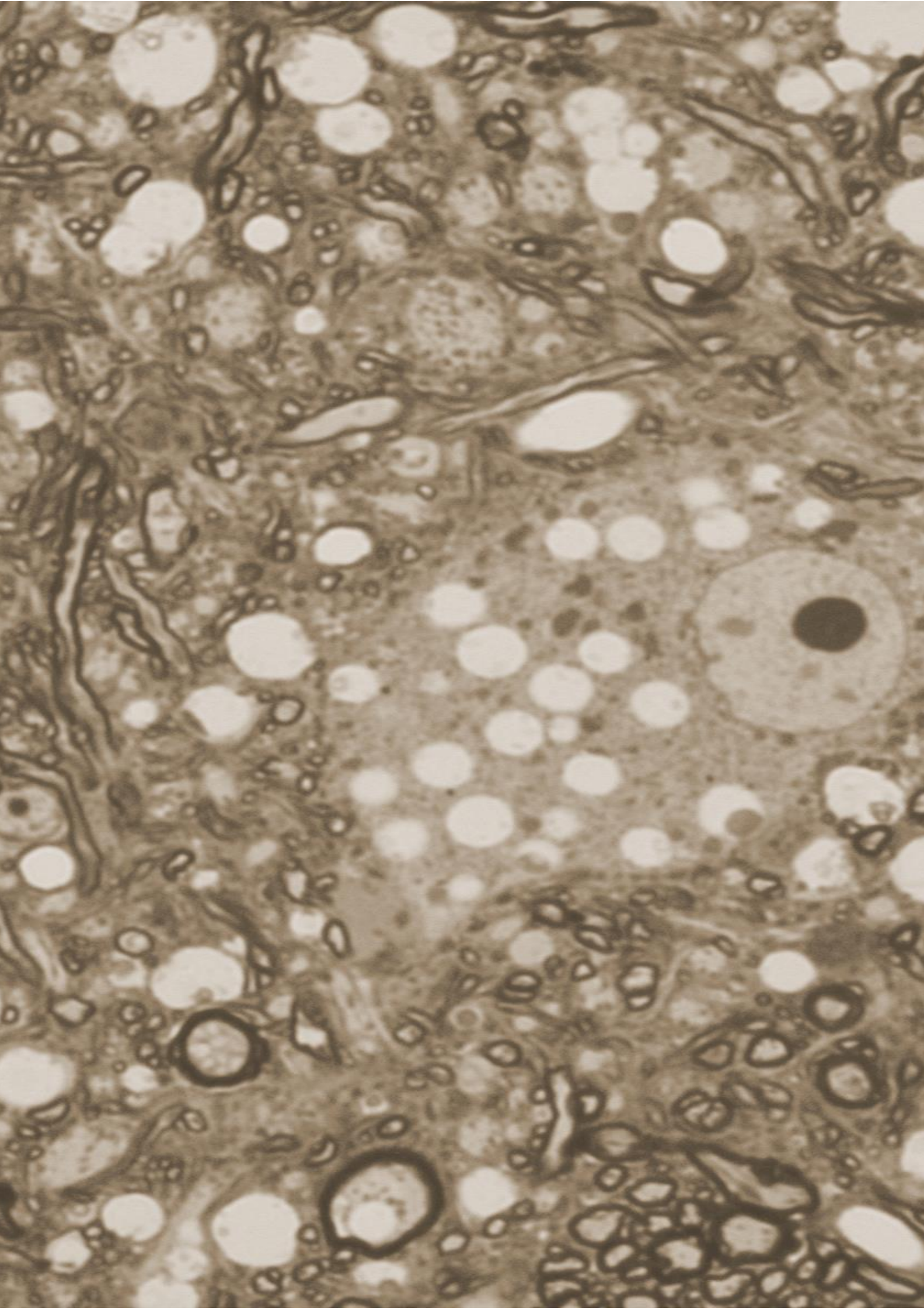
La primera hipòtesi del present treball, és que els BC poden tenir un rol rellevant en la fisiopatologia de l'ELA, concretament que la seva alteració pot reflexar o contribuir a la degeneració de les MNs de la medul·la espinal. En aquest context, la NRG1, proteïna associada al BC pel grup de recerca on s'ha dut a terme la tesi (Gallart-Palau *et al.*, 2014) i de funció desconeguda en aquesta localització, podria ser de vital importància en aquests terminals, ja que la via de senyalització en la que està involucrada s'ha vist mutada en un tipus d'ELA (Takahashi *et al.*, 2013).

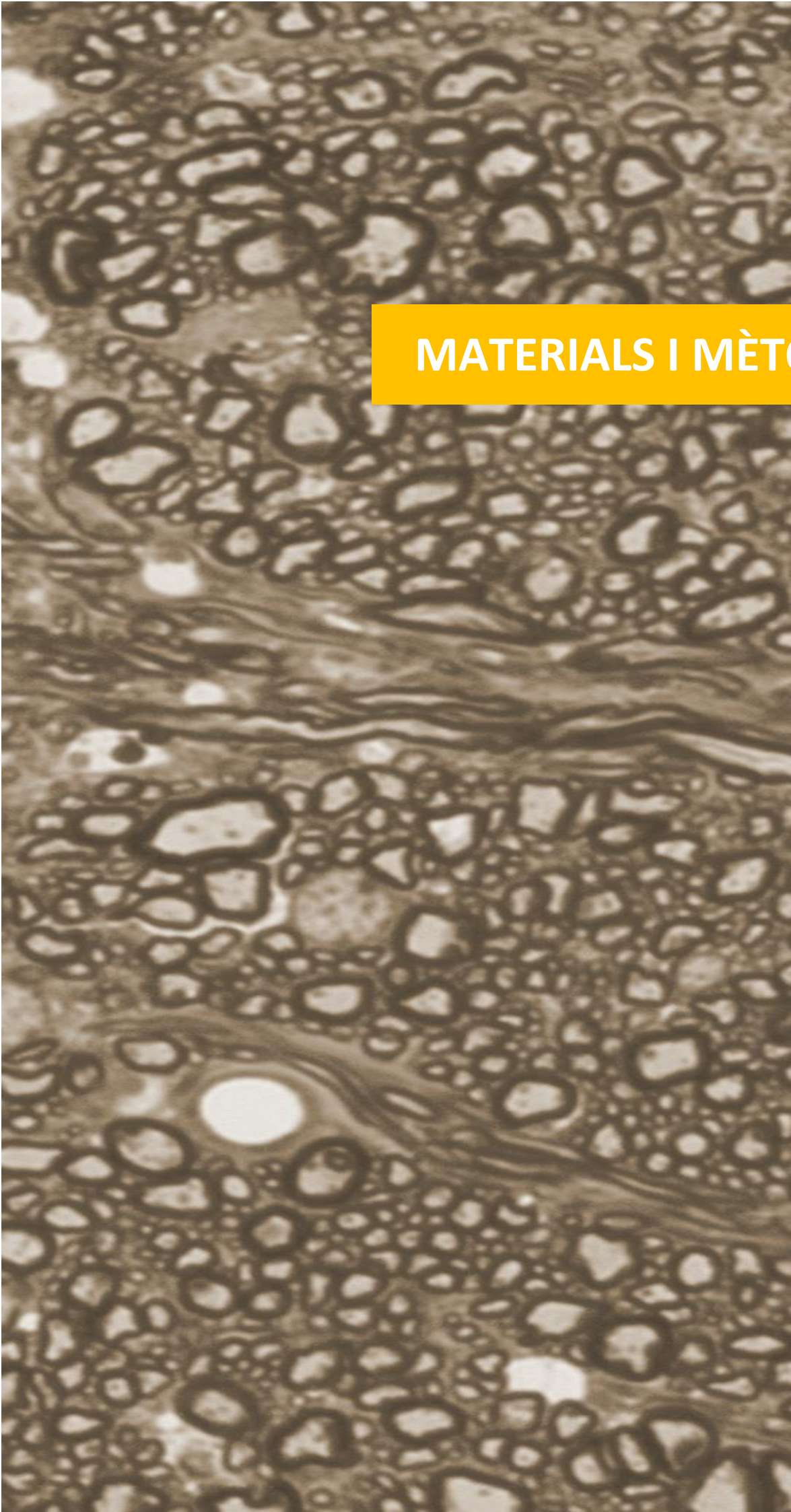
D'altra banda, en l'ELA no només hi intervenen mecanismes intrínsecos de les MNs, sinó que s'ha vist que factors extrínsecos com les cèl·lules no neuronals contribueixen de forma significativa a la degeneració de les MNs. És per això, que una segona hipòtesi en la que ens fonamentem, fa referència a que la neuroinflamació a través de la micròglia, pot influir de forma significativa l'estabilitat dels terminals sinàptics, i en definitiva, a la neurodegeneració.

Estudiar la fisiologia dels BC així com les alteracions que aquests sofreixen en l'ELA i la seva relació amb la neuroinflamació, podria ajudar a esclarir el mecanisme pel qual les MNs degeneren en aquesta malaltia així com contribuir a desenvolupar noves dianes moleculars per una futura aproximació terapèutica per l'ELA.

Partint de les hipòtesis exposades prèviament, en el present treball vàrem establir els següents objectius:

1. Analitzar l'organització estructural del BC i la compartmentalització subcel·lular dels seus components moleculars
 - 1.1 Definir les característiques estructurals d'aquests terminals en condicions fisiològiques
 - 1.2 Estudiar els BC durant la seva formació en etapes prenatals, la maduració en fases postnatals i adults, així com els canvis que pateixen durant l'enveliment
2. Realitzar una aproximació al significat funcional de la senyalització NRG1/ErbBs en els BC de les alfa-motoneurones
 - 2.1 Determinar l'efecte de la sobreexpressió de les isoformes I i III de la NRG1 així com de la forma truncada de NRG1 III (GIEF) sobre els BC
3. Explorar la participació dels BC en la patologia degenerativa de les motoneurones i la seva relació amb la neuroinflamació
 - 3.1 Estudiar els efectes d'estressos aïllats en el BC tals com l'estrés de reticle, la modulació farmacològica de la seva activitat o l'estimulació elèctrica
 - 3.2 Investigar l'affectació dels BC en el model d'axotomia i caracteritzar la implicació de la micròglia en la degeneració dels terminals sinàptics
 - 3.3 Analitzar la relació entre les alteracions del BC, la neuroinflamació, l'acumulació progressiva de mfSOD1 i la conseqüent degeneració de MNs individuals en el model de ratolí d'ELA SOD1^{G93A}





MATERIALS I MÈTODES

1. Models animals

Per caracteritzar els BC en condicions fisiològiques, així com per l'estudi dels fenòmens que succeeixen després de l'axotomia del nervi ciàtic, s'han utilitzat ratolins de la soca CD1, obtinguts de *Envigo* (*East Millstone, NJ, USA*). També s'ha utilitzat aquesta soca per realitzar cultius cel·lulars i pels experiments de les *slices in vitro*.

La instauració de la colònia de ratolins transgènics sobreexpressors de la NRG1 tipus III cedits pel Dr. Markus Schwab i el Dr. Klaus-Armin Nave (*Max-Planck-Institute of Experimental Medicine, Göttingen, Alemanya*) a l'estabulari de la Universitat de Lleida, ens ha permès estudiar les funcions específiques d'aquesta isoforma en el BC. Aquests animals transgènics sobreexpressen la NRG1 tipus III conjugada a la proteïna hemaglutinina (HA-NRG1^{FL}). El transgèn es manté en heterozigosi creuant animals transgènics (TG) amb animals de la soca C57BL/6J. La descendència TG s'identifica mitjançant el genotipatge amb la tècnica de la Reacció en Cadena de la Polimerasa (*Polymerase Chain Reaction; PCR*) de l'ADN extret de la cua d'aquests animals en els primers dies postnatals i utilitzant els *primers* descrits (Velanac *et al.*, 2012).

També s'ha treballat amb mostres de medul·la espinal de ratolins sobreexpressors de la isoforma I de NRG1 (NRG1^{type I}) (Michailov *et al.*, 2004), així com amb un transgènic que expressa la variant processada per la proteasa BACE1 de la NRG1 tipus III (HA-NRG1^{GIEF}). Les mostres d'aquests animals transgènics van ser cedides pel grup de recerca dels investigadors anteriorment mencionats.

El model animal que s'ha utilitzat per estudiar l'ELA són els ratolins transgènics que sobreexpressen la proteïna humana mutada SOD1^{G93A} (B6SJL-Tg(SOD1-G93A)1Gur/J), obtinguts de *Jackson Laboratory* (Sacramento, CA, USA). Aquesta línia transgènica es manté amb el creuament de masclles SOD1^{G93A} TG amb femelles de la soca B6SJL. Les noves generacions també s'identifiquen mitjançant el genotipatge amb la PCR de l'ADN extret de la cua dels animals pocs dies després d'haver nascut utilitzant *primers* específics (Ripps *et al.*, 1995). Es considera que els animals TG d'entre p0-p30 són asimptomàtics, entre p30-p60 són presimptomàtics, esdevenen simptomàtics de forma progressiva entre p60-p90 i entren en la fase terminal a p90 fins a p120 ± 10 (Mancuso *et al.*, 2012; Sábado *et al.*, 2013). Sobretot en aquest model transgènic considerat sever, però també en els altres, es van establir criteris de punt final per tal de minimitzar el patiment de l'animal si aquest existís (Günther *et al.*, 2012).

En tots els procediments que han involucrat ratolins TG, els animals de la mateixa camada que no han adquirit el transgèn (considerats WT) s'han tractat en paral·lel respecte els TG i s'han utilitzat com a controls en els diferents procediments.

En tots els casos, s'ha treballat preferentment amb masclles per evitar la dispersió provocada pel sexe. Els animals estaven allotjats en gàbies de 5-6 ratolins amb accés permanent i lliure al pinso estàndard de laboratori i a aigua, i amb un cicle de llum/fosc de 12 hores. D'acord a criteris prèviament definits (Burkholder *et al.*, 2012; R. A. Miller & Nadon, 2000), els animals que en algun moment hagin presentat tumors o anormalitats físiques, s'excloïen dels experiments i es procedia a l'eutanàsia per sobredosi de pentobarbital (30 mg, intraperitoneal). Es van realitzar tots els esforços necessaris per tal de reduir el número d'animals utilitzats d'acord amb la Normativa de la Unió Europea (24 de Novembre de 1986, 86/609/EEC).

Tots els procediments amb animals d'experimentació es van dur a terme d'acord a la normativa de la Comissió Europea i a les normes estableertes per la Generalitat de Catalunya (publicades com a llei en el Diari Oficial de la Generalitat de Catalunya 2073, 1995). Tots els experiments han estat prèviament avaluats i aprovats pel Comitè Ètic d'Experimentació Animal (CEEA) de la Universitat de Lleida.

Pel que fa als animals no rosegadors que s'han utilitzat per estudiar l'homologia entre espècies del BC, es va treballar amb mostres fixades de medul·la espinal de granota (*Xenopus Laevis*) cedides pel Dr. Jesús María López (Universitat Complutense de Madrid, Madrid); de llangardaix (*Timon Lepidus*) proveïdes per la Dra. Ester Desfilis (Universitat de Lleida); i de porc (*Sus scrofa domesticus*), proporcionades pel Dr. José Antonio Moreno (Universitat de Lleida).

2. Procediments quirúrgics i farmacològics *in vivo*

Axotomia del nervi ciàtic: Aquesta intervenció quirúrgica s'ha realitzat en animals CD1 adults (entre p60 – p90) i en animals SOD1^{G93A} de p30, p60 i p90. Els animals s'anestesiaven utilitzant una combinació de ketamina (100 mg/kg) i xilacina (10 mg/kg) i es mantenien amb anestèsia inhalada (1% isoflurà) durant el procediment.

Després de l'exposició del nervi ciàtic a nivell medio-femoral abans de la seva bifurcació, es seccionava aquest nervi prèvia lligadura del segment proximal per tal d'evitar la reinnervació espontània. Per minimitzar el dolor derivat de la secció del nervi, s'administrava analgèsia postoperatoria consistent en dos dosis subcutànies de buprenorfina (0.05 mg/kg): una immediatament després de la cirurgia i una altra a les 24h després de la intervenció. Si l'animal presentava signes de dolor (postura corporal encorbada, autolesions,...) s'administrava una tercera dosi d'analgèsia a les 48 h després de l'operació. Les mostres de medul·la espinal s'obtenien a diferents punts temporals després de la intervenció: 1, 3, 7, 15, 30, 90, 120 i 180 dies. En un altre grup d'animals CD1 adults, es va seguir el mateix procediment, però enllloc de l'axotomia, es va

realitzar l'aixafament (*crush*) del nervi ciàtic durant 1 minut utilitzant microfòrceps, amb la mateixa pauta d'analgèsia posterior.

Marcatge retrògrad: Es va utilitzar la toxina colèrica B (CTB) conjugada amb el fluorocrom AlexaFluor 555 pel múscul tibial anterior o marcada amb el fluorocrom AlexaFluor 488 pel múscul solí (1 µg/µl en tampó fosfat (*phosphate buffer*; PB), (*Molecular Probes*, Eugene, OR, United States) per marcar retrògradament les MNs que innerven aquests músculs.

Després de l'exposició quirúrgica dels músculs, amb l'ajuda d'un micromanipulador es va injectar un volum de 6 µl de la solució de CTB en el múscul tibial anterior dret, i, 3 µl en el múscul solí esquerre, mitjançant un capil·lar de vidre acoblat a una xeringa *Hamilton*. Un dia després de la injecció, els animals es van perfondre transcardíacament, tal com es descriu més endavant. Aquest procediment es va dur a terme sota les mateixes condicions d'anestèsia i analgèsia descrits per l'axotomia.

Experiments farmacològics: Per dur a terme l'agonisme i l'antagonisme dels receptors M2 muscarínics, es va utilitzar Oxotremorina M (agonista) (Ref. 1067, *Tocris Bioscience*, Minneapolis, MN, USA), administrada en una dosi diària intraperitoneal a 30-50 µg/kg diluït en sèrum fisiològic (salí) durant 15 dies; i Metoctramina (antagonista) (Ref. M105, *Sigma-Aldrich*, Saint Louis, Missouri, USA), també una única dosi diària intraperitoneal durant 15 dies dissolta en salí a 200 µg/kg. Els protocols d'administració estan basats en articles publicats (Saxena *et al.*, 2013). Aquests dos tractaments s'han dut a terme en animals SOD1^{G93A} en edat adulta (entre p60 i p75) (Fig. 19).



Figura 19 | Esquema de la pauta farmacològica seguida pels tractaments amb l'agonista Oxotremorina i l'antagonista Metoctramina dels receptors M2 muscarínics. Creat amb Biorender.

Per tal d'estudiar els efectes de l'estrés de reticle en el BC, es va realitzar un tractament farmacològic amb un inductor com és la Tunicamicina (Ref. T7765, *Sigma-Aldrich*, Saint Louis, Missouri, USA), injectant una dosi diària intraperitonealment a 1 mg/kg en salí durant 2 dies; i amb un inhibidor com el Salubrinal (Ref. 2347, *Tocris Bioscience*, Minneapolis, MN, USA), injectat intraperitonealment a una

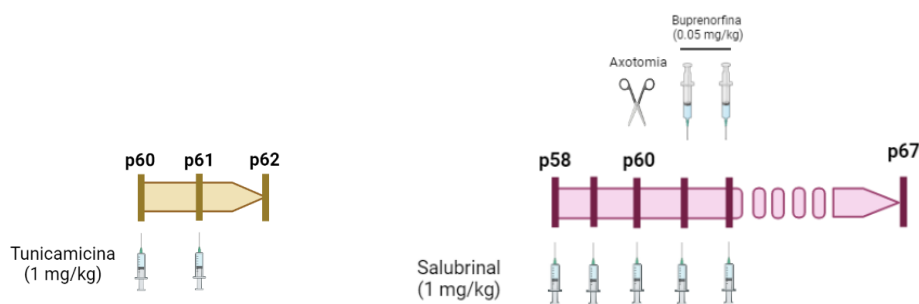


Figura 20 | Esquema de la pauta farmacològica seguida amb els fàrmacs Tunicamicina i Salubrinal (inductor i inhibidor de l'estrés de reticle respectivament). Creat amb Biorender.

concentració de 1 mg/kg en salí en una única dosi diària, començant 2 dies abans de l’axotomia (inductor de l’estrès), continuant el mateix dia de la intervenció i durant el següents 7 dies (Fig. 20).

Amb la intenció de bloquejar la inducció microglial que es produeix després de l’axotomia del nervi perifèric en ratolins CD1, així com la microgliosis que té lloc intrínsecament en animals SOD1^{G93A} a mesura que progressa la malaltia, es va administrar l’inhibidor específic del factor estimulant de la colònia-1 (*Colony Stimulating Factor-1; CSF-1*) anomenat PLX5622 (Elmore *et al.*, 2014), proveït per Plexxikon Inc. (Berkeley, CA) i formulat en pinso estàndard AIN-76 per Research Diets Inc. (New Brunswick, NJ). Aquest pinso amb l’inhibidor, es va administrar a animals CD1 p60 durant 7 dies abans de l’axotomia i els 7 dies postintervenció; d’altra banda, també s’ha administrat a animals SOD1^{G93A} durant 1 mes (p30-p60). Tots els animals estaven en un ambient lliure de patògens durant el tractament i se’ls alimentava amb el pinso que contenia 1,200 mg/kg de PLX5622 o amb pinso control. Per comprovar que els animals consumien el pinso, es va monitoritzar el pes dels ratolins, i

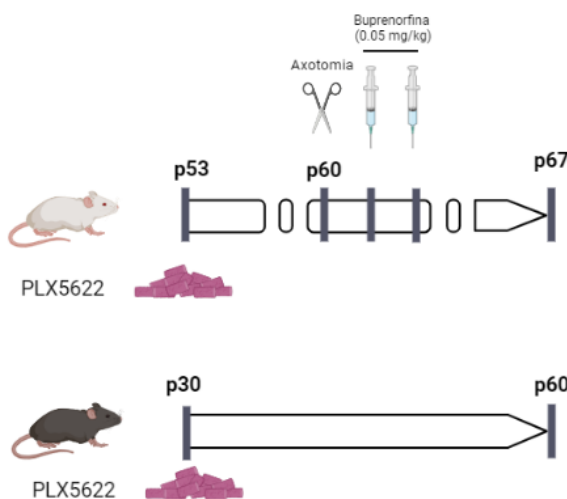


Figura 21 | Esquema de la pauta farmacològica seguida amb l’inhibidor del CSF-1 anomenat PLX5622 per tal d’inhibir la proliferació microglial. Creat amb Biorender.

es va observar que no hi havia una pèrdua significativa de pes (Fig. 21).

Després del procediment quirúrgic o del tractament farmacològic oportú, els animals s'anestesiaven amb ketamina i xilacina, es perfonien transcardíacament amb 4% paraformaldehid (PFA) i es processaven per dur-hi a terme immunohistoquímiques tal com es detalla en els apartats posteriors.

3. Estimulació elèctrica

Pels experiments d'estimulació elèctrica, tant per l'estimulació del nervi ciàtic com de la medul·la espinal, es van utilitzar agulles d'acupuntura (0.3 x 30 mm; *Acupuncture Shop, Varde*, Dinamarca) com elèctrodes estimuladors i una unitat d'estimulació Cibertec (CS-20, *Cibertec*, Madrid).

Per a estimular elèctricament el nervi ciàtic, després d'exposar-lo, se li va aplicar electroestimulació (5 V a 10 o 100 Hz) amb la unitat estimuladora. Amb això es van provocar potencials d'acció en direcció retrògrada, els quals van causar la despolarització del soma de les MNs localitzades en la medul·la espinal.

D'altra banda, l'estimulació elèctrica directa de la medul·la espinal es va dur a terme utilitzant 2 agulles d'acupuntura inserides en la regió dorsal de la medul·la espinal toràcica-lumbar. Llavors, es va aplicar estimulació elèctrica amb la unitat estimuladora (5 V a 10 Hz).

En cada cas, com a control intern de l'experiment, es van sotmetre 3 animals a les mateixes condicions però sense aplicar electroestimulació.

Tant en l'estimulació del nervi ciàtic com de la medul·la espinal, es va dur a terme un control electromiogràfic de la pota de l'animal per tal de comprovar l'efectivitat de l'electroestimulació. Amb aquest propòsit, l'elèctrode enregistrator es va inserir en la zona plantar de la pota, i l'elèctrode de referència, es va situar subcutàniament a prop de la cua.

4. Preparació de les mostres i ànalisi histològic

Els ratolins, prèvia anestèsia, es perfonien transcardíacament amb una solució salina (0.9% NaCl) seguida de 4% PFA en 0.1M PB pH 7.4 . Després de la fixació inicial, els teixits d'interès, generalment

la medul·la espinal a nivell lumbar (L1 – L6), es dissecava ràpidament i es postfixava amb la mateixa solució de fixació durant 24h a 4°C.

Les mostres de medul·la espinal humana (fixades també amb 4% PFA) es van obtenir del Banc de Teixits Neurològics de l'Hospital Universitari de Bellvitge (Dr. Isidre Ferrer, Barcelona). Els teixits d'animals diferents al ratolí, també es van fixar amb 4% PFA. Totes les mostres es van postfixar durant 24h amb la mateixa solució de fixació.

Després de la fixació, si les mostres s'havien de tallar amb el criòstat, es submergien en 30% sucrosa en 0.1M PB contenint 0.02% d'azida sòdica per tal de crioprotegir-les abans de congelar-les. Posteriorment, es realitzaven seccions transversals de les medul·les amb un gruix de 16 µm mitjançant el criòstat (*Leica, Wetzlar, Alemanya*). Els talls es recollien i dipositaven en portaobjectes gelatinitzats per realitzar les tincions o immunohistoquímiques corresponents, o per emmagatzemar-los a -80°C.

Pels anàlisis dels BC mitjançant les reconstruccions 3D, les mostres enlloc de tallar-les al criòstat, es processaven per *squash* (Pena *et al.*, 2001). Aquesta tècnica alternativa al criòstat no necessita de crioprotecció, amb la qual cosa després de la postfixació, es submergien les medul·les en 0.1M PB contenint 0.02% d'azida sòdica. Posteriorment, es tallaven seccions transversals amb el vibratom (*Leica, Wetzlar, Alemanya*) a un gruix de 200 µm. Les seccions es dipositaven sobre portaobjectes *Superfrost Plus* (*Menzel-Glaser, Germany*), es cobrien amb un cobreobjecte i s'aixafaven (*squash*) amb unes pinces. A continuació, les preparacions es sotmetien a una congelació ràpida amb nitrogen líquid, i posteriorment es retirava el cobreobjecte. Les mostres aixafades i adherides al portaobjecte es fixaven durant 10 minuts en metanol a -20°C. Després de rentar-les amb tampó fosfat salí (*phosphate-buffered saline (PBS)*), les mostres estaven preparades per realitzar-hi immunohistoquímiques (procediment descrit en l'apartat següent) o per emmagatzemar-les a -80°C.

Pels comptatges de MNs així com per l'anàlisi histològic, s'escollien varis seccions de criòstat a l'atzar, tenint en compte que fossin representatives de tota la regió lumbar (L1-L6), les quals es tenyien amb la tinció Violeta de Cresil. Les α-MNs, localitzades a nivell de la banya ventral, s'identificaven per la seva mida (diàmetre del soma de > 20 µm), morfologia (aspecte multipolar, nucli prominent i abundants grànuls de Nissl en el citoplasma) i topografia (làmina IX de Rexed). Les MNs es comptaven a cegues i cada dos seccions, d'acord amb criteris prèviament establerts (Calderó *et al.*, 1997; P. G. Clarke & Oppenheim, 1995). Només es comptabilitzaven les MNs amb un nucli gran, amb nuclèols i amb un citoplasma basofílic intens. Amb aquests criteris estrictes de comptatge no es va fer necessari utilitzar cap factor de correcció per evitar el comptatge doble d'una MN (P. G. Clarke & Oppenheim, 1995).

5. Immunohistoquímica de fluorescència i captura d'imatges

Les seccions de criòstat o *squash* es permeabilitzaven amb 0.1% tritó X-100 en PBS durant 30 minuts, es bloquejaven segons corresponia amb sèrum de cabra (*Normal Goat Serum (NGS)*) o de cavall (*Normal Horse Serum (NHS)*) al 10% en PBS durant 1 hora a temperatura ambient, i després s'incubaven amb la combinació d'anticossos primaris d'interès tota la nit a 4°C. Els anticossos primaris utilitzats estan indicats en la Taula 2.

Després de rentar amb PBS, les seccions s'incubaven amb la barreja d'anticossos secundaris fluorescents adients durant 1h a temperatura ambient, cada un d'ells marcats amb un dels següents fluorocroms: Alexa Fluor 488, DyLight 549, DyLight 649 (*Jackson Immuno Research Laboratories, West Grove, PA, Estats Units*). Tots ells a una dilució de 1/500.

Finalment, les seccions de medul·la espinal es tenyien amb la tinció de Nissl fluorescent (*NeuroTrace Nissl*) (1:150; *Molecular Probes*) i es muntaven utilitzant un medi de muntatge que evitava l'esvaïment de la senyal fluorescent (*anti-fading*), el qual contenia 0.1M de tampó Tris-HCl (pH 8.5), 20% glicerol, 10% Mowiol i 0.1% 1,4-diazabicyclo[2.2.2]octà. Per la visualització dels ErbBs, algunes seccions es van processar utilitzant un kit d'amplificació de la senyal per Tiramida, seguint el procediment recomanat pel fabricant (*Thermo Fisher Scientific, Waltham, MA, Estats Units*).

Les seccions s'examinaven amb el microscopi confocal d'escaneig làser *FluoView FV-500* o amb el *FluoView FV-1000* (*Olympus, Hamburg, Alemanya*). Les imatges del soma de les MNs estaven formades per l'empilament de múltiples seccions òptiques de 0.5 o 1 µm.

Per realitzar les comparacions, els teixits dels diferents animals en les diverses condicions experimentals, es processaven en paral·lel tant pel que fa a la realització de les immunohistoquímiques, com a la captura de les imatges, les quals s'adquirien amb els mateixos paràmetres d'escaneig. Les imatges digitals s'analitzaven utilitzant el programa *FV10-ASW 3.1 Viewer* (*Olympus*) i el software *ImageJ* (*US National Institutes of Health, Bethesda, MD, Estats Units*).

Les característiques dels perfils immunomarcats corresponents a les diferents proteïnes, s'examinaven i es comptaven manualment amb el programa *ImageJ* establint com a referència el soma de les MNs. Els experiments que involucraven axotomies, només s'analitzava la làmina IX de Rexed corresponent a la columna motora del ciàtic (L6) (Watson, et al, 2009). Aquesta agrupació de MNs s'identificava per la seva relació amb la micròglia reclutada, aquesta última marcada amb l'anticòs anti-Iba1.

Les reconstruccions 3D es van realitzar amb el programa *Imaris* (*Bitplane*, CT, Estats Units) a partir de imatges seqüencials de 0.5 µm de gruix obtingudes amb el microscopi confocal. Les imatges digitals es van editar utilitzant el programa informàtic FV10-ASW 3.1 *Viewer* (*Olympus*) i el Adobe Photoshop CS4 (*Adobe Systems Inc*, San Jose, CA, Estats Units).

Antigen	Espècie d'obtenció	Clonalitat	Casa comercial (nº de referència)	Dilució
ATP5A	Ratolí	Monoclonal	Abcam (ab14748)	1:100
C1q	Conill	Monoclonal	Abcam (182451)	1:1000
CD11c	Hàmster	Monoclonal	AbDserotec (MCA1369T)	1:50
CD63	Conill	Monoclonal	Abcam (ab217345)	1:100
CD68	Rata	Monoclonal	AbDserotec (MCA1957T)	1:100
CD81	Conill	Policlonal	Abcam (ab155760)	1:100
CD9	Conill	Monoclonal	Abcam (ab92726)	1:350
ChAT Transferasa d'acetilcolina (<i>Choline acetyltransferase</i>)	Conill	Policlonal	Millipore (AB143)	1:200
ChAT Transferasa d'acetilcolina (<i>Choline acetyltransferase</i>)	Cabra	Policlonal	Millipore (AB144)	1:250
Flotilina	Conill	Policlonal	Abcam (ab41927)	1:150
GFAP Proteïna acídica fibrilar glial (<i>Glial fibrillary acidic protein</i>)	Pollastre	Policlonal	Abcam (ab4674)	1:1000
Grp78 / BiP Proteïna 78 regulada per glucosa (<i>Glucose-regulated protein 78</i>)	Conill	Policlonal	Enzo Life Sciences (SPA-826)	1:1000
HA-tag Pèptid HA	Rata	Monoclonal	Roche (11 867 423 001)	1:500
Her4 / ErbB4	Conill	Monoclonal	Cell Signaling (#4795)	1:50
Iba1 Molècula adaptadora ionitzant d'unió a calci 1 (<i>Ionised calcium-Binding Adaptor molecule 1</i>)	Cabra	Policlonal	Abcam (ab5076)	1:500

Kv2.1 Canal de potassi dependent de voltagge Kv2.1 (<i>Kv2.1 voltage gated potassium channel</i>)	Ratolí	Monoclonal	NeuroMab (73-014)	1:100
M2 Receptor M2 muscarínic (<i>M2 muscarinic receptor</i>)	Conill	Policlonal	Alomone Labs (AMR-002)	1:100
Mac2 Mac2 / Galectina-3	Rata	Monoclonal	Cedarlane (CL8942AP)	1:800
mfSOD1 Superòxid Dismutasa 1 humana malplegada (<i>Misfolded Human SOD1</i>)	Conill	Policlonal	AbBcn (4251/4252) (AJ10)	1:1000
mfSOD1 Superòxid Dismutasa 1 humana malplegada (<i>Misfolded Human SOD1</i>)	Ratolí	Monoclonal	MediMabs 2B Scientific (MM-00070-2-P) (C4F6)	1:100
MLKL (phospho S345) Domini mixt de llinatge cinasa fosforilat en la serina 345 (<i>Mixed Lineage Kinase domain Like</i>)	Conill	Monoclonal	Abcam (196436)	1:100
Neu (C-18) (ErbB2)	Conill	Policlonal	Santa Cruz Biotechnology (Sc-284)	1:50
Neu/N	Ratolí	Monoclonal	Thermo Fisher Scientific (MAB377)	1:100
NRG1 1α /β 1/2 Neuregulina-1	Conill	Policlonal	Santa Cruz (sc-348)	1:300
NRG1 III extracel·lular Neuregulina-1 tipus III extracel·lular	Conill	Policlonal	Alomone Labs (ANR-113)	1:250
NRG1-CRD tipus III Domini Ric en Cisteïnes de la Neuregulina-1 tipus III (<i>Neuregulin-1 type III Cysteine Rich Domain</i>)	Ratolí	Monoclonal	Millipore (MABN534)	1:250
P2RY12	Rata	Monoclonal	Biolegend (848002)	1:100
PDC6IP-Àlix Proteïna interactuant de la mort cel·lular programada 6 (<i>Programmed Cell Death 6 Interacting Protein</i>)	Conill	Policlonal	Sigma-Aldrich (HPA011905)	1:50
p-ErbB2 tyr1248 Neu fosforilat en la tirosina 1248 (<i>phospho Neu tyr 1248; p-Neu tyr1248</i>)	Conill	Policlonal	Santa Cruz Biotechnology (Sc-293110)	1:100

p-ErbB4 Her4/ErbB4 fosforilat en la tirosina 1248 (phospho- Her4/ErbB4 tyr1248)	Conill	Monoclonal	Cell Signaling (#4757)	1:50
Rab10	Conill	Monoclonal	Abcam (ab237703)	1:500
Rab4	Conill	Monoclonal	Abcam (ab109009)	1:170
Rab5	Conill	Monoclonal	Abcam (ab218624)	1:1000
Rab7	Conill	Monoclonal	Abcam (ab137029)	1:100
Rab8A	Conill	Monoclonal	Abcam (188574)	1:500
Rab9	Ratolí	Monoclonal	Abcam (ab2810)	1:200
S1R Receptor Sigma-1 (Sigma-1 receptor)	Ratolí	Monoclonal	Santa Cruz Biotechnology (Sc-137075)	1:50
Serotonin	Rata monoclonal	Monoclonal	Chemicon (MAB 352)	1:100
Sinaptofisina 1	Conillet d'índies	Policlonal	Synaptic Systems (101 004)	1:500
SK3 Canal de potassi activat per calci SK3 (calcium-activated potassium channel SK3)	Conill	Policlonal	Alomone Labs (APC-025)	1:100
SMI-32	Ratolí	Monoclonal	Covance Research Products Inc. (SMI32)	1:5000
SV2 Glicoproteïna 2A de vesícules sinàptiques (Synaptic Vesicle glycoprotein 2A)	Ratolí	Monoclonal	Developmental Studies Hybridoma Bank (SV2)	1:1000
TMEM119 Proteïna Transmembrana 119	Conill	Policlonal	Abcam (ab209064)	1:300
VACHT Transportador vesicular d'acetilcolina (Vesicular Acetylcholine Transporter)	Conillet d'índies	Policlonal	Synaptic Systems (139 105)	1:500
VGAT Transportador vesicular de GABA (Vesicular GABA transporter)	Conillet d'índies	Policlonal	Synaptic Systems (131 004)	1:200
VGluT1 Transportador vesicular de glutamat 1 (Vesicular Glutamate transporter 1)	Conillet d'índies	Policlonal	Synaptic Systems (135 304)	1:500

VGluT2 Transportador vesicular de glutamat 2 (<i>Vesicular Glutamate transporter 2</i>)	Conillet d'índies	Policlonal	Synaptic Systems (135 404)	1:500
--	--------------------------	-------------------	-----------------------------------	--------------

En referència als anticossos contra la proteïna NRG1, la nostra experiència ens ha demostrat que el millor anticòs comercial disponible per visualitzar-la en els BC és el pan-NRG1 (sc-348, *Santa Cruz Biotechnology*). Degut a que aquest anticòs va ser descatalogat durant el transcurs de la tesi, vam haver de buscar alternatives. Només amb l'anticòs de conill anti-NRG1 tipus III extracel·lular (ANR113, *Alomone Labs*) hem estat capaços de detectar marcatge positiu en els BC, però aquesta senyal és menys intensa que la que s'obté amb el sc-348. L'anticòs monoclonal de ratolí anti-NRG-CRD tipus III (MABN534, *Millipore Sigma*) també és capaç de detectar tenuement la NRG1 associada als BC.

6. Microscòpia electrònica

En alguns casos concrets i en condicions específiques, alguns animals es van perfondre amb 2% PFA i 2% glutaraldehid en 0.1M PB (pH 7.4) per observar els teixits mitjançant microscòpia electrònica convencional. Alternativament i en condicions puntuals, la solució fixadora va ser 4% PFA en 0.1% de glutaraldehid en 0.1M PB per realitzar immunomarcatges ultraestructurals. Després de la fixació, els teixits es dissecaven ràpidament i es postfixaven 24h a 4°C en la mateixa solució de fixació.

Per la microscòpia electrònica convencional, les mostres es seccionaven a 200 µm de gruix utilitzant el vibratom. Els teixits es postfixaven en un 1% OsO₄ durant 2h, i després es contrastaven amb 0.5% d'acetat d'uranil durant 30 minuts, tot a 4°C. Posteriorment, les mostres s'inclouen en la reïna Epoxy Embed 812 (*Electron Microscopy Sciences, Hatfield, PA, Estats Units*), d'acord amb el protocol estàndard. Una vegada les mostres estaven incloses en la reïna, es feien els talls semi-fins (1 µm de gruix) i es tenyien amb blau de Richardson. En alguns articles, les imatges dels semi-fins es van realitzar utilitzant un microscopi convencional (*Olympus*) i una càmera digital DMX 1200 Nikon (*Tokyo, Japó*). Un cop localitzada la zona d'interès amb els semi-fins, es procedia a realitzar talls ultrafins (80 nm), els quals es contrastaven amb la solució de citrat de plom de Reynold's. Les observacions de les mostres es van fer amb un microscopi electrònic

Taula 2. Anticossos utilitzats per immunohistoquímica de fluorescència. JEOL JE;1010 (*Alkishima, Tokyo, Japó*).

Per fer l'immunomarcatge abans de la inclusió en la reïna, les mostres es seccionaven amb el vibratom a un gruix de 50 µm i es bloquejaven en una solució de 10% albúmina sèrica de boví (*Bovin Serum Albumin (BSA)*) i 0.02% saponina en PBS durant 1 hora. Després, es procedia amb la incubació amb un únic anticòs primari (Taula 3) en una solució formada per 10% BSA en PBS i 0.004% de saponina, durant 2 dies a 4°C. A continuació, les mostres es rentaven amb 1% BSA en PBS i s'incubaven durant 2 hores amb el corresponent anticòs secundari biotinilat (1:100, *Vector Laboratories*). Per visualitzar el marcatge, s'utilitzava el *Vectastain Elite ABC* (*Vector Laboratories*), i finalment es revelava mitjançant la incubació de les seccions en 0.05% de 3,3-diaminobenzidina/0.01% H₂O₂. En alguns casos, les regions reactives a la peroxidasa s'amplificaven amb plata mitjançant la incubació de les seccions en una solució de 2.6% d'hexametiletramina (*Merck, Darmstadt, Alemanya*), 0.2% de nitrat de plata (*Merck*) i 0.2% de tetraborat disòdic (*Merck*) durant 10 minuts a 60°C. Posteriorment, les seccions es rentaven amb aigua destil·lada i es tractaven amb 0.05% de clorit d'or durant 2 minuts. Finalment, les seccions es tornaven a rentar i s'incubaven 2 minuts en 2.5% de tiosulfat sòdic (*Merck*). El teixit es postfixava en 1% OsO₄ i s'incluïa en la reïna Embed 812.

Antigen	Espècie d'obtenció	Clonalitat	Casa comercial (nº de referència)	Dilució
Iba1	Cabra	Policlonal	Abcam (ab5076)	1:500

Taula 3. Anticossos utilitzats per l'immunomarcatge ultraestructural abans de la inclusió en la reïna.

Per la immunohistoquímica amb partícules d'or col·loïdal, aquesta es realitza després de la inclusió de les mostres en la reïna. Prèviament, les mostres es tallen a 200 µm utilitzant l'aparell *McIlwain Tissue Chopper* (*Campden Instruments LTD, Loughborough, Leics, Anglaterra*). Després de la crioprotecció amb glicerol, les mostres es submergeixen ràpidament en propà líquid refredat utilitzant nitrogen líquid (-184°C) i es processa per realitzar una criosubstitució utilitzant el sistema Leica EM System (*Leica Microsystems, Wetzlar, Alemanya*). Les mostres s'incrosten en la reïna Lowicryl HM20 (*Electron Microscopy Sciences*) mantenint la baixa temperatura i seguint un protocol similar al descrit en altres estudis (Rubio & Wentholt, 1999). Els talls ultrafins es realitzen en un Ultracut UC6 ultramicròtom (*Leica*) i es dipositen en reixes de níquel. A continuació es renten amb 50mM de glicina en PBS, es bloquegen en 5 i 1% de BSA, i s'incuben a temperatura ambient durant 1h amb els anticossos primaris seleccionats (Taula 4). Aquesta tècnica permet utilitzar un únic anticòs o una barreja de dos anticossos. En aquest últim cas, s'incuben els teixits amb partícules d'or col·loïdal de dos mides diferents per després poder distingir els marcatges de les proteïnes en les imatges.

Antigen	Espècie d'obtenció	Clonalitat	Casa comercial (nº de referència)	Dilució
MLKL (phospho S345)	Conill	Monoclonal	Abcam (196436)	1:100
NRG1	Conill	Policlonal	Santa Cruz (sc-348)	1:300
S1R	Ratolí	Monoclonal	Santa Cruz Biotechnology (Sc-137075)	1:50
Kv2.1	Ratolí	Monoclonal	NeuroMab (73-014)	1:100

Taula 4. Anticossos utilitzats per l'immunomarcatge ultraestructural després de la inclusió en la reïna.

Després de rentar les seccions amb 0.25% Tween 20 en PBS, es bloquegen amb 1% BSA i s'incuben amb els anticossos secundaris conjugats a partícules d'or de 12 nm (1:30, *Sigma-Aldrich, St. Louis, MO, Estats Units*) i/o partícules de 5 nm (1:30; *Sigma-Aldrich*) durant 30 minuts a temperatura ambient. Previ rentat en PBS i aigua destil·lada, les seccions es contrasten amb acetat d'urani i citrat de plom. En paral·lel, es van processar mostres controls en les quals es va ometre la incubació amb l'anticòs primari. Les observacions també es van dur a terme amb un microscopi de transmissió electrònica JEOL JE1010 (*Akishima, Tokyo, Japó*).

En alguns casos, per facilitar la localització dels BC de les MNs en les crioseccions ultrafines, s'utilitzava el nucli hipoglòs del tronc de l'encèfal en lloc de la medul·la espinal, ja que en aquest nucli hi ha més densitat de MNs.

7. Cultius de medul·la espinal

Es preparaven cultius primaris provinents de la dissociació de la medul·la espinal d'embrions de ratolí CD1 (dia embrionari 13) tal com es descriu en protocols anteriors (Roy *et al.*, 1998) amb lleugeres modificacions. Les medul·les espinals es dissecaven i es netejaven de meninges i ganglis. Les cèl·lules dissociades es plantaven a una densitat de 300.000 cèl·lules/pou en plaques de cultiu de 4 poues les quals contenien cobreobjectes rodons de vidre tractats amb poli-D-lisina i Matrigel (*Corning, Bedford, MA, Estats Units*). Les cèl·lules es mantenien en un medi essencial mínim (*Gibco, Waltham, Estats Units*) enriquit amb 5 g/l de glucosa i suplementat amb un 3% de NHS, 10 ng/ml de factor de creixement neural (*Nerve Growth Factor (NGF)*), 0.5-1% de penicil·lina i estreptomicina (*Sigma-Aldrich, #P4458*) i medi B27 (*Gibco*). Al dia 6, els cultius es tractaven amb 1.4 µg/ml de citosina-β-arabinosa (*Sigma-Aldrich*) per tal de minimitzar el creixement de les cèl·lules no neuronals. Els cultius es mantenien durant 14-28 dies *in vitro* i després es rentaven amb PBS, es fixaven amb 4% PFA en 0.1

M de PB (pH 7.4) durant 1 hora, i es procedia a realitzar una immunohistoquímica de fluorescència seguint el protocol descrit anteriorment.

8. *Slices in vitro*

Els animals es van perfondre transcardíacament amb líquid cefalorraquídi artificial (*artificial cerebrospinal fluid (ACSF)*) fred oxigenat (95% O₂, 5% CO₂), per després extreure'n la medul·la espinal hidràulicament aplicant pressió amb una xeringa amb ACSF. La xeringa es situava a l'obertura de la regió caudal del canal vertebral tal com es descriu en (Chéry *et al.*, 2000).

Un cop s'obtenia la medul·la, els segments medul·lars lumbars s'aïllaven i es seccionaven ràpidament en talls transversals de 300-400 µm amb el *Tissue Chopper*. A continuació, la medul·la espinal lumbar neta de meninges i en fred (0-4°C), es submergia en ACSF oxigenat (95% O₂, 5% CO₂) el qual contenia 130 mM NaCl, 26 mM NaHCO₃, 2 mM MgCl₂, 1.25 mM NaPO₄, 2 mM CaCl₂, 3 mM KCl i 10 mM de glucosa. Posteriorment els talls es transferien (o no) a una càmera de perfusió amb ACSF oxigenat durant 10 minuts abans de la fixació amb 4% PFA.

Després, es processaven les mostres per *squash* per tal de realitzar-hi immunohistoquímiques de fluorescència contra diferents proteïnes.

9. *Western Blot*

Per a realitzar la tècnica del *Western Blot* (WB), la medul·la espinal dels animals s'estreia hidràulicament aplicant pressió amb una xeringa omplerta amb PBS situada a l'obertura de la regió caudal del canal vertebral tal com es descriu en (Chéry *et al.*, 2000). Immediatament després de l'extracció, el teixit es sotmetia a una congelació ràpida amb nitrogen líquid (-196°C) per tal d'aconseguir una òptima preservació de les proteïnes i, després, es guardava a -80°C.

Es disagregaven en fred 5-6 mg de teixit congelat procedent de la medul·la espinal lumbar utilitzant un homogenitzador elèctric (*Tissue Grinder*, Coyote Bioscience Co., Ltd, Yixing City, Xina) utilitzant 150 µl del tampó de lisis de radioimmunoprecipitació (*Radioimmunoprecipitation assay buffer (RIPA)*) (150 mM NaCl; 1 % NP-40; 0.5% Na-deoxycolat; 0.1% dodecilsulfat sòdic (*Sodium dodecyl sulfate (SDS)*)); 50 mM Tris-HCl [pH 7.4]), supplementat amb inhibidors de proteases (*Sigma-Aldrich*, cat. #P8340) i inhibidors de fosfatases (*PhosphoSTOP*, Roche, Laval, QC, Canadà). Els homogenats es centrifugaven a 12.000 rpm durant 15 minuts a 4°C. A continuació, s'obtenia el sobredendant i se'n determinava la

concentració de proteïna obtinguda mitjançant el kit BIO-RAD Micro DC *protein assay* (BIO-RAD, Laboratories Inc., Hercules, CA, Estats Units). La quantitat concreta de proteïna que es necessitava, normalment entre 15-50 µg, es barrejava amb el tampó de càrrega 4 x SDS (0.250 M Tris, 8% SDS, 40% glicerol, 0.4% blau de bromofenol, 20% β-mercaptoetanol) i es carregava en un gel de poliacrilamida al 10% (el percentatge variava en funció del pes molecular de la proteïna d'interès) per dur a terme l'electroforesi.

Les proteïnes s'electrotransferien del gel a una membrana de PVDF (Immobilon TM-P, Millipore, Burlington, MA, USA) utilitzant el tampó de transferència el qual contenia 48 mM Tris, 39 mM glicina, 20% metanol i 0.04% SDS. A continuació, les membranes es bloquejaven amb 5% llet desnatada en 0.1% *Tween* 20 i tampó Tris salí (TBST) pH 8 durant 1 h a temperatura ambient i, després, es rentaven abundantment amb TBST.

La immunodetecció es duia a terme mitjançant la incubació de les membranes tota la nit a 4°C amb l'anticòs d'interès (Taula 5).

Les membranes es rentaven en TBST i s'incubaven durant 1 h a temperatura ambient amb l'anticòs secundari conjugat a peroxidasa (1:15000; *Cell Signaling*, Danvers, MA, Estats Units; cat. #7074; cat. #7076), es rentaven en TBST i es visualitzaven utilitzant el revelador *ECL Prime Western Blotting Detection Reagent Detection Kit* (GE Healthcare, Buckinghamshire, Anglaterra), seguint les instruccions del fabricant.

Es tornava a repetir la immunodetecció en la mateixa membrana, aquesta vegada incubant les membranes amb un segon anticòs primari, normalment, contra la proteïna *β-actina* de conill o de ratolí en funció de quin fos el més apropiat, amb l'objectiu de tenir un control de càrrega amb el que normalitzar els resultats.

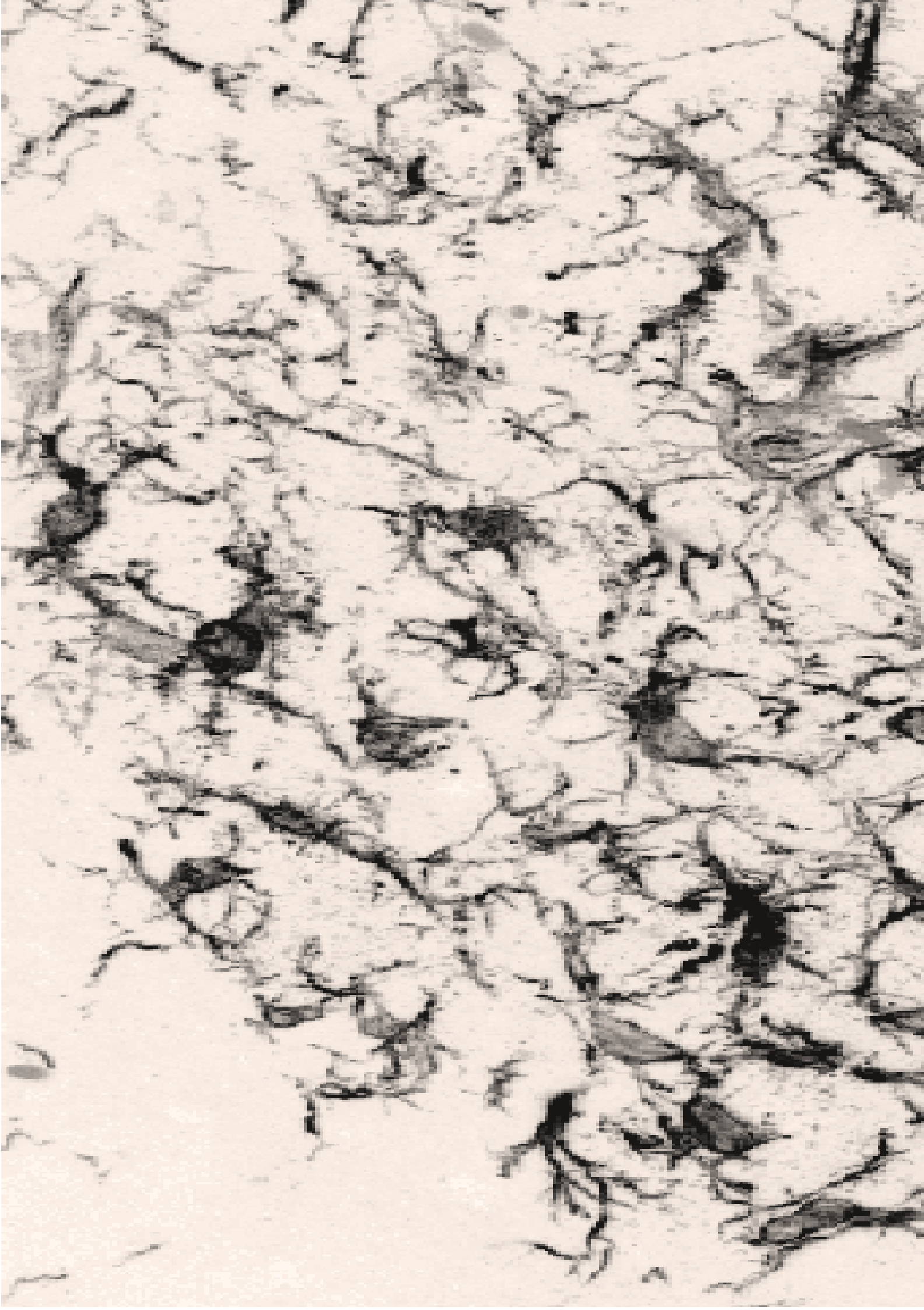
Finalment, la quantificació de la intensitat de les bandes es realitzava utilitzant el programa *Chemidoc MP Imaging System* (BIO-RAD Laboratories Inc., Hercules, CA, Estats Units).

Antigen	Espècie d'obtenció	Clonalitat	Casa comercial (nº de referència)	Dilució
MLKL (phospho S345)	Conill	Monoclonal	Abcam (196436)	1:2500
Mac2	Rata	Monoclonal	Cedarlane (CL8942AP)	1:800

Taula 5. Anticossos utilitzats per WB.

10. Anàlisi estadístic

Les dades estan expressades com a mitjana \pm SEM. Pel que fa als anàlisis estadístics, quan es comparava dos valors, s'escollia el test *Student's t-test*; quan es comparaven varíes dades, es realitzava 1- o 2-way analysis of variance (ANOVA) seguit de la correcció de *post hoc* Bonferroni. El nivell de significança es va establir a $p < 0.05$. Tant per dur a terme els anàlisis estadístics com la representació gràfica de les dades, s'ha utilitzat el programa GraphPad Prism 6.



RESULTATS

Article I**Neuregulin 1-ErbB module in C-bouton synapses on somatic motor neurons:
molecular compartmentation and response to peripheral nerve injury**

**Anna Casanovas, Sara Salvany, Víctor Lahoz, Olga Tarabal, Lídia Piedrafita, Raimundo
Sabater, Sara Hernández, Jordi Calderó i Josep E. Esquerda**

Scientific Reports

(2017) Jan 9, 7(1), 40155; Q1, IF: 4.122

SCIENTIFIC REPORTS



OPEN

Neuregulin 1-ErbB module in C-bouton synapses on somatic motor neurons: molecular compartmentation and response to peripheral nerve injury

Received: 07 September 2016

Accepted: 02 December 2016

Published: 09 January 2017

Anna Casanovas, Sara Salvany, Víctor Lahoz, Olga Tarabal, Lídia Piedrafita,
Raimundo Sabater, Sara Hernández, Jordi Calderó & Josep E. Esquerda

The electric activity of lower motor neurons (MNs) appears to play a role in determining cell-vulnerability in MN diseases. MN excitability is modulated by cholinergic inputs through C-type synaptic boutons, which display an endoplasmic reticulum-related subsurface cistern (SSC) adjacent to the postsynaptic membrane. Besides cholinergic molecules, a constellation of proteins involved in different signal-transduction pathways are clustered at C-type synaptic sites (M2 muscarinic receptors, Kv2.1 potassium channels, Ca^{2+} activated K^+ [SK] channels, and sigma-1 receptors [S1R]), but their collective functional significance so far remains unknown. We have previously suggested that neuregulin-1 (NRG1)/ErbBs-based retrograde signalling occurs at this synapse. To better understand signalling through C-boutons, we performed an analysis of the distribution of C-bouton-associated signalling proteins. We show that within SSC, S1R, Kv2.1 and NRG1 are clustered in highly specific, non-overlapping, microdomains, whereas ErbB2 and ErbB4 are present in the adjacent presynaptic compartment. This organization may define highly ordered and spatially restricted sites for different signal-transduction pathways. SSC associated proteins are disrupted in axotomised MNs together with the activation of microglia, which display a positive chemotaxis to C-bouton sites. This indicates that C-bouton associated molecules are also involved in neuroinflammatory signalling in diseased MNs, emerging as new potential therapeutic targets.

Skeletal muscle contractions mediating motor behaviour involves the coordinated activity of distinct brain stem and spinal cord motor neuron (MN) populations. The firing rates of individual MNs results from the integration of a variety of excitatory and inhibitory MN synaptic inputs, which involve a range of different neurotransmitter systems. During rhythmic motor behaviour (e.g. locomotion), the highly organized pattern of MN activity is modulated by cholinergic inputs¹. These are delivered through C-type synaptic boutons originating from spinal interneurons. C-boutons are intriguing synaptic structures that are present in α - (but not in γ -) MNs, and that were first morphologically identified over 45 years ago². C-boutons are unusually large nerve terminals (3–5 μm long) which contain a high number of densely packed, round clear synaptic vesicles. In the postsynaptic region, C-terminals display a unique structure, consisting of a subsurface cistern (SSC) immediately adjacent (at 10–20 nm distance) to the MN membrane, and associated with a stack of underlying lamellae of endoplasmic reticulum (ER). There has recently been increased interest in C-boutons. After recognizing the cholinergic phenotype of C-boutons and their association with M2 muscarinic receptors^{3,4}, other molecular aspects of these synapses, such as the expression of: voltage-gated K^+ channels Kv2.1⁵, Ca^{2+} activated K^+ (SK) channels⁶, vesicle-associated membrane protein 2 (VAMP-2)³ and sigma-1 receptors (S1Rs)⁷, have been described. The gap junction protein connexin 32 has also been localized postsynaptically at the SSC^{8,9}. The neuronal origin of C-bouton inputs was recently identified as a small cluster of cholinergic interneurons (VOc interneurons)

Departament de Medicina Experimental, Patologia Neuromuscular Experimental, Facultat de Medicina, Universitat de Lleida/IRBLLEIDA, Av. Rovira Roura 80, 25198 Lleida, Catalonia, Spain. Correspondence and requests for materials should be addressed to J.E.E. (email: josep.esquerda@mex.udl.cat)

www.nature.com/scientificreports/

located near the central canal of the spinal cord, which modulate MN activity during locomotor behaviour^{1,10}. Metabotropic M2 transmission in C-type synapses may inhibit Ca^{2+} dependent K^+ channels, reducing the spike afterhyperpolarization, instead of after hyperpolarization and enhancing MN firing frequency through a local intermediary effect of $[\text{Ca}^{2+}]_{\text{in}}$ ^{1,10}.

The neuregulin-1 (NRG1) family includes more than 15 membrane-associated and secreted growth factors generated by alternative RNA splicing that interact with ErbB receptor tyrosine kinases. All NRG1 isoforms share an epidermal growth factor (EGF)-like signalling domain, and control many aspects of development. In the nervous system, the most abundant forms of NRG1 are types I and III. These, have been detected in MNs, dorsal root ganglion (DRG) neurons and, in particular in glia. NRG1 is involved in glia-axon interactions (myelination), the development of motor endplates, neuronal migration, synaptogenesis and plasticity in the CNS^{11–14}. NRG1 is also involved in psychiatric disorders, including schizophrenia^{15,16}. In a study examining the expression of NRG1 in phrenic spinal cord MNs, it was reported that this trophic protein is expressed in nearly all cholinergic nerve terminals¹⁷; however, its precise subcellular localization was not addressed by these investigators. We have recently examined this issue and found that NRG1 is associated with C-boutons, concentrated in postsynaptic sites within the ER at the SSC¹⁸. We have also demonstrated that ErbB2 and ErbB4 receptors are present in the presynaptic compartment, suggesting that NRG1 acts as a retrograde signalling molecule in C-type synapses. C-boutons are scarcely investigated structures¹⁹, which have been reported to suffer plastic changes in sick MNs after spinal cord injury^{20,21}, peripheral nerve lesion²², and amyotrophic lateral sclerosis (ALS)^{18,23–29}. In addition, mutations in S1R are considered risk factors for familial ALS, and abnormal accumulations of this protein in C-terminals have also been observed in patients with sporadic ALS^{30–32}. Altered SSCs also appear to be present in ALS-linked mutations of vesicle-associated membrane protein-associated protein B (VAPB, ALS8), which is abnormally targeted to C boutons³³.

The relevance of the NRG1/ErbB pathway in MN diseases has been further underlined by the discovery of a new type of familial ALS caused by a loss of function mutation of ErbB4³⁴, and by the reported neuroprotective effects of NRG1 supplementation³⁵ and/or altered NRG1 expression³⁶ in ALS mice. MNs in oculomotor nuclei, which are spared in ALS, lack both C-boutons and SSC-associated NRG1^{4,18}.

Thus, at C-type synaptic sites, in addition to the presence of cholinergic molecules, a constellation of proteins involved in different signal-transduction pathways are specifically clustered, although their functional significance remains largely unknown. In order to better understand synaptic signalling through C-boutons, we undertook a structural analysis of the spatial organization of distinct C-bouton-associated signalling proteins, and especially the NRG1-ErbBs module, in different MN populations. We also examined changes in NRG1-ErbB expression during development and following peripheral nerve injury.

Results

Ultrastructure of C-bouton synapse in mouse spinal cord MNs. C-boutons can be morphologically distinguished from other afferent synaptic terminals contacting MN soma or dendrites in the spinal cord ventral horn. The C-bouton presynaptic element contains spherical and electron lucent synaptic vesicles, some endosome-like bodies and mitochondria. In the postsynaptic compartment, and in close apposition with the postsynaptic membrane, the ER-related SSC is the main structural hallmark of C-boutons. The distance between the SSC and postsynaptic membrane is about 10–15 nm. C-boutons with large SSCs were also observed in MNs of newborn (P1) animals (Supplementary Fig. 1a–d). Our observations are consistent with the classical description of C-boutons in cat spinal cord².

The NRG1-ErbB module is found in C-boutons and is differentially compartmentalised with other signalling proteins. Using several specific antibodies we analysed the precise distribution of several proteins that are known to be clustered at the C-type synapse. C-bouton sites were identified by labelling presynaptic terminals with vesicular acetylcholine transporter (VACHT, Figs 1 and 2). In close association with VACHT-positive spots, we confirmed the presence of NRG1, M2-type muscarinic acetylcholine receptors (M2 AChRs), S1Rs, the Kv2.1 delayed rectifier K^+ channel (Kv2.1), and the postsynaptic SK channel SK3. All of these were present in oval patches distributed throughout the soma and in proximal dendrites of large spinal cord MNs, representing the postsynaptic compartment of C-bouton (Fig. 1a–d). In agreement with our previous work¹⁸, non-cholinergic (i.e. glutamatergic, serotonergic and GABAergic) afferent synapses on MNs did not express the particular assembly of postsynaptic molecules seen in cholinergic terminals (not shown). In addition, ultrastructural immunolabelling (Fig. 1e,f) followed by the stereological analysis³⁷ of gold nanoparticles distribution confirmed that, within C-bouton, NRG1 was accumulated postsynaptically in the SSC (for total Chi-square = 19,337.8 and df = 4, $p < 0.0001$, there is a preferential labelling in SSC, n = 20 C-bouton synapses; see Fig. 1f).

C-bouton-associated protein molecules were assembled in a highly ordered manner and segregated into specific microdomains. This was clearly shown after confocal imaging of multi-labelled C-boutons using the highest resolution settings. Our results complement those reported by Deardorff *et al.*¹⁹. Postsynaptic sites enriched in M2 cholinergic receptors were precisely aligned with the strongest signal for VACHT, indicating the areas with the maximum concentration of cholinergic vesicles at the presynaptic terminal (Fig. 2a–f). The areas most enriched in NRG1 were intercalated with microdomains displaying the maximal intensity for Kv2.1 or S1R immunolabelling (Fig. 2g–p). In orthogonal projections of C-boutons, the S1R signal was usually detected in the form of a central saccule-like structure surrounded by smaller NRG1-containing spots (Fig. 2g–i). In addition, in some MNs, Kv2.1 immunoreactivity formed an additional bell-like line, externally surrounding the whole C-bouton area (Fig. 2q–s). This is in agreement with observations made in hippocampal neurons^{38,39}. The segregated localization of NRG1 and Kv2.1 in C-type synapses was further assessed after double immunolabelling. This analysis suggested that Kv2.1 subunits were located both in the postsynaptic membrane and in the SSC, although they

www.nature.com/scientificreports/

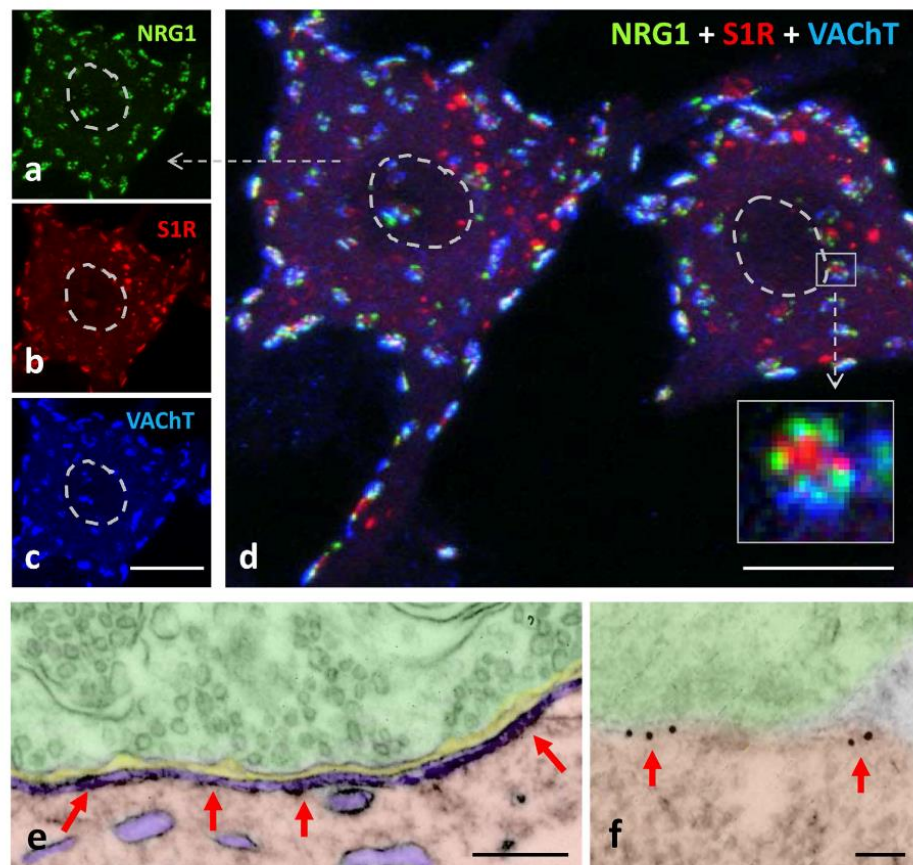


Figure 1. NRG1 protein is associated with the C-bouton proteins VACHT and S1R, and localized in SSC at postsynaptic region. (a–d) Squashed MNs triple immunolabelled for NRG1 (green), S1R (red) and VACHT (blue). The three molecules colocalise at C-boutons, but S1R is also present as non-synaptically-associated particles. The nuclei are delimited by a dashed line. Individual RGB channels of the indicated MN (arrow) are shown in (a–c). When individual C-boutons are observed at high magnification (square delimited in (d)), sites containing S1R are segregated from NRG1-positive patches, and delimited by presynaptic VACHT. (e and f) NRG1 accumulates in the SSC (arrows) as shown in spinal cord MNs after ultrastructural immunolabelling by a pre-embedding (e) or post-embedding (f) procedure. Scale bars: in (c) = 10 μm; (d) = 20 μm; in (e) = 250 nm; in (f) = 50 nm.

were clustered in separate domains than NRG1 (Fig. 2p). SK3 channel protein was also clustered in C-boutons from some, but not all, MNs; these, probably correspond to MNs innervating slow-twitch muscles⁶. In our samples, SK3 and Kv2.1 potassium channels appear to be localized in separate domains (Fig. 2t–y). All these results indicate that the postsynaptic machinery at C-boutons contains a unique mosaic of proteins that are spatially arranged in highly ordered, interdigitated, non-overlapping, microclusters. Using double immunogold labelling, the regions within the SSC enriched in NRG1 and S1R were clearly segregated; most of the particles were located at the SSC membrane. A minor proportion (9.7 ± 2.59%, n = 14 synapses) of nanogold particles were seen associated with the postsynaptic membrane, suggesting that NRG1 may have been translocated from the SSC to the postsynaptic membrane (Fig. 3a–c). Double immunogold labelling was also applied to identify NRG1 in conjunction with Kv2.1; results confirmed that both proteins reside postsynaptically in separate regions, with Kv2.1 located at the periphery of clustered NRG1 (Fig. 3d). These data extend previous observations on the ultrastructural localization of Kv2.1 channels^{5,38}. To improve C-bouton sampling in ultrathin cryosections, all these double labelling experiments were performed in hypoglossal MNs, as these are more densely packed than ventral horn MNs. We have already described that both morphological and immunocytochemical properties of C-boutons in hypoglossal MNs are virtually identical to those in spinal cord¹⁸.

By using several anti-ErbB2 or ErbB4 antibodies, positive immunolabelling in the presynaptic compartment of C-boutons was unambiguously observed in contrast to the postsynaptic localisation of NRG1 (Fig. 4a–c). Although this immunoreaction was sometimes faint and imprecise, it became more prominent when

www.nature.com/scientificreports/

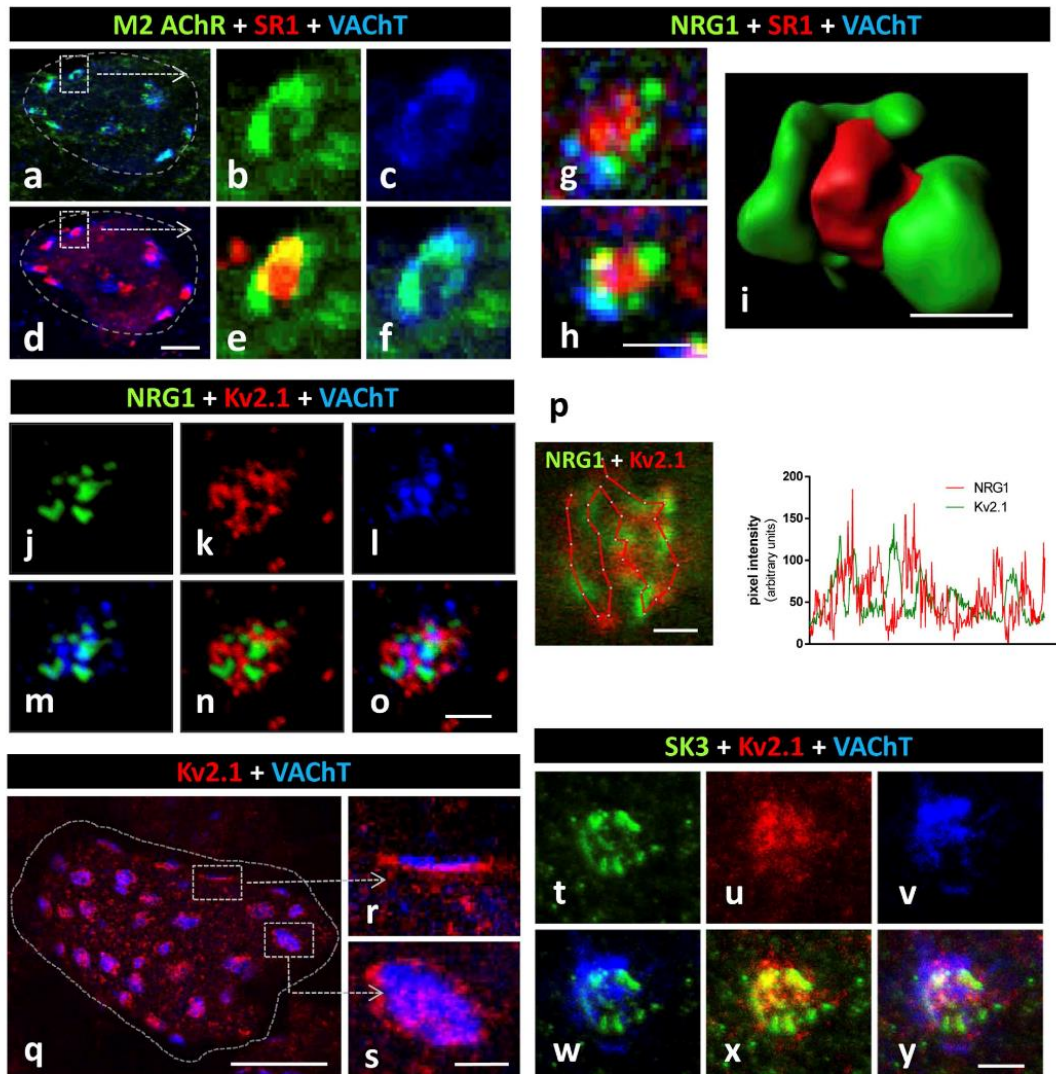


Figure 2. C-bouton proteins NRG1, S1R, Kv2.1 and SK3 are differentially clustered at the postsynaptic region. (a–f) MN somata (encircled in (a) and (d)) showing C-bouton synapses immunostained for simultaneous visualisation of M2 AChR (green), SR1 (red) and VACHT (blue); an enlargement of the square delimited C-bouton is shown in (b,c,e,f) in either separate or combined channels; note the similar distribution of the M2 AChR and VACHT sites; this contrasts with the differential localisation of M2 AChR and SR1; two channel merged images are shown in (a,d,e and f). (g,h) Sites containing S1R locate in a central region surrounded by NRG1-positive patches, separately delimited from presynaptic VACHT. (h) Volume rendering of a C-bouton site showing the differential distribution of NRG1 (green) and S1R (red) is depicted. (j–o) Clusters of NRG1 (green) and Kv2.1 (red) display a complementary distribution within the VACHT-positive (blue) C-bouton; two and three channel merged images are shown in (m,n) and (o), respectively. (p) A detail of a C-bouton, double labelled for NRG1 (green) and Kv2.1 (red), is subjected to pixel profile analysis along the depicted line; note the absence of colocalisation between the two interdigitating signals. (q–s) Surface of squashed MN cell body (delimited by a dotted line) displaying the distribution of clustered Kv2.1 (red) potassium channels in VACHT-immunolabelled C-boutons (blue) (q); the lateral and orthogonal projections of enlarged C-boutons are shown in (r) and (s), respectively; the postsynaptic localisation of Kv2.1 channels is shown in front of a VACHT-positive terminal in (r); the belt like arrangement of Kv2.1 potassium channels around the VACHT-labelled C-bouton can be seen in (s). (t–y) A triple immunolabelled C-bouton showing the differential distribution of SK3 Ca^{2+} -dependent K^+ (green) with respect to Kv2.1 K^+ (red) channels in a VACHT-delimited (blue) synaptic region; two and three channel merged images are shown in (w,x), and (y) respectively. Scale bars: in (d)=10 μm (also applicable to (a)); in (h) (valid for (g)), (i), (o), (p), (s) (valid for (r)) and (y)=1 μm ; in (q)=20 μm .

www.nature.com/scientificreports/

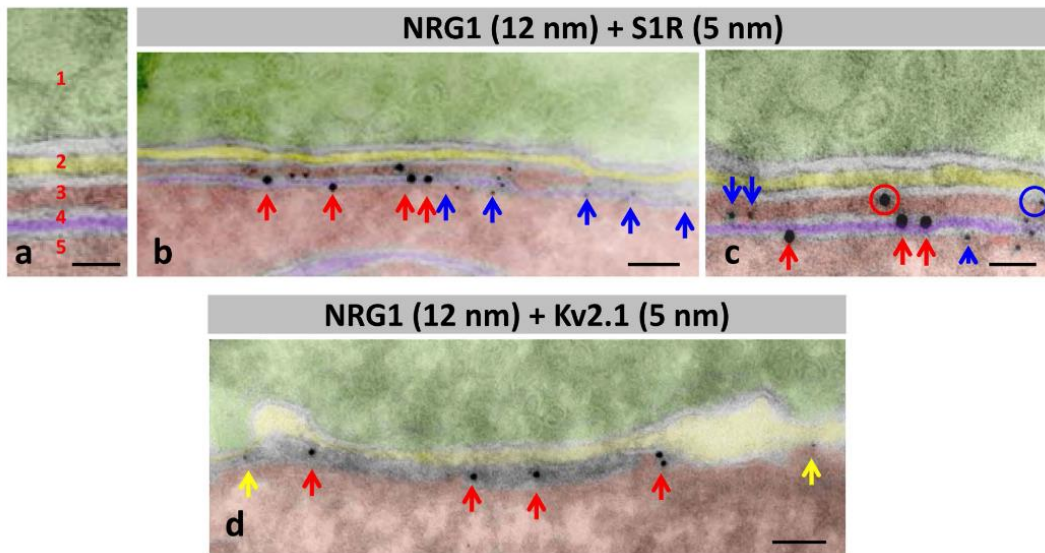


Figure 3. Immunolabelling using nanogold particles of ultrathin cryosection for the ultrastructural localisation of NRG1, S1R and Kv2.1 channels at C-boutons. To facilitate the localisation of C-boutons, the analysis was performed in hypoglossal MNs. A detail of the organization of compartments at C-bouton synapses in negatively stained cryosections is depicted in (a) 1 = presynaptic (green), 2 = intersynaptic extracellular space (yellow), 3 = postsynaptic cytoplasmic compartment lodged between postsynaptic membrane and subsynaptic cistern (SSC, red), 4 = SSC (violet), and 5 = MN cytoplasm (red). The same colour code is used in (b–d). (b,c) Double immunolabelling for NRG1 and S1R; NRG1 (red arrows) is mainly associated with SSC forming a cluster segregated from S1R (blue arrows). (c) A minor proportion of gold particles (encircled) are located at the postsynaptic membrane. (d) nanogold particles labelling Kv2.1 are located on the periphery (yellow arrows) of C-bouton enriched with a NRG1 cluster (red arrows). Scale bar: in (a,c) = 25 nm; in (b,d) = 50 nm.

phosphospecific antibodies were used and, in particular, after performing tyramide signal amplification (TSA) (Fig. 4d–f, and Supplementary Fig. 2). The immunostaining obtained with the anti-phosphorylated ErbB2 or ErbB4 antibodies overlapped the presynaptic VACHT positivity in most, although not all, C-boutons (Fig. 4d). However, unphosphorylated ErbB2 and ErbB3 were not detected in association with VACHT-positive puncta. The plot profile and co-localization analysis showed a high degree of coincidence between phospho-ErbB2 and VACHT signals (Pearson's $R = 0.72$, Fig. 4i,j). By contrast, the same analysis confined NRG1 to the postsynaptic compartment, and as being clearly distinct from the VACHT signal (Pearson's $R = 0.33$, Fig. 4g,h). The intensity of ErbB immunoreactivity varied among the individual cholinergic terminals, ranging from negative or very weak to intense. In addition to the synaptic immunolabelling, ErbB2 and ErbB4 were also detected in MN cell bodies and neuropil, particularly when TSA was used. The association between either NRG1 or p-ErbB2 with VACHT immunolabelled C-boutons can be further appreciated after volume rendering imaging (Fig. 4k,l).

This overall spatial distribution of C-bouton-associated proteins is depicted in Fig. 5(a,b), based on a model that we proposed after examining 3D reconstructions of multi-labelled C-bouton synapses.

The total number of C-boutons per MN soma was calculated from 3D reconstructed squash preparations of thick ($200\text{ }\mu\text{m}$) spinal cord slices from adult mice. After analysing 14 MNs, we found an average of 3.11 ± 0.30 ($100\text{ }\mu\text{m}^2$ of MN soma surface; C-type synapses were visualized by VACHT immunostaining). Similar numbers were found after evaluating clustered NRG1-positive particles ($3.60 \pm 0.29/100\text{ }\mu\text{m}^2$ of MN soma surface) and synaptically-associated S1R-positive spots ($2.92 \pm 0.28/100\text{ }\mu\text{m}^2$). The average size of the synaptic area containing the distinct C-bouton markers was as follows: VACHT = 6.87 ± 0.25 , $n = 184$; NRG1 = 5.41 ± 0.20 , $n = 203$; S1R = 4.30 ± 0.20 , $n = 153$ (all in μm^2 ; with n corresponding to the number of C-bouton examined). We further determined whether these morphometric parameters differed when the analysis was specifically performed in MN subtypes innervating fast or slow muscles. MN pools were identified after retrograde tracing by injecting fluorescent cholera toxin B into either tibialis anterior (TA) or soleus muscles (Supplementary Fig. 3). The results indicated that NRG1-positive puncta were more abundant, although smaller, in fast type TA-innervating MNs than in slow type MNs contacting the soleus muscle.

Development of C-bouton-associated NRG1. Developmental changes in C-bouton associated proteins such, as Kv2.1 and M2 AChRs occur postnatally, together with the functional maturation of the motor system⁴⁰. We analysed the developmental expression of NRG1 in the spinal cord in relation to the other C-bouton associated molecules, such as VACHT and S1R (Fig. 6a–f). Small ($< 1\text{ }\mu\text{m}^2$), but abundant, NRG1 positive discrete puncta were detected prenatally at E18 (Fig. 6c,d). Many of these particles did not show any association with

www.nature.com/scientificreports/

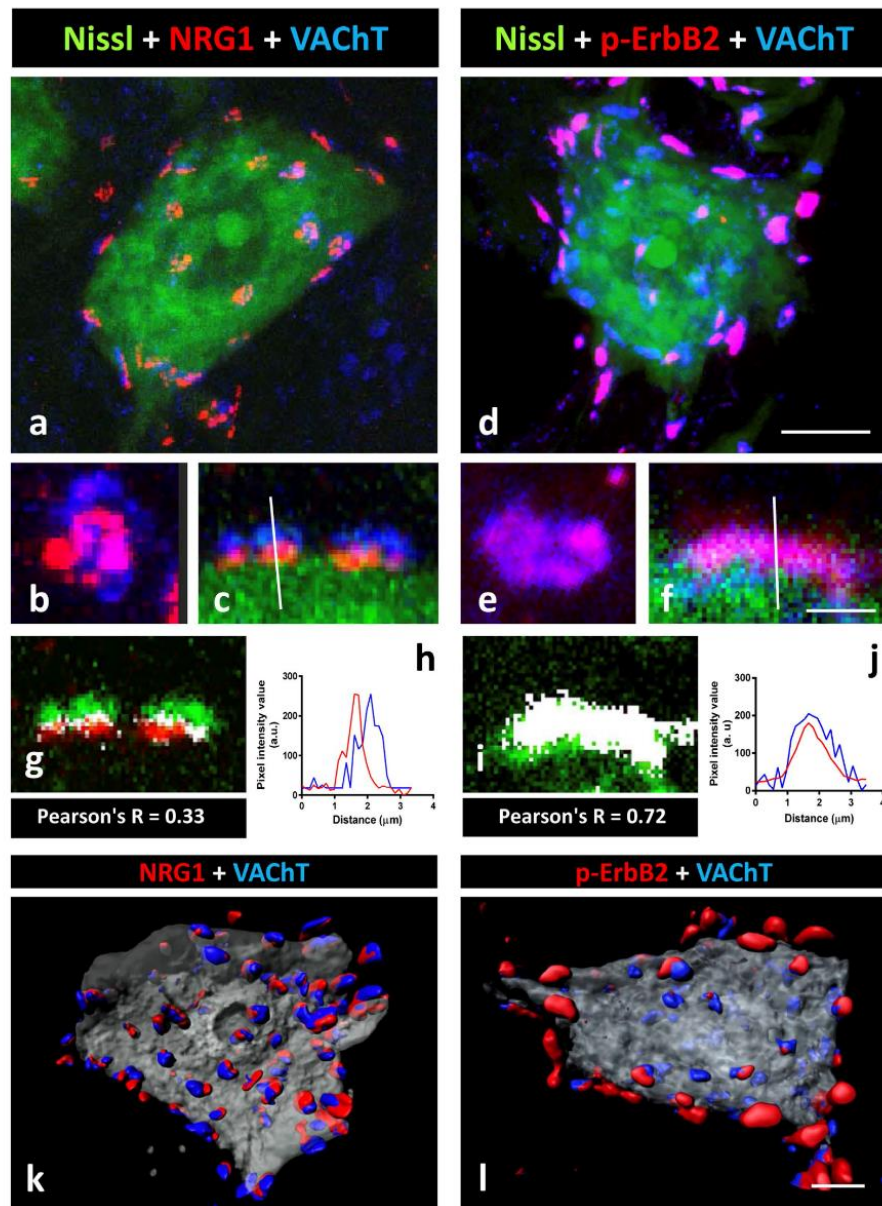


Figure 4. C-bouton type synapses contain the NRG1/ErbB signalling module. (a,b,c) NRG1 (red) is concentrated at the C-bouton postsynaptic site adjacent to VACHT (blue) positive cholinergic terminals. (d,e,f) show that p-ErbB2 (red) is present in the presynaptic site of many, but not all, cholinergic terminals labelled with VACHT antibody (blue). In (a,c,d,f) MN somata are visualised with fluorescent Nissl staining (green). In (b) and (c), orthogonal and lateral projections, respectively, of a C-bouton immunolabelled for NRG1 and VACHT are shown; the dissociation of the two signals is evidenced after colocalisation (g) and pixel profile analysis (i). In (e) and (f) orthogonal and lateral projections, respectively, of a C-bouton immunolabelled for p-ErbB2 and VACHT are also shown; the overlapping of two signals is evidenced after a colocalisation (h) and pixel profile analysis (j). Colocalised pixels are displayed in white in (g) and (i); the low numbers of white pixels in (g) corresponds to the boundary between pre- and post-synaptic compartments, which are overlapped due to mechanical folding and compression inherent to tissue processing. (k,l) represents the volume rendering of serial optical sections (0.5- μm thick) from a MN showing the distribution of NRG1 (red in (k)) and p-ErbB2 (red in (l)), and VACHT (blue) co-labelled C-boutons. Scale bars: in (d) = 10 μm (also applicable to (a)); in (f) = 3 μm (also applicable to (b, c, e)); in (l) = 5 μm (valid for (k)).

www.nature.com/scientificreports/

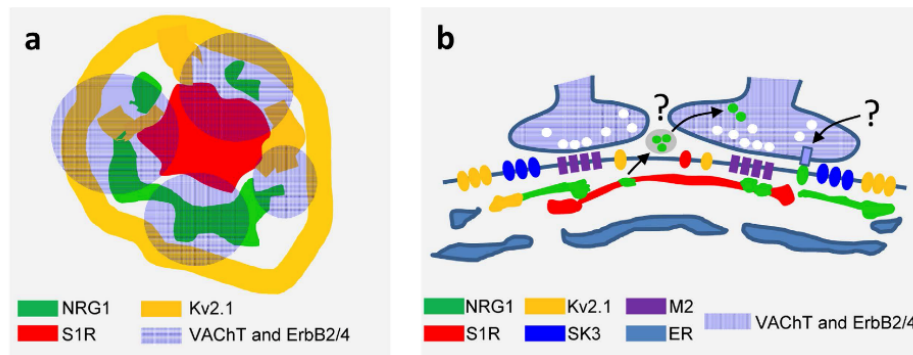


Figure 5. Model showing the possible distribution of some proteins specifically concentrated at C-type synapses. The synapse is displayed in orthogonal (a) and lateral (b) views. The different sub-compartments in which proteins accumulate are depicted according to the indicated colour code. Since the mechanism by which postsynaptic NRG1 and presynaptic ErbBs interact is unknown, two possible routes are indicated with question marks: one mediated by exosomes, and the other involving a juxtarcline interaction.

VACHT-positive presynaptic terminals. In addition, at this stage, large patches of NRG1 ($>3\mu\text{m}^2$) were often seen adjacent to the MN surface, although they were not related to VACHT-labelled nerve terminals. These NRG1 clusters, underwent a conspicuous remodelling becoming virtually absent from P1 onwards (Fig. 6c,e). During the postnatal period, the size of the NRG1 clusters increased progressively, reaching a plateau at P18 (Fig. 6a,b,f). At this age, virtually all of the NRG1 clusters were associated with presynaptic cholinergic terminals. In agreement with Mavlyutov *et al.*⁴¹, C-bouton-associated S1R immunoreactivity began only after the second week of postnatal development (Fig. 6a,b). In the spinal cord MNs of aged mice, the density and size of the C-bouton presynaptic terminals were markedly reduced, whereas this did not occur for the postsynaptic proteins NRG1 and S1R.

In order to analyse NRG1 and C-bouton synapse formation in an *in vitro* model, we performed long-term cultures of dissociated spinal cord neurons. We assumed that the presence of a mixed neuronal population would be necessary to develop C-bouton-like cholinergic afferents and that the presence of glial cells would provide trophic support for promoting long-term MN survival and differentiation. In these cultures, highly branched and large MNs were identified after immunostaining with either SMI32 or anti-ChAT antibodies following 14–28 days *in vitro* (Fig. 7a,b). These MNs exhibited neurite outgrowth over long distances and formed an interconnected network with abundant neuritic-neuritic and neuritic-somatic junctures, which displayed the synaptic marker synaptophysin (Syn) and appeared distributed in discrete puncta. Many of these were glutamatergic boutons because they also contained VGLUT1 or VGLUT2 (Fig. 7d–f). Very few MNs showed VACHT-positive axo-somatic or axo-dendritic synaptic contacts adjacent to spots containing NRG1 (Fig. 7g,h). By contrast, a variable number of spots with a prominent NRG1 signal was observed in many MNs without any association with the presynaptic nerve terminal markers Syn and VACHT (Fig. 7i–j). These non-synaptic associated NRG1 patches were often in close proximity to GFAP-positive astroglial processes (Fig. 7c). It is interesting to note that somato-dendritic NRG2 puncta have been described in association with astroglia in cultured hippocampal neurons³⁹. Overall, this *in vitro* model recapitulates some of the early events leading to C-bouton formation *in vivo*, but it is only able to generate afferent cholinergic synapses on a minor proportion of MNs.

Disruption of postsynaptically-clustered NRG1 in axotomised MNs together with microglial activation. The retrograde response of neurons to peripheral nerve interruption is associated with prominent changes in ER organisation⁴², in the plasticity of synaptic inputs combined with the activation of perineuronal glial cells^{43,44}, and increased excitability²². As these changes may be related to altered C-bouton function²², we analysed the impact of sciatic nerve transection on postsynaptic NRG1. In spinal cord sections, the pool of axotomised MNs was readily identifiable after IBA1 immunostaining due to the notable and early recruitment of microglia around lesioned MN somata (Fig. 8a). As shown in Fig. 8b–f, a progressive and transient disintegration of NRG1 clusters occurred in axotomised MNs associated with perisomatic microglial activation starting 24 h after nerve injury. Although the reduction in size of NRG1 immunoreactive profiles reached its maximum 14 days following axotomy, the density of individual clusters was only slightly changed. By 30 days post-lesion, the size of the NRG1 profiles found in basal conditions showed a recovery, reaching similar values to controls. Correlative ultrastructural alterations have been reported in the SSC of axotomised MNs⁴⁵. The size of the VACHT immunoreactive profiles present in the presynaptic compartment of afferent nerve terminals contacting axotomised MNs showed changes similar to those found for NRG1 (area of VACHT-delimited C-bouton in μm^2 : control = 6.80 ± 0.20 [n = 184], 14 days post-axotomy = 3.08 ± 0.14 [n = 114], and 30 days post-axotomy = 7.45 ± 0.32 [n = 153]; control vs. 14 days post-axotomy, p < 0.001; control vs. 30 days post-axotomy, non-significant; Student's *t*-test). By contrast, the number of VACHT positive terminals declined more markedly (>45%, 7 days after axotomy) than that of NRG1 clusters (number of VACHT positive profiles per $100\mu\text{m}^2$: control = 3.19 ± 0.3 [n = 14], 7 days post-axotomy = 1.46 ± 0.16 [n = 10]; p < 0.001, Student's *t*-test). We observed that during microglial recruitment and activation around axotomised MNs, C-bouton sites exerted an apparent chemoattractant-like effect

www.nature.com/scientificreports/

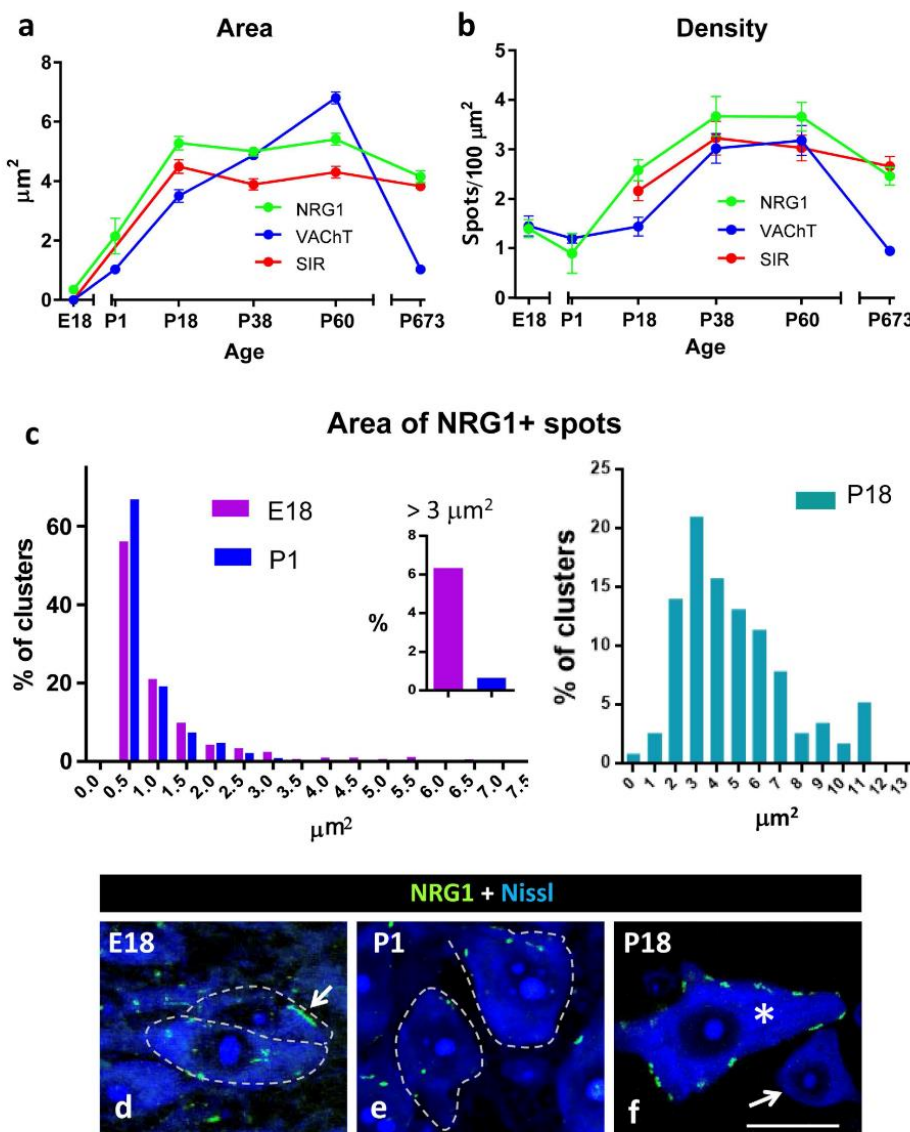


Figure 6. Age-related changes in the morphometrical parameters of the C-bouton associated proteins NRG1, VACHT and SIR. The area and density of the immunolabelled protein profiles are shown in (a) and (b), respectively. (c) Relative frequency histogram of NRG1 clusters for late embryonic (E18), newborn (P1) and P18 MNs; note that the large ($> 3 \mu\text{m}^2$) NRG1 clusters seen on E18 animals are substantially reduced by P1. (d-f) Representative images of MN somata used for quantification in (c); arrow in (d) indicates a large cluster of NRG1 on an E18 MN; MN somata are delimited by dashed lines; note that at P18 (f), C-bouton-associated clusters of NRG1 were only seen on large MNs (*), but not on smaller cell bodies corresponding to interneurons (arrow). In all the graphs, the data are shown as mean \pm SEM. One-way analysis of variance (Bonferroni's post-hoc test) was used for statistical analysis. Scale bar in (f) 20 μm (valid for (d,e)).

on microglial profiles (Figs 8b,c and 9a–c). When the proportion of distinct types of presynaptic terminals contacted by microglial profiles was measured in MN somata 7 days after axotomy (Fig. 9d–g), we found that more than 50% of VACHT-positive or VGlut1-positive terminals were intimately associated with microglial processes, whereas a much lower proportion of microglial profiles were in contact with GABAergic or serotoninergic synapses (Fig. 9h); data concerning the relative density of the distinct types of afferents do not account for these differences (not shown). In addition to motor axons, peripheral nerve injury leads to the interruption of the sensory proprioceptive axons that establish monosynaptic VGlut1-positive afferent connections with MNs⁴⁶. It would not

www.nature.com/scientificreports/

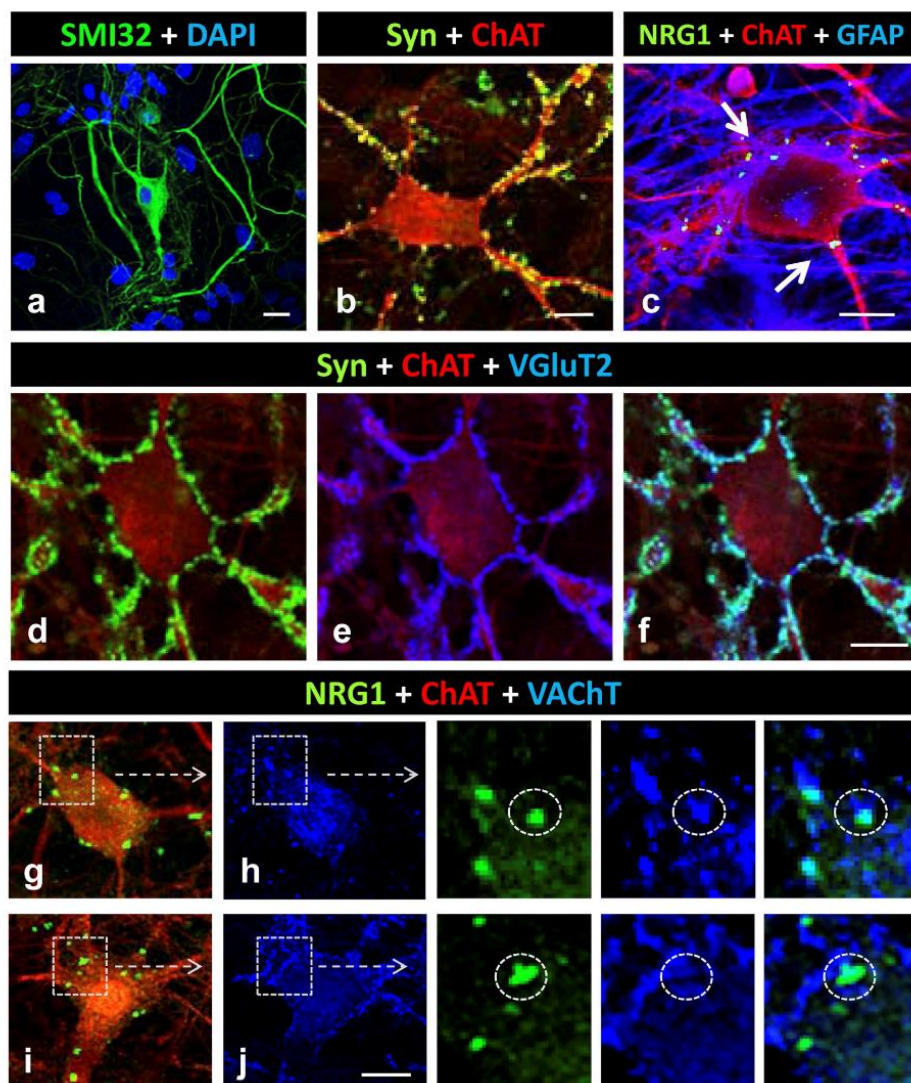


Figure 7. Formation of synaptic afferents in long-term cultures of spinal cord neurons. MNs are identified with SMI32 or ChAT immunostaining. (a) A representative highly branched SMI32 (green) positive MN. (b) A ChAT positive (red) MN showing multiple afferent synaptic boutons detected by synaptophysin (Syn, green) labelling. (c) A ChAT positive (red) MN displaying NRG1 clusters (green) which, in some cases, are in contact with GFAP positive (blue) astroglial profiles (arrows). (d–f) A ChAT positive (red) MN with multiple Syn positive (green) synaptic contacts in which many contain VGlutT2 (blue). (g,h) A ChAT positive MN (red) showing VACHT positive (blue) cholinergic afferent boutons in close association with NRG1 (green) positive clusters, as detailed (encircled) in the enlarged region delimited in (h). (i,j) A ChAT positive MN (red) showing NRG1 (green) positive clusters which are not associated with VACHT (blue) positive puncta, as shown (encircled) in the enlarged region delimited in (j). Scale bars: in (a and b) = 20 µm; in (c) = 10 µm; in (f) = 20 µm (valid for (d,e)); in (j) = 20 µm (valid for (g,h,i)).

be surprising if there were an association between microglia with degenerating and presumably chemoattractant VGlutT1-containing terminals⁴⁷. Nevertheless, the C-bouton spatial specificity as a target for microglial migration is less expected, because the interneurons, from which these terminals originate, are not directly damaged by axotomy. This apparent chemotactic activity is probably related to the complex arrangement of molecules and signal-transduction pathways inherent to C-boutons. This may represent an early event in the inflammatory response to injured MNs that could contribute to the generation of a perisynaptic environment that could play a

www.nature.com/scientificreports/

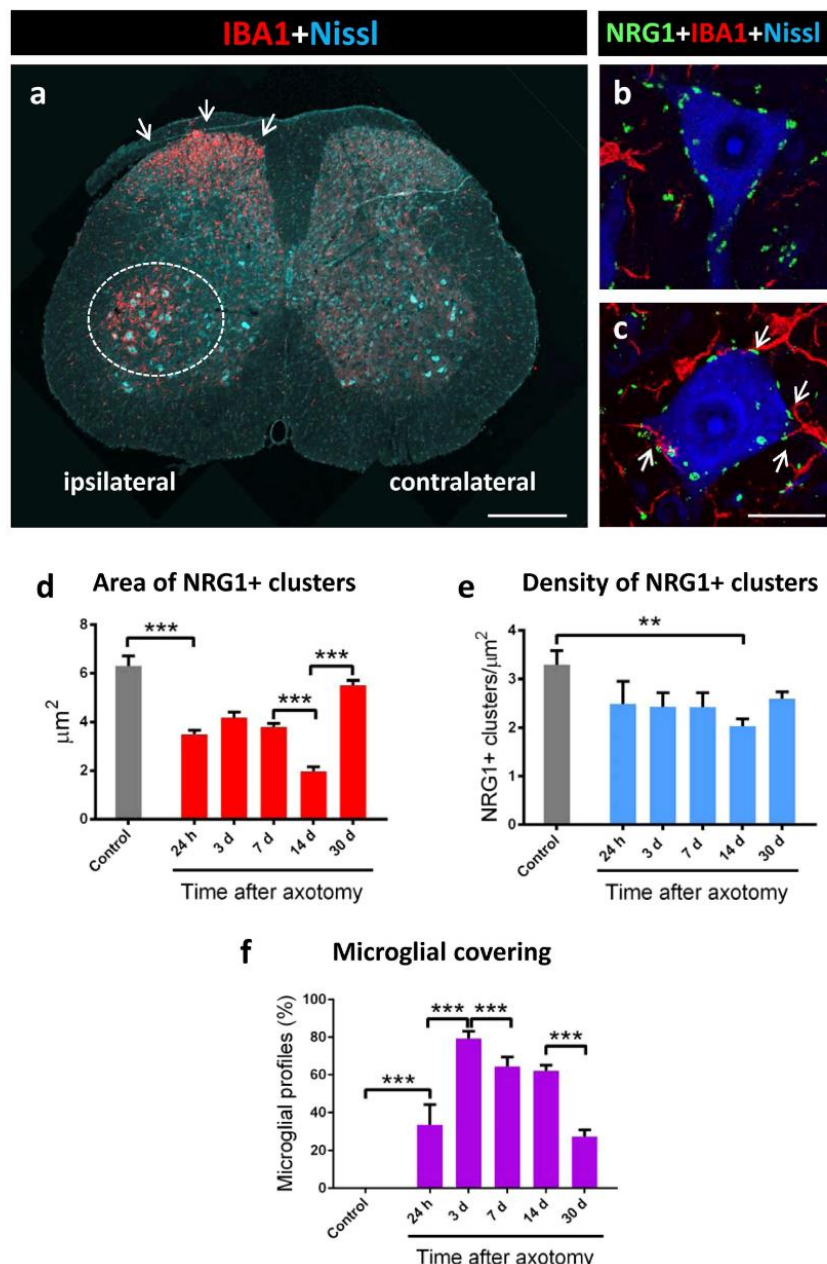


Figure 8. C-bouton-associated NRG1 clusters are disrupted after peripheral nerve transection together with microglial activation. (a) A lumbar spinal cord transverse section 7 days after unilateral sciatic nerve transection; note the microglial reaction (IBA1, red) around the ventral horn MNs (encircled) and in the dorsal horn (arrows); the section was Nissl-counterstained (blue). (b,c) Detail of spinal MNs corresponding to the contralateral (b) and ipsilateral (c) ventral horns following nerve axotomy stained for NRG1 (green), IBA1 (red) and Nissl (blue); microglial cells are recruited around axotomised MNs (c), in which NRG1 clusters are in the process of fragmentation. Note the tendency of microglial profiles to contact altered NRG1 clusters. The time course of changes in the morphometrical parameters of NRG1 clusters after sciatic nerve axotomy are shown in (d,e). Changes in the perisomatic-microglial covering of MNs are measured at the same time points (f). In all the graphs, data are shown as mean \pm SEM. $^{**}p < 0.01$, $^{***}p < 0.001$, one-way analysis of variance (Bonferroni's post-hoc test); n = 27–113 (d); n = 7–15 (e) and n = 10–18 (f). Scale bar: in (a) = 250 μm ; in (c) = 20 μm (valid for (b)).

www.nature.com/scientificreports/

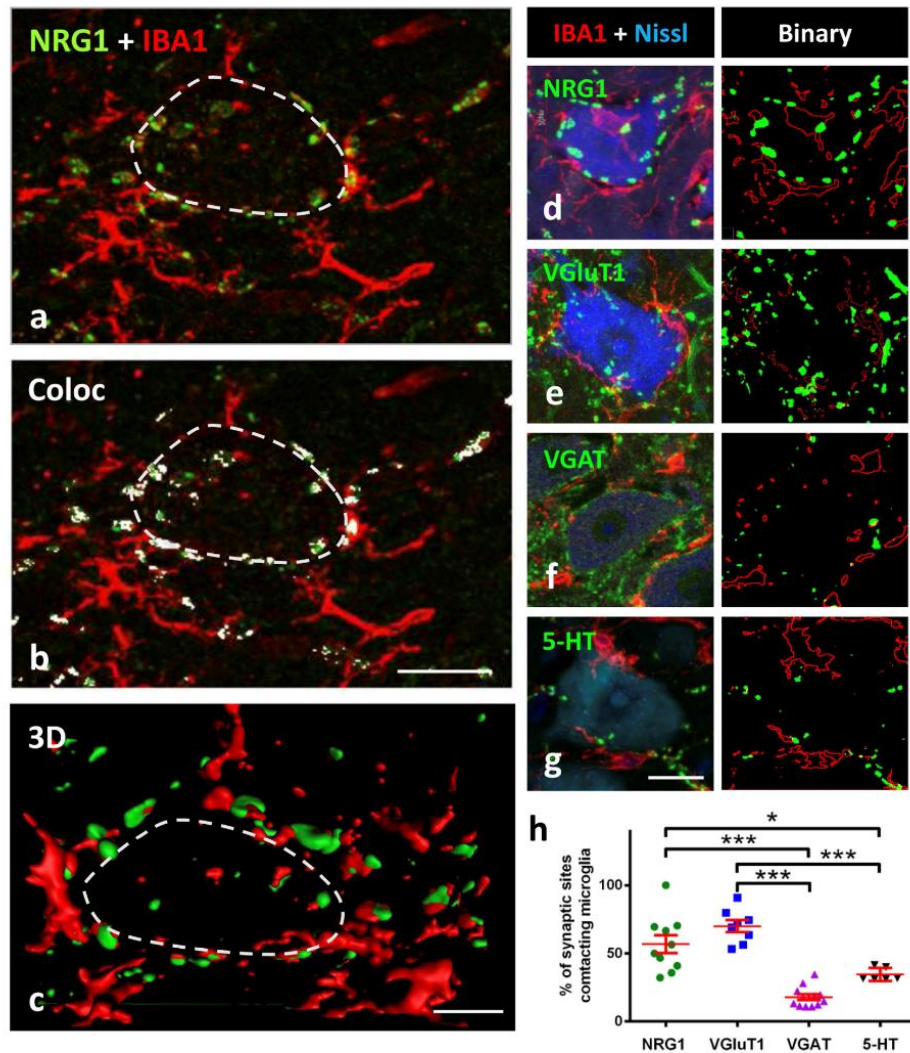


Figure 9. Recruitment of microglial cells to axotomised MNs exhibits apparent positive chemoattraction to C-bouton sites. (a) IBA1 positive microglial profiles (red) near the soma of a 24 h axotomised MN show a high number of contacts with NRG1 positive C-bouton sites (green). (b) After colocalisation analysis, NRG1 clusters enwrapped by microglia are displayed in white. (c) 3D volume rendering showing the relationship between microglial processes and NRG1 clusters in the MN displayed in (a); the limit of MN soma is delineated (dashed lines). (d–g) The spatial relationship between microglial profiles and different afferent boutons on 7-day axotomised MNs is analysed after immunostaining for IBA1 (red) and the indicated synaptic proteins (green); MN somata were identified by Nissl staining (blue). The green and red signals were binarised for analysis as shown in each adjacent panel. (h) Graph showing that microglial profiles exhibit a preference to contact NRG1-labelled C-boutons and/or VGlut1-containing synapses, rather than to VGAT-immunolabelled GABAergic or serotonergic (5-HT) synapses; plotted data are also shown as mean \pm SEM; * p < 0.05, *** p < 0.001, one-way analysis of variance (Bonferroni's post-hoc test). Scale bars: in (b) = 20 μ m (valid for (a)); in (c) = 5 μ m; in (g) = 20 μ m (valid for (d,e,f)).

role in determining MN survival or degeneration. Further work is necessary to determine the molecular cues that attract microglial processes to C-type synapses following nerve injury.

Discussion

With the emergence of new data about the C-bouton structure and function, and its possible relevance to MN pathology, there has been considerable recent interest in this type of synapses^{19,48}. Here, we extend our previous report showing that the NRG1-ErbB2/3 signalling module is expressed at C-boutons¹⁸, by providing a more

www.nature.com/scientificreports/

detailed analysis of the compartmentation of these molecules and their relation with other proteins that are known to be specifically clustered at this synaptic site. The SSC, the ER-related organelle that anatomically defines C-boutons, is the site at which some of these proteins accumulate. This is the case of SR1, Kv2.1 and NRG1. In addition, we show that, within the SSC, these proteins reside in segregated regions that probably represent distinct, highly specific spatial domains. This may define spatially-restricted fields for different signal-transduction pathways in the post-synaptic compartment, which are specifically arranged in relation to presynaptic proteins. This would be consistent with the emerging concept of “trans-synaptic nanocolumns”⁴⁹. One so far unsolved question that deserves further attention is whether SSC-resident proteins can translocate and/or interact with the post-synaptic membrane, as appears to be the case for Kv2.1 and SR1. Kv2.1 is a major component of delayed rectifier K⁺ channels which are involved in the modulation of neuronal excitability in various neuronal types⁵. In agreement with our findings, Kv2.1 channels have sometimes been identified in the most peripheral region of the SSC^{38,39}. These data indicate that Kv2.1 clusters are strategically situated at specific somatic synapses in conjunction with other signalling proteins including S1R and NRG1. S1R is a highly dynamic chaperone-like protein present in the SSC, which is involved in ALS when mutated⁵⁰. S1R may operate here in a similar way to that described for mitochondrion-associated ER membrane in Ca²⁺ signalling via IP3 receptors, perhaps in collaboration with M2-receptor cholinergic activation^{50–52}. Thus, by modulating spatiotemporal calcium signals, S1Rs may regulate either voltage-gated calcium channels or potassium channels⁵³, both of which have an impact on neuronal excitability through a mechanism that acts via either G-protein-dependent M2 receptor activation or channel phosphorylation. In addition, it should be taken into account that highly clustered Kv2.1 phosphorylated proteins may have non-conducting, as yet undefined, functions⁵⁴. It has been suggested that these Kv2.1 clusters could be sites for the delivery of membrane proteins to the cell surface⁵⁵. Accordingly, Kv2.1 platforms may play a role as an organizer of the complex molecular assembly at the C-bouton postsynaptic site, regulating site-directed vesicle-membrane trafficking. This would perhaps explain the particular, belt-like, distribution of Kv2.1 protein, surrounding the whole oval-shaped C-bouton site.

The existence of NRG1 within the SSC facing ErbBs in association with cholinergic terminals is a recently described observation¹⁸ that we have extended on here. It has also been recently shown that NRG2 accumulates in the SSCs of cortical interneurons expressing ErbB4³⁹. In this case, NRG2/ErbB4 signalling appears to regulate NMDA receptors in an autocrine manner. Although our data indicate that the main pathway for NRG1-ErbBs signalling at C-boutons may be retrogradely directed from post- to pre-synaptic compartments, we cannot rule out the possibility of additional autocrine NRG1 mediated signalling in MNs, as ErbBs are also expressed in these cells. Although our results concerning the localization of ErbBs contrast with those reported by Lasiene *et al.*³⁵ using non-phosphospecific anti-ErbBs antibodies, we are confident of our results since they were extensively replicated and analysed using several different antibodies. The strongest presynaptic ErbB signal was obtained when phosphospecific anti-ErbB2 and ErbB4 antibodies were used; this points to the activation of this pathway in a particular subset of C-boutons. Furthermore, the NRG1/ErbB signalling system is also involved in a variety of well-established roles within the neuromuscular system. For example the MN-derived NRG1 pathway is critical: (i) to the development of Schwann cells and myelination⁵⁶, (ii) to the development and plasticity of neuromuscular junctions⁵⁷ and, (iii) perhaps also, to the induction of local AChR synthesis^{58,59}. The anti-NRG1 antibody used in this work recognises a C-terminal epitope which is common within the different NRG-1 isoforms. The above mentioned actions are mainly mediated by the type III NRG1 (NRG1-III), which is the main isoform expressed in MNs^{58,60–63}. It is therefore likely that the isoform we detected in C-boutons corresponds to NRG1-III, which is characterised by a cysteine-rich domain (CRD) determining a second N-terminal transmembrane domain. Signalling mediated by this membrane-anchored isoform may take place in a contact-dependent juxtaacrine manner, through either the full length or truncated protein. Paracrine signalling via the proteolytic liberation of the EGF-like domain has also been described⁶⁴. How post-synaptic NRG1 at C-boutons gains access to presynaptic ErbB receptors is not yet understood. Intercellular vesicular transmission mediated by exosomes may have a role in some forms of trans-synaptic communication⁶⁵. We have observed intersynaptic multivesicular bodies at C-boutons with exosome-like vesicles containing NRG1¹⁸. It should be noted that the intersynaptic trafficking of large vesicles has already been documented in C-type synaptic terminals⁶⁶. Another aspect that should be taken into account is the possibility of ErbBs-elicited NRG1 back signalling after the proteolytic release of the intracellular domain of NRG1, which may act as a transcriptional factor capable of regulating neuronal survival⁶⁷.

Surface-associated NRG1 spots appeared in developing MNs on E18, at the same time as VACHT-positive perisomatic puncta. This is consistent with reported data on the development of cholinergic terminals in MNs⁶⁸. However, the transient existence of large and un-innervated NRG1 spots in immature MNs suggests that SSC development is a cell autonomous process, which undergoes remodelling induced by nerve terminals during cholinergic synaptogenesis. In adults, SSC markers, including NRG1, are progressively lost after peripheral nerve section, together with microglial activation and synaptic loss. This is consistent with the decrease in NRG1-III expression found in the facial nucleus after axotomy¹⁴ and also with the redistribution of C-bouton-associated Kv2.1 channels after peripheral nerve injury²².

Another interesting question that has derived from our study is whether C-bouton has a particular role in the orchestration of a neuroinflammatory response. Our results suggest that C-bouton associated molecules act as cues for the attraction of microglial processes which, in turn, remove the synaptic terminals. In addition to motor axons, peripheral nerve injury leads to the interruption of the sensory proprioceptive axons that establish monosynaptic VGlut1-positive afferent connections with MNs⁴⁶. It would not be surprising if there were an association between microglia with degenerating and presumably chemoattractant VGlut1-containing terminals⁴⁷. Nevertheless, the C-bouton spatial specificity as a target for microglial migration is less expected, because the interneurons, from which these terminals originate, are not directly damaged by axotomy. This apparent chemotactic activity is probably related to the complex arrangement of molecules and signal-transduction pathways inherent to C-boutons. At the molecular level, one candidate for this action could be the NRG1/ErbBs signalling

www.nature.com/scientificreports/

pathway. It has been shown that ErbB receptors are expressed in microglia and that NRG1 is a chemotactic factor for microglia *in vitro*; the NRG1/ErbBs module is specifically activated in spinal cord dorsal horn during microglial reaction following peripheral nerve injury⁶⁹. This may represent an early event in the inflammatory response to injured MNs that could contribute to the generation of a perisynaptic environment that could play a role in determining MN survival or degeneration. However, we did not observe ErbB positive immunostaining in activated microglia around axotomised MN somata (data not shown).

Our findings reveal the highly specific arrangement of C-bouton-associated proteins, their disruption in acutely lesioned MNs and their putative role in regulating the neuroinflammatory response, and emphasize the relevance of this hitherto poorly understood structure in the physiology and pathology of MNs. The significance of NRG1-ErbBs retrograde signalling in C-type synapse deserves particular attention in the future as a putative new target for therapy in ALS.

Material and Methods

Animals, surgical procedures and tissue preparation. CD1 mice were purchased from Harlan Laboratories (Castellar del Vallès, Barcelona, Catalonia, Spain). All the animal experimentation procedures were performed according to the European Committee Council Directive and the norms established by the *Generalitat de Catalunya* (published as a law in the *Diari Oficial de la Generalitat de Catalunya* [DOGC] 2073, 1995). All the experiments were previously evaluated and approved by the Committee for Animal Care and Use of the University of Lleida.

For axotomy experiments in adult mice (postnatal day 60), the sciatic nerve was transected at the femoral level and its proximal stump was ligated in order to prevent spontaneous reinnervation.

To retrograde label MNs innervating the tibialis anterior (TA) and soleus muscles, cholera toxin B conjugated with either AlexaFluor 555 (for TA) or AlexaFluor 488 (for soleus) (1 µg/µl in phosphate buffer [PB], Molecular Probes, Eugene, OR, United States) was used. After surgical exposure of the muscles, volumes of 6 or 3 µl of CTB solution were respectively injected into the right TA or left soleus. One day after injection, the animals were fixed by transcardial perfusion, as described below.

All surgical manipulations were performed under anaesthesia, with a combination of ketamine (100 mg/Kg) and xylazine (10 mg/Kg). To minimise suffering, the animals were subjected to postoperative analgesia with intra-peritoneally injected buprenorphine (0.05 mg/Kg).

Spinal cord cultures. Primary cultures of dissociated spinal cord from CD1 mouse embryos (embryonic day 13) were prepared as previously described⁷⁰ with minor modifications. Briefly, the lumbar spinal cords were dissected and the meninges and ganglia removed. Dissociated cells were plated at a density of 300,000 per well in 12-well Nunclon culture dishes containing round glass coverslips coated with a poly-D-lysine plus Matrigel basement membrane matrix (Corning, Bedford, MA). The cells were then maintained in minimum essential medium (Gibco, Waltham, USA) enriched with 5 g/l glucose and supplemented with 3% horse serum, 10 ng/ml nerve growth factor and B27 medium (Gibco). On day 6, the cultures were treated with 1.4 µg/ml cytosine-β-arabinoside (Sigma-Aldrich, Saint Louis, MO) in order to minimise the growth of non-neuronal cells. Cultures kept for 14–28 days *in vitro* were washed in PBS, fixed in 4% paraformaldehyde (PFA) in 0.1 M PB (pH 7.4) for 1 h, and processed for immunofluorescence.

Multiple fluorescent labelling and confocal microscopy. Tissue samples were obtained from mice transcardially perfused with 4% PFA in 0.1 M PB, pH 7.4. Lumbar spinal cord samples were dissected, post-fixed in the same fixative overnight at 4°C, and then cryoprotected with 30% sucrose in 0.1 M PB containing 0.02% sodium azide. Transverse cryostat sections (16-µm thick) were collected on gelatin-coated glass slides.

Sections were then permeabilised with phosphate-buffered saline (PBS) containing 0.1% Triton X-100 for 1 h, blocked with either 10% normal goat serum or normal horse serum in PBS for 1 h at room temperature, and then incubated overnight at 4°C with an appropriate primary antibody mixture. The primary antibodies used are indicated in Table 1.

Once previously washed with PBS, sections were incubated for 1 h with a combination of appropriate secondary fluorescent antibodies labelled with one of the following fluorochromes (1/500): Alexa Fluor 488, Alexa Fluor 546, (Molecular Probes, Eugene, OR, United States), Cy3, or Cy5 (Jackson Immuno Research Laboratories, West Grove, PA, United States). Finally, the spinal cord sections were labelled with blue fluorescent NeuroTrace Nissl staining (1:150; Molecular Probes) and mounted using an anti-fading medium containing 0.1 M Tris-HCl buffer (pH 8.5), 20% glycerol, 10% Moviol, and 0.1% 1,4-diazabicyclo[2.2.2]octane. For ErbB visualisation, some sections were processed using the tyramide signal amplification (TSA), following the procedure recommended by the manufacturer (ThermoFisher, Waltham, MA).

For the 3D analysis of C-boutons in individual MNs, a squash procedure⁷¹ was used. Fixed spinal cords were sectioned with a vibratome (200-µm thick). Sections were collected in PB, and placed on SuperfrostPlus microscope slides (Menzel-Glaser, Germany). A coverslip was then applied to the tissue which was squashed with forceps. The preparations were then frozen in liquid N₂, and, after removing the coverslip, the slides with the retained tissue were fixed in methanol at -20°C for 10 min. After washing with PBS, immunocytochemistry was performed as described above.

The slides were then examined under a Fluoview FV-500 or Fluoview FV-1000 Olympus laser-scanning confocal microscopes (Olympus, Hamburg, Germany). The MNs were imaged after obtaining optical sections (0.5 or 1 µm) of cell bodies. Digital images were analysed with either Visilog 6.3 software (Noesis, Orsay, France) or ImageJ software (US National Institutes of Health, Bethesda, MD, USA). For colocalization analysis the ImageJ plugin developed by Pierre Bourdoncle (bourdoncle@ijm.jussieu.fr) was used.

www.nature.com/scientificreports/

Target	Source	Host species	Used concentration
Choline acetyltransferase (ChAT)	Millipore (Tamecula, CA) (AB 143)	Rabbit polyclonal	1:200
Glial fibrillary acidic protein (GFAP)	Abcam (ab4674)	Chicken polyclonal	1:1000
Her4/ErbB4	Cell Signalling (#4795)	Rabbit monoclonal	1:50
Ionised calcium-binding adaptor molecule 1 (IBA1)	Abcam (ab5076)	Goat polyclonal	1:500
Kv 2.1 voltage-gated potassium channel (Kv2.1)	NeuroMab (73-014)	Mouse monoclonal	1:100
M2 muscarinic receptor	Alomone Labs (AMR-002)	Rabbit polyclonal	1:100
Neu (C-18) (ErbB2)	Santa Cruz Biotechnology (Sc-284)	Rabbit polyclonal	1:50
NRG1 1 α /3 β 1/2	Santa Cruz (sc-348)	Rabbit polyclonal	1:200
Phospho-Her4/ErbB4 tyr1248	Cell Signalling (#4757)	Rabbit monoclonal	1:50
p-Neu tyr1248 (p-ErbB2)	Santa Cruz (sc-293110-R)	Rabbit polyclonal	1:100
Sigma-1 receptor (S1R)	Santa Cruz (sc-137075)	Mouse monoclonal	1:50
Serotonin	Chemicon (MAB352)	Rat monoclonal	1:100
SK3 calcium-activated potassium channel (SK3)	Alomone Labs (APC-025)	Rabbit polyclonal	1:100
SMI32	Covance Research Products Inc (SMI32)	Mouse monoclonal	1:5000
Synaptophysin	Synaptic Systems (101 004)	Guinea pig polyclonal	1:500
Vesicular acetylcholine transporter (VAcHT)	Synaptic Systems (139 105)	Guinea pig polyclonal	1:500
Vesicular GABA transporter (VGAT)	Synaptic Systems (131 004)	Guinea pig polyclonal	1:200
Vesicular glutamate transporter 1 (VGluT1)	Synaptic Systems (135 304)	Guinea pig polyclonal	1:500
Vesicular glutamate transporter 2 (VGluT2)	Synaptic Systems (135 404)	Guinea pig polyclonal	1:500

Table 1. Antibodies used for immunocytochemistry.

Immunlabelled profiles of NRG1 and of the different protein markers examined were then manually counted on the screen for each MN soma. The area and perimeter of MN somata, and microglial profiles covering the MNs were also manually measured. The number of synaptic boutons contacting activated microglia in axotomised MNs was evaluated by image analysis (ImageJ). After application of the outline tool on binarised IBA1 images, these were merged with those corresponding to binarised synaptic boutons; the number of boutons contacting perisomatic microglial profiles was manually counted. Three-dimensional reconstructions were performed using Bitplane (Imaris, Bitplane, CT, USA) on 0.5- μ m thick Z step obtained with the confocal microscope. The digital images were edited using FV10-ASW 3.1 Viewer (Olympus) and Adobe Photoshop CS4 (Adobe Systems Inc, San Jose, CA).

Electron microscopy. Some of the animals were perfused either with 1% PFA and 1% glutaraldehyde in 0.1 M PB (pH 7.4) for conventional electron microscopy or with 4% PFA and 0.2% glutaraldehyde in 0.1 M PB for immunoelectron microscopy.

For conventional electron microscopy, dissected tissues were postfixed in 1% OsO₄ and processed for Embed 812 embedding according to standard procedures. Ultrathin sections were counterstained with uranyl acetate and lead citrate.

For ultrastructural immunolabelling of NRG1, either pre-embedding or post-embedding (freeze substitution and low temperature embedding in Lowicryl HM20 resin [Electron Microscopy Sciences, Hatfield, PA, USA]) procedures were used, as previously described¹⁸. Double immunolabelling of NRG1 in combination with SR1 or Kv2.1 was performed in ultrathin cryosections obtained with a Leica EM FC cryoultramicrotome and processed according to established methods^{72,73}. To facilitate the localisation of C-boutons in ultrathin cryosections, hypoglossal, instead of spinal cord, MNs were analysed in some cases. To do this, samples from brainstem or spinal cord were sectioned with a vibratome (200- μ m thick), and regions containing either hypoglossal nuclei or ventral horn were microdissected. Ultrathin cryosections were labelled using rabbit anti-NRG1 antibody (1:50; Santa Cruz Biotechnology, sc-348) in combination with either mouse anti-Kv2.1 (1:30; NeuroMab, 73014) or mouse anti-S1R (1:10; Santa Cruz Biotechnology, sc-137075). After washing, samples were incubated with 12 nm gold-conjugated goat anti-rabbit IgG (1:30; Sigma Aldrich) and 5 nm gold-conjugated goat anti-mouse IgG (1:30; Sigma Aldrich). Controls, omitting the primary antibody, were also performed. Observations were performed with either a Jeol JEM 1400 (Jeol, Tokyo, Japan) or a Zeiss EM 910 (Zeiss, Jena, Germany) transmission electron microscope. The subcellular distribution of immunogold labelling of NRG1 in MNs was evaluated by the stereological analysis described by Mayhew³⁷.

Statistical analysis. The data are expressed as means \pm SEM. The statistical analysis was assessed by either the Student's *t*-test or one-way analysis of variance (ANOVA) followed by *post hoc* Bonferroni's test. Chi-square was used for the stereological analysis of immunogold labelling. The level of significance was established at $p < 0.05$.

References

- Zagoraiou, L. et al. A cluster of cholinergic premotor interneurons modulates mouse locomotor activity. *Neuron* **64**, 645–662, doi: 10.1016/j.neuron.2009.10.017 (2009).
- Conradi, S. Ultrastructure and distribution of neuronal and glial elements on the surface of the proximal part of a motoneuron dendrite, as analyzed by serial sections. *Acta Physiol Scand Suppl* **332**, 49–64 (1969).
- Hellstrom, J., Arvidsson, U., Elde, R., Cullheim, S. & Meister, B. Differential expression of nerve terminal protein isoforms in VACHT-containing varicosities of the spinal cord ventral horn. *The Journal of comparative neurology* **411**, 578–590 (1999).
- Hellstrom, J., Oliveira, A. L. R., Meister, B. & Cullheim, S. Large cholinergic nerve terminals on subsets of motoneurons and their relation to muscarinic receptor type 2. *Journal of Comparative Neurology* **460**, 476–486, doi: 10.1002/cne.10648 (2003).
- Muennich, E. A. L. & Fyffe, R. E. W. Focal aggregation of voltage-gated, Kv2.1 subunit-containing, potassium channels at synaptic sites in rat spinal motoneurons. *J Physiol-London* **554**, 673–685, doi: 10.1113/jphysiol.2003.056192 (2004).
- Deardorff, A. S. et al. Expression of postsynaptic Ca²⁺-activated K⁺ (SK) channels at C-bouton synapses in mammalian lumbar a-motoneurons. *J Physiol-London* **591**, 875–897, doi: 10.1113/jphysiol.2012.240879 (2013).
- Mavlyutov, T. A. et al. Lack of sigma-1 receptor exacerbates ALS progression in mice. *Neuroscience* **240**, 129–134, doi: 10.1016/j.neuroscience.2013.02.035 (2013).
- Yamamoto, T., Hertzberg, E. L. & Nagy, J. I. Subsurface cisterns in alpha-motoneurons of the rat and cat: immunohistochemical detection with antibodies against connexin32. *Synapse* **8**, 119–136, doi: 10.1002/syn.890080206 (1991).
- Zampieri, N., Jessell, T. M. & Murray, A. J. Mapping sensory circuits by anterograde transsynaptic transfer of recombinant rabies virus. *Neuron* **81**, 766–778, doi: 10.1016/j.neuron.2013.12.033 (2014).
- Miles, G. B., Hartley, R., Todd, A. J. & Brownstone, R. M. Spinal cholinergic interneurons regulate the excitability of motoneurons during locomotion. *Proceedings of the National Academy of Sciences of the United States of America* **104**, 2448–2453, doi: 10.1073/pnas.0611134104 (2007).
- Falls, D. L. Neuregulins: functions, forms, and signaling strategies. *Experimental cell research* **284**, 14–30 (2003).
- Stassart, R. M. et al. A role for Schwann cell-derived neuregulin-1 in remyelination. *Nature neuroscience* **16**, 48–54, doi: 10.1038/nn.3281 (2013).
- Nave, K. A. & Salzer, J. L. Axonal regulation of myelination by neuregulin 1. *Current opinion in neurobiology* **16**, 492–500, doi: 10.1016/j.conb.2006.08.008 (2006).
- Kerber, G., Streif, R., Schwaiger, F. W., Kreutzberg, G. W. & Hager, G. Neuregulin-1 isoforms are differentially expressed in the intact and regenerating adult rat nervous system. *J Mol Neurosci* **21**, 149–165, doi: 10.1385/JMN:21:2:149 (2003).
- Mei, L. & Xiong, W. C. Neuregulin 1 in neural development, synaptic plasticity and schizophrenia. *Nature reviews. Neuroscience* **9**, 437–452, doi: 10.1038/nrn2392 (2008).
- Karl, T. Neuregulin 1: a prime candidate for research into gene-environment interactions in schizophrenia? Insights from genetic rodent models. *Front Behav Neurosci* **7**, 106, doi: 10.3389/fnbeh.2013.00106 (2013).
- Issa, A. N., Zhan, W. Z., Sieck, G. C. & Mantilla, C. B. Neuregulin-1 at Synapses on Phrenic Motoneurons. *Journal of Comparative Neurology* **518**, 4213–4225, doi: 10.1002/cne.22449 (2010).
- Gallart-Palau, X. et al. Neuregulin-1 is concentrated in the postsynaptic subsurface cistern of C-bouton inputs to alpha-motoneurons and altered during motoneuron diseases. *Faseb Journal* **28**, 3618–3632, doi: 10.1096/fj.13-248583 (2014).
- Deardorff, A. S., Romer, S. H., Sonner, P. M. & Fyffe, R. E. Swimming against the tide: investigations of the C-bouton synapse. *Frontiers in neural circuits* **8**, 106, doi: 10.3389/fncir.2014.00106 (2014).
- Pullen, A. H. & Sears, T. A. Trophism between C-Type Axon Terminals and Thoracic Motoneurones in the Cat. *J Physiol-London* **337**, 373–& (1983).
- Novikov, L. N., Novikova, L. N., Holmberg, P. & Kellerth, J. Exogenous brain-derived neurotrophic factor regulates the synaptic composition of axonally lesioned and normal adult rat motoneurons. *Neuroscience* **100**, 171–181 (2000).
- Romer, S. H. et al. Redistribution of Kv2.1 ion channels on spinal motoneurons following peripheral nerve injury. *Brain research* **1547**, 1–15, doi: 10.1016/j.brainres.2013.12.012 (2014).
- Pullen, A. H. Presynaptic terminal loss from alpha-motoneurones following the retrograde axonal transport of diphtheria toxin. *Acta Neuropathol* **83**, 488–498 (1992).
- Nagao, M., Misawa, H., Kato, S. & Hirai, S. Loss of cholinergic synapses on the spinal motor neurons of amyotrophic lateral sclerosis. *Journal of neuropathology and experimental neurology* **57**, 329–333 (1998).
- Pullen, A. H. & Athanasiou, D. Increase in presynaptic territory of C-terminals on lumbar motoneurons of G93A SOD1 mice during disease progression. *The European journal of neuroscience* **29**, 551–561, doi: 10.1111/j.1460-9568.2008.06602.x (2009).
- Saxena, S. et al. Neuroprotection through Excitability and mTOR Required in ALS Motoneurons to Delay Disease and Extend Survival. *Neuron* **80**, 80–96, doi: 10.1016/j.neuron.2013.07.027 (2013).
- Vinsant, S. et al. Characterization of early pathogenesis in the SOD1(G93A) mouse model of ALS: part II, results and discussion. *Brain and behavior* **3**, 431–457, doi: 10.1002/brb3.142 (2013).
- Milan, L. et al. Age-Related Changes in Pre- and Postsynaptic Partners of the Cholinergic C-Boutons in Wild-Type and SOD1G93A Lumbar Motoneurons. *PLoS one* **10**, e0135525, doi: 10.1371/journal.pone.0135525 (2015).
- Herron, L. R. & Miles, G. B. Gender-specific perturbations in modulatory inputs to motoneurons in a mouse model of amyotrophic lateral sclerosis. *Neuroscience* **226**, 313–323, doi: 10.1016/j.neuroscience.2012.09.031 (2012).
- Al-Saif, A., Al-Mohanna, F. & Bohlega, S. A mutation in sigma-1 receptor causes juvenile amyotrophic lateral sclerosis. *Annals of neurology* **70**, 913–919, doi: 10.1002/ana.22534 (2011).
- Prause, J. et al. Altered localization, abnormal modification and loss of function of Sigma receptor-1 in amyotrophic lateral sclerosis. *Human molecular genetics* **22**, 1581–1600, doi: 10.1093/hmg/ddt008 (2013).
- Mavlyutov, T. A., Guo, L. W., Epstein, M. L. & Ruoho, A. E. Role of the Sigma-1 receptor in Amyotrophic Lateral Sclerosis (ALS). *Journal of pharmacological sciences* **127**, 10–16, doi: 10.1016/j.jphs.2014.12.013 (2015).
- Aliaga, L. et al. Amyotrophic lateral sclerosis-related VAPB P56S mutation differentially affects the function and survival of corticospinal and spinal motor neurons. *Human molecular genetics* **22**, 4293–4305, doi: 10.1093/hmg/ddt279 (2013).
- Takahashi, Y. et al. ERBB4 Mutations that Disrupt the Neuregulin-ErbB4 Pathway Cause Amyotrophic Lateral Sclerosis Type 19. *Am J Hum Genet* **93**, 900–905, doi: 10.1016/j.ajhg.2013.09.008 (2013).
- Lasiene, J. et al. Neuregulin 1 confers neuroprotection in SOD1-linked amyotrophic lateral sclerosis mice via restoration of C-boutons of spinal motor neurons. *Acta neuropathologica communications* **4**, 15, doi: 10.1186/s40478-016-0286-7 (2016).
- Song, F., Chiang, P., Wang, J., Ravits, J. & Loeb, J. A. Aberrant neuregulin 1 signaling in amyotrophic lateral sclerosis. *Journal of neuropathology and experimental neurology* **71**, 104–115, doi: 10.1097/NEN.0b013e3182423c43 (2012).
- Mayhew, T. M. Mapping the distributions and quantifying the labelling intensities of cell compartments by immunoelectron microscopy: progress towards a coherent set of methods. *Journal of anatomy* **219**, 647–660, doi: 10.1111/j.1469-7580.2011.01438.x (2011).

38. Du, J., Tao-Cheng, J. H., Zerfas, P. & McBain, C. J. The K⁺ channel, Kv2.1, is apposed to astrocytic processes and is associated with inhibitory postsynaptic membranes in hippocampal and cortical principal neurons and inhibitory interneurons. *Neuroscience* **84**, 37–48, doi: 10.1016/S0306-4522(97)00519-8 (1998).
39. Vullhorst, D. *et al.* A negative feedback loop controls NMDA receptor function in cortical interneurons via neuregulin 2/ErbB4 signalling. *Nature communications* **6**, 7222, doi: 10.1038/ncomms8222 (2015).
40. Wilson, J. M., Rempel, J. & Brownstone, R. M. Postnatal development of cholinergic synapses on mouse spinal motoneurons. *The Journal of comparative neurology* **474**, 13–23, doi: 10.1002/cne.20089 (2004).
41. Matlyutov, T. A. *et al.* Development of the sigma-1 receptor in C-terminals of motoneurons and colocalization with the N,N'-dimethyltryptamine forming enzyme, indole-N-methyl transferase. *Neuroscience* **206**, 60–68, doi: 10.1016/j.neuroscience.2011.12.040 (2012).
42. Lieberman, A. R. The axon reaction: a review of the principal features of perikaryal responses to axon injury. *International review of neurobiology* **14**, 49–124 (1971).
43. Blinzingger, K. & Kreutzberg, G. Displacement of synaptic terminals from regenerating motoneurons by microglial cells. *Zeitschrift für Zellforschung und mikroskopische Anatomie* **85**, 145–157 (1968).
44. Aldskogius, H. & Kozlova, E. N. Central neuron-glial and glial-glial interactions following axon injury. *Progress in neurobiology* **55**, 1–26 (1998).
45. Sumner, B. E. A quantitative analysis of boutons with different types of synapse in normal and injured hypoglossal nuclei. *Experimental neurology* **49**, 406–417 (1975).
46. Alvarez, F. J. *et al.* Permanent central synaptic disconnection of proprioceptors after nerve injury and regeneration. I. Loss of VGLUT1/IA synapses on motoneurons. *Journal of neurophysiology* **106**, 2450–2470, doi: 10.1152/jn.01095.2010 (2011).
47. Kettenmann, H., Kirchhoff, F. & Verkhratsky, A. Microglia: new roles for the synaptic stripper. *Neuron* **77**, 10–18, doi: 10.1016/j.neuron.2012.12.023 (2013).
48. Witts, E. C., Zagoraiou, L. & Miles, G. B. Anatomy and function of cholinergic C bouton inputs to motor neurons. *Journal of anatomy* **224**, 52–60, doi: 10.1111/joa.12063 (2014).
49. Tang, A. H. *et al.* A trans-synaptic nanocolumn aligns neurotransmitter release to receptors. *Nature* **536**, 210–214, doi: 10.1038/nature19058 (2016).
50. Watanabe, S. *et al.* Mitochondria-associated membrane collapse is a common pathomechanism in SIGMAR1- and SOD1-linked ALS. *EMBO molecular medicine*, doi: 10.15252/emmm.201606403 (2016).
51. Fernandez de Sevilla, D., Nunez, A., Borde, M., Malinow, R. & Buno, W. Cholinergic-mediated IP3-receptor activation induces long-lasting synaptic enhancement in CA1 pyramidal neurons. *The Journal of neuroscience: the official journal of the Society for Neuroscience* **28**, 1469–1478, doi: 10.1523/JNEUROSCI.2723-07.2008 (2008).
52. Hayashi, T. & Su, T. P. Sigma-1 receptor chaperones at the ER-Mitochondrion interface regulate Ca²⁺ signaling and cell survival. *Cell* **131**, 596–610, doi: 10.1016/j.cell.2007.08.036 (2007).
53. Aydar, E., Palmer, C. P., Klyachko, V. A. & Jackson, M. B. The sigma receptor as a ligand-regulated auxiliary potassium channel subunit. *Neuron* **34**, 399–410, doi: 10.1016/S0896-6273(02)00677-3 (2002).
54. Fox, P. D., Loftus, R. J. & Tamkun, M. M. Regulation of Kv2.1 K(+) conductance by cell surface channel density. *The Journal of neuroscience: the official journal of the Society for Neuroscience* **33**, 1259–1270, doi: 10.1523/JNEUROSCI.3008-12.2013 (2013).
55. Deutsch, E. *et al.* Kv2.1 cell surface clusters are insertion platforms for ion channel delivery to the plasma membrane. *Molecular biology of the cell* **23**, 2917–2929, doi: 10.1091/mbc.E12-01-0047 (2012).
56. Birchmeier, C. & Nave, K. A. Neuregulin-1, a Key Axonal Signal that Drives Schwann Cell Growth and Differentiation. *Glia* **56**, 1491–1497, doi: 10.1002/glia.20753 (2008).
57. Lee, Y. I. *et al.* Neuregulin1 displayed on motor axons regulates terminal Schwann cell-mediated synapse elimination at developing neuromuscular junctions. *Proceedings of the National Academy of Sciences of the United States of America* **113**, E479–E487, doi: 10.1073/pnas.1519156113 (2016).
58. Falls, D. L., Rosen, K. M., Corfas, G., Lane, W. S. & Fischbach, G. D. Aria, a Protein That Stimulates Acetylcholine-Receptor Synthesis, Is a Member of the Neu Ligand Family. *Cell* **72**, 801–815, doi: 10.1016/0092-8674(93)90407-H (1993).
59. Trinidad, J. C., Fischbach, G. D. & Cohen, J. B. The agrin/MuSK signaling pathway is spatially segregated from the neuregulin/ErbB receptor signaling pathway at the neuromuscular junction. *Journal of Neuroscience* **20**, 8762–8770 (2000).
60. Meyer, D. *et al.* Isoform-specific expression and function of neuregulin. *Development* **124**, 3575–3586 (1997).
61. Loeb, J. A., Khurana, T. S., Robbins, J. T., Yee, A. G. & Fischbach, G. D. Expression patterns of transmembrane and released forms of neuregulin during spinal cord and neuromuscular synapse development. *Development* **126**, 781–791 (1999).
62. Wolpowitz, D. *et al.* Cysteine-rich domain isoforms of the neuregulin-1 gene are required for maintenance of peripheral synapses. *Neuron* **25**, 79–91 (2000).
63. Velanac, V. *et al.* Bace1 processing of NRG1 type III produces a myelin-inducing signal but is not essential for the stimulation of myelination. *Glia* **60**, 203–217, doi: 10.1002/glia.21255 (2012).
64. Fleck, D. *et al.* Dual cleavage of neuregulin 1 type III by BACE1 and ADAM17 liberates its EGF-like domain and allows paracrine signaling. *The Journal of neuroscience: the official journal of the Society for Neuroscience* **33**, 7856–7869, doi: 10.1523/JNEUROSCI.3372-12.2013 (2013).
65. Korkut, C. *et al.* Trans-Synaptic Transmission of Vesicular Wnt Signals through Evi/Wntless. *Cell* **139**, 393–404, doi: 10.1016/j.cell.2009.07.051 (2009).
66. Ronnevi, L. O. Spontaneous phagocytosis of C-type synaptic terminals by spinal alpha-motoneurons in newborn kittens. An electron microscopic study. *Brain research* **162**, 189–199 (1979).
67. Bao, J., Wolpowitz, D., Role, L. W. & Talmage, D. A. Back signaling by the Nrg-1 intracellular domain. *The Journal of cell biology* **161**, 1133–1141, doi: 10.1083/jcb.200212085 (2003).
68. Wetts, R. & Vaughn, J. E. Development of cholinergic terminals around rat spinal motor neurons and their potential relationship to developmental cell death. *Journal of Comparative Neurology* **435**, 171–183, doi: Doi 10.1002/Cne.1200 (2001).
69. Calvo, M. *et al.* Neuregulin-ErbB signaling promotes microglial proliferation and chemotaxis contributing to microgliosis and pain after peripheral nerve injury. *The Journal of neuroscience: the official journal of the Society for Neuroscience* **30**, 5437–5450, doi: 10.1523/JNEUROSCI.5169-09.2010 (2010).
70. Roy, J., Minotti, S., Dong, L., Figlewicz, D. A. & Durham, H. D. Glutamate potentiates the toxicity of mutant Cu/Zn-superoxide dismutase in motor neurons by postsynaptic calcium-dependent mechanisms. *The Journal of neuroscience: the official journal of the Society for Neuroscience* **18**, 9673–9684 (1998).
71. Pena, E., Berciano, M. T., Fernandez, R., Ojeda, J. L. & Lafarga, M. Neuronal body size correlates with the number of nucleoli and Cajal bodies, and with the organization of the splicing machinery in rat trigeminal ganglion neurons. *The Journal of comparative neurology* **430**, 250–263 (2001).
72. Tokuyasu, K. T. *Immunocytochemistry on ultrathin cryosections*. Vol. 131 (Cold Spring Harbor Laboratory Press, 1997).
73. Slot, J. W. & Geuze, H. J. Cryosectioning and immunolabeling. *Nature protocols* **2**, 2480–2491, doi: 10.1038/nprot.2007.365 (2007).

www.nature.com/scientificreports/

Acknowledgements

We would like to thank Dr. Ronald W. Oppenheim for his critical reading of the manuscript and for helpful comments and suggestions. We would also like to thank Marta Hereu for her technical assistance, Lidia Delgado, Gema Marta Martínez and M. Yolanda Muella, from the *Unitat de Criomicroscòpia Electrònica (Centres Científics i Tecnològics de la Universitat de Barcelona)*, for their technical support with ultrastructural immunolabelling, Daniel Cabezas for his help in some experiments, and the SCT animal facility of the *Universitat de Lleida* for mouse care and housing. This work was supported by grants from the *Ministerio de Economía y Competitividad* cofinanced by FEDER (SAF2015-70801-R to J.E.E. and J.C.), and from Jack Van den Hoek a la *investigació de l'ELA - Fundació Miquel Valls* (to J.E.E.).

Author Contributions

J.E.E. and A.C. conceived and designed the experiments. A.C., S.S., V.L., O.T., L.P., S.H., R.S., J.C. and J.E.E. performed the experiments and analysed the data. J.E.E. and J.C. wrote the paper.

Additional Information

Supplementary information accompanies this paper at <http://www.nature.com/srep>

Competing financial interests: The authors declare no competing financial interests.

How to cite this article: Casanovas, A. *et al.* Neuregulin 1-ErbB module in C-bouton synapses on somatic motor neurons: molecular compartmentation and response to peripheral nerve injury. *Sci. Rep.* 7, 40155; doi: 10.1038/srep40155 (2017).

Publisher's note: Springer Nature remains neutral with regard to jurisdictional claims in published maps and institutional affiliations.



This work is licensed under a Creative Commons Attribution 4.0 International License. The images or other third party material in this article are included in the article's Creative Commons license, unless indicated otherwise in the credit line; if the material is not included under the Creative Commons license, users will need to obtain permission from the license holder to reproduce the material. To view a copy of this license, visit <http://creativecommons.org/licenses/by/4.0/>

© The Author(s) 2017

Supplementary Information

Neuregulin 1-ErbB module in C-bouton synapses on somatic motor neurons: molecular compartmentation and response to peripheral nerve injury

Anna Casanovas, Sara Salvany, Víctor Lahoz, Olga Tarabal, Lídia Piedrafita,
Raimundo Sabater, Sara Hernández, Jordi Calderó & Josep E. Esquerda*

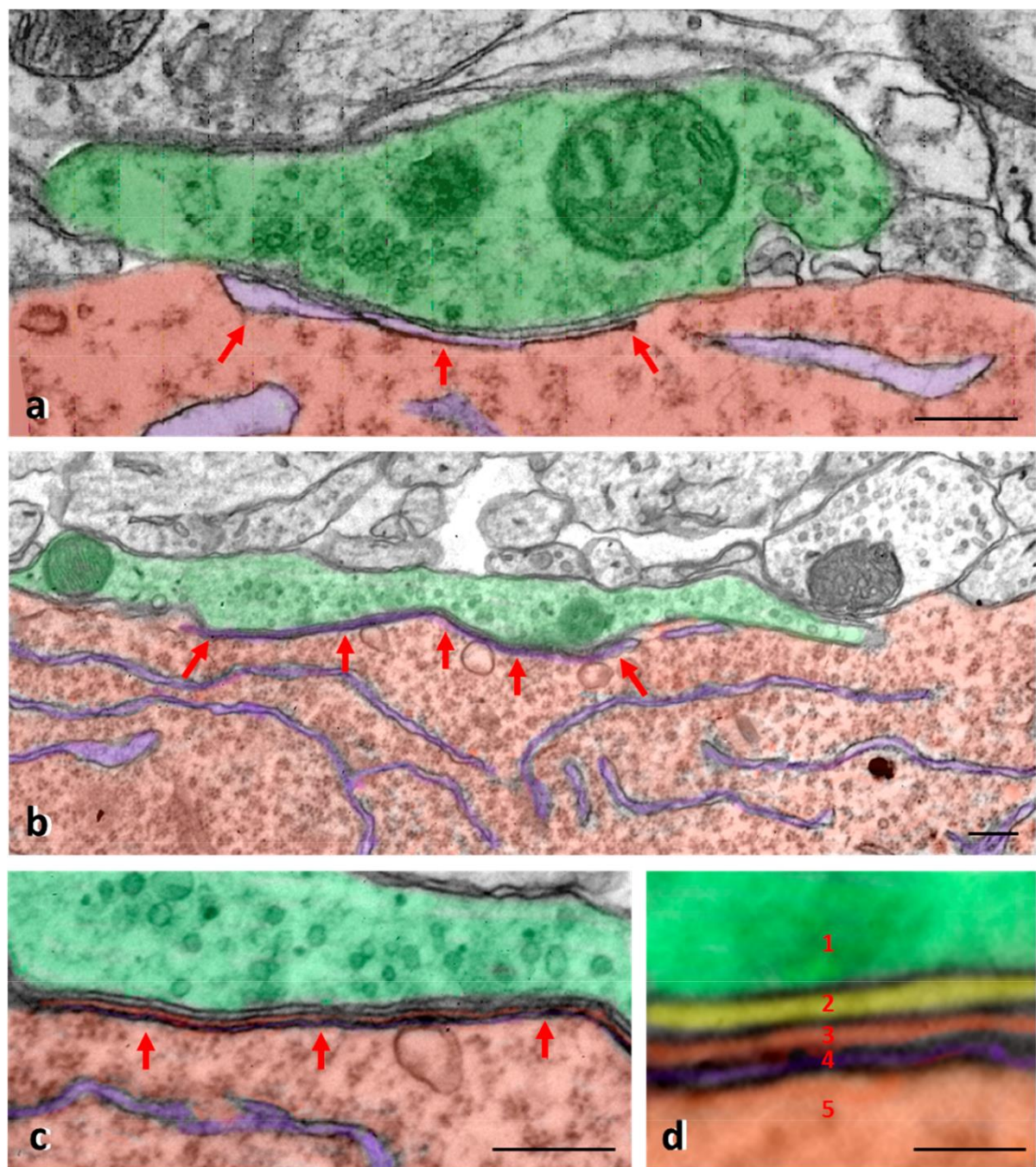
Supplementary Figure 1. Ultrastructure of C-type synapses at the surface of MN soma. (a-d)

Synaptic compartments were pseudo-coloured: presynaptic terminals, green; MN soma (postsynaptic), red; subsynaptic cistern (SSC), and ER, blue; intersynaptic space, yellow. Presynaptic terminals show some mitochondria and synaptic vesicles; in the postsynaptic compartment, the ER-related SSC is seen closely adjacent to postsynaptic membrane (arrows in **a, b and c**). The C-bouton in **(a)** was taken from an adult mouse whereas in **(b)** and **(c)** it came from a newborn mouse. A detail of the organisation of the compartments at the C-bouton synapse is depicted in **(d)**: 1 = presynaptic, 2 = intersynaptic extracellular space, 3 = postsynaptic cytoplasmic compartment lodged between the postsynaptic membrane and the SSC, 4 = SSC, and 5 = MN cytoplasm. Scale bars: in **(a, b, and c)** = 250 nm; in **(d)** = 40 nm.

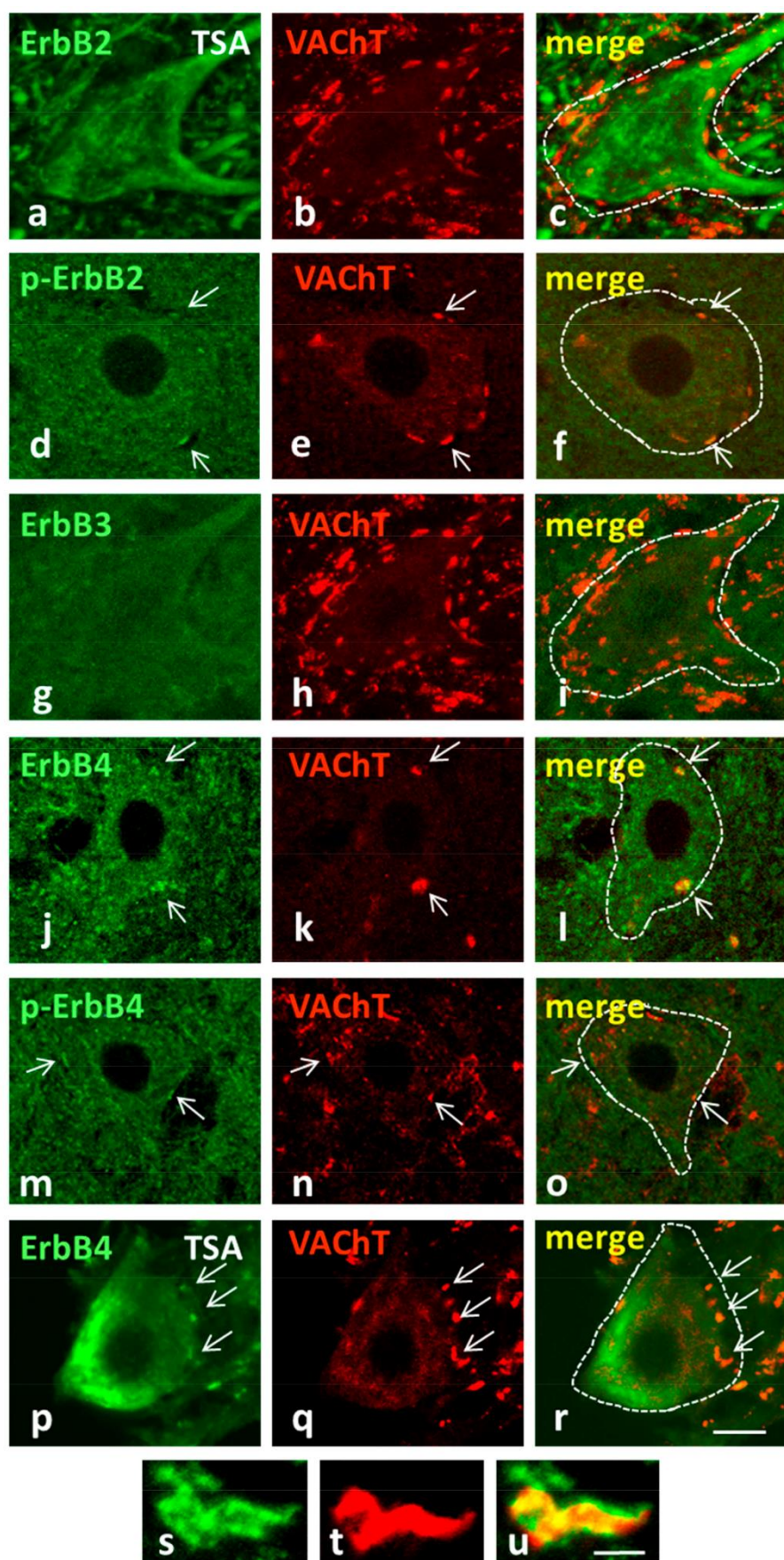
Supplementary Figure 2. Immunostaining of NRG1 receptors ErbBs (green) in conjunction with VACHT (red) demonstrates the presynaptic localisation of ErbBs. (a-c) ErbB2 immunoreactivity after applying the tyramide signal amplification (TSA) procedure shows positive signal in MN somata and neuropil, without association with VACHT positive C-boutons. **(d-f)** By using a phosphospecific anti-ErbB2 antibody a faint signal is detected in association with C-boutons (arrows). **(g-i)** ErbB3 immunoreactivity is low in MNs, without any trace of

positive immunoreactivity in association with presynaptic VACHT. **(j-o)** Both unphosphorylated **(j-l)** and phosphorylated **(m-o)** ErbB4 immunoreactivity can be detected in association with some VACHT positive C-boutons (arrows) **(p-r)** ErbB4 immunoreactivity unambiguously colocalises with VACHT (arrows) after using the TSA procedure. **(s-u)** An enlarged C-bouton showing the colocalisation of ErbB4 **(s)** and VACHT **(t)**. Scale bars: in **(r)** = 20 µm (also valid for **(a-q)**); in **(u)** = 2 µm (valid for **(s,t)**).

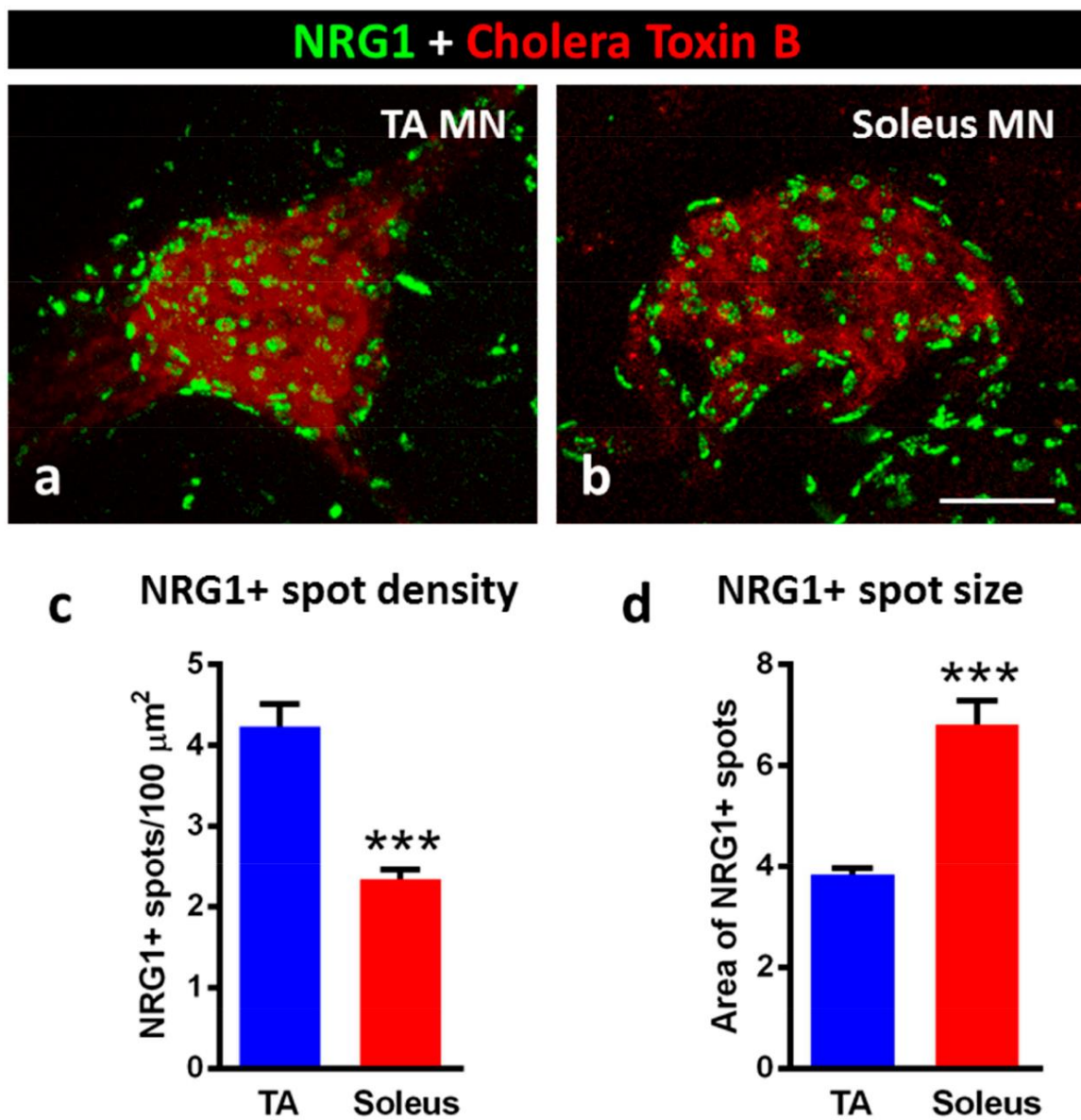
Supplementary Figure 3. Fast and slow MNs display differential morphometrical parameters on C-bouton-associated NRG1. **(a,b)** Fast **(a)** and slow **(b)** MNs were identified after cholera toxin B (red) retrograde tracing following its injection into the tibialis anterior(TA) or soleus muscles, respectively. NRG1 (green) immunolabelling was analysed in both MN populations. **(c,d)** Graphs showing the density **(c)** and size **(d)** of C-boutons containing NRG1 on TA and soleus MNs. The data are expressed as mean ± SEM of n=15-22 3D reconstructed MNs **(c)** and n=199-322 spots **(d)**. *** $p<0.001$ (Student's t-test). Scale bar: in **(b)** = 20 µm (valid for **(a)**).



Supplementary Fig. 1



Supplementary Fig. 2



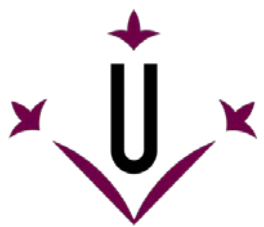
Supplementary Fig. 3

Article II**Localization and dynamic changes of neuregulin-1 at C-type synaptic boutons
in association with motor neuron injury and repair**

Sara Salvany, Anna Casanovas, Olga Tarabal, Lídia Piedrafita, Sara Hernández, Manuel Santafé, María Clara Soto-Bernardini, Jordi Calderó, Markus H. Schwab i Josep E. Esquerda

The FASEB Journal

(2019) Jul; 33(7), 7833–7851; Q1, IF: 4.966



Universitat de Lleida

Document downloaded from:

<http://hdl.handle.net/10459.1/67775>

The final publication is available at:

<https://doi.org/10.1096/fj.201802329R>

Copyright

(c) Federation of American Societies for Experimental Biology, 2019

Localization and dynamic changes of neuregulin-1 at C-type synaptic boutons in association with motor neuron injury and repair

Sara Salvany¹, Anna Casanovas¹, Olga Tarabal¹, Lídia Piedrafita¹, Sara Hernández¹, Manuel Santafé², María Clara Soto-Bernardini³, Jordi Calderó¹, Markus H. Schwab^{4,5,*} Josep E. Esquerda^{1,*}

¹Unitat de Neurobiologia Cel·lular, Departament de Medicina Experimental, Facultat de Medicina, Universitat de Lleida and Institut de Recerca Biomèdica de Lleida (IRBLLEIDA), Lleida, Catalonia, Spain

²Unitat d'Histologia i Neurobiologia (UHN), Facultat de Medicina i Ciències de la Salut, Universitat Rovira i Virgili, Reus, Catalonia, Spain.

³Instituto Tecnológico de Costa Rica (TEC), Cartago, Costa Rica

⁴Hannover Medical School, Hannover, Germany.

⁵Center for Systems Neuroscience (ZSN), Hannover, Germany

Sara Salvany and Anna Casanovas equally contributed to this work

*Corresponding author: Josep E. Esquerda, Unitat de Neurobiologia Cel·lular, Departament de Medicina Experimental, Facultat de Medicina, IRBLLEIDA, Universitat de Lleida, Av. Rovira Roure 80, 25198 Lleida, Catalonia, Spain. Phone: +34-973-702427. E-mail address: josep.esquerda@mex.udl.cat

*Co-corresponding author: Markus H. Schwab, Hannover Medical School, Hannover, Germany. E-mail address: schwab.markus@mh-hannover.de

Running title: Neuregulin-1 at C-type synapses on motor neurons

Non-standard abbreviations

AChR, acetylcholine receptor

ACSF, artificial cerebrospinal fluid

AHP, afterhyperpolarization

ALS, amyotrophic lateral sclerosis

BACE1, β -site amyloid precursor protein–cleaving enzyme1

BiP, binding immunoglobulin protein

CSF, cerebrospinal fluid

CTB, cholera toxin-B

EGF, epidermal growth factor

EM, electron microscopy

ER, endoplasmic reticulum

HA-NRG1^{FL}, HA-tagged full-length NRG1 type III

HA-NRG1^{GIEF}, HA-tagged NRG1 type III processing by BACE1 cleavage

i.p., intraperitoneally

ICD, intracellular domain

MN, motor neuron

NRG1, neuregulin 1

OCM, oculomotor

PB, phosphate buffer

PFA, paraformaldehyde

Pi-eIF2 α , phosphorylated-eukaryotic initiation factor 2

PM, plasma membrane

S1R, sigma-1 receptor

SOD1, superoxide dismutase 1

SSC, subsynaptic cistern

TSA, tyramide signal amplification

VACHT, vesicular acetylcholine transporter

VGLUT1, vesicular glutamate transporter 1

WT, wild-type

Abstract

C-type synaptic boutons are cholinergic motor neuron (MN) afferents displaying an endoplasmic reticulum-related subsynaptic cistern (SSC) adjacent to the postsynaptic membrane. A constellation of proteins is clustered at C-boutons, including M2 muscarinic receptors, potassium channels and sigma-1 receptors. We previously found that neuregulin (NRG) 1 is associated with C-boutons at postsynaptic SSCs, whereas its ErbB receptors are located at the presynaptic compartment. C-bouton-mediated regulation of MN excitability has been implicated in MN vulnerability. To address the involvement of C-boutons during pathological conditions, we investigated their plastic changes after electrical stimulation, pharmacological treatments and peripheral nerve axotomy. NRG1 clusters were disrupted in acutely stressed MNs and after tunicamycin-induced ER stress. In axotomized MNs C-bouton loss occurred in concomitance with microglial recruitment and was prevented by the ER-stress inhibitor salubrinal. Activated microglia displayed a positive chemotaxis to C-boutons. Analysis of transgenic mice overexpressing NRG1 type I and type III isoforms revealed that NRG1 type III acts as a specific organizer of SSC-like structures, whereas NRG1 type I promotes cholinergic synaptogenesis. Thus, distinct NRG1 isoform-mediated signaling functions regulate the complex matching between pre- and postsynaptic elements at C-boutons. Overall, these data provide new insights into C-bouton-associated molecules as therapeutic targets in MN disease.

Keywords: spinal cord; motor neuron; C-bouton; neuregulin; nerve transection; microglia

Introduction

Lower motor neurons (MNs) in the ventral spinal cord and brain stem project to skeletal muscles and govern the final efferent pathway that determines motor behavior. To achieve a coordinated control of muscle activity, MNs receive a variety of synaptic inputs, which shape appropriate patterns of discharge of muscle-specific MN pools (1, 2). Among the synaptic afferents involved in the regulation of MN excitability, C-boutons are particularly relevant due to their capacity to modulate the strength of the action potential afterhyperpolarization (AHP) via a reduction of outward K⁺ currents (3). C-boutons originate from cholinergic V0_c interneurons located close to the central canal (4) and display a particular postsynaptic morphology with a prominent endoplasmic reticulum (ER)-related subsynaptic cistern (SSC) (3, 5). In addition to M2 muscarinic acetylcholine receptors (AChRs) at the postsynaptic plasma membrane (PM) (6), a specific constellation of signaling proteins in the PM and SSC of C-boutons has been described. These include: the voltage-gated K⁺ channel Kv2.1 (7), Ca²⁺ activated K⁺ (SK) channels (8), and sigma-1 receptors (S1Rs, (9). Most of these proteins are clustered in non-overlapping microdomains within SSC (10, 11), but their exact roles and functional organization are largely unknown. One novel intriguing aspect of the molecular assembly at C-boutons is the accumulation of neuregulin (NRG) 1 in the SSC (11, 12). The NRG1 family of pleiotropic signaling proteins serve as epidermal growth factor (EGF)-like ligands for transmembrane tyrosine kinase receptors of the ErbB family and regulate multiple neurodevelopmental processes, including myelination and synaptic plasticity (13, 14). NRG1 comprises a variety of isoforms, grouped into three main ‘types’. NRG1 type I and type II variants contain an immunoglobulin-like domain, whereas type III variants harbor a cysteine-rich domain located N-terminal to the EGF-like domain, which serves as a second transmembrane domain (15). Thus, proteolytic processing in the extracellular domain by several proteases, including β-site amyloid precursor protein–cleaving enzyme1 (BACE1), releases the EGF-like domain in types I and II, resulting in paracrine signaling. In contrast, the EGF-like domain of type III variants remains membrane-anchored following BACE1 cleavage and has been implicated in juxtacrine signaling (16). MNs prominently express NRG1 type III isoforms during perinatal development (17-19). In addition, using an isoform-specific antibody, it has recently been reported that NRG1 type II is targeted to C-boutons (20). Nevertheless, NRG1 isoform-specific functions during C-bouton development have not been addressed.

C-boutons are involved in diseases affecting MNs and spinal cord. Their reversible loss occurs following spinal cord injury (21). Although debated (22), C-boutons have also been reported to display pronounced changes in rodent and human MNs affected by amyotrophic

lateral sclerosis (ALS, (12, 23-27). MN subtype-specific differences in vulnerability during disease conditions are driven by endogenous neuroprotective mechanisms linked to their synaptic activity and excitability, including those related with C-boutons; for example, blocking cholinergic neurotransmission via C-boutons results in increased neurotoxic misfolded SOD1 in MNs of an ALS mouse model (Saxena et al., 2013). Several C-boutons-associated proteins are also directly linked to ALS, as demonstrated for S1R (28-30) and VAPB (31). In addition, a mutation in the ErbB4 receptor has been identified as a genetic cause of ALS (32), suggesting a role of impaired NRG1 signaling in ALS pathophysiology. Another intriguing aspect of C-boutons is the absence of this type of afferent synapses in ALS-resistant MNs of oculomotor (OCM) nuclei (Hellström et al., 2003; Gallart-Palau et al., 2014).

Given the putative relevance of C-boutons for the understanding of spinal cord and MN pathology, and their potential as targets for therapy, a more detailed knowledge of C-bouton organization and reactivity to well-defined conditions of experimental injury is required. For instance, it has not been explored how the arrangement and stability of SSC-associated molecules (i.e., NRG1) are altered when afferent inputs are lost in target-deprived (axotomized) MNs and to which extent the ER-derived C-bouton-associated SSC is altered under these conditions. The effects of axotomy also extend to the perineuronal environment, including synaptic inputs and glial cells. Activated microglia following axotomy appear to displace synaptic terminals from the soma and dendrites, a phenomenon usually recognized as “synaptic striping” (33). C-boutons are also partially lost in response to axotomy (34), and a positive influence of C-bouton sites on recruitment of microglial processes has been observed in axotomized MNs (11). However, the role of microglia in C-bouton disruption and recovery in lesioned MNs is still poorly defined.

Here, we systematically investigated the impact of nerve crush, irreversible peripheral nerve transection and pharmacological induction or attenuation of ER-stress on cholinergic presynaptic terminals, postsynaptic NRG1 clusters, and activation of perisynaptic glial cells. These studies revealed the involvement of ER-stress and microglial activation in pathological C-bouton disruption. In addition, based on findings in transgenic mice overexpressing specific NRG1 isoforms, we show that juxtacrine NRG1 type III accumulates at C-boutons and may act as an organizer of SSC-like ER-plasma membrane contacts. In contrast, paracrine NRG1 type I promotes the differentiation of presynaptic components of C-type synapses, suggesting that distinct NRG1 isoforms govern the architectural and functional organization of C-boutons.

Material and Methods

Animals, surgical procedures and tissue preparation

Wild-type (WT) mice (CD1 strain) were purchased from Harlan Laboratories (Castellar del Vallès, Barcelona, Catalonia, Spain). Mice were housed five to six per cage with permanent access to food and water under a 12-h light/12-h dark. All animal experimentation procedures were performed according to the European Committee Council Directive and the norms established by the *Generalitat de Catalunya* (published as a law in the *Diari Oficial de la Generalitat de Catalunya* [DOGC] 2073, 1995). All experiments were previously evaluated and approved by the Committee for Animal Care and Use of our Universities.

Transgenic mice overexpressing full-length NRG1 type I (35), as well as HA-tagged full-length NRG1 type III (HA-NRG1FL) and a HA-tagged variant that mimics NRG1 type III processing by BACE1 cleavage (HA-NRG1GIEF) were used and genotyped as described previously (36).

All surgical manipulations were performed under anesthesia, with a combination of ketamine (100 mg/Kg) and xylazine (10 mg/Kg). To minimize suffering, mice were subjected to postoperative analgesia with intraperitoneally (i.p.) injected buprenorphine (0.05 mg/Kg). In one group of animals, the sciatic nerve at femoral level was exposed, transected and its proximal stump was ligated in order to prevent spontaneous reinnervation; in another group the sciatic nerve was crushed for 30 seconds using microforceps.

For the pharmacological experiments, mice (postnatal day 60) has been used. Drug delivery regimes were i.p. injected based on published reports (26): methocramine (Sigma-Aldrich, Madrid, Spain), 200 µg/kg, daily for 15 days; tunicamycin (Sigma-Aldrich), 1 mg/Kg in saline for 2 days; and salubrinal (Alexis Biochemicals, San Diego, CA reconstituted at 2.6mM with PBS containing 0.1%BSA and 10% DMSO) 100 µl, daily , two days before the sciatic nerve axotomy and the next 7 days post-surgery.

Electrical stimulation

We used acupuncture steel needles (0.30x30mm, Acupuncture Shop Aps, Varde, Denmark) as stimulation electrodes and a Cibertec stimulation unit (CS-20, Cibertec S.A., Madrid, Spain) at both sciatic nerve and spinal cord.

The whole lumbosacral area and the leg were shaved and an incision through the skin and musculature made until visualizing the sciatic nerve. Then electrostimulation (5V at 10 Hz or

100Hz) was applied with the stimulator unit. Electrical stimulation of the sciatic nerve causes action potentials in a retrograde direction which leads to a depolarization of the cell body of the MN in the spinal cord. Direct electrical stimulation of the spinal cord was performed using two acupuncture needles inserted immediately on each side of the dorsal spinal cord. Then, the electrical stimulation was applied with a stimulator unit (5 V at 10 Hz). Three animals in the same conditions but without electrical stimulation were used as sham controls.

In both, sciatic and spinal cord stimulation, an electromyographic record of the foot pad was used to check out the electrostimulation accuracy. For this purpose, the recording electrode was inserted into the foot pad and the reference electrode was inserted subcutaneously near the tail.

***In vitro* slices**

The spinal cord, with the pia mater rapidly removed and immersed in cold (0–4 °C), oxygenated (95% O₂/5% CO₂) artificial cerebrospinal fluid (ACSF), containing (in mM): NaCl, 130; NaHCO₃, 26; MgCl₂, 2; NaPO₄, 1.25; CaCl₂, 2; KCl, 3; glucose, 10. In some experiments, isolation of spinal cords were performed with sucrose-ACSF (in mM): NaHCO₃, 26; MgCl₂, 2; NaPO₄, 1.25; CaCl₂, 0.5; KCl, 3; sucrose, 218, and later transferred to normal ACSF (37). Some experiments were performed in a 0 Ca²⁺ ACSF; in this case, 4 mM EGTA was added. The spinal cord was hydraulically extruded by applying pressure on a syringe filled with ACSF placed on the caudal opening of the vertebral canal as described (38). Prior to excision, the animals were briefly perfused transcardially with ice-cold oxygenated (95% O₂, 5% CO₂) ACSF. Isolated lumbar segments were rapidly sliced (300-400 µm transversal sections) with a McIlwain tissue chopper tissue. The slices were subsequently transferred (or not) to a storage perfusion chamber filled with oxygenated normal ACSF, until their fixation in 4% paraformaldehyde (PF) at the desired experimental time.

Multiple fluorescent labeling and confocal microscopy

Tissue samples were obtained from anaesthetized mice, transcardially perfused with 4% PF in 0.1 M phosphate buffer (PB), pH 7.4. Human spinal cord samples (4% PF fixed) were obtained from the *Banc de Teixits Neurològics de l'Hospital Universitari de Bellvitge* (Dr. Isidre Ferrer, Barcelona, Catalonia, Spain). Tissues from animal species other than rodents were also fixed in 4% PF. Samples were post-fixed overnight in the same fixative at 4°C, and then cryoprotected with 30% sucrose in 0.1 M PB containing 0.02% sodium azide. Transverse cryostat sections (16-µm thick) were collected on gelatin-coated glass slides.

Sections were then permeabilized with phosphate-buffered saline (PBS) containing 0.1% Triton X-100 for 30 minutes, blocked with either 10% normal goat serum or normal horse serum in PBS for 1 h at room temperature, and then incubated overnight at 4 °C with an appropriate primary antibody mixture. The primary antibodies used are indicated in Table 1.

Once previously washed with PBS, sections were incubated for 1 hour with a combination of appropriate secondary fluorescent antibodies labeled with one of the following fluorochromes (1/500): Alexa Fluor 488, Alexa Fluor 546, (Molecular Probes, Eugene, OR, United States), Cy3, or Cy5 (Jackson Immuno Research Laboratories, West Grove, PA, United States). Finally, the spinal cord sections were labeled with blue fluorescent NeuroTrace Nissl staining (1:150; Molecular Probes) and mounted using an anti-fading medium containing 0.1 M Tris-HCl buffer (pH 8.5), 20% glycerol, 10% Mowiol, and 0.1% 1,4-diazabicyclo[2.2.2]octane. For ErbB visualization, some sections were processed using the tyramide signal amplification (TSA), following the procedure recommended by the manufacturer (ThermoFisher, Waltham, MA).

Concerning anti-NRG1 antibodies, in our hands, the best commercially available antibody that can be used to visualize NRG1 at C-boutons is the pan-NRG1 antibody sc-348 (Santa Cruz Biotechnology, Dallas, TX). As this product has been recently discontinued, we looked for other alternatives. Only the rabbit anti-NRG1 type III (extracellular, ANR113, from Alomone, Jerusalem, Israel) gives a positive labeling at C-bouton sites, but this was weaker than that obtained with sc-348. The mouse monoclonal anti-NRG-CDR type III antibody (MABN534, from Millipore, Temecula, CA) is also able to dimly detect C-bouton NRG1 (Suppl. Fig. 1).

Retrograde tracing of MNs was performed with fluorescent-labeled cholera toxin-B subunit (CTB-AlexaFluor 555; Molecular Probes) at 1 µg/µl in PBS. Tracer (5 µl) was injected in leg muscles by means of glass capillary tubes attached to a Hamilton syringe. Animals were perfused 24 h later, and tissues were processed for immunolabeling as above described.

The slides were then examined under a Fluoview FV-500 or Fluoview FV-1000 Olympus laser-scanning confocal microscopes (Olympus, Hamburg, Germany). The MNs were imaged after obtaining optical sections (0.5 or 1 µm) of cell bodies. Digital images were analyzed with either Visilog 6.3 software (Noesis, Orsay, France) or ImageJ software (US National Institutes of Health, Bethesda, MD, USA). For colocalization analysis, the ImageJ plugin developed by Pierre Bourdoncle (bourdoncle@ijm.jussieu.fr) was used.

Immunolabeled profiles of NRG1 and of the different protein markers examined were then manually counted on the screen for each MN soma. In axotomy experiments, we only analyzed cell bodies located in pes 9 region of L6 spinal cord segment, which corresponds to the sciatic

motor column, according to (39) The area and perimeter of MN somata, and microglial profiles covering MNs were also manually measured. The number of synaptic boutons contacting activated microglia in axotomized MNs was evaluated by image analysis (ImageJ). After application of the outline tool on binarized Iba1 images, these were merged with those corresponding to binarized synaptic boutons: the number of boutons contacting perisomatic microglial profiles was manually counted. In some cases, three-dimensional reconstructions were performed using Bitplane (Imaris, Bitplane, CT, USA) on 0.5- μ m thick Z step obtained with the confocal microscope. The digital images were edited using FV10-ASW 3.1 Viewer (Olympus) and Adobe Photoshop CS4 (Adobe Systems Inc, San Jose, CA).

Electron microscopy

Some of the animals were perfused either with 1% PFA and 1% glutaraldehyde in 0.1 M PB (pH 7.4) for conventional electron microscopy or with 4% PFA. Dissected tissues were postfixed in 1% OsO₄ and processed for Embed 812 embedding according to standard procedures. Ultrathin sections were counterstained with uranyl acetate and lead citrate.

Statistical analysis

The data are expressed as means \pm SEM. The statistical analysis was assessed by either the Student's *t*-test or either one-way or two-way analysis of variance (ANOVA) followed by post-hoc Bonferroni's test. The level of significance was established at $p < 0.05$.

Results

Molecular architecture of C-boutons in vertebrate spinal MNs

In agreement with our previous studies (11), we corroborated that ventral horn α -MN in adult mouse spinal cord are innervated by large, cholinergic (VACHT-positive) presynaptic terminals, which juxtapose a highly organized postsynaptic compartment harboring a specific set of distinct proteins, including M2 AChRs, Kv2.1 K⁺ channels, S1R, and NRG1. Postsynaptic regions delimited by NRG1 were often aligned with several VACHT positive terminal bulbs, indicating that individual C-terminals form branches that share a common postsynapse (Fig. 1a-d). Expression of the NRG1 receptor ErbB2 and its phosphorylated form colocalized with VACHT in the presynaptic compartment of C-boutons (Fig. 1e).

In addition to mouse spinal cord, we observed the characteristic punctate accumulation of NRG1 in the postsynaptic compartment of C-boutons in all vertebrate species analyzed,

including frog, lizard, chicken, pig, and human (Suppl. Fig. 2a-g), consistent with evolutionary conserved NRG1 functions in C-type synapses in the vertebrate lineage.

Upon inspection by electron microscopy (EM), large afferent nerve terminals were identified as C-boutons if they coaligned with a postsynaptic SSC, a hallmark for this type of synapse (Fig. 2a-d). Large aggregates of spherical or flattened clear synaptic vesicles were often concentrated at active zone-like sites close to the presynaptic PM, whereas presumably endocytic “coated” vesicles tended to accumulate at the most peripheral areas of terminals (Fig. 2b). Large membrane-bound vacuoles sequestering synaptic vesicles were also frequently seen within the presynaptic compartment, resembling either late endosomes/multivesicular bodies or phagosomal structures (Fig. 2c). To trace endocytic compartments of MN, intramuscular injections were performed using either fluorescent cholera toxin B or the Hc fragment of tetanus toxin. Although both tracers were extensively incorporated into the vacuolar system of MN somata, no association was found between labeled compartments and NRG1-marked postsynaptic regions of C-boutons (Suppl. Fig. 3).

MN stimulation alters C-bouton-associated NRG1 clusters

We next ask whether physiological or pathological changes in MN activity could affect C-bouton-associated NRG1 expression domains. Electrical stimulation of sciatic nerve results in antidromic propagation of action potentials and MN cell body depolarization, whereas electrical stimulation adjacent to the spinal cord causes orthodromic activation of MN axons that can be assessed by EMG recordings of distal leg and foot muscles. Moderate antidromic stimulation (10 Hz, 60 min) produced a modest increase in the size of both pre- and postsynaptic C-bouton compartments delineated by VACHT and NRG1, respectively (NRG1 cluster size in μm^2 : contralateral, 4.26 ± 0.22 , n = 28 MNs; ipsilateral, 5.48 ± 0.24 , n = 37 MNs; $p < 0.05$). Cholinergic transmission at C-boutons is mediated by M2 AChRs, which can be pharmacologically targeted by treatment with the M2 agonist oxotremorine. Similar to antidromic stimulation, oxotremorine treatment caused an increase in size of postsynaptic NRG1 clusters (NRG1 cluster size in μm^2 : saline, 4.37 ± 0.18 , n = 103 clusters; oxotremorine, 5.97 ± 0.37 , n = 62; $p < 0.01$).

In contrast to moderate stimulation, pathologic antidromic stimulation (100 Hz, 60 min) or direct orthodromic spinal cord stimulation at lower frequency and shorter time period (10 Hz, 30 min) resulted in a severe depletion of NRG1 clusters, whereas VACHT-positive terminals were largely spared (Fig. 3a-k). Examination by EM (Fig. 3j) showed that, as a consequence of extreme spinal cord stimulation, the SSC was disrupted in many C-boutons, and SSC remnants

in identifiable C-boutons had a shortened contact area with the postsynaptic membrane; in line with SSC disruption, we observed an increased number of vacuoles at variable sizes, multivesicular bodies and vesicles in subsynaptic regions of the MN cortical cytoplasm.

ER-disruption was largely confined to cortical regions of MN cell bodies, but was absent from Nissl-like ER stacks located in more central cytoplasmic areas (Fig. 3j). We conclude that pathological exacerbation of synaptic activity at C-boutons heavily impacts on the stability of postsynaptic SSCs. This notion was supported by a dramatic loss of SSC-associated NRG1 clusters at C-boutons in an *in vitro* acute spinal cord slice preparation maintained in ACSF. Even after reducing the preparation time from anesthesia to slicing and paraformaldehyde fixation to ~9 min (with or without ulterior recovery in an oxygenated-superfusion slice chamber), most MNs were completely devoid of NRG1-positive puncta. In those few cases, in which NRG1 clusters persisted, they appeared heavily fragmented and dispersed. Small-sized VACHT puncta were still present juxtaposed to a fraction of de-clustered NRG1-containing SSC remnants (Fig. 3l-s). These findings identify an extreme SSC instability as a major component of adult MN vulnerability in response to slicing procedures, most likely due to their large dendritic arbor (40). While similar experiments performed with Ca²⁺-free CSF did not improve the preservation of NRG1 clusters (Fig. 3t), we suggest that massive Ca²⁺ release from intracellular Ca²⁺ stores is sufficient to disrupt SSC integrity in cortical areas of MN cell bodies.

To further analyze the dependence of C-boutons and their associated NRG1 clusters on ER integrity *in vivo*, we induced ER-stress by parenteral administration of tunicamycin (26). The effectiveness of drug administration was assessed by the demonstration that BiP was upregulated in MN somata (BiP intensity in arbitrary units: saline, 116.38 ± 6.76, n = 58 MNs; tunicamycin, 217.10 ± 6.42, n = 57 MNs; p < 0.001). EM analysis confirmed disrupted Golgi and ER membranes (not shown). Concomitant with widespread ER stress, tunicamycin treatment also disrupted SSC-associated NRG1 clusters (NRG1 cluster size in μm²: saline, 3.11 ± 0.12, n = 278 clusters [from 58 MNs]; tunicamycin, 2.42 ± 0.06, n = 444 clusters [from 57 MNs], p < 0.001), and these postsynaptic changes were matched by an equivalent but attenuated response at the corresponding VACHT-delimited presynaptic terminal (VACHT cluster size in μm²: saline, 3.73 ± 0.13, n = 514 clusters [from 58 MNs]; tunicamycin, 3.19 ± 0.13, n = 226 clusters [from 57 MNs]; p < 0.01). Thus, we conclude that pharmacologically-induced ER-stress diminishes the integrity of SSC-associated NRG1 clusters, which in turn affects the size of presynaptic C-boutons.

Glial reactivity and C-bouton plasticity after reversible and irreversible axonal interruption

Distal axon transection leads to rapid and drastic changes in MNs and their synaptic and glial environment (41). We recently showed that C-boutons of axotomized MNs rapidly attract microglial processes (11). Here, we extended these findings by performing a long-term analysis in both reversible (crush) and irreversible (axotomy) axonal interruption paradigms (Fig. 4a-d). A rapid microglial and astroglial recruitment to MNs occurred 1-3 days after axotomy, in concomitance with C-bouton disruption. Most microglial profiles interacted with NRG1-positive C-boutons 1 day after nerve injury, but subsequently the number of microglia interacting with NRG1-positive C-boutons rapidly declined (Fig. 4e-i, Suppl. Fig. 4 and movie). Importantly, the disruption of VACHT-labeled presynaptic terminals was temporally dissociated from the disorganization of postsynaptic NRG1-clusters. Whereas at 7 days after axotomy we observed a loss of 72% of VACHT profiles, the number of postsynaptic NRG1 clusters was only reduced by 32%. This indicates that the elimination of the presynaptic component of C-boutons implies a disorganization and subsequent reorganization of their postsynaptic SSC-associated NRG1 clusters. A recovery of some C-boutons was seen 15 days after axotomy, which occurred in conjunction with a sustained decline of microglial recruitment. However, an opposite profile was seen for astrogliosis, which, after a transient decline, is again triggered 30 days post irreversible nerve injury (Fig. 4b). Regenerated VACHT-positive C-boutons displayed a marked, but transient, reduction in size of postsynaptic NRG1 clusters (Fig. 4b-d). To further assess the involvement of microglia in the elimination of the presynaptic compartment of C-boutons, we compared the juxtaposed expression of VACHT and NRG1 in individual synapses in the presence and absence of nearby Iba1-labeled microglial processes 14 days postaxotomy. NRG1 clusters contacting microglia showed VACHT depletion, whereas those in the absence of microglial processes exhibited a positive VACHT signal (Fig. 4j,k). Together, we conclude that the axotomy-mediated loss of C-boutons is a consequence of a selective microglial recruitment to these synaptic sites, in concordance with the ability of microglia to engulf synaptic inputs during normal and pathological conditions (42, 43).

The pronounced atrophy seen in axotomized non-reinnervating MNs, was less severe after nerve crush (Fig. 4a-d). Moreover, the severe and long-term astroglial reaction following nerve transection was also significantly milder after crush. Compared to irreversible axotomy, an improvement in the restoration of C-bouton density was present 120 days after crush, however, this was no longer sustained.

A further indication of a microglia-mediated removal of presynaptic terminals following axotomy was obtained from ultrastructural analysis (Fig. 5a-k). We noticed that a considerable number of axo-somatic presynaptic terminals showed degenerative changes; some of these

terminals, which often appeared in close proximity to microglial cells, displayed a complete disintegration (Fig 5f and h). However, due to the advanced stage of degeneration, it was impossible to unambiguously identify the morphological subtype of affected synaptic boutons. Nevertheless, in some cases remnants of postsynaptic SSCs were still present adjacent to microglia-covered MN surface areas (or to degenerating synapses), indicating that those correspond to “denervated” C-bouton sites, which underwent degeneration post-axotomy (Fig. 5g and i-k). Based on these data, we conclude that, at least in part, microglia-mediated elimination of C-boutons following axotomy causes a rapid disintegration of presynaptic compartments. This observation contrasts the generally accepted concept that synaptic elimination from axotomized MNs results from the detachment of presynaptic terminals from perykaria by activated microglia, which physically separate pre- and post-synaptic elements in the absence of synaptic degeneration (“synaptic striping”, (33)). The exact role of activated microglia in the destruction of synaptic terminals is difficult to assess here. However, PM apposition of microglia to SSC remnants at sites devoid of synaptic boutons most likely marks areas previously occupied by C-boutons, and this finding is consistent with a more rapid postaxotomy loss of VACHT-positive puncta compared to their postsynaptic counterpart as defined by NRG1 immunolabeling.

Neuronal damage induced by peripheral or central axonal injury comprises unfolded protein response and ER-stress that can promote a regenerative response or apoptotic cell death (44, 45). Salubrinal provides neuroprotection by inhibition of P_i-eIF2α dephosphorylation and ER-stress (46) and salubrinal treatment results in attenuation of microgliosis and neurodegeneration in SOD1^{G93A} mice (47). Using a similar treatment protocol we found that salubrinal administration significantly reduced BiP elevation and nearly abolished the massive microglial recruitment to MN somata 7 days post-axotomy (Fig 6a-p). Moreover, the loss of presynaptic VACHT and postsynaptic NRG1 that concomitantly occurred in axotomized MNs was strongly attenuated by salubrinal. This indicates that unfolded protein response is coupled with microglial activation and synaptic loss in distally lesioned MNs.

Distinct NRG1 isoforms mediate specific pre- and postsynaptic functions at cholinergic C-boutons

Transgenic mice with Thy1.2 promoter-mediated neuronal overexpression of distinct NRG1 isoforms have previously been employed to study axonal control mechanisms during myelination of spinal MNs (35, 36). Considering NRG1 as a prominent and spatially restricted component of C-boutons, we took advantage of these mouse lines to examine NRG1 isoform-

specific functions in C-bouton development and architecture. These studies included transgenic mice which overexpress full-length NRG1 type I (35), N-terminally HA epitope-tagged full-length NRG1 type III (HA-NRG1^{FL}) or a HA-tagged NRG1 type III variant that mimics the product of BACE1 cleavage in the juxtamembrane ‘stalk’ region (HA-NRG1^{GIEF}; (36), which separates an N-terminal (EGF-like domain-containing) transmembrane protein from the C-terminal ICD (Suppl. Fig. 5).

First, we performed simultaneous fluorescent immunostainings for the N-terminal HA-tag and either the C-terminal ICD of NRG1 or the C-bouton postsynaptic markers S1R, Kv2.1 and M2 AChR, in conjunction with presynaptic VACHT on spinal cord sections (Fig. 7a-f). Samples from HA-NRG1^{FL} mice showed highly overlapping immunostaining for the HA-tag and the ICD on the surface of MN cell bodies, which was frequently associated with presynaptic VACHT-positive C-boutons (Fig. 7a). These findings are consistent with the accumulation of unprocessed NRG1 type III at postsynaptic sites of C-boutons. To assess possible consequences of the postsynaptic accumulation of NRG1 type III on the organization of C-type synapses, we performed an examination of HA-NRG1^{FL} mice by EM. Remarkably, we observed an accumulation of abnormally expanded surface-associated ER membranes, which were arranged like redundant SSCs (Fig. 9a). As the number of cholinergic C-boutons contacting MN somata was not altered (Fig. 8a), only a fraction of plasma membrane presenting apposed ER membranes was associated with afferent synaptic C-boutons in HA-NRG1^{FL} mice. We also analyzed whether the pattern of S1R and Kv2.1, two molecules that normally concentrate in C-bouton-associated SSCs, were altered in HA-NRG1^{FL} mice. We found that both, S1R and Kv2.1, were notably increased, displaying a similar pattern to that found for NRG1 type III detected by HA staining (Fig. 7b and e, and 8d and e). Thus, the induction of redundant SSC-like membrane compartments by NRG1 type III overexpression was linked to an increased production and insertion of other SSC-associated partner molecules, such as S1R and Kv2.1. Nevertheless, a more detailed examination revealed that although S1R and NRG1 were closely associated, they did not occupy identical micro-domains (Fig. 8c-d), very similar to their configuration in C-boutons from WT mice (11). In contrast, a tight co-localization between NRG1 and Kv2.1 was observed (Fig. 7e). Importantly, expression of M2 muscarinic receptors, which presumably reside mainly in the postsynaptic membrane, also expanded beyond synaptic areas, as defined by the absence of VACHT-positive terminals, in HA-NRG1^{FL} mice (Fig. 7f and 8c). Together, the redundancy and enlargement of SSC-like structures in HA-NRG1^{FL} mice suggest that full-length NRG1 type III acts as an organizer of ER-membrane contacts, including SSCs, in α-MNs. These findings also indicate that SSCs are involved in organizing the size and molecular layout of the

postsynaptic membrane, whereas SSC architecture has no major direct effects on presynaptic elements of C-boutons.

To address a specific role of the cytoplasmic ICD in organizing SSC architecture in C-boutons, we next investigated HA-NRG1^{GIEF} mice. Although extensive HA-NRG1^{GIEF} expression was observed in MN cell bodies and dendrites, the BACE1-processed variant of NRG1 type III was completely excluded from C-bouton sites. This was unambiguously corroborated when HA-tag detection was combined with antibodies against VACHT and pan-NRG1 (sc-348) to localize C-boutons (Fig. 7g). Consistent with this finding, no expansion of SCC structures, S1R and M2 expression domains was observed in HA-NRG1^{GIEF} mice (not shown). Taken together, these data strongly suggest that the C-terminal ICD is required for SSC accumulation of NRG1 type III and that full-length NRG1 type III exerts specific postsynaptic, SSC organizing functions in spinal α-MNs.

NRG1 type I shares the same ICD with NRG1 type III, but lacks a second transmembrane domain, therefore BACE1 processing results in shedding of the N-terminal EGF-like domain and paracrine signaling. To identify possible consequences of enhanced NRG1 type I-mediated paracrine signaling on C-bouton development, we next examined transgenic mice with Thy1.2 promoter-driven NRG1 type I overexpression (*NRG1^{typeI}*) in spinal MNs (35). As this transgene lacks an N-terminal HA-tag, a specific immunostaining for transgene-derived NRG1 type I could not be performed. However, immunostaining for the ICD produced an extensive signal at the MN surface of *NRG1^{typeI}* mice (Fig. 7h) analogous to that obtained in *HA-NRG1^{FL}* mice. Moreover, immunostaining for M2 AChRs showed their enlarged distribution on the MN surface, similar to that observed in *HA-NRG1^{FL}* mice (Fig. 7i). However, in stark contrast to *HA-NRG1^{FL}* mice, VACHT immunostaining revealed a profound increase in the number and size of presynaptic cholinergic terminals innervating the MN surface (Fig. 8a, b). Nevertheless, we found no concomitant increase in the number of ChAT-positive V0_C neurons in *NRG1^{typeI}* mice (V0_C interneuron numbers per section, expressed as mean ± SEM: WT, 2.37 ± 0.32, n = 8 sections; *NRG1^{typeI}* 1.74 ± 0.32, n = 14 sections; p > 0.05), strongly suggesting that C-bouton synaptogenesis was abnormally stimulated in *NRG1^{typeI}* mice. Many of these VACHT-positive puncta were associated with neighboring postsynaptic S1R-positive patches, which did not overlap with pan-NRG1 signal, in the same way as occurs in WT (Fig. 7h). In addition, S1R clusters in *NRG1^{typeI}* mice were not enlarged when compared with those in WT (Fig. 8d). This is in contrast to that was observed in *HA-NRG1^{FL}* mice, in which surface-associate S1R labeling is largely expanded together with NRG1. Kv2.1 clusters were not detected in *NRG1^{typeI}* mouse MNs (Fig. 8e).

Ultrastructural examination confirmed the presence of enlarged presynaptic terminals on the MN soma surface, matching only partially with post-synaptic SSC; moreover, the amplified formation of SSC-like ER-plasma membrane contacts in *HA-NRG1^{FL}* mice was not observed in *NRG1^{typeI}* mice (Fig. 9b). This suggests that NRG1 type I is mainly targeted to the MN plasma membrane, whereas NRG1 type III is preferentially located to C-bouton SSCs. As Kv2.1 is a protein specifically linked to ER-plasma-membrane junctions (e.g. at SSCs) (48), its expanded or, alternatively, reduced expression detected in *HA-NRG1^{FL}* or *NRG1^{typeI}* mice, respectively, is consistent with this interpretation. A summary of idealized C-bouton phenotypes in NRG1 transgenic mice is depicted in Fig. 9c.

C-boutons and associated NRG1 clusters are absent in ALS-resistant OCM (abducens cranial nerve [CN] VI) MNs (12), but present in other brainstem motor nuclei. Therefore, we next examined the impact of NRG1 overexpression in brainstem MNs of NRG1 transgenic mouse lines (Suppl. Fig. 6a-f). Consistent with our above findings, non-OCM MNs (facial [CNVII], hypoglossus [CNXII] and ambiguous [CNX] nuclei) displayed similar effects of NRG1 overexpression on C-bouton structure as described for spinal cord MNs, including an increased number of VACHT-containing synaptic afferents in NRG1 type I overexpressing transgenic mice (Suppl. Fig. 6c). NRG1 labeling patterns in OCM MNs of *NRG1^{typeI}* *HA-NRG1^{FL}* mice were also comparable to those observed in non-OCM MNs. However, as in WT (Suppl. Fig. 6d), we never observed VACHT-positive C-boutons on the surface of transgenic OCM MNs (Suppl. Fig. 6e-f). These findings strongly suggest that NRG1 type I promotes C-bouton synaptogenesis also at non-OCM MNs, but that additional factors are required to promote cholinergic synaptogenesis in OCM MNs.

Altogether, these findings suggest that: 1) full-length NRG1 type III acts as a specific organizer of postsynaptic SSC-like membrane compartments without a major impact on the C-bouton presynaptic counterpart, 2) NRG1 type I promotes presynaptic C-bouton synaptogenesis, with no influence on biogenesis or molecular architecture of co-aligned SSC, and 3) there is partial independence of pre- and postsynaptic C-bouton development. Thus, specific signaling functions related to the distinct spatial arrangement of NRG1 isoforms are involved in the complex matching of pre- and postsynaptic elements at C-boutons.

Discussion

To provide a better understanding of the role of C-boutons and associated NRG1 assemblies in MN diseases, we describe here novel aspects of their biology and responses when subjected to

distinct paradigms of experimental MN injury. Stimulation and *ex vivo* slicing experiments revealed that C-bouton-associated NRG1 assemblies are extremely sensitive to acute cellular stress. This probably reflects their tight association with SSCs, a specialized form of highly dynamic cortical ER, which is closely apposed to the postsynaptic plasma membrane of C-boutons. In fact, rapid and reversible ER fission occurs after neuronal depolarization, and synaptic activity modulates ER structure via Ca^{2+} transients (49, 50). In addition, Kv2.1 clusters in ER-plasma-membrane junctions, which are homologous structures to SSCs, are highly dynamic and unstable when exposed to moderate stress (48). We report here that moderate levels of either electrical or chemical stimulation induce an enlargement of VACHT-labeled presynaptic terminals and their associated postsynaptic NRG1 clusters. This is in congruence with data reported in the context of electrical stimulation of proprioceptive afferents to MNs (51). The dependence of NRG1 clusters on the structural integrity of cortical ER was further confirmed by induction of ER-stress with tunicamycin, which severely disrupted NRG1 clusters without affecting the number and size of VACHT-positive terminals. This observation is distinct from our findings in MNs following axotomy in which the dispersion of NRG1 clusters at C-boutons takes place at a slower time scale compared to the loss of presynaptic terminals, the latter presumably being mediated by reactive microglia.

We also confirm our previous observations that C-boutons are preferred sites to be contacted by reactive microglia in injured MNs post-axotomy (11) and provide new data concerning the involvement of microglial cells in synaptic removal in this pathological condition. At present, the molecular substrate of this positive chemotactic effect is unknown. NRG1/ErbB signaling promotes microglial chemotaxis *in vitro* and in spinal cord dorsal horn after peripheral nerve injury (52, 53), and antagonizing NRG1 signaling results in a reduction of microgliosis and MN death in mutant SOD1 ALS mice (54). Thus, whether NRG1/ErbB signaling also operates during C-bouton-directed microglial sensing after axotomy should be further explored.

We found no evidence for the engulfment of presynaptic elements by microglial processes recruited in the vicinity of axotomized MNs. This is in accordance with the classical description of microglial activation and synaptic removal that occurs during the response of MN cell bodies to axotomy (33). However, in contrast to these studies, we unambiguously observed degenerating presynaptic boutons contacting lesioned MNs in close association with perineuronally-recruited microglia. This suggests an active role of microglia in the disintegration of presynaptic terminals by means of a target-directed toxic mechanism instead of bulk phagocytosis. Activated microglia produce free oxygen radicals, nitric oxide, proteases

and cytokines (55), all of which could be neurotoxic in a local microenvironment and induce extrinsic apoptosis (56) or extracellular digestion (“exophagy”) of synaptic debris (57). In congruence with this idea, superoxide ions produced by microglial cells induce apoptotic death of Purkinje neurons in organotypic slice cultures (58), and macrophage-derived TNF α signals developmental MN death (59). Since axons can activate degenerative/apoptotic molecular pathways without resulting in cell death of the parent neuron (60), it is plausible that a similar, spatially restricted mechanism operates at presynaptic axon terminals (61).

Our data suggest that NRG1 ‘declustering’ is related to a microglia-dependent disruption of cholinergic presynaptic terminals, in conjunction with ER-stress/reorganization inherent to a chromatolytic reaction. We demonstrate that C-bouton disruption in axotomized MNs is prevented when ER-stress or microglial activation is inhibited by salubrinal treatment. Our data also indicate that removal of afferent terminals, including C-boutons, precedes postsynaptic NRG1 declustering and removal. This interpretation is supported by the presence of activated microglia in close proximity to denervated, SSC-containing postsynaptic sites of MN somata. Resting microglia perform specific and transient mutual contacts and serve as a vigilant surveyor of synaptic activity. During pathological conditions, microglial processes extensively enwrap synaptic boutons that will be later removed (42). However, in agreement with a classic study (33), we found no ultrastructural evidence for the engulfment of embraced axon terminals into phagosomes of activated microglia adjacent to axotomized MN somata.

Axonal regeneration following nerve crush frequently results in restored peripheral nerve function 6-8 weeks after injury (34, 62). Our analysis of cholinergic C-boutons are comparable with previous studies (34) showing their recovery after either irreversible transection or crush. However, to which extend their function is restored is currently unclear. In fact, the size of postsynaptic NRG1 clusters was not fully restored after irreversible nerve transection, but almost completely reestablished after (more permissive) injury following nerve crush. This is another example of the relative independence of pre- and postsynaptic components of C-boutons during development and adult plasticity. C-bouton density in MNs also depends on competition with other types of synapses in an activity and space-dependent manner (63). For instance, the loss of vesicular glutamate transporter 1 (VGLUT1)-containing boutons (derived from proprioceptive sensory afferents) from axotomized MNs is not restored during peripheral regeneration (34). This indicates that peripheral nerve injury induces permanent deficits in the function and plasticity of central synaptic connections, but the inability to restore proprioceptive afferent may favor regeneration of cholinergic inputs to lesioned MNs.

Our findings in NRG1 transgenic mice demonstrate that altered expression levels (and most likely signaling activities) of NRG1 isoforms differentially affect molecular and structural features of C-boutons. These results reveal a previously unknown role of distinct NRG1 isoforms as selective organizers of pre- and post-synaptic components of cholinergic C-boutons at the receptive somatodendritic compartment of spinal MNs and adds to established functions of NRG1 in the neuromuscular system, such as: 1) differentiation and survival of Schwann cells (64); 2) myelination of peripheral axons (35, 36, 65, 66); 3) terminal Schwann cell-mediated remodeling of neuromuscular junctions (19); and 4) regulation nicotinic AChRs clustering at the neuromuscular junction (67).

Specifically, we show that NRG1 type III serves as a postsynaptic SSC organizer with no major impact on the formation or structure of presynaptic VACHT-positive terminals. In contrast, NRG1 type I stimulates a substantial increase in the number and size of cholinergic inputs without driving the development of an equally enlarged SSC. The exact mechanism and functional consequences of NRG1 type I-mediated effects on presynaptic terminal growth and NRG1 type III-induced SSC enlargement are currently unknown and require further investigation. ER-plasma membrane contacts are involved in calcium homeostasis by means of a mechanism referred to as “store operated calcium entry” (SOCE). An essential protein in this process is STIM1, which, when overexpressed, induces multilayered stacks of cortical ER (68) comparable to those produced in MNs of NRG1 type III overexpressing mice. In our study, enlarged ER-derived planar stacks displayed distinct subdomains that, in addition to NRG1, were enriched in SR1 and Kv2.1, as expected for redundant SSCs. It is interesting to note that the sole overexpression of Kv2.1 is sufficient to induce ER-plasma-membrane junctions (48). Since S1R plays a role as a SOCE regulator in a variety of systems, this suggests that SSC at C-boutons serve as a Ca^{2+} microdomain and that NRG1 type III-mediated changes of SSC architecture could recruit STIM1 functions, thereby shaping the temporal and spatial fine-tuning of intracellular Ca^{2+} at this specific site (69). Stimulation of both NRG1 type I and type III-mediated signaling impacts on the accumulation of M2 AChRs at the postsynaptic plasma membrane. Thus, the concept of NRG1-regulated functional interactions of M2 AChRs with other postsynaptic components of C-type synapses, e. g. Kv2.1 potassium channels (7) requires further investigations. Kv2.1 channels form highly dynamic clusters on the plasma membrane of cortical neurons (70), may contribute to homeostatic adaptation of MN excitability during pathologic conditions, and axotomy results in a loss of Kv2.1 clusters at C-boutons (71). Of note, NRG2, which is structurally related to NRG1 type I, accumulates in close proximity to Kv2.1 clusters in the plasma membrane atop intracellular SSCs in cortical interneurons and

NRG2/ErbB4 serve a negative feedback loop that controls NMDA function (72). Moreover, NRG1 type I colocalizes with NRG2 and Kv2.1 channel clusters in cultured hippocampal neurons (20). These findings indicate that NRG isoforms constitute a diverse set of spatially compartmentalized postsynaptic signaling molecules that play an important role during C-bouton differentiation. Possible additional functions in the modulation of plasma membrane/SSC interactions and chemical transmission at C-boutons and cortical synapses will require further studies.

Altered spinal cord expression of NRG1 isoforms occurs in a SOD1 ALS mouse model (73), and loss of C-bouton-associated NRG1 assemblies in this mouse model and in human ALS have been observed (12, 74). Similarly, increased activation of ErbB receptors was found in inflammatory microglia in ALS mouse models and human patients (73, 75). Recently, NRG1 signaling was directly targeted in SOD1-ALS mice by virus-mediated delivery of NRG1 type III to the spinal cord, which resulted in an extended survival time and reduced C-bouton loss, whereas NRG1 type I expression had no effect (74). NRG1 type I overexpression confined to the muscle promoted axonal collateral sprouting and muscle reinnervation, but failed to improve clinical outcome (76). On the other hand, blocking NRG1 signaling reduced microglial activation and slowed disease progression (54). Taken together, these data indicate that pleiotropic NRG1 activities may account for the variable and to some extend discrepant outcomes when analyzed in the context of distinct therapeutic approaches.

In conclusion, our study identifies plastic C-bouton changes in well-defined experimental models of MN injury and reveals previously unknown functions of distinct NRG1 isoforms in C-bouton architecture. Our data provide a refined framework for the involvement of C-boutons in the pathophysiology of MN diseases, such as ALS. Since C-boutons regulate MN excitability, contribute to MN vulnerability and orchestrate neuroinflammatory glial responses after nerve injury, the targeting of C-bouton-embedded signaling modules, such as the NRG1/ErbB axis, should be further explored in support of novel treatment strategies for ALS and other MN disorders.

Acknowledgements

We would like to thank Klaus A. Nave for advice and kindly supplying NRG1 mutant mice, Jesús María López, Ester Desfilis and José Antonio Moreno for providing spinal cord samples from non-rodent animals. Anaïs Panosa and Xavier Calomarde for technical support with confocal and electron microscopy, and the SCT animal facility of the University of Lleida for

mouse care and housing. This work was supported by grants to JEE and JC from the Spanish *Ministerio de Economía y Competitividad* co-financed by FEDER (SAF2015-70801-R). SS holds a grant from Spanish *Ministerio de Educación, Cultura y Deporte* (FPU). MHS holds a Heisenberg Fellowship from the Deutsche Forschungsgemeinschaft (DFG) and acknowledges funding by a DFG research grant (SCHW741/4-1).

Author contributions: JEE, MHS, AC and JC conceived and designed research. SS, AC, OT, LP, MCS-B, MS, SH and JEE performed research. AC, SS, JC, MHS and JEE analyzed data. JEE, JC, AC and MHS wrote the paper.

Conflict of interest: The authors declare that no conflict of interest exists.

References

1. Rekling, J. C., Funk, G. D., Bayliss, D. A., Dong, X. W., and Feldman, J. L. (2000) Synaptic control of motoneuronal excitability. *Physiol Rev* **80**, 767-852
2. Kanning, K. C., Kaplan, A., and Henderson, C. E. (2010) Motor neuron diversity in development and disease. *Annu Rev Neurosci* **33**, 409-440
3. Miles, G. B., Hartley, R., Todd, A. J., and Brownstone, R. M. (2007) Spinal cholinergic interneurons regulate the excitability of motoneurons during locomotion. *Proc Natl Acad Sci U S A* **104**, 2448-2453
4. Zagoraiou, L., Akay, T., Martin, J. F., Brownstone, R. M., Jessell, T. M., and Miles, G. B. (2009) A cluster of cholinergic premotor interneurons modulates mouse locomotor activity. *Neuron* **64**, 645-662
5. Conradi, S. (1969) Ultrastructure of dorsal root boutons on lumbosacral motoneurons of the adult cat, as revealed by dorsal root section. *Acta Physiol Scand Suppl* **332**, 85-115
6. Hellström, J., Oliveira, A. L. R., Meister, B., and Cullheim, S. (2003) Large cholinergic nerve terminals on subsets of motoneurons and their relation to muscarinic receptor type 2. *Journal of Comparative Neurology* **460**, 476-486
7. Muennich, E. A., and Fyffe, R. E. (2004) Focal aggregation of voltage-gated, Kv2.1 subunit-containing, potassium channels at synaptic sites in rat spinal motoneurones. *J Physiol* **554**, 673-685

8. Deardorff, A. S., Romer, S. H., Deng, Z., Bullinger, K. L., Nardelli, P., Cope, T. C., and Fyffe, R. E. (2013) Expression of postsynaptic Ca²⁺-activated K⁺ (SK) channels at C-bouton synapses in mammalian lumbar α-motoneurons. *J Physiol* **591**, 875-897
9. Mavlyutov, T. A., Epstein, M. L., Verbny, Y. I., Huerta, M. S., Zaitoun, I., Ziskind-Conhaim, L., and Ruoho, A. E. (2013) Lack of sigma-1 receptor exacerbates ALS progression in mice. *Neuroscience* **240**, 129-134
10. Deardorff, A. S., Romer, S. H., Sonner, P. M., and Fyffe, R. E. (2014) Swimming against the tide: investigations of the C-bouton synapse. *Front Neural Circuits* **8**, 106
11. Casanovas, A., Salvany, S., Lahoz, V., Tarabal, O., Piedrafita, L., Sabater, R., Hernandez, S., Caldero, J., and Esquerda, J. E. (2017) Neuregulin 1-ErbB module in C-bouton synapses on somatic motor neurons: molecular compartmentation and response to peripheral nerve injury. *Sci Rep* **7**, 40155
12. Gallart-Palau, X., Tarabal, O., Casanovas, A., Sabado, J., Correa, F. J., Hereu, M., Piedrafita, L., Calderó, J., and Esquerda, J. E. (2014) Neuregulin-1 is concentrated in the postsynaptic subsurface cistern of C-bouton inputs to alpha-motoneurons and altered during motoneuron diseases. *Faseb Journal* **28**, 3618-3632
13. Buonanno, A., and Fischbach, G. D. (2001) Neuregulin and ErbB receptor signaling pathways in the nervous system. *Curr Opin Neurobiol* **11**, 287-296
14. Mei, L., and Nave, K. A. (2014) Neuregulin-ERBB signaling in the nervous system and neuropsychiatric diseases. *Neuron* **83**, 27-49
15. Wolpowitz, D., Mason, T. B., Dietrich, P., Mendelsohn, M., Talmage, D. A., and Role, L. W. (2000) Cysteine-rich domain isoforms of the neuregulin-1 gene are required for maintenance of peripheral synapses. *Neuron* **25**, 79-91
16. Willem, M. (2016) Proteolytic processing of Neuregulin-1. *Brain Res Bull* **126**, 178-182
17. Meyer, D., Yamaai, T., Garratt, A., Riethmacher-Sonnenberg, E., Kane, D., Theill, L. E., and Birchmeier, C. (1997) Isoform-specific expression and function of neuregulin. *Development* **124**, 3575-3586
18. Yang, X., Kuo, Y., Devay, P., Yu, C., and Role, L. (1998) A cysteine-rich isoform of neuregulin controls the level of expression of neuronal nicotinic receptor channels during synaptogenesis. *Neuron* **20**, 255-270
19. Lee, Y. I., Li, Y., Mikesh, M., Smith, I., Nave, K. A., Schwab, M. H., and Thompson, W. J. (2016) Neuregulin1 displayed on motor axons regulates terminal Schwann cell-mediated synapse elimination at developing neuromuscular junctions. *Proceedings of the National Academy of Sciences of the United States of America* **113**, E479-E487

20. Vullhorst, D., Ahmad, T., Karavanova, I., Keating, C., and Buonanno, A. (2017) Structural Similarities between Neuregulin 1-3 Isoforms Determine Their Subcellular Distribution and Signaling Mode in Central Neurons. *Journal of Neuroscience* **37**, 5232-5249
21. Kitzman, P. (2006) Changes in vesicular glutamate transporter 2, vesicular GABA transporter and vesicular acetylcholine transporter labeling of sacrocaudal motoneurons in the spastic rat. *Exp Neurol* **197**, 407-419
22. Dukkipati, S. S., Chihi, A., Wang, Y., and Elbasiouny, S. M. (2017) Experimental Design and Data Analysis Issues Contribute to Inconsistent Results of C-Bouton Changes in Amyotrophic Lateral Sclerosis. *eNeuro* **4**
23. Nagao, M., Misawa, H., Kato, S., and Hirai, S. (1998) Loss of cholinergic synapses on the spinal motor neurons of amyotrophic lateral sclerosis. *J Neuropathol Exp Neurol* **57**, 329-333
24. Pullen, A. H., and Athanasiou, D. (2009) Increase in presynaptic territory of C-terminals on lumbar motoneurons of G93A SOD1 mice during disease progression. *Eur J Neurosci* **29**, 551-561
25. Herron, L. R., and Miles, G. B. (2012) Gender-specific perturbations in modulatory inputs to motoneurons in a mouse model of amyotrophic lateral sclerosis. *Neuroscience* **226**, 313-323
26. Saxena, S., Roselli, F., Singh, K., Leptien, K., Julien, J. P., Gros-Louis, F., and Caroni, P. (2013) Neuroprotection through Excitability and mTOR Required in ALS Motoneurons to Delay Disease and Extend Survival. *Neuron* **80**, 80-96
27. Milan, L., Courtand, G., Cardoit, L., Masmejean, F., Barriere, G., Cazalets, J. R., Garret, M., and Bertrand, S. S. (2015) Age-Related Changes in Pre- and Postsynaptic Partners of the Cholinergic C-Boutons in Wild-Type and SOD1G93A Lumbar Motoneurons. *PLOS One* **10**, e0135525
28. Luty, A. A., Kwok, J. B., Dobson-Stone, C., Loy, C. T., Coupland, K. G., Karlstrom, H., Sobow, T., Tchorzewska, J., Maruszak, A., Barcikowska, M., Panegyres, P. K., Zekanowski, C., Brooks, W. S., Williams, K. L., Blair, I. P., Mather, K. A., Sachdev, P. S., Halliday, G. M., and Schofield, P. R. (2010) Sigma nonopioid intracellular receptor 1 mutations cause frontotemporal lobar degeneration-motor neuron disease. *Ann Neurol* **68**, 639-649
29. Al-Saif, A., Al-Mohanna, F., and Bohlega, S. (2011) A mutation in sigma-1 receptor causes juvenile amyotrophic lateral sclerosis. *Ann Neurol* **70**, 913-919

30. Mavlyutov, T. A., Guo, L. W., Epstein, M. L., and Ruoho, A. E. (2015) Role of the Sigma-1 receptor in Amyotrophic Lateral Sclerosis (ALS). *J Pharmacol Sci* **127**, 10-16
31. Aliaga, L., Lai, C., Yu, J., Chub, N., Shim, H., Sun, L., Xie, C., Yang, W. J., Lin, X., O'Donovan, M. J., and Cai, H. (2013) Amyotrophic lateral sclerosis-related VAPB P56S mutation differentially affects the function and survival of corticospinal and spinal motor neurons. *Hum Mol Genet* **22**, 4293-4305
32. Takahashi, Y., Fukuda, Y., Yoshimura, J., Toyoda, A., Kurppa, K., Moritoyo, H., Belzil, V. V., Dion, P. A., Higasa, K., Doi, K., Ishiura, H., Mitsui, J., Date, H., Ahsan, B., Matsukawa, T., Ichikawa, Y., Moritoyo, T., Ikoma, M., Hashimoto, T., Kimura, F., Murayama, S., Onodera, O., Nishizawa, M., Yoshida, M., Atsuta, N., Sobue, G., Fifita, J. A., Williams, K. L., Blair, I. P., Nicholson, G. A., Gonzalez-Perez, P., Brown, R. H., Nomoto, M., Elenius, K., Rouleau, G. A., Fujiyama, A., Morishita, S., Goto, J., Tsuji, S., and JaCALs. (2013) ERBB4 Mutations that Disrupt the Neuregulin-ErbB4 Pathway Cause Amyotrophic Lateral Sclerosis Type 19. *American Journal of Human Genetics* **93**, 900-905
33. Blinzingher, K., and Kreutzberg, G. (1968) Displacement of synaptic terminals from regenerating motoneurons by microglial cells. *Z Zellforsch Mikrosk Anat* **85**, 145-157
34. Alvarez, F. J., Titus-Mitchell, H. E., Bullinger, K. L., Kraszpulski, M., Nardelli, P., and Cope, T. C. (2011) Permanent central synaptic disconnection of proprioceptors after nerve injury and regeneration. I. Loss of VGLUT1/IA synapses on motoneurons. *J Neurophysiol* **106**, 2450-2470
35. Michailov, G. V., Sereda, M. W., Brinkmann, B. G., Fischer, T. M., Haug, B., Birchmeier, C., Role, L., Lai, C., Schwab, M. H., and Nave, K. A. (2004) Axonal neuregulin-1 regulates myelin sheath thickness. *Science* **304**, 700-703
36. Velanac, V., Unterbarnscheidt, T., Hinrichs, W., Gummert, M. N., Fischer, T. M., Rossner, M. J., Trimarco, A., Brivio, V., Taveggia, C., Willem, M., Haass, C., Mobius, W., Nave, K. A., and Schwab, M. H. (2012) Bace1 processing of NRG1 type III produces a myelin-inducing signal but is not essential for the stimulation of myelination. *Glia* **60**, 203-217
37. Carp, J. S., Tennissen, A. M., Mongeluzi, D. L., Dudek, C. J., Chen, X. Y., and Wolpaw, J. R. (2008) An in vitro protocol for recording from spinal motoneurons of adult rats. *J Neurophysiol* **100**, 474-481
38. Chery, N., Yu, X. H., and de Koninck, Y. (2000) Visualization of lamina I of the dorsal horn in live adult rat spinal cord slices. *J Neurosci Methods* **96**, 133-142
39. Watson, C., Paxinos, G., G., K., and Heise, C. (2009) *The spinal cord*, Elsevier, Amsterdam

40. Moghaddasi, M., Velumian, A. A., Zhang, L., and Fehlings, M. G. (2007) An ex vivo preparation of mature mice spinal cord to study synaptic transmission on motoneurons. *J Neurosci Methods* **159**, 1-7
41. Aldskogius, H., and Kozlova, E. N. (1998) Central neuron-glial and glial-glial interactions following axon injury. *Progress in neurobiology* **55**, 1-26
42. Wake, H., Moorhouse, A. J., Jinno, S., Kohsaka, S., and Nabekura, J. (2009) Resting microglia directly monitor the functional state of synapses in vivo and determine the fate of ischemic terminals. *The Journal of neuroscience : the official journal of the Society for Neuroscience* **29**, 3974-3980
43. Schafer, D. P., Lehrman, E. K., Kautzman, A. G., Koyama, R., Mardinaly, A. R., Yamasaki, R., Ransohoff, R. M., Greenberg, M. E., Barres, B. A., and Stevens, B. (2012) Microglia sculpt postnatal neural circuits in an activity and complement-dependent manner. *Neuron* **74**, 691-705
44. Penas, C., Pascual-Font, A., Mancuso, R., Fores, J., Casas, C., and Navarro, X. (2011) Sigma receptor agonist 2-(4-morpholinethyl)1 phenylcyclohexanecarboxylate (Pre084) increases GDNF and BiP expression and promotes neuroprotection after root avulsion injury. *Journal of neurotrauma* **28**, 831-840
45. Li, S., Yang, L., Selzer, M. E., and Hu, Y. (2013) Neuronal endoplasmic reticulum stress in axon injury and neurodegeneration. *Annals of neurology* **74**, 768-777
46. Boyce, M., Bryant, K. F., Jousse, C., Long, K., Harding, H. P., Scheuner, D., Kaufman, R. J., Ma, D., Coen, D. M., Ron, D., and Yuan, J. (2005) A selective inhibitor of eIF2alpha dephosphorylation protects cells from ER stress. *Science* **307**, 935-939
47. Saxena, S., Cabuy, E., and Caroni, P. (2009) A role for motoneuron subtype-selective ER stress in disease manifestations of FALS mice. *Nature neuroscience* **12**, 627-636
48. Fox, P. D., Haberkorn, C. J., Akin, E. J., Seel, P. J., Krapf, D., and Tamkun, M. M. (2015) Induction of stable ER-plasma-membrane junctions by Kv2.1 potassium channels. *Journal of cell science* **128**, 2096-2105
49. Kucharz, K., Krogh, M., Ng, A. N., and Toresson, H. (2009) NMDA receptor stimulation induces reversible fission of the neuronal endoplasmic reticulum. *PLoS One* **4**, e5250
50. Kucharz, K., Wieloch, T., and Toresson, H. (2011) Potassium-induced structural changes of the endoplasmic reticulum in pyramidal neurons in murine organotypic hippocampal slices. *J Neurosci Res* **89**, 1150-1159
51. Gajewska-Wozniak, O., Grycz, K., Czarkowska-Bauch, J., and Skup, M. (2016) Electrical Stimulation of Low-Threshold Proprioceptive Fibers in the Adult Rat Increases Density

- of Glutamatergic and Cholinergic Terminals on Ankle Extensor alpha-Motoneurons.
PLoS One **11**, e0161614
52. Calvo, M., Zhu, N., Tsantoulas, C., Ma, Z., Grist, J., Loeb, J. A., and Bennett, D. L. (2010) Neuregulin-ErbB signaling promotes microglial proliferation and chemotaxis contributing to microgliosis and pain after peripheral nerve injury. *The Journal of neuroscience : the official journal of the Society for Neuroscience* **30**, 5437-5450
53. Calvo, M., Zhu, N., Grist, J., Ma, Z., Loeb, J. A., and Bennett, D. L. (2011) Following nerve injury neuregulin-1 drives microglial proliferation and neuropathic pain via the MEK/ERK pathway. *Glia* **59**, 554-568
54. Liu, M., Solomon, W., Cespedes, J. C., Wilson, N. O., Ford, B., and Stiles, J. K. (2018) Neuregulin-1 attenuates experimental cerebral malaria (ECM) pathogenesis by regulating ErbB4/AKT/STAT3 signaling. *J Neuroinflammation* **15**, 104
55. Madry, C., Kyrargyri, V., Arancibia-Carcamo, I. L., Jolivet, R., Kohsaka, S., Bryan, R. M., and Attwell, D. (2018) Microglial Ramification, Surveillance, and Interleukin-1beta Release Are Regulated by the Two-Pore Domain K(+) Channel THIK-1. *Neuron* **97**, 299-312 e296
56. Galluzzi, L., Vitale, I., Aaronson, S. A., Abrams, J. M., Adam, D., Agostinis, P., Alnemri, E. S., Altucci, L., Amelio, I., Andrews, D. W., Annicchiarico-Petruzzelli, M., Antonov, A. V., Arama, E., Baehrecke, E. H., Barlev, N. A., Bazan, N. G., Bernassola, F., Bertrand, M. J., Bianchi, K., Blagosklonny, M. V., Blomgren, K., Borner, C., Boya, P., Brenner, C., Campanella, M., Candi, E., Carmona-Gutierrez, D., Cecconi, F., Chan, F. K., Chandel, N. S., Cheng, E. H., Chipuk, J. E., Cidlowski, J. A., Ciechanover, A., Cohen, G. M., Conrad, M., Cubillos-Ruiz, J. R., Czabotar, P. E., D'Angiolella, V., Dawson, T. M., Dawson, V. L., De Laurenzi, V., De Maria, R., Debatin, K. M., DeBerardinis, R. J., Deshmukh, M., Di Daniele, N., Di Virgilio, F., Dixit, V. M., Dixon, S. J., Duckett, C. S., Dynlacht, B. D., El-Deiry, W. S., Elrod, J. W., Fimia, G. M., Fulda, S., Garcia-Saez, A. J., Garg, A. D., Garrido, C., Gavathiotis, E., Golstein, P., Gottlieb, E., Green, D. R., Greene, L. A., Gronemeyer, H., Gross, A., Hajnoczky, G., Hardwick, J. M., Harris, I. S., Hengartner, M. O., Hetz, C., Ichijo, H., Jaattela, M., Joseph, B., Jost, P. J., Juin, P. P., Kaiser, W. J., Karin, M., Kaufmann, T., Kepp, O., Kimchi, A., Kitsis, R. N., Klionsky, D. J., Knight, R. A., Kumar, S., Lee, S. W., Lemasters, J. J., Levine, B., Linkermann, A., Lipton, S. A., Lockshin, R. A., Lopez-Otin, C., Lowe, S. W., Luedde, T., Lugli, E., MacFarlane, M., Madeo, F., Malewicz, M., Malorni, W., Manic, G., Marine, J. C., Martin, S. J., Martinou, J. C., Medema, J. P., Mehlen, P., Meier, P., Melino, S., Miao, E. A., Molkentin, J. D., Moll, U. M., Munoz-Pinedo, C., Nagata, S., Nunez, G., Oberst, A., Oren, M., Overholtzer, M., Pagano, M.,

- Panaretakis, T., Pasparakis, M., Penninger, J. M., Pereira, D. M., Pervaiz, S., Peter, M. E., Piacentini, M., Pinton, P., Prehn, J. H. M., Puthalakath, H., Rabinovich, G. A., Rehm, M., Rizzuto, R., Rodrigues, C. M. P., Rubinsztein, D. C., Rudel, T., Ryan, K. M., Sayan, E., Scorrano, L., Shao, F., Shi, Y., Silke, J., Simon, H. U., Sistigu, A., Stockwell, B. R., Strasser, A., Szabadkai, G., Tait, S. W. G., Tang, D., Tavernarakis, N., Thorburn, A., Tsujimoto, Y., Turk, B., Vanden Berghe, T., Vandenabeele, P., Vander Heiden, M. G., Villunger, A., Virgin, H. W., Vousden, K. H., Vucic, D., Wagner, E. F., Walczak, H., Wallach, D., Wang, Y., Wells, J. A., Wood, W., Yuan, J., Zakeri, Z., Zhivotovsky, B., Zitvogel, L., Melino, G., and Kroemer, G. (2018) Molecular mechanisms of cell death: recommendations of the Nomenclature Committee on Cell Death 2018. *Cell Death Differ* **25**, 486-541
57. Acharjee, S., Verbeek, M., Gomez, C. D., Bisht, K., Lee, B., Benoit, L., Sharkey, K. A., Benediktsson, A., Tremblay, M. E., and Pittman, Q. J. (2018) Reduced Microglial Activity and Enhanced Glutamate Transmission in the Basolateral Amygdala in Early CNS Autoimmunity. *The Journal of neuroscience : the official journal of the Society for Neuroscience* **38**, 9019-9033
58. Marin-Teva, J. L., Dusart, I., Colin, C., Gervais, A., van Rooijen, N., and Mallat, M. (2004) Microglia promote the death of developing Purkinje cells. *Neuron* **41**, 535-547
59. Sedel, F., Bechade, C., Vyas, S., and Triller, A. (2004) Macrophage-derived tumor necrosis factor alpha, an early developmental signal for motoneuron death. *The Journal of neuroscience : the official journal of the Society for Neuroscience* **24**, 2236-2246
60. Cusack, C. L., Swahari, V., Hampton Henley, W., Michael Ramsey, J., and Deshmukh, M. (2013) Distinct pathways mediate axon degeneration during apoptosis and axon-specific pruning. *Nat Commun* **4**, 1876
61. Mattson, M. P., Keller, J. N., and Begley, J. G. (1998) Evidence for synaptic apoptosis. *Exp Neurol* **153**, 35-48
62. Nguyen, Q. T., Sanes, J. R., and Lichtman, J. W. (2002) Pre-existing pathways promote precise projection patterns. *Nature neuroscience* **5**, 861-867
63. Jiang, Y. Q., Zaaimi, B., and Martin, J. H. (2016) Competition with Primary Sensory Afferents Drives Remodeling of Corticospinal Axons in Mature Spinal Motor Circuits. *The Journal of neuroscience : the official journal of the Society for Neuroscience* **36**, 193-203
64. Syroid, D. E., Maycox, P. R., Burrola, P. G., Liu, N., Wen, D., Lee, K. F., Lemke, G., and Kilpatrick, T. J. (1996) Cell death in the Schwann cell lineage and its regulation by neuregulin. *Proc Natl Acad Sci U S A* **93**, 9229-9234

65. Nave, K. A., and Salzer, J. L. (2006) Axonal regulation of myelination by neuregulin 1. *Curr Opin Neurobiol* **16**, 492-500
66. Stassart, R. M., Fledrich, R., Velanac, V., Brinkmann, B. G., Schwab, M. H., Meijer, D., Sereda, M. W., and Nave, K. A. (2013) A role for Schwann cell-derived neuregulin-1 in remyelination. *Nature neuroscience* **16**, 48-54
67. Ngo, S. T., Cole, R. N., Sunn, N., Phillips, W. D., and Noakes, P. G. (2012) Neuregulin-1 potentiates agrin-induced acetylcholine receptor clustering through muscle-specific kinase phosphorylation. *Journal of cell science* **125**, 1531-1543
68. Orci, L., Ravazzola, M., Le Coadic, M., Shen, W. W., Demaurex, N., and Cosson, P. (2009) From the Cover: STIM1-induced precortical and cortical subdomains of the endoplasmic reticulum. *Proc Natl Acad Sci U S A* **106**, 19358-19362
69. Giordano, F., Saheki, Y., Ideval-Hagren, O., Colombo, S. F., Pirruccello, M., Milosevic, I., Gracheva, E. O., Bagriantsev, S. N., Borgese, N., and De Camilli, P. (2013) PI(4,5)P(2)-dependent and Ca(2+)-regulated ER-PM interactions mediated by the extended synaptotagmins. *Cell* **153**, 1494-1509
70. Misonou, H., Thompson, S. M., and Cai, X. (2008) Dynamic regulation of the Kv2.1 voltage-gated potassium channel during brain ischemia through neuroglial interaction. *Journal of Neuroscience* **28**, 8529-8538
71. Romer, S. H., Dominguez, K. M., Gelpi, M. W., Deardorff, A. S., Tracy, R. C., and Fyffe, R. E. (2014) Redistribution of Kv2.1 ion channels on spinal motoneurons following peripheral nerve injury. *Brain Res* **1547**, 1-15
72. Vullhorst, D., Mitchell, R. M., Keating, C., Roychowdhury, S., Karavanova, I., Tao-Cheng, J. H., and Buonanno, A. (2015) A negative feedback loop controls NMDA receptor function in cortical interneurons via neuregulin 2/ErbB4 signalling. *Nat Commun* **6**, 7222
73. Song, F., Chiang, P., Wang, J., Ravits, J., and Loeb, J. A. (2012) Aberrant neuregulin 1 signaling in amyotrophic lateral sclerosis. *J Neuropathol Exp Neurol* **71**, 104-115
74. Lasiene, J., Komine, O., Fujimori-Tonou, N., Powers, B., Endo, F., Watanabe, S., Shijie, J., Ravits, J., Horner, P., Misawa, H., and Yamanaka, K. (2016) Neuregulin 1 confers neuroprotection in SOD1-linked amyotrophic lateral sclerosis mice via restoration of C-boutons of spinal motor neurons. *Acta Neuropathol Commun* **4**, 15
75. Song, F., Chiang, P., Ravits, J., and Loeb, J. A. (2014) Activation of microglial neuregulin1 signaling in the corticospinal tracts of ALS patients with upper motor neuron signs. *Amyotroph Lateral Scler Frontotemporal Degener* **15**, 77-83

76. Mancuso, R., Martinez-Muriana, A., Leiva, T., Gregorio, D., Ariza, L., Morell, M., Esteban-Perez, J., Garcia-Redondo, A., Calvo, A. C., Atencia-Cibreiro, G., Corfas, G., Osta, R., Bosch, A., and Navarro, X. (2016) Neuregulin-1 promotes functional improvement by enhancing collateral sprouting in SOD1(G93A) ALS mice and after partial muscle denervation. *Neurobiol Dis* **95**, 168-178

Figure legends

Figure 1. C-boutons on normal spinal cord MNs (visualized by Nissl staining, blue) after double fluorescent immunolabeling. **a)** A MN soma showing the concentration of M2 AChR (green) in close apposition with VACHT-labeled synaptic terminals (red); in the enlarged insets the displacement of the presynaptic VACHT-signal with respect to the postsynaptic M2 AChR labeling can be seen. **b)** MN soma showing the close relationship of S1R (green) with VACHT-labeled synaptic terminals (red); note in the insets the displacement of S1R signal respect to VACHT reflecting the postsynaptic localization of S1R; S1R is also present on MN soma in non-synaptically associated particles (encircled), which presumably correspond to ER stacks. **c)** A MN soma showing the association between NRG1 patches (green) with VACHT-labeled synaptic terminals (red); in the enlarged insets the displacement of the presynaptic VACHT-signal with respect to the postsynaptic NRG1 labeling can be observed. **d)** A MN soma showing that clusters of NRG1 (green) co-localize with Kv2.1 potassium channels (red) at C-bouton sites; in the enlarged insets the co-localizing signal is seen in yellow. **e)** A MN somata showing the co-localization between p-ErbB2 (green) and most of the VACHT-labeled synaptic terminals (red); the enlarged insets show a detail of two VACHT-positive terminals (red), one of them colocalizing with p-ErbB2 immunolabeling (yellow). Scale bars: 10 µm in e (valid for a-d).

Figure 2. Ultrastructure of C-bouton synaptic terminals. **a)** A presynaptic terminal (colored green) apposed to the surface of a MN cell body (colored red) displaying a SSC (delimited by arrows). **b)** A coated endocytic vesicle located at the periphery of the terminal in (a) (delimited by the dotted circle) is shown. **c)** A detail of a presumably endocytic/autophagic structure (*) within the nerve terminal is shown. **d)** A detail of compartmentation of pre- and postsynaptic elements in C-bouton is shown; the extracellular space (yellow) is interposed between the presynaptic terminal (green) and the postsynaptic MN cell body (red); the postsynaptic membrane displays an intimately associated SSC (blue) that exhibits continuity with ER membranes at the MN cell body (arrow). Scale bars: 250 nm.

Figure 3. Disruption of NRG1 clusters at C-boutons in acutely stressed MNs. **a-e)** Lumbar spinal cord MNs were antidromically stimulated by electrical pulses delivered through sciatic nerve (5V, 10 Hz, 60 min). Double immunolabeling for NRG1 (green) and VACHT (blue) shows an important disruption of NRG1 clusters in stimulated MNs (**c,d)** versus those in the control side (**a,b)**. Densitometric measurements of NRG1 labeling at VACHT-positive C-bouton sites shows the presence of a NRG1-depleted population of cholinergic synapses (**e**). **f-k)** MNs in lumbar

spinal cords were subjected to orthodromic electrical field stimulation (5V, 10 Hz, 30 min). Double immunolabeling for NRG1 (green) and VACHT (blue) shows an important depletion of NRG1 in stimulated MNs (**h,i**) versus control ones (**f,g**). **j**) Ultrastructural morphology of C-bouton area from a stimulated MN shows a disrupted SSC (arrows and colored blue in the inset), and the accumulation of large vesicles and vacuoles (red * in the inset), presumably representing disorganized ER at the cortical areas (delimited by double arrows) of the MN; presynaptic terminals are colored green, whereas postsynaptic MN is colored red; ER stacks in the deeper regions of MN soma appear not altered (yellow *). **k**) Densitometric analysis of VACHT and NRG1 in individual C-boutons demonstrates the huge depletion of NRG1 after stimulation. **l-t)** Effects of acute spinal cord slicing on C-bouton organization; MN cell bodies double immunolabeled for NRG1 (green) and VACHT (blue) in a spinal cord slice from a whole body PF-perfused mouse used as control (**l,m**) and in a sample obtained from an acute spinal cord oxygenated in artificial LCR and subsequently fixed by immersion in PF for 10 min (**n,q**). Note the dispersion and fragmentation of NRG1 clusters after slicing in conjunction with a depletion of VACHT-positive puncta (**n,o**) or the near complete depletion of NRG1 clusters (**p,q**). **r,s)** Semithin plastic sections of a control-fixed MN (**r**) and a MN fixed after 10 min of slicing (**s**) showing the cytoplasmic microvacuolization induced by the slicing process. **t)** The quantification of NRG1 cluster size (in μm^2) shows its reduction after slicing, which is not prevented when a 0 Ca^{2+} medium is used. Values in graphs are shown as mean \pm SEM; *** $p < 0.001$ (Student's *t*-test [**e** and **k**] and one way ANOVA, Bonferroni's post-hoc test [**t**]); n in **e** = 184, contralateral and 219, ipsilateral; n in **k** = 117, cont. and 53, stim., and n in **t** = 42-151. Scale bar: 500 nm in **j** (250 nm in inset); 20 μm in **q** (valid for **a-d**; **f-l** and **l-p**); 10 μm in **s** (valid for **r**).

Figure 4. Correlative changes in MN cell bodies, glial cells and NRG1 clusters, and VACHT-positive C-bouton synaptic sites after axotomy (either peripheral nerve irreversible transection or crush); only data from long-term (120-180 days) crush experiments allowing permissive reinnervation are shown. **a)** Measurements of MN soma size (* $p < 0.05$ and *** $p < 0.001$ vs. 0 day, or crush vs. respective transection time point), one-way ANOVA, Bonferroni's post-hoc test); n = 14-52 MNs from 2-4 animals. **b)** Time course of microglial and astrogliol activation around axotomized MNs; * $p < 0.05$ and *** $p < 0.001$ vs. 0 day, or crush vs. respective transection time point (two-way ANOVA, Bonferroni's post-hoc test); n = 5-25 sections from 2-4 animals. **c, d)** Time course of density (**c**) and size (**d**) of VACHT- and NRG1-labeled C-boutons in axotomized MNs; * $p < 0.05$, ** $p < 0.01$ and *** $p < 0.001$ vs. respective time-point of VACHT after axotomy, or crush vs. respective transection time point (two-way ANOVA, Bonferroni's

post-hoc test); n = in **c** = 10-52 and in **d** = 25-180 MNs, from 2-4 animals. **e-h)** Microglial reaction adjacent to MN cell bodies in the axotomized (ipsi) side (7 days after lesion) (**f, g**) compared to the unoperated (contra) side (**e**); MN cell bodies are delimited by Nissl staining (blue), C-bouton sites and microglia are visualized by NRG1 (green) and Iba1 (red) immunolabeling, respectively; note the prominent microglial recruitment seen around axotomized MN cell bodies (**f, g**). A detail of the spatial relation between microglial processes (Iba1, red) and clustered NRG1 (green) at C-bouton after a 3D reconstruction is shown in **h**. **i)** Number of NRG1-positive spots interacting with microglial processes; note their rapid reduction 24 h after axotomy, indicating that C-boutons are disrupted following the initial and rapid microglial recruitment; * $p < 0.05$ and *** $p < 0.001$ vs. 0 days (one-way ANOVA, Bonferroni's post-hoc test); n = 10-21 3D reconstructed MNs. **j-k)** Interaction between microglial processes and C-bouton sites in 14 days-axotomized MNs; **j**) shows MN cell bodies (delimited by dashed lines) exhibiting microglial recruitment (Iba1, red) in relation with VACHT- (blue) and NRG1- (green) labeled puncta; note that the NRG1 spots, which are more intimately in contact with microglial processes, are devoid of VACHT immunolabeling (see the insets), suggesting that they correspond to denervated C-bouton sites; this aspect is quantified in **k**, showing the ratio between NRG1 and VACHT immunoreactivity in spots associated or not with Iba1 microglial profiles; note that postsynaptic NRG1 positive clusters still persisted in sites in which presynaptic VACHT is already removed by microglia. ** $p < 0.01$ (Student's *t*-test); n = 27 clusters in the 2 3D reconstructed MNs showed in **j**. Data in graphs are shown as mean \pm SEM. Scale bars: 50 μ m in **f** (valid for **e**); 20 μ m in **g**; 5 μ m in **h**; 20 μ m in **j**.

Figure 5. Ultrastructural alterations of MN afferent synapses in concomitance with microglial recruitment at the surface of MN somata 7days after peripheral nerve transection. **a-b)** Semithin plastic sections of control (**a**) and axotomized (**b**) MN somata; note the recruitment of microglial cells (arrows), some of them, in close contact with the MN cell body surface of the injured MN. **c-e)** Electron micrographs of cell bodies and dendrites (colored red) of unaxotomized MNs showing abundant afferent synaptic boutons (colored violet and indicated with *); normal C-type synapses are shown in (**d** and **e**); observe that presynaptic terminals filled with synaptic vesicles are in front of the postsynaptic membrane which is in close association with SSC (arrows in **d**, and colored blue in **d** and **e**); the extracellular space, interposed between pre- and postsynaptic structures, was marked in yellow in **d** and **e**. **f-l)** Ultrastructural morphology of an axotomized MN cell body (colored red) in contact with recruited microglial cell (colored green); a degenerating dark terminal synaptic bouton is interposed between both cells (*); a portion of MN surface containing a presumably

denervated SSC is seen contacting a microglial cell (delimited by a rectangle and enlarged in **g**). Another example of degenerating synaptic bouton (*), interposed between a recruited microglial cell (colored green) and an axotomized MN soma (dashed in red) is shown in **(h)**. **i-k**) A recruited microglial cell (colored green) over a denervated postsynaptic site of a C-bouton on an axotomized MN (colored red) is shown in **i**; this postsynaptic locus was formerly occupied by a presynaptic terminal which, once removed, its adjacent postsynaptic SSC structure remains as an indicator of the denervated C-bouton site; the relationship between these compartments are depicted in **j** and **k** as follows: MN soma red; microglia, green; SSC, blue; and extracellular space, yellow. Scale bars: 10 μm in **b** (valid for **a**), 500 nm in **c** and **d**, 200 nm in **e**, 1 μm in **f** and **h**, 2.5 μm in **I**, and 200 nm in **h**.

Figure 6. Animals were treated with vehicle or the ER-stress inhibitor salubrinal, subjected to sciatic nerve transection and examined 7 days later. **a-f)** The axotomized MN pool was analyzed by double immunofluorescent staining for BiP (green) and Iba1 (red). **g-l)** The same samples were labeled for Nissl (blue), NRG1 (green), VACHT (blue) and Iba1 (red). **m-p)** Quantitative analysis of changes in BiP-immunostaining intensity (**m**), microglial covering of MN soma perimeter (**n**) and density of VACHT- and NRG1-positive spots (per 100 μm^2) (**o** and **p**, respectively); note that the treatment with salubrinal significantly reverts the BiP upregulation, microglial activation and C-bouton loss that occurs in/or adjacent to axotomized MNs; Data are shown as mean \pm SEM. *** $p < 0.001$ vs. vehicle (Student's *t*-test), n (vehicle and salubrinal, respectively) = 203 and 179 MNs (in **m**); 41 and 66 MNs (in **n**); 22 and 47 MNs (in **o** and **p**), from 3 animals. Scale bars: 40 μm in **f** (valid for **a-e**) and 10 μm in **I** (valid for **g-k**).

Figure 7. Impact of the overexpression of different NRG1 isoforms in C-boutons on spinal cord MNs. **a)** Multiple fluorescent analysis of C-bouton-associated proteins in adult transgenic mice overexpressing HA-tag labeled NRG1 type III. The distribution of HA tag (red) NRG1 (visualized with an anti-pan-NRG1 antibody, green), and VACHT (blue) was detected in a Nissl-delimited MN cell body (gray); HA immunostaining exactly matches the anti-pan NRG1 signal and shows an extensive labeling along the whole MN surface; the VACHT-delimited C-bouton presynaptic sites display also association with NRG1, as detailed in the inset. **b)** The expression S1R, a protein focally concentrated in normal C-bouton SSCs, is largely expanded along the MN surface in NRG1 type III overexpressors: the extensive surface labeling of HA tag (red) and NRG1 (green) is associated with wide S1R immunostaining (blue). However, whereas there was an exact colocalization between HA and NRG1, sites containing S1R belong to separate microdomains, as evidenced after the plot profile analysis of fluorescence intensity depicted in

c and d. e) The enlarged expression of NRG1 (green) at the MN surface is associated with the expansion of the SSC marker Kv2.1 (red); both signals are largely co-localized (yellow, in merge panel, and white, after co-localization analysis, Person's R = 0.67). **f)** Show the altered distribution of M2 muscarinic AChRs in the NRG1 type III overexpressors. The extensive surface immunolabeling of M2 AChRs (green) exceeds the area corresponding to VACHT-labeled cholinergic terminals (red), as seen detailed in the inset. **g)** Multiple immunofluorescent analysis of C-boutons on a spinal cord MN from a transgenic mouse overexpressing HA-NRG1-GIEF, a BACE1-cleaved variant of NRG1 type III [36]. The Nissl-delimited MN cell body (gray) displays abundant HA-tag signal inside the MN cytoplasm and adjacent dendrites (red); HA-tag signal does not colocalize with either the NGR1, when detected with an anti-pan-NRG1 antibody, (green), or VACHT-positive terminals (blue); however, C-bouton sites displaying VACHT puncta associated with postsynaptic NRG1, do not contain HA-positive signal, indicating the absence of BACE1-processed NRG1 type III (insets). The white granules in the merge image are lipofuscin particles emitting unspecific fluorescence visible in the three channels. **h,i)** Multiple fluorescent analysis of C-bouton-associated proteins in adult transgenic mice overexpressing NRG1 type I; **h)** A MN, visualized after Nissl staining (gray), the anti-pan-NRG1 antibody (green) shows an extensive surface-associated immunolabeling; abundant C-bouton sites are visualized by S1R (red) and VACHT (blue) immunolabeling; NRG1 labeling at the MN surface exceeds out of the VACHT and S1R-containing synaptic sites (insets); **i)** A MN delimited by Nissl (gray) was immunolabeled for M2 AChR (green) and VACHT (red), showing the extensive surface expression of postsynaptic M2 AChR (inset). Both the number and size of C-boutons were dramatically increased, in NRG1 type I overexpressors. Scale bars: 10 µm in i (valid for a-h).

Figure 8. Quantification of C-bouton-associated markers in WT and transgenic mice overexpressing either NRG1 type I or type III as indicated. The number and size of C-boutons in NRG1 type III overexpressors are not different from those in WT animals. However, in NRG1 type I overexpressors, both the number and size of C-boutons are dramatically increased. The postsynaptic expression of M2 AChRs, S1R and Kv2.1 are also largely increased in type III NRG1 overexpressors, whereas in NRG1 type I animals only M2 AChRs significantly increased. In all graphs values are shown as mean ± SEM; *** $p < 0.001$ (one-way ANOVA, Bonferroni's post-hoc test); n (WT, NRG1 type I and NRG1 type III, respectively) = 13, 13, and 9 MNs (in a); 92, 88, and 44 MNs (in b); 11, 10, and 13 MNs (in c); 8, 17 and 10 (in d), 5, 10 and 7 MNs (in e) from 2-3 animals per condition.

Figure 9. a-b) Electron micrographs of the cell body MN surface in transgenic mice overexpressing either NRG1 type III (**a**) or type I (**b**) isoforms. MN cytoplasm is dashed in red and C-bouton presynaptic terminals are marked in green. **a)** In NRG type III transgenic MNs, presynaptic terminals (*) are normal in size and located in face of enlarged and reduplicated SSC-like membranes (red arrows and bottom inset) in the postsynaptic MN; SSC-like membranes are extended far away from C-bouton sites. **b)** In NRG1 type I transgenic MNs the C-bouton presynaptic terminal (*) is highly enlarged and extends on the MN surface far away from the SSC-delimited area (colored blue) and detailed in the inset. **c)** The proposed changes in the structural and molecular organization of C-bouton synaptic sites, induced by overexpression of either NRG1 type III or type I isoforms, are depicted and compared to WT. Scale bar: 500 nm in **b** (valid for **a**).

Target	Source	Host species	Used concentration
Grp78 (BiP)	Stressgene (SPA-826), San Diego, CA, USA	Rabbit polyclonal	1:1000
Choline acetyltransferase (ChAT)	Millipore (AB144), Darmstadt, Germany	Goat polyclonal	1:250
Glial fibrillary acidic protein (GFAP)	Abcam (ab4674), Cambridge, UK	Chicken polyclonal	1:1000
Her4/ErbB4	Cell Signalling (#4795) Danvers, MA, USA	Rabbit monoclonal	1:50
HA Tag	Roche Diagnostics (11 867 423 001), Sant Cugat del Vallès, Barcelona	Rat monoclonal	1:500
Ionised calcium-binding adaptor molecule 1 (IBA1)	Abcam (ab5076)	Goat polyclonal	1:500
Kv2.1 α-subunit	NeuroMab (73-014), Davis, CA, USA	Mouse monoclonal	1:100
M2 muscarinic receptor	Alomone Labs (AMR-002), Jerusalem, Israel	Rabbit polyclonal	1:100
Neu (C-18) (ErbB2)	Santa Cruz Biotechnology (Sc-284), Dallas, TX, USA	Rabbit polyclonal	1:50
Neu/N	Chemicon International (MAB377), Temecula, CA, USA	Mouse monoclonal	1:100
NRG1 1α /β 1/2	Santa Cruz (sc-348)	Rabbit polyclonal	1:300
Neuregulin-1 Type III (extracellular)	Alomone labs (ANR-113)	Rabbit polyclonal	1:250
Neuregulin-CRD, Type III, clone N126B/31	Millipore (MABN534)	Mouse Monoclonal	1:250
p-Neu tyr1248 (p-ErbB2)	Santa Cruz (sc-293110)	Rabbit polyclonal	1:100
Sigma-1 receptor (S1R)	Santa Cruz (sc-137075)	Mouse monoclonal	1:50
SV2	Hybridoma bank (SV2), Iowa City, IA, USA	Mouse monoclonal	1:1000
Vesicular acetylcholine transporter (VACHT)	Synaptic Systems (139 105), Goettingen, Germany	Guinea pig polyclonal	1:500

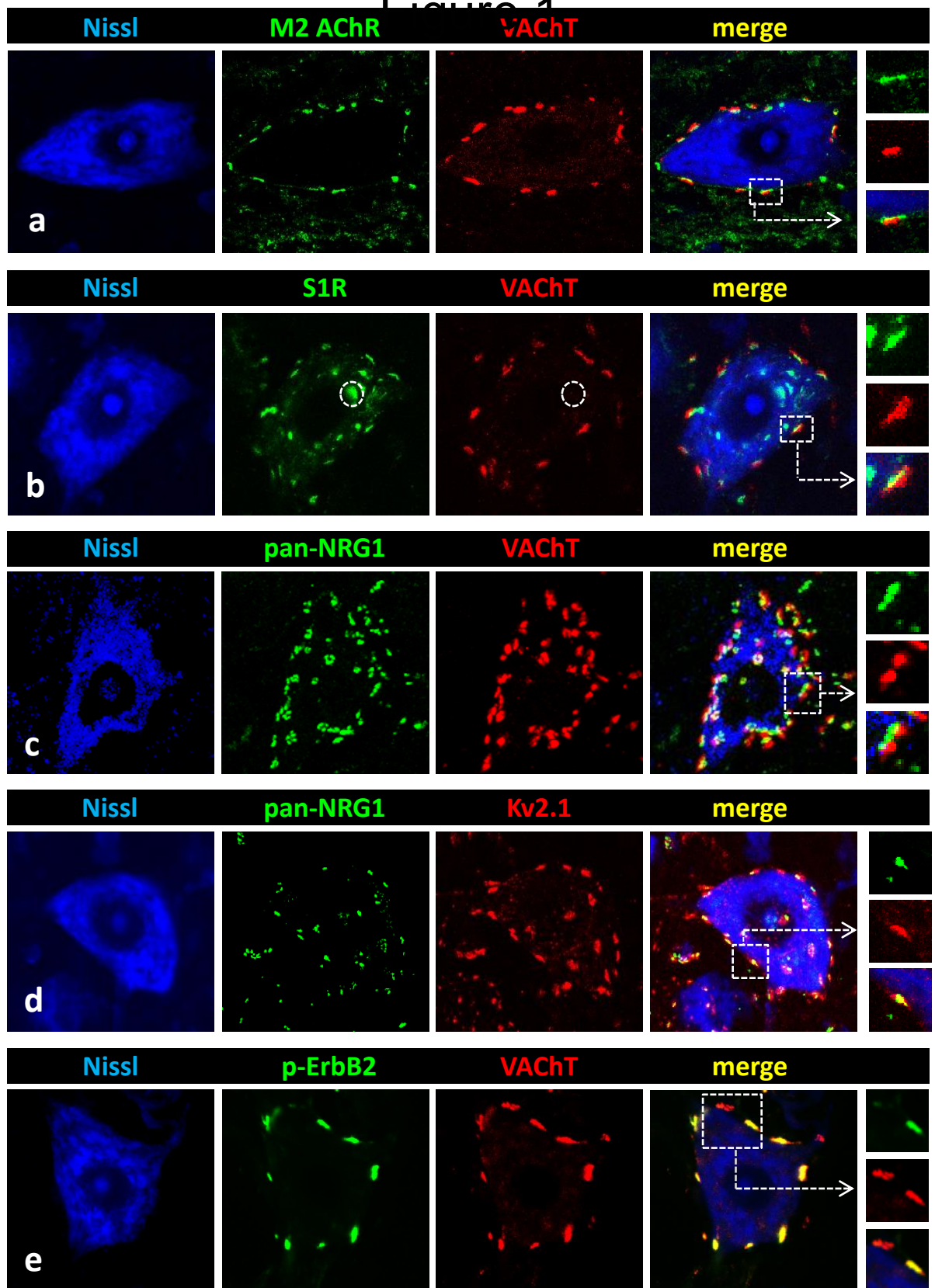
Figure 1**Figure 1**

Figure 2

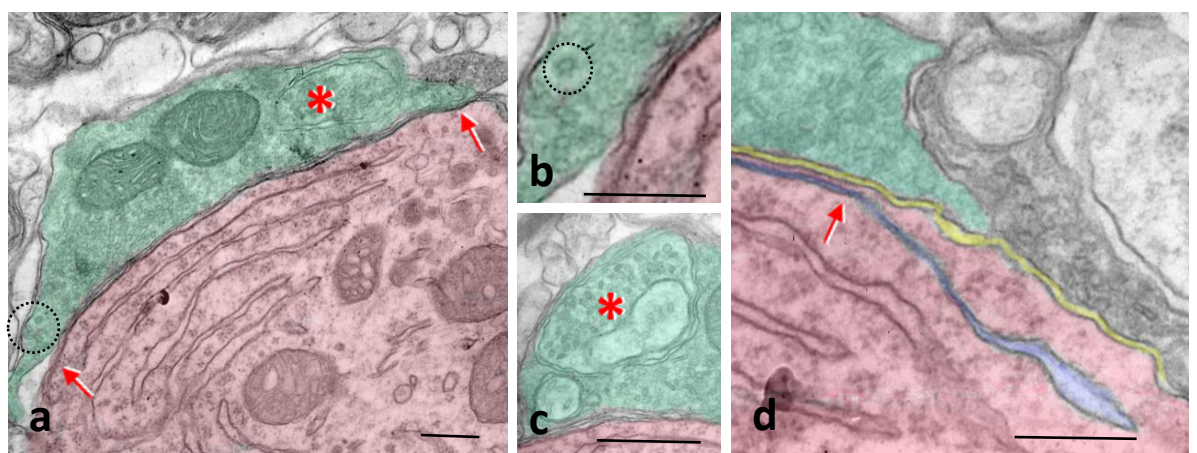
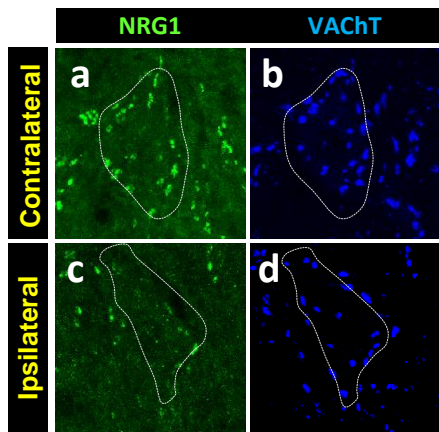


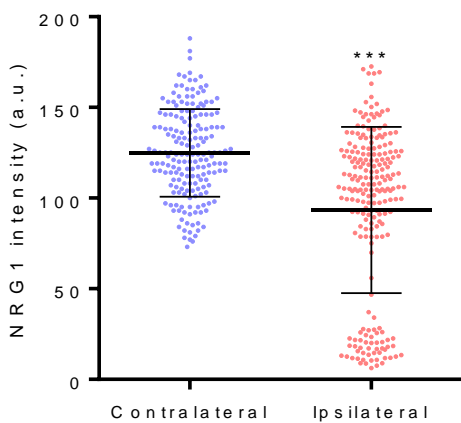
Figure 2

Figure 3

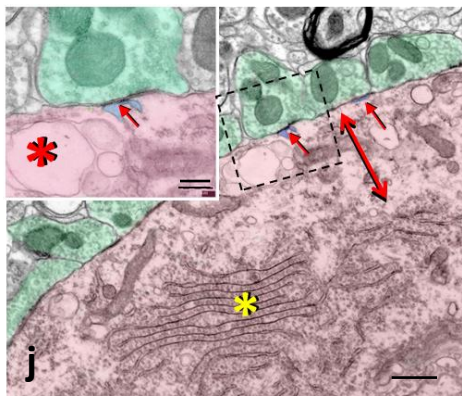
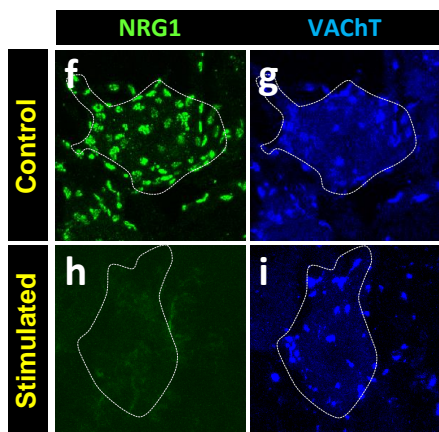
Antidromic stimulation



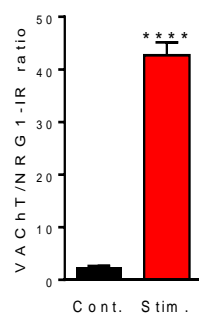
e



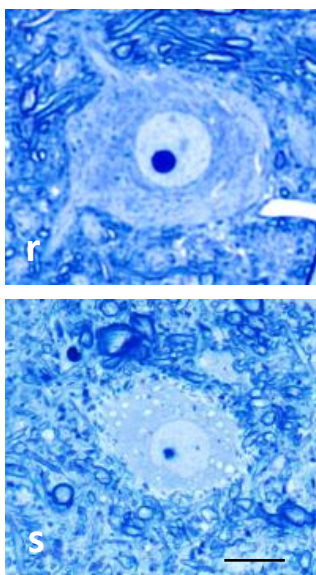
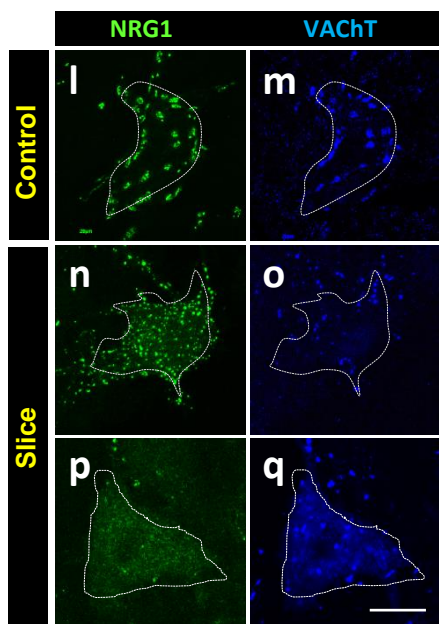
Orthodromic stimulation



k



Ex vivo slice



t

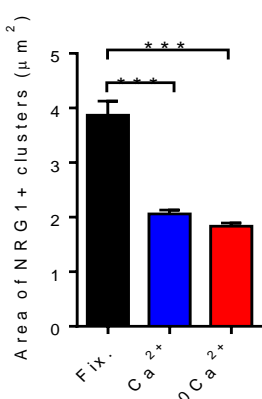


Figure 3

Figure 4

b

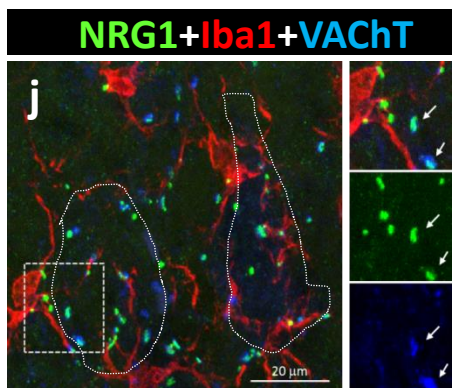
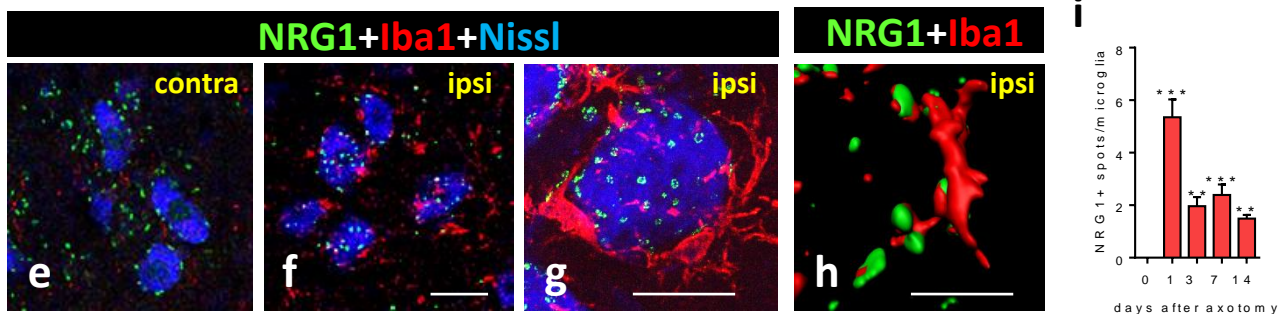
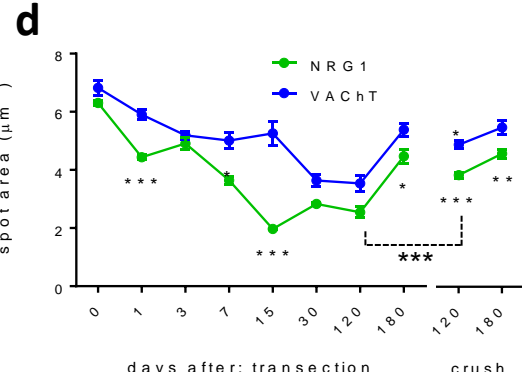
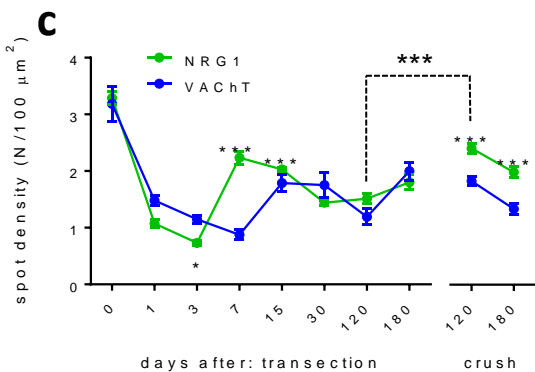
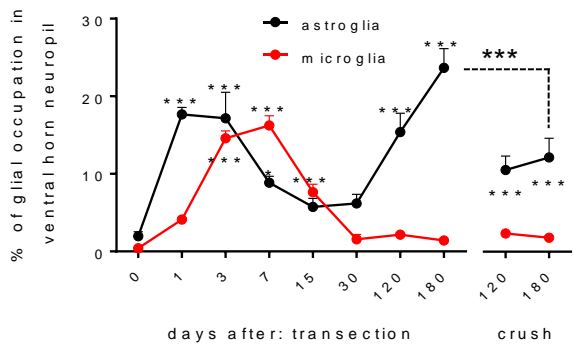
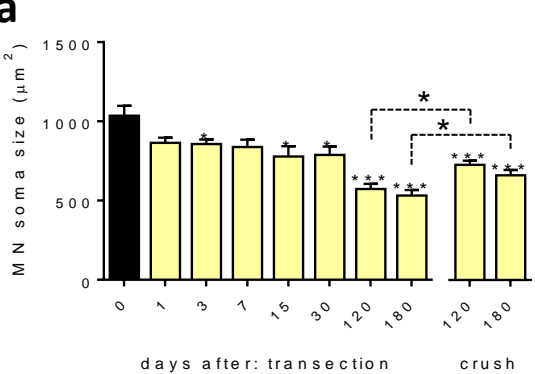


Figure 4

Figure 5

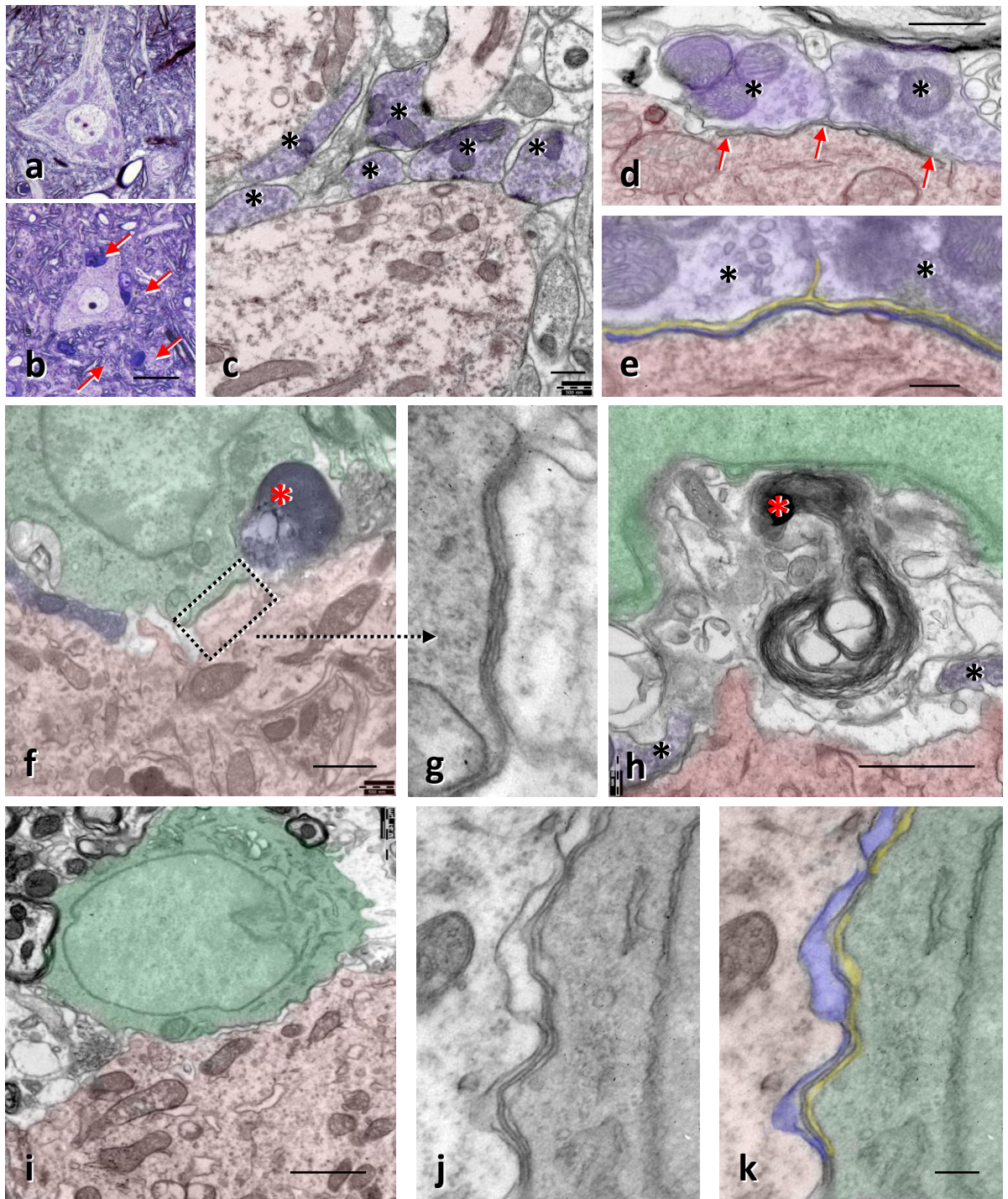


Figure 5

Figure 6

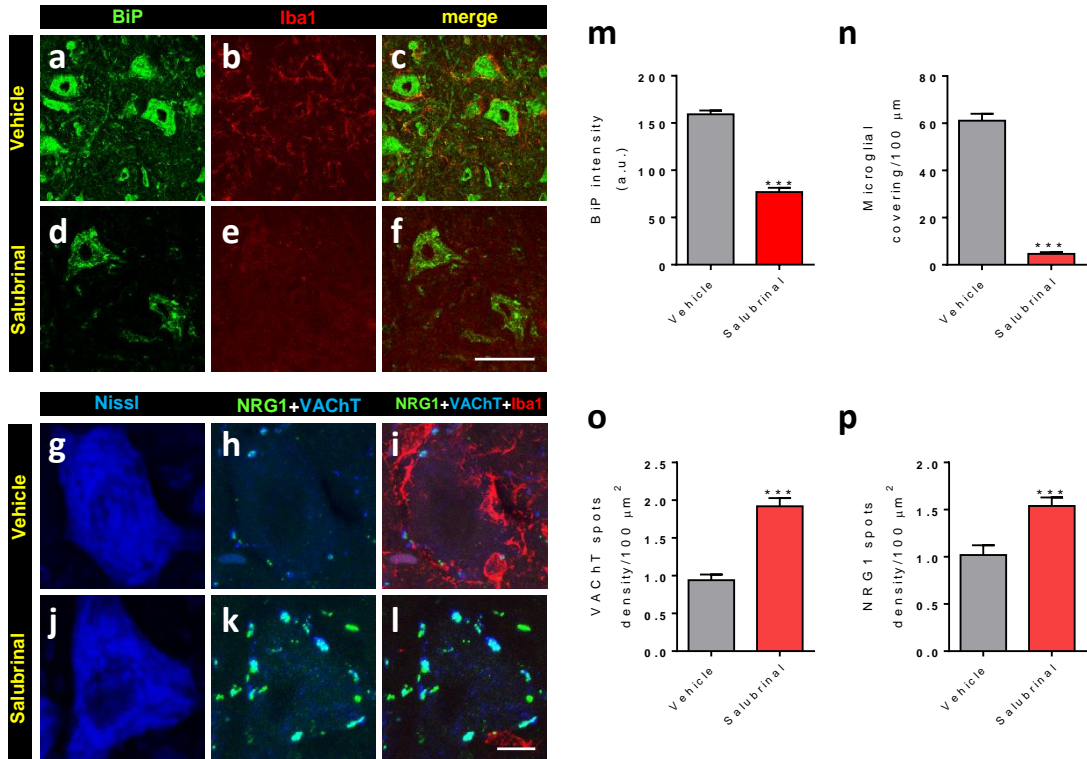


Figure 6

Figure 7

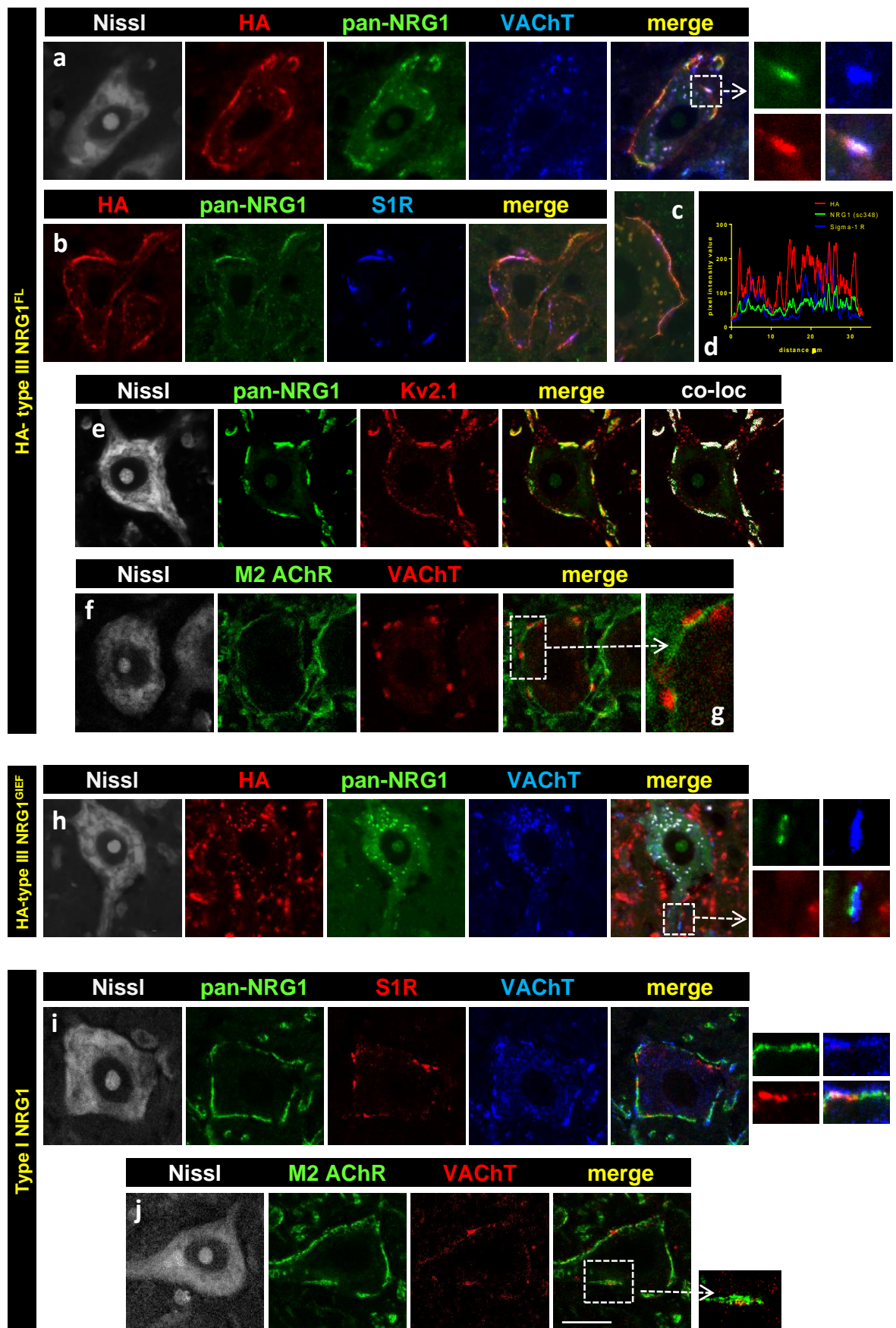


Figure 7

Figure 8

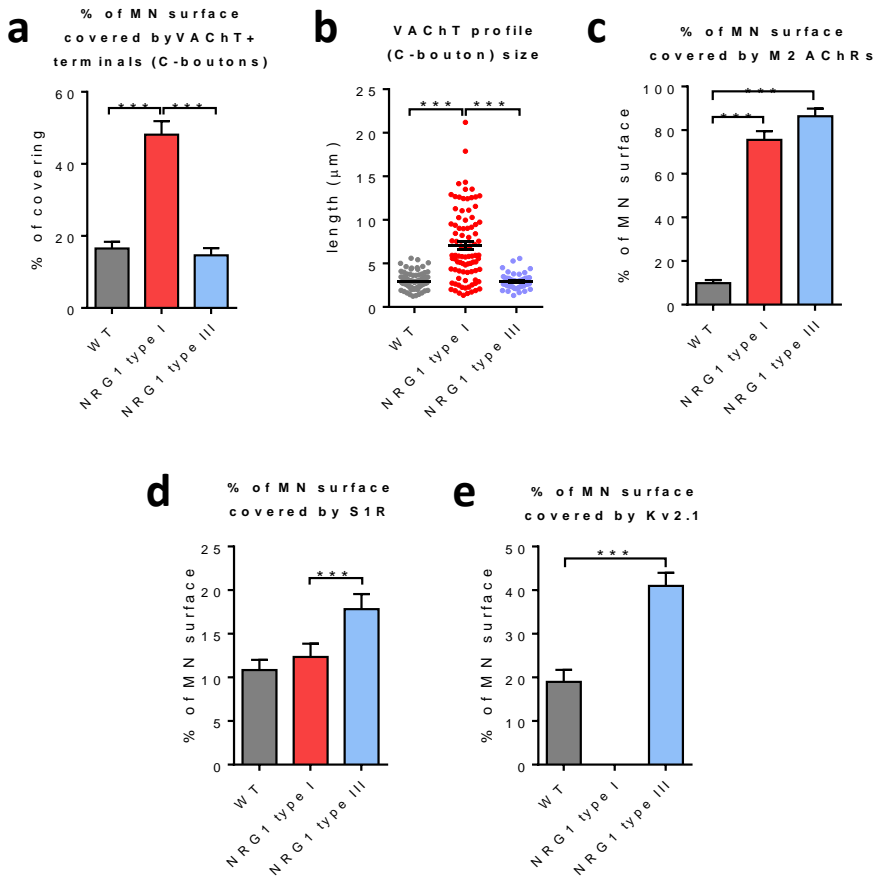


Figure 8

Figure 9

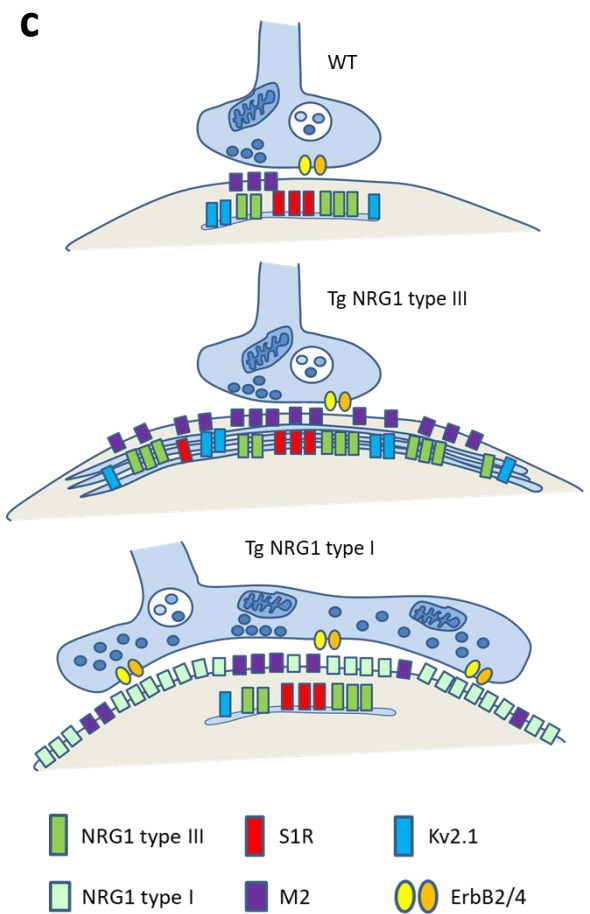
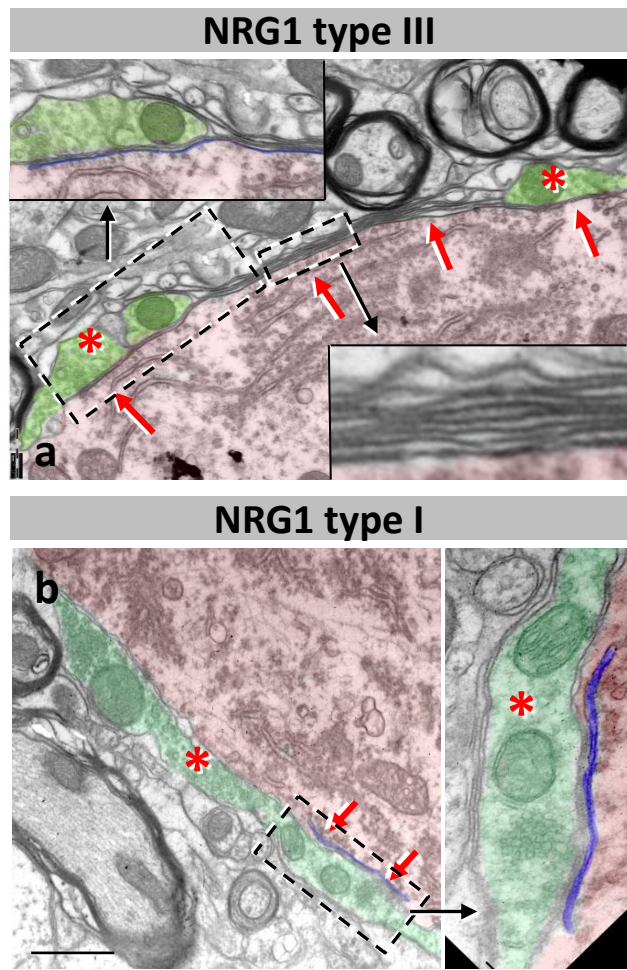
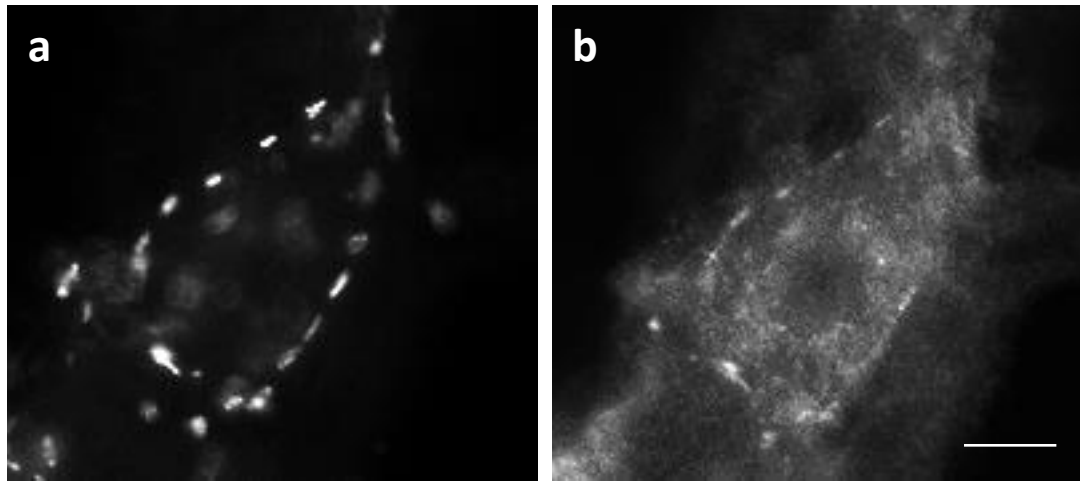


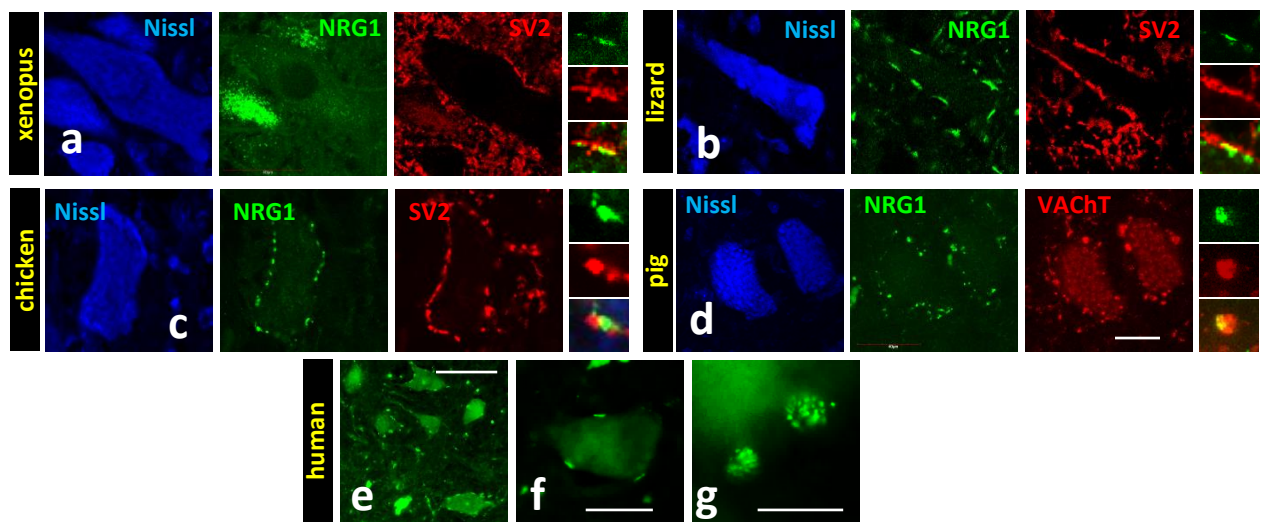
Figure 9



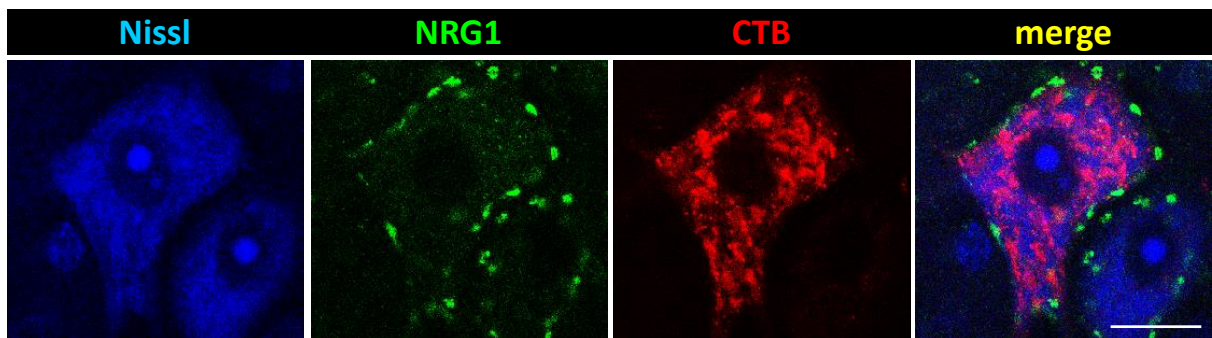
Neuregulin-1 α / β 1/2 (C-20)
sc-348
Santa Cruz, 1:200

Neuregulin-CRD, Type III
MABN534
Millipore, 1:250

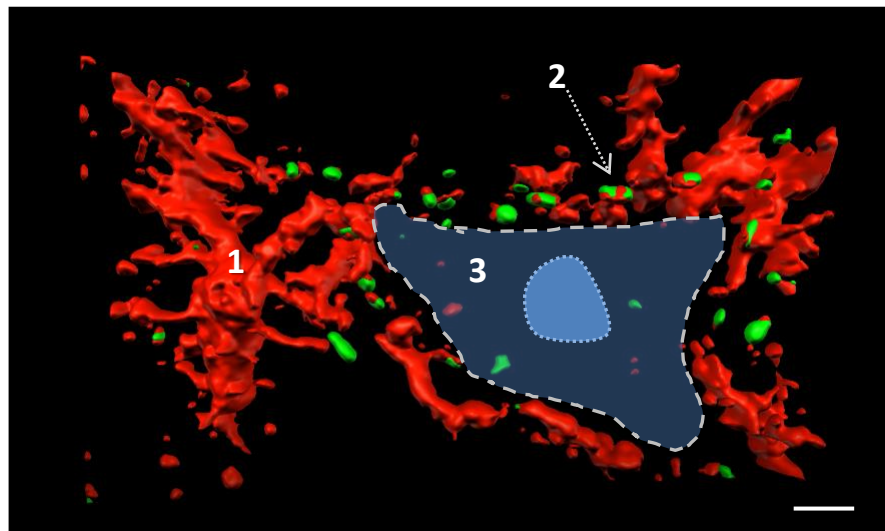
Supplementary Figure 1. **a** and **b**) Spinal cord MN somata showing NRG1 immunoreactivity obtained by the two indicated antibodies simultaneously used. Note that both antibodies detect clusters of NRG1 representing C-bouton synaptic sites. However, the rabbit pan-anti-NRG1 antibody sc-348 displays more intense and clean immunolabeling than the mouse monoclonal MABN534, which is directed against type III NRG1-CRD. Scale bar: 10 μ m in **b** (valid for **a**).



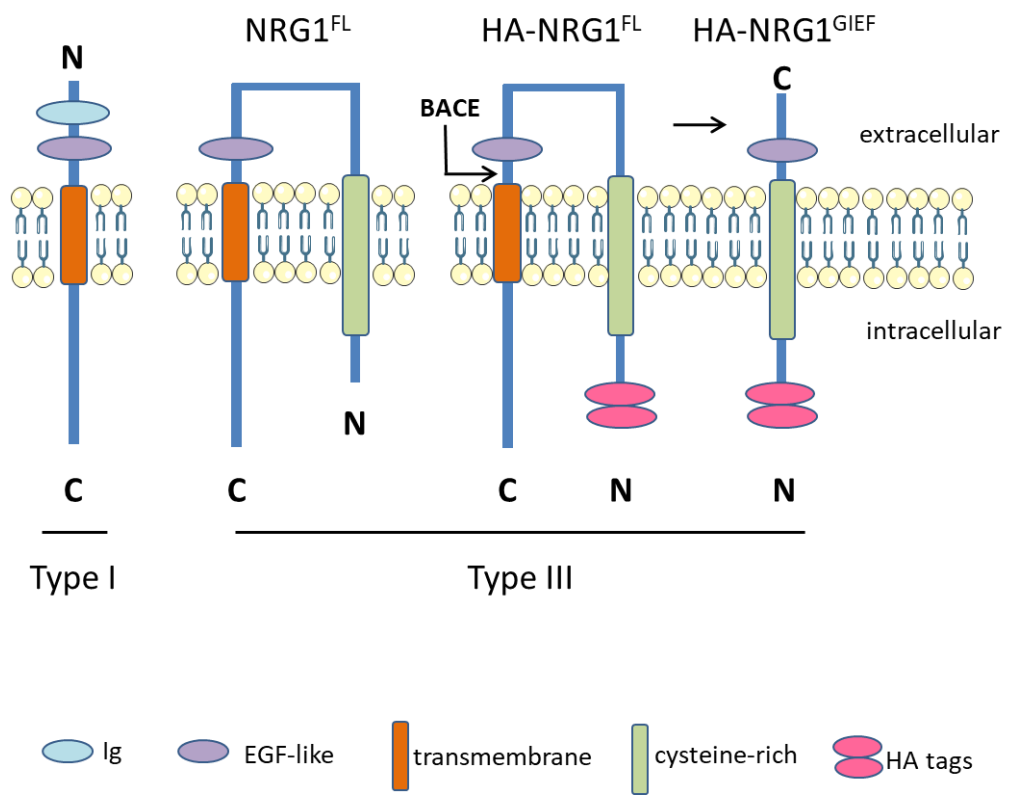
Supplementary Figure 2. Clusters of NRG1 are present in association with MN synaptic afferents in distinct indicated animal species. As anti-VACHT antibodies were not reactive in species different from mammals, synaptic sites were labeled with anti-SV2 antibodies in xenopus (**a**), lizard (**b**) and chicken (**c**) samples; in pig samples (**d**) C-boutons were labeled with anti-VACHT antibodies, in human tissues (**e-g**), NRG1-positive spots were seen adjacent to MN surface, in an identical pattern as observed in mice. MN cell bodies were delimited with fluorescent Nissl staining (blue). Scale bars: 20 μ m in **d** (valid for **a-c**), 100 μ m in **e**, 20 μ m in **f** and 10 μ m in **g**.



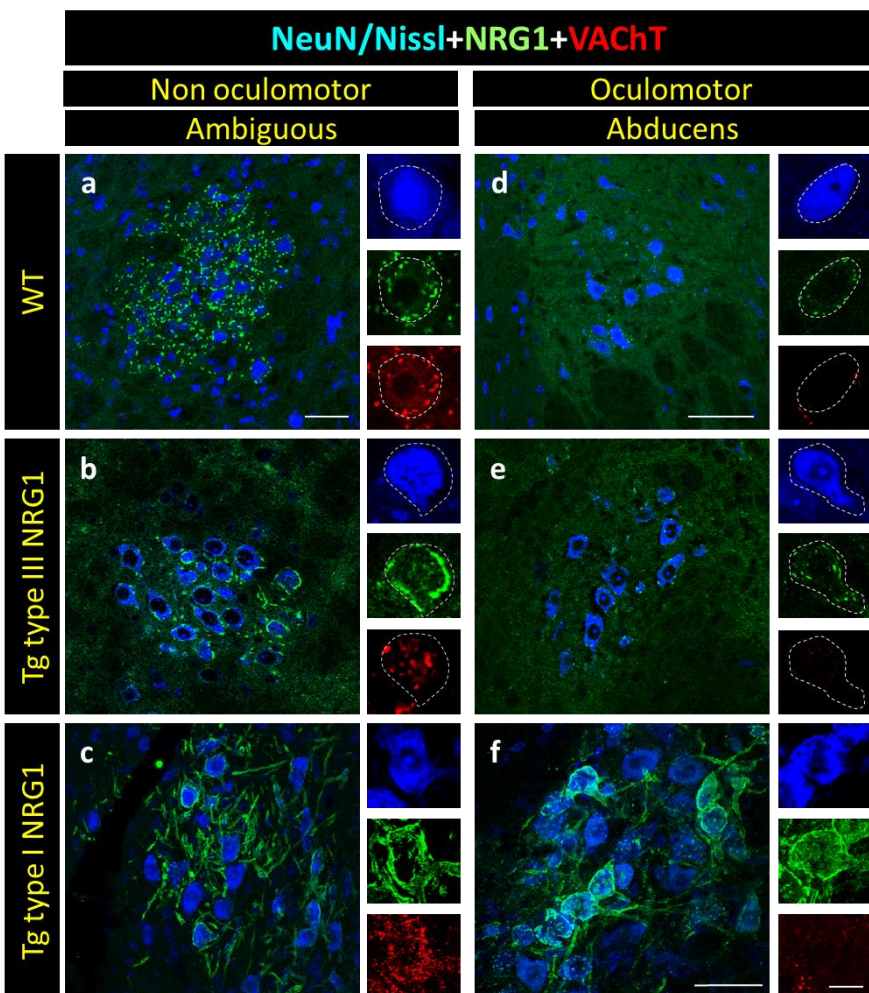
Supplementary Figure 3. Spinal cord MN somata, retrograde labeled by intramuscular injection of fluorescent CTB (red) was immunostained with anti-NRG1 antibody (green) and counterstained with Nissl (blue). Note that the extensive incorporation of CTB in MN cytoplasm does not overlap with NRG1 clustered at C-bouton sites. Scale bar: 20 μ m.



Supplementary Figure 4. 3D volume rendering displaying the close relationship between microglial processes and C-bouton associated NRG1 clusters. Image was obtained from stacked 0.5 μ m optical confocal sections. A massive recruitment of microglia (red, 1) is seen around the MN soma (depicted, 3) 24 h after sciatic nerve axotomy. Microglial cells intimately interact with NRG1 clusters (green, 2). Scale bar: 5 μ m.



Supplementary Figure 5. Membrane disposition of NRG1 isoforms (adapted from [36,65]).



Supplementary Figure 6. Impact of NRG1 overexpression in C-bouton organization of brainstem (non-oculomotor [non-OCM, **a**, **b** and **c**] and oculomotor [OCM, **d**, **e** and **f**]) MNs. Selected sections were triple fluorescent labeled with NRG1 (green), VACHT (red) and MN cell bodies were delimited by either Nissl (**a**, and **d**) or NeuN (**b**, **c**, **e** and **f**) staining (blue). **a)** Non-OCM (ambiguous, cranial nerve [CN] X) MNs display NRG1 clusters associated with VACHT positive terminals, in an identical pattern to that observed in ventral horn spinal cord MNs. **b** and **c)** In samples from transgenic mice overexpressing either NRG1 type III or NRG1 type I, the observed changes are the same as those observed for ventral horn spinal cord MNs: the expanded superficial expression of postsynaptic NRG1 is detected in both models (green in **b** and **c**), whereas an important increase in the number of cholinergic VACHT positive terminals is noticed in NRG1 type I overexpressors (red in **c**). Identical results were observed in other brainstem non-OCM MN nuclei, such as: facial (CNVII), motor trigeminal (CNV) and hypoglossus (CNXII) (not shown). **d)** WT OCM (abducens, CNVI) MNs are devoid of VACHT positive C-bouton afferents, and clusters of NRG1 are scarce and not associated to cholinergic synapses. **e)** After overexpression of NRG1 type III, an increase in NRG1 clusters in OCM MN somata, which are non-associated to VACHT-positive terminals, are noticed. **f)** After NRG1 type I overexpression a dramatic increase in surface associated NRG1 in OCM MNs are detected, however, contrasting to that found in non-OCM MNs, excess of NRG1 is not able to induce cholinergic (VACHT-positive) synaptogenesis. Scale bars: 50 µm in **a**, **d** and **f** (valid for **b**, **c** and **e**), 10 µm in the inset in **f** (valid for all insets).

Article III**Microglial recruitment and mechanisms involved in the disruption of afferent synaptic terminals on spinal cord motor neurons after acute peripheral nerve injury**

Sara Salvany, Anna Casanovas, Lídia Piedrafita, Olga Tarabal, Sara Hernández, Jordi Calderó, i Josep E. Esquerda

Glia

(2021) Jan 2; 69(5), 1216–1240; Q1, IF: 7.452

Received: 14 August 2020 | Revised: 11 December 2020 | Accepted: 14 December 2020
DOI: 10.1002/glia.23959

GLIA



WILEY

RESEARCH ARTICLE

Microglial recruitment and mechanisms involved in the disruption of afferent synaptic terminals on spinal cord motor neurons after acute peripheral nerve injury

Sara Salvany | Anna Casanovas | Lídia Piedrafita | Olga Tarabal |
Sara Hernández | Jordi Calderó | Josep E. Esquerda

Patología Neuromuscular Experimental
Departament de Medicina Experimental,
Facultat de Medicina, Universitat de Lleida and
Institut de Recerca Biomèdica de Lleida
(IRBLleida), Lleida, Catalonia, Spain

Correspondence

Josep E. Esquerda, Departament de Medicina Experimental, Facultat de Medicina, Universitat de Lleida-IRBLleida, Av. Rovira Roure 80, 25198 Lleida, Catalonia, Spain.
Email: josep.esquerda@udl.cat

Funding information

Ministerio de Ciencia, Innovación y Universidades (MICIU) and Fondo Europeo de Desarrollo Regional (FEDER), Grant/Award Number: RTI2018-099278-B-I00; Spanish Ministerio de Educación, Cultura y Deporte; Jack Van den Hock a la Investigació de l'ELA - Fundació Miquel Valls

Abstract

Peripheral nerve section with subsequent disconnection of motor neuron (MN) cell bodies from their skeletal muscle targets leads to a rapid reactive response involving the recruitment and activation of microglia. In addition, the loss of afferent synapses on MNs occurs in concomitance with microglial reaction by a process described as synaptic stripping. However, the way in which postaxotomy-activated microglia adjacent to MNs are involved in synaptic removal is less defined. Here, we used confocal and electron microscopy to examine interactions between recruited microglial cells and presynaptic terminals in axotomized MNs between 1 and 15 days after sciatic nerve transection in mice. We did not observe any bulk engulfment of synaptic boutons by microglia. Instead, microglial cells internalized small membranous-vesicular fragments which originated from the acute disruption of synaptic terminals involving the activation of the necrototic pathway. The presence of abundant extracellular vesicles in the perineuronal space after axotomy, together with the increased expression of phospho-mixed lineage kinase domain-like protein and, later, of extracellular vesicle markers, such as CD9, CD63, and flotillin, indicate that the vesicles mainly originated in synapses and were transferred to microglia. The upregulation of Rab7 and Rab10 in microglia interacting with injured MNs, indicated the activation of endocytosis. As activated microglia and synaptic boutons displayed positive C1q immunoreactivity, a complement-mediated opsonization may also contribute to microglial-mediated synaptic disruption. In addition to the relevance of our data in the context of neuroinflammation and MN disease, they should also be taken into account for understanding functional recovery after peripheral nerve injury.

KEY WORDS

afferent synapses, extracellular vesicles, exosomes, microglia, motor neuron, nerve axotomy, necroptosis

Sara Salvany and Anna Casanovas contributed equally to this work. Jordi Calderó and Josep E. Esquerda are senior co-authors.

This is an open access article under the terms of the Creative Commons Attribution-NonCommercial-NoDerivs License, which permits use and distribution in any medium, provided the original work is properly cited, the use is non-commercial and no modifications or adaptations are made.
© 2021 The Authors. *Glia* published by Wiley Periodicals LLC.

1 | INTRODUCTION

The disconnection of motor neuron (MN) cell bodies from their skeletal muscle targets, as occurs after peripheral nerve injury, leads to rapid and profound reactive responses in the affected regions of the spinal cord. These reactive changes involve not only the severed neuronal cell bodies, but also their neighboring astroglial and microglial cells. In addition, the distal stump of injured peripheral nerve undergoes progressive disintegration in the context of Wallerian degeneration (Coleman & Freeman, 2010; Conforti, Gilley, & Coleman, 2014); conversely, the proximal stump regenerates as a consequence of the intrinsic growth capacity of the injured MN and of locally derived growth promoting factors (Chen, Yu, & Strickland, 2007). It seems that changes in retrograde signaling along with proximal axonal events inform the cell body of the distally located injury in order to activate a complex cellular response, which is eventually directed either to regeneration or, in certain cases, to cell death (Pollin, McHanwell, & Slater, 1991; Rishal & Fainzilber, 2014). The conspicuous structural changes that MN cell bodies suffer after axonal interruption are classically described within the concept of chromatolysis: a retrograde response mainly focused on alterations in the endoplasmic reticulum (ER) and in other organelles (Lieberman, 1971). Nevertheless, peripheral nerve transection also affects the stability of synaptic inputs on the corresponding MN cell bodies (Alvarez et al., 2020; Brannstrom & Kellerth, 1998; Sumner, 1975; Sumner & Sutherland, 1973). Pioneering studies by Blinzingier and Kreutzberg (1968) have shown that the loss of the afferent synaptic boutons on MNs following axotomy is mediated by recruited perineuronal microglial cells, leading to the introduction of the synaptic stripping concept. This notion is usually referred to as the glial-mediated detachment of presynaptic terminals from the cell bodies or dendrites of axotomized MNs, and has been extended to other damaged CNS neurons (Kettenmann, Kirchhoff, & Verkhratsky, 2013). This process has been considered as favorable for the survival and functional recovery of injured neurons and, thereby, microglia should act in a protective manner (Cullheim & Thams, 2007; Kettenmann et al., 2013). In the seminal article on this subject (Blinzingier & Kreutzberg, 1968), it is stated that, in axotomized facial MNs, microglia-mediated synaptic removal occurs in the absence of presynaptic bouton degeneration or phagocytosis. Conversely, microglia-mediated phagocytosis of synaptic elements has been frequently reported within the context of both the postnatal remodeling of synapses and under a variety of pathologic conditions (Cullheim & Thams, 2007; Tremblay, Lowery, & Majewska, 2010). It has been suggested that, during development, microglia engulf and phagocytose synaptic boutons in order to eliminate supernumerary synapses by a mechanism involving complement (Paolicelli et al., 2011; Schafer et al., 2012; Sipe et al., 2016). However, the direct investigation of the way by which microglia ingest and destroy synaptic terminals has been barely addressed. This has been examined in detail by correlative advanced microscopical techniques in the hippocampus during developmental synaptic

remodeling (Weinhard et al., 2018); although, interestingly, these authors have not reported any evidence for phagocytosis of dendritic spines. Instead, synaptic pruning occurs by selective partial phagocytosis of synaptic structures. The term trogocytosis, a name borrowed from the immune system process in which cells ingest small parts of their targets, was adopted to describe this process (Dopfer, Minguet, & Schamel, 2011).

Although the elimination of synaptic inputs in axotomized MNs and its association with microglial cell activation have been widely described for some time, the mechanism by which the afferent synaptic terminals disappear from the surface of injured MNs needs to be reexamined in depth. In a recent study (Salvany et al., 2019), we have reported that the degeneration of synaptic inputs on axotomized MNs occurs in a close relationship with processes of recruited microglia. This involves bouton terminal disruption and fragmentation into vesicular structures that seems to be "ingested" by microglia. It was suggested that this process may be comparable to that described as synaptic trogocytosis.

Here, by using ultrastructural and confocal microscope imaging, we revisited this issue by performing a more detailed examination of changes in perineuronal afferent inputs and glial cells in injured spinal cord MNs following sciatic nerve transection. We provide new data concerning the way in which synapses disintegrate during the local sterile neuroinflammation induced by a distal axonal lesion. It is known that peripheral nerve injury entails permanent changes within the spinal cord and brain circuitry that makes incomplete the functional restoration and clinical recovery (Alvarez et al., 2011; Delgado-Garcia, Del Pozo, Spencer, & Baker, 1988; Lundborg, 2003; Navarro, Vivo, & Valero-Cabré, 2007). For this reason, a more precise knowledge of the biological process involved in the loss and remodeling of afferent MN synaptic boutons after traumatic nerve lesions will provide new understanding and help to improve therapeutic interventions.

2 | MATERIALS AND METHODS

2.1 | Animals, surgical procedures, and tissue preparation

All the experiments were performed using adult CD1 mice obtained from Envigo (East Millstone, NJ). Mice were housed five to six per cage with ad libitum access to food and water under a 12 hr light/dark cycle. All animal experimentation procedures were performed according to the European Committee Council Directive and the norms established by the Generalitat de Catalunya (published as law in the *Diari Oficial de la Generalitat de Catalunya* 2073, 1995). All experiments were previously evaluated and approved by the Committee for Animal Care and Use of our university.

Adult (postnatal day [P] 60–90) mice were subjected to unilateral sciatic nerve transection. Animals were anaesthetized using a solution consisting of a combination of ketamine (100 mg/kg) and xylazine (10

mg/kg). The sciatic nerve was exposed at the femoral level and transected; a ligature was performed in the proximal segment in order to prevent spontaneous reinnervation. To minimize suffering, mice were subjected to postoperative analgesia with two subcutaneous injections of buprenorphine (0.05 mg/kg): one immediately after surgery and the other 24 hr after the intervention. Lumbar spinal cord samples were obtained 1, 3, 7, and 15 days after axotomy.

The colony stimulating factor 1 receptor (CSF-1R) specific kinase inhibitor (PLX5622, Elmore et al., 2014) was generously provided by Plexxikon Inc. (Berkeley, CA), and formulated in AIN-76A standard chow by Research Diets Inc. (New Brunswick, NJ). Two-month-old male CD1 mice, specific-pathogen-free housed, were treated with either vehicle or 1,200 mg/kg chow PLX5622 for 7 days. After that time, the mice had their sciatic nerves surgically intervened according to the procedure described above. The mice were then treated with the same dose of chow PLX5622 for a further 7 days. To verify PLX5622 consumption by the mice, their weight was monitored; no significant weight reduction was observed. To assess the effectiveness of PLX5622 in depleting microglial cells, the number of Iba1-positive glial cells was assessed in serially sectioned brain striatal area. The treatment with PLX5622 resulted in a ~45% reduction in brain-resident microglial cells evaluated after Iba1 immunostaining.

Mice were anesthetized and transcardially perfused with 4% PFA in 0.1 M phosphate buffer (PB) pH 7.4. Samples were postfixed for

24 hr in the same fixative, at 4°C, and then cryoprotected at 4°C with 30% sucrose in 0.1 M PB containing 0.02% sodium azide. Transverse cryostat sections (16 mm thick) were collected on gelatin-coated glass slides.

2.2 | Multiple fluorescent labeling and confocal microscopy

Cryostat sections were permeabilized with PBS containing 0.1% Triton X-100 for 30 min, blocked with either 10% normal goat serum or normal horse serum in PBS for 1 hr at room temperature, and then incubated overnight at 4°C with an appropriate primary antibody mixture. The primary antibodies used are listed in Table 1.

Once previously washed with PBS, sections were incubated for 1 hr with a combination of appropriate secondary antibodies labeled with one of the following fluorochromes (1:500): Alexa Fluor 488, Alexa Fluor 546 (ThermoFisher Scientific, Waltham, MA), cyanine 3, or cyanine 5 (Jackson Immuno-Research Laboratories, West Grove, PA). Finally, the spinal cord sections were labeled with blue fluorescent NeuroTrace Nissl staining (1:150; Thermo Fisher Scientific) and mounted using an antifading medium containing 0.1 M Tris-HCl buffer (pH 8.5), 20% glycerol, 10% Mowiol, and 0.1% 1,4-diazabicyclo [2.2.2]octane.

TABLE 1 Primary antibodies used for immunocytochemistry

Target	Source	Host species	Used concentration
C1q	Abcam (ab182451)	Rabbit monoclonal	1:1,000
CD9	Abcam (ab92726)	Rabbit monoclonal	1:350
CD11c	AbDserotec (MCA1369T)	Hamster monoclonal	1:50
CD63	Abcam (ab217345)	Rabbit monoclonal	1:100
CD68	AbDserotec (MCA1957T)	Rat monoclonal	1:100
Flotillin	Abcam (ab41927)	Rabbit polyclonal	1:150
Ionized calcium-binding adaptor molecule 1 (IBA1)	Abcam (ab5076)	Goat polyclonal	1:500
Mac2	Cerdalane (CL8942AP)	Rat monoclonal	1:800
MLKL (phospho S345)	Abcam (ab196436)	Rabbit monoclonal	1:100
PDC6IP-Alix	Sigma-Aldrich (HPA011905)	Rabbit polyclonal	1:50
Rab4	Abcam (ab109009)	Rabbit monoclonal	1:170
Rab5	Abcam (ab218624)	Rabbit monoclonal	1:1,000
Rab7	Abcam (ab137029)	Rabbit monoclonal	1:100
Rab8A	Abcam (188574)	Rabbit monoclonal	1:500
Rab9	Abcam (ab2810)	Mouse monoclonal	1:200
Rab10	Abcam (ab237703)	Rabbit monoclonal	1:500
SV2	Developmental Studies Hybridoma Bank	Mouse monoclonal	1:1,000
Synaptophysin	Synaptic Systems (101004)	Guinea pig polyclonal	1/500
TMEM119	Abcam (ab209064)	Rabbit polyclonal	1:300
VACHT	Synaptic Systems (139105)	Guinea pig polyclonal	1:500

Abbreviation: VACHT, vesicular acetylcholine transporter.

The slides were then examined under a Fluoview FV-500 or Fluoview FV-1000 Olympus laser-scanning confocal microscope (Olympus, Tokyo, Japan). The MNs were imaged after obtaining optical sections (0.5 or 1 mm) of cell bodies. Digital images were analyzed using FV10-ASW 3.1 Viewer (Olympus) and the ImageJ (National Institutes of Health [NIH], Bethesda, MD) software.

Immunolabeled profiles of the different protein markers examined were then manually counted on a screen for each MN soma. In axotomy experiments, we only analyzed cell bodies located in the pes 9 region of the lumbar 6 spinal cord segment, which corresponds to the sciatic motor column (Watson, Paxinos, Kayalioglu, & Heise, 2009). The pool of axotomized MNs was identified by their close interaction with recruited Iba1-stained microglial cells. The intensity of microgliosis was evaluated by analyzing the percentage of either MN perimeter covered by microglia or the neuropile area adjacent to MNs occupied by microglia. The expression of CD68 in microglia was measured as the percentage of the area of CD68-positive puncta with respect to Iba1-positive profiles. The complexity of microglial branching was calculated as the number of triple-point branches after analysis of the skeleton using ImageJ software (AnalyzeSkeleton [2D/3D] from <http://imagej.net/AnalyzeSkeleton>) in 3D projected images of Iba1-immunostained cells. The number of afferent synaptic boutons contacting MNs was evaluated on synaptophysin-immunolabeled sections after tracing a line along the periphery of the cell soma and manually counting the number of pixel profile picks. The colocalization of presynaptic markers with the other proteins that were examined was evaluated after pixel profiling around a line traced at the periphery of the MNs using the ImageJ plugin developed by Pierre Bourdoncle (bourdoncle@ijm.jussieu.fr).

2.3 | Electron microscopy

Animals were perfused with either 2% PFA and 2% glutaraldehyde in PB (for conventional electron microscopy [EM]) or 4% PFA and 0.1% glutaraldehyde in PB (for ultrastructural immunolabeling). Dissected tissues were postfixed for 24 hr, at 4°C, in the same fixative solution. The samples were sectioned at 200 μm using a vibratome and postfixed with 1% OsO₄ for 2 hr, and then contrasted with 0.5% uranyl acetate for 30 min; all these procedures were conducted at 4°C. After that, the samples were processed for Embed 812 (Electron Microscopy Sciences, Hatfield, PA) according to standard procedures. Ultrathin sections were counterstained with Reynold's lead citrate. For Iba1 ultrastructural immunolabeling with the preembedding procedure, 50-μm-thick vibratome sections were blocked in a solution containing: 10% BSA and 0.02% saponin in PBS, for 1 hr, prior to incubation with goat polyclonal anti-Iba1 antibody (diluted 1:500 in 10% BSA/PBS containing 0.004% saponin), at 4°C, for 2 days, and washed five times in 1% BSA/TBS (3 × 1 min and 2 × 10 min). The sections were then incubated for 2 hr with a secondary anti-goat biotinylated antibody (1:100, Vector Laboratories) and visualized using Vectastain Elite ABC (Vector Laboratories), followed by incubation in a 0.05% 3,3-diaminobenzidine /0.01% H₂O₂ mixture. In some cases, peroxidase reactive sites were subjected to silver

enhancement by incubating the sections in a solution containing 2.6% hexamethylenetetramine (Merck, Darmstadt, Germany), 0.2% silver nitrate (Merck), and 0.2% disodium tetraborate (Merck) for 10 min, at 60°C. Sections were rinsed in distilled water and treated with 0.05% gold chloride for 2 min. Finally, the sections were rinsed and incubated in 2.5% sodium thiosulfate (Merck) for 2 min. Tissue was postfixed in 2% OsO₄ and flat embedded in Embed 812.

For postembedding immunogold analysis, lumbar spinal cords were sectioned at 200 μm using a McIlwain Tissue Chopper (Mickle Laboratory Engineering, Gomshall, UK). After glycerol cryoprotection, samples were plunged rapidly into liquid propane (−184°C) cooled by liquid nitrogen and processed for freeze substitution, using a Leica EM system (Leica Microsystems, Wetzlar, Germany). Tissues were low temperature embedded in Lowicryl HM20 resin (Electron Microscopy Sciences), following a protocol similar to that described elsewhere (Rubio & Wenthold, 1999). Ultrathin sections were collected using an Ultracut UC6 ultramicrotome (Leica) and picked up on formvar-coated nickel grids. They were washed in PBS and in 50 mM glycine, and then blocked in 5 and 1% BSA. Sections were incubated for 1 hr with anti-phospho-mixed lineage kinase domain-like protein (MLKL; 1:10) at room temperature. After being rinsed in 0.25 Tween 20, they were blocked in 1% BSA and incubated in 12 nm gold-conjugated goat anti-rabbit IgG (1:30, Sigma-Aldrich, St. Louis, MO), for 30 min at room temperature. After being washed in PBS and distilled water, sections were counterstained with uranyl acetate and lead citrate. All observations were performed on a transmission electron microscope JEOL JEM 1010 (Akishima, Tokyo, Japan).

2.4 | Statistical analysis

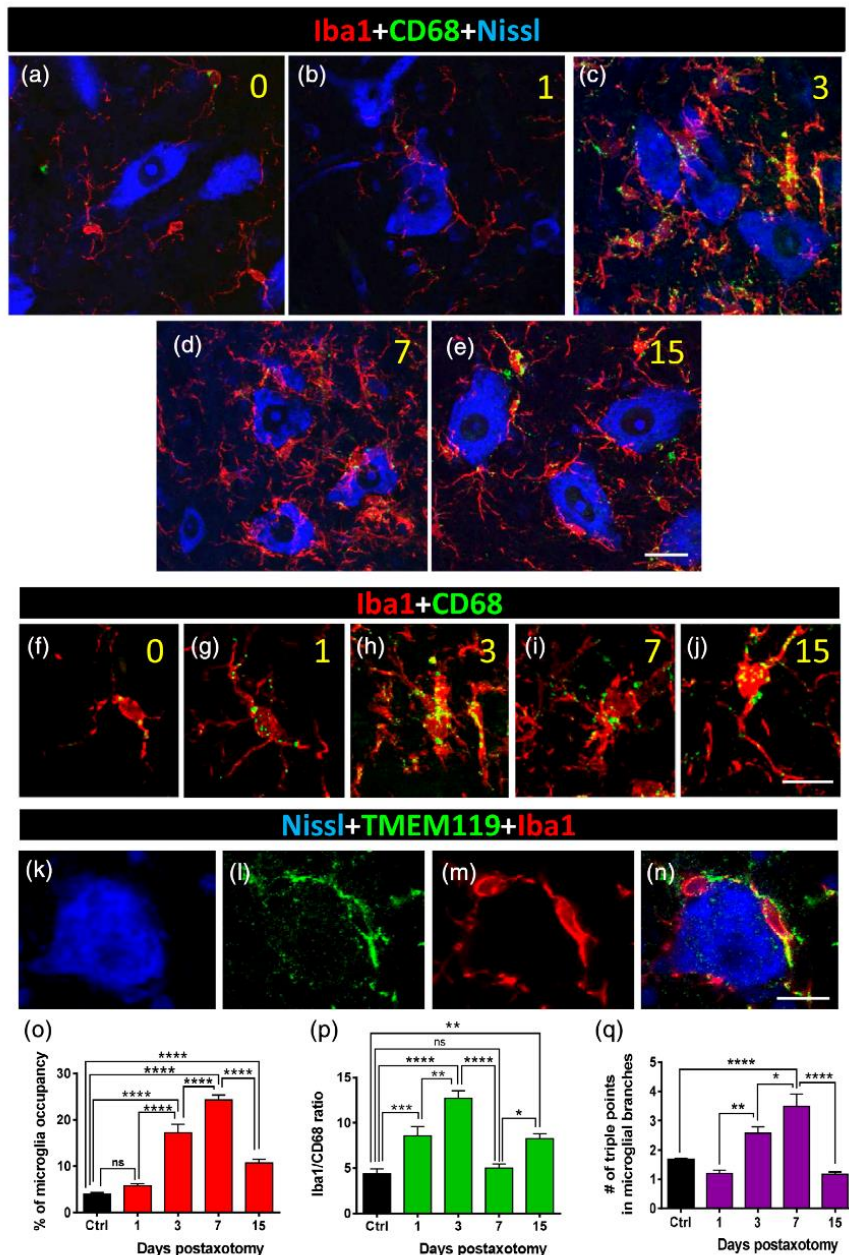
The data were expressed as the mean ± SEM. The statistical analysis was assessed by a Student's *t* test, or by one- or two-way analysis of variance followed by the post hoc Bonferroni's test. The level of significance was established at *p* ≤ .05. GraphPad Prism 6 software was used for statistical analysis and graph presentation of data.

3 | RESULTS

3.1 | Microglial recruitment to axotomized MNs

Twenty four hours after nerve transection, Iba1, a pan-marker for both resting and activated microglia (Ito et al., 1998), revealed a noticeable accumulation of these cells in areas of the spinal cord surrounding injured MNs. Recruited microglia extended large filopodia, which tended to contact MN surfaces, and increased in number and complexity from 1 to 7 days after axotomy (Figure 1a–e,o–q). Moreover, microglial morphology evolved from an amoeboid-like pattern, seen 1 day after axotomy, to a highly ramified form 7 days post-axotomy (Figure 1q). Double labeling for Iba1 and the lysosomal-

FIGURE 1 Microglial recruitment and activation around motor neuron (MN) somata after sciatic nerve axotomy. (a–e) Spinal cord sections displaying Nissl stained axotomized MN pools (blue) in combination with both Iba1 (red, as a general marker of microglia) and CD68 (green, for detection of lysosomes in activated microglia). Representative images taken on Days 0, 1, 3, 7, and 15 (numbers in yellow) after lesion are shown. (f–j) Details of size and distribution of CD68-positive particles in individual Iba1-positive microglial cells are shown after 0, 1, 3, 7, and 15 days postaxotomy (numbers in yellow). (k–n) In recruited microglial cells, Iba1-immunolabeling (red) colocalizes with TMEM119 (green), as shown. (o–q) Quantification of MN surface occupancy by microglial cell processes, ratio of Iba1/CD68 occupied area (p), and complexity of microglial processes measured as a number of triple-point branches (q) at different times after axotomy. Data in graph are shown as mean \pm SEM, from 9 to 14 MNs (o,p), and 1,900–2,300 microglial branches (q), from nine mice, in projected Z-stacks; * $p < .05$; ** $p < .01$; *** $p < .001$; **** $p < .0001$, one-way analysis of variance (ANOVA), Bonferroni's post hoc test. Scale bars: e = 20 μ m (valid for a–d); j = 10 μ m (valid for f–i); n = 10 μ m (valid for k–m) [Color figure can be viewed at wileyonlinelibrary.com]



associated protein CD68, which is present in phagocytic cells (da Silva & Gordon, 1999), demonstrated that once recruited, microglial cells displayed significant phagocytic activity in very close proximity to axotomized MN cell bodies (Figure 1f,j). The number of CD68-positive particles within the microglial cytoplasm was observed to be already increased at 1 day postaxotomy and reached their maximum number 3 days postlesion, before a subsequent decline (Figure 1p). The reduction in the number of CD68 particles found at 7 and 15 days after surgery did not entail a decrease in microgliosis during

this period; in fact, the opposite occurred: microglial mobilization was observed to increase until 7 days after lesion (Figure 1o). Microglia enwrapping axotomized MNs displayed positive TMEM119 immunostaining (Figure 1k–n), a specific marker of resident adult microglia, which is absent in peripheral macrophages (Bennett et al., 2016). Whereas recruited microglial cells did not express activation markers such as CD11c or Mac-2 (not shown), they exhibited other features indicative of an inflammatory response. For example, these cells were coated by endogenous IgGs, probably as a consequence of the local

disruption of the blood brain barrier, and of the increased expression of Fc receptors at the microglial membrane (Supplementary Figure 1a–c). This finding is in agreement with previous observations (Liu, Aldskogius, & Svensson, 1998). In addition, the component of the classic complement pathway C1q was also notably upregulated in the recruited perineuronal microglia as early as 24 hr after axotomy, with a further and transient increase at 7 days postlesion (Figure 2a–i). C1q mediates synapse elimination during normal development and the

aberrant activation of this mechanism may account for synaptic destruction in neurodegenerative diseases (Hong et al., 2016; Schafer et al., 2012; Stevens et al., 2007). We therefore wondered whether unwanted synaptic boutons on axotomized MNs could also be tagged by complement before loss. C1q immunoreactivity was analyzed for its colocalization with the general presynaptic protein marker synaptophysin. At the peak of C1q immunoreactivity, 7 days post-axotomy, there was partial colocalization (Pearson's correlation

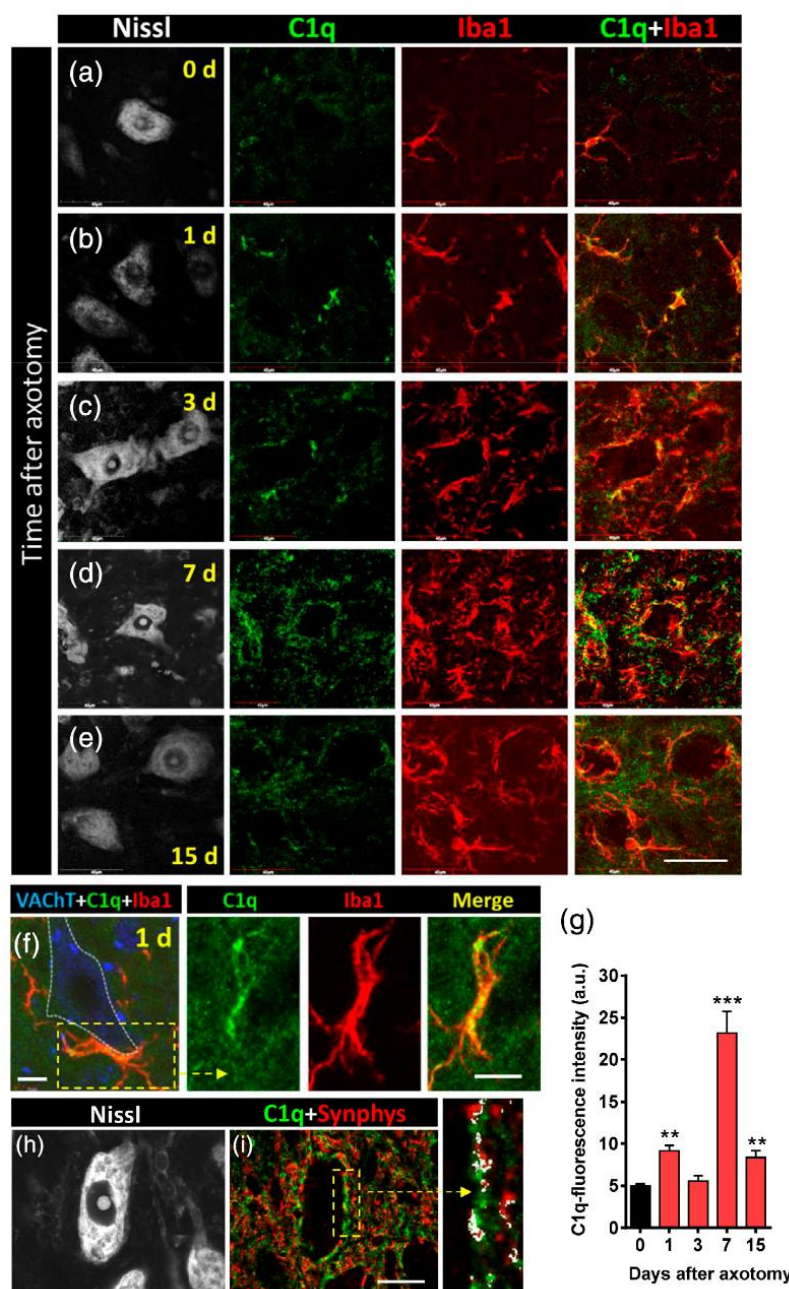


FIGURE 2 C1q expression is upregulated during microglial activation and recruitment that occurs in the vicinity of axotomized motor neurons (MNs). (a–e) Spinal cord MNs are visualized with fluorescent Nissl staining (gray) in conjunction with C1q- (green) and Iba1-immunostaining (red) at different times after axotomy, as indicated (d = days). (f) Detail of recruited microglial cells adjacent to 1-day-axotomized MN soma (delimited by a dotted line); the boxed area is shown at a higher magnification in split and merged green and red channels (VACHT is shown in blue). (g) Quantification of the intensity of C1q fluorescence in Iba1-positive profiles; data are shown as mean \pm SEM; ** p < .01, and *** p < .001 versus 0 days (control; Student's t test; n = 4–7 mice per condition). (h,i) C1q-immunoreactivity (green) partially colocalizes with afferent synaptophysin-immunostained synaptic boutons (red, Synphys) surrounding a 7-day-axotomized MN (visualized by Nissl staining, gray); the colocalized pixels are depicted in white in the enlarged panel. Scale bars: e = 40 μ m (valid for a–d); (f) and enlarged boxed area = 10 μ m; i = 20 μ m (valid for h) [Color figure can be viewed at wileyonlinelibrary.com]

coefficient = .28) between C1q and the synaptophysin signal at the surface of the MN cell bodies (Figure 2h,i).

3.2 | Loss of synaptic inputs on axotomized MNs

The loss of afferent synapses on MNs, induced by peripheral axotomy, was assessed after quantification of presynaptic synaptophysin puncta on the periphery of lesioned MN somas (Supplementary Figure 2a-d). The number of synaptophysin-positive spots per 100 μm of MN perimeter was: control = 162.4 ± 2.74 , and 7 days postaxotomy = 87.03 ± 2.2 (mean \pm SEM, $n = 85$ and 109 measurements, respectively, from three animals; $p < .0001$). This agreed with the reported data which refer to the loss of about 50% of presynaptic terminals during the first week postaxotomy (Oliveira et al., 2004). We next evaluated the impact of the pharmacologically induced reduction of the microglial cell population on MN synaptic loss after nerve transection. To do this, we orally administered the selective CSF1R inhibitor PLX5622 (Elmore et al., 2014). The recruitment of microglia on the periphery of MN somata at 7 days postaxotomy was also substantially reduced by PLX5622 (percentage of microglial occupancy: axotomy = 25.98 ± 1.03 [$n = 43$], and axotomy + PLX5622 = 10.53 ± 0.61 [$n = 22$]; $p < .0001$; from six control and four PLX5622-treated animals). In parallel, the effects of PLX5622 treatment on MN synapse loss were quantified after synaptophysin immunostaining, resulting in a moderate (~10%) increase in the number of synapses that remained after 7 days of peripheral nerve injury. The number of synaptophysin-positive spots per 100 μm of MN perimeter was: axotomy = 87.03 ± 2.2 ($n = 109$), and axotomy + PLX5622 = 95.57 ($n = 173$), from three animals ($p < .001$).

We next analyzed the organization of synaptic terminals contacting the surface of normal and injured (axotomized) MN cell bodies of adult mouse by transmission EM. In intact MNs, almost the entire surface of the cell bodies and their proximal dendrites was covered by densely packed synaptic terminals and cellular processes separated by a very narrow cleft (~20 nm wide) of extracellular space (Figure 3a). Applying the classical morphological criteria previously established (Bodian, 1975; Conradi, 1969), it was possible to recognize the S, F, C, and M types of afferent bouton (Supplementary Figure 3a-e). This arrangement was noticeably altered as a consequence of peripheral nerve transection.

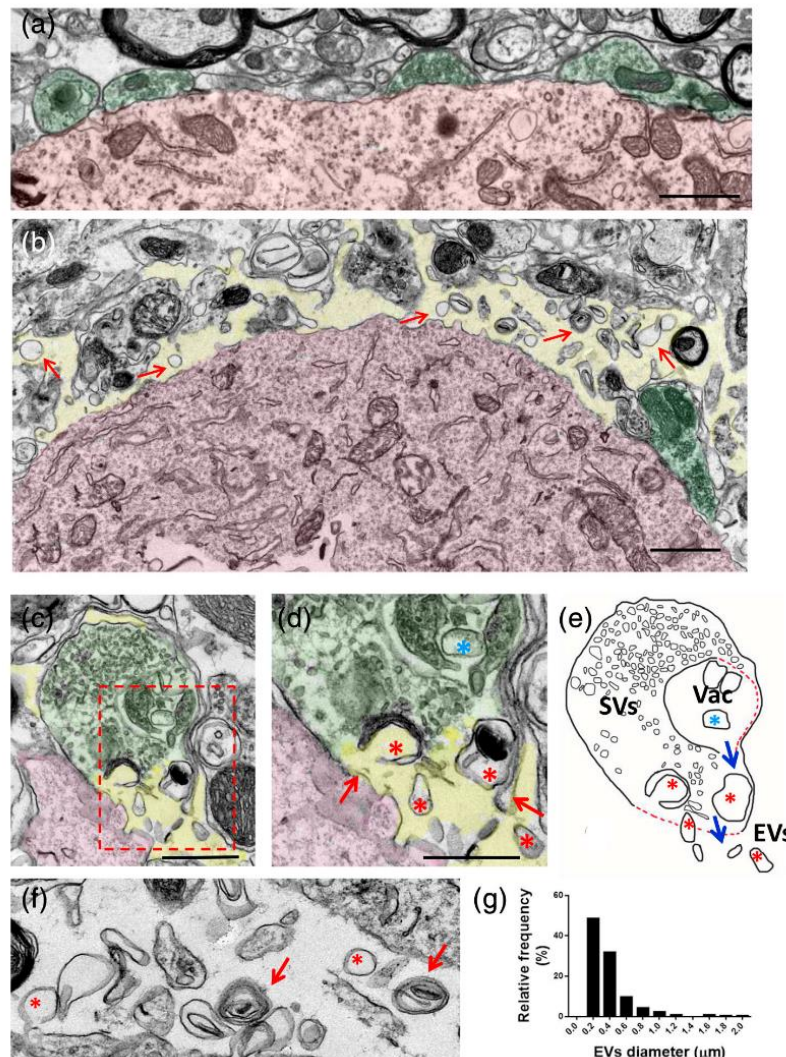
In contrast to the normal organization of synaptic afferents contacting MN surface, early (1–3 days) after lesion, a conspicuous detachment of the presynaptic membrane from its postsynaptic counterpart was observed in many nerve terminals (Figure 3a,b and Supplementary Figure 4a-f). Additionally, the narrow extracellular space seen in normal CNS was found to be highly enlarged. When the presynaptic compartment was partially detached, axosomatic terminals maintained some focal adherence to the MN surface at the puncta adherentia sites, which are considered to be purely adhesive structures (Peters, Palay, & Webster, 1976) (Supplementary Figure 4b). Many synaptic terminals, including C-boutons, displayed noticeable changes in the distribution and size of their synaptic vesicles and related vacuolar structures. An increased

accumulation of large endocytic-like, or autophagosomal-like, vesicles was found, irrespective of the synapse subtypes, at all the time-points examined (1–15 days postlesion).

Due to the synapse detachment and loss, large areas of MN plasma membrane were devoid of presynaptic terminals. The widened extracellular space surrounding MN cell bodies contained a considerable amount of free vesicular-like particles (Figure 3b and Supplementary Figure 4a-f). The accumulation of extracellular vesicles (EVs) was particularly prominent near MN surfaces denuded of synaptic terminals, suggesting that they resulted from the disruption of synaptic boutons. This was confirmed by examining the ultrastructural changes in synaptic boutons at early stages of the disruption (24 hr after nerve injury). At this time-point, some afferent boutons undergoing cellular membrane rupture leading to the release of intracellular vesicular components to the extracellular space were observed (Figure 3c-e). The EVs displayed a marked variability in size, ranging from 100 to 2,000 nm (Figure 3g), and a great diversity of shapes. However, they were usually circular in appearance and exhibited either unilamellar or multilamellar organization (Figure 3f and Supplementary Figure 4d-f). As expected, recruited microglial cells were seen adjacent to injured MNs, and EVs were also abundant near the surface of some of these glial cells (Supplementary Figure 4c). Overall, these alterations affected S and F synaptic types at a similar degree, although C-boutons appeared to be reluctant to the acute disruption.

Many remaining synaptic terminals displayed remarkable changes in the distribution and size of their vesicles and endocytic-autophagosomal like vacuolar structures. This was found at all time-points examined (1–15 days postlesion) and irrespective of the synapse subtypes. During microglial recruitment, some Iba1-labeled microglial end-foot profiles contacted still well preserved, but partially detached, presynaptic boutons (Figure 4a-i); in this case, the nerve terminals usually exhibited an abnormal accumulation of vacuoles regionally segregated from the areas in where the synaptic vesicles accumulated (Figure 4h,i). Other microglial profiles appeared adjacent to extracellular multilamellar bodies. Many structurally preserved nerve terminals, which withstand the acute (1–3 days) lytic disruption, exhibited an abnormal accumulation of multivesicular bodies (MVBs), and endocytic and double-membrane bounded autophagosomal-like structures. This suggests that an imbalance in the turnover of synaptic vesicles occurs prior to full synaptic degeneration seen at more advanced stages postlesion. Figure 5a-c, shows a striking example of Iba1-labeled microglia, taken 7 days after axotomy, exhibiting a continuous sequence of early interaction, and posterior engulfment and internalization of EVs near the surface of an axotomized MN. The panels in Figure 5d-h show vacuoles of identical morphology in different locations, including inside synaptic terminals, in the extracellular space and in double-membrane bounded intracellular microglial inclusions. This strongly suggests a sequential trafficking process from synapses to microglia by means of extracellular intermediaries. Several microglial processes, seen at 7 days postaxotomy, and extensive accumulations of this type of vesicle are depicted in Figure 5i.

The structural alterations in the postsynaptic regions facing damaged presynaptic terminals were more difficult to assess and to



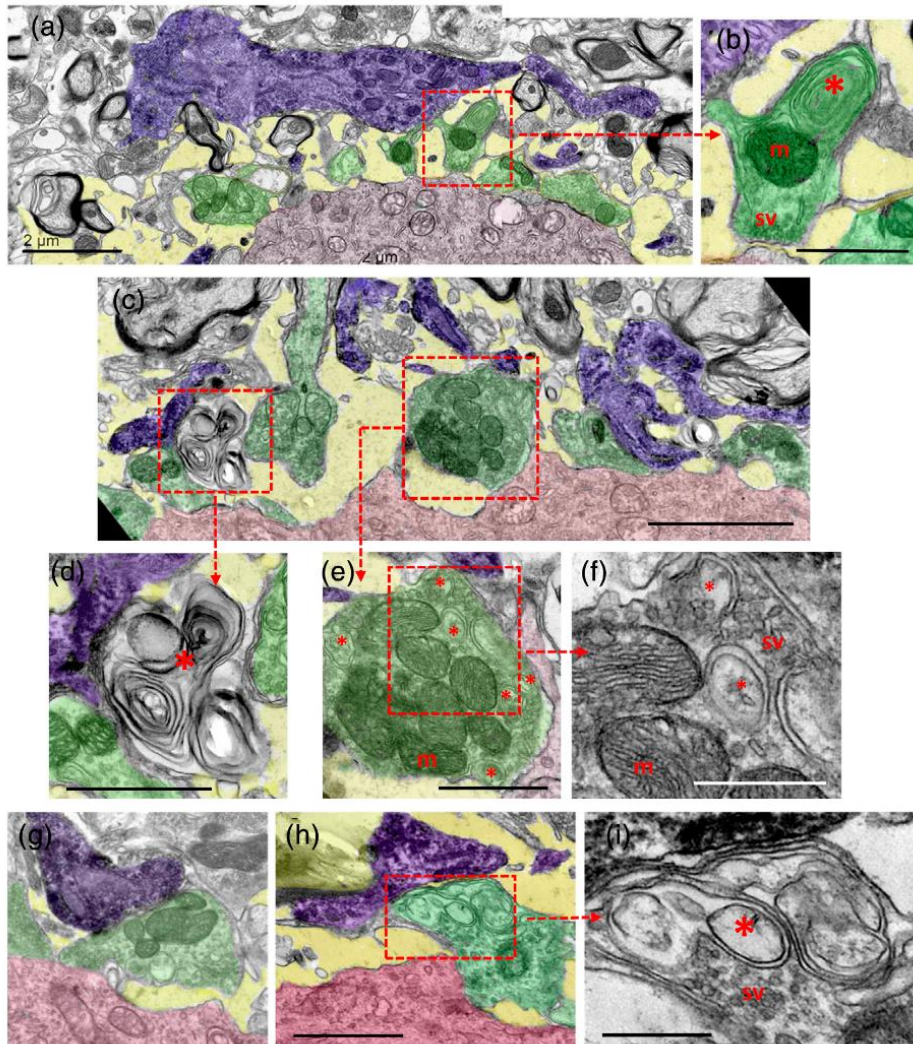


FIGURE 4 Ultrastructural analysis of the interactions of Iba1-immunostained microglial profiles (shaded in blue) with synaptic afferents (shaded in green) on motor neuron (MN) cell bodies (shaded in red) 7 days postaxotomy. (a) Microglial processes in close proximity to altered synaptic boutons and a widened extracellular space (shaded in yellow) are depicted. (b) A higher magnification detail of a synaptic bouton (delimited by a dotted square) in (a) containing clustered synaptic vesicles (sv), normal mitochondria (m) and abnormal concentrically arranged membranes of presumably endocytic origin (*). (c) Microglial cell processes (blue) interacting with altered and disrupted presynaptic boutons (green) on a 7-day-axotomized MN (red). (d) A higher magnification view of the corresponding area delimited in (c) showing a complex multilamellar body located near the MN surface and in close contact with a microglial process, presumably derived from a disrupted presynaptic bouton. (e) A detail of a partially detached presynaptic terminal contacted by microglial processes (which is delimited in (c)), showing abnormal accumulation of endocytic-like vesicles (*), enlarged in (f); m = mitochondria. (g,h) Microglial processes (blue) contacting an altered afferent synaptic bouton (green) at the surface of MN cell bodies (red). (i) A detail of the area delimited in (h) showing an abnormal accumulation of membranous structures (*) in the region in which the synaptic terminal is closest to the microglial end-foot process; note the normal clustering of synaptic vesicles in the zone contacting the postsynaptic MN. Scale bars: a = 2 μm, b = 1 μm, c = 2.5 μm, d and e = 1 μm, f = 500 nm, g = 1 μm (valid for h), and i = 500 nm [Color figure can be viewed at wileyonlinelibrary.com]

expanded. Additionally, microglial cells recruited to the vicinity of MNs, emitted processes that contacted to some of the remaining axosomatic synaptic boutons or to the synaptically denuded MN surface (Figure 5j). EVs were also present in the perineuronal space, but

at a lower density than that observed at 1–3 days postaxotomy. Many of the remaining axosomatic terminal boutons displayed a variety of involutive changes. These included: global darkening, the clumping of synaptic vesicles, and the accumulation of endosomal-

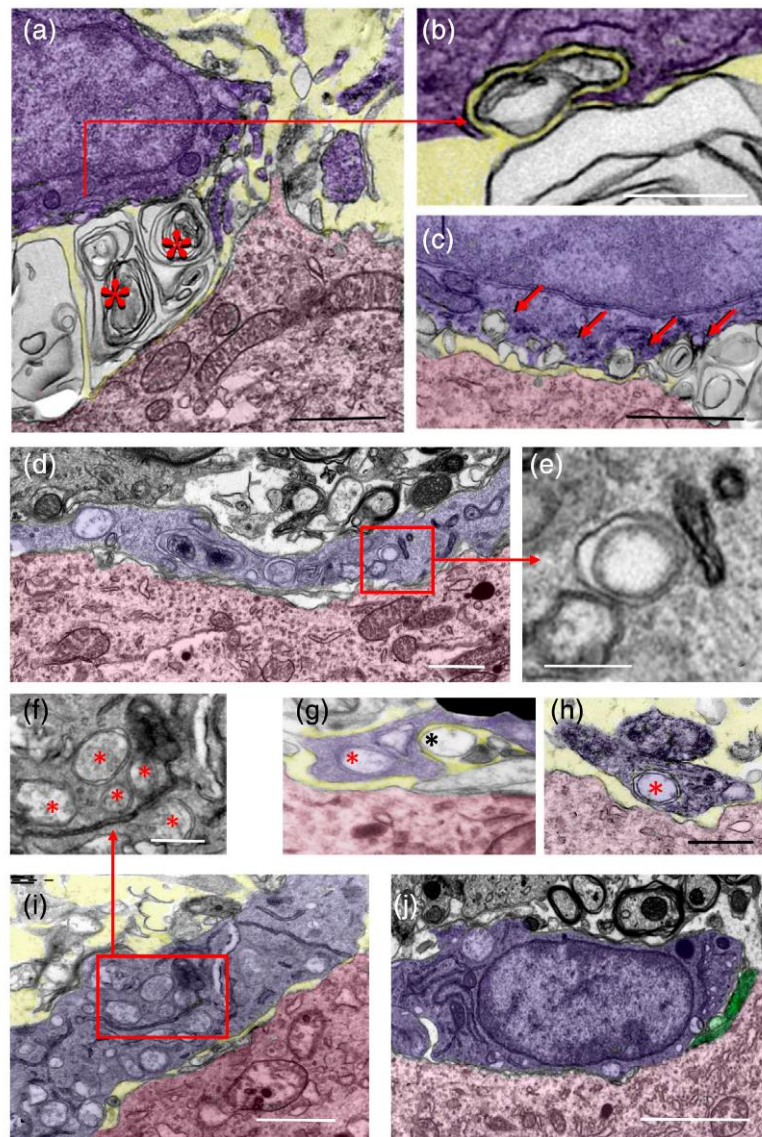


FIGURE 5 Ultrastructural analysis of the interactions of microglial cell bodies (shaded in blue) with motor neuron (MN) cell bodies (shaded in red) 7 days after axotomy. (a) Extracellular multilamellar bodies and vesicles (*) are seen interposed between an Iba1-immunostained microglial cell and an axotomized MN cell body; note that extracellular membranous structures appear in sites that would normally be occupied by presynaptic boutons on an uninjured MN soma. This suggests that the extracellular material came from disrupted synaptic terminals. (b,c) Extracellular vesicles interact with microglial cell surfaces and undergo a process of enwrapping (b, [a high magnification detail of the indicated region in a]) and engulfment; in (c) there is a sequence of early contacts leading to a final engulfment (shown by the arrows). (d) A microglial cell profile (blue) covering the surface of an axotomized MN cell body (red), which appears to be completely denuded of synaptic terminals; note the presence of abundant double-membrane endocytic/phagocytic inclusions inside the microglial cytoplasm (detailed in e). (g,h) An example of a microglial process (blue) close to an axotomized MN cell body (red); microglia interact with a single-membrane-bounded extracellular vesicle (black *) and contain a double-membrane vesicular inclusion (red *), presumably resulting from extracellular vesicle endocytosis (g). The microglial nature of the processes containing a double-membrane bounded inclusion (red *) is demonstrated by Iba1 ultrastructural immunolabeling (h). (i) A microglial cell process (blue) interacting with a surface of an axotomized MN cell body (red), which is depleted of afferent synaptic terminals; note the abundance of double membrane-bounded inclusions (enlarged in f)), presumably resulting from phagocytosis of EVs. (j) A microglial cell (blue) covering large areas of an axotomized MN surface (red) depleted of synaptic afferents (only a few of them remain, shaded in green); the microglial cell displays few phagocytic inclusions and a cytoplasmic organization suggestive of a less activated state. The extracellular space found in some panels is shaded in yellow. Scale bars: (a, c, d, and i) = 1 μ m; (b) 250 nm; (e-h) = 500 nm; and (j) = 2.5 μ m [Color figure can be viewed at wileyonlinelibrary.com]

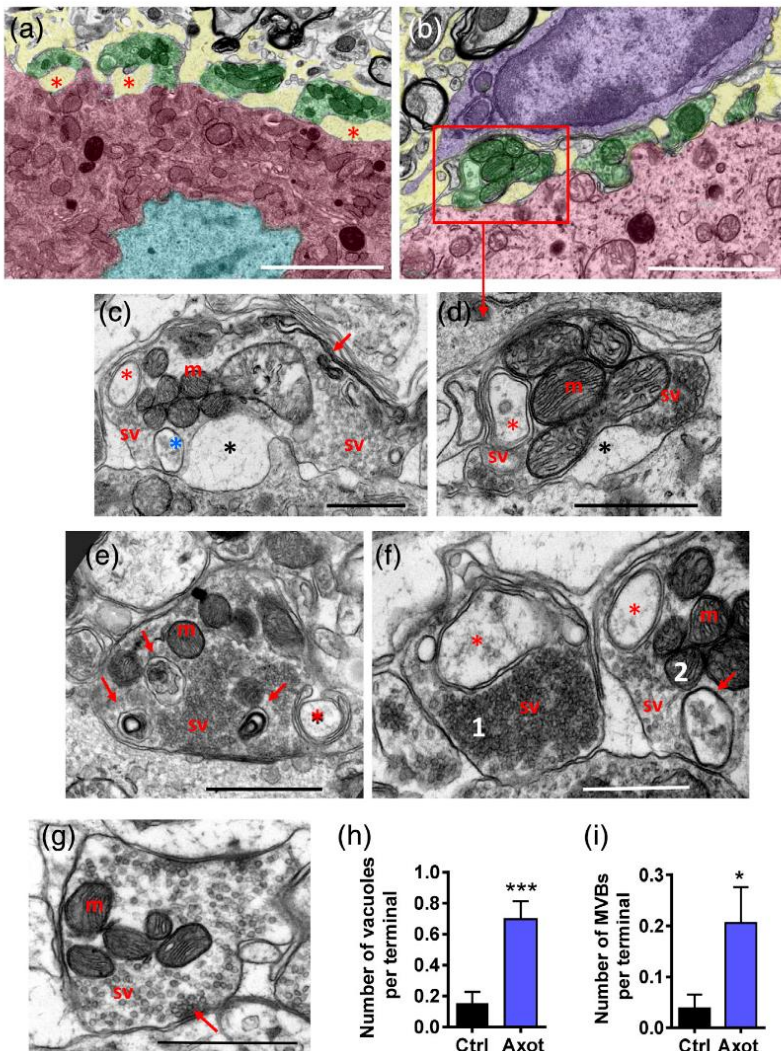


FIGURE 6 Changes in the organization of afferent synaptic terminals on motor neuron (MN) surfaces at 15 days postaxotomy. (a) An MN cell body displaying a wrinkled nucleus (light blue) and several detached synaptic terminals (green) with a widened extracellular space (yellow). (b) Another area of an axotomized MN (red) covered by altered synaptic boutons (green, detailed in d) interacting with a recruited microglial cell (blue); note that the microglial cell cytoplasm is devoid of endocytic/phagocytic inclusions, which is suggestive of a resting state. (c–f) Details of structural alterations observed in afferent synaptic terminals on a 15-day-axotomized MN; partial detachments of presynaptic and postsynaptic membranes (black asterisks), synaptic vesicles (sv) and mitochondria (m). Double-membrane encircled-endocytic-like structures are indicated by red asterisks. A multivesicular body (blue, *) is shown in (c); the accumulation of highly folded intracellular membranes (c, arrows). (e) An accumulation of phagosome/lysosome inclusions (arrows). (f) An example of abnormally clustered and densely packed synaptic vesicles (sv) is depicted in terminal 1, in conjunction with an endocytic-like vacuole; compare with the less clustered arrangement of synaptic vesicles (sv) in terminal 2, which also shows a multivesicular body (arrow), a double-membrane containing endocytic-like vesicles (*), and several mitochondria (m). (g) A control afferent synapse containing round synaptic vesicles (sv) clustered at the active zone (arrow); m = mitochondria. (h,i) Quantification of the number of endocytic/autophagosome-like vacuoles (h) and multivesicular bodies (MVBs, i) in synaptic terminals contacting 15-day-axotomized MN bodies. Data are presented as mean \pm SEM; * $p < .05$, and *** $p < .001$ versus Ctrl, Student's *t* test; $n = 52$ –73 terminals from two animals per condition. Scale bars: a = 5 μ m, b = 2 μ m, and c–g = 1 μ m [Color figure can be viewed at wileyonlinelibrary.com]

autophagosomal-like vacuoles, as well as MVBs containing distinctive intraluminal vesicles.

Moreover, at 15 days after axotomy, recruited microglial cells were often seen covering extensive areas of the surface of

axotomized MN cell bodies. These areas were completely devoid of synaptic terminals and displayed a narrow gap between the neuronal and microglial cell membranes, similarly to that occasionally seen at 7 days postaxotomy (Figure 5j).

It is known that axonal interruption in adult rats does not entail MN death, as occurs in young rats. In contrast, in adult mice, there is a slow loss of axotomized MNs in association with exacerbated microglia (Kiryu-Seo, Gamo, Tachibana, Tanaka, & Kiyama, 2006; Yamada, Nakanishi, & Jinno, 2011). In concordance with these observations, we occasionally found some MNs that displayed a completely disrupted ultrastructural organization (Supplementary Figure 5a,b).

These dying neurons were usually spatially related with altered microglial cells showing extensive vacuolation, and distended ER and perinuclear spaces, which are signs of cellular stress (Bisht et al., 2016).

At 15 days postlesion, axotomized cell bodies displayed hyperconvoluted nuclei (Figure 6a) and a reduced number of afferent synaptic terminals exhibiting a variety of structural alterations:

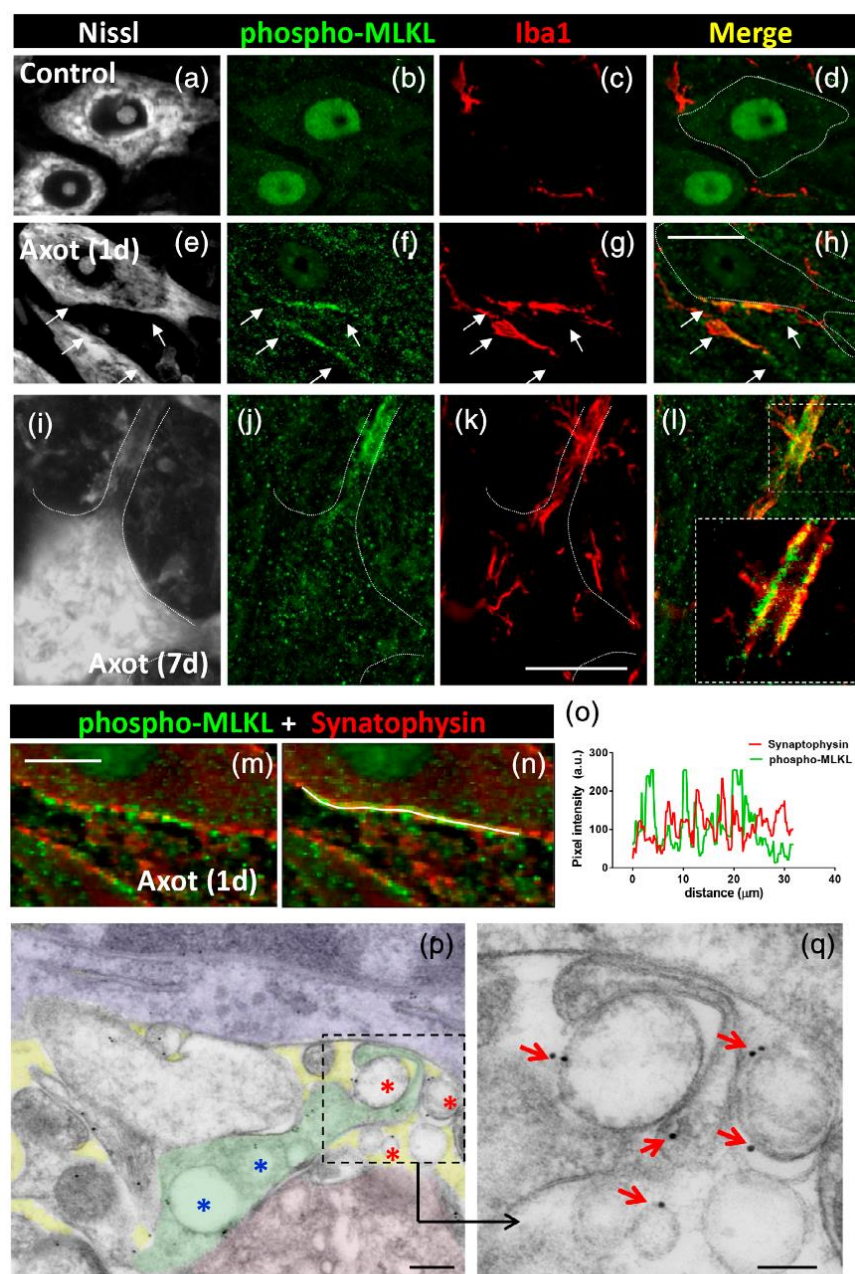


FIGURE 7 Legend on next page.

detachment from the postsynaptic membrane, and a conspicuous accumulation of endosome and autophagosome-lysosome-like inclusions. Some terminals appeared to be clearly degenerated, appearing dark in color and with clumped synaptic vesicles (Figure 6b-i).

3.3 | Activation of the necroptotic pathway is involved in synaptic disruption on axotomized MNs

Necroptosis is a regulated form of caspase-independent cell death that is mediated by receptor-interacting protein kinase 3 (RIPK3) and MLKL. In this type of programmed cell death, a rupture of cellular membranes occurs leading to the release of intracellular components; phosphorylation of MLKL by RIPK3 and its targeting to cell membranes is directly involved in the disruption of membrane integrity (Gong, Guy, Crawford, & Green, 2017; Grootjans, Vanden Berghe, & Vandenebeele, 2017; Wang et al., 2014). Broken plasma membrane may determine the formation of “bubbles” at the cell surface and the secretion of necroptotic EVs (Gong, Guy, Olauson, et al., 2017; Raden, Shlomovitz, & Gerlic, 2020). Interestingly, all these events fit very well with the ultrastructural observations we made during early stages (1–3 days) of afferent synapse acute disruption in axotomized MNs. For this reason, we explored, by immunolocalization of phospho-MLKL (Figure 7a-l), whether the activation of the necroptotic pathway is involved in central synapse loss on injured MNs. In fact, a monoclonal antibody against phospho-MLKL has been used as specific immunocytochemical marker for necroptosis in human diseased tissue (Wang et al., 2014). Using the same antibody, a positive phospho-MLKL immunoreactivity was detected near the surface of axotomized MNs early (24 hr) after peripheral nerve injury; this was not seen in control noninjured MNs. The phospho-MLKL signal was noticed in form of small puncta clustered at discrete regions of MN surface and closely related to processes of reactive microglia (Figure 7a-l). When individual sections of confocal z-stacks were analyzed in detail, it was noticed that many phospho-MLKL positive puncta were located in the narrow gap interposed between microglial and neuronal cells. Synaptophysin-positive puncta, which normally surround MN

cell bodies, were depleted at points in which phospho-MLKL-positive particles accumulated (Figure 7m-o). This is consistent with the assumption that phospho-MLKL-positive particles are derived from disrupted synaptic terminals. This was further corroborated by *in situ* localization of phospho-MLKL by means of postembedding immunogold EM. A selective labeling of vacuoles in presynaptic bouton contacting MNs and in EVs located near MN surfaces was noticed (Figure 7p-q). Negligible labeling was observed in control sections after omitting the primary antibody. A positive immunofluorescence signal was also detected in the nuclei of neuronal cells both in control and axotomized conditions; although it is known that MLKL can translocate to the nucleus during necroptosis (Yoon, Bogdanov, Kovalenko, & Wallach, 2016, this aspect, was not further explored in our context.

3.4 | Identification of EV protein markers in association with an inflammatory response and synaptic disruption adjacent to axotomized MN cell bodies

EM analysis revealed that synaptic damage and local microglial recruitment, occurring near axotomized MNs, involved the generation and probable transcytosis of EVs. We therefore further explored whether any of the already identified proteins enriched in EVs, other than necroptotic EVs (Raden et al., 2020), were locally accumulated during this form of aseptic neuroinflammation. According to the ExoCarta database (<http://www.exocarta.org>), which catalogs molecular EVs components, we used antibodies against CD9, CD63, flotillin, and PDC6IP-Alix in order to explore their presence in the ventral horn of the spinal cord during the neuroinflammatory response. Tissue samples were taken from mice at 7 days after sciatic nerve transection. Each EV marker was combined with Iba1 and VACHT immunolabeling to simultaneously visualize microglia and cholinergic synaptic profiles. In some cases, either the general synaptic bouton marker SV2 or synaptophysin was used instead of VACHT.

CD9, a member of tetraspanin family, is the protein most frequently identified in exosomes. Small CD9-positive profiles were seen

FIGURE 7 Activation of the necroptotic protein effector phospho-MLKL near the surface of injured motor neuron (MN) cell bodies and dendrites, 24 hr after axotomy. (a-d) In noninjured MN cytoplasm, phospho-MLKL-immunoreactivity (green) is weak; only a positive signal is detected in nuclei; some Iba1-positive microglial profiles (red) can be observed; MN somata were visualized by fluorescent Nissl staining (gray). (e-h) Twenty-four hours after axotomy, clusters (delimited by arrows) of phospho-MLKL-positive particles (green) can be observed near the surface of injured MN cell bodies. Recruited Iba1-positive microglial cell profiles (red) are seen in a close relationship with clustered phospho-MLKL-positive particles (green); MN somata are visualized with fluorescent Nissl staining (gray). (i-l) Clustered phospho-MLKL-positive particles (green) are seen at a site enwrapped by a recruited Iba1-positive microglial cell (red), which is located on a dendrite of an MN (delimited by dashed line on a fluorescent Nissl stained image, gray) 24 hr postaxotomy; a detail of the distribution of Iba1 and phospho-MLKL is shown in the enlarged inset in (l). (m-o) Clusters of MLKL positive particles (green), adjacent to the surface of a MN soma 24 hr postaxotomy, are interposed between the still remaining synaptophysin positive puncta (red), indicating that activated MLKL was associated to sites with disrupted synaptic boutons. The absence of colocalization of both phospho-MLKL-positive and synaptophysin-positive puncta is shown in the pixel intensity profile (o) obtained along the line drawn in (n). (p) Postembedding immunogold localization of phospho-MLKL at the membrane of extracellular vesicles (red *) interposed between an axotomized MN (red) and a microglial cell (blue); a synaptic terminal (green) displaying some labeled vacuoles (blue *) is also seen; extracellular space is shown shaded in yellow. The area delimited by dashed line in (p) is shown enlarged in (q), in which gold particles are more clearly visible in association with the membrane of EVs (arrows). Scale bars: (h) = 20 μm (valid for a-g), (k) = 20 μm (valid for i-l), (m) = 10 μm, (p) = 200 nm, and (q) = 100 nm [Color figure can be viewed at wileyonlinelibrary.com]

inside MN cytoplasm and also scattered in the adjacent neuropile (profile diameter = $0.53 \pm 0.01 \mu\text{m}$, $n = 163$) (Figure 8a). A slight CD9-positive signal was also present in VACHT-labeled cholinergic afferent terminals. However, after axotomy, there was a notable accumulation of CD9-immunoreactive particles in association with cholinergic terminals, but not with any of the other afferent synaptic

boutons (Figure 8b,e,f). In addition, CD9-positive particles were noticed attached to the surface of processes of microglial cells recruited near axotomized MN cell bodies (Figure 8c,d). An ultrastructural examination of C boutons on 7-day-axotomized MNs showed increased pleomorphism in their synaptic vesicular content; this included an accumulation of large double-membrane bounded vesicles

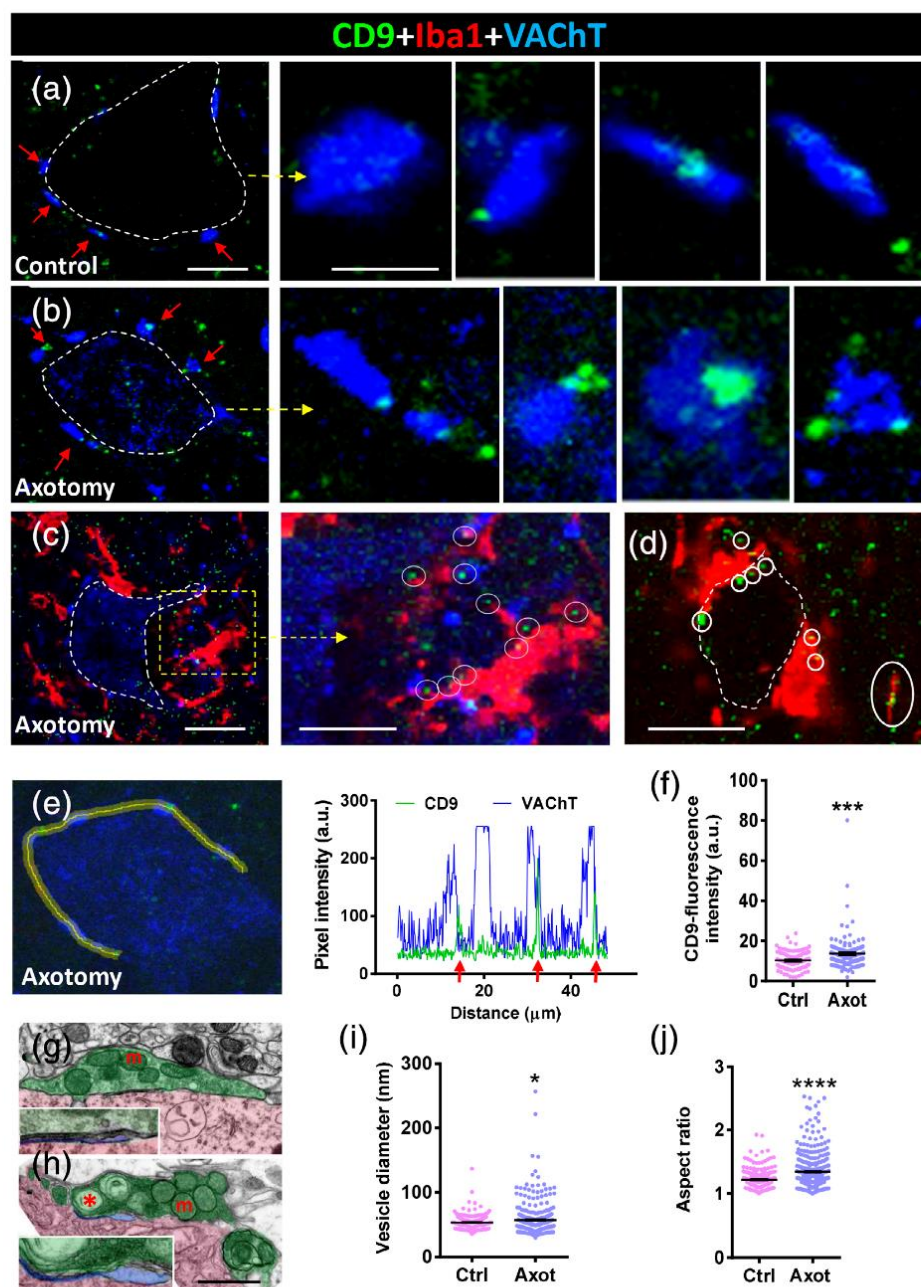


FIGURE 8 Legend on next page.

(Figure 8g–j), which presumably corresponded to the CD9-positive puncta observed under the confocal microscope.

CD63 is another protein belonging to the tetraspanin family which is enriched in EVs and has been used in the characterization of EV subtypes and found in neuronal exosomes (Kowal et al., 2016; Men et al., 2019). In control MNs, CD63 immunostaining revealed a perinuclear punctate pattern that was reinforced at the MN periphery (Figure 9a). Overall, the CD63-positive puncta were more abundant and larger than the CD9 positive particles (diameter: $0.71 \pm 0.01 \mu\text{m}$, $n = 993$). Axotomized MNs (7 days after nerve transection) showed an increased number of CD63 puncta surrounding their injured somata; they were otherwise covered by recruited microglial cells (Figure 9b–f). In sharp contrast to the CD9 immunostaining, no association of CD63-positive particles and afferent cholinergic terminals was observed. However, when CD63 immunolabeling was combined with SV2 immunostaining, it was possible to observe a close relationship between CD63 puncta located at the MN surface and axosomatic synaptic terminals (Supplementary Figure 6a,b).

Flotillin is another protein often used as an exosomal marker which has been detected in all types of EVs, baring or not tetraspanins (Baietti et al., 2012; Kowal et al., 2016). Flotillin is associated with "lipid rafts," which are membrane subdomains that are enriched in cholesterol and sphingolipids and also localized in human neuronal cell bodies (Bickel et al., 1997; Girardot et al., 2003). It has also been shown that flotillin is involved in recycling the vesicle-mediated trafficking of synaptic proteins and synaptogenesis (Bodrikov, Pauschert, Kochlamazashvili, & Stuermer, 2017). In spinal cord MNs, we noted that flotillin immunostaining displayed a particulate pattern (diameter profile: $0.59 \pm 0.01 \mu\text{m}$, $n = 424$). In axotomized cell bodies with extensive microglial covering, flotillin-positive particles were seen to accumulate on the surface of neuronal cell bodies and, in particular, at the microglia-neuronal interface (Figure 9g–l).

Another abundant component in the exosome proteome is PDC6IP-Alix, a protein originally identified in relation to the apoptotic signaling pathway and later found to be connected to endocytic membrane trafficking and exosome formation (Odorizzi, 2006). On sections

of spinal cord tissue, Alix-immunoreactivity was detected in the form of small particles distributed within the MN cytoplasm; the particles delineated subdomains that probably represent intracellular membrane compartments such as ER or Golgi areas. In addition, the antibody used strongly detected intranuclear inclusions, which probably corresponded to nuclear speckles; we suggest that this localization could have been due to an unspecific cross reaction of the antibody used. This pattern of MN immunostaining did not change very much in the axotomized MNs that were covered by microglial cell processes (Supplementary Figure 7a,b).

3.5 | Altered distribution of Rab GTPase proteins in MNs and microglia after axotomy

The Rab GTPase family of small-molecular-weight proteins comprises more than 60 gene products, with most of its members playing a role in vesicular trafficking in eukaryote cells (Zerial & McBride, 2001). They are also critically involved in the regulation of the synaptic function at presynaptic and postsynaptic sites (Mignogna & D'Adamo, 2018). Taking into account the dramatic changes that occur in the structural organization of the synaptic vesicular compartment observed in the synaptic terminals of axotomized MNs by EM, we used immunocytochemistry to analyze whether the localization of some of the Rab-GTPase proteins in MNs and adjacent cells changed as a consequence of axotomy. Antibodies against Rab 4, 5, 7, 8A, 9, and 10 were used in sections of spinal cord taken from mice 3 or 7 days after sciatic nerve axotomy. Ventral horn MNs from both the ipsilateral (lesioned) and contralateral (control) sides were examined, after triple fluorescent immunostaining, for the simultaneous identification of each Rab protein. This was performed in combination with Iba1 and VACHT, which were, respectively, used as microglial and cholinergic synapse markers.

Rab4-immunoreactivity revealed a pattern in the form of small particles scattered within the MN cell bodies, with no overt changes being found after axotomy. The Rab4 signal was, however,

FIGURE 8 CD9-immunoreactive puncta accumulate into VACHT-positive synaptic afferents (C-boutons) on motor neurons (MN) at 7 days postaxotomy; CD9-positive particles also interact with recruited microglia. (a) A control MN cell body (delimited by a dotted line) displaying VACHT-positive synaptic terminals (blue, arrowed) and faint CD9-positive puncta (green); arrowed synapses are shown at higher magnification in the neighboring panels (a). (b) A 7-day-axotomized MN (delimited by a dotted line) displaying VACHT-positive synaptic terminals (blue, arrowed) and faint CD9-positive puncta (green); arrowed synapses are shown at higher magnification in the right-hand panels (b); note the increase in size and number of CD9 particles compared to the control. (c) Microglial cells (Iba1 immunostained, red) recruited in close proximity to a 7-day-axotomized MN (delimited by a dotted line) interact with CD9-containing particles (encircled), as shown at higher magnification in the right-hand panel (c). (d) Another example of an axotomized MN showing recruited microglia (red) contacting CD9-positive particles (green, encircled). (e) Pixel intensity (arbitrary units [a.u.]) profile along a line (yellow) traced on the VACHT-positive synapses (blue) contacting MN surface, in order to simultaneously analyze CD9-immunoreactivity (green) as depicted; arrows point out the association between the CD9-signal and VACHT-positive peaks. (f) Quantification of CD9 fluorescence intensity on VACHT-positive C-boutons on 7-day-axotomized MN. (g,h) Electron microscope micrographs showing C-boutons on a control (g) and a 7-day-axotomized MN (h); synaptic terminals, shaded in green; MN cell body, shaded in red; and postsynaptic subsynaptic cistern, shaded in blue and enlarged in the insets; abnormally large vesicular structures (*) and dilated SSC are seen after axotomy in (h); m = mitochondria; (i,j) Quantification of the size (i) and shape (j, aspect ratio of vesicular membranous structures in C-boutons; data are shown as mean \pm SEM; * $p < .05$, ** $p < .001$, and *** $p < .0001$ versus Ctrl, Student's t test; $n = 95$ –140 C-boutons (f), and 262–351 C-bouton synaptic vesicles (i,j) (two animals per condition). Scale bars: a = $10 \mu\text{m}$ (valid for b); enlarged areas from a = $2 \mu\text{m}$ (valid for enlarged areas from b); c = $20 \mu\text{m}$; enlarged area from c = $10 \mu\text{m}$; d = $15 \mu\text{m}$; and h = $1 \mu\text{m}$ (valid for g) [Color figure can be viewed at wileyonlinelibrary.com]

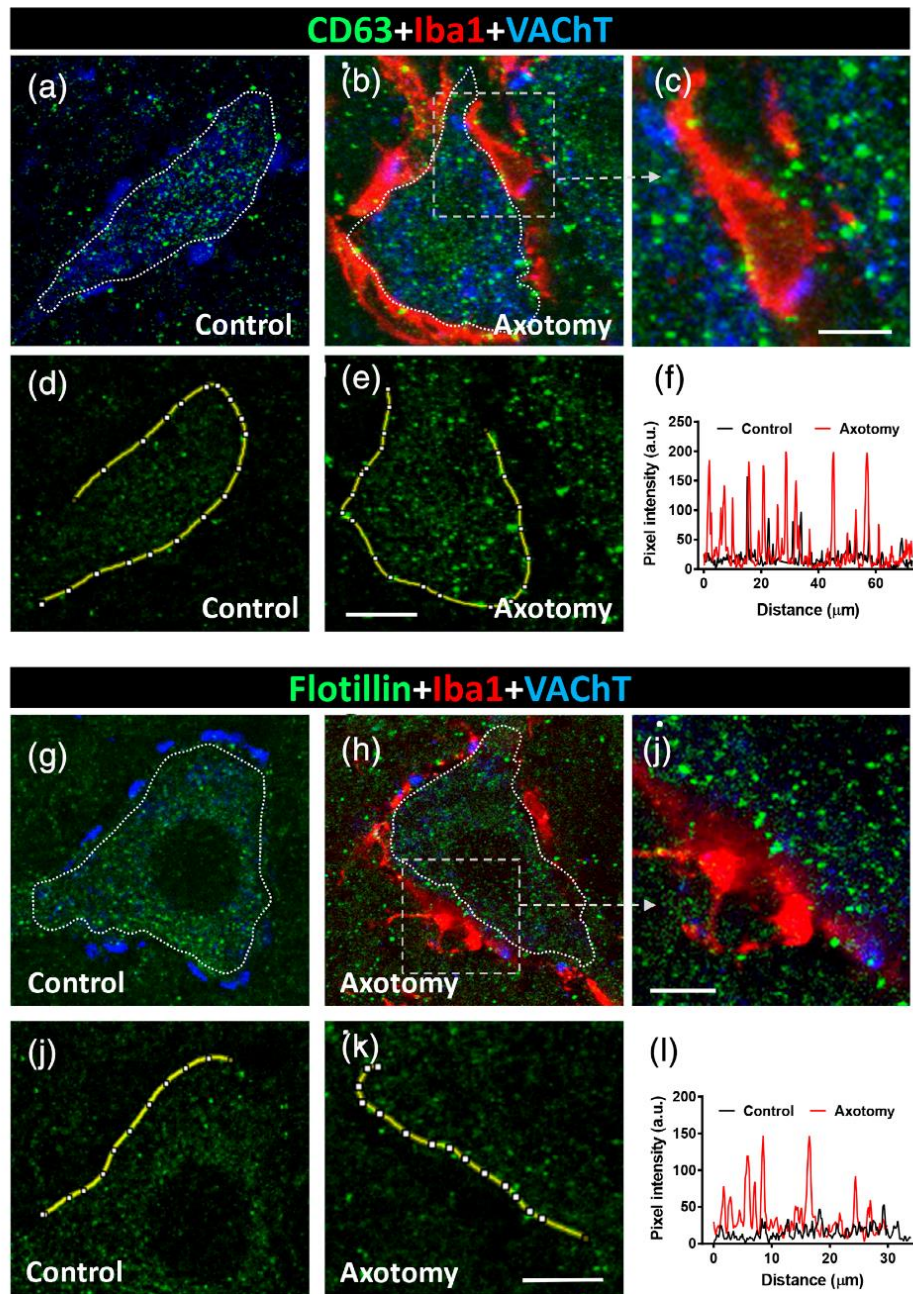


FIGURE 9 (a–f) CD63-immunoreactivity in control and 7-day-axotomized motor neurons (MNs). (a) A control MN showing CD63-immunolabeling in the form of abundant particles (green); no association is found with VACHT-positive synaptic terminals (blue). (b) After axotomy, many CD63-positive particles (green) are seen interacting with microglial cells (Iba1-immunolabeled, red) recruited at the MN surface; the boxed area is shown enlarged in (c). (d–f) Pixel intensity (arbitrary units [a.u.]) profile along a line (yellow) traced along the periphery of the control and axotomized MN cell bodies, showing the increase in CD63-positive particles postaxotomy. (g–l) Flotillin-immunoreactivity in control and 7-day-axotomized MNs. (g) A control MN showing flotillin-immunolabeling in the form of abundant particles (green); no association is found with VACHT-positive synaptic terminals (blue). (h) After axotomy, many flotillin-positive profiles (green) are seen in close proximity to microglial cells (Iba1-immunolabeled, red) recruited at the MN surface; the boxed area is shown enlarged in (j). (i–l) Pixel intensity (arbitrary units [a.u.]) profile along a line (yellow) traced along the periphery of the control and axotomized MN cell bodies, showing the increase in flotillin-positive particles postaxotomy. Scale bars: e = 10 μm (valid for a, b, d); c = 5 μm; k = 15 μm (valid for g, h, j); and i = 5 μm [Color figure can be viewed at wileyonlinelibrary.com]

higher in the neuronal processes occupying the MN neuropile (including the MN axons), and this was substantially increased following axotomy. Similar results were found for Rab5 (Supplementary Figure 8a-d).

Rab7 is a factor which is recruited by nascent phagosomes and is essential for their fusion with late endosomes and/or lysosomes (Bucci, Thomsen, Nicoziani, McCarthy, & van Deurs, 2000; Harrison, Bucci, Vieira, Schroer, & Grinstein, 2003). In microglial cells, it has

been shown that Rab7 is required for the fusion between pinosomes and lysosomes and for their size-based sorting (Chen et al., 2015). In sections of spinal cord, Rab7 displayed a noticeable punctate pattern of immunoreactivity in the MN soma, under both control and axotomized conditions. The size of the Rab7-positive particles was: $0.50 \pm 0.01 \mu\text{m}$ ($n = 220$). Recruited microglia close to axotomized MNs displayed a notable accumulation of Rab7-positive particles (Figure 10a-c). It should be noted that Rab7-positive particles located

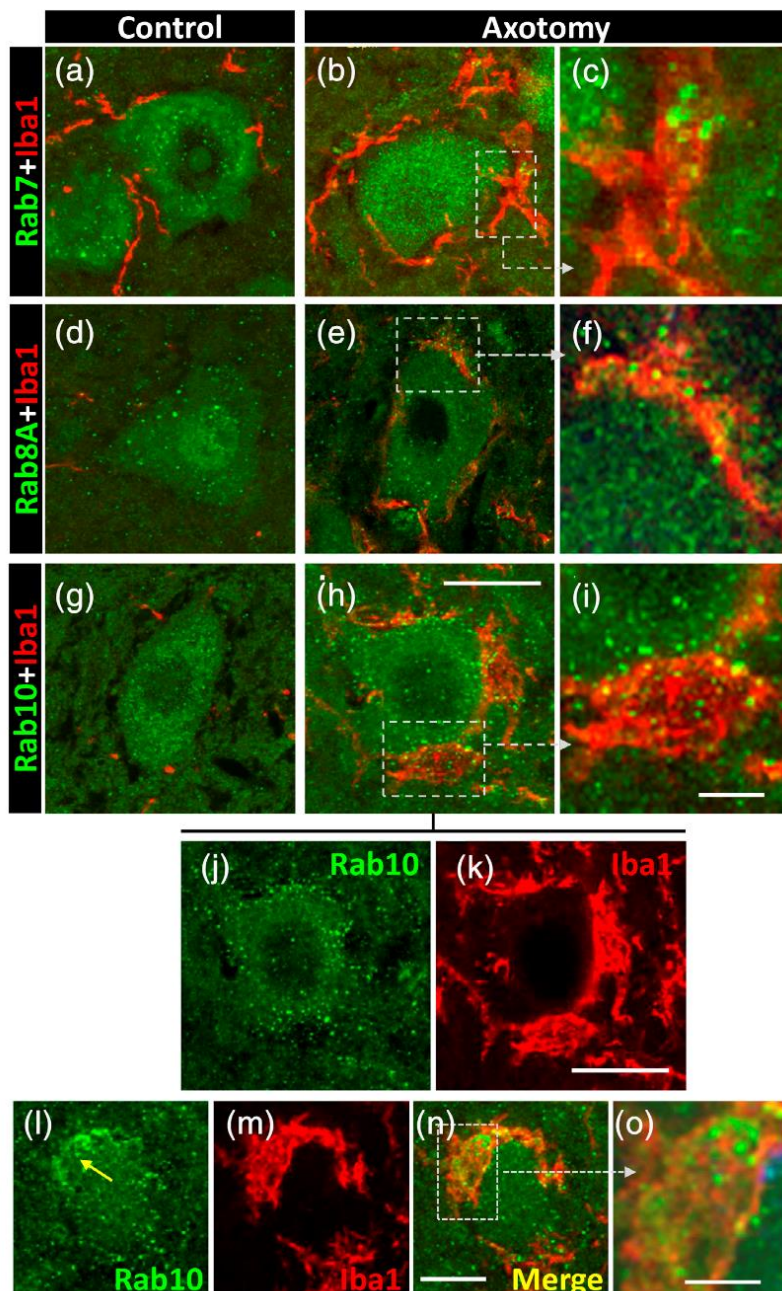


FIGURE 10 Expression of Rab GTPase proteins (green) in motor neurons (MN) and microglia (red) in a basal condition and after axotomy, as indicated. (a–c) Compared to control, Rab7-positive particles accumulate in recruited microglial cells adjacent to 3-day-axotomized MNs, as depicted in the enlarged boxed area in (c). (d–f) Abundant small Rab8A-positive profiles are seen inside microglial cells covering a 7-day-axotomized MN; the area delimited by a square is shown at higher magnification in (f). (g–k) Numerous Rab10-positive particles are mainly seen at the interface between microglia and the soma of a 7-day-axotomized MN; the area delimited by a square is shown enlarged in (i); (j,k) corresponds to spliced green and red channels from (h); the peripheral distribution of Rab10-positive particles on MN soma is clearly visible in (j). (l–o) Illustrate the accumulation of Rab10-positive particles inside microglia covering the surface of a 7-day-axotomized MN; an enlargement of the boxed area is shown in (o). Scale bars: $h = 20 \mu\text{m}$ (valid for a, b, d, e, g, j, and k); $i = 5 \mu\text{m}$ (valid for c and f); $n = 20 \mu\text{m}$ (valid for l,m); and $o = 5 \mu\text{m}$ [Color figure can be viewed at wileyonlinelibrary.com]

inside microglial cells were significantly larger than those present in MN somata ($1.13 \pm 0.15 \mu\text{m}$, $n = 13$, $p < .0001$).

Rab8A has been shown to be enriched in macropinocytotic vesicles of activated macrophages (Wall et al., 2019). It has also been reported that Rab8A interacts with flotillin in the tubulovesicular recycling compartment (Solis et al., 2013). We found that Rab8A-immunoreactivity was present in MN somata in the form of small puncta (diameter: $0.55 \pm 0.01 \mu\text{m}$, $n = 209$), under both control and axotomized conditions. Some postaxotomy-activated microglial cells, which interacted with MN somata, showed an accumulation of small Rab8A-positive particles (Figure 10d–f). It is interesting to note that this location was highly comparable with the one that we found for flotillin in microglial cells after axotomy.

Rab10 has been identified as a novel protein which is predominantly localized in tubular endosomes (Etoh & Fukuda, 2019). As far as we know, no data have previously been published regarding Rab10 in microglia. Our findings relating to Rab10 after axotomy would seem to be of particular interest. Under control conditions, Rab10 was present in the form of small, homogeneously distributed, dots (diameter: $0.49 \pm 0.008 \mu\text{m}$, $n = 543$) within the MN soma, while no particular association was observed with microglial cells. Seven days after axotomy, the Rab10 particles migrated to the periphery of the MN cell body and many particles were also observed in association with microglial cells covering lesioned MNs (Figure 10g–o).

4 | DISCUSSION

During the developmental establishment of neuronal networks, microglia play a fundamental role via a process of activity-dependent synaptic pruning and remodeling in order to achieve a stable neural function and establish robust behavior. In adults, however, synaptic loss is considered an early sign of various neurodegenerative conditions, including MN diseases (Fogarty, 2019; Vukojicic et al., 2019). It has been suggested that a reactivation of synaptic elimination mechanisms similar to those operating during development may occur in these disorders (Stephan, Barres, & Stevens, 2012). Accepting the putative relevance of the synaptic alteration within the context of MN pathology, we used a peripheral nerve lesion paradigm, which resulted in prominent microglial activation, to explore its impact on the fate of MN synaptic inputs. Microglial activation around axotomized MNs is an extensively documented process, but its effect on afferent synaptic bouton organization has been poorly addressed with rather confusing results. For a long time, it was assumed that activated microglia recruited close to MN cell bodies play a role as “synaptic strippers”; however, whether stripping represents a simple and reversible synaptic withdrawal or, conversely, leads to the degeneration and phagocytosis of synapses, has yet to be clearly established (Aldskogius, 2011; Alvarez et al., 2020; Linda et al., 2000; Möller et al., 1996; Moran & Graeber, 2004; Sumner, 1975). In axotomized facial MNs, Blinzing and Kreutzberg (1968) have described how active microglia displaced intact synaptic terminals from neuronal perikarya; the absence of degenerating synaptic boutons and lack of apparent

phagocytosis by microglia have also been reported. Our results in spinal cord, unambiguously demonstrate that a severe disruption of synaptic afferents to MNs occurs early after peripheral nerve transection in conjunction with prominent distant aseptic microglial mediated neuroinflammation. In agreement with the description Blinzing and Kreutzberg (1968), we observed that in advanced stages of microglial migration toward axotomized MNs, large areas of the MN cell body surface appeared to be completely devoid of synaptic contacts and the vacant spaces were occupied by flattened microglial cells. In these areas, signs of synaptic degeneration were rarely visible. Nevertheless, this clearly contrasts with what occurs during the early steps of interaction between recruited microglial cells and axotomized MN cell bodies and their synapses. The partial discordance between observations could therefore have resulted from limited spatial and temporal sampling in different models of MN axotomy.

We observed that the way in which synaptic terminals are eliminated in the MN axotomy paradigm did not comprise their bulk engulfment by microglia. Instead of this, microglial cells internalize small membranous vesicular fragments arising from the disruption of synaptic terminals, which, presumably, were previously primed by their close proximity with microglial processes. It should be noted that processes from early recruited microglial cells postaxotomy preferentially contacted presynaptic boutons rather than the MN surface. Other microglial filopodia interacted with vesicular elements coming from the disassembly of previously altered synaptic boutons.

The ultrastructural organization of the area adjacent to the surface of MN somata abruptly changes as soon as 24 hr after peripheral nerve transection. During this early acute alteration, some synaptic terminals exhibit a rupture of presynaptic membranes with the concomitant release of intracellular vesicles that further accumulate at the extracellular space. This overall picture fits well with a process of necroptosis, and this was corroborated by the localization of the membrane-disrupting effector MLKL at sites where presynaptic terminals degenerate and in neighboring EVs. Our negative results after western blot analysis could be because only a proportion of MNs in ventral horn belong to the axotomized sciatic nerve pool, and the corresponding synaptic disruption occurs in restricted subcompartments at a given time. Thus, the expression of necroptotic molecular markers such as phospho-MLKL, would be hard to detect in the whole extracts. In any case, we think that, the accuracy of data from the *in situ* immunolocalization, both at the confocal and EM levels, are enough robust to show the involvement of the necroptotic pathway in the acute synaptic disruption occurring on axotomized MNs. As this probably occurs in the absence of the death of its parent neuron, we must assume that a necroptotic program may be locally activated in presynaptic axon terminals, as described for a form of apoptosis spatially confined to axons or synapses (Cusack, Swahari, Hampton Henley, Michael Ramsey, & Deshmukh, 2013; Mattson, Keller, & Begley, 1998).

Sites where phospho-MLKL-containing vesicles accumulate were usually closely associated with microglia that was attracted to axotomized MNs. One of the possible microglial-derived factor that

SALVANY ET AL.

may initiate the activation of necrotic pathway is tumor necrosis factor, as occurs in other neuropathological conditions (Chen et al., 2019; Ito et al., 2016; Pasparakis & Vandenabeele, 2015). However, one important aspect not resolved here is whether activated microglia induces a synaptic damage that precedes synaptic disruption or, conversely, an altered, neuronal-autonomous, synaptic function, is as a primary event which promotes a chemotactic effect on microglia.

Experiments in which microglial proliferation has been prevented by means of antimitotic agents have not demonstrated any significant change in afferent synaptic loss on axotomized MNs (Graeber, Streit, & Kreutzberg, 1989; Svensson & Aldskogius, 1993). Our results obtained with the CSF1R blocking agent PLX5622 showed only ~10% of synaptic loss prevention, despite the ~46% reduction in microgliosis; this suggests a poor correlation between the strength of the microglial reaction and the number of synaptic boutons which are eliminated. A lack of correlation between synaptic stripping and microglial function has also been observed in MNs devoid of CSF1 (Akhter, Griffith, English, & Alvarez, 2019; Rotterman et al., 2019) and also in other conditions involving synaptic degeneration or plasticity (Perry & O'Connor, 2010; Tremblay & Majewska, 2011).

To a variable degree, nonacutely disrupted synaptic terminals contacting axotomized MNs showed an accumulation of membrane-bound organelles, such as endosome-like and phagosome-like vacuoles, which are indicative of altered vesicle recycling and synaptic function. Early studies on synaptic structure and function have described how increased synaptic activity results in an accumulation of extensive presynaptic membrane infoldings which are generated as a consequence of the blocking of the vesicle recycling process (Haimann, Torri-Tarelli, Fesce, & Ceccarelli, 1985; Solsona, Esquerda, & Marsal, 1981). Along these lines, it should also be noted that changes in the activity of MN afferent synapses occurs soon after peripheral nerve injury (Bichler et al., 2007). An accumulation of comparable vacuolar intermediates has been observed in presynaptic terminals when the conversion of bulk endosomes into synaptic vesicle is inhibited (Wu et al., 2014). We have also observed double-membrane autophagosome-like vesicles similar to those found after autophagy promotion by rapamycin (Hernandez et al., 2012), or by Sonic hedgehog (Petralia et al., 2013) or Basson depletion (Okerlund et al., 2017; Waites et al., 2013). In synaptic terminals, synaptic vesicles or proteins are eliminated by autophagy (Lüningschrör & Sendtner, 2018). Since the induction of reactive oxygen species (ROS) rapidly provokes a pre-synaptic promotion of autophagy (Hoffmann et al., 2019), it could be assumed that activated microglia in the proximity of synaptic terminals would release ROS (Block, Zecca, & Hong, 2007), resulting in local protein and organelle damage and in the activation of autophagic pathways. In addition, massive and spatially restricted microglial over-activation state may result in more extensive neurotoxic damage affecting MN survival as it is occasionally seen after axotomy.

Additionally, it should be taken into account that activation of MLKL does not definitively result in an irreversible commitment to cell death. In certain conditions, MLKL-dependent membrane damage can be repaired to promote cell survival. In these circumstances, active MLKL induce the formation of bubbles at the surface of the cells that

are released extracellularly (Gong, Guy, Olaison, et al., 2017). MLKL also associates to endosomes to facilitate the generation and release of EVs, independently of death induction (Yoon, Kovalenko, Bogdanov, & Wallach, 2017). These data are of interest because they may also account for the vacuolar changes we observed in synaptic terminals that escape from the acute "explosive" disruption. These terminals remain, at least several days, in contact with MNs, display abundant MVBs and endosome-like vesicles, and are often in contact with microglial processes. Thus, in these terminals, the enhanced endosomal trafficking may be also a source of EVs other than "lytic EVs." These EVs would correspond, based on their molecular composition, to exosomes. In these cases, phospho-MLKL, would work antagonizing, instead of stimulating, the execution of lysis during necroptosis (see Yoon et al., 2017); this would result in the structural maintenance of synaptic terminals exhibiting a conspicuous alteration in their vacuolar system. Moreover, this scenario is in concordance with the increased density of particles displaying positive immunoreactivity for exosomal markers we found near the surface of axotomized MN somata 7 days postlesion. Thus, different populations of EVs such as necroptotic vesicles, plasma membrane-derived vesicles, and vesicles derived from MVBs should be produced in a separate spatiotemporal sequence during the complex reactive cellular events occurring near the surface of axotomized MNs. However, we cannot exclude that a part of EVs may be secreted by microglia (Paolicelli, Bergamini, & Rajendran, 2019). Another point that should be considered here is the existing link between necroptosis and inflammation, by increasing the production and release of cytokines and chemokines (Orozco et al., 2019), as well as by activating the inflammasomal pathway, involving caspase 1 activation and cytokine IL-1 β secretion (Conos et al., 2017).

The degenerative signs we found in synaptic terminals 2 weeks after nerve transection are very similar to those described in other "synaptopathies" in the context of human prion diseases (Sikorska, Liberski, Giraud, Kopp, & Brown, 2004). Dark degenerating terminals have also been described in the initial stages of prion disease pathology (Jeffrey et al., 2000; Šíšková, Reynolds, O'Connor, & Perry, 2013), even in the absence of the direct involvement of microglial cells (Šíšková et al., 2009). This suggests that, at least in this case, synaptic degeneration and removal may be part of an autonomous neuronal process. Nevertheless, delayed microglia activation occurs in these models.

In the MN axotomy paradigm, the disconnection of cell bodies from the periphery is the stimulus that rapidly changes the MN status in a way that is coped with its immediate environment: that is, extracellular matrix, afferent synapses and glial cells. For example, it is conceivable that MNs or synapses rapidly switch from "do not eat me" to "eat me" signals, which are sensed by microglia. Mobilized microglia may release various factors, including matrix metalloproteinases (Kim et al., 2007; Konnecke & Bechmann, 2013), thrombospondin (Möller et al., 1996), and free radicals, which affect the extracellular matrix in the immediate MN environment (perineuronal net; Fawcett, Oohashi, & Pizzorusso, 2019). This may have consequences such as the widening of the extracellular space (i.e., local edema) or the

detachment of presynaptic from postsynaptic structures. This would also contribute to weakening the blood-spinal cord barrier, which has been shown to be disrupted in spinal cord after peripheral nerve lesions and to contribute to the influx of inflammatory mediators (Echeverry, Shi, Rivest, & Zhang, 2011); this is consistent with the endogenous IgGs that we have seen surrounding capillary vessels near axotomized MNs and also decorating the surface of recruited microglial cells. It is interesting to note that IgG extravasation exists during the initial stages of disease in ALS mouse models, in conjunction with muscle denervation and before MN death (Zhong et al., 2008). At the same time as escaped IgGs bind to the surface of microglial cells, presumably through Fc receptor upregulation, C1q also becomes overexpressed in microglia. It is conceivable that C1q produced by microglia binds vesicular debris coming from disrupted synaptic terminals in order to promote their opsonization and phagocytosis, in a comparable way to what happens during the clearance of apoptotic cells (Galvan, Greenlee-Wacker, & Bohlson, 2012) or developmental synaptic remodeling and pathological synaptic loss (Hong et al., 2016; Schafer et al., 2012; Stevens et al., 2007). However, we must also point out that, in the absence of C1q, synapse elimination on MNs following axotomy is not reduced (Berg et al., 2012). This is probably due to a redundancy mechanism involved in the loss of afferent synapses on lesioned MNs.

We observed a type of double-membrane-bound vacuoles with an analogous morphology inside of synaptic terminals and internalized within microglial cells. This suggested that they could form part of a category of membrane vesicles that originated in nonacutely broken synapses and were subsequently transferred to microglia. In line with this interpretation, it was possible to detect free intercellular intermediates of this particular morphological type of vesicles. This observation is in concordance with the presynaptic secretion of EVs. The increased expression of EV markers such as CD9 and CD63, together with the presence of flotillin adjacent to neuronal surface and in close relation with microglial processes, would be concordant with this hypothesis. In an "in vitro" model of synaptic elimination, exosomes released by PC12 cells promoted microglial activation, with subsequent synaptic phagocytosis and pruning (Bahrini, Song, Diez, & Hanayama, 2015).

The increase in CD9-containing particles restricted to the C-boutons contacting axotomized MNs, is particularly intriguing. Several quite particular properties of vesicular trafficking and transcytotic transfer have been identified in this type of terminals (Caleo et al., 2018). We noticed that a pattern of vacuole accumulation in conjunction with dark degeneration predominated in C-boutons of axotomized MNs; this phenotype is not usually seen in other types of synapses. C-boutons are also preferential chemoattractive sites for microglial filopodia during their mobilization postaxotomy (Salvany et al., 2019). This indicates that the fate of afferent synaptic terminals on axotomized MNs is not entirely homogeneous and depends on their neurotransmitter-specificity. It has also been reported that axotomy in MNs favors the predominant loss of excitatory inputs with respect to other input types (Alvarez et al., 2011; Spejo & Oliveira, 2015).

The ultrastructural morphology that we observed in the EVs "floating" in the perineuronal net of axotomized MNs was highly pleomorphic and exhibited a broad variation in size. These vesicles appear to belong to a heterogeneous population of EVs which includes exosomes and other EVs (in example, lytic or necroptotic vesicles). Used in a restrictive form, the term "exosome" is usually applied to small vesicles (50–100 nm) of endosomal or MVB origin that are released from cells. Other membrane vesicles released by the outward budding of cells include a heterogeneous population of elements without this size limitation that can even exceed 1 μm in length and that have sometimes been referred to as microvesicles or ectosomes. The more general term of EVs has been used for a collective denomination of these elements (Cocucci & Meldolesi, 2015; Colombo, Raposo, & Thery, 2014; Kowal et al., 2016). Exosomes can be released from neurons in an activity-dependent manner (Fauré et al., 2006). In our system, we have seen synaptic boutons displaying a prominent concentration of MVBs; this suggests that they could be a source of exosome secretion in the perineuronal milieu. Other larger and pleomorphic vesicles observed in this enlarged extracellular space originate from a disruption of synaptic terminals and should be considered as cellular debris (Baxter et al., 2019). Similar alterations in membrane integrity may be induced by complement-mediated cytolysis, a condition that should be further evaluated in MNs postaxotomy. We demonstrate that the fate of most of the EVs generated in the perineuronal space of axotomized MNs is their elimination by microglial cell phagocytosis. These data are in concordance with the progressive and transient accumulation of CD68-positive puncta inside recruited and perisomatic microglia which, in turn, is indicative of lysosomal activity. However, the intimate relationship between exosomal markers such as CD9, CD63, and flotillin with the microglial cell surface indicates a previous process involving the endocytic trapping of EVs. The presence of Rab7 and Rab10 in microglia interacting with injured MNs is an indicator of the activation of endocytic activity by these cells.

Overall, our data reveal new mechanisms by which afferent synapses are removed from acutely injured MNs after peripheral nerve transection. Although microglial cells are actively involved in eliminating fragments of damaged presynaptic terminals, there is a lack of evidence to support any bulk engulfment of synaptic boutons. EVs are intermediate elements in this process of synaptic removal, which presents certain homologies with those described under the concept of synaptic trogocytosis during microglia-mediated synaptic removal during development (Weinhard et al., 2018). Nevertheless, further studies are required for a more general validation of this phenomenon of synaptic piecemeal phagocytosis. Since the reduction of synaptic inputs in MNs is an early event in amyotrophic lateral sclerosis (ALS) (Chang & Martin, 2009; Jiang, Schuster, Fu, Siddique, & Heckman, 2009; Sasaki & Iwata, 1996; Schutz, 2005; Sunico et al., 2011; Vaughan, Kemp, Hatzipetros, Vieira, & Valdez, 2015) and spinal muscular atrophy (SMA) pathology (Cerveró et al., 2018; Menthis et al., 2011; Tarabal et al., 2014; Vukojicic et al., 2019), a more precise understanding of the fundamental mechanisms involved in the microglia-synapse interaction in the injured MNs may help to define new therapeutic interventions. The impact of our observation on the

SALVANY ET AL.

pathogenetic mechanisms underlying ALS deserves further attention since the role of necroptosis in this disease remains controversial (Dermentzaki et al., 2019; Ito et al., 2016; Re et al., 2014). In any case, our results may prove significantly relevant in the context of functional recovery after peripheral nerve injury, in which the restoration of synaptic inputs to MNs is incomplete in spite of successful nerve regeneration and muscle reinnervation (Rotterman, Nardelli, Cope, & Alvarez, 2014).

ACKNOWLEDGMENTS

The authors thank Alaó Gatus, Alba Blasco, and Sílvia Gras for their help in some experiments, Anaïs Panosa from the SCT of Microscopy of the *Universitat de Lleida* for technical support with confocal microscopy, and the staff from the SCT Animal Facility of the *Universitat de Lleida* for mouse care and housing. The authors thank Lidia Delgado and M. Yolanda Muela, from the *Unitat de Criomicroscòpia Electrònica (Centres Científics i Tecnològics de la Universitat de Barcelona)*, for technical support with ultrastructural immunolabeling, and Plexxikon Inc. for providing the CSFR1 inhibitor PLX5622. This work was supported by grants from the *Ministerio de Ciencia, Innovación y Universidades* cofinanced by *Fondo Europeo de Desarrollo Regional (FEDER)*; RTI2018-099278-B-I00 J. C. and J. E.), and from Jack Van den Hock a la Investigació de l'ELA – Fundació Miquel Valls. S. S. holds a grant from the Spanish *Ministerio de Educación, Cultura y Deporte (FPU)*.

CONFLICT OF INTEREST

The authors declare no conflict of interest.

DATA AVAILABILITY STATEMENT

All the data and original images of this article are available upon reasonable request by e-mailing to the corresponding author.

ORCID

Josep E. Esquerda  <https://orcid.org/0000-0003-1413-2103>

REFERENCES

- Akhter, E. T., Griffith, R. W., English, A. W., & Alvarez, F. J. (2019). Removal of the potassium chloride co-transporter from the somatodendritic membrane of axotomized motoneurons is independent of BDNF/TrkB signaling but is controlled by neuromuscular innervation. *eNeuro*, 6(5), ENEURO.0172-19.2019. <https://doi.org/10.1523/ENEURO.0172-19.2019>
- Aldskogius, H. (2011). Mechanisms and consequences of microglial responses to peripheral axotomy. *Frontiers in Bioscience (Scholar Edition)*, 3, 857–868. <https://doi.org/10.2741/192>
- Alvarez, F. J., Rotterman, T. M., Akhter, E. T., Lane, A. R., English, A. W., & Cope, T. C. (2020). Synaptic plasticity on motoneurons after axotomy: A necessary change in paradigm. *Frontiers in Molecular Neuroscience*, 13, 68. <https://doi.org/10.3389/fnmol.2020.00068>
- Alvarez, F. J., Titus-Mitchell, H. E., Bullinger, K. L., Kraszpulski, M., Nardelli, P., & Cope, T. C. (2011). Permanent central synaptic disconnection of proprioceptors after nerve injury and regeneration. I. Loss of VGLUT1/IA synapses on motoneurons. *Journal of Neurophysiology*, 106(5), 2450–2470. <https://doi.org/10.1152/jn.01095.2010>
- Bahrini, I., Song, J. H., Diez, D., & Hanayama, R. (2015). Neuronal exosomes facilitate synaptic pruning by up-regulating complement factors in microglia. *Scientific Reports*, 5, 7989. <https://doi.org/10.1038/srep07989>
- Baietti, M. F., Zhang, Z., Mortier, E., Melchior, A., Degeest, G., Geeraerts, A., ... David, G. (2012). Syndecan-syntenin-Alix regulates the biogenesis of exosomes. *Nature Cell Biology*, 14(7), 677–685. <https://doi.org/10.1038/ncb2502>
- Baxter, A. A., Phan, T. K., Hanssen, E., Liem, M., Hulett, M. D., Mathivanan, S., & Poon, I. K. H. (2019). Analysis of extracellular vesicles generated from monocytes under conditions of lytic cell death. *Scientific Reports*, 9(1), 7538. <https://doi.org/10.1038/s41598-019-44021-9>
- Bennett, M. L., Bennett, F. C., Liddelow, S. A., Ajami, B., Zamanian, J. L., Fernhoff, N. B., ... Barres, B. A. (2016). New tools for studying microglia in the mouse and human CNS. *Proceedings of the National Academy of Sciences of the United States of America*, 113(12), E1738–E1746. <https://doi.org/10.1073/pnas.1525528113>
- Berg, A., Zelano, J., Stephan, A., Thams, S., Barres, B. A., Pekny, M., ... Cullheim, S. (2012). Reduced removal of synaptic terminals from axotomized spinal motoneurons in the absence of complement C3. *Experimental Neurology*, 237(1), 8–17. <https://doi.org/10.1016/j.expneuro.2012.06.008>
- Bichler, E. K., Nakanishi, S. T., Wang, Q. B., Pinter, M. J., Rich, M. M., & Cope, T. C. (2007). Enhanced transmission at a spinal synapse triggered in vivo by an injury signal independent of altered synaptic activity. *The Journal of Neuroscience*, 27(47), 12851–12859. <https://doi.org/10.1523/JNEUROSCI.1997-07.2007>
- Bickel, P. E., Scherer, P. E., Schnitzer, J. E., Oh, P., Lisanti, M. P., & Lodish, H. F. (1997). Flotillin and epidermal surface antigen define a new family of caveolae-associated integral membrane proteins. *Journal of Biological Chemistry*, 272(21), 13793–13802. <https://doi.org/10.1074/jbc.272.21.13793>
- Bisht, K., Sharma, K. P., Lecours, C., Sanchez, M. G., El Hajj, H., Milior, G., ... Tremblay, M. E. (2016). Dark microglia: A new phenotype predominantly associated with pathological states. *Glia*, 64(5), 826–839. <https://doi.org/10.1002/glia.22966>
- Blinzinger, K., & Kreutzberg, G. (1968). Displacement of synaptic terminals from regenerating motoneurons by microglial cells. *Zeitschrift für Zellforschung und Mikroskopische Anatomie*, 85(2), 145–157. <https://doi.org/10.1007/bf00325030>
- Block, M. L., Zecca, L., & Hong, J. S. (2007). Microglia-mediated neurotoxicity: Uncovering the molecular mechanisms. *Nature Reviews. Neuroscience*, 8(1), 57–69. <https://doi.org/10.1038/nrn2038>
- Bodian, D. (1975). Origin of specific synaptic types in the motoneuron neuropil of the monkey. *The Journal of Comparative Neurology*, 159(2), 225–243. <https://doi.org/10.1002/cne.901590205>
- Bodrikov, V., Pauschert, A., Kochlamazashvili, G., & Stuermer, C. A. O. (2017). Corrigendum to "Reggie-1 and reggie-2 (flotillins) participate in Rab11a-dependent cargo trafficking, spine synapse formation and LTP-related AMPA receptor (GluA1) surface exposure in mouse hippocampal neurons" [Exp. Neurol. 289, pages 31–45]. *Experimental Neurology*, 293, 200. <https://doi.org/10.1016/j.expneuro.2017.02.016>
- Brannstrom, T., & Kellerth, J. O. (1998). Changes in synaptology of adult cat spinal alpha-motoneurons after axotomy. *Experimental Brain Research*, 118(1), 1–13. <https://doi.org/10.1007/s002210050249>
- Bucci, C., Thomsen, P., Nicoziani, P., McCarthy, J., & van Deurs, B. (2000). Rab7: A key to lysosome biogenesis. *Molecular Biology of the Cell*, 11(2), 467–480. <https://doi.org/10.1091/mbc.11.2.467>
- Caleo, M., Spinelli, M., Colosimo, F., Matac, I., Rossetto, O., Lackovic, Z., & Restani, L. (2018). Transsynaptic action of botulinum neurotoxin type A at central cholinergic boutons. *Journal of Neuroscience*, 38(48), 10329–10337. <https://doi.org/10.1523/Jneurosci.0294-18.2018>
- Cerveró, C., Blasco, A., Tarabal, O., Casanovas, A., Piedrafita, L., Navarro, X., ... Calderó, J. (2018). Glial activation and central synapse loss, but not motoneuron degeneration, are prevented by the sigma-1 receptor agonist PRE-084 in the Smn2B/- mouse model of spinal

- muscular atrophy. *Journal of Neuropathology and Experimental Neurology*, 77(7), 577–597. <https://doi.org/10.1093/jnen/nly033>
- Chang, Q., & Martin, L. J. (2009). Glycinergic innervation of motoneurons is deficient in amyotrophic lateral sclerosis mice A quantitative confocal analysis. *American Journal of Pathology*, 174(2), 574–585. <https://doi.org/10.2353/ajpath.2009.080557>
- Chen, A. Q., Fang, Z., Chen, X. L., Yang, S., Zhou, Y. F., Mao, L., ... Hu, B. (2019). Microglia-derived TNF-alpha mediates endothelial necroptosis aggravating blood brain-barrier disruption after ischemic stroke. *Cell Death & Disease*, 10(7), 487. <https://doi.org/10.1038/s41419-019-1716-9>
- Chen, C., Li, H. Q., Liu, Y. J., Guo, Z. F., Wu, H. J., Li, X., ... Duan, S. M. (2015). A novel size-based sorting mechanism of pinocytic luminal cargoes in microglia. *The Journal of Neuroscience*, 35(6), 2674–2688. <https://doi.org/10.1523/JNEUROSCI.4389-14.2015>
- Chen, Z. L., Yu, W. M., & Strickland, S. (2007). Peripheral regeneration. *Annual Review of Neuroscience*, 30, 209–233. <https://doi.org/10.1146/annurev.neuro.30.051606.094337>
- Cocucci, E., & Meldolesi, J. (2015). Ectosomes and exosomes: Shedding the confusion between extracellular vesicles. *Trends in Cell Biology*, 25(6), 364–372. <https://doi.org/10.1016/j.tcb.2015.01.004>
- Coleman, M. P., & Freeman, M. R. (2010). Wallerian degeneration, wld(s), and nmnat. *Annual Review of Neuroscience*, 33, 245–267. <https://doi.org/10.1146/annurev-neuro-060909-153248>
- Colombo, M., Raposo, G., & Thery, C. (2014). Biogenesis, secretion, and intercellular interactions of exosomes and other extracellular vesicles. *Annual Review of Cell and Developmental Biology*, 30, 255–289. <https://doi.org/10.1146/annurev-cellbio-101512-122326>
- Conforti, L., Gilley, J., & Coleman, M. P. (2014). Wallerian degeneration: An emerging axon death pathway linking injury and disease. *Nature Reviews Neuroscience*, 15(6), 394–409. <https://doi.org/10.1038/nrn3680>
- Conos, S. A., Chen, K. W., de Nardo, D., Hara, H., Whitehead, L., Nunez, G., ... Vince, J. E. (2017). Active MLKL triggers the NLRP3 inflammasome in a cell-intrinsic manner. *Proceedings of the National Academy of Sciences of the United States of America*, 114(6), E961–E969. <https://doi.org/10.1073/pnas.1613305114>
- Conradi, S. (1969). Ultrastructure and distribution of neuronal and glial elements on the surface of the proximal part of a motoneuron dendrite, as analyzed by serial sections. *ACTA Physiologica Scandinavica Supplement*, 332, 49–64.
- Cullheim, S., & Thams, S. (2007). The microglial networks of the brain and their role in neuronal network plasticity after lesion. *Brain Research Reviews*, 55(1), 89–96. <https://doi.org/10.1016/j.brainresrev.2007.03.012>
- Cusack, C. L., Swahari, V., Hampton Henley, W., Michael Ramsey, J., & Deshmukh, M. (2013). Distinct pathways mediate axon degeneration during apoptosis and axon-specific pruning. *Nature Communications*, 4, 1876. <https://doi.org/10.1038/ncomms2910>
- da Silva, R. P., & Gordon, S. (1999). Phagocytosis stimulates alternative glycosylation of macrosialin (mouse CD68), a macrophage-specific endosomal protein. *The Biochemical Journal*, 338(Pt 3), 687–694.
- Delgado-Garcia, J. M., del Pozo, F., Spencer, R. F., & Baker, R. (1988). Behavior of neurons in the abducens nucleus of the alert cat—III. Axotomized motoneurons. *Neuroscience*, 24(1), 143–160. [https://doi.org/10.1016/0306-4522\(88\)90319-3](https://doi.org/10.1016/0306-4522(88)90319-3)
- Dermentzaki, G., Politis, K. A., Lu, L., Mishra, V., Perez-Torres, E. J., Sosunov, A. A., ... Przedborski, S. (2019). Deletion of Ripk3 prevents motor neuron death in vitro but not in Vivo. *eNeuro*, 6(1), ENEURO.0308-18.2018. <https://doi.org/10.1523/ENEURO.0308-18.2018>
- Dopfer, E. P., Minguet, S., & Schamel, W. W. (2011). A new vampire saga: The molecular mechanism of T cell trogocytosis. *Immunity*, 35(2), 151–153. <https://doi.org/10.1016/j.immuni.2011.08.004>
- Echeverry, S., Shi, X. Q., Rivest, S., & Zhang, J. (2011). Peripheral nerve injury alters blood-spinal cord barrier functional and molecular integrity through a selective inflammatory pathway. *Journal of Neuroscience*, 31(30), 10819–10828. <https://doi.org/10.1523/Jneurosci.1642-11.2011>
- Elmore, M. R., Najafi, A. R., Koike, M. A., Dagher, N. N., Spangenberg, E. E., Rice, R. A., ... Green, K. N. (2014). Colony-stimulating factor 1 receptor signaling is necessary for microglia viability, unmasking a microglia progenitor cell in the adult brain. *Neuron*, 82(2), 380–397. <https://doi.org/10.1016/j.neuron.2014.02.040>
- Etoh, K., & Fukuda, M. (2019). Rab10 regulates tubular endosome formation through KIF13A and KIF13B motors. *Journal of Cell Science*, 132(5), jcs226977. <https://doi.org/10.1242/jcs.226977>
- Fauré, J., Lachenal, G., Court, M., Hirrlinger, J., Chatellard-Causse, C., Blot, B., ... Sadoul, R. (2006). Exosomes are released by cultured cortical neurones. *Molecular and Cellular Neurosciences*, 31(4), 642–648. <https://doi.org/10.1016/j.mcn.2005.12.003>
- Fawcett, J. W., Oohashi, T., & Pizzorusso, T. (2019). The roles of perineuronal nets and the perinodal extracellular matrix in neuronal function. *Nature Reviews Neuroscience*, 20(8), 451–465. <https://doi.org/10.1038/s41583-019-0196-3>
- Fogarty, M. J. (2019). Amyotrophic lateral sclerosis as a synaptopathy. *Neural Regeneration Research*, 14(2), 189–192. <https://doi.org/10.4103/1673-5374.244782>
- Galvan, M. D., Greenlee-Wacker, M. C., & Bohlson, S. S. (2012). C1q and phagocytosis: The perfect complement to a good meal. *Journal of Leukocyte Biology*, 92(3), 489–497. <https://doi.org/10.1189/jlb.0212099>
- Girardot, N., Allinquant, B., Langui, D., Laquerriere, A., Dubois, B., Hauw, J. J., & Duyckaerts, C. (2003). Accumulation of flotillin-1 in tangle-bearing neurones of Alzheimer's disease. *Neuropathology and Applied Neurobiology*, 29(5), 451–461. <https://doi.org/10.1046/j.1365-2990.2003.00479.x>
- Gong, Y. N., Guy, C., Crawford, J. C., & Green, D. R. (2017). Biological events and molecular signaling following MLKL activation during necroptosis. *Cell Cycle*, 16(19), 1748–1760. <https://doi.org/10.1080/15384101.2017.1371889>
- Gong, Y. N., Guy, C., Olaison, H., Becker, J. U., Yang, M., Fitzgerald, P., ... Green, D. R. (2017). ESCRT-III acts downstream of MLKL to regulate necroptotic cell death and its consequences. *Cell*, 169(2), 286–300 e216. <https://doi.org/10.1016/j.cell.2017.03.020>
- Graeber, M. B., Streit, W. J., & Kreutzberg, G. W. (1989). Formation of microglia-derived brain macrophages is blocked by adriamycin. *Acta Neuropathologica*, 78(4), 348–358. <https://doi.org/10.1007/BF00688171>
- Grootjans, S., Vanden Berghe, T., & Vandendaele, P. (2017). Initiation and execution mechanisms of necroptosis: An overview. *Cell Death and Differentiation*, 24(7), 1184–1195. <https://doi.org/10.1038/cdd.2017.65>
- Haimann, C., Torri-Tarelli, F., Fesce, R., & Ceccarelli, B. (1985). Measurement of quantal secretion induced by ouabain and its correlation with depletion of synaptic vesicles. *The Journal of Cell Biology*, 101(5 Pt 1), 1953–1965. <https://doi.org/10.1083/jcb.101.5.1953>
- Harrison, R. E., Bucci, C., Vieira, O. V., Schroer, T. A., & Grinstein, S. (2003). Phagosomes fuse with late endosomes and/or lysosomes by extension of membrane protrusions along microtubules: Role of Rab7 and RILP. *Molecular and Cellular Biology*, 23(18), 6494–6506. <https://doi.org/10.1128/mcb.23.18.6494-6506.2003>
- Hernandez, D., Torres, C. A., Setlik, W., Cebrian, C., Mosharov, E. V., Tang, G., ... Sulzer, D. (2012). Regulation of presynaptic neurotransmission by macroautophagy. *Neuron*, 74(2), 277–284. <https://doi.org/10.1016/j.neuron.2012.02.020>
- Hoffmann, S., Orlando, M., Andrzejak, E., Bruns, C., Trimbuch, T., Rosenmund, C., ... Ackermann, F. (2019). Light-activated ROS production induces synaptic autophagy. *The Journal of Neuroscience*, 39(12), 2163–2183. <https://doi.org/10.1523/JNEUROSCI.1317-18.2019>

- Hong, S., Beja-Glasser, V. F., Nfonoyim, B. M., Frouin, A., Li, S., Ramakrishnan, S., ... Stevens, B. (2016). Complement and microglia mediate early synapse loss in Alzheimer mouse models. *Science*, 352 (6286), 712–716. <https://doi.org/10.1126/science.aad8373>
- Ito, D., Imai, Y., Ohsawa, K., Nakajima, K., Fukuuchi, Y., & Kohsaka, S. (1998). Microglia-specific localisation of a novel calcium binding protein, Iba1. *Brain Research. Molecular Brain Research*, 57(1), 1–9. [https://doi.org/10.1016/S0169-328X\(98\)00040-0](https://doi.org/10.1016/S0169-328X(98)00040-0)
- Ito, Y., Ofengheim, D., Najafov, A., Das, S., Saberi, S., Li, Y., ... Yuan, J. (2016). RIPK1 mediates axonal degeneration by promoting inflammation and necroptosis in ALS. *Science*, 353(6299), 603–608. <https://doi.org/10.1126/science.aaf6803>
- Jeffrey, M., Halliday, W. G., Bell, J., Johnston, A. R., MacLeod, N. K., Ingham, C., ... Fraser, J. R. (2000). Synapse loss associated with abnormal PrP precedes neuronal degeneration in the scrapie-infected murine hippocampus. *Neuropathology and Applied Neurobiology*, 26(1), 41–54. <https://doi.org/10.1046/j.1365-2990.2000.00216.x>
- Jiang, M., Schuster, J. E., Fu, R., Siddique, T., & Heckman, C. J. (2009). Progressive changes in synaptic inputs to motoneurons in adult sacral spinal cord of a mouse model of amyotrophic lateral sclerosis. *The Journal of Neuroscience*, 29(48), 15031–15038. <https://doi.org/10.1523/JNEUROSCI.0574-09.2009>
- Kettenmann, H., Kirchhoff, F., & Verkhratsky, A. (2013). Microglia: New roles for the synaptic stripper. *Neuron*, 77(1), 10–18. <https://doi.org/10.1016/j.neuron.2012.12.023>
- Kim, Y. S., Choi, D. H., Block, M. L., Lorenzl, S., Yang, L., Kim, Y. J., ... Joh, T. H. (2007). A pivotal role of matrix metalloproteinase-3 activity in dopaminergic neuronal degeneration via microglial activation. *The FASEB Journal*, 21(1), 179–187. <https://doi.org/10.1096/fj.06-5865com>
- Kiryu-Seo, S., Gamo, K., Tachibana, T., Tanaka, K., & Kiyama, H. (2006). Unique anti-apoptotic activity of EAAC1 in injured motor neurons. *The EMBO Journal*, 25(14), 3411–3421. <https://doi.org/10.1038/sj.emboj.7601225>
- Konnecke, H., & Bechmann, I. (2013). The role of microglia and matrix metalloproteinases involvement in neuroinflammation and gliomas. *Clinical & Developmental Immunology*, 2013, 914104–914115. <https://doi.org/10.1155/2013/914104>
- Kowal, J., Arras, G., Colombo, M., Jouve, M., Morath, J. P., Primdal-Bengtson, B., ... Thery, C. (2016). Proteomic comparison defines novel markers to characterize heterogeneous populations of extracellular vesicle subtypes. *Proceedings of the National Academy of Sciences of the United States of America*, 113(8), E968–E977. <https://doi.org/10.1073/pnas.1521230113>
- Lieberman, A. R. (1971). The axon reaction: A review of the principal features of perikaryal responses to axon injury. *International Review of Neurobiology*, 14, 49–124. [https://doi.org/10.1016/s0074-7742\(08\)60183-x](https://doi.org/10.1016/s0074-7742(08)60183-x)
- Linda, H., Shupliakov, O., Ornung, G., Ottersen, O. P., Storm-Mathisen, J., Risling, M., & Cullheim, S. (2000). Ultrastructural evidence for a preferential elimination of glutamate-immunoreactive synaptic terminals from spinal motoneurons after intramedullary axotomy. *The Journal of Comparative Neurology*, 425(1), 10–23.
- Liu, L., Aldskogius, H., & Svensson, M. (1998). Ultrastructural localization of immunoglobulin G and complement C9 in the brain stem and spinal cord following peripheral nerve injury: An immunoelectron microscopic study. *Journal of Neurocytology*, 27(10), 737–748. <https://doi.org/10.1023/a:1006950917973>
- Lundborg, G. (2003). Richard P. Bunge memorial lecture. Nerve injury and repair—A challenge to the plastic brain. *Journal of the Peripheral Nervous System*, 8(4), 209–226. <https://doi.org/10.1111/j.1085-9489.2003.03027.x>
- Lüningschrör, P., & Sendtner, M. (2018). Autophagy in the presynaptic compartment. *Current Opinion in Neurobiology*, 51, 80–85. <https://doi.org/10.1016/j.conb.2018.02.023>
- Mattson, M. P., Keller, J. N., & Begley, J. G. (1998). Evidence for synaptic apoptosis. *Experimental Neurology*, 153(1), 35–48. <https://doi.org/10.1006/exnr.1998.6863>
- Men, Y., Yelick, J., Jin, S., Tian, Y., Chiang, M. S. R., Higashimori, H., ... Yang, Y. (2019). Exosome reporter mice reveal the involvement of exosomes in mediating neuron to astroglia communication in the CNS. *Nature Communications*, 10(1), 4136. <https://doi.org/10.1038/s41467-019-11534-w>
- Mentis, G. Z., Blivis, D., Liu, W., Drobac, E., Crowder, M. E., Kong, L., ... O'Donovan, M. J. (2011). Early functional impairment of sensory-motor connectivity in a mouse model of spinal muscular atrophy. *Neuron*, 69(3), 453–467. <https://doi.org/10.1016/j.neuron.2010.12.032>
- Mignogna, M. L., & D'Adamo, P. (2018). Critical importance of RAB proteins for synaptic function. *Small GTPases*, 9(1-2), 145–157. <https://doi.org/10.1080/21541248.2016.1277001>
- Möller, J. C., Klein, M. A., Haas, S., Jones, L. L., Kreutzberg, G. W., & Raivich, G. (1996). Regulation of thrombospondin in the regenerating mouse facial motor nucleus. *Glia*, 17(2), 121–132. [https://doi.org/10.1002/\(SICI\)1098-1136\(199606\)17:2<121::AID-GLIA4>3.0.CO;2-5](https://doi.org/10.1002/(SICI)1098-1136(199606)17:2<121::AID-GLIA4>3.0.CO;2-5)
- Moran, L. B., & Graeber, M. B. (2004). The facial nerve axotomy model. *Brain Research. Brain Research Reviews*, 44(2-3), 154–178. <https://doi.org/10.1016/j.brainresrev.2003.11.004>
- Navarro, X., Vivo, M., & Valero-Cabré, A. (2007). Neural plasticity after peripheral nerve injury and regeneration. *Progress in Neurobiology*, 82 (4), 163–201. <https://doi.org/10.1016/j.pneurobio.2007.06.005>
- Odorizzi, G. (2006). The multiple personalities of Alix. *Journal of Cell Science*, 119(Pt 15), 3025–3032. <https://doi.org/10.1242/jcs.03072>
- Okerlund, N. D., Schneider, K., Leal-Ortiz, S., Montenegro-Venegas, C., Kim, S. A., Garner, L. C., ... Garner, C. C. (2017). Bassoon controls pre-synaptic autophagy through Atg5. *Neuron*, 93(4), 897–913 e897. <https://doi.org/10.1016/j.neuron.2017.01.026>
- Oliveira, A. L., Thams, S., Lidman, O., Piehl, F., Hokfelt, T., Karre, K., ... Cullheim, S. (2004). A role for MHC class I molecules in synaptic plasticity and regeneration of neurons after axotomy. *Proceedings of the National Academy of Sciences of the United States of America*, 101(51), 17843–17848. <https://doi.org/10.1073/pnas.0408154101>
- Orozco, S. L., Daniels, B. P., Yatim, N., Messmer, M. N., Quarato, G., Chen-Harris, H., ... Oberst, A. (2019). RIPK3 activation leads to cytokine synthesis that continues after loss of cell membrane integrity. *Cell Reports*, 28(9), 2275–2287 e2275. <https://doi.org/10.1016/j.celrep.2019.07.077>
- Paolicelli, R. C., Bergamini, G., & Rajendran, L. (2019). Cell-to-cell communication by extracellular vesicles: Focus on microglia. *Neuroscience*, 405, 148–157. <https://doi.org/10.1016/j.neuroscience.2018.04.003>
- Paolicelli, R. C., Bolasco, G., Pagani, F., Maggi, L., Scianni, M., Panzanelli, P., ... Gross, C. T. (2011). Synaptic pruning by microglia is necessary for normal brain development. *Science*, 333(6048), 1456–1458. <https://doi.org/10.1126/science.1202529>
- Pasparakis, M., & Vandeneabeele, P. (2015). Necroptosis and its role in inflammation. *Nature*, 517(7534), 311–320. <https://doi.org/10.1038/nature14191>
- Perry, V. H., & O'Connor, V. (2010). The role of microglia in synaptic stripping and synaptic degeneration: A revised perspective. *ASN Neuro*, 2 (5), e00047. <https://doi.org/10.1042/AN20100024>
- Peters, A., Palay, S. L., & Webster, H. d. F. (1976). The fine structure of the nervous system: Neurons and their supporting cells. Philadelphia: Saunders Co.
- Petralia, R. S., Schwartz, C. M., Wang, Y. X., Kawamoto, E. M., Mattson, M. P., & Yao, P. J. (2013). Sonic hedgehog promotes autophagy in hippocampal neurons. *Biology Open*, 2(5), 499–504. <https://doi.org/10.1242/bio.20134275>
- Pollin, M. M., McHanwell, S., & Slater, C. R. (1991). The effect of age on motor neurone death following axotomy in the mouse. *Development*, 112(1), 83–89.

- Raden, Y., Shlomovitz, I., & Gerlic, M. (2020). Necroptotic extracellular vesicles—Present and future. *Seminars in Cell & Developmental Biology*. (in press). <https://doi.org/10.1016/j.semcdb.2020.08.011>
- Re, D. B., le Verche, V., Yu, C., Amoroso, M. W., Politi, K. A., Phani, S., ... Przedborski, S. (2014). Necroptosis drives motor neuron death in models of both sporadic and familial ALS. *Neuron*, 81(5), 1001–1008. <https://doi.org/10.1016/j.neuron.2014.01.011>
- Rishal, I., & Fainzilber, M. (2014). Axon-soma communication in neuronal injury. *Nature Reviews Neuroscience*, 15(1), 32–42. <https://doi.org/10.1038/nrn3609>
- Rotterman, T. M., Akhter, E. T., Lane, A. R., MacPherson, K. P., Garcia, V. V., Tansey, M. G., & Alvarez, F. J. (2019). Spinal motor circuit synaptic plasticity after peripheral nerve injury depends on microglia activation and a CCR2 mechanism. *The Journal of Neuroscience*, 39(18), 3412–3433. <https://doi.org/10.1523/JNEUROSCI.2945-17.2019>
- Rotterman, T. M., Nardelli, P., Cope, T. C., & Alvarez, F. J. (2014). Normal distribution of VGLUT1 synapses on spinal motoneuron dendrites and their reorganization after nerve injury. *Journal of Neuroscience*, 34(10), 3475–3492. <https://doi.org/10.1523/Jneurosci.4768-13.2014>
- Rubio, M. E., & Wenthold, R. J. (1999). Differential distribution of intracellular glutamate receptors in dendrites. *The Journal of Neuroscience*, 19(13), 5549–5562.
- Salvany, S., Casanovas, A., Tarabal, O., Piedrafita, L., Hernandez, S., Santafe, M., ... Esquerda, J. E. (2019). Localization and dynamic changes of neuregulin-1 at C-type synaptic boutons in association with motor neuron injury and repair. *The FASEB Journal*, 33(7), 7833–7851. <https://doi.org/10.1096/fj.201802329R>
- Sasaki, S., & Iwata, M. (1996). Synaptic loss in anterior horn neurons in lower motor neuron disease. *Acta Neuropathologica*, 91(4), 416–421. <https://doi.org/10.1007/s004010050444>
- Schafer, D. P., Lehrman, E. K., Kautzman, A. G., Koyama, R., Mardinly, A. R., Yamasaki, R., ... Stevens, B. (2012). Microglia sculpt postnatal neural circuits in an activity and complement-dependent manner. *Neuron*, 74(4), 691–705. <https://doi.org/10.1016/j.neuron.2012.03.026>
- Schutz, B. (2005). Imbalanced excitatory to inhibitory synaptic input precedes motor neuron degeneration in an animal model of amyotrophic lateral sclerosis. *Neurobiology of Disease*, 20(1), 131–140. <https://doi.org/10.1016/j.nbd.2005.02.006>
- Sikorska, B., Liberski, P. P., Giraud, P., Kopp, N., & Brown, P. (2004). Autophagy is a part of ultrastructural synaptic pathology in Creutzfeldt-Jakob disease: A brain biopsy study. *International Journal of Biochemistry & Cell Biology*, 36(12), 2563–2573. <https://doi.org/10.1016/j.biocel.2004.04.014>
- Sipe, G. O., Lowery, R. L., Tremblay, M. E., Kelly, E. A., Lamantia, C. E., & Majewska, A. K. (2016). Microglial P2Y12 is necessary for synaptic plasticity in mouse visual cortex. *Nature Communications*, 7, 10905. <https://doi.org/10.1038/ncomms10905>
- Šišková, Z., Page, A., O'Connor, V., & Perry, V. H. (2009). Degenerating synaptic boutons in prion disease microglia activation without synaptic stripping. *American Journal of Pathology*, 175(4), 1610–1621. <https://doi.org/10.2353/ajpath.2009.090372>
- Šišková, Z., Reynolds, R. A., O'Connor, V., & Perry, V. H. (2013). Brain region specific pre-synaptic and post-synaptic degeneration are early components of neuropathology in prion disease. *PLoS One*, 8(1), e55004. <https://doi.org/10.1371/journal.pone.0055004>
- Solis, G. P., Hulbusch, N., Radon, Y., Katanaev, V. L., Plattner, H., & Stuermer, C. A. (2013). Reggies/flotillins interact with Rab11a and SNX4 at the tubulovesicular recycling compartment and function in transferrin receptor and E-cadherin trafficking. *Molecular Biology of the Cell*, 24(17), 2689–2702. <https://doi.org/10.1091/mbc.E12-12-0854>
- Solsona, C., Esquerda, J. E., & Marsal, J. (1981). Effects of ouabain and electrical stimulation on the fine structure of nerve endings in the electric organ of *Torpedo marmorata*. *Cell and Tissue Research*, 220(4), 857–871. <https://doi.org/10.1007/BF00210467>
- Spejo, A. B., & Oliveira, A. L. (2015). Synaptic rearrangement following axonal injury: Old and new players. *Neuropharmacology*, 96(Pt A), 113–123. <https://doi.org/10.1016/j.neuropharm.2014.11.002>
- Stephan, A. H., Barres, B. A., & Stevens, B. (2012). The complement system: An unexpected role in synaptic pruning during development and disease. *Annual Review of Neuroscience*, 35, 369–389. <https://doi.org/10.1146/annurev-neuro-061010-11380>
- Stevens, B., Allen, N. J., Vazquez, L. E., Howell, G. R., Christopherson, K. S., Nouri, N., ... Barres, B. A. (2007). The classical complement cascade mediates CNS synapse elimination. *Cell*, 131(6), 1164–1178. <https://doi.org/10.1016/j.cell.2007.10.036>
- Sumner, B. E. (1975). A quantitative analysis of boutons with different types of synapse in normal and injured hypoglossal nuclei. *Experimental Neurology*, 49(2), 406–417. [https://doi.org/10.1016/0014-4886\(75\)90097-7](https://doi.org/10.1016/0014-4886(75)90097-7)
- Sumner, B. E., & Sutherland, F. I. (1973). Quantitative electron microscopy on the injured hypoglossal nucleus in the rat. *Journal of Neurocytology*, 2(3), 315–328. <https://doi.org/10.1007/bf01104033>
- Sunico, C. R., Dominguez, G., Garcia-Verdugo, J. M., Osta, R., Montero, F., & Moreno-Lopez, B. (2011). Reduction in the motoneuron inhibitory/excitatory synaptic ratio in an early-symptomatic mouse model of amyotrophic lateral sclerosis. *Brain Pathology*, 21(1), 1–15. <https://doi.org/10.1111/j.1750-3639.2010.00417.x>
- Svensson, M., & Aldskogius, H. (1993). Infusion of cytosine-arabinoside into the cerebrospinal-fluid of the rat-brain inhibits the microglial cell-proliferation after hypoglossal nerve injury. *Glia*, 7(4), 286–298. <https://doi.org/10.1002/glia.440070404>
- Tarabal, O., Caraballo-Miralles, V., Cardona-Rossinyol, A., Correa, F. J., Olmos, G., Llado, J., ... Calderó, J. (2014). Mechanisms involved in spinal cord central synapse loss in a mouse model of spinal muscular atrophy. *Journal of Neuropathology and Experimental Neurology*, 73(6), 519–535. <https://doi.org/10.1097/NEN.0000000000000074>
- Tremblay, M. E., Lowery, R. L., & Majewska, A. K. (2010). Microglial interactions with synapses are modulated by visual experience. *PLoS Biology*, 8(11), e1000527. <https://doi.org/10.1371/journal.pbio.1000527>
- Tremblay, M. E., & Majewska, A. K. (2011). A role for microglia in synaptic plasticity? *Communicative & Integrative Biology*, 4(2), 220–222. <https://doi.org/10.4161/cib.4.2.14506>
- Vaughan, S. K., Kemp, Z., Hatzipetros, T., Vieira, F., & Valdez, G. (2015). Degeneration of proprioceptive sensory nerve endings in mice harboring amyotrophic lateral sclerosis-causing mutations. *The Journal of Comparative Neurology*, 523(17), 2477–2494. <https://doi.org/10.1002/cne.23848>
- Vukojicic, A., Delestree, N., Fletcher, E. V., Pagiazitis, J. G., Sankaranarayanan, S., Yednock, T. A., ... Mentis, G. Z. (2019). The classical complement pathway mediates microglia-dependent remodeling of spinal motor circuits during development and in SMA. *Cell Reports*, 29(10), 3087–3100 e3087. <https://doi.org/10.1016/j.celrep.2019.11.013>
- Waites, C. L., Leal-Ortiz, S. A., Okerlund, N., Dalke, H., Fejtova, A., Altrock, W. D., ... Garner, C. C. (2013). Bassoon and piccolo maintain synapse integrity by regulating protein ubiquitination and degradation. *The EMBO Journal*, 32(7), 954–969. <https://doi.org/10.1038/emboj.2013.27>
- Wall, A. A., Condon, N. D., Luo, L., & Stow, J. L. (2019). Rab8a localisation and activation by Toll-like receptors on macrophage macropinosomes. *Philosophical Transactions of the Royal Society B: Biological Sciences*, 374(1765), 20180151. <https://doi.org/10.1098/rstb.2018.0151>
- Wang, H. Y., Sun, L. M., Su, L. J., Rizo, J., Liu, L., Wang, L. F., ... Wang, X. D. (2014). Mixed lineage kinase domain-like protein MLKL causes necrotic membrane disruption upon phosphorylation by RIP3. *Molecular Cell*, 54(1), 133–146. <https://doi.org/10.1016/j.molcel.2014.03.003>

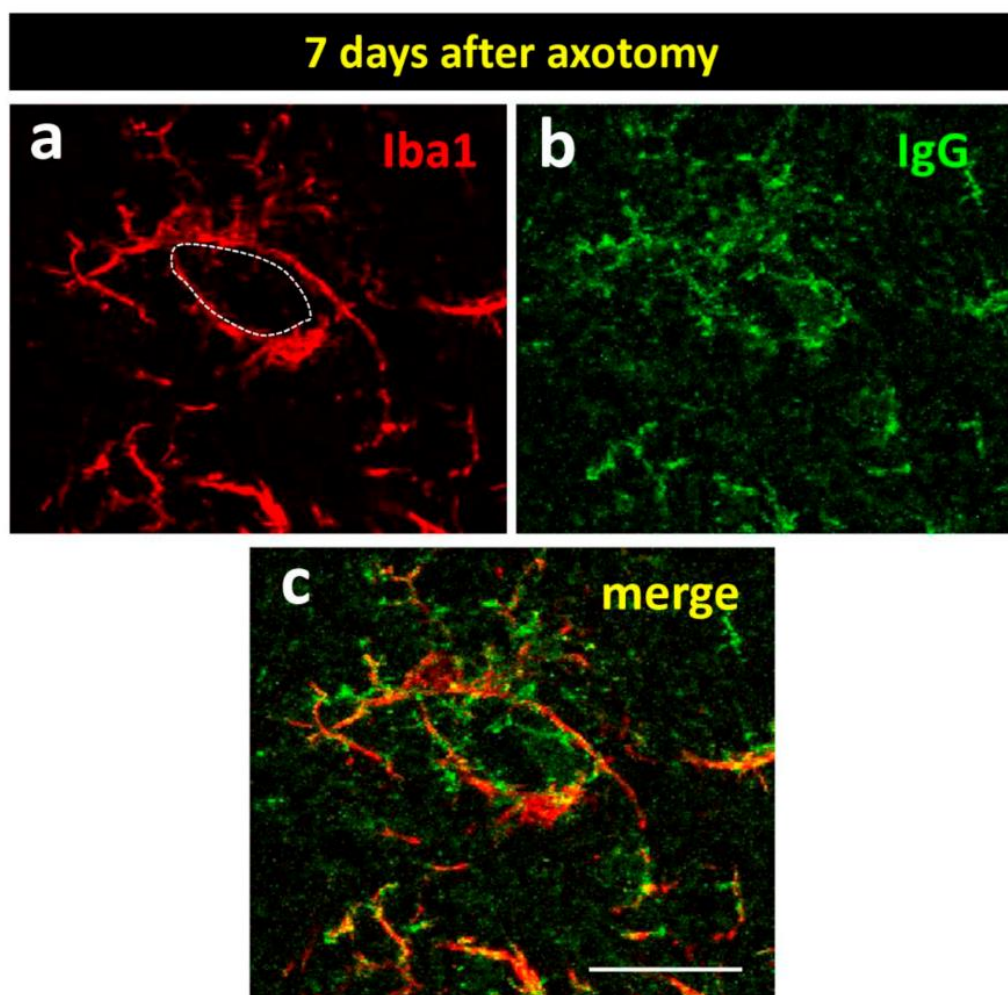
SALVANY ET AL.

- Watson, C., Paxinos, G., Kayalioglu, G., & Heise, C. (2009). In C. Watson, G. Paxinos, & K. G (Eds.), *The spinal cord* (1st ed.). Amsterdam: Elsevier.
- Weinhard, L., di Bartolomei, G., Bolasco, G., Machado, P., Schieber, N. L., Neniskyte, U., ... Gross, C. T. (2018). Microglia remodel synapses by presynaptic trogocytosis and spine head filopodia induction. *Nature Communications*, 9(1), 1228. <https://doi.org/10.1038/s41467-018-03566-5>
- Wu, Y., O'Toole, E. T., Girard, M., Ritter, B., Messa, M., Liu, X., ... de Camilli, P. (2014). A dynamin 1-, dynamin 3- and clathrin-independent pathway of synaptic vesicle recycling mediated by bulk endocytosis. *eLife*, 3, e01621. <https://doi.org/10.7554/eLife.01621>
- Yamada, J., Nakanishi, H., & Jinno, S. (2011). Differential involvement of perineuronal astrocytes and microglia in synaptic stripping after hypoglossal axotomy. *Neuroscience*, 182, 1–10. <https://doi.org/10.1016/j.neuroscience.2011.03.030>
- Yoon, S., Bogdanov, K., Kovalenko, A., & Wallach, D. (2016). Necroptosis is preceded by nuclear translocation of the signaling proteins that induce it. *Cell Death & Differentiation*, 23(2), 253–260. <https://doi.org/10.1038/cdd.2015.92>
- Yoon, S., Kovalenko, A., Bogdanov, K., & Wallach, D. (2017). MLKL, the protein that mediates necroptosis, also regulates endosomal trafficking and extracellular vesicle generation. *Immunity*, 47(1), 51–65 e57. <https://doi.org/10.1016/j.jimmuni.2017.06.001>
- Zerial, M., & McBride, H. (2001). Rab proteins as membrane organizers. *Nature Reviews. Molecular Cell Biology*, 2(2), 107–117. <https://doi.org/10.1038/35052055>
- Zhong, Z., Deane, R., Ali, Z., Parisi, M., Shapovalov, Y., O'Banion, M. K., ... Zlokovic, B. V. (2008). ALS-causing SOD1 mutants generate vascular changes prior to motor neuron degeneration. *Nature Neuroscience*, 11(4), 420–422. <https://doi.org/10.1038/nn2073>

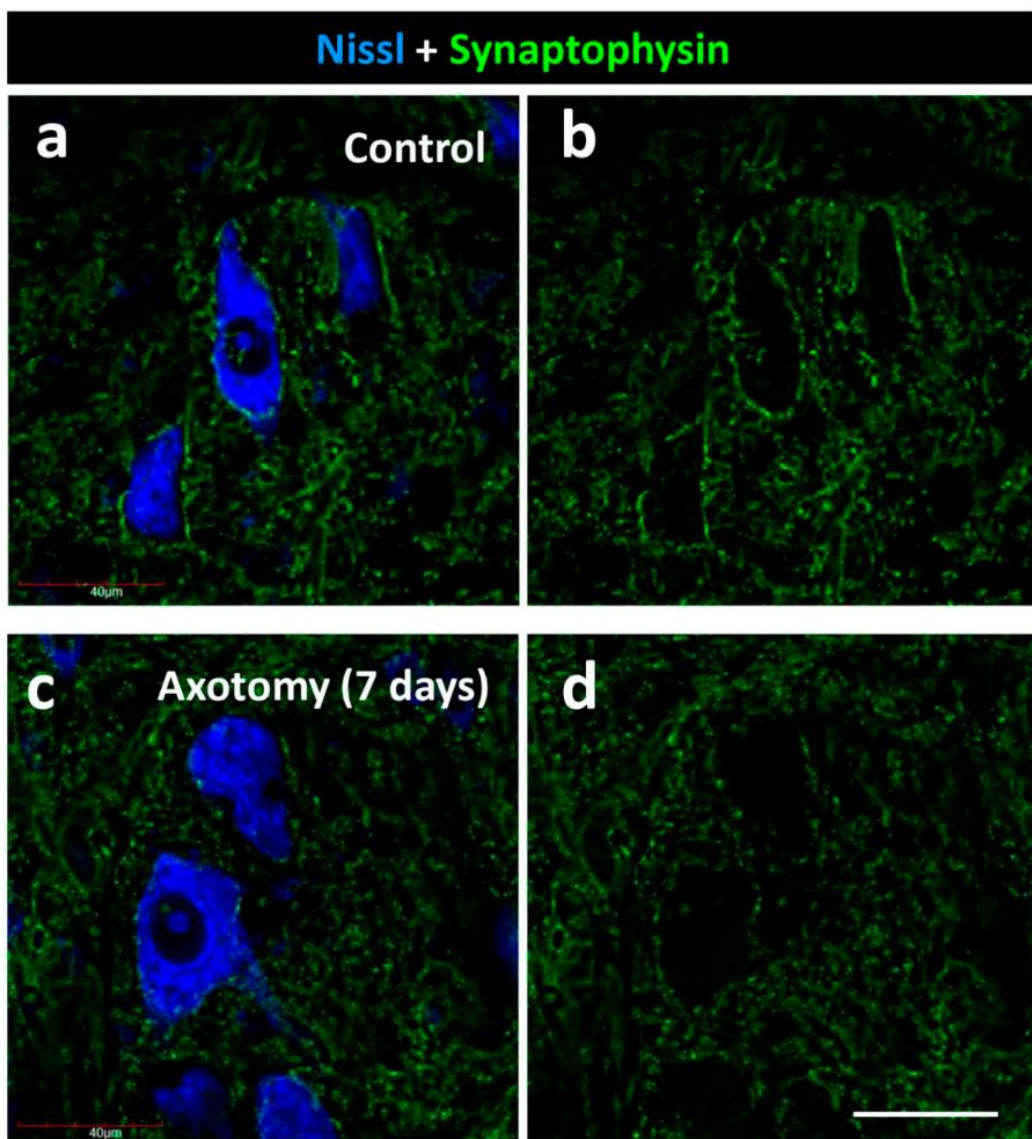
SUPPORTING INFORMATION

Additional supporting information may be found online in the Supporting Information section at the end of this article.

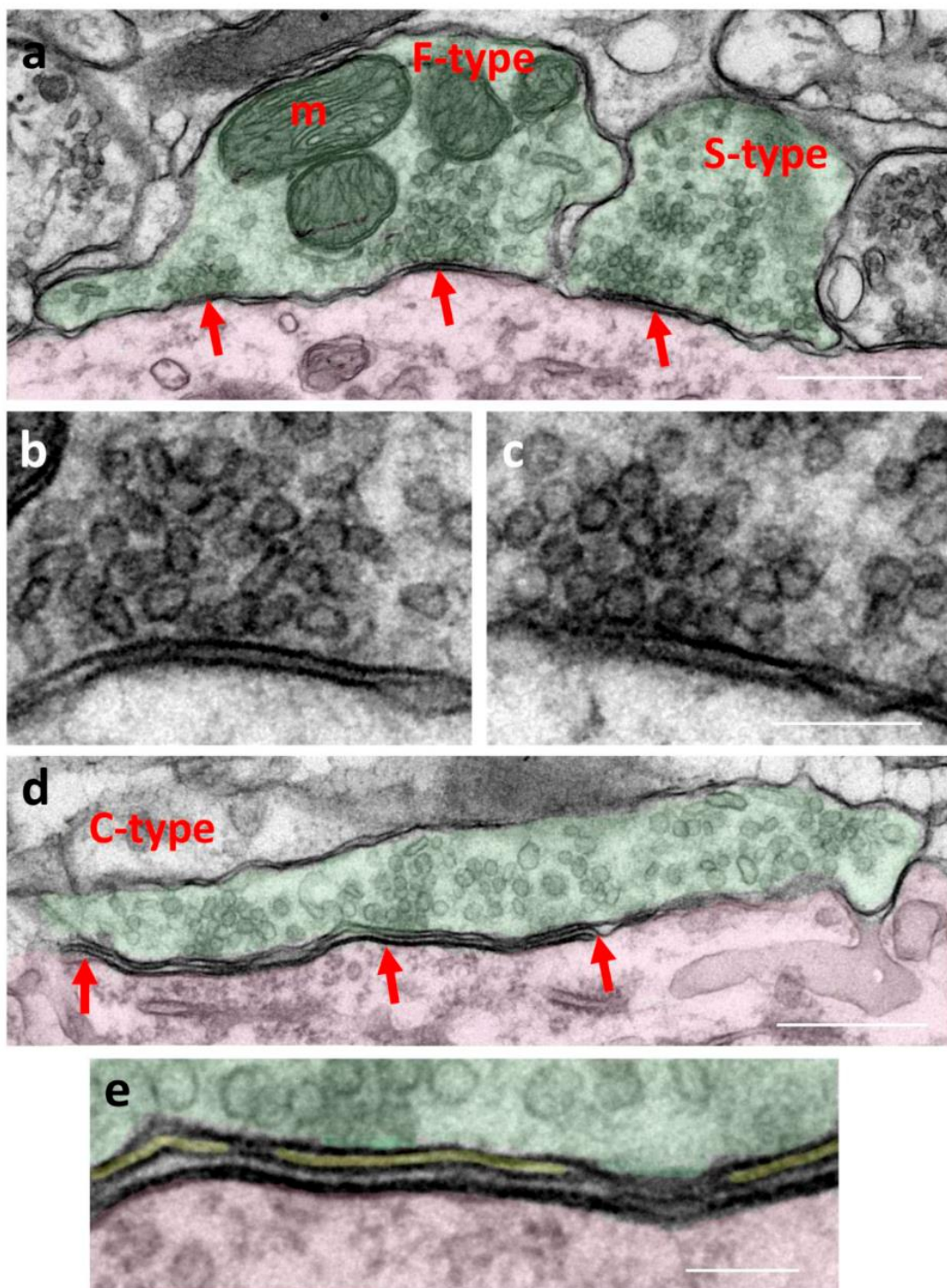
How to cite this article: Salvany S, Casanovas A, Piedrafita L, et al. Microglial recruitment and mechanisms involved in the disruption of afferent synaptic terminals on spinal cord motor neurons after acute peripheral nerve injury. *Glia*. 2021;1–25. <https://doi.org/10.1002/glia.23959>



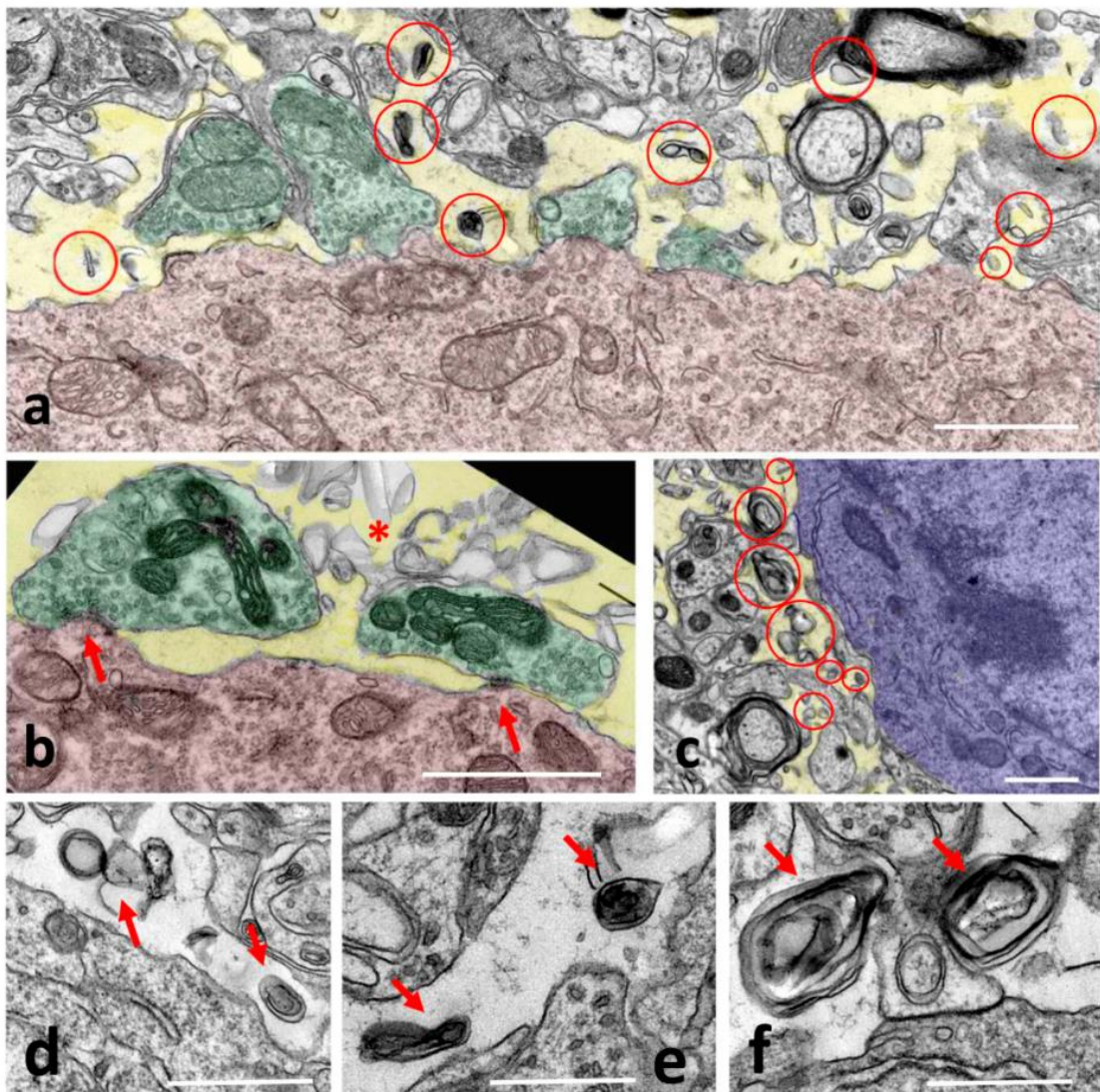
Supplementary Figure 1 Endogenous IgGs decorate recruited microglial cells at the MN surface 7 days postaxotomy. (a-c) Spinal cord section showing an axotomized MN (delimited by a dashed line) covered by Iba1-immunostained microglia (red); note the association of endogenous IgGs (green) with microglial profiles. Scale bar: 20 μ m



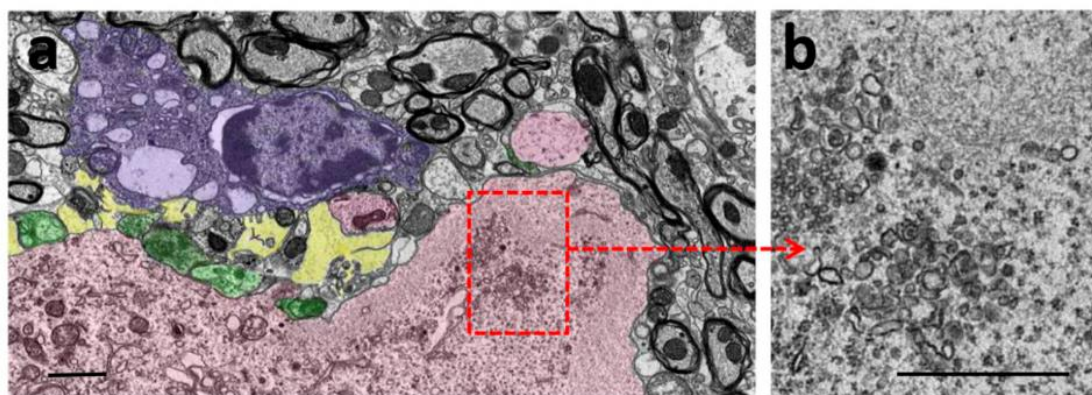
Supplementary Figure 2 Spinal cord section immunostained for synaptophysin (green) showing ventral horn MN cell bodies (visualized by fluorescent Nissl staining, blue) in control (a and b) and postaxotomy (c and d) conditions, as indicated. Note the reduction of synaptophysin positive puncta near the surface of MN cell bodies after axotomy. Scale bar: 40 μ m (valid for a-c)



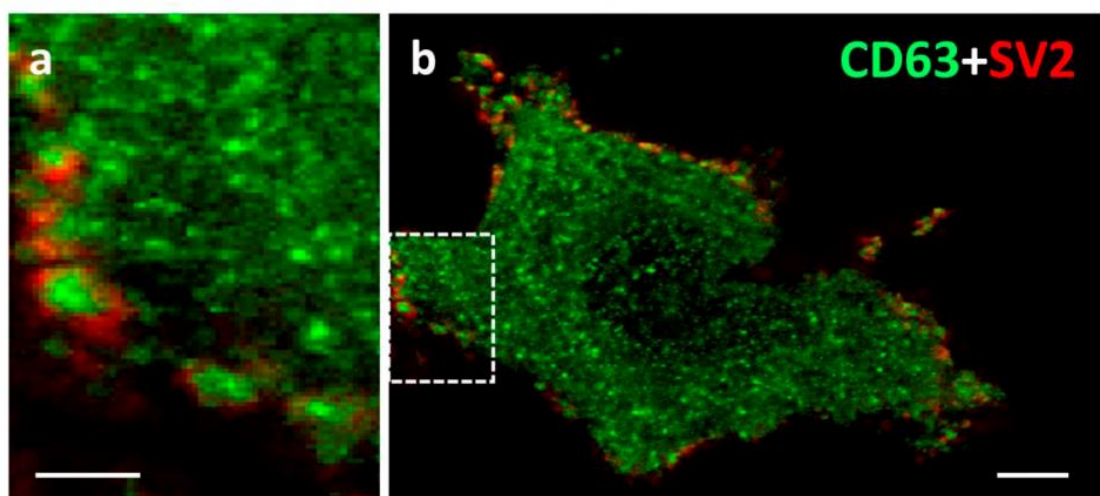
Supplementary Figure 3 Ultrastructural morphology of normal synaptic boutons (shaded in green) contacting MN cell bodies (shaded in red). (a) Two presynaptic boutons containing synaptic vesicles clustered in the active zones (arrows); details of synaptic vesicle morphology are seen in the enlarged panels (b and c), showing flattened (b) and round (c) vesicles characteristic of F-type and S-type terminals, respectively. (d) A C-type synaptic bouton is shown, displaying the characteristic subsynaptic cistern (arrows) that can be observed enlarged in (e); the intersynaptic extracellular gap is shaded in yellow. m = mitochondria. Scale bars: 0.5 μ m in (a) and (d); 150 nm in (b), (c) and (e)



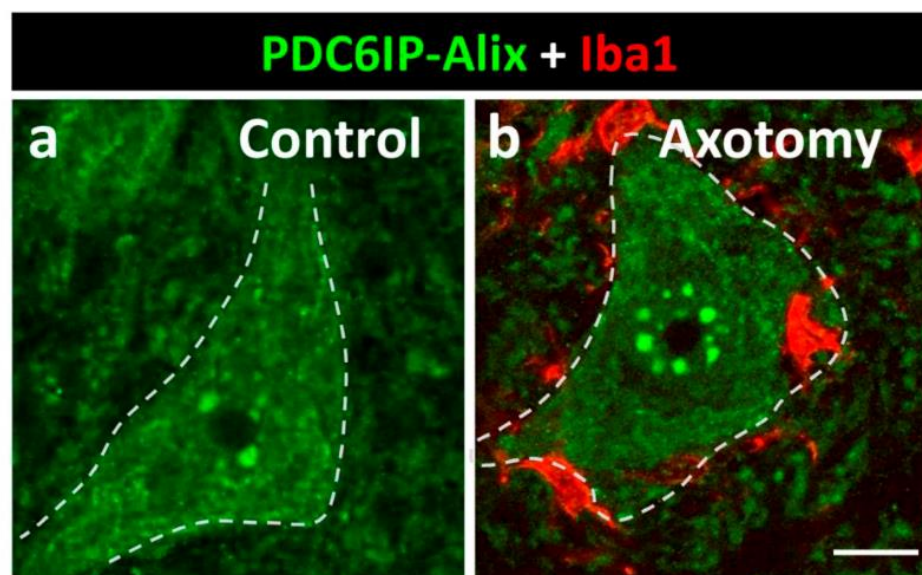
Supplementary Figure 4 Ultrastructural analysis of the periphery of MN cell bodies, and adjacent synaptic afferents and cell structures in the spinal cord. (a) Three days after axotomy, the extracellular space (shaded in yellow) is widened and synaptic terminals (green) are partially detached from the MN surface (red); in addition, a number of extracellular membrane-bound vesicles (encircled in red) can be seen “floating” in the extracellular space. (b) A detail of two terminal synaptic boutons (green) contacting MN surface (red) are partially detached but maintain focal adherence at the puncta adherentia sites (red arrows); note the presence of abundant extracellular vesicles (*) in the extracellular space (yellow). (c) A recruited microglial cell (shaded in blue) in the proximity of the MN surface and interacting with abundant extracellular pleomorphic vesicles (indicated with red circles), 3 days after axotomy. (d-f) A high magnification detail of the morphology of extracellular vesicles (arrows) near the MN surface, 3 days after axotomy. Scale bars: 1 μ m (a-c) and 500 nm (d-f)



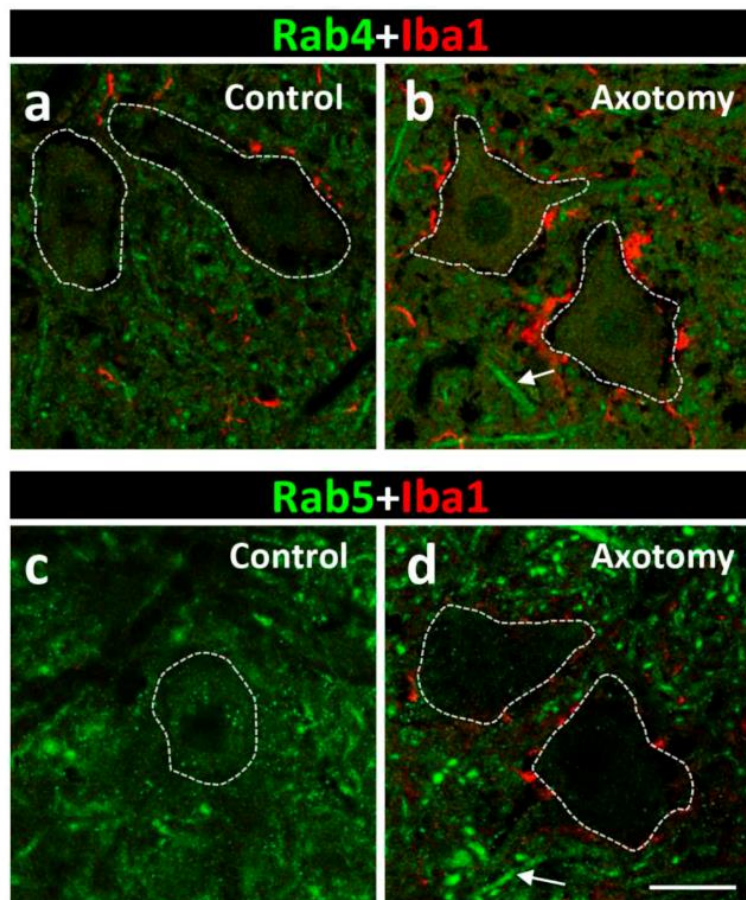
Supplementary Figure 5 Electron micrograph of a MN cell body (shaded in red) showing a marked disruption of intracellular organelle organization. (a) In the vicinity of the MNs, an altered microglial cell is seen displaying vacuolar changes in the endoplasmic reticulum and other organelles. Altered synaptic afferents are shaded in green, and the extracellular space at the MN-microglia interface (shaded in yellow) can be seen expanded. A detailed view of MN cytoplasmic disorganization is shown at higher magnification in (b). Scale bars: (a) and (b) = 2.5 μ m



Supplementary Figure 6 (a,b) An isolated MN cell body, 7 days postaxotomy, in a squash preparation immunostained for CD63 (green) and SV2 (red). Red spots, corresponding to afferent synaptic boutons, are seen covering the surface of the MN soma, in which abundant CD63 positive puncta can be seen. In the enlarged boxed area (a), the relationship between larger CD63-positive spots and afferent boutons can be observed. Scale bars: a = 2 μ m, b = 10 μ m



Supplementary Figure 7 (a,b) Ventral horn MN cell bodies (delimited by dashed lines) double immunostained for PDC6IP-Alix (green) and Iba1 (red) in control and 7 days postaxotomy. The axotomized MN can be identified by recruited Iba1-positive microglial cells. However, the pattern of PDC6IP-Alix does not show identifiable changes following axotomy. Scale bar: 20 μ m (valid for a)



Supplementary Figure 8 Control and 7-day axotomized MN cell bodies (delimited by dotted lines) immunostained for either Rab4 (a, b) or Rab5 (c, d) (green) combined with Iba1 (red). Note that the recruitment of Iba1-positive microglial cells around axotomized MNs (b and d). Rab4 and Rab5-immunoreactivity is increased in neuronal processes (arrows) adjacent to injured MNs. Scale bars: Scale bar: d = 20 μ m (valid for a-c)

Article IV

Accumulation of misfolded SOD1 outlines distinct patterns of motor neuron pathology and death during disease progression in SOD1^{G93A} mouse model of amyotrophic lateral sclerosis

Sara Salvany, Anna Casanovas, Sílvia Gras, Lídia Piedrafita, Jordi Calderó, i Josep E. Esquerda

S'està ultimant la seva preparació pel sotmetre'l a *Acta Neuropathologica Communications*
(Q1 , IF: 6.47)

Accumulation of misfolded SOD1 outlines distinct patterns of motor neuron pathology and death during disease progression in SOD1^{G93A} mouse model of amyotrophic lateral sclerosis

Sara Salvany, Anna Casanovas, Sílvia Gras, Lídia Piedrafita, Jordi Calderó, Josep E. Esquerda

Patologia Neuromuscular Experimental Group, Departament de Medicina Experimental, Facultat de Medicina, Universitat de Lleida and Institut de Recerca Biomèdica de Lleida (IRBLleida), Lleida, Catalonia, Spain

Corresponding author: Josep E. Esquerda, Grup de Patologia Neuromuscular Experimental, Departament de Medicina Experimental, Facultat de Medicina, Universitat de Lleida-IRBLleida, Av. Rovira Roure 80, 25198 Lleida, Spain. Phone: +34-973-702427. E-mail address: josep.esquerda@udl.cat

ABSTRACT

Early misfolded SOD1 (mfSOD1) accumulation, motor neuron (MN) degeneration and microgliosis are hallmark pathological features in SOD1^{G93A} ALS mice. Due to the different vulnerability of distinct MN subtypes, degenerating and surviving MNs coexist in a different proportion during disease progression. Furthermore, since MN degeneration in SOD1 mice is non-cell autonomous, the role of immediate MN environment including astrocytes, microglia and afferent synapses are of singular relevance. Based on the examination of mfSOD1 expression we have defined distinct MN phenotypes that have been evaluated during the disease progression and the local neuroinflammatory reaction. The effects of the experimental increase or decrease of microglial response on the expression of MN phenotypes was also evaluated. The expression of mfSOD1 was analysed in SOD1^{G93A(fast)} mice after immunolabelling with conformational-specific antibodies, C4F6 and AJ10. Neuroinflammatory response was exacerbated or decreased by means of the sciatic nerve axotomy or by treatment with PLX5622 respectively. Multiple fluorescent immunolabelling was performed on spinal cord sections and observed under the confocal microscope. Some samples were also processed for electron microscopy. By mfSOD1 immunohistochemistry we have defined three MN phenotypes. The most severe (phenotype 3) correspond to MN somas showing highly positive mfSOD1 immunostaining; these MNs are extremely vacuolated as a result of massive mitochondrial and endoplasmic reticulum swelling. These features fit well with those described under the concept of paraptosis. Paraptotic-like MNs display an accumulation of Flotillin and CD81 particles which are considered as markers for extracellular vesicles. These degenerating MNs display pMLKL positivity, the effector protein of the necroptotic pathway. Paraptotic MNs showed a significant loss of afferent synapsis and recruit microglial cells. We have established the type 2 phenotype when mfSOD1 accumulation and vacuolization was restricted to MN processes, and type 1 when mfSOD1 accumulation was not evident neither in MN somas or processes. The most severe type 3 phenotype appears to be more frequent between P60 and P90 than in the terminal stages. We have also found a progressive microgliosis displaying neurotoxic markers of activation. The relative amount of mfSOD1 phenotypes can be experimentally altered by modulating the microglial neuroinflammatory response. This study reveals a dissociation between mfSOD1 accumulation in degenerating MNs and the clinical progression of the disease. We show that at presymptomatic stages (p60) a substantial amount of MNs with phenotype type 3 (paraptotic-like) exist which can be determinant for the ulterior spread of the disease by an exosome-based mechanism. There is also a link between mfSOD1 expression in MNs and neuroinflammation.

INTRODUCTION

Amyotrophic lateral sclerosis (ALS) is a fatal degenerative disease mainly involving spinal cord and brain motor neurons (MNs) leaving muscles denervated (Rowland, 1995). Most of ALS cases are sporadic while 10% are familial and, among of them, 20% have been linked to mutations of the superoxide dismutase 1 (SOD1) gene (Rosen et al., 1993). It has been shown that, rather via its loss-of-function, mutant SOD1 determines ALS phenotype via a gain of neurotoxic properties, which includes oxidative stress, protein aggregation, mitochondrial dysfunction and neuroinflammation (Brujin et al., 2004). The SOD1G93A ALS mouse model overexpresses ~25 copies of the human gene encoding the enzyme SOD1 carrying a mutation (mSOD1G93A) causative of familial ALS. Since its development in 1994, this model has been extensively used to investigate the pathogenic mechanisms leading to ALS, because it recapitulates many phenotypic features observed in ALS patients (Gurney et al., 1994; Saeed et al., 2009). SOD1G93A mice exhibit progressive paralysis starting at ~90 days, with death occurring at ~135 days, depending on the genetic background. In this mutant mouse model, the decrease in motor function occurs in concomitance with the development of conspicuous and severe pathological changes that include the loss of α-MN and reactive astrocytosis and microgliosis. MN pathology and dysfunction progress with notable temporal reproducibility, a condition that is essential for correlation of data from individuals of different ages in longitudinal studies. This has led to the demarcation of presymptomatic (P30-P90), symptomatic (P90-P120) and end-stage (P120 to death) periods in the time-course of the disease, as a reference in many experimental studies (Chiu et al., 1995; Hall et al., 1998; Turner & Talbot, 2008). One intriguing aspect of ALS pathology is the distinct degrees of vulnerability among the different MN groups or subtypes: in example, fast-twitch, fast-fatigable MNs are severely affected and degenerate first, while slow-twitch MNs are less vulnerable in ALS (Hegedus et al., 2007; Nijssen et al., 2017; Pun et al., 2006). In addition, MNs that innervate extraocular muscles or external sphincters are considered as ALS-resistant (reviewed in (Kanning et al., 2010; Nijssen et al., 2017)). Low MN excitability correlates with ALS-resistance (Saxena et al., 2013) and γ-MNs, which innervate muscle spindles, are completely spared from ALS (Lalancette-Hebert et al., 2016). After the early loss of most vulnerable MNs, the axons of the remaining ones sprout in order to compensate for those that have degenerated (Schaefer et al., 2005). This entails that, at a given time, degenerating and surviving (perhaps regenerating) MNs coexist at the spinal cord ventral horn in variable proportions during the disease progression. Thus, the corresponding pathomorphological status of individual MNs should be heterogeneous and dissociated from the clinical outcome of the disease. In example, severely damaged MNs could be present (although in a minor proportion) at the early stages and vice versa, some apparently healthy MNs would be present at the end-stage period. Given our limited

knowledge about the sequence of cellular events during disease progression, we tried to categorize ALS MN pathology at a single cell level by establishing distinct phenotypic patterns of damage based on the expression of toxic forms of misfolded SOD1. It is known that MN degeneration in mutant SOD1 mouse models is non-cell-autonomous, and the participation of adjacent cells appears to be essential in the process of disease pathogenesis (Boillée et al., 2006; Clement et al., 2003; Ilieva et al., 2009). For this reason, the examination of MN neuropile, including afferent synapses, astrocytes and microglia, in relation to defined cell body phenotypes were included in our analysis. A better characterization of how degenerative and reactive changes are spatially and temporally distributed would help to evaluate the effects of putative therapeutic agents in preclinical assays in the SOD1G93A fast mouse model of ALS. In addition, it seems that before NM degeneration, a motor axon dying-back process determines an early disconnection of MNs from their muscle targets (Fischer et al., 2004; Hegedus et al., 2007). The interruption of nerve-muscle interaction occurs also in healthy animals after peripheral nerve transection (axotomy), resulting in a CNS response that includes glial activation around axotomized MNs and a loss of synaptic afferents contacting MN cell bodies (Aldskogius, 2011; Rotterman & Alvarez, 2020; Salvany et al., 2021). Thus, the reactive response seen in axotomized MNs could share some common pathogenic mechanisms with ALS. However, contrasting with what occurs in ALS, MN cell body activation in response to peripheral nerve axotomy in adults is not usually followed by MN death (Lowrie & Vrbová, 1992; Pollin et al., 1991). Instead of this, axotomy triggers the expression of “regeneration associated genes” shifting neurons from “transmitting” to a “growth” mode, which provides MNs with the structural and molecular machinery for restoration of neuromuscular connectivity (Aldskogius, 2011). Although it may be deleterious in some aspects (Rotterman et al., 2019; Salvany et al., 2021), the glial neuroinflammatory response at the vicinity of axotomized MNs is also considered as neuroprotective (Oliveira et al., 2004; Svensson & Aldskogius, 1993). Therefore, the analysis of afferent synapses and the glial response in axotomized MNs under WT and mutant SOD1 genetic backgrounds may provide new cues for understanding the mechanisms of MN degeneration in ALS.

MATERIALS AND METHODS

Animals, surgical procedures and pharmacological treatments

SOD1^{G93A} (B6SJL-Tg(SOD1-G93A)1Gur/J) mice were purchased from Jackson Laboratory (Sacramento, CA, USA) and maintained as hemizygotes by breeding transgenic males with B6SJL females. Transgenic progeny were identified by PCR genotyping of DNA extracted from the tail by using specific primers as described previously (Ripps et al., 1995). Age-matched wildtype (WT) littermates of transgenic animals were used as controls. Briefly, asymptomatic mice were considered at 0-30 postnatal days [P], presymptomatic at p30 - p60 days, symptomatic at p60 - p90 days and in terminal phase at p90 - p120 ± 10 days (Mancuso et al., 2012). Endpoint criteria previously described (Günther et al., 2012) were used to minimize suffering. To avoid potential bias due to gender, only male animals were used in this study. Mice were housed 5-6 per cage having *ad libitum* access to standard laboratory chow and water and under a 12-h light/dark cycle. According to previous defined criteria (Burkholder et al., 2012; Miller & Nadon, 2000), mice displaying tumours or physical abnormalities were excluded from the study and euthanized by an overdose of pentobarbital (30 mg, intraperitoneally). All efforts were made to reduce the number of animals in agreement with the European Communities Council Directive (24 November 1986, 86/609/EEC).

All the animal experimentation procedures were performed according to the European Committee Council Directive and the norms established by the Generalitat de Catalunya (published as a law in the *Diari Oficial de la Generalitat de Catalunya* 2073, 1995). All the experiments were previously evaluated and approved by the Committee for Animal Care and Use of the University of Lleida.

Young and adult (p30, p60 and p90) mice were subjected to unilateral sciatic nerve transection. Animals were anaesthetized using a solution consisting of a combination of ketamine (100 mg/kg) and xylazine (10 mg/kg) and maintained with inhalant anaesthesia (1% isoflurane). The sciatic nerve was exposed at the femoral level and transected; a ligature was performed in the proximal segment in order to prevent spontaneous reinnervation. To minimize suffering, mice were subjected to postoperative analgesia with two subcutaneous injections of buprenorphine (0.05 mg/kg): one immediately after surgery and the other 24 hr after the intervention. Lumbar spinal cord samples were obtained 7 days after axotomy.

For the pharmacological approaches adult mice (p60) has been used. Drug delivery regimes were based on published reports (Saxena et al., 2013) and the delivery protocols were as follows. Methocramine (Sigma): a daily dose during 15 days injected intraperitoneally (i.p.) in saline at 200

µg/kg; Oxotremorine M (Tocris Bioscience): a daily dose during 15 days injected i.p. in saline at 30-50 µg/kg.

The colony stimulating factor 1 receptor (CSF-1R) specific kinase inhibitor (PLX5622) (Elmore et al., 2014) was generously provided by Plexxikon Inc. (Berkeley, CA), and formulated in AIN-76 standard chow by Research Diets Inc. (New Brunswick, NJ). One-month-old male mice, specific-pathogen-free housed, were treated with 1,200 mg/kg chow PLX5622 for 30 days. To verify PLX5622 consumption by the mice, their weight was monitored; no significant weight reduction was observed.

Tissue sample preparation, histological analysis and motoneuron counts

Mice were anaesthetized and transcardially perfused with 4% PFA in 0.1M phosphate buffer (PB) pH 7.4. Lumbar spinal cord samples were postfixed for 24 hr at 4°C in the same fixative solution and then cryoprotected at 4°C with 30% sucrose in 0.1 M PB containing 0.02% sodium azide. Transverse cryostat sections (16 µm thick) were collected on gelatin-coated glass slides.

For MN counts, several randomly cryostat sections representing the lumbar spinal cord (L1 – L5) were chose and stained with Cresyl Violet. α-MNs, located in the ventral horn, were identified by their size (soma diameter > 20 µm), morphology (multipolar appearance, prominent nucleolus, and abundant Nissl granules in cytoplasm) and topography (Lamina IX of grey matter). MNs were counted blindly on one side of every 2nd section, according to previously described criteria (Calderó et al., 1997; P. G. Clarke & Oppenheim, 1995). Briefly, only MNs with a large nucleus and a visible clump of nuclear material and a substantial intense basophilic cytoplasm were included in the counts. These stringent criteria make not necessary the use of a correction factor for double counting (P. G. Clarke & Oppenheim, 1995).

Immunocytochemistry and imaging

Cryostat sections were permeabilized with phosphate-buffered saline (PBS) containing 0.1% Triton X-100 for 30 min, blocked with either 10% normal goat serum or normal horse serum in PBS for 1 h at room temperature, and then incubated overnight at 4°C with an appropriate primary antibody mixture. The primary antibodies used are indicated in *Table 1*.

Once previously washed with PBS, sections were incubated for 1 hour with a combination of appropriate secondary fluorescent antibodies labelled with one of the following fluorochromes (1/500): Alexa Fluor 488, DyLight 549 or DyLight 649 (Jackson Immuno Research Laboratories, West Grove, PA, United States). Finally, the spinal cord sections were labelled with blue fluorescent NeuroTrace Nissl staining (1:150; Molecular Probes) and mounted using an anti-fading medium

containing 0.1 M Tris-HCl buffer (pH 8.5), 20% glycerol, 10% Mowiol, and 0.1% 1,4-diazabicyclo[2.2.2]octane.

The slides were then examined under a FluoView FV-500 or FluoView FV-1000 Olympus laser-scanning confocal microscopes (Olympus, Hamburg, Germany). The MNs were imaged after obtaining optical sections (0.5 or 1 µm) of cell bodies. For comparisons, slides from different animals and experimental conditions were processed in parallel for immunocytochemistry and subsequent imaging. The same scanning parameters were used for the acquisition of images corresponding to different experimental groups. Digital images were analysed using FV10-ASW 3.1 Viewer (Olympus) and the ImageJ software (US National Institutes of Health, Bethesda, MD, USA).

Immunolabelled profiles of the different protein markers were examined and then were manually counted on the screen for each MN soma. The area and perimeter of MN somata, and both microglial and astroglial profiles covering or physically closed to MNs were also manually measured. In axotomy experiments, we only analysed cell bodies located in the pes 9 region of the lumbar 6 spinal cord segment, which corresponds to the sciatic motor column (Watson, et al. 2009). The pool of axotomized MNs was identified by their close interaction with recruited Iba1-stained microglial cells. The number of synaptic boutons contacting activated microglia in axotomized MNs was evaluated by image analysis (ImageJ).

The digital images were edited using FV10-ASW 3.1 Viewer (Olympus) and Adobe Photoshop CS4 (Adobe Systems Inc, San Jose, CA).

Electron microscopy

Some of the animals were perfused either with 2% PFA and 2% glutaraldehyde in 0.1 M PB (pH 7.4) for conventional electron microscopy. Dissected tissues were postfixed for 24 hr at 4°C in the same fixative solution.

For conventional electron microscopy, dissected tissues were sectioned at 200 µm using a vibratome. Then, the tissues were postfixed in 1% OsO₄ for 2 hr, and then contrasted with 0.5% uranyl acetate for 30 min; all these procedures were conducted at 4°C. After that, the samples were processed for Embed 812 (Electron Microscopy Sciences, Hatfield, PA, USA) epoxy resin, according to standard procedures. Semithin transversal sections (1 µm thick) were stained with Richardson stain and imaged using an Olympus 60x/1.4NA PlanApo oil immersion objective (Olympus) and a DMX 1200 Nikon (Tokyo, Japan) digital camera. Ultrathin sections were counterstained with Reynold's lead citrate. All observations were performed on a transmission electron microscope JEOL JE; 1010 (Akishima, Tokyo, Japan).

Statistical analysis

The data is expressed as means \pm SEM. The statistical analysis was assessed by a Student's t-test or by 1- or 2-way analysis of variance (ANOVA) followed by *post hoc* Bonferroni's test. The level of significance was established at $p < 0.05$. GraphPad Prism 6 software was used for statistical analysis and graph presentations of data.

RESULTS

Three patterns of MN pathology established on the basis of accumulation of misfolded SOD1G93A

The accumulation of misfolded SOD1 (mfSOD1) is a hallmark feature of spinal cord pathology in mutant SOD1-mediated ALS animal models. mfSOD1 can be detected by conformational-specific antibodies able to distinguish this form of SOD1 from those with native conformation (Bosco et al., 2010; Brotherton et al., 2012; Fujisawa et al., 2012; Hernández et al., 2010; Maier et al., 2018b; Paré et al., 2018; Pickles & Vande Velde, 2012; Rakhit et al., 2007; Javier Sábado et al., 2013; Urushitani et al., 2007). Due to its neurotoxicity, mfSOD1 is a key element in the pathogenesis of SOD1-mediated familial ALS (Redler et al., 2014) and it has been suggested that may also play a role in sporadic ALS when wild-type SOD1 adopt a "toxic conformation" by post-translational modifications (Bosco et al., 2010; Forsberg et al., 2010; Maier et al., 2018b; Paré et al., 2018; Rotunno & Bosco, 2013). Thus, the evaluation of SOD1 expression by means of antibodies like C4F6 or AJ10 (Brotherton et al., 2012; Javier Sábado et al., 2013; Urushitani et al., 2007) in individual MNs may provide a valuable readout of their pathologic status (Saxena et al., 2013). For this purpose, after analyzing mfSOD1 immunostaining, we defined three distinct patterns of its distribution in spinal cords sections in SOD1G93A mice, that were categorized as follows (see Fig. 1 a-h): i) absence or very low levels of mfSOD1-positive immunoreactivity (phenotype 1); ii) scattered mfSOD1 positive specks in the ventral horn surrounding MN cell bodies largely devoid of mfSOD1 labeling (phenotype 2); and iii) MN cell bodies showing highly positive mfSOD1 immunostaining (phenotype 3). Mitochondria have been identified as a main target for misfolded SOD1 in spinal cord (Liu et al., 2004; Vande Velde et al., 2008). Translocation of mutant SOD1 to mitochondria results in swelling and ulterior massive vacuolization, which were remarkably detectable under EM), but also identifiable with light

microscopy, particularly in semithin sections (Higgins et al., 2003; Jaarsma et al., 2001; Wong et al., 1995). As shown in Fig. 1 (e-n), we observed these vacuolated MNs in a pattern which coincides with that described in previous reports (Fischer et al., 2004; Kong & Xu, 1998; Vinsant et al., 2013). This type of degeneration allowed to perform a correlation between the above mentioned mfSOD1-based phenotypes and the cellular structure; for instance: i) in the phenotype 1, vacuolar degeneration is scarce or absent; ii) in the phenotype 2, vacuolar degeneration is conspicuous and mainly delimited to MN dendrites and axons; iii) in the phenotype 3, vacuolar degeneration is also extensive within MN somas. EM observations pointed out that vacuolar degeneration originated from both massive mitochondrial swelling and endoplasmic reticulum (ER) vesicular fragmentation (Fig. 1, i-n and Suppl Fig 1).

The longitudinal analysis of distribution of the three MN phenotypes during the time course of disease showed that phenotype 2 is highly predominant at P30, whereas phenotype 3 appeared at around P60 and extended until the end-stages of disease. Most of the phenotype 3 MNs disappeared during a time interval ranging from P90 and end-stage, a period in which MN loss reached its maximum (Fig. 1, o-s and Suppl Fig 2). In concordance with the phenotype 2, ultrastructural examination at P30 showed a mitochondrial vacuolar degeneration restricted to MN processes (dendrites and axons), with only minimal changes detectable in MN somata. These alterations consisted of a focal enlargement of mitochondrial intermembrane space and early vacuolar changes in the ER (Supp Fig 1 a-d). These data are in concordance with those previously reported (Bendotti et al., 2001; Kong & Xu, 1998; Vinsant et al., 2013). In addition, some MNs occasionally showed massive fragmentation of their ER into individual vesicles, which probably reflected a sustained ER-stress and intracellular calcium homeostasis disturbance prior to overt neuronal degeneration and death. Although the MN type 3 phenotype corresponded to a severe cellular damage, chromatin condensation was never seen in these neurons. In addition, as expected, MN cell bodies with type 3 phenotype did not show positive signal for active caspase 3, this confirming the lack of apoptotic machinery activation in these cells (not shown). The ultrastructural morphology of these highly vacuolated MNs fitted well in the concept of paraptosis, in which cytoplasmic vacuolation arising from altered mitochondria and/or ER are key features (Kim et al., 2021; Sperandio et al., 2000). The maximal rise in the emergence of type 3 phenotype appears between P30 and P90. In this time interval, a moderate but sustained, MN loss occurred, indicating that MNs with massive mfSOD1 accumulation die notably at presymptomatic or early symptomatic stages of the disease. Co-immunostaining of mfSOD1 with the MMP9 showed that MNs with vacuolar degeneration correspond to ALS-vulnerable MNs subtype (Kaplan et al., 2014). Type 3 phenotype was further characterized by co-localizing mfSOD1 with mitochondrial and ER markers, showing that mfSOD1 was

accumulated in large vacuoles of mitochondrial origin and did not share any compartmentation with the ER markers PDI or BiP. This is consistent with the EM observations suggesting that enlargement of vacuoles of mitochondrial origin is produced by coalescence of several less-sized membrane-bounded elements; in this way, the very large vacuoles (5-10 um of diameter) like those we seen in MNs can be generated (Supp Fig 1 e-i) The multi-mitochondrial origin of these giant vacuoles can be proved by the presence of several segregated units of internal mitochondrial membrane complexes that were seen accumulated in a corner of a vacuole and sharing a single highly-enlarged external membrane (Supp Fig 1h).

We hypothesized that the fate of vacuoles massively accumulated in degenerating MNs should be their release to the extracellular space in form of extracellular vesicles (EVs). For this reason we further explored the association of some selected markers in vacuolated MNs (Fig 2). A strong positive immunoreactivity for chromogranin was observed in the lumen of many, but not all, large cytoplasmatic vacuoles of MNs with type 3 phenotype. Chromogranin is a protein found in secretory vesicles in neurons and neuroendocrine system that interact with mutant SOD1 in ALS (Urushitani et al., 2006). In agreement with (Rudnick et al., 2017) we have observed some round bodies of about 3 um of diameter (2.98 ± 0.09 um n=16) in vacuolated MNs that display a positive p62-immunoreactivity indicating the dysregulation of autophagy also exist in these early degenerating MNs (not shown). Also a highly positive CD81 immunoreactivity was observed in association with large cytoplasmatic vacuoles of degenerating MNs overexpressing mfSOD1. CD81 is a member of tetraspannin family of proteins that it was found enriched in extracellular vesicles or (EVs) or exosomes (Kowal et al., 2016) including those of neuronal origin. However, other members of tetraspannin family such as CD9 or CD63, were not found imitating a pattern described in some EVs subtypes (Kowal et al., 2016). A positive signal for flotillin, another well established EV marker, was also detected in relation to MN vacuolar degeneration. In addition, these paraptotic-like MNs contained some pMLKL-positive granules, suggesting their involvement in a membrane rupture in a similar way that occurs during execution of necroptotic cell death (H. Wang et al., 2014). If this was the case, the ultimate fate of vacuolated MNs would be the membrane rupture and massive release of vacuolar structures.

Thus, the significant (~60%) reduction of type 3 phenotype at the end-stage is a consequence of the massive MN cell death that takes place once symptomatology has been started after P90. This indicates that ALS-resistant MNs, which still remain at the end-stages of the disease, do not particularly accumulate large amounts of mfSOD1. Importantly, the scarcity of type 3 phenotype at end-stages, did not indicate a reduction of neuronal death. Conversely, since MN death is maximal in this period, the phenotype of dying neurons did not involve mfSOD1 accumulation associated to

vacuolar (paraprototic) morphology. Instead, most of degenerating MNs seen in ventral horn at end-stages displayed disorganization of the normal intracellular organelle architecture, with a marked reduction in the size of Golgi network, and prominent accumulation of small presumably transport vesicles; these vesicles are clearly distinct in size and shape from those described in phenotype 3 MNs. In addition, in these MNs, almost all mitochondria virtually displayed a nearly normal morphology, which greatly contrasted with that typically occurring in MN type 3 phenotype. Other MNs at the end-stage displayed complete organelle disruption and amorphous intracellular inclusions, which corresponded likely to large protein aggregates. Overall, these results indicate the coexistence of a diversity of mechanisms of neuronal death during ALS progression.

Synaptic inputs to MNs and mfSOD1 accumulation

Alterations in synaptic inputs and MN excitability have been reported as early events in ALS (Bączyk et al., 2020; Chang & Martin, 2009; Delestrée et al., 2014; Martínez-Silva et al., 2018; Roselli & Caroni, 2015; Saxena et al., 2013; Schutz, 2005; Vinsant et al., 2013; Zang et al., 2005; P. Zhao et al., 2008). By examining the density of synaptic terminals on MN cell bodies by synaptophysin immunolabeling, we did not observe any significant change between SOD1G93A and WT animals at P60 (synaptic puncta/100 µm MN perimeter: WT = 102.1 ± 1.55 , SOD1G93A = 106.1 ± 1.39 [mean ± SEM]; n = 299 and 383 MNs, respectively, from 3 animals per condition; p > 0.05). However, a significant loss of afferent axosomatic synapses was detected in SOD1G93A mice when the analysis was restricted to MNs displaying the type 3 phenotype with extensive vacuolization and mfSOD1 accumulation (synaptic puncta/100 µm MN soma perimeter: SOD1G93A MNs with type 3 phenotype = 91.01 ± 2.3 vs. the entire population of SOD1G93A MNs = 106.1 ± 1.39 [mean ± SEM], p < 0.0001; n = 147 MNs from 3 animals). However, it appeared that the activity of afferent inputs on SOD1G93A MNs underwent more widespread changes, which were reflected by alterations in the ultrastructural organization of presynaptic organelles (Fig Supp 3, a-f). Indeed, the density of small (< 100 nm) vesicles contained within afferent synaptic boutons on MNs was markedly reduced at P60, but not at P30, SOD1G93A mice (Fig Supp 3, e); This vesicle depletion occurred irrespective to S (excitatory) or F (inhibitory) synaptic type (Conradi & Skoglund, 1969). In addition, many synaptic terminals at P60 contained an abnormal accumulation of large endosome-like vacuoles (> 100 nm of diameter), which presumably indicates an altered synaptic vesicle recycling due to a dysregulation in neurotransmitter release. Pioneering studies on the relationship between synaptic structure and function have shown that increased synaptic activity results in an accumulation of complex vesicles and presynaptic endocytic structures generated as a consequence of the blockade of the vesicle recycling process (Christensen, 1976; Haimann et al., 1985; Heuser & Reese, 1973; Soykan et al., 2017).

The ultrastructure of presynaptic boutons in advanced stages of the disease show extreme degenerative changes and also presynaptic membrane disruption with release of vesicular structures to the extracellular space (Fig Supp 3). Some of this changes have reported to occur in acute degeneration of synaptic terminals in axotomized MNs and involve the activation of necroptotic pathway (Salvany et al., 2021).

Regulation of MN excitability particularly depends on the activity of cholinergic C-type synapses (C-boutons) throughout a decrease in the after-hyperpolarization (AHP) potential (Miles et al., 2007). Although controversial (Dukkipati et al., 2017), changes in C-bouton size or density have been reported in ALS (Casas et al., 2013; Herron & Miles, 2012; Lasiene et al., 2016; Milan et al., 2015; Nagao et al., 1998; Pullen & Athanasiou, 2009; Saxena et al., 2013). By means of double immunolabeling for VACHT and NRG1, the pre- and postsynaptic compartments of C-type synapses can be delimited (Casanovas et al., 2017; Gallart-Palau et al., 2014), and their changes in relation to the already defined misfolded SOD1G93A MN phenotypes can be examined. After co-immunostaining with anti-mfSOD1 antibodies, we found that quantitative alterations in VACHT were only observed in MNs showing type 3 phenotype, whereas postsynaptic organization, visualized by NRG1 labeling, was already altered in less severe phenotypes and also in presymptomatic stages of disease (Fig. 3 a - f). NRG1 is a protein co-clustered with other molecules forming part of the signaling complex associated to the subsynaptic cistern of C-boutons (Casanovas et al., 2017; Deardorff et al., 2021; Witts et al., 2014). It should be noted that in MNs at early stages of disease (P30) or in those exhibiting middle severity alteration (type 2 phenotype), presynaptic VACHT-positive C-bouton terminals are moderately, but significantly, enlarged in SOD1G93A animals. This is consistent with previously reported findings (Herron & Miles, 2012; Milan et al., 2015; Pullen & Athanasiou, 2009; Saxena et al., 2013). Thus, alteration in C-bouton signaling may be relevant in determining MN dysfunction prior to cell death. For this reason, we analyzed the impact of a C-bouton signaling-pharmacological intervention on mfSOD1 accumulation by means of a treatment with the M2 muscarinic cholinergic receptor agonist (oxotremorine) or antagonist (methocramine), according to established protocols (Saxena et al., 2013). The effects of these interventions on the expression of mfSOD1 and C-bouton morphological parameters were examined after 15 days of treatment started at p60. Methocramine significantly promoted the expression of mfSOD1 in ventral horn (Fig. 3 g). Both treatments resulted in a similar effect increasing the number and size of VACHT-positive C-bouton terminals (Fig. 3 h-i). Similar changes were found in the size of NRG1 spots (Fig. 3 j), representing the postsynaptic side of C-boutons; however, no changes were noticed in the density of NRG1 spots on MN somata after these treatments.

Glial responses and mfSOD1 accumulation

A critical aspect of ALS pathology is glial activation, which affects the onset and progression of disease (Beers et al., 2011; B. E. Clarke & Patani, 2020; D'Erchia et al., 2017; Frakes et al., 2014; Hall et al., 1998; Nagai et al., 2007; Philips & Robberecht, 2011). Microglial activation results in a cell proliferation and phenotype switching from a protective anti-inflammatory state to another with neurotoxic pro-inflammatory features (Geloso et al., 2017; W. Zhao et al., 2013). Microgliosis is particularly prominent at advanced stages of disease but has also been detected presymptomatically either by histological analysis or by molecular signature (Maniatis et al., 2019; Sanagi et al., 2010). The extent of astrogliosis and microgliosis in relation to mfSOD1 expression in spinal cord ventral horn was analyzed in SOD1G93A mice along the disease progression. This was accomplished after triple fluorescent immunolabeling for GFAP, Iba1 and C4F6. All these markers showed a progressive and parallel rise, indicative of both astrogliosis and microgliosis, from P30 to the end-stages of disease (Fig. 4 a-b). However, the expression of mfSOD1 did not follow a similar parallel course, with a rapid rise between P30 and P60 and ulterior gradual decline (Fig. 4 c). It is interesting to note that, at the end-stage period, the content in mfSOD1 is importantly reduced, probably due to a substantial loss of MNs involving those of type 3 phenotype.

A more detailed analysis of the microglial reaction occurring in close apposition with MN cell bodies was also performed in relation with their mfSOD1 content and MN phenotypes. These results are depicted in Fig. 4. MN cell bodies closely interacted with recruited microglial cells in a positive correlation with the disease progression. Moreover, MN cell bodies expressing high levels of mfSOD1 are largely covered by microglia (Fig. 4 d). A parallel increase in the amount of CD68+ lysosomal particles within Iba1-delimited microglia profiles, indicative of their phagocytic activity, were observed (Fig. 4 e). A similar profile was found for the expression of galectin-3/Mac-2, which is a marker for a subset of activated-phagocytizing microglial cells (Reichert & Rotshenker, 2019), and for the inflammatory molecule C1q (Fig. 4 f and g). However, when Iba1-positive microglia was co-immunolabeled for the P2Y12R, an inverse time course profile was observed, with a maximal expression at presymptomatic stages (P60) and a subsequent decline reaching minimal levels at end-stages (Fig. 4 h). P2Y12R is a subtype of G-coupled purinergic receptor uniquely expressed in CNS microglia (Sasaki et al., 2003) and strongly downregulated in their activated states, when microglia progress from ramified to amoeboid morphology (Haynes et al., 2006); this assumption is fully consistent with our data in ALS mice. In addition to longitudinal analysis during evolution of ALS, when microglia was analyzed topologically in relation to MN mfSOD1 phenotypes, it was found that all markers of activation were moderately elevated around MNs with type 3 phenotype, whereas the levels of P2Y12R were not affected by the proximity of mfSOD1 deposits (Fig. 4 h).

Elimination of microglia reduces the severity of MN phenotypes of mfSOD1

PLX5622 is a CSF1R inhibitor that, administered orally in mice, results in a virtual elimination of the whole microglial population (Elmore et al., 2014). By applying this drug, we examined how the absence of microglial cells affected the expression of mfSOD1 in SOD1G93A animals. Iba1 immunostaining was performed at P30 in animals that were treated with PLX5622 for 30 days, which resulted in the lack of detectable microglia on spinal cord sections. This treatment also provoked a reduction of mfSOD1 expression when analyzed at P60. The percentage (mean ± SEM) mfSOD1-immunoreactivity occupancy found in ventral horn was: WT = 0.18 ± 0.02 [n = 32]; SOD1G93A P60 = 7.4 ± 0.86 [n = 29]; SOD1G93A P60-PLX5622 = 3.45 ± 0.39 [n = 52] (SOD1G93A P60 vs. SOD1G93A P60-PLX5622, p < 0.05 [one-way ANOVA]; n = number of measurements from 3 animals per condition). It is interesting to note that mfSOD1-immunoreactive vacuolated (type 3 phenotype) MNs were markedly depleted in the absence of microglia, as shown by the analysis of C4F6 signal occupancy on P60 MN somata (WT = 0.23 ± 0.04 [n = 62]; SOD1G93A P60 = 12.69 ± 1.75 [n = 54]; SOD1G93A P60-PLX5622 = 2.4 ± 0.21 [n = 95]; p < 0.0001, SOD1G93A P60 vs. SOD1G93A P60-PLX5622 [one-way ANOVA]; n = number of measurements from 3 animals per condition).

Effects of peripheral nerve injury in SOD1G93A mice on the progression of MN pathology

According to the “dying back” hypothesis, it has been proposed that ALS is initiated as a distal axonopathy which evolves to proximal axonal degeneration; this would lead to an altered retrograde-signaling cascade resulting in a MN death (Fischer et al., 2004). The interruption of neuromuscular connection due to a peripheral nerve injury is also a strong negative modifier of ALS phenotype in animal models (Mariotti et al., 2002; Schram et al., 2019; Sharp et al., 2005). Nevertheless, some positive effects promoting regenerative events and MN survival were also observed after nerve crush in SOD1G93A mice (Kong & Xu, 1998; Sharp et al., 2018).

Here, we examined whether sciatic nerve transection (axotomy), performed in SOD1G93A mice, alters the expression of mfSOD1 MN phenotypes and promotes neuroinflammation in spinal cord. MN anterolateral pool located at lumbar spinal cord, which corresponds to the location of the injured MNs, was analyzed 7 days following axotomy performed at distinct time points of disease progression (P30, P60 and P90). In all conditions, we observed that a shift of the relative amount of the three MN phenotypes to those more harmful occurred as a consequence of nerve transection. For example, at a presymptomatic stage (P30) in which the MN phenotype type 3 (paraptotic-like) was not yet appeared in unoperated SOD1G93A mice, sciatic nerve axotomy resulted in an induction of this worse cytopathological phenotype affecting 14% of MNs. Nerve axotomy performed at later stages, such as P60 or P90, also entailed a worsening in the MN phenotype score (Fig. 5 a-d). It is well known that peripheral nerve lesion induces a plethora of changes in axotomized MN cell bodies and,

also in adjacent synaptic afferents and glial cells (Salvany et al., 2019, 2021). Thus, the strong neuroinflammatory response induced prematurely by axotomy in SOD1G93A animals may act as a synergic mechanism in promoting non-cell-autonomous MN degeneration and mfSOD1 expression (Fig. 5 e and f). This also indicates a link between the expression of neurotoxic forms of SOD1 in MNs and neuroinflammation. It is conceivable that the injury-mediated microgliosis, when produced under a SOD1G93A background, may exacerbate the endogenous neurotoxicity of microglia that basally exists as a consequence of the disease (Beers et al., 2006; Clement et al., 2003). Conversely, mfSOD1 accumulated in degenerating MNs, could be released at the extracellular medium via exosomal or necroptotic-like extracellular vesicles; since extracellular mfSOD1 is a potent trigger of microgliosis (W. Zhao et al., 2010), a harmful feedback loop potentiating neuroinflammation and neurotoxicity in SOD1G93A mice could be established at local level.

To determine whether axotomy potentiates the acquisition of a harmful microglial phenotype, the expression of CD68, Mac-2, and C1q were examined within Iba1-positive cells recruited around axotomized MN cell bodies. This analysis was performed in SOD1G93A animals at presymptomatic (P60) and symptomatic (P90) stages and 7 days postaxotomy. It is interesting to note that at P60 the density of microglial cells with phagocytic activity, based on the CD68-expression analysis, was either not changed or tended to be reduced as a consequence of axotomy. A similar result was seen when CD68 was evaluated in relation to mfSOD1 MN phenotypes. A comparable profile was found for Mac-2 expression. However, the opposite was observed at P90; at this age, the microglial neuroinflammatory response induced by axotomy, entailed the acquisition of a worse microglial phenotype, which included the upregulation of CD68-positive particles and the acquisition of Mac-2 expression (not shown).

DISCUSSION

The availability of conformational-specific mfSOD1 antibodies allowed us to explore in some detail the cellular distribution of these toxic SOD1 conformers and their association with MN degeneration and gliosis during ALS progression in SOD1G93A mice. Since targeting mutant SOD1 neurotoxicity is a significant approach for ALS therapy (Gros-Louis et al., 2010; Maier et al., 2018a; Raoul et al., 2005; Sun et al., 2012; Urushitani et al., 2007), the new information we provide here on the involvement of mfSOD1 in MN pathology may be relevant in future designs of SOD1-based ALS treatments. Most of our data on mfSOD1 localization were obtained using the C4F6 monoclonal antibody and are highly

coincident with those previously reported using this antibody (Brotherton et al., 2012); additionally, according to animal species requirements, for multilabeling experiments, our rabbit anti-mfSOD1 AJ10 antibody was also applied when needed. Both antibodies give the same pattern of immunoreactivity when analyzed together in spinal cord sections of SOD1G93A mice (J Sábado et al., 2015). We found that mfSOD1 immunoreactivity was mainly associated to MNs, starting on their dendritic and axonal expansions with a later accumulation on cell bodies. This sequential distribution allowed us the delimitation, for operative purposes in this work, of the above described three phenotypes. There is also a good correlation between mfSOD1 signal and the presence of vacuoles in MNs. Vacuolar degeneration has been largely described in degenerating MNs in mutant SOD1 transgenic mouse models, with both mitochondria and ER as the main organelles involved in vacuole formation (Bendotti et al., 2001; Dal Canto & Gurney, 1994; Higgins et al., 2003; Jaarsma et al., 2001; Kong & Xu, 1998; Wong et al., 1995). Since these are the hallmark features of paraptosis (Kim et al., 2021; Sperandio et al., 2000), we propose to apply this concept to vacuolated MNs in the context of mutant SOD1 ALS. Thus, the extensive and emerging data about the molecular pathways involved in the parapoptotic cell death in a variety of contexts may eventually help to find new targets for SOD1-mediated therapy in ALS. Vacuolated MN degeneration has been also observed during glutamate-mediated excitotoxic cell death, and ER dilatation and fragmentation is also a prominent ultrastructural feature of this form of neuronal death (Calderó et al., 1997). However, the mitochondrial swelling in this excitotoxic paradigm is not as massive as in ALS SOD1 MNs; moreover, some degree of chromatin clumping, which we did not observe in ALS-SOD1 parapoptotic-like MNs, is usually present in excitotoxic MNs.

It has been observed that massive mitochondrial swelling in the SOD1G93A mice results from an expansion on the intermembrane space in which the involvement of peroxisomes has been suggested as membrane donors (Higgins et al., 2003). This is in contrast with the more common mechanism of pathological mitochondrial swelling that occurs by the increase of matrix volume due to the altered ionic fluxes, osmotic imbalance and opening the permeability transition pore at the inner mitochondrial membranes (Javadov et al., 2018). This form of mitochondrial swelling is also seen in damaged cells present in the spinal cord of SOD1G93A mice, but also co-exists with a prominent intermembrane swelling of vacuolated MNs. Thus, mitochondrial damage in these mfSOD1-containing MNs seems to entail specific mechanisms, and could be the consequence of a tissue-specific interaction of mutant SOD1 with molecular components of the surface of outer mitochondrial membrane (Israelson et al., 2010; Pedrini et al., 2010; Vande Velde et al., 2008).

The ultrastructure appearance of the larger vacuoles (>10 um diameter) suggests they are formed by fusion of some units of already vacuolated mitochondria. As a consequence of fusion of outer

mitochondrial membranes, single giant vacuoles were formed. This giant vacuole contains several highly folded inner mitochondrial membrane units gathered at the wall of a big vacuole, which presumably originates by the fusion of several vacuolated mitochondria carrying their extended outer membrane. It should be noted that large vacuolated spheroidal mitochondria, present in axons and dendrites in concomitance with mfSOD1 accumulation, is an early event in SOD1G93A MN pathology; this corresponds with the pattern designated as type 2 phenotype in this work, which is prominent at P30, long time before the onset of symptoms. It is possible that the spatially restricted environmental conditions, characteristic of MN processes in relation to cell bodies, made the mitochondria present in axon and dendrites more vulnerable to mfSOD1 pathology. In this line, it has been shown that pathological elevations of neuronal Ca²⁺ starts in dendrites and later propagate to somas (Vande Velde et al., 2008). Imbalance of intracellular Ca²⁺, perturbation of ER-mitochondrial signaling and protein misfolding are crucial elements in determining paraptosis (Kim et al., 2021), which seems to be also shared by mfSOD1-containing MNs.

Alterations in the activity of afferent synaptic inputs may modulate the time course and severity of these early degenerative changes in mfSOD1-containing MNs. This is consistent with our results detecting premature structural alterations in synaptic terminals contacting MNs, and the observed effects of a pharmacological alteration of C-bouton-mediated neurotransmission. Our results showed that treatment with methocarbamol, to block muscarinic cholinergic inputs, results in a significant promotion of the mfSOD1 expression in ventral horn and change the relative distribution of mfSOD1 MN phenotypes during ALS progression in SOD1G93A mice. This is consistent with data previously reported (Saxena et al., 2013) and with the idea that the hypoexcitability is a positive factor in the promotion of MN vulnerability in ALS (Bączyk et al., 2020; Delestrée et al., 2014; Filipchuk et al., 2021; Martínez-Silva et al., 2018; Ruegsegger & Saxena, 2016; Saxena et al., 2013). It has been shown that the organization of postsynaptic glutamate receptors in synaptic afferents on MNs is critically disrupted before the alteration of their presynaptic partners in SOD1G93A mice (Bączyk et al., 2020). We observed an early dismantlement of the sub-synaptic cistern associated to C-boutons, which presumably results in a dysfunctional synaptic signaling in this particular type of synapse that critically regulates MN excitability. As the normal organization of the ER appears severely disrupted in vacuolated MNs, it should be expected that the sub-synaptic cistern, as specific ER sub-compartment, may be also involved in the change. Thus, we must conclude that the decreased functionality of glutamatergic and cholinergic synapses contributes to MN hypoexcitability, mfSOD1 burden and MN vacuolar degeneration.

We have surprisingly found that paraptotic-like MNs exhibit positive immunoreactivity for flotillin and CD81 located within the large vacuoles of mitochondrial origin. Flotillin and CD81 are members

of tetraspanin family that regulate membrane morphology and dynamics, affect intracellular trafficking, exocytosis-endocytosis and intercellular signaling (Hemler, 2005), and are also recognized as markers for extracellular vesicles (Kowal et al., 2016). The mitochondrial origin of vacuoles containing CD81 has been confirmed by its positive co-staining with ATP5A (complex V) antibody. The identification of mitochondrial components in extracellular vesicles displaying tetraspanin exosomal markers has been recently reported (D'Acunzo et al., 2021; Picca et al., 2020). Thus, the existence of vacuoles containing mfSOD1 associated with tetraspanins and mitochondrial components in degenerating MNs, points out about the possibility that they may be involved in the generation of extracellular vesicles which once release contribute to local neuroinflammation and prion-like spreading of the disease (Bellingham et al., 2012; Grad et al., 2014; Silverman et al., 2019). Another possibility is that, once generated, vacuolated mitochondria may be disrupted as a consequence of a promotion of fission molecular mechanisms that seem to be activated in ALS (Joshi et al., 2019). Thus, mitochondrial fragments may be eventually transferred to other neighboring cells (Hayakawa et al., 2016; Joshi et al., 2019).

Another intriguing aspect of vacuolated MNs is their content in pMLKL-positive particles, which is indicative of activation of the terminal effector of necroptotic pathways. Using the same antibody against pMLKL, it has been demonstrated the translocation of this protein from the cytosol to membrane fractions, including mitochondria, during necroptosis; pMLKL-positive puncta have also been observed by immunofluorescence in cells undergoing necroptosis (H. Wang et al., 2014). Since, once translocated, pMLKL is a membrane integrity disruptor, its role in the formation and release of mfSOD1-containing vesicles from vacuolated MNs should be further analyzed. Previous studies examining the involvement of necroptosis in ALS have resulted unclear: necroptosis has been proposed as a mechanism for MN death induced by ALS-astrocytes “*in vitro*” (Re et al., 2014), and elevation of necroptotic markers including MLKL has been observed in spinal cords from SOD1G93A mice and patients with sporadic ALS (Ito et al., 2016). However, deletion of MLKL or either RIP1 or RIP3 kinases does not improve either the neuropathology or the clinical course of ALS in transgenic SOD1 mouse models (Dermentzaki et al., 2019; Dominguez et al., 2021; T. Wang et al., 2020). In any case, the pathogenic role of necroptosis in ALS cannot be totally excluded, since the activation of compensatory mechanisms may account for the lack of beneficial effects obtained by the deletion of some necroptotic mediators on transgenic mouse models (Dermentzaki et al., 2019). In addition, other cell death mechanisms appear to be activated in non-vacuolated MNs in the more advanced stages of the disease that could not be abolished in these mutants.

Extracellular mfSOD1 does not kill MNs “*per se*” but, when derived from neurons and astrocytes, is a potent inducer of microglial activation and microglia-mediated neurotoxicity (Urushitani et al., 2006;

W. Zhao et al., 2010). In concordance with our data, it has been shown that extracellular vesicles of neuronal and astroglial origin may carry abundant mfSOD1 in SOD1-mediated ALS in humans and mouse models (Silverman et al., 2019). Neurosecretory proteins such as chromogranins interact with mutant SOD1 and mediate its secretion to the extracellular space where becomes indirectly toxic for MNs following microglial activation (Urushitani et al., 2006; W. Zhao et al., 2010). Given our data on the coexistence of mfSOD1 with chromogranin, the EVs markers flotillin and CD81, and the membrane disruptor pMLKL in vacuolated MNs, it is suggested that they might act as microglial attractors in the immediate vicinity of vacuolated MNs. For this reason, we analyzed topographically the microglial recruitment in relation to the above defined patterns of mfSOD1 expression in MNs. A good correlation between the severity of mfSOD1 accumulation in MNs and local microglial recruitment has been observed among the distinct MN phenotypes (Fig. 4 d). These locally positioned microglia display an activation profile with increased expression of CD68, Mac-2 and C1q (Fig. 4 e - g), and vice versa, the status of microglia also impacts on the extension of mfSOD1 accumulation and vacuolar degeneration of MNs. This can be concluded from our experiments in which microgliosis in the immediate MN environment was altered either by pharmacological elimination of microglia or by promoting a supplementary axotomy-induced chemotaxis. This points out to the crucial role of non-neuronal cells contributing to MN death via non-cell-autonomous mechanisms (Clement et al., 2003). In this line, it has been shown that microglia expressing mutant SOD1 is neurotoxic for MNs (Frakes et al., 2014; Xiao et al., 2007; W. Zhao et al., 2010), and probably play a distinct pathogenic role according to the natural history of the disease. By eliminating the expression of mutant SOD1 in MNs it is concluded that the protein is a primary determinant of disease onset, whereas decreasing mutant SOD1 levels in microglia slows disease progression (Clement et al., 2003). Our data may fit with this concept if we consider that vacuolar MN degeneration, which predominates at the early presymptomatic stages, is followed by a progressive glial activation and more extensive neurotoxicity, triggered by the release mfSOD1 and EVs from degenerating or disrupted vacuolar MNs. This second phase would be linked to the paralysis onset and disease progression, in which microglial-derived neurotoxicity affects the less vulnerable MN subtypes. It is interesting to note that according to our results and others (Kong & Xu, 1998), the vacuolation is a transient process mainly affecting the MMP9-positive fast-twitch, vulnerable, MNs. We deduce that since, once disrupted, vacuolar degeneration does not affect the rest of less vulnerable MNs that also undergo a degenerative pathology with a clearly distinct non-vacuolar phenotype may be expressive of a glial-mediated neurotoxic attack instead a cell autonomous mutant-SOD1-mediated damage. But the more exact mechanism involved in the MN degeneration and death in the later phases of ALS progression remain to be determined.

In conclusion, our results more precisely map the neuropathological events occurring in the early and late stages of ALS progression in the SOD1G93A mouse model. In particular, we focused our attention on the location of mfSOD1 as a crucial determinant of the initial steps of MN degeneration, in which the ER and mitochondrial vacuolation are the main hallmarks. The association of mfSOD1-containing vacuoles with chromogranin, EVs markers and, also, pMLKL points out to a new mechanism in which EVs derived from damaged MNs, via cellular secretion or necroptotic disruption, may be the triggers for the initial steps in neuroinflammation, glial-mediated neurotoxicity and disease spreading. A more detailed knowledge of these processes occurring long before end-stages of the disease will allow us to identify new molecular targets to be further investigated in future preclinical trials.

ACKNOWLEDGMENTS

The authors thank Alaó Gatius, Alba Blasco, Olga Tarabal and Sara Hernández for their help in some experiments, Anaïs Panosa from the SCT of Microscopy of the *Universitat de Lleida* for technical support with confocal microscopy, and the staff form the SCT Animal Facility of the *Universitat de Lleida* for mouse care and housing. The authors thank Lidia Delgado and M. Yolanda Muela, from the Unitat de Criomicroscòpia Electrònica (Centres Científics i Tecnològics de la Universitat de Barcelona), for technical support with ultrastructural immunolabeling, and Plexxikon Inc. for providing the CSFR1 inhibitor PLX5622. This work was supported by grants from the Ministerio de Ciencia, Innovación y Universidades cofinanced by Fondo Europeo de Desarrollo regional (FEDER; RTI2018-099278-B100 J.C. and J.E.) and from Jack Van den Hock a la Investigació de l'ELA – Fundació Miquel Valls. S.S. holds predoctoral fellowship “Ajuts 2020 de Promoció de la Recerca en Salut-8^a edició” from IRBLleida/Diputació de Lleida.

REFERENCES

- Aldskogius, H. (2011). Mechanisms and consequences of microglial responses to peripheral axotomy. *Frontiers in Bioscience*, 3, 857–868.
- Bączyk, M., Alami, N. O., Delestrée, N., Martinot, C., Tang, L., Commissio, B., Bayer, D., Doisne, N., Frankel, W., Manuel, M., Roselli, F., & Zytnicki, D. (2020). Synaptic restoration by cAMP/PKA drives activity-dependent neuroprotection to motoneurons in ALS. *Journal of Experimental Medicine*, 217(8). <https://doi.org/10.1084/jem.20191734>

- Beers, D. R., Henkel, J. S., Xiao, Q., Zhao, W., Wang, J., Yen, A. A., Siklos, L., McKercher, S. R., & Appel, S. H. (2006). Wild-type microglia extend survival in PU.1 knockout mice with familial amyotrophic lateral sclerosis. *Proceedings of the National Academy of Sciences*, 103(43), 16021–16026. <https://doi.org/10.1073/pnas.0607423103>
- Beers, D. R., Zhao, W., Liao, B., Kano, O., Wang, J., Huang, A., Appel, S. H., & Henkel, J. S. (2011). Neuroinflammation modulates distinct regional and temporal clinical responses in ALS mice. *Brain, Behavior, and Immunity*, 25(5), 1025–1035. <https://doi.org/10.1016/j.bbi.2010.12.008>
- Bellingham, S. A., Guo, B. B., Coleman, B. M., & Hill, A. F. (2012). Exosomes: Vehicles for the Transfer of Toxic Proteins Associated with Neurodegenerative Diseases? *Frontiers in Physiology*, 3(May), 1–12. <https://doi.org/10.3389/fphys.2012.00124>
- Bendotti, C., Calvaresi, N., Chiveri, L., Prelle, A., Moggio, M., Braga, M., Silani, V., & De Biasi, S. (2001). Early vacuolization and mitochondrial damage in motor neurons of FALS mice are not associated with apoptosis or with changes in cytochrome oxidase histochemical reactivity. *Journal of the Neurological Sciences*, 191(1–2), 25–33. [https://doi.org/10.1016/S0022-510X\(01\)00627-X](https://doi.org/10.1016/S0022-510X(01)00627-X)
- Boillée, S., Yamanaka, K., Lobsiger, C. S., Copeland, N. G., Jenkins, N. A., Kassiotis, G., Kollias, G., & Cleveland, D. W. (2006). Onset and progression in inherited ALS determined by motor neurons and microglia. *Science*, 312(5778), 1389–1392. <https://doi.org/10.1126/science.1123511>
- Bosco, D. A., Morfini, G., Karabacak, N. M., Song, Y., Gros-Louis, F., Pasinelli, P., Goolsby, H., Fontaine, B. A., Lemay, N., McKenna-Yasek, D., Frosch, M. P., Agar, J. N., Julien, J., Brady, S. T., & Brown, R. H. (2010). Wild-type and mutant SOD1 share an aberrant conformation and a common pathogenic pathway in ALS. *Nature Neuroscience*, 13(11), 1396–1403. <https://doi.org/10.1038/nn.2660>
- Brotherton, T. E., Li, Y., Cooper, D., Gearing, M., Julien, J.-P., Rothstein, J. D., Boylan, K., & Glass, J. D. (2012). Localization of a toxic form of superoxide dismutase 1 protein to pathologically affected tissues in familial ALS. *Proceedings of the National Academy of Sciences*, 109(14), 5505–5510. <https://doi.org/10.1073/pnas.1115009109>
- Bruijn, L. I., Miller, T. M., & Cleveland, D. W. (2004). UNRAVELING THE MECHANISMS INVOLVED IN MOTOR NEURON DEGENERATION IN ALS. *Annual Review of Neuroscience*, 27(1), 723–749. <https://doi.org/10.1146/annurev.neuro.27.070203.144244>
- Burkholder, T., Foltz, C., Karlsson, E., Linton, C. G., & Smith, J. M. (2012). Health Evaluation of Experimental Laboratory Mice. *Current Protocols in Mouse Biology*, 2(2), 145–165. <https://doi.org/10.1002/9780470942390.mo110217>
- Calderó, J., Ciutat, D., Lladó, J., Castán, E., Oppenheim, R. W., & Esquerda, J. E. (1997). Effects of excitatory amino acids on neuromuscular development in the chick embryo. *The Journal of Comparative Neurology*, 387(1), 73–95. [https://doi.org/10.1002/\(SICI\)1096-9861\(19971013\)387:1<73::AID-CNE7>3.3.CO;2-G](https://doi.org/10.1002/(SICI)1096-9861(19971013)387:1<73::AID-CNE7>3.3.CO;2-G)
- Casanovas, A., Salvany, S., Lahoz, V., Tarabal, O., Piedrafita, L., Sabater, R., Hernández, S., Calderó, J., & Esquerda, J. E. (2017). Neuregulin 1-ErbB module in C-bouton synapses on somatic motor neurons: molecular compartmentation and response to peripheral nerve injury. *Scientific Reports*, 7(1), 40155. <https://doi.org/10.1038/srep40155>

- Casas, C., Herrando-grabulosa, M., Manzano, R., Mancuso, R., Osta, R., & Navarro, X. (2013). *Early presymptomatic cholinergic dysfunction in a murine model of amyotrophic lateral sclerosis.* <https://doi.org/10.1002/brb3.104>
- Chang, Q., & Martin, L. J. (2009). Glycinergic Innervation of Motoneurons Is Deficient in Amyotrophic Lateral Sclerosis Mice. *The American Journal of Pathology*, 174(2), 574–585. <https://doi.org/10.2353/ajpath.2009.080557>
- Chi, A. Y., Zhai, P., Dal Canto, M. C., Peters, T. M., Kwon, Y. W., Prattis, S. M., & Gurney, M. E. (1995). Age-Dependent Penetrance of Disease in a Transgenic Mouse Model of Familial Amyotrophic Lateral Sclerosis. *Molecular and Cellular Neuroscience*, 6(4), 349–362. <https://doi.org/10.1006/mcne.1995.1027>
- Christensen, B. N. (1976). Morphological correlates of synaptic transmission in lamprey spinal cord. *Journal of Neurophysiology*, 39(2), 197–212. <https://doi.org/10.1152/jn.1976.39.2.197>
- Clarke, B. E., & Patani, R. (2020). The microglial component of amyotrophic lateral sclerosis. *Brain*, 143(12), 3526–3539. <https://doi.org/10.1093/brain/awaa309>
- Clarke, P. G., & Oppenheim, R. W. (1995). Neuron death in vertebrate development: in vitro methods. *Methods in Cell Biology*, 46, 277–321.
- Clement, A. M., Nguyen, M. D., Roberts, E. A., Garcia, M. L., Boillée, S., Rule, M., McMahon, A. P., Doucette, W., Siwek, D., Ferrante, R. J., Brown Jr., R. H., Julien, J.-P., Goldstein, L. S. B., & Cleveland, D. W. (2003). Wild-Type Nonneuronal Cells Extend Survival of SOD1 Mutant Motor Neurons in ALS Mice. *Science*, 302(5642), 113–117. <https://doi.org/10.1126/science.1086071>
- Conradi, S., & Skoglund, S. (1969). Observations on the ultrastructure and distribution of neuronal and glial elements on the motoneuron surface in the lumbosacral spinal cord of the cat during postnatal development. *Acta Physiologica Scandinavica. Supplementum*, 333, 5–52. <http://www.ncbi.nlm.nih.gov/pubmed/5386538>
- D'Acunzo, P., Pérez-González, R., Kim, Y., Hargash, T., Miller, C., Alldred, M. J., Erdjument-Bromage, H., Penikalapati, S. C., Pawlik, M., Saito, M., Saito, M., Ginsberg, S. D., Neubert, T. A., Goulbourne, C. N., & Levy, E. (2021). Mitovesicles are a novel population of extracellular vesicles of mitochondrial origin altered in Down syndrome. *Science Advances*, 7(7), eabe5085. <https://doi.org/10.1126/sciadv.abe5085>
- D'Erchia, A. M., Gallo, A., Manzari, C., Raho, S., Horner, D. S., Chiara, M., Valletti, A., Aiello, I., Mastropasqua, F., Ciaccia, L., Locatelli, F., Pisani, F., Nicchia, G. P., Svelto, M., Pesole, G., & Picardi, E. (2017). Massive transcriptome sequencing of human spinal cord tissues provides new insights into motor neuron degeneration in ALS. *Scientific Reports*, 7(1), 10046. <https://doi.org/10.1038/s41598-017-10488-7>
- Dal Canto, M. C., & Gurney, M. E. (1994). Development of central nervous system pathology in a murine transgenic model of human amyotrophic lateral sclerosis. *American Journal of Pathology*, 145(6), 1271–1279.
- Deardorff, A. S., Romer, S. H., & Fyffe, R. E. W. (2021). Location, location, location: the organization and roles of potassium channels in mammalian motoneurons. *The Journal of Physiology*, 599(5), 1391–1420. <https://doi.org/10.1113/JP278675>
- Delestrée, N., Manuel, M., Iglesias, C., Elbasiouny, S. M., Heckman, C. J., & Zytnicki, D. (2014). Adult spinal motoneurones are not hyperexcitable in a mouse model of inherited amyotrophic lateral sclerosis. *The Journal of Physiology*, 592(7), 1687–1703.

<https://doi.org/10.1113/jphysiol.2013.265843>

Dermentzaki, G., Politi, K. A., Lu, L., Mishra, V., Pérez-Torres, E. J., Sosunov, A. A., McKhann, G. M., Lotti, F., Shneider, N. A., & Przedborski, S. (2019). Deletion of Ripk3 Prevents Motor Neuron Death In Vitro but not In Vivo. *Eneuro*, 6(1), ENEURO.0308-18.2018. <https://doi.org/10.1523/ENEURO.0308-18.2018>

Dominguez, S., Varfolomeev, E., Brendza, R., Stark, K., Tea, J., Imperio, J., Ngu, H., Earr, T., Foreman, O., Webster, J. D., Easton, A., Vucic, D., & Bingol, B. (2021). Genetic inactivation of RIP1 kinase does not ameliorate disease in a mouse model of ALS. *Cell Death & Differentiation*, 28(3), 915–931. <https://doi.org/10.1038/s41418-020-00625-7>

Dukkipati, S. S., Chihi, A., Wang, Y., & Elbasiouny, S. M. (2017). Experimental Design and Data Analysis Issues Contribute to Inconsistent Results of C-Bouton Changes in Amyotrophic Lateral Sclerosis. *Eneuro*, 4(1), ENEURO.0281-16.2016. <https://doi.org/10.1523/ENEURO.0281-16.2016>

Elmore, M. R. P., Najafi, A. R., Koike, M. A., Dagher, N. N., Spangenberg, E. E., Rice, R. A., Kitazawa, M., Matusow, B., Nguyen, H., West, B. L., & Green, K. N. (2014). Colony-Stimulating Factor 1 Receptor Signaling Is Necessary for Microglia Viability, Unmasking a Microglia Progenitor Cell in the Adult Brain. *Neuron*, 82(2), 380–397. <https://doi.org/10.1016/j.neuron.2014.02.040>

Filipchuk, A., Pambo-Pambo, A., Gaudel, F., Liabeuf, S., Brocard, C., Gueritaud, J. P., & Durand, J. (2021). Early Hypoexcitability in a Subgroup of Spinal Motoneurons in Superoxide Dismutase 1 Transgenic Mice, a Model of Amyotrophic Lateral Sclerosis. *Neuroscience*, 463, 337–353. <https://doi.org/10.1016/j.neuroscience.2021.01.039>

Fischer, L. R., Culver, D. G., Tennant, P., Davis, A. A., Wang, M., Castellano-Sanchez, A., Khan, J., Polak, M. A., & Glass, J. D. (2004). Amyotrophic lateral sclerosis is a distal axonopathy: evidence in mice and man. *Experimental Neurology*, 185(2), 232–240. <https://doi.org/10.1016/j.expneurol.2003.10.004>

Forsberg, K., Jonsson, P. A., Andersen, P. M., Bergemalm, D., Graffmo, K. S., Hultdin, M., Jacobsson, J., Rosquist, R., Marklund, S. L., & Brännström, T. (2010). Novel antibodies reveal inclusions containing non-native SOD1 in sporadic ALS patients. *PLoS ONE*, 5(7), 1–9. <https://doi.org/10.1371/journal.pone.0011552>

Frakes, A. E., Ferraiuolo, L., Haidet-Phillips, A. M., Schmelzer, L., Braun, L., Miranda, C. J., Ladner, K. J., Bevan, A. K., Foust, K. D., Godbout, J. P., Popovich, P. G., Guttridge, D. C., & Kaspar, B. K. (2014). Microglia induce motor neuron death via the classical NF-κB pathway in amyotrophic lateral sclerosis. *Neuron*, 81(5), 1009–1023. <https://doi.org/10.1016/j.neuron.2014.01.013>

Fujisawa, T., Homma, K., Yamaguchi, N., Kadokami, H., Tsuburaya, N., Naguro, I., Matsuzawa, A., Takeda, K., Takahashi, Y., Goto, J., Tsuji, S., Nishitoh, H., & Ichijo, H. (2012). A novel monoclonal antibody reveals a conformational alteration shared by amyotrophic lateral sclerosis-linked SOD1 mutants. *Annals of Neurology*, 72(5), 739–749. <https://doi.org/10.1002/ana.23668>

Gallart-Palau, X., Tarabal, O., Casanovas, A., Sábado, J., Correa, F. J., Hereu, M., Piedrafita, L., Calderó, J., & Esquerda, J. E. (2014). Neuregulin-1 is concentrated in the postsynaptic subsurface cistern of C-bouton inputs to α-motoneurons and altered during motoneuron diseases. *The FASEB Journal*, 28(8), 3618–3632. <https://doi.org/10.1096/fj.13-248583>

Geloso, M. C., Corvino, V., Marchese, E., Serrano, A., Michetti, F., & D'Ambrosi, N. (2017). The Dual Role of Microglia in ALS: Mechanisms and Therapeutic Approaches. *Frontiers in Aging*

Neuroscience, 9(JUL). <https://doi.org/10.3389/fnagi.2017.00242>

Grad, L. I., Pokrishevsky, E., Silverman, J. M., & Cashman, N. R. (2014). Exosome-dependent and independent mechanisms are involved in prion-like transmission of propagated Cu/Zn superoxide dismutase misfolding. *Prion*, 8(5), 331–335. <https://doi.org/10.4161/19336896.2014.983398>

Gros-Louis, F., Soucy, G., Larivière, R., & Julien, J.-P. (2010). Intracerebroventricular infusion of monoclonal antibody or its derived Fab fragment against misfolded forms of SOD1 mutant delays mortality in a mouse model of ALS. *Journal of Neurochemistry*, 113(5), 1188–1199. <https://doi.org/10.1111/j.1471-4159.2010.06683.x>

Günther, R., Suhr, M., Koch, J. C., Bähr, M., Lingor, P., & Tönges, L. (2012). Clinical Testing and Spinal Cord Removal in a Mouse Model for Amyotrophic Lateral Sclerosis (ALS). *Journal of Visualized Experiments*, 61, 4–7. <https://doi.org/10.3791/3936>

Gurney, M. E., Pu, H., Arlene Y, C., Canto, M. C. D., Polchow, C. Y., Alexander, D. D., Caliendo, Ja., Hentati, A., Kwon, Y. W., Deng, H.-X., Chen, W., Zhai, P., Sufit, R. L., & Siddique, T. (1994). Motor neuron degeneration in mice that express a human Cu , Z. *Science*, 264, 1772–1775.

Haimann, C., Torri-Tarelli, F., Fesce, R., & Ceccarelli, B. (1985). Measurement of quantal secretion induced by ouabain and its correlation with depletion of synaptic vesicles. *The Journal of Cell Biology*, 101(5), 1953–1965. <https://doi.org/10.1083/jcb.101.5.1953>

Hall, E. D., Oostveen, J. A., & Gurney, M. E. (1998). Relationship of microglial and astrocytic activation to disease onset and progression in a transgenic model of familial ALS. *Glia*, 23(3), 249–256. [https://doi.org/10.1002/\(sici\)1098-1128\(199803\)23:3<249::aid-glia1002>3.0.co;2-1](https://doi.org/10.1002/(sici)1098-1128(199803)23:3<249::aid-glia1002>3.0.co;2-1)

Hayakawa, K., Esposito, E., Wang, X., Terasaki, Y., Liu, Y., Xing, C., Ji, X., & Lo, E. H. (2016). Transfer of mitochondria from astrocytes to neurons after stroke. *Nature*, 535(7613), 551–555. <https://doi.org/10.1038/nature18928>

Haynes, S. E., Hollopeter, G., Yang, G., Kurpius, D., Dailey, M. E., Gan, W.-B., & Julius, D. (2006). The P2Y12 receptor regulates microglial activation by extracellular nucleotides. *Nature Neuroscience*, 9(12), 1512–1519. <https://doi.org/10.1038/nn1805>

Hegedus, J., Putman, C. T., & Gordon, T. (2007). Time course of preferential motor unit loss in the SOD1G93A mouse model of amyotrophic lateral sclerosis. *Neurobiology of Disease*, 28(2), 154–164. <https://doi.org/10.1016/j.nbd.2007.07.003>

Hemler, M. E. (2005). Tetraspanin functions and associated microdomains. *Nature Reviews Molecular Cell Biology*, 6(10), 801–811. <https://doi.org/10.1038/nrm1736>

Hernández, S., Casanovas, A., Piedrafita, L., Tarabal, O., & Esquerda, J. E. (2010). Neurotoxic Species of Misfolded SOD1 G93A Recognized by Antibodies Against the P2X 4 Subunit of the ATP Receptor Accumulate in Damaged Neurons of Transgenic Animal Models of Amyotrophic Lateral Sclerosis. *Journal of Neuropathology & Experimental Neurology*, 69(2), 176–187. <https://doi.org/10.1097/NEN.0b013e3181cd3e33>

Herron, L. R., & Miles, G. B. (2012). Gender-specific perturbations in modulatory inputs to motoneurons in a mouse model of amyotrophic lateral sclerosis. *Neuroscience*, 226, 313–323. <https://doi.org/10.1016/j.neuro.2012.09.031>

<https://doi.org/10.1016/j.neuroscience.2012.09.031>

Heuser, J. E., & Reese, T. S. (1973). Evidence for recycling of synaptic vesicle membrane during transmitter release at the frog neuromuscular junction. *Journal of Cell Biology*, 57(2), 315–344. <https://doi.org/10.1083/jcb.57.2.315>

Higgins, C. M. J., Jung, C., & Xu, Z. (2003). ALS-associated mutant SOD1G93A causes mitochondrial vacuolation by expansion of the intermembrane space by involvement of SOD1 aggregation and peroxisomes. *BMC Neuroscience*, 4. <https://doi.org/10.1186/1471-2202-4-16>.

Ilieva, H., Polymenidou, M., & Cleveland, D. W. (2009). Non-cell autonomous toxicity in neurodegenerative disorders: ALS and beyond. *Journal of Cell Biology*, 187(6), 761–772. <https://doi.org/10.1083/jcb.200908164>

Israelson, A., Arbel, N., Da Cruz, S., Ilieva, H., Yamanaka, K., Shoshan-Barmatz, V., & Cleveland, D. W. (2010). Misfolded Mutant SOD1 Directly Inhibits VDAC1 Conductance in a Mouse Model of Inherited ALS. *Neuron*, 67(4), 575–587. <https://doi.org/10.1016/j.neuron.2010.07.019>

Ito, Y., Ofengeim, D., Najafov, A., Das, S., Saberi, S., Li, Y., Hitomi, J., Zhu, H., Chen, H., Mayo, L., Geng, J., Amin, P., DeWitt, J. P., Mookhtiar, A. K., Florez, M., Ouchida, A. T., Fan, J., Pasparakis, M., Kelliher, M. A., ... Yuan, J. (2016). RIPK1 mediates axonal degeneration by promoting inflammation and necroptosis in ALS. *Science*, 353(6299), 603–608. <https://doi.org/10.1126/science.aaf6803>

Jaarsma, D., Rognoni, F., van Duijn, W., Verspaget, H. W., Haasdijk, E. D., & Holstege, J. C. (2001). CuZn superoxide dismutase (SOD1) accumulates in vacuolated mitochondria in transgenic mice expressing amyotrophic lateral sclerosis-linked SOD1 mutations. *Acta Neuropathologica*, 102(4), 293–305. <https://doi.org/10.1007/s004010100399>

Javadov, S., Chapa-Dubocq, X., & Makarov, V. (2018). Different approaches to modeling analysis of mitochondrial swelling. *Mitochondrion*, 38, 58–70. <https://doi.org/10.1016/j.mito.2017.08.004>

Joshi, A. U., Minhas, P. S., Liddelow, S. A., Haileselassie, B., Andreasson, K. I., Dorn, G. W., & Mochly-Rosen, D. (2019). Fragmented mitochondria released from microglia trigger A1 astrocytic response and propagate inflammatory neurodegeneration. *Nature Neuroscience*, 22(10), 1635–1648. <https://doi.org/10.1038/s41593-019-0486-0>

Kanning, K. C., Kaplan, A., & Henderson, C. E. (2010). Motor Neuron Diversity in Development and Disease. *Annual Review of Neuroscience*, 33(1), 409–440. <https://doi.org/10.1146/annurev.neuro.051508.135722>

Kaplan, A., Spiller, K. J., Towne, C., Kanning, K. C., Choe, G. T., Geber, A., Akay, T., Aebsicher, P., & Henderson, C. E. (2014). Neuronal Matrix Metalloproteinase-9 Is a Determinant of Selective Neurodegeneration. *Neuron*, 81(2), 333–348. <https://doi.org/10.1016/j.neuron.2013.12.009>

Kim, E., Lee, D. M., Seo, M. J., Lee, H. J., & Choi, K. S. (2021). Intracellular Ca²⁺ Imbalance Critically Contributes to Paraptosis. *Frontiers in Cell and Developmental Biology*, 8(January). <https://doi.org/10.3389/fcell.2020.607844>

Kong, J., & Xu, Z. (1998). Massive Mitochondrial Degeneration in Motor Neurons Triggers the Onset of Amyotrophic Lateral Sclerosis in Mice Expressing a Mutant SOD1. *The Journal of Neuroscience*, 18(9), 3241–3250. <https://doi.org/10.1523/JNEUROSCI.18-09-03241.1998>

- Kowal, J., Arras, G., Colombo, M., Jouve, M., Morath, J. P., Primdal-Bengtson, B., Dingli, F., Loew, D., Tkach, M., & Théry, C. (2016). Proteomic comparison defines novel markers to characterize heterogeneous populations of extracellular vesicle subtypes. *Proceedings of the National Academy of Sciences*, 113(8), E968–E977. <https://doi.org/10.1073/pnas.1521230113>
- Lalancette-Hebert, M., Sharma, A., Lyashchenko, A. K., & Shneider, N. A. (2016). Gamma motor neurons survive and exacerbate alpha motor neuron degeneration in ALS. *Proceedings of the National Academy of Sciences*, 113(51), E8316–E8325. <https://doi.org/10.1073/pnas.1605210113>
- Lasiene, J., Komine, O., Fujimori-Tonou, N., Powers, B., Endo, F., Watanabe, S., Shijie, J., Ravits, J., Horner, P., Misawa, H., & Yamanaka, K. (2016). Neuregulin 1 confers neuroprotection in SOD1-linked amyotrophic lateral sclerosis mice via restoration of C-boutons of spinal motor neurons. *Acta Neuropathologica Communications*, 4(1), 15. <https://doi.org/10.1186/s40478-016-0286-7>
- Liu, J., Lillo, C., Jonsson, P. A., Velde, C. Vande, Ward, C. M., Miller, T. M., Subramaniam, J. R., Rothstein, J. D., Marklund, S., Andersen, P. M., Bränström, T., Gredal, O., Wong, P. C., Williams, D. S., & Cleveland, D. W. (2004). Toxicity of Familial ALS-Linked SOD1 Mutants from Selective Recruitment to Spinal Mitochondria. *Neuron*, 43(1), 5–17. <https://doi.org/10.1016/j.neuron.2004.06.016>
- Lowrie, M. B., & Vrbová, G. (1992). Dependence of postnatal motoneurones on their targets: review and hypothesis. *Trends in Neurosciences*, 15(3), 80–84. [https://doi.org/10.1016/0166-2236\(92\)90014-y](https://doi.org/10.1016/0166-2236(92)90014-y)
- Maier, M., Welt, T., Wirth, F., Montrasio, F., Preisig, D., McAfoose, J., Vieira, F. G., Kulic, L., Späni, C., Stehle, T., Perrin, S., Weber, M., Hock, C., Nitsch, R. M., & Grimm, J. (2018a). A human-derived antibody targets misfolded SOD1 and ameliorates motor symptoms in mouse models of amyotrophic lateral sclerosis. *Science Translational Medicine*, 10(470). <https://doi.org/10.1126/scitranslmed.aah3924>
- Maier, M., Welt, T., Wirth, F., Montrasio, F., Preisig, D., McAfoose, J., Vieira, F. G., Kulic, L., Späni, C., Stehle, T., Perrin, S., Weber, M., Hock, C., Nitsch, R. M., & Grimm, J. (2018b). A human-derived antibody targets misfolded SOD1 and ameliorates motor symptoms in mouse models of amyotrophic lateral sclerosis. *Science Translational Medicine*, 10(470), eaah3924. <https://doi.org/10.1126/scitranslmed.aah3924>
- Mancuso, R., Oliván, S., Mancera, P., Pastén-Zamorano, A., Manzano, R., Casas, C., Osta, R., & Navarro, X. (2012). Effect of genetic background on onset and disease progression in the SOD1-G93A model of amyotrophic lateral sclerosis. *Amyotrophic Lateral Sclerosis*, 13(3), 302–310. <https://doi.org/10.3109/17482968.2012.662688>
- Maniatis, S., Äijö, T., Vickovic, S., Braine, C., Kang, K., Mollbrink, A., Fagegaltier, D., Andrusiová, Ž., Saarenpää, S., Saiz-Castro, G., Cuevas, M., Watters, A., Lundeberg, J., Bonneau, R., & Phatnani, H. (2019). Spatiotemporal dynamics of molecular pathology in amyotrophic lateral sclerosis. *Science*, 364(6435), 89–93. <https://doi.org/10.1126/science.aav9776>
- Mariotti, R., Cristina, L., Bressan, C., Boscolo, S., & Bentivoglio, M. (2002). Altered reaction of facial motoneurons to axonal damage in the presymptomatic phase of a murine model of familial amyotrophic lateral sclerosis. *Neuroscience*, 115(2), 331–335. [https://doi.org/10.1016/S0306-4522\(02\)00448-7](https://doi.org/10.1016/S0306-4522(02)00448-7)

- Martínez-Silva, M. de L., Imhoff-Manuel, R. D., Sharma, A., Heckman, C. J. C., Shneider, N. A., Roselli, F., Zytnicki, D., & Manuel, M. (2018). Hypoexcitability precedes denervation in the large fast-contracting motor units in two unrelated mouse models of ALS. *eLife*, 7(2007), 1–26. <https://doi.org/10.7554/eLife.30955>
- Milan, L., Courtand, G., Cardoit, L., Masmejean, F., Barrière, G., Cazalets, J.-R., Garret, M., & Bertrand, S. S. (2015). Age-Related Changes in Pre- and Postsynaptic Partners of the Cholinergic C-Boutons in Wild-Type and SOD1G93A Lumbar Motoneurons. *PLOS ONE*, 10(8), e0135525. <https://doi.org/10.1371/journal.pone.0135525>
- Miles, G. B., Hartley, R., Todd, A. J., & Brownstone, R. M. (2007). Spinal cholinergic interneurons regulate the excitability of motoneurons during locomotion. *Proceedings of the National Academy of Sciences*, 104(7), 2448–2453. <https://doi.org/10.1073/pnas.0611134104>
- Miller, R. A., & Nadon, N. L. (2000). Principles of Animal Use for Gerontological Research. *The Journals of Gerontology Series A: Biological Sciences and Medical Sciences*, 55(3), B117–B123. <https://doi.org/10.1093/gerona/55.3.B117>
- Nagai, M., Re, D. B., Nagata, T., Chalazonitis, A., Jessell, T. M., Wichterle, H., & Przedborski, S. (2007). Astrocytes expressing ALS-linked mutated SOD1 release factors selectively toxic to motor neurons. *Nature Neuroscience*, 10(5), 615–622. <https://doi.org/10.1038/nn1876>
- Nagao, M., Misawa, H., Kato, S., & Hirai, S. (1998). Loss of Cholinergic Synapses on the Spinal Motor Neurons of Amyotrophic Lateral Sclerosis. *Journal of Neuropathology and Experimental Neurology*, 57(4), 329–333. <https://doi.org/10.1097/00005072-199804000-00004>
- Nijssen, J., Comley, L. H., & Hedlund, E. (2017). Motor neuron vulnerability and resistance in amyotrophic lateral sclerosis. *Acta Neuropathologica*, 133(6), 863–885. <https://doi.org/10.1007/s00401-017-1708-8>
- Oliveira, A. L. R., Thams, S., Lidman, O., Piehl, F., Hokfelt, T., Karre, K., Linda, H., & Cullheim, S. (2004). From The Cover: A role for MHC class I molecules in synaptic plasticity and regeneration of neurons after axotomy. *Proceedings of the National Academy of Sciences*, 101(51), 17843–17848. <https://doi.org/10.1073/pnas.0408154101>
- Paré, B., Lehmann, M., Beaudin, M., Nordström, U., Saikali, S., Julien, J.-P., Gilthorpe, J. D., Marklund, S. L., Cashman, N. R., Andersen, P. M., Forsberg, K., Dupré, N., Gould, P., Brännström, T., & Gros-Louis, F. (2018). Misfolded SOD1 pathology in sporadic Amyotrophic Lateral Sclerosis. *Scientific Reports*, 8(1), 14223. <https://doi.org/10.1038/s41598-018-31773-z>
- Pedrini, S., Sau, D., Guareschi, S., Bogush, M., Brown, R. H., Naniche, N., Kia, A., Trott, D., & Pasinelli, P. (2010). ALS-linked mutant SOD1 damages mitochondria by promoting conformational changes in Bcl-2. *Human Molecular Genetics*, 19(15), 2974–2986. <https://doi.org/10.1093/hmg/ddq202>
- Philips, T., & Robberecht, W. (2011). Neuroinflammation in amyotrophic lateral sclerosis: role of glial activation in motor neuron disease. *The Lancet Neurology*, 10(3), 253–263. [https://doi.org/10.1016/S1474-4422\(11\)70015-1](https://doi.org/10.1016/S1474-4422(11)70015-1)
- Picca, A., Beli, R., Calvani, R., Coelho-Júnior, H. J., Landi, F., Bernabei, R., Bucci, C., Guerra, F., & Marzetti, E. (2020). Older Adults with Physical Frailty and Sarcopenia Show Increased Levels of Circulating Small Extracellular Vesicles with a Specific Mitochondrial Signature. *Cells*, 9(4), 973. <https://doi.org/10.3390/cells9040973>
- Pickles, S., & Vande Velde, C. (2012). Misfolded SOD1 and ALS: zeroing in on mitochondria.

- Amyotrophic Lateral Sclerosis : Official Publication of the World Federation of Neurology Research Group on Motor Neuron Diseases*, 13(4), 333–340. <https://doi.org/10.3109/17482968.2012.648645>
- Pollin, M. M., McHanwell, S., & Slater, C. R. (1991). The effect of age on motor neurone death following axotomy in the mouse. *Development (Cambridge, England)*, 112(1), 83–89.
- Pullen, A. H., & Athanasiou, D. (2009). Increase in presynaptic territory of C-terminals on lumbar motoneurons of G93A SOD1 mice during disease progression. *European Journal of Neuroscience*, 29(3), 551–561. <https://doi.org/10.1111/j.1460-9568.2008.06602.x>
- Pun, S., Santos, A. F., Saxena, S., Xu, L., & Caroni, P. (2006). Selective vulnerability and pruning of phasic motoneuron axons in motoneuron disease alleviated by CNTF. *Nature Neuroscience*, 9(3), 408–419. <https://doi.org/10.1038/nn1653>
- Rakhit, R., Robertson, J., Vande Velde, C., Horne, P., Ruth, D. M., Griffin, J., Cleveland, D. W., Cashman, N. R., & Chakrabarty, A. (2007). An immunological epitope selective for pathological monomer-misfolded SOD1 in ALS. *Nature Medicine*, 13(6), 754–759. <https://doi.org/10.1038/nm1559>
- Raoul, C., Abbas-Terki, T., Bensadoun, J.-C., Guillot, S., Haase, G., Szulc, J., Henderson, C. E., & Aebsicher, P. (2005). Lentiviral-mediated silencing of SOD1 through RNA interference retards disease onset and progression in a mouse model of ALS. *Nature Medicine*, 11(4), 423–428. <https://doi.org/10.1038/nm1207>
- Re, D. B., Le Verche, V., Yu, C., Amoroso, M. W., Politi, K. A., Phani, S., Ikiz, B., Hoffmann, L., Koolen, M., Nagata, T., Papadimitriou, D., Nagy, P., Mitsumoto, H., Kariya, S., Wichterle, H., Henderson, C. E., & Przedborski, S. (2014). Necroptosis Drives Motor Neuron Death in Models of Both Sporadic and Familial ALS. *Neuron*, 81(5), 1001–1008. <https://doi.org/10.1016/j.neuron.2014.01.011>
- Redler, R. L., Fee, L., Fay, J. M., Caplow, M., & Dokholyan, N. V. (2014). Non-native Soluble Oligomers of Cu/Zn Superoxide Dismutase (SOD1) Contain a Conformational Epitope Linked to Cytotoxicity in Amyotrophic Lateral Sclerosis (ALS). *Biochemistry*, 53(14), 2423–2432. <https://doi.org/10.1021/bi500158w>
- Reichert, F., & Rotshenker, S. (2019). Galectin-3 (MAC-2) controls microglia phenotype whether amoeboid and phagocytic or branched and non-phagocytic by regulating the cytoskeleton. *Frontiers in Cellular Neuroscience*, 13(March), 1–9. <https://doi.org/10.3389/fncel.2019.00090>
- Ripps, M. E., Huntley, G. W., Hof, Pa. R., Morrison, J. H., & Gordon, J. W. (1995). Transgenic mice expressing an altered murine superoxide dismutase gene provide an animal model of amyotrophic lateral sclerosis. *Proc. Natl. Acad. Scie.*, 92, 689–693.
- Roselli, F., & Caroni, P. (2015). From Intrinsic Firing Properties to Selective Neuronal Vulnerability in Neurodegenerative Diseases. *Neuron*, 85(5), 901–910. <https://doi.org/10.1016/j.neuron.2014.12.063>
- Rosen, D. R., Siddique, T., Patterson, D., Figlewicz, D. A., Sapp, P., Hentati, A., Donaldson, D., Goto, J., O'Regan, J. P., Deng, H. X., Rahmani, Z., Krizus, A., McKenna-Yasek, D., Cayabyab, A., Gaston, S. M., Berger, R., Tanzi, R. E., Halperin, J. J., Herzfeldt, B., ... Brown, R. H. (1993). Mutations in Cu/Zn superoxide dismutase gene are associated with familial amyotrophic lateral sclerosis. *Nature*, 362(6415), 59–62.
- Rotterman, T. M., Akhter, E. T., Lane, A. R., MacPherson, K. P., García, V. V., Tansey, M. G., & Alvarez,

- F. J. (2019). Spinal motor circuit synaptic plasticity after peripheral nerve injury depends on microglia activation and a CCR2 mechanism. *Journal of Neuroscience*, 39(18), 3412–3433. <https://doi.org/10.1523/JNEUROSCI.2945-17.2019>
- Rotterman, T. M., & Alvarez, F. J. (2020). Microglia Dynamics and Interactions with Motoneurons Axotomized After Nerve Injuries Revealed By Two-Photon Imaging. *Scientific Reports*, 10(1), 1–22. <https://doi.org/10.1038/s41598-020-65363-9>
- Rotunno, M. S., & Bosco, D. A. (2013). An emerging role for misfolded wild-type SOD1 in sporadic ALS pathogenesis. *Frontiers in Cellular Neuroscience*, 7(DEC), 1–16. <https://doi.org/10.3389/fncel.2013.00253>
- Rowland, L.P., 1995. Hereditary and acquired motor neuron diseases. In: Rowland, LP (Ed.), Merritt's Textbook of Neurology. Williams & Wilkins, Philadelphia, pp. 742–749.
- Rudnick, N. D., Griffey, C. J., Guarnieri, P., Gerbino, V., Wang, X., Piersant, J. A., Tapia, J. C., Rich, M. M., & Maniatis, T. (2017). Distinct roles for motor neuron autophagy early and late in the SOD1 G93A mouse model of ALS. *Proceedings of the National Academy of Sciences*, 114(39), E8294–E8303. <https://doi.org/10.1073/pnas.1704294114>
- Ruegsegger, C., & Saxena, S. (2016). Proteostasis impairment in ALS. *Brain Research*, 1648, 571–579. <https://doi.org/10.1016/j.brainres.2016.03.032>
- Sábado, J., Casanovas, A., Rodrigo, H., Arqué, G., & Esquerda, J. E. (2015). Adverse effects of a SOD1-peptide immunotherapy on SOD1G93A mouse slow model of amyotrophic lateral sclerosis. *Neuroscience*, 310, 38–50. <https://doi.org/10.1016/j.neuroscience.2015.09.027>
- Sábado, Javier, Casanovas, A., Hernández, S., Piedrafita, L., Hereu, M., & Esquerda, J. E. (2013). Immunodetection of Disease-Associated Conformers of Mutant Cu/Zn Superoxide Dismutase 1 Selectively Expressed in Degenerating Neurons in Amyotrophic Lateral Sclerosis. *Journal of Neuropathology & Experimental Neurology*, 72(7), 646–661. <https://doi.org/10.1097/NEN.0b013e318297fd10>
- Saeed, M., Yang, Y., Deng, H.-X., Hung, W.-Y., Siddique, N., Dellefave, L., Gellera, C., Andersen, P. M., & Siddique, T. (2009). Age and founder effect of SOD1 A4V mutation causing ALS. *Neurology*, 72(19), 1634–1639. <https://doi.org/10.1212/01.wnl.0000343509.76828.2a>
- Salvany, S., Casanovas, A., Piedrafita, L., Tarabal, O., Hernández, S., Calderó, J., & Esquerda, J. E. (2021). Microglial recruitment and mechanisms involved in the disruption of afferent synaptic terminals on spinal cord motor neurons after acute peripheral nerve injury. *Glia*, 69(5), 1216–1240. <https://doi.org/10.1002/glia.23959>
- Salvany, S., Casanovas, A., Tarabal, O., Piedrafita, L., Hernández, S., Santafé, M., Soto-Bernardini, M. C., Calderó, J., Schwab, M. H., & Esquerda, J. E. (2019). Localization and dynamic changes of neuregulin-1 at C-type synaptic boutons in association with motor neuron injury and repair. *The FASEB Journal*, 33(7), 7833–7851. <https://doi.org/10.1096/fj.201802329R>
- Sanagi, T., Yuasa, S., Nakamura, Y., Suzuki, E., Aoki, M., Warita, H., Itoyama, Y., Uchino, S., Kohsaka, S., & Ohsawa, K. (2010). Appearance of phagocytic microglia adjacent to motoneurons in spinal cord tissue from a presymptomatic transgenic rat model of amyotrophic lateral sclerosis. *Journal of Neuroscience Research*, 88(12), 2736–2746. <https://doi.org/10.1002/jnr.22424>
- Sasaki, Y., Hoshi, M., Akazawa, C., Nakamura, Y., Tsuzuki, H., Inoue, K., & Kohsaka, S. (2003). Selective expression of Gi/o-coupled ATP receptor P2Y12 in microglia in rat brain. *Glia*, 44(3), 242–250.

<https://doi.org/10.1002/glia.10293>

- Saxena, S., Roselli, F., Singh, K., Leptien, K., Julien, J.-P., Gros-Louis, F., & Caroni, P. (2013). Neuroprotection through Excitability and mTOR Required in ALS Motoneurons to Delay Disease and Extend Survival. *Neuron*, 80(1), 80–96. <https://doi.org/10.1016/j.neuron.2013.07.027>
- Schaefer, A. M., Sanes, J. R., & Lichtman, J. W. (2005). A compensatory subpopulation of motor neurons in a mouse model of amyotrophic lateral sclerosis. *The Journal of Comparative Neurology*, 490(3), 209–219. <https://doi.org/10.1002/cne.20620>
- Schram, S., Chuang, D., Schmidt, G., Piponov, H., Helder, C., Kerns, J., Gonzalez, M., Song, F., & Loeb, J. A. (2019). Mutant SOD1 prevents normal functional recovery through enhanced glial activation and loss of motor neuron innervation after peripheral nerve injury. *Neurobiology of Disease*, 124(December 2018), 469–478. <https://doi.org/10.1016/j.nbd.2018.12.020>
- Schutz, B. (2005). Imbalanced excitatory to inhibitory synaptic input precedes motor neuron degeneration in an animal model of amyotrophic lateral sclerosis. *Neurobiology of Disease*, 20(1), 131–140. <https://doi.org/10.1016/j.nbd.2005.02.006>
- Sharp, P. S., Dick, J. R., & Greensmith, L. (2005). The effect of peripheral nerve injury on disease progression in the SOD1(G93A) mouse model of amyotrophic lateral sclerosis. *Neuroscience*, 130(4), 897–910. <https://doi.org/10.1016/j.neuroscience.2004.09.069>
- Sharp, P. S., Tyreman, N., Jones, K. E., & Gordon, T. (2018). Crush injury to motor nerves in the G93A transgenic mouse model of amyotrophic lateral sclerosis promotes muscle reinnervation and survival of functionally intact nerve-muscle contacts. *Neurobiology of Disease*, 113, 33–44. <https://doi.org/10.1016/j.nbd.2018.01.019>
- Silverman, J. M., Christy, D., Shyu, C. C., Moon, K.-M., Fernando, S., Gidden, Z., Cowan, C. M., Ban, Y., Stacey, R. G., Grad, L. I., McAlary, L., Mackenzie, I. R., Foster, L. J., & Cashman, N. R. (2019). CNS-derived extracellular vesicles from superoxide dismutase 1 (SOD1)G93A ALS mice originate from astrocytes and neurons and carry misfolded SOD1. *Journal of Biological Chemistry*, 294(10), 3744–3759. <https://doi.org/10.1074/jbc.RA118.004825>
- Soykan, T., Kaempf, N., Sakaba, T., Vollweiter, D., Goerdeler, F., Puchkov, D., Kononenko, N. L., & Haucke, V. (2017). Synaptic Vesicle Endocytosis Occurs on Multiple Timescales and Is Mediated by Formin-Dependent Actin Assembly. *Neuron*, 93(4), 854–866.e4. <https://doi.org/10.1016/j.neuron.2017.02.011>
- Sperandio, S., de Belle, I., & Bredesen, D. E. (2000). An alternative, nonapoptotic form of programmed cell death. *Proceedings of the National Academy of Sciences*, 97(26), 14376–14381. <https://doi.org/10.1073/pnas.97.26.14376>
- Sun, L., Wang, H., Wang, Z., He, S., Chen, S., Liao, D., Wang, L., Yan, J., Liu, W., Lei, X., & Wang, X. (2012). Mixed Lineage Kinase Domain-like Protein Mediates Necrosis Signaling Downstream of RIP3 Kinase. *Cell*, 148(1–2), 213–227. <https://doi.org/10.1016/j.cell.2011.11.031>
- Svensson, M., & Aldskogius, H. (1993). Regeneration of hypoglossal nerve axons following blockade of the axotomy-induced microglial cell reaction in the rat. *The European Journal of Neuroscience*, 5(1), 85–94. <https://doi.org/10.1111/j.1460-9568.1993.tb00208.x>
- Turner, B., & Talbot, K. (2008). Transgenics, toxicity and therapeutics in rodent models of mutant SOD1-mediated familial ALS. *Progress in Neurobiology*, 85(1), 94–134.

<https://doi.org/10.1016/j.pneurobio.2008.01.001>

- Urushitani, M., Ezzi, S. A., & Julien, J.-P. (2007). Therapeutic effects of immunization with mutant superoxide dismutase in mice models of amyotrophic lateral sclerosis. *Proceedings of the National Academy of Sciences*, 104(7), 2495–2500. <https://doi.org/10.1073/pnas.0606201104>
- Urushitani, M., Sik, A., Sakurai, T., Nukina, N., Takahashi, R., & Julien, J.-P. (2006). Chromogranin-mediated secretion of mutant superoxide dismutase proteins linked to amyotrophic lateral sclerosis. *Nature Neuroscience*, 9(1), 108–118. <https://doi.org/10.1038/nn1603>
- Vande Velde, C., Miller, T. M., Cashman, N. R., & Cleveland, D. W. (2008). Selective association of misfolded ALS-linked mutant SOD1 with the cytoplasmic face of mitochondria. *Proceedings of the National Academy of Sciences*, 105(10), 4022–4027. <https://doi.org/10.1073/pnas.0712209105>
- Vinsant, S., Mansfield, C., Jimenez-Moreno, R., Moore, V. D. G., Yoshikawa, M., Hampton, T. G., Prevette, D., Caress, J., Oppenheim, R. W., & Milligan, C. (2013). Characterization of early pathogenesis in the SOD1 G93A mouse model of ALS: part II, results and discussion. *Brain and Behavior*, 3(4), 431–457. <https://doi.org/10.1002/brb3.142>
- Wang, H., Sun, L., Su, L., Rizo, J., Liu, L., Wang, L.-F., Wang, F.-S., & Wang, X. (2014). Mixed Lineage Kinase Domain-like Protein MLKL Causes Necrotic Membrane Disruption upon Phosphorylation by RIP3. *Molecular Cell*, 54(1), 133–146. <https://doi.org/10.1016/j.molcel.2014.03.003>
- Wang, T., Perera, N. D., Chiam, M. D. F., Cuic, B., Wanniarachchilage, N., Tomas, D., Samson, A. L., Cawthorne, W., Valor, E. N., Murphy, J. M., & Turner, B. J. (2020). Necroptosis is dispensable for motor neuron degeneration in a mouse model of ALS. *Cell Death & Differentiation*, 27(5), 1728–1739. <https://doi.org/10.1038/s41418-019-0457-8>
- Watson, C., Paxinos, G., Kayalioglu, G., & Heise, C. (2009). In C. Watson, G. Paxinos, & K. G (Eds.), *The spinal cord* (1st ed.). Amsterdam: Elsevier
- Witts, E. C., Zagoraiou, L., & Miles, G. B. (2014). Anatomy and function of cholinergic C bouton inputs to motor neurons. *Journal of Anatomy*, 224(1), 52–60. <https://doi.org/10.1111/joa.12063>
- Wong, P. C., Pardo, C. A., Borchelt, D. R., Lee, M. K., Copeland, N. G., Jenkins, N. A., Sisodia, S. S., Cleveland, D. W., & Price, D. L. (1995). An adverse property of a familial ALS-linked SOD1 mutation causes motor neuron disease characterized by vacuolar degeneration of mitochondria. *Neuron*, 14(6), 1105–1116. [https://doi.org/10.1016/0896-6273\(95\)90259-7](https://doi.org/10.1016/0896-6273(95)90259-7)
- Xiao, Q., Zhao, W., Beers, D. R., Yen, A. A., Xie, W., Henkel, J. S., & Appel, S. H. (2007). Mutant SOD1 G93A microglia are more neurotoxic relative to wild-type microglia. *Journal of Neurochemistry*, 102(6), 2008–2019. <https://doi.org/10.1111/j.1471-4159.2007.04677.x>
- Zang, D. W., Lopes, E. C., & Cheema, S. S. (2005). Loss of synaptophysin-positive boutons on lumbar motor neurons innervating the medial gastrocnemius muscle of the SOD1G93A G1H transgenic mouse model of ALS. *Journal of Neuroscience Research*, 79(5), 694–699. <https://doi.org/10.1002/jnr.20379>
- Zhao, P., Ignacio, S., Beattie, E. C., & Abood, M. E. (2008). Altered presymptomatic AMPA and cannabinoid receptor trafficking in motor neurons of ALS model mice: implications for excitotoxicity. *European Journal of Neuroscience*, 27(3), 572–579.

<https://doi.org/10.1111/j.1460-9568.2008.06041.x>

Zhao, W., Beers, D. R., & Appel, S. H. (2013). Immune-mediated Mechanisms in the Pathoprotection of Amyotrophic Lateral Sclerosis. *Journal of Neuroimmune Pharmacology*, 8(4), 888–899. <https://doi.org/10.1007/s11481-013-9489-x>

Zhao, W., Beers, D. R., Henkel, J. S., Zhang, W., Urushitani, M., Julien, J.-P., & Appel, S. H. (2010). Extracellular mutant SOD1 induces microglial-mediated motoneuron injury. *Glia*, 58(2), 231–243. <https://doi.org/10.1002/glia.20919>

FIGURE LEGENDS AND TABLES

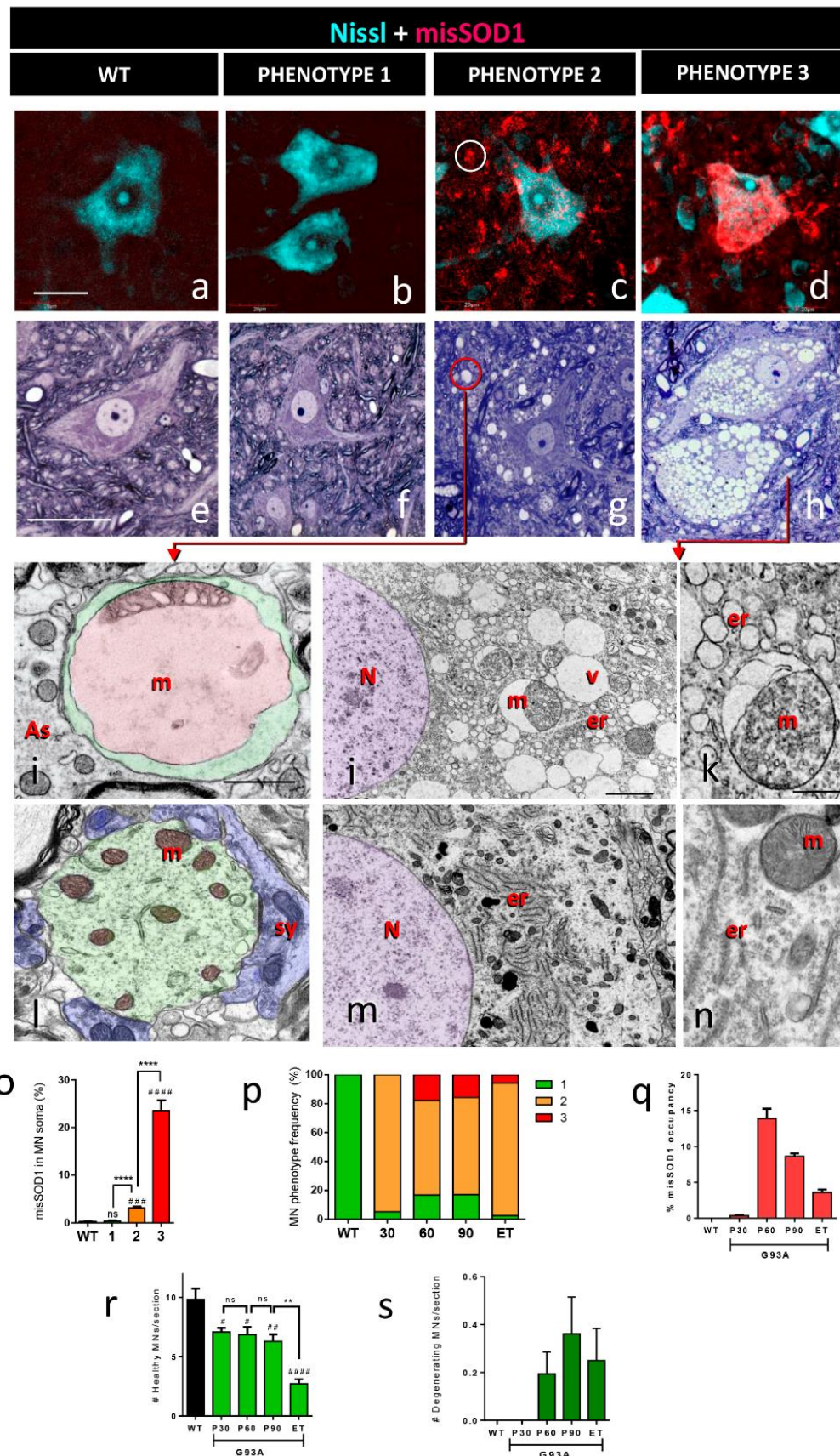


Fig 1. Demarcation of MN phenotypes in spinal cord ventral horn we described in SOD1G93A ALS mice in basis of their immunostaining of mfSOD1 using the conformational-specific antibody C4F6 (**a-d**); mfSOD1 signal (red) is depicted in combination of Nissl-staining (blue) in the indicated conditions and taken from p60 mouse. mfSOD1 was absent or very low in WT or phenotype 1 (**a, b**) and predominates in MN neuropile (encircled in **c**) or MN somas respectively in the phenotypes 2 and 3 (**c, d**). The mfSOD1 phenotypes can be correlated with vacuolar changes observed in 1 um plastic semithin sections (**e-h**); vacuoles are virtually absent in WT or type 1 phenotype (**e, f**), abundant in the neuropile in type 2 phenotype (**g**) and in the soma of MNs presenting massive vacuolization in the type 3 phenotype (**h**): note the absence on chromatin condensation in MNs undergoing advanced stages of vacuolar degeneration. Ultrastructural analysis of vacuolar degeneration in SOD1G93A MNs at p60 (**i-k**) vs control WT (**l-n**) in which representative images of dendrites (**i** and **l**) and somas (**j** and **m**) are depicted. Equivalent regions in semithin section of EM-imaged areas are indicated by arrows. In (**i**) the mitochondrial origin of vacuoles in dendrites is shown; the cytoplasm of the dendrite (dashed in green) is largely occupied by an enlarged and swollen mitochondria (**m** and dashed in red) caused by a huge expansion of the outer mitochondrial membrane. Compare with the ultrastructure of a dendrite seen in a control animal (dashed in green) containing several normal mitochondria (**m**) and receiving several axodendritic synaptic contacts (**sy** and dashed in blue); by contrast, synaptic contacts are not seen in vacuolated dendrite which is contacted, instead, by some glial processes (**As**). The ultrastructure of the soma of vacuolated MNs is shown in (**j**) and detailed in (**k**); equivalent areas taken from control MNs are depicted in (**m**) and (**n**). MNs undergoing vacuolar degeneration (**v**) display a massive fragmentation of endoplasmic reticulum (**er**) and mitochondrial expansive enlargement of intermembrane space (**m**). It is remarkable that within the nuclei (**N**, dashed in violet) chromatin ultrastructure remains intact in massively vacuolated MNs as seen by comparing (**j**) and (**m**). Quantification of misSOD1 in MN soma according phenotypes (**o**), MN phenotype frequency among postnatal days (**p**), and misSOD1 occupancy along postnatal days. (**r-s**) Quantification of healthy (**r**) or degenerating (**s**) MNs in spinal cord sections stained with Nissl stain. Data in graph are shown as mean \pm SEM, from 31 to 107 MNs ($n=3$ animals) in (**o**); (**p**) total MNs of different cryostat sections of 3 different animals in each condition; and from 15-18 spinal cord sections ($n=3$); images from (**o and q**) were projected Z-stacks; (**r-s**) total MNs of different cryostat sections ($n=3$) in each condition; * $p < .05$; ** $p < .01$; *** $p < .001$; **** $p < .0001$, one-way analysis of variance (ANOVA), Bonferroni's post hoc test. Scale bars: **a** = 20 μ m (valid for **b-d**); **e** = 20 μ m (valid for **f-h**); **i** = 1 μ m (valid for **m**); **j** = 250 nm (valid for **m**); **k** = 100 nm (valid for **n**).

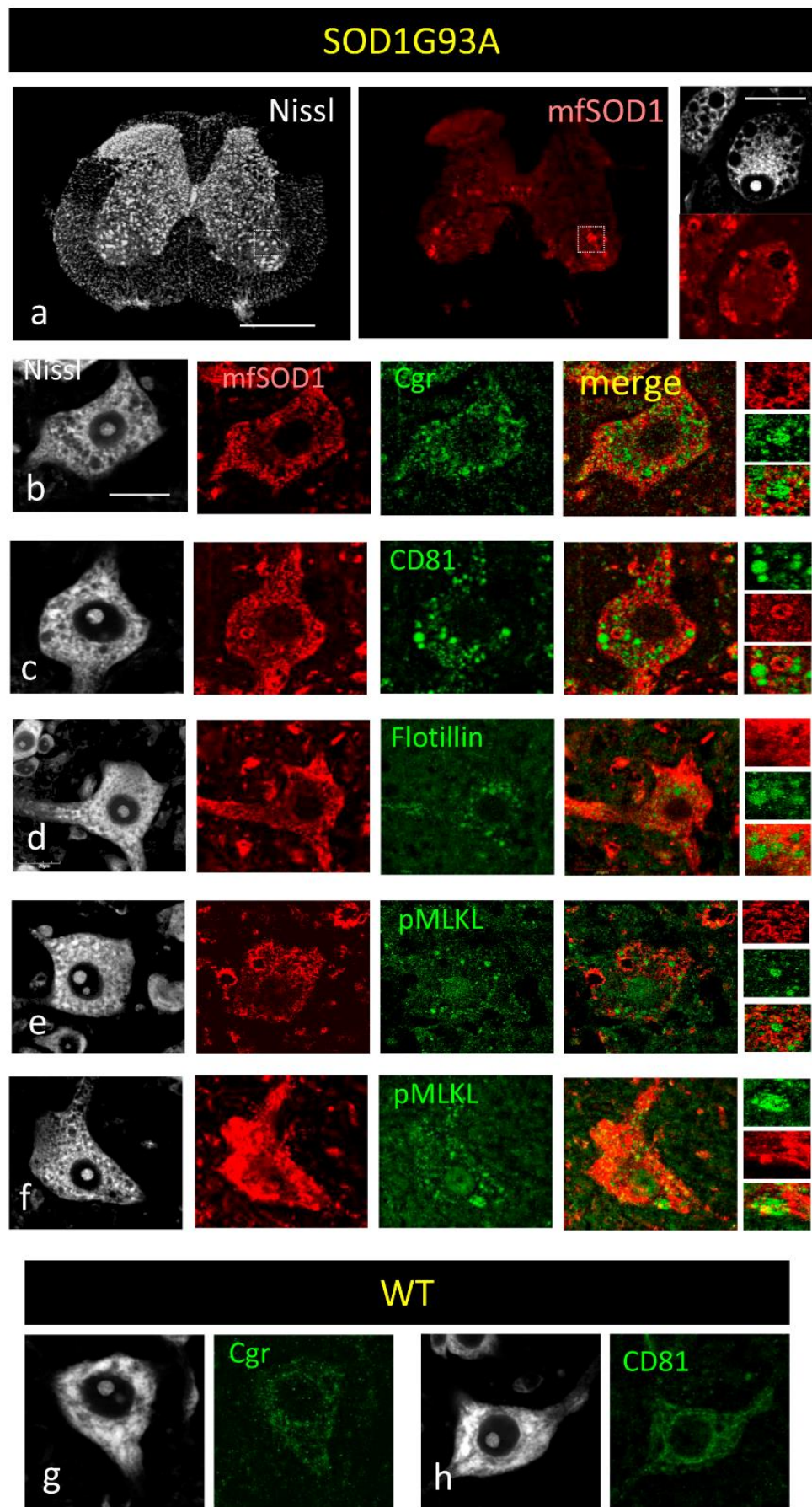


Fig 2 Immunocytochemical characterization of MN vacuolar degeneration. MNs displaying high immunoreactivity to mfSOD1 using C4F6 antibody (red) were co-immunostained with several antibodies as indicated (green). Samples were taken from p60 SOD1G93A or WT mouse and counterstained by Nissl (gray). In low magnification micrographs of whole spinal cord, a number of neurons displaying strong mfSOD1 are seen located at the ventral horn (**a**); in the enlarged inset a detail of a mfSOD1 positive MN showing its associated vacuolar degeneration evidenced after Nissl co-staining. On each row, a detail of mSOD1 (red) and the corresponding protein signal is depicted in separate and combined image in the insets. Scale bars: a = 500 μ (valid for b); c = 20 μ m (valid for d); e = μ m (valid for f-k).

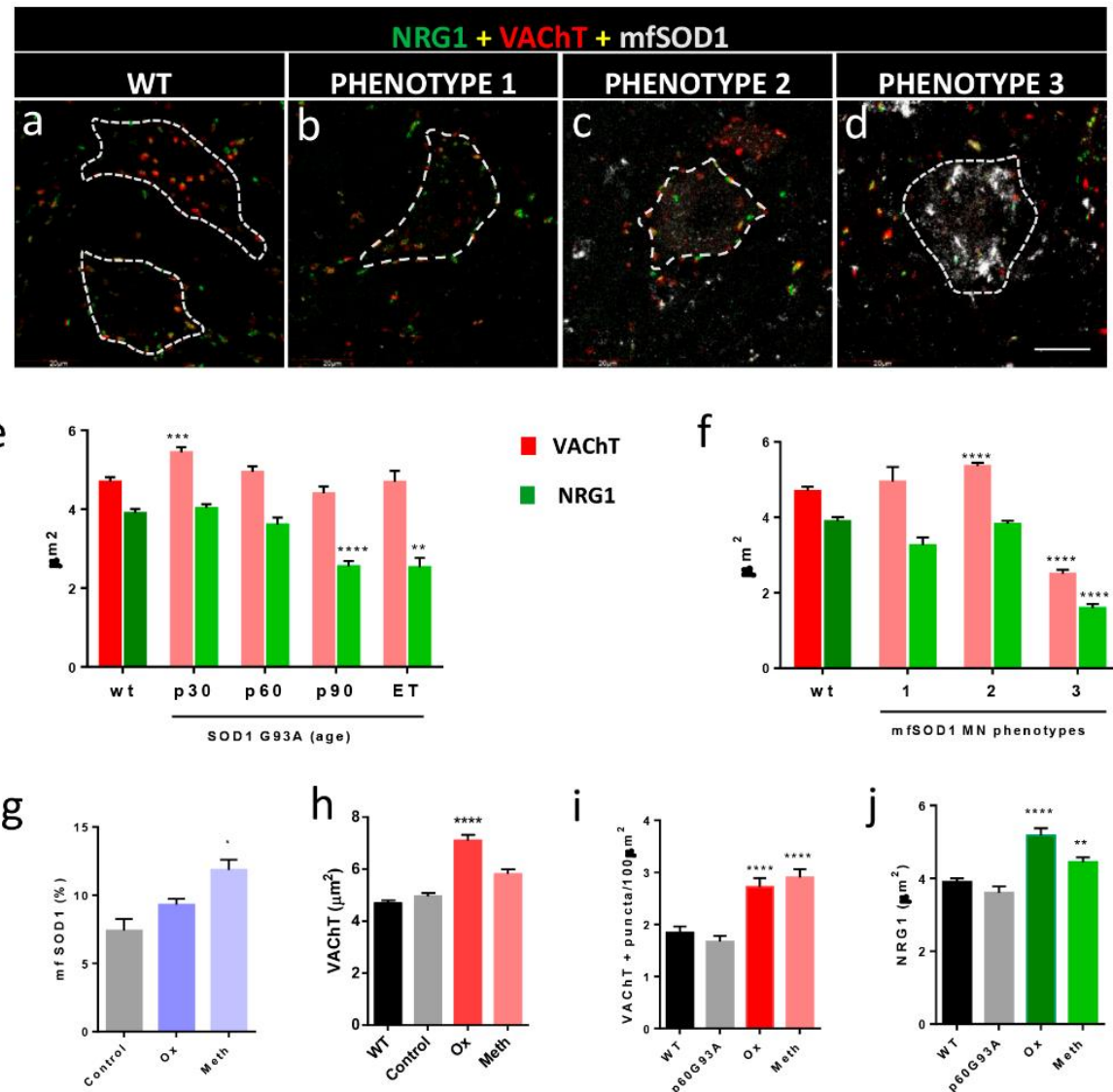


Fig. 3. MNs triple immunolabeled for BC proteins NRG1 (green) and VACHT (red) and mfSOD1 (grey). The MN profile is delimited by a dashed line. MNs are classified according the defined phenotypes. Quantification of VACHT and NRG1 area, according postnatal days (**e**) or MN phenotype (**f**). Quantification of mfSOD1 neuropile occupancy, VACHT spot area, VACHT density, and NRG1 spot area (**g-j**), after the treatment with Oxotremorine (Ox) and Methroctamine (Meth) compared with aged-matched transgenic animals and with a wt animal. Data in graphs are shown as mean \pm SEM, from 70 – 200 MN spots in (**a, b**); from 24 to 29 MN neuropile (**g**); from 167-219 VACht spots (**h**); 24 to 59 MN (**i**); and from 73-206 NRG1 spots (**j**); from three mice in each condition, in projected Z-stacks; * $p < .05$; ** $p < .01$; *** $p < .001$; **** $p < .0001$, one-way analysis of variance (ANOVA), Bonferroni's post hoc test. Scale bars: e = 20 μ m (valid for a-c).

RESULTS

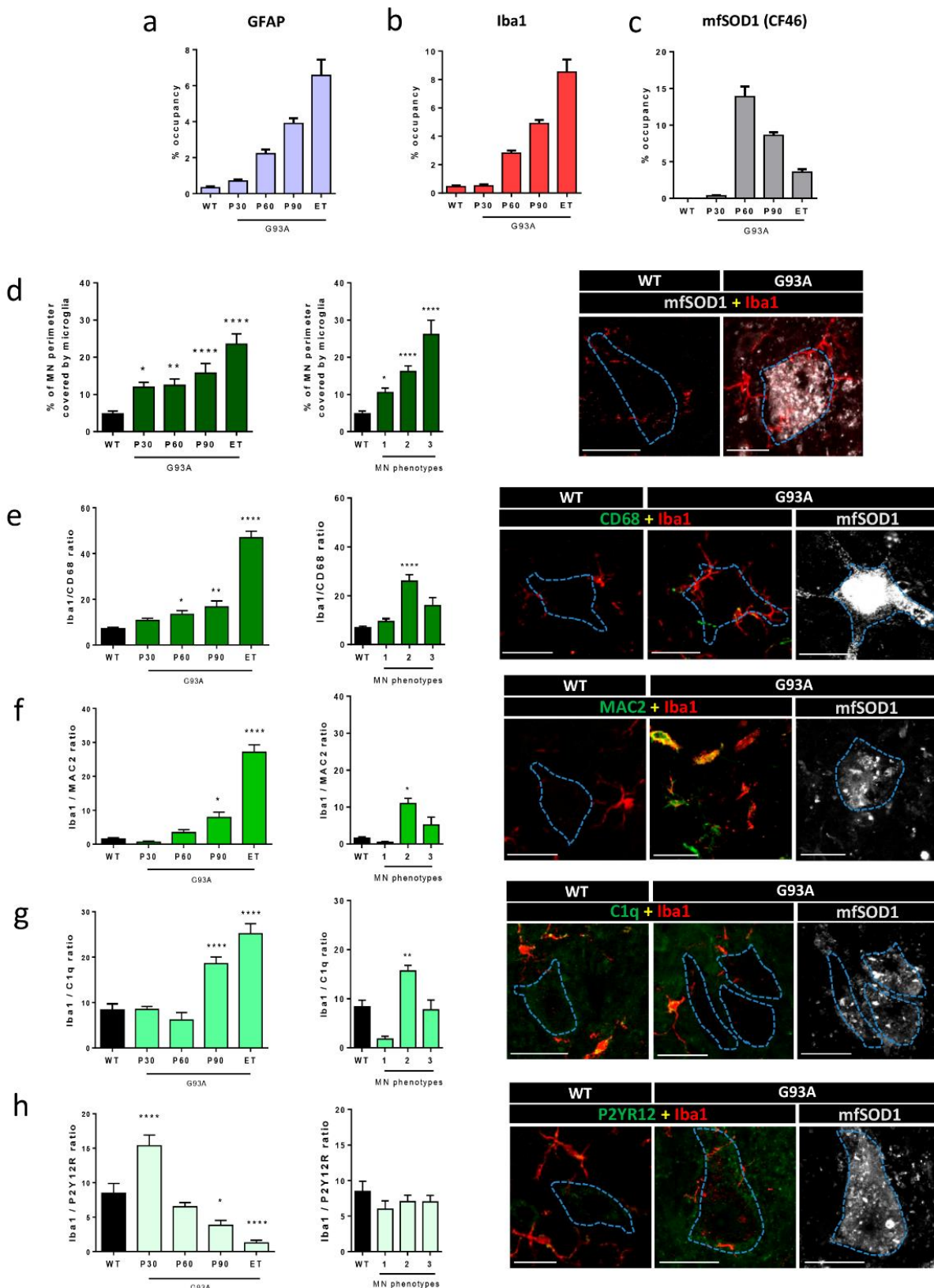


Fig. 4. Quantification of MN neuropile occupancy of GFAP (**a**), Iba1 (**b**) and mfSOD1 (**c**). Quantification of the MN perimeter covered by microglia (**d**) and the ratios of Iba1/CD68 (**e**), Iba1/MAC2(**f**), Iba1/C1q (**g**) and Iba1/P2Y12R(**h**) during the time point course of ALS or along our established phenotypes. In each condition, Iba1 is showed in red and mfSOD1 in grey. The different microglial markers are shown in green. The MN profile is shown by dashed line. Data in graph are shown as mean \pm SEM, from 15 to 20 MN neuropile sections (**a-c**); and from 20 to 50 MN neuropile (**d-h**), from three mice, in projected Z-stacks; * $p < .05$; ** $p < .01$; *** $p < .0001$, one-way analysis of variance (ANOVA), Bonferroni's post hoc test. Scale bars: a = 30 μ m (valid for d-h).

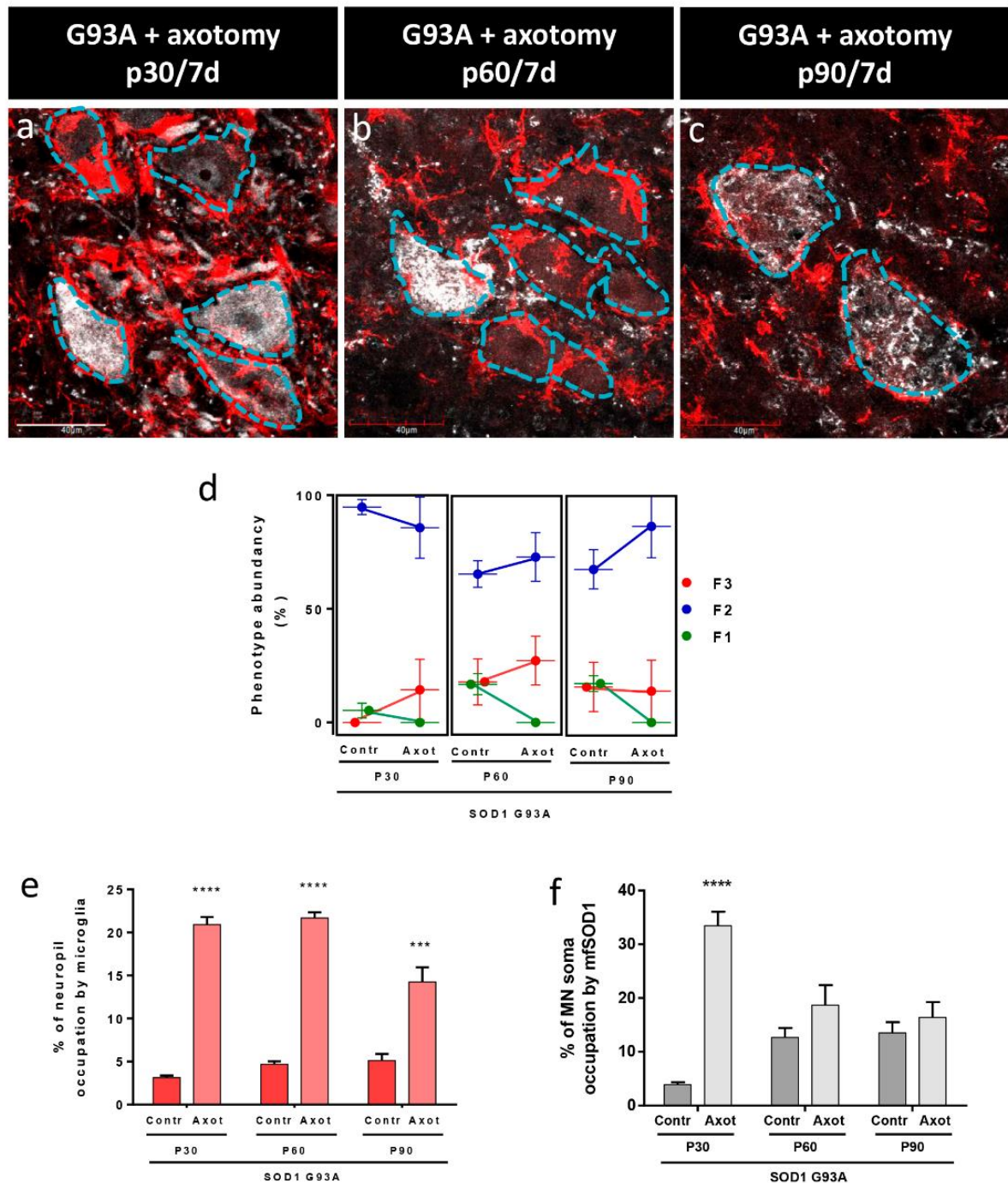


Fig. 5. Axotomized MNs immunolabeled for microglia (red) and mfSOD1 (grey) at 7 days after axotomies, which were performed at different time points (**a-c**). Quantification of the phenotype abundance (**d**), the MN neuropile occupied by microglia (**e**) and the MN soma occupied by mfSOD1 (**f**) at 7 days after axotomy performed in different time points. Each condition is compared with the age-matched mice. Data in graphs are shown as mean \pm SEM, from the total amount of MN of several cryostat sections of 3 different animals (**d**); from 17 to 82 MN neuropile (**e**); from 20 – 60 MN soma (**f-h**); from 3 mice, in projected Z-stacks; * $p < .05$; *** $p < .001$; **** $p < .0001$, one-way analysis of variance (ANOVA), Bonferroni's post hoc test. Scale bars: a = 40 μ m (valid for b and c).

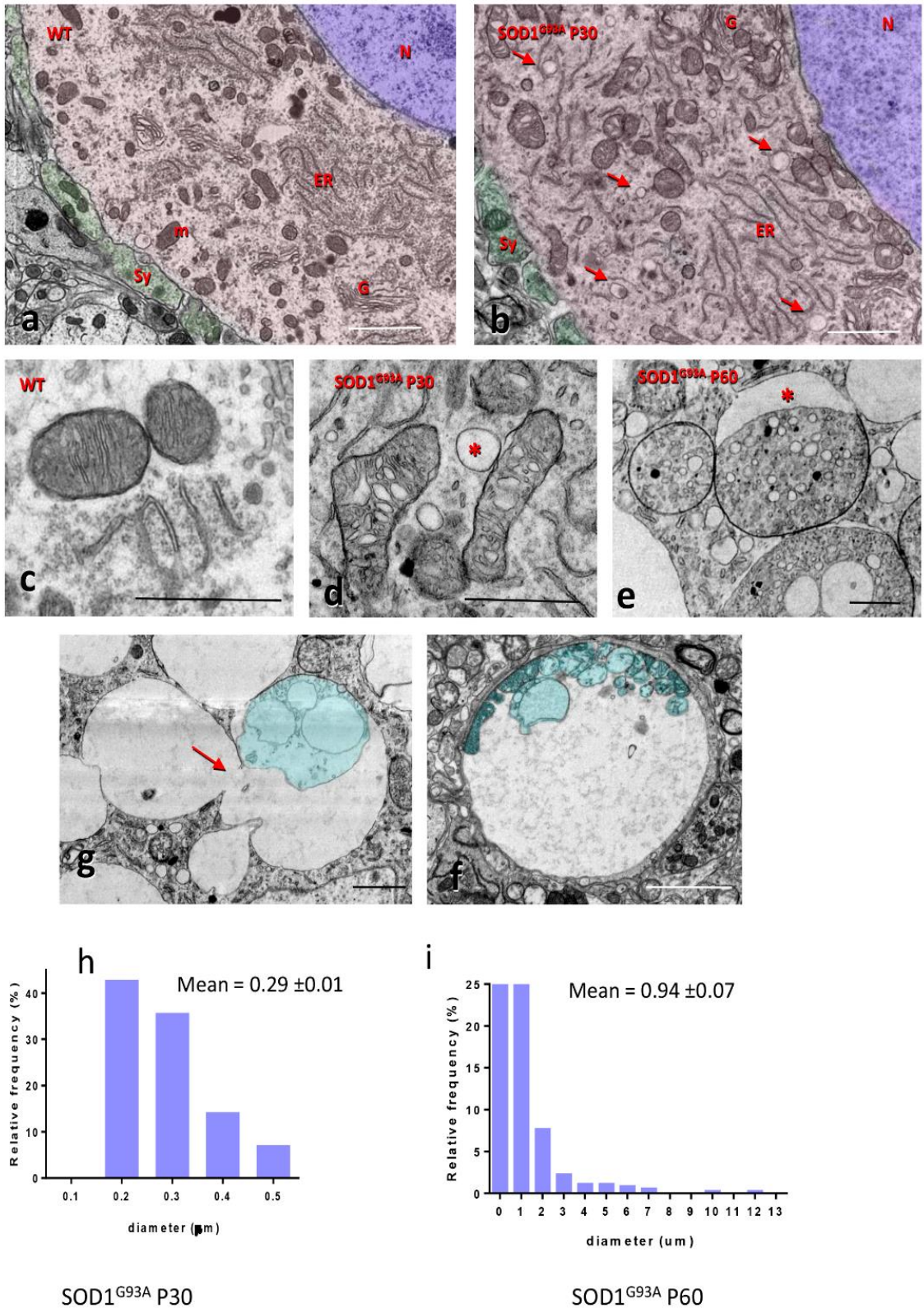


Fig Supp 1. Ultrastructure of vacuolar degeneration in SOD1G93A MNs. A low magnification EM view of WT and p30 SOD1G93A MN somas (**a,b**) showing early vacuolar changes (arrows); MN somas, nuclei and afferent synapses are dashed in blue, red and green respectively (N, nuclei; ER, endoplasmic reticulum; G, golgi, Sy, afferent synapses). A detail of mitochondrial ultrastructure within MN somas from WT and SOD1G93A at p30 and p60, as indicated, is shown (**c-e**); note the early swelling of mitochondrial matrix within the inner mitochondrial membranes in conjunction with early cytoplasmic vacuolization (*) at p30 (**d**) and its progression reaching massive vacuolization with enlargement of intermembrane space (*) observed at p60 (**e**). An example of coalescence and fusion of vacuoles seen p60 is shown (arrow in **g**) in which swollen remnants of inner mitochondrial membrane can be seen (dashed in blue). A big dendric vacuole presumably generated by fusion of several expanded outer mitochondrial membranes that delimitate a single vacuole containing several units of inner membrane complexes clustered at the periphery of vacuole (dashed in blue) (**h**). Frequency distribution of the size of vacuoles measured on p30 and p60 MN somas is shown (**i, j**). Scale bars: a = 2 μ m (valid for b, g, f); c = 1 μ m (valid for d-e).

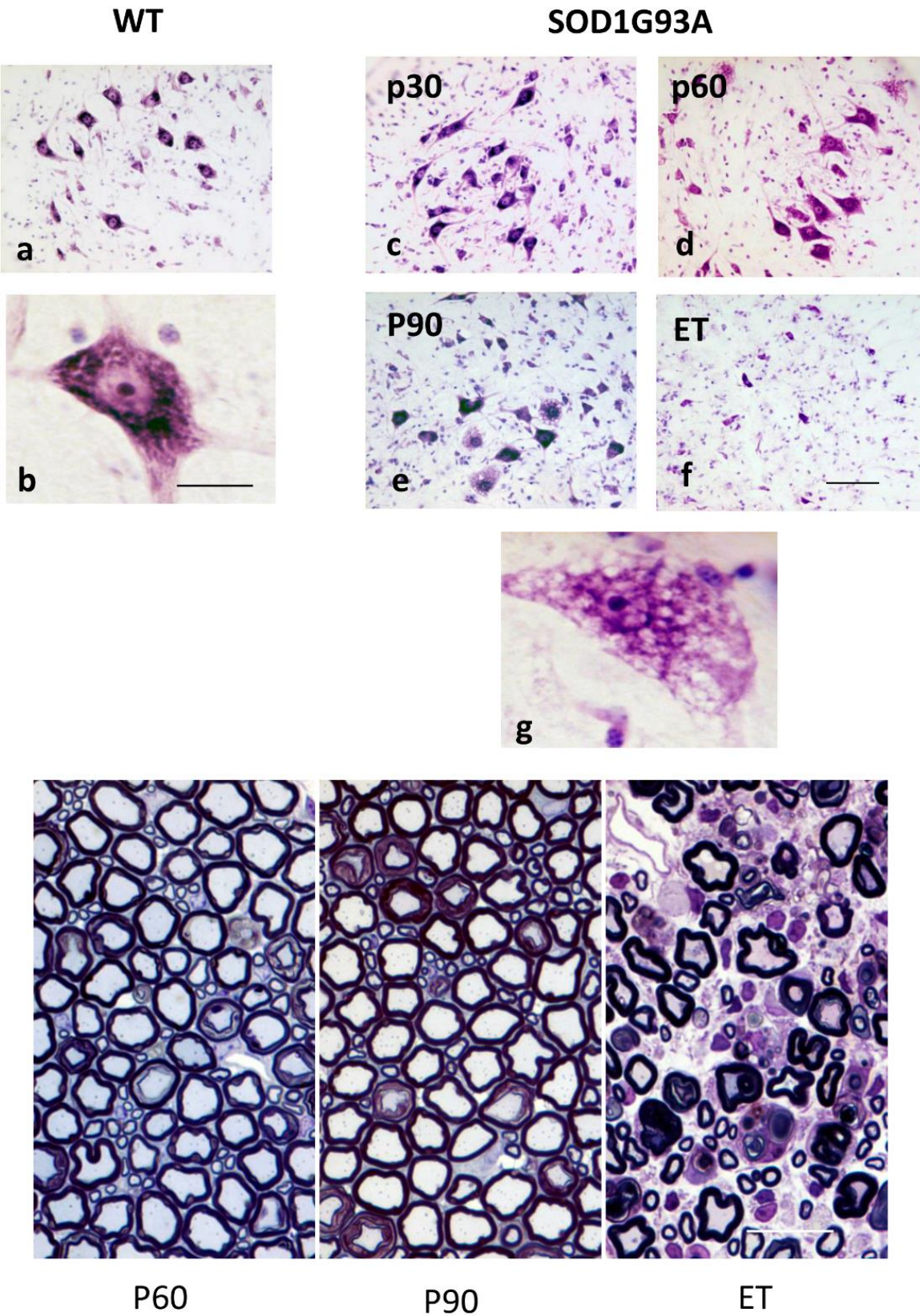


Fig. Supp 2. Nissl staining of spinal cord sections where MNs of WT (a-b) compared with those from p30, p60, p90 and end terminal states (c-f) can be observed. Note the decrease of MN somata according to the advance of the disease. A magnification of a vacuolated MN is shown in (g). Axons from the ventral root sections of p60, p90 and end terminal animals are shown (h-j) showing a different degree of degeneration. Scale bars: f = 100 µm (valid for a, c, d, e); b = 25 µm (valid for g).

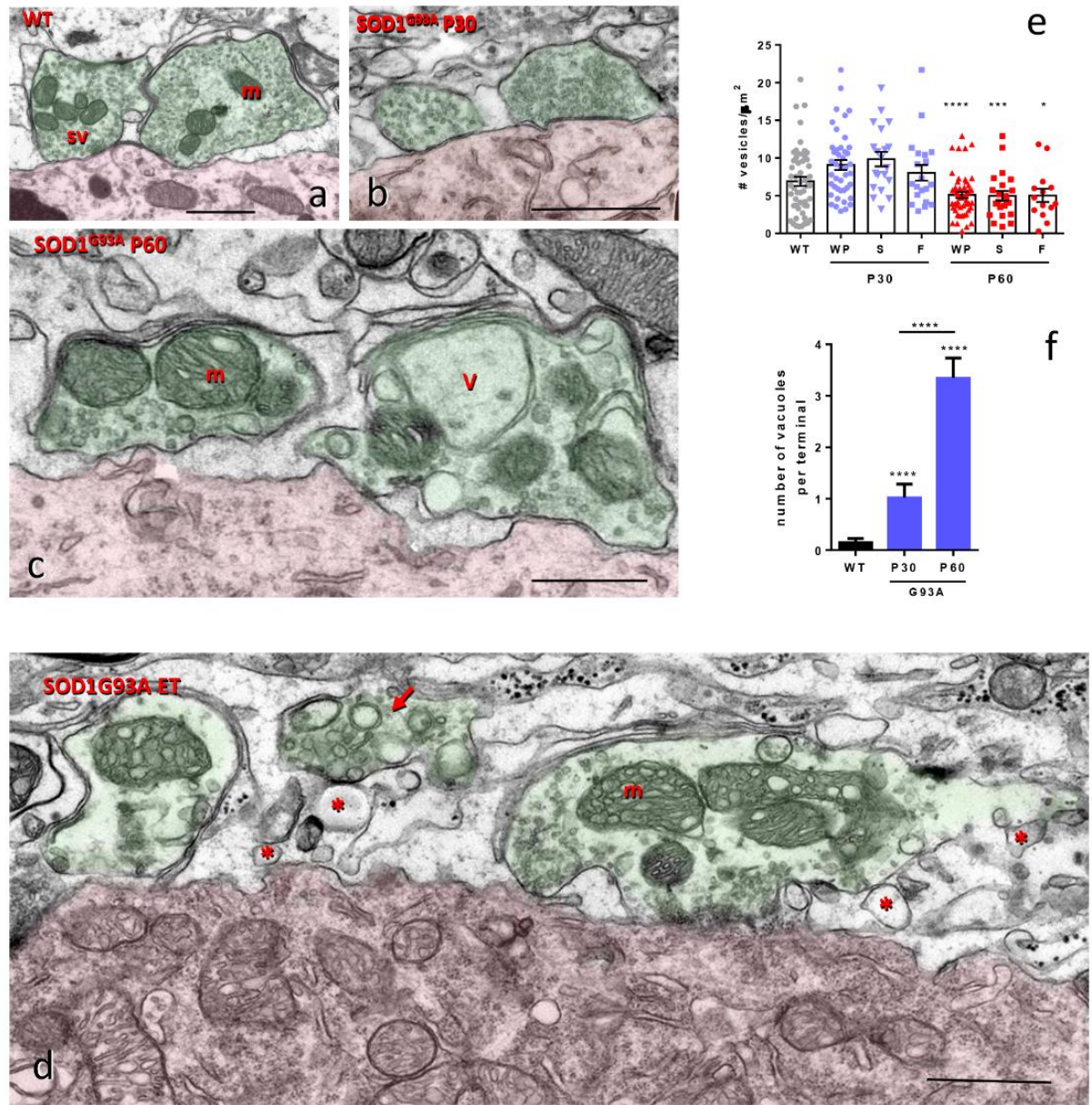
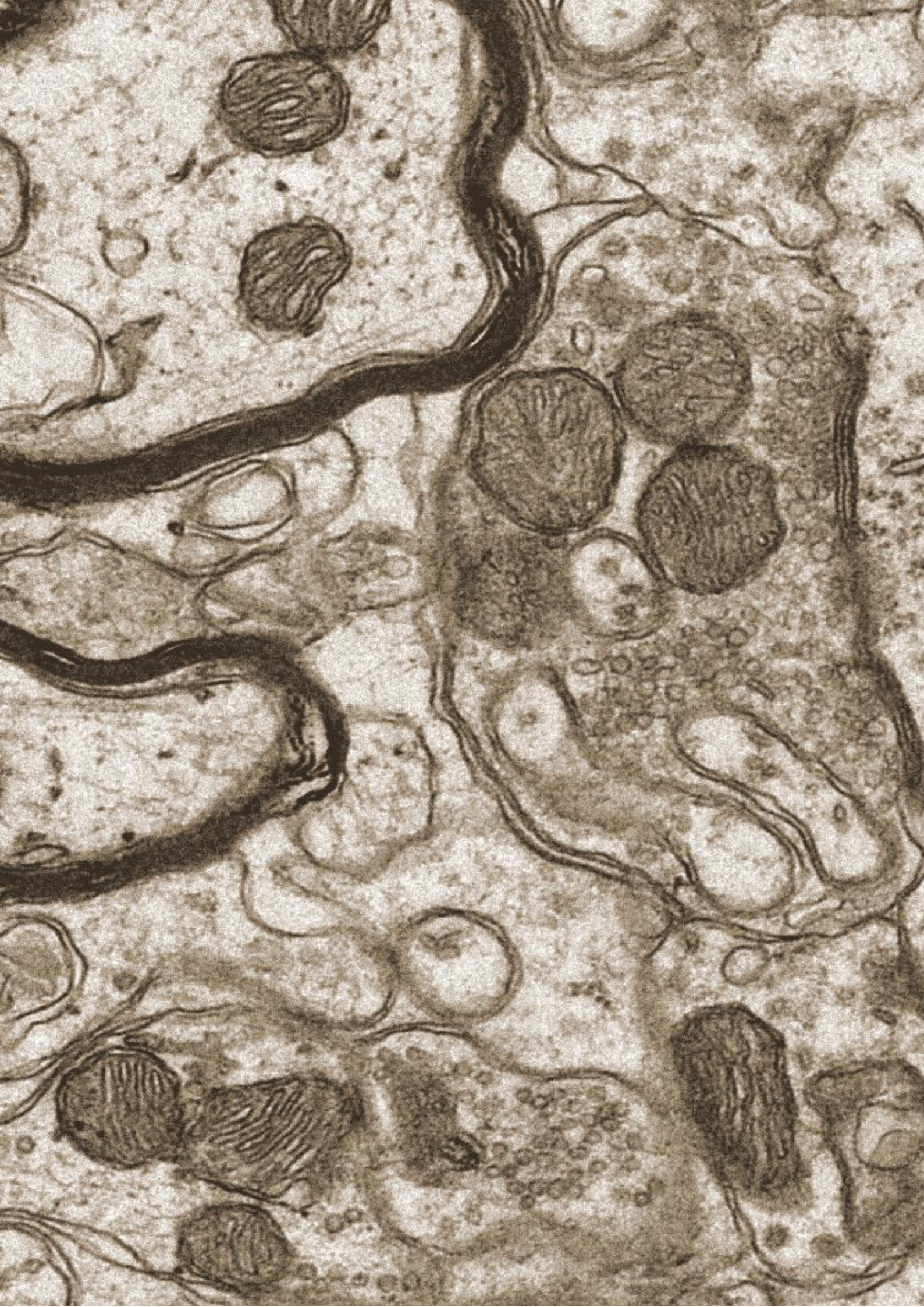
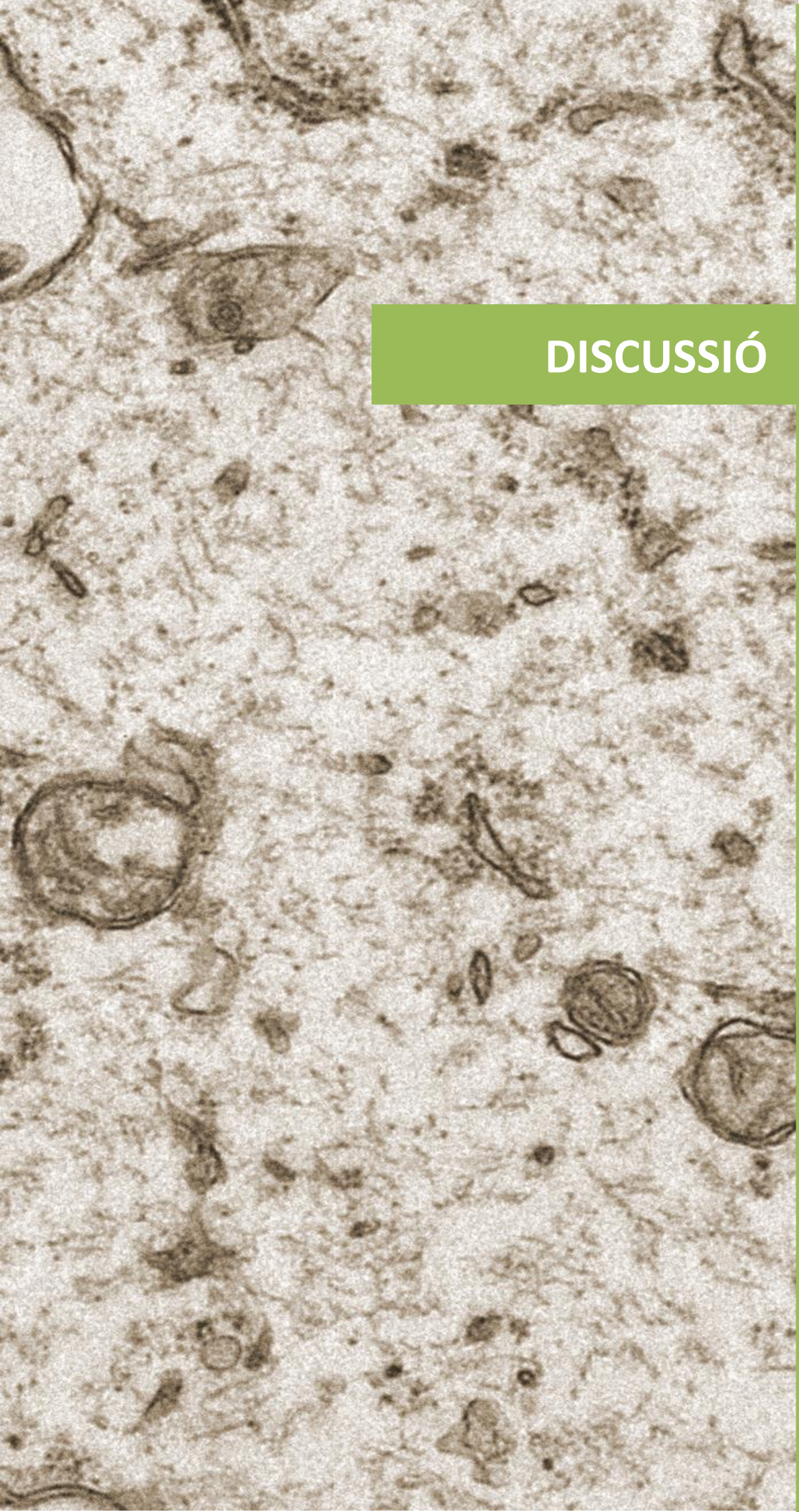


Fig Supp 3. Ultrastructural analysis of synaptic afferent boutons on MN cell bodies in WT (**a**) and SOD1G93A animals at p30 (**b**), p60 (**c**) and end-terminal (**d**) animals. Note the presence of large endocytic-like large vesicles inside some terminals (**v**) at p60 and their disruption at the end-terminal stages which include the release of extracellular vesicles (*). In (**e**), the density of synaptic vesicles in MN afferent terminals was quantified considering the whole synaptic vesicle population (WP), and the synapses containing spherical (S) or flattened (F) synaptic vesicles. In (**f**) the number of endocytic-like vesicles (>100 μm) in presynaptic afferent terminals was quantified. Data are presented as mean $\pm \text{SEM}$; * $p < .05$; *** $p < .001$; **** $p < .0001$, one-way analysis of variance (ANOVA), Bonferroni's post hoc test. n = xx – xx terminals from xxx animals per condition. Scale bars: a = 1 μm (valid for b-d).

Target	Host species	Source (catalogue n°)	Dilution
ATP5A	Mouse monoclonal	Abcam (ab14748)	1:100
C1q	Rabbit monoclonal	Abcam (182451)	1:1000
CD11c	Hamster monoclonal	AbDserotec (MCA1369T)	1:50
CD63	Rabbit monoclonal	Abcam (ab217345)	1:100
CD68	Rat monoclonal	AbDserotec (MCA1957T)	1:100
CD81	Rabbit polyclonal	Abcam (ab155760)	1:100
CD9	Rabbit monoclonal	Abcam (ab92726)	1:350
Glial fibrillary acidic protein (GFAP)	Chicken polyclonal	Abcam (ab4674)	1:1000
Ionised calcium-binding adaptor molecule 1 (IBA1)	Goat polyclonal	Abcam (ab5076)	1:500
Mac-2	Rat monoclonal	Cedarlane (Burlington, Canada) (CL8942AP)	1:800
MLKL (phospho S345)	Rabbit monoclonal	Abcam (196436)	1:100
NRG1 1 α / β 1/2	Rabbit polyclonal	Santa Cruz (sc-348)	1:300
P2RY12	Rat monoclonal	Biolegend (848002)	1:100
SOD1 (AJ10) Anti-Misfolded Human SOD1	Rabbit polyclonal	AbBcn (4251/4252)	1:1000
SOD1 (C4F6) Anti-Misfolded Human SOD1	Mouse monoclonal	MediMabs 2B Scientific (MM-00070-2-P)	1:100
Synaptophysin 1	Guinea pig polyclonal	Synaptic Systems (101 004)	1:500
Vesicular acetylcholine transporter (VACHT)	Guinea pig polyclonal	Synaptic Systems (139 105)	1:500

Table 1. Antibodies used for immunocytochemistry.





A black and white photomicrograph of a brain tissue section. The image shows various cellular structures, some of which contain dark, electron-dense deposits characteristic of Lewy bodies and Lewy neurites, often associated with neurodegenerative diseases like Alzheimer's or Parkinson's.

DISCUSSIÓ

1. Caracterització molecular i estructural dels terminals de tipus C

En els últims anys, els BC, principals reguladors de l'excitabilitat de les α -MN, han anat guanyant un considerable interès en relació a la patologia de la MN. Arran de la descripció de mutacions en proteïnes associades als BC i la seva relació amb casos d'ELA familiar (S. Watanabe *et al.*, 2016), diversos autors han analitzat aspectes d'aquests aferents com són la seva funció, estructura i composició proteica, tant en condicions fisiològiques com patològiques (Deardorff *et al.*, 2014; Witts *et al.*, 2014).

El primer objectiu de la present tesi era aprofundir en els estudis previs del grup en els que es va demostrar l'existència de la NRG1 associada als terminals colinèrgics de les MNs, concretament ubicada en la SSC (Gallart-Palau *et al.*, 2014). Es va dur a terme un análisis detallat de la compartimentalització de les proteïnes ubicades en el BC, posant especial atenció en la NRG1 i utilitzant la SSC, estructura altament característica i ultraestructuralment definitòria dels BC, com a referència. Vam observar que tant el SR1, el Kv2.1 com la NRG1, es localitzaven específicament en el compartiment postsinàptic. Addicionalment vam descriure que aquestes proteïnes ocupaven microdominis espacials altament definits i no solapats entre ells (Fig. 22).

Aquesta especificitat en la sublocalització podria estar definint diferents microdominis dins del BC, els quals podrien estar actuant mitjançant vies de senyalització diferents, i per tant, duent a terme funcions plurals dins del component postsinàptic, i en definitiva, en la MN. Aquesta teoria concordaria amb el concepte emergent de “nano-columnes transinàptiques” (A.-H. Tang *et al.*, 2016). Inclús en alguns casos, les proteïnes associades al BC podrien estar duent a terme funcions diferents a les descrites com a canòniques.

Un exemple que dóna suport a l'anterior hipòtesi fa referència al canal Kv2.1, el qual en els nostres estudis, hem identificat en la regió més externa de la SSC (Fig. 22). La funció fisiològica més estudiada

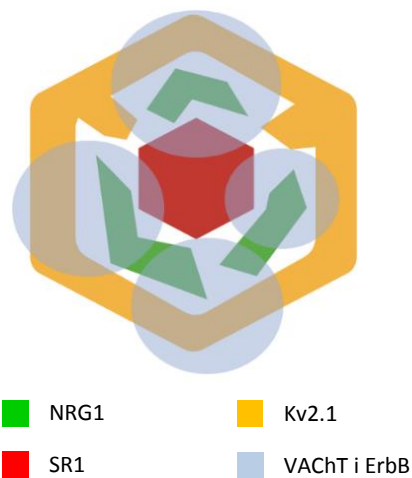


Figura 22 | Esquema de la possible distribució d'algunes de les proteïnes específicament concentrades als BC. La sinapsi està representada en una vista ortogonal. En verd està representada la NRG1; en vermell, el S1R; en taronja, el Kv2.1; i en blau, el VACHT i ErbBs. Creat amb Biorender.

d'aquest canal voltatge dependent, és la relacionada amb la modulació de l'excitabilitat neuronal en diversos tipus neuronals (Muennich & Fyffe, 2004). Aquesta funció, tot i ser la principal, no és la única. S'ha vist que agrupacions fosforilades de Kv2.1 poden tenir funcions no conductores alternatives a les pròpies d'un canal iònic, les quals encara no estan suficientment definides (Fox *et al.*, 2013). S'ha suggerit que aquestes acumulacions poden ser llocs pel traspàs de proteïnes de membrana a la superfície cel·lular (Deutsch *et al.*, 2012). D'acord amb això, el Kv2.1, en el context del BC podria estar orquestrant l'organització de les altres proteïnes localitzades en el compartiment postsinàptic dels BC, regulant el tràfic de vesícules cap i des de la membrana cel·lular, cosa que donaria una possible explicació a la seva peculiar localització.

Per la seva banda, el S1R és una xaperona situada també en la SSC, de la que s'han descrit mutacions causants d'ELA familiar (S. Watanabe *et al.*, 2016). En el context del BC, el S1R enllot de desenvolupar la funció normal de les xaperones, podria estar actuant de la mateixa manera que ho fa en les unions mitocondri-RE, on està implicat en la senyalització a través de calci mitjançant els receptors IP3 (de Sevilla *et al.*, 2008; T. Hayashi & Su, 2007; S. Watanabe *et al.*, 2016). Així doncs, ja que el SR1 té un paper rellevant en la modulació dels fluxos de calci en una gran varietat de sistemes, la seva presència en la SSC, estructura derivada del RE, suggereix que aquesta podria servir com un reservori de calci (Giordano *et al.*, 2013).

Així doncs, aquests resultats suggereixen que aquests dos proteïnes podrien estar desenvolupant funcions molt diferents a les seves habituals quan es localitzen en els BC, actuant mitjançant vies de senyalització independents, amb efectes en la cèl·lula també diferents.

D'altra banda, l'exploració dels BC dels animals transgènics sobreexpressors de les diferents isoformes de NRG1, ha demostrat que l'alteració dels nivells d'expressió i, probablement de l'activitat de la senyalització conseqüent, de les isoformes I i III de NRG1, afecten de forma diferencial la composició i l'estructura dels BC.

Concretament, hem descrit que la NRG1 tipus III modula l'organització postsinàptica del BC, específicament de la SSC, sense tenir efectes rellevants en la formació o estructura dels terminals presinàptics colinèrgics. Aquest animal transgènic sobreexpressor de la isoforma III de NRG1, induceix la formació de SSC redundants apilades les quals no només estan enriquides amb NRG1 tipus III, sinó també amb SR1 i Kv2.1. En canvi, la NRG1 tipus I, estimula substancialment l'increment del nombre i la mida dels aferents presinàptics VACHT positius, sense que això impliqui un engrandiment equivalent de la SSC. D'altra banda, tant la sobreexpressió de la NRG1 tipus I com la de tipus III, promouen l'acumulació de receptor M2 en la membrana postsinàptica.

Aquests resultats revelen un rol anteriorment desconegut de la NRG1 tipus I i la NRG1 tipus III com a organitzadors selectius del comportament pre- i postsinàptic respectivament dels BC en les MNs espinals. El mecanisme exacte i les conseqüències funcionals, actualment es desconeixen.

2. Mòdul NRG1/ErbB

La via de senyalització NRG1/ErbB s'ha vist involucrada en diferents processos ben definits en el sistema neuromuscular, com per exemple, en el desenvolupament de les cèl·lules de Schwann i la mielinització (Birchmeier & Nave, 2008), en el desenvolupament i plasticitat de les unions neuromusculars (Y. Il Lee *et al.*, 2016) i, en la inducció local de la síntesis d'acetilcolina (Falls *et al.*, 1993; Trinidad *et al.*, 2000).

Els nostres resultats utilitzant anticossos contra ErbB2 i ErbB4, constataren clarament la localització dels receptors de la NRG1 en el compartiment presinàptic dels BC. No es va poder determinar si ocupaven un microdomini en concret ja que, probablement degut a la seva escassa abundància, només es podien detectar si s'utilitzava un kit d'amplificació del senyal, cosa que dificultava poder distingir més finament la seva sublocalització. La major intensitat del senyal d'ErbB es va obtenir utilitzant anticossos contra ErbB2/4, ambdós fosforilats. El marcatge no era homogeni en tots els BC, sinó que només es detectava en un subgrup de BC, cosa que podria estar indicant diferents estats d'activació de la via NRG1/ErbB en els diferents BC d'una MN, corresponents a diferències *in vivo* de la funcionalitat de la via.

Tenint en compte els nostres resultats i els antecedents coneguts, suggerim l'existència d'un possible mecanisme de senyalització retrògrada NRG1/ErbB en els BC. Es desconeix però, com la NRG1 postsinàptica, té accés als ErbBs localitzats en el compartiment presinàptic. Degut a la proximitat dels compartiments, podria produir-se una senyalització juxtacrina que posés en contacte lligand i receptor. No obstant, en algunes ocasions i en concordança amb les descripcions d'altres autors (Caleo *et al.*, 2018; Ronnevi, 1979), hem observat mitjançant microscòpia electrònica, cossos multivesiculars intersinàptics semblants a exosomes entre el compartiment pre- i postsinàptic en els BC. Inesperadament, en aquestes vesícules semblants a exosomes, vam descriure la presència de NRG1, suggerint que aquests podrien ser els que facilitessin la comunicació intersinàptica per a que es pugui dur a terme la senyalització NRG1/ErbB. Aquest mecanisme de comunicació intrasinàptic, tot i ser infreqüent, no seria estrany ja que s'ha descrit en altres contexts (Korkut *et al.*, 2009). Tot els resultats anirien a favor d'una possible senyalització retrògrada NRG1/ErbB des del compartiment postsinàptic cap al presinàptic en el BC (Fig. 23).

Una altra possibilitat plausible i no excloent amb l'anterior, seria una senyalització ErbB-NRG1 anterògrada (des del presinàptic cap al postsinàptic), que tindria lloc després de la interacció juxtacrina entre els components. En aquest cas, després de la proteòlisis de la NRG1, el fragment intracel·lular restant en la MN, podria estar actuant com un factor de transcripció capaç de regular la supervivència neuronal.

Recentment s'ha descrit que la NRG2 s'acumula en la SSC d'interneurones corticals les quals expressen ErbB4 (Vullhorst *et al.*, 2015). En aquest cas la senyalització NRG2/ErbB4 sembla regular de forma autocrina els receptors NMDA. És per això, que no es pot descartar tampoc la possibilitat d'una senyalització autocrina en les MNs mediada per la NRG1.

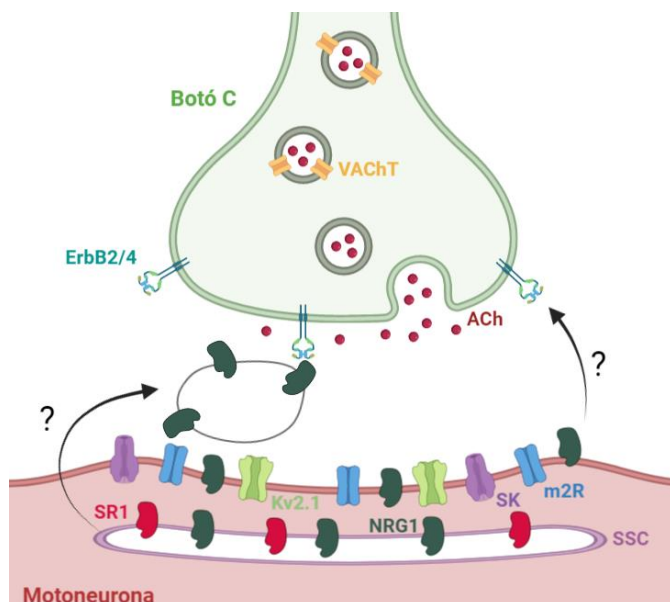


Figura 23 | Esquema dels possibles mecanismes de comunicació transinàptica que farien possible el contacte NRG1 – ErbB: la senyalització via exosomal o la interacció juxtacrina. Creat amb Biorender.

3. Resposta del BC a diferents paradigmes de dany experimental en les MNs

Per comprendre millor el paper dels BC i, per extensió de la NRG1, en l'activitat de les MNs, tant en condicions fisiològiques com patològiques, vam descriure els canvis que experimentava aquesta sinapsi en resposta a diferents paradigmes de dany experimental.

L'estimulació elèctrica intensa i els experiments *ex vivo*, van revelar que la NRG1 associada als BC és extremadament sensible als estressos cel·lulars aguts. Aquestes observacions van en concordança

amb els resultats d'altres estudis que han demostrat que el RE es fisiona ràpidament però de forma reversible després de la despolarització, i que l'activitat sinàptica en modula l'estructura de forma calci dependent (Kucharz *et al.*, 2009, 2011). Per tant, és lògic pensar que davant de canvis abruptes aguts, s'afecti el RE, i per tant, la SSC, que en el nostre cas es reflexa en la NRG1. Els mateixos canvis es van observar quan s'administrava el tractament farmacològic amb Tunicamicina, un inductor de l'estrés de reticle, corroborant la hipòtesis anterior.

Aquests experiments demostren que el BC, concretament el compartiment postsinàptic, és molt sensible a diversos agents estressants exercits de forma aïllada. Les axotomies, ens han permès simular diferents processos patològics, com són la neuroinflamació, l'estrés de reticle i la deafferentació associada a la medul·la espinal, en una situació controlada, que alhora reproduïa alguns dels mecanismes fisiopatològics que estarien succeint en l'ELA d'acord amb la teoria del *dying-back*.

Una qüestió interessant que deriva del nostre estudi és el possible paper dels BC en l'orquestració de la resposta neuroinflamatòria que té lloc al voltant de les MNs lesionades. Els nostres resultats suggereixen que les molècules associades al BC actuen com a senyals que atrauen processos microglials. Aquesta preferència de la micròglia per determinats tipus de sinapsis, s'havia descrit en relació als aferents excitadors vGlut1 (Alvarez *et al.*, 2011; Spejo & Oliveira, 2015). En aquest cas, aquest fenomen es podria explicar per l'affectació dels axons sensitius propioceptius que estableixen connexions monosinàptiques amb les MNs i que també s'affecten directament en l'axotomia del nervi ciàtic (Kettenmann *et al.*, 2013).

L'especificitat espacial pels BC era menys esperable, ja que les interneurones a partir de les quals s'originen aquests terminals no estan directament danyades per l'axotomia. Suggerim, que en aquest model experimental, el que atrau a la micròglia cap als BC, probablement sigui la complexa disposició de les molècules i les vies de senyalització inherents al BC. No obstant, de moment, el substrat molecular concret d'aquest efecte quimiotàctic de la micròglia híper-reactiva cap al BC es desconeix. Tot i això, estudis *in vitro* i *in vivo* suggereixen que aquesta quimiotaxis pot estar mediada per la senyalització NRG1-ErbB, concretament per la NRG1, ja que si aquesta es sobreexpressa, s'exacerba la microgliosi basal i, si s'antagonitza, es produeix una reducció de la microgliosi (Calvo *et al.*, 2010, 2011; M. Liu *et al.*, 2018).

Per altra banda, els nostres resultats demostren la desintegració de forma aguda de la NRG1 en els BC després de la lesió de les MNs. L'estudi realitzat suggerix que aquesta disruptió podria estar relacionada amb l'estrés de reticle i la reacció cromatolítica que es desencadena després l'axotomia, ja que aquesta desintegració es pot prevenir quan s'inhibeix l'estrés de reticle produït per la lesió del

nervi perifèric amb el fàrmac Salubrinal. En aquest mateix experiment, vam observar que el component presinàptic tampoc patia la disagregació que també s'observa quan es realitza una axotomia. Sorprenentment, amb el Salubrinal també evitàvem el reclutament de micròglia al voltant de les MNs lesionades, suggerint algun tipus de relació entre l'estrés de reticle, l'aferent sinàptic i la micròglia.

Està molt ben caracteritzat que la micròglia durant el desenvolupament juga un paper fonamental en l'eliminació de sinapsis no actives amb l'objectiu d'establir una xarxa neuronal estable. Algunes evidències apunten a que la pèrdua sinàptica que es produeix en l'adult, signe inicial de diverses malalties neurodegeneratives incloent aquelles que afecten a les MNs (Fogarty, 2019; Vukojicic *et al.*, 2019), es podria dur a terme a través de la reactivació patològica dels mecanismes que actuen durant el desenvolupament, on la micròglia hi podria tenir un paper rellevant (Stephan *et al.*, 2012).

En els últims anys, la teoria predominant per explicar l'eliminació dels aferents per part de la micròglia, era la que proposava la micròglia amb un rol de *stripper* sinàptic (Blinzinger & Kreutzberg, 1968): la micròglia activa desplaça terminals sinàptics intactes de la superfície de MNs axotomitzades del nucli facial, sense que aquests presentin signes de degeneració i sense que siguin fagocitats per la micròglia.

Els nostres resultats en la medul·la espinal, demostren una disruptió severa dels terminals aferents de les MNs en fases molt inicials després de la transecció del nervi perifèric, acompanyada ja d'una prominent neuroinflamació per part de la micròglia. Aquests resultats contrasten amb el *stripping* sinàptic, però aquesta discordança podria ser resultat de la diferent correlació temporal en el mostreig: en el nostre estudi estudiàvem l'efecte de l'axotomia sobre les MNs començant al dia següent de la intervenció, en contrast amb l'estudi del 1968 on observaven els efectes diversos dies després de la cirurgia.

A les 24 h després de la lesió, alguns terminals sinàptics exhibien la ruptura de les membranes presinàptiques amb la conseqüent alliberació de les vesícules intracel·lulars a l'espai extracel·lular. Aquesta imatge concordava amb el procés de necroptosi, mecanisme que es va descriure involucrat en la disruptió dels terminals ja que es va localitzar la proteïna p-MLKL en els llocs on els aferents presinàptics degeneraven. Aquest procés necroptòtic probablement succeeix de forma localitzada en els axons terminals, sense que acabi provocant la mort de les cèl·lules originaries dels terminals, tal com succeeix en una forma d'apoptosi espacialment confinada als axons o a les sinapsis (Cusack *et al.*, 2013; Mattson *et al.*, 1998).

En aquest punt, ens sorgeixen dos possibles explicacions del paper primari que pot tenir la micròglia en el procés de disruptió presinàptica.

Segons la nostra primera hipòtesi, el procés que explicaria el reclutament de la micròglia cap a les MNs lesionades és que aquestes alliberen factors derivats de l'estrés de reticle tals com ATP/ADP

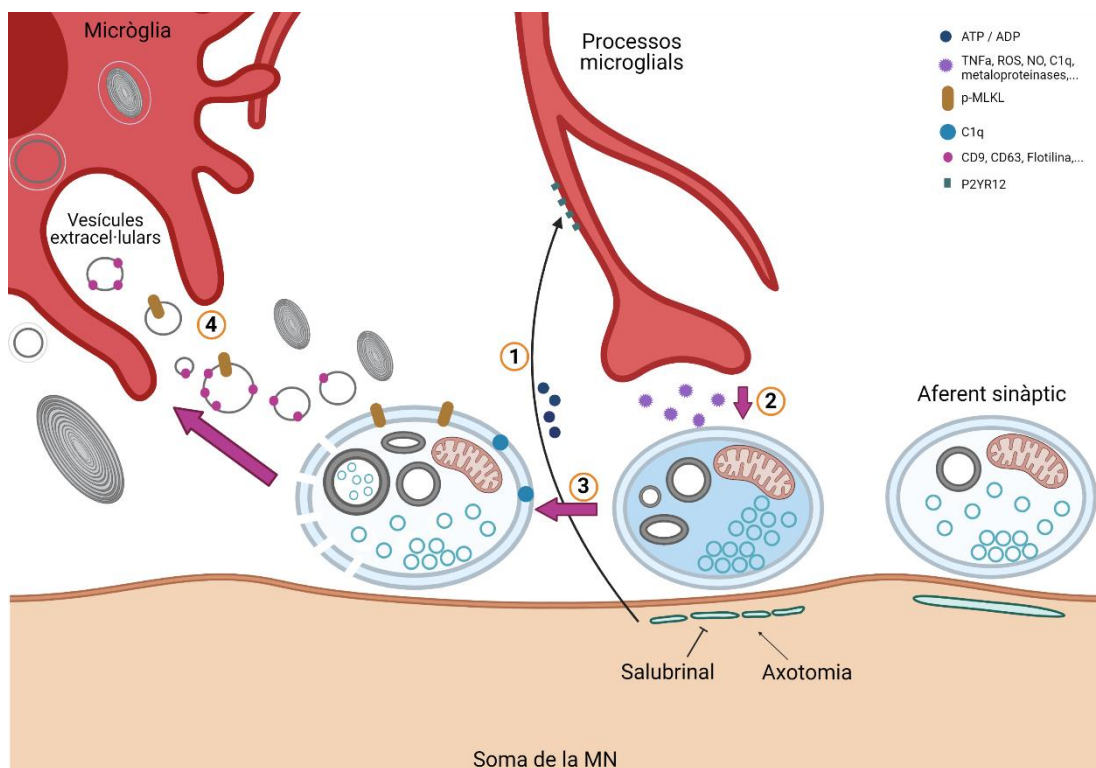


Figura 24 | Representació esquemàtica del possible rol primari de la micròglia en la deafferentació sinàptica postaxotomia. Segons aquesta hipòtesi, a les 24h després de l'axotomia, l'alliberació de factors derivats de l'estrés de reticle tals com ATP/ADP (1), poden ser els responsables de reclutar la micròglia cap a les MNs lesionades, a través de receptors com el P2YR12. Aquesta, alliberaria factors tòxics pel terminal tals com TNF- α , ROS, C1q,... (2), que provocarien la ruptura dels terminals presinàptics via necroptosi localitzada (3), amb la conseqüent alliberació de vesícules intracel·lulars a l'espai extracel·lular (4). Creat amb Biorender.

(Badimon *et al.*, 2020; Patritti-Cram *et al.*, 2021) que siguin els responsables d'atreure la micròglia per quimiotaxi a través dels receptors P2YR12. Aquestes cèl·lules microglials mobilitzades podrien estar alliberant diversos factors (Block *et al.*, 2007; Fawcett *et al.*, 2019; Y. S. Kim *et al.*, 2007; Könnecke & Bechmann, 2013) que alterin de forma negativa el compartiment presinàptic (Fig. 24).

D'altra banda, una possible alternativa seria que la micròglia no contribuís al dany sinàptic directament, sinó que aquesta es reclutés secundàriament en resposta, per exemple de l'alliberació de components presinàptics tals com vesícules sinàptiques. Segons aquesta hipòtesi, les alteracions en les sinapsis s'originarien per processos inherents a la neurona (Fig. 25), els quals col·lateralment serien exacerbades pels factors neurotòxics que podria estar secretant la micròglia activa reclutada.

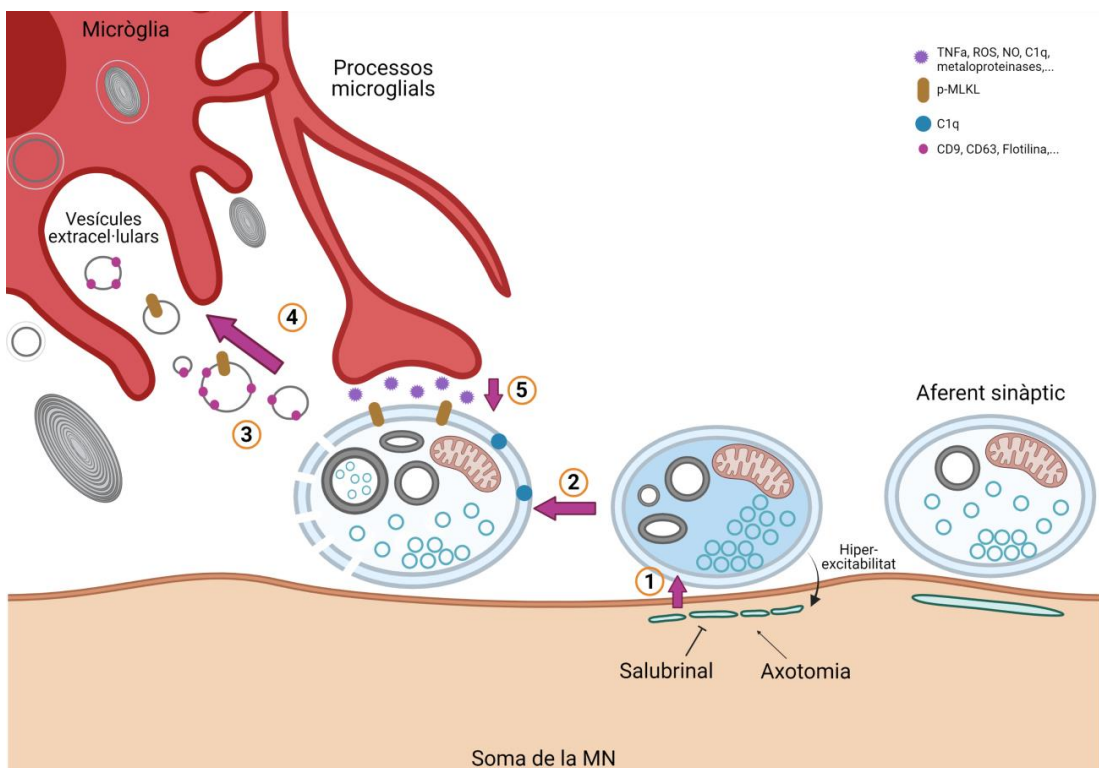


Figura 25 | Representació esquemàtica del possible rol tardà de la micròglia en la deafferentació sinàptica postaxotomia. D'acord a aquesta hipòtesi, les alteracions en el terminal presinàptics observades a les 24h després de la lesió s'originarien per processos inherent a la neurona (1). Secundàriament a aquestes pertorbacions, es produiria la ruptura dels terminals (2) amb la conseqüent alliberació de vesícules (3), les quals serien el senyal quimiotàctic que promouria el reclutament de la micròglia (4). La micròglia reclutada, mitjançant l'alliberació de factors tòxics (5) podria estar exacerbant les alteracions sinàptiques. Creat amb Biorender.

De forma variable, aquests terminals sinàptics trencats, presenten una acumulació d'òrgànuls membranosos semblants a vesícules endosomals, la qual cosa és indicativa d'una funció de reciclatge de les vesícules alterada i, en definitiva, d'una funció sinàptica anòmala. Estudis inicials sobre l'estrucció sinàptica i la seva funció, van descriure que una activitat elèctrica incrementada donava com a resultat l'acumulació de membranes presinàptiques mal plegades, les quals es generaven a conseqüència del bloqueig del reciclatge de les vesícules (Haimann *et al.*, 1985; Solsona *et al.*, 1981). No descartem doncs, que aquest sigui l'origen de l'alteració vesicular observada en els terminals.

Tot i les diferents possibilitats sobre el paper primari de la micròglia, els nostres resultats suggereixen que aquesta participa activament en l'eliminació de les sinapsis. Els llocs on s'acumulen les vesícules que contenen p-MLKL procedents de la disruptió dels terminals, acostumen a estar a prop de zones

on la micròglia ha estat atreta. Una possible teoria que se'n deriva és que la micròglia secreti factors que inicien la via necroptòtica, emulant al que succeeix en altres condicions neuropatològiques (A.-Q. Chen *et al.*, 2019; Ito *et al.*, 2016; Pasparakis & Vandenabeele, 2015). De la mateixa manera, el factor del complement C1q també es veu sobreexpressat en la micròglia en el context de les axotomies. És conceivable que el C1q produït per la micròglia s'uneixi alsdebris vesiculars formats a partir de terminals sinàptics desintegrats per tal de promoure la seva opsonització i posterior fagocitosis, d'una manera comparable al que succeeix durant l'eliminació de cèl·lules apoptòtiques (Galvan *et al.*, 2012) o en el remodelat sinàptic que té lloc durant el desenvolupament i en condicions patològiques de pèrdua sinàptica (Hong *et al.*, 2016; Schafer *et al.*, 2012; Stevens *et al.*, 2007). No obstant, en absència de C1q, l'eliminació sinàptica que segueix a l'axotomia no es redueix (Berg *et al.*, 2012), probablement degut a l'existència de mecanismes redundants implicats en l'eliminació d'aferents sinàptics de les MNs lesionades.

La morfologia ultraestructural que hem observat en les vesícules extracel·lulars lliures en l'espai perineuronal de MNs axotomitzades, era molt pleomòrfica i exhibia una gran varietat de mides. A part de les vesícules producte de la lisis o necroptosis dels terminals sinàptics, en el nostre sistema també hem vist botons sinàptics presentant una prominent concentració de cossos multivesiculars, els quals també podrien ser secretats a l'entorn perineuronal.

S'ha de tenir en compte que l'activació del p-MLKL no compromet de forma irreversible les cèl·lules a morir. En determinades circumstàncies, la inducció de p-MLKL promou la formació de bombolles a la superfície de les cèl·lules que són alliberades a l'espai extracel·lular (Gong *et al.*, 2017; Yoon *et al.*, 2017) per tal de promoure la restauració de l'estructura danyada. Aquest fenomen pot correlacionar amb els canvis vacuolars que observem en el terminal sinàptic que escapan de la disrupció aguda. Aquests aferents romanen, almenys alguns dies, en contacte amb les MNs, i desenvolupen abundants cossos multivesiculars i vesícules semblants a endosomes, els quals sovint estan en contacte amb processos microglials. Aquestes vesícules també poden alliberar-se i barrejar-se en l'espai extracel·lular amb les vesícules lítiques. Això no obstant, aquestes, en base a la seva composició molecular, poden correspondre a exosomes (Fig. 26).

Per tant, diferents poblacions de vesícules extracel·lulars tals com les derivades de la necroptosi o les procedents dels cossos multivesiculars, es poden produir en una seqüència espai-temporal diferent durant els complexos esdeveniments cel·lulars que es produeixen a prop de la superfície de la MN axotomitzada.

Hem demostrat que el destí de la majoria de les vesícules extracel·lulars generades en l'espai perineuronal de MNs axotomitzades és la seva eliminació per fagocitosis per cèl·lules microglials.

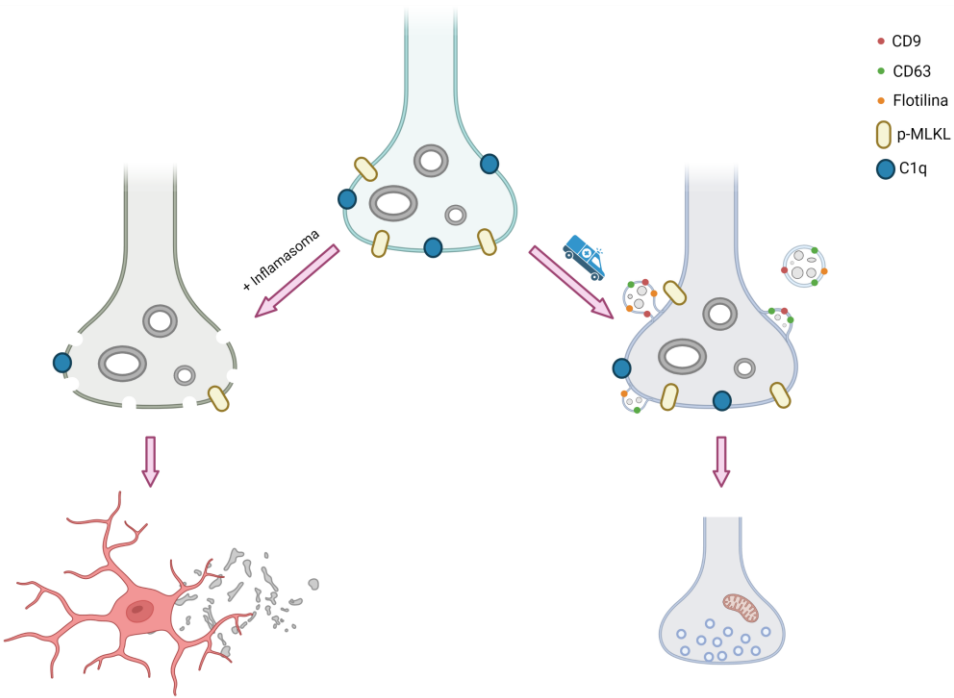


Figura 26 | Representació esquemàtica de les dos funcions que poden derivar de l'activació del p-MLKL. L'activació del p-MLKL no compromet de forma irreversible les cèl·lules a morir. En determinades circumstàncies, promou la formació de bombolles a la superfície de les cèl·lules, les quals són alliberades a l'espai extracel·lular en forma de vesícules per tal de promoure la restauració de l'estructura danyada. En el context d'axotomia, aquestes vesícules presenten marcadors d'exosomes (CD9, CD63 i flotilina). Creat amb Biorender.

Aquestes dades concorden amb la progressiva i transitòria acumulació de punts CD68 positius dins de les cèl·lules microglials perisomàtiques, el qual és un indicatiu d'activitat lisosomal. No obstant, la íntima relació entre els marcadors exosomals i la superfície de la micròglia, indica un procés previ que involucra l'atrapament amb la finalitat d'endocitar les vesícules extracel·lulars.

Les nostres dades indiquen que les cèl·lules microglials estan involucrades activament en l'eliminació dels fragments procedents de terminals presinàptics danyats. No hem recollit evidències que recolzin l'engoliment massiu dels botons sinàptics per part de la micròglia. Enlloc d'això, els nostres resultats suggereixen que les cèl·lules microglials internalitzen petits fragments de vesícules extracel·lulars resultants de la disruptió dels terminals sinàptics, concepte reminiscent de la trogocitosi sinàptica que té lloc durant el desenvolupament per part de la micròglia (Weinhard *et al.*, 2018).

4. Degeneració de les MNs en el model SOD1^{G93A}

El següent pas en la línia d'investigació, va ser extrapolar els resultats obtinguts en el model d'axotomia al model SOD1^{G93A}, per tal d'estudiar com s'altera el BC durant l'evolució de l'ELA i el paper que té la micròglia en el procés.

Un aspecte intrigant de la patologia de l'ELA són els diversos graus de vulnerabilitat dels diferents tipus de MNs envers la malaltia. Durant el curs de l'ELA i després de la pèrdua de les MNs més vulnerables, els axons romanents broten (*sprout*) per tal de compensar aquells que han degenerat (Schaefer *et al.*, 2005). Això implica que en un moment determinat, MNs degenerants i supervivents, o inclús regenerants, coexisteixen en diferent proporció en la banya ventral de la medul·la espinal.

Donat el limitat coneixement sobre la seqüència d'esdeveniments cel·lulars que tenen lloc durant la progressió de l'ELA, hem intentat categoritzar la patologia de MNs individuals establint diferents patrons fenotípics de dany basats en l'expressió de formes tòxiques mal plegades de la SOD1 en el model de ratolí SOD1^{G93A}. La disponibilitat d'anticossos específics de conformació de mfSOD1 com l'anticòs monoclonal C4F6 (Brotherton *et al.*, 2012; Urushitani *et al.*, 2007) o el nostre anticòs policlonal AJ10 (Sábado *et al.*, 2013), ens ha permès explorar en detall la distribució d'aquests components tòxics de SOD1 i la seva relació amb la degeneració de les MNs.

Hem trobat immunoreactivitat principalment associada a MNs començant en les seves expansions dendrítiques o axonals en etapes inicials, amb la posterior acumulació en els cossos cel·lulars en fases més avançades de degeneració. Aquesta distribució seqüencial de mfSOD1 ens ha permès delimitar tres fenotips: l'absència o nivells molt baixos d'immunoreactivitat per mfSOD1, l'hem categoritzat com fenotip 1; la presència de mfSOD1 dispersa en el neuròpil al voltant dels somes de les MNs, l'hem definit com fenotip 2; i finalment, el fenotip 3, l'hem caracteritzat com aquell en que

no només trobem agregats de mfSOD1 en el neuròpil, sinó que les pròpies MNs presenten somes altament positius a mfSOD1.

L'anàlisi longitudinal de la distribució dels tres fenotips durant el curs natural de la malaltia demostra que el fenotip 2 ja és molt prominent a p30, suggerint una important alteració patològica ja en etapes asimptomàtiques. D'altra banda, el fenotip 3 apareix des de p60, denotant la degeneració de les MNs més vulnerables en estadis presimptomàtics inicials, fins a etapes terminals. En aquest interval es produeix una pèrdua moderada però sostinguda de MNs indicant que les MNs amb acumulació massiva de mfOD1 moren notablement en etapes presimptomàtiques o inicialment simptomàtiques. Això suggereix que les MNs resistentes a l'ELA, les quals encara són presents en les etapes terminals de la malaltia, no acumulen grans quantitats de mfSOD1.

La degeneració de les MNs en models animals de SOD1 mutada és un procés que tant depèn de factors intrínsecos de la MN (acumulació de mfSOD1) com de factors extrínsecos, fent-se essencial la participació de les cèl·lules no neuronals (Boillée *et al.*, 2006; Clement *et al.*, 2003; Ilieva *et al.*, 2009). Per aquesta raó, l'estudi del neuròpil de les MNs incloent els aferents sinàptics, els astròcits i la micròglia és igualment rellevant.

Pel que fa a l'estructura del BC, i en relació al compartiment postsinàptic, els nostres resultats demostren una disruptió de la SSC en etapes asimptomàtiques, la qual cosa suggereix alteracions en la senyalització sinàptica dels BC en fases molt inicials de l'ELA. Ja que l'organització normal del RE resulta severament alterada en etapes prematures de la malaltia (Walker & Atkin, 2011), seria esperable que la SSC com a subcompartiment específic del RE, també estigui afectada.

Recentment, la manipulació de la senyalització per NRG1 ha estat objecte d'estudi en ratolins SOD1. S'han realitzat estudis on es promovia l'expressió de NRG1 tipus III en la medul·la espinal mitjançant virus, experiment que va resultar en un augment de la supervivència i una reducció en la pèrdua de BC. Per altra banda, el bloqueig de la senyalització de la NRG1 reduïa l'activació microglial i alentia la progressió de la malaltia (M. Liu *et al.*, 2018). Aquestes dades en conjunt, indiquen que la NRG1 té activitats pleiotòpiques i que de la seva manipulació se'n deriven resultats variables i en alguns casos controvertits, fent-se necessaris més estudis per esclarir el rol de la NRG1 en l'ELA.

En referència al compartiment presinàptic dels BC, només hem detectat alteracions en el VACHT en el fenotip 3, és a dir, quan les MNs presenten els canvis més severs i la microgliosi és molt elevada. En relació als aferents sinàptics en general, diversos estudis han descrit la presència d'alteracions en aquests com esdeveniments inicials en l'ELA (Bączyk *et al.*, 2020; Delestrée *et al.*, 2014; Martínez-Silva *et al.*, 2018; Roselli & Caroni, 2015; Saxena *et al.*, 2013; Schutz, 2005; Vinsant *et al.*, 2013; Zang

et al., 2005; P. Zhao *et al.*, 2008). Aquestes descripcions són consistents amb els nostres resultats on hem detectat una disminució d'aferents sinàptics en les MNs amb el fenotip més sever ja a p60. A més, en aquestes etapes primerenques, a nivell ultraestructural es podien distingir terminals amb una acumulació anormal de vacuoles i endosomes indicant, com succeïa en les axotomies, una alteració del reciclatge de vesícules a conseqüència de la desregulació de l'alliberació de neurotransmissors.

Donada la similitud d'algunes observacions entre el model G93A-f i les axotomies, ens vam disposar a analitzar l'expressió de diferents marcadors relacionats amb exosomes i amb la necroptosi en el model G93A, per establir mecanismes homòlegs entre els dos models.

En el model SOD1^{G93A} vam observar l'acumulació de partícules positives a la Flotilina relacionades amb el lumen de grans vacuoles citoplasmàtiques presents en les MNs amb fenotip 3. Ja que la degeneració vacuolar s'ha descrit àmpliament en MNs en procés de degeneració en aquest model de ratolí, varem decidir indagar sobre la relació d'aquestes vacuoles amb marcadors de vesícules extracel·lulars.

En concordança amb estudis previs, amb els nostres resultats immunohistoquímics i ultraestructurals hem corroborat la prominent degeneració vacuolar que presenten les MNs en decadència en el model de ratolí SOD1^{G93A} (Bendotti *et al.*, 2001; Dal Canto & Gurney, 1994; Higgins *et al.*, 2003; Jaarsma *et al.*, 2001; Kong & Xu, 1998; Wong *et al.*, 1995). Aquestes vacuoles hem vist que procedeixen de mitocondris massivament inflats i de la fragmentació del RE en vesícules, patró coincident amb publicacions anteriors (Fischer *et al.*, 2004; Kong & Xu, 1998; Vinsant *et al.*, 2013). L'estrucció morfològica d'aquestes MNs altament vacuolitzades encaixa bé amb el concepte de paraptosi, el qual es caracteritza precisament per la vacuolització del citoplasma a partir dels mitocondris i/o d'alteracions en el RE (E. Kim *et al.*, 2021; Sperandio *et al.*, 2000). Degut a aquestes similituds, proposem aplicar el concepte de paraptosi a les MNs vacuolitzades i altament positives a mfSOD1 en el context d'ELA deguda a mutacions en la SOD1.

Aquesta morfologia mitocondrial alterada en el model SOD1^{G93A} es deu a la translocació específica de la SOD1 mutada a aquest orgànul (J. Liu *et al.*, 2004; Vande Velde *et al.*, 2008). Les grans vacuoles que s'observen a nivell ultraestructural es probable que es formin a partir de mitocondris vacuolitzats i com a conseqüència de la fusió de les seves membranes mitocondrials externes, donant lloc a una única vacuola gegant la qual conté varies membranes mitocondrials internes plegades i agrupades a la paret de la gran vacuola. Les grans vacuoles esferoidals mitocondrials presents en els axons i les dendrites juntament amb l'acumulació de mfSOD1, és un esdeveniment inicial en la patologia de les MNs en el SOD1^{G93A}. Aquestes observacions concorden amb el patró designat com a

fenotip 2, el qual és prominent a p30, temps abans del debut dels símptomes. És possible que degut a les restringides condicions espacials de les dendrites i els axons, aquests siguin més vulnerables a la patologia de mfSOD1 i sigui on es manifestin en primer lloc els canvis patològics. Aquests fenòmens concordarien amb la teoria del *dying-back*.

Hem descrit que les vacuoles d'origen mitocondrial de les MNs paraptòtiques, a més de contenir Flotilina, també són positives per la proteïna CD81 i estan associades a la cromogranina. Aquestes proteïnes, entre altres funcions, es relacionen amb l'excreció de vesícules cel·lulars a l'exterior (Hemler, 2005; Kowal *et al.*, 2016; Urushitani *et al.*, 2006; W. Zhao *et al.*, 2010). Aquestes troballes, juntament amb estudis recents que localitzen marcadors exosomals i de tràfic vesicular com els anteriors en vesícules extracel·lulars lliures provinents de mitocondris (D'Acunzo *et al.*, 2021; Picca *et al.*, 2020), suggereixen la possibilitat de l'alliberació d'aquestes vacuoles d'origen mitocondrial carregades amb mfSOD1 a l'exterior de les MNs. Aquestes vacuoles lliures en el neuròpil i en proximitat a MNs, podrien contribuir a la neuroinflamació local i a la propagació priònica de l'ELA (Bellingham *et al.*, 2012; Grad *et al.*, 2014; Silverman *et al.*, 2019). Una altra possibilitat apuntaria a que una vegada generats els mitocondris vacuolitzats, es trenquin a conseqüència de la promoció de la fissió mitocondrial (Joshi *et al.*, 2019) i que aquests fragments amb mfSOD1 adherida puguin ser eventualment transferits a altres cèl·lules veïnes (Hayakawa *et al.*, 2016; Joshi *et al.*, 2019).

Un altre aspecte intrigant de les MNs paraptòtiques és el seu contingut en partícules positives a p-MLKL, indicatiu de l'activació de l'efector terminal de la via necroptòtica (H. Wang *et al.*, 2014). El p-MLKL podria estar destruint la integritat de la membrana de les MNs i alliberar vesícules que contenen mfSOD1. Hi ha indicis que suggereixen que la necroptosi podria ser la causa de la lisi i mort de la MN paraptòtica (Re *et al.*, 2014), propiciant així la propagació *prion-like* de l'ELA (Fig. 27). Corroborant aquesta hipòtesis, s'ha detectat l'elevació de marcadors necroptòtics incloent el MLKL en medul·les espinals de ratolins SOD1^{G93A} i en pacients amb ELA esporàdica (Ito *et al.*, 2016). No obstant, la delecio de MLKL o de les kinases RIP1 o RIP3 (implicades en la via necroptòtica) no millora ni la neuropatologia ni el curs clínic de l'ELA en el ratolí model transgènic SOD1 (Dermentzaki *et al.*, 2019; Dominguez *et al.*, 2021; T. Wang *et al.*, 2020).

Aquesta absència de millora del curs de l'ELA en els ratolins deficientes en factors que intervenen en la via necroptòtica, es podria deure a que molt probablement existeixin altres mecanismes que condueixin a la mort de les MNs, compensant així la necroptosi quan aquesta no es pot dur a terme. Això concordaria amb la ultraestructura que mostren la majoria de MNs presents en les etapes terminals, les quals degeneren amb característiques diferents i, per tant, per mecanismes distints als observats en les MNs vulnerables a la patologia per mfSOD1.

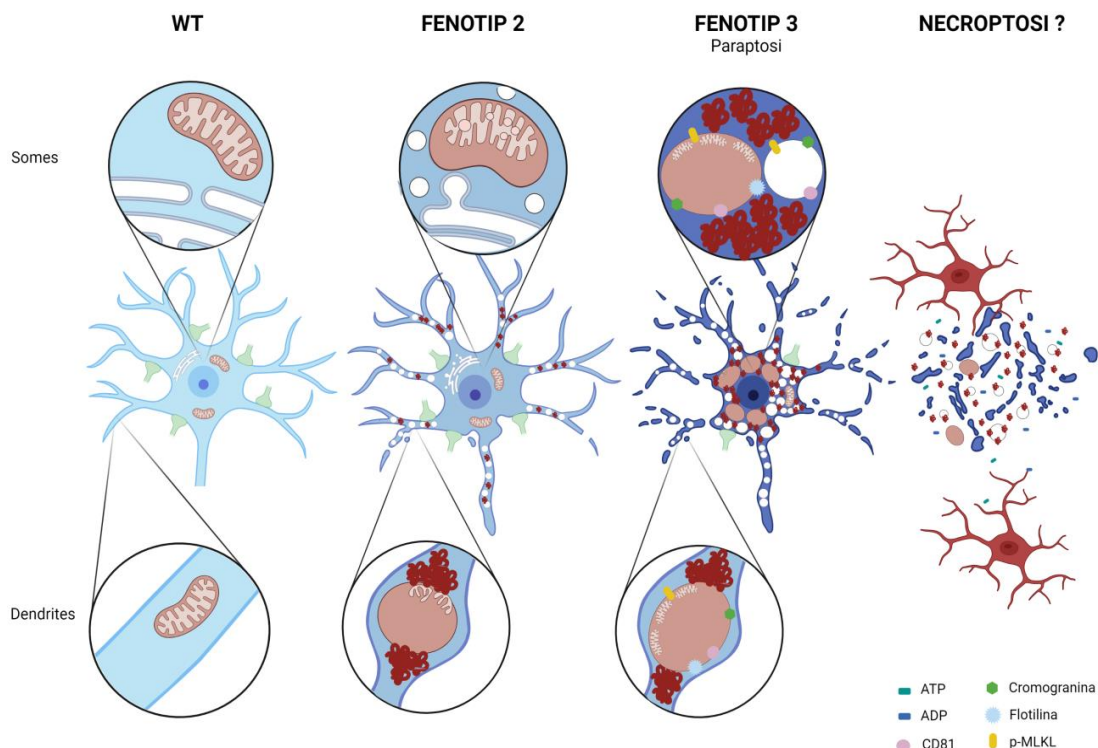


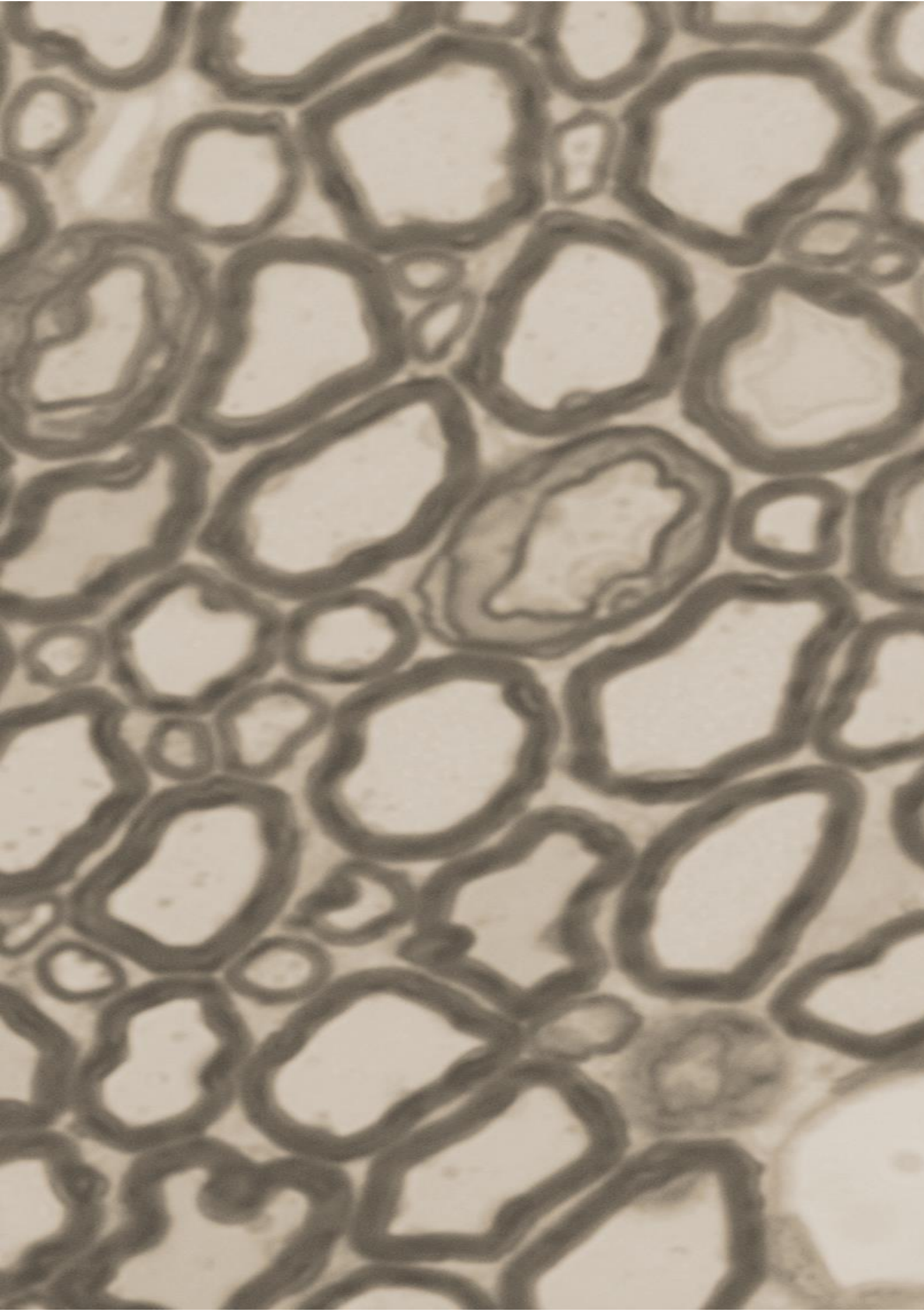
Figura 27 | Esquema representatiu de l'evolució de les MNs durant el curs de l'ELA segons els fenotips definits. En el fenotip 2, juntament amb la vacuolització del RE, s'observen grans vacuoles esfèriodals d'origen mitocondrial presents sobretot en axons i dendrites i amb una important acumulació de mfSOD1. En el fenotip 3, les MNs presenten característiques paraptòtiques tals com una gran vacuolització mitocondrial i de RE amb una gran acumulació de mfSOD1 en l'axó, en les dendrites i en el soma. Les vacuoles d'aquestes MNs són positives a marcadors com el CD81, la cromogranina o la flotilina, tots ells relacionats amb l'excreció de vesícules cel·lulars a l'exterior, suggerint la possibilitat de l'alliberació d'aquestes vacuoles carregades amb mfSOD1 a l'exterior de les MNs. Aquestes vacuoles lliures en el neuròpil i en proximitat a MNs, podrien contribuir a la neuroinflamació local i a la propagació priònica de l'ELA. Creat amb Biorender.

D'altra banda, és coneix que la mfSOD1 extracel·lular no provoca neurotoxicitat en les MNs per sí sola, però es sap que és un potent inductor de l'activació microglial (Urushitani *et al.*, 2006; W. Zhao *et al.*, 2010). Hem descrit topogràficament el reclutament microglial en relació amb els fenotips anteriorment descrits. En els diferents fenotips de MNs, hem observat una bona correlació entre l'acumulació de mfSOD1 en les MNs i el reclutament local de la micròglia. Aquestes cèl·lules microglials reclutades mostren un increment progressiu de marcadors d'activitat fagocítica tals com el CD68, MAC-2 i C1q.

D'altra banda, els experiments amb els que manipulàvem la microglia, ja sigui eliminant-la farmacològicament o induint-la mitjançant les axotomies, suggereixen que la neuroinflamació promou l'acumulació de la mfSOD1 i la degeneració vacuolar de les MNs. Aquests estudis recolzen el rol crucial de les cèl·lules no neuronals tals com la micròglia a l'hora de contribuir a la mort de MNs (Clement *et al.*, 2003).

Estudis previs d'altres autors proposaven l'acumulació de mfSOD1 com la causa primària que determina el debut de la malaltia, mentre que la micròglia contribuïa a la progressió de l'ELA (Clement *et al.*, 2003). Les nostres dades concorden amb aquesta teoria, ja que en etapes presimptomàtiques hem observat una destacable vacuolització degenerativa d'origen mitocondrial associada a mfSOD1 en les MNs vulnerables (positives a la proteïna matriu metallopeptidasa-9 (*Matrix metallopeptidase-9 (MMP-9)*)). Aquestes vacuoles, possiblement s'alliberen a l'espai perineuronal via exosomal o mitjançant vesícules extracel·lulars, o directament s'alliberen degut a la mort per necroptosi de les MNs. L'acumulació extracel·lular de mfSOD1 seria el que desencadenaria la resposta neuroinflamatòria, on la micròglia, en un intent d'eliminar els agregats, acabaria tenint efectes neurotòxics per les MNs, la qual cosa podria provocar, que aquestes, al seu torn, es tornin més disfuncionals i generin més mfSOD1. D'aquesta manera s'establiria un bucle de realimentació en el que s'estaria potenciant la neuroinflamació i la neurotoxicitat a nivell local al voltant de les MNs vulnerables, i que tot junt, contribuís a la mort progressiva d'aquestes.

És interessant notar que, d'acord amb els nostres resultats i els d'altres autors (Kong & Xu, 1998), la vacuolització sembla ser un procés transitori que afecta principalment les MN més vulnerables a l'ELA. No obstant, els altres subtipus de MNs també pateixen una patologia degenerativa amb característiques diferents a les anteriors, potser degut a la neurotoxicitat derivada de la resposta microglial enllot de ser degut a un mecanisme intrínsec d'aquestes MNs, les quals semblen ser més resistentes a l'acumulació de mfSOD1. Tot i això, el mecanisme exacte involucrat en la degeneració i mort de les MNs menys vulnerables a l'ELA en les fases tardanes està encara per determinar.



CONCLUSIONS

1. Els BC tenen una estructura altament complexa, específica, característica i única que els confereix unes propietats molt singulars. La NRG1, el SR1 i el canal de potassi Kv2.1 estan situats en el compartiment postsinàptic, concretament, es troben associats a la SSC ocupant microdominis espacials altament definits i no solapats entre ells. En canvi, els receptors de la neuregulina-1, ErbB2 i ErbB4, es localitzen en el compartiment presinàptic.
2. Suggerim l'existència d'un possible mecanisme de senyalització retrògrada NRG1/ErbB en els BCs mediat per exosomes, els quals facilitarien la comunicació intersinàptica posant en relació receptor i lligand.
3. La sobreexpressió de les isoformes I i III de la neuregulina-1 afecten de forma diferencial la composició, l'estructura i, probablement, l'activitat de la senyalització dels BC en les MNs espinals. Mentre que la NRG1 tipus I actua com a organitzador selectiu del compartiment presinàptic en el BC, la NRG1 tipus III té el seu efecte en el compartiment postsinàptic.
4. Els BC són terminals molt sensibles a estressors cel·lulars, sobretot el compartiment postsinàptic, el qual s'altera notablement i molt ràpidament després d'insults aguts així com de forma molt inicial en estressos crònics.
5. Després de realitzar una axotomia, els BC resulten quimioatraients per processos microglials, suggerint un possible rol dels BC en l'orquestració de la resposta neuroinflamatòria que té lloc al voltant de les MNs lesionades.
6. Després de la lesió aguda deguda a l'axotomia, no només s'esmicola el compartiment postsinàptic, si no que el terminal aferent de les MNs lesionades també es descomposa poc temps després de la transecció del nervi perifèric. Tot aquest procés va acompanyat d'una prominent neuroinflamació per part de la micròglia.
7. Posteriorment a la lesió del nervi perifèric, es poden observar vesícules extracel·lulars en l'ambient perineuronal provinents de la disruptió per necroptosi d'alguns terminals sinàptics; altres vesícules, procedeixen de cossos multivesiculars també amb origen en els aferents. Aquestes diferents poblacions de vesícules extracel·lulars es produeixen en una seqüència espai-temporal diferent durant els complexos esdeveniments cel·lulars que tenen lloc a prop de la superfície de les MNs axotomitzades.
8. Tot i les diferents possibilitats sobre el paper primari de la micròglia, els nostres resultats evidencien que aquesta participa activament en l'eliminació de les sinapsis, ja que el destí de la

majoria de les vesícules extracel·lulars secretades a l'espai perineuronal de MNs axotomitzades, és la seva eliminació per fagocitosis per part de les cèl·lules microglials.

9. De forma equiparable a les axotomies, en el model SOD1^{G93A} es produeix la disruptió de la SSC en etapes asimptomàtiques, la qual cosa suggereix alteracions en la senyalització sinàptica dels BC en fases molt inicials de l'ELA. En referència al comportament presinàptic, només hem detectat alteracions quan les MNs presenten els canvis més severs i la microgliosis és molt elevada.

10. En el model SOD1^{G93A} es produeix una prominent degeneració vacuolar d'origen mitocondrial localitzada en les MNs degenerants altament positives a mfSOD1. L'estructura morfològica d'aquestes MNs altament vacuolitzades encaixa bé amb el concepte de paraptosi. La vacuolització sembla ser un procés transitori que afecta principalment les MNs més vulnerables a l'ELA. No obstant, els altres subtipus de MNs també pateixen una patologia degenerativa amb característiques diferents.

11. Aquestes vacuoles d'origen mitocondrial carregades amb mfSOD1 podrien ser alliberades a l'exterior de les MNs mitjançant la pròpia maquinària secretora de la cèl·lula o per mitjà de la necroptosi, la qual alhora, podria ser la causa de la lisi i mort de les MNs paraptòtiques. Aquestes vacuoles lliures en el neuròpil i en proximitat a altres MNs, podrien contribuir a la neuroinflamació local i a la propagació priònica de l'ELA.

12. A nivell local al voltant de les MNs vulnerables, s'estableix un bucle de realimentació en el que la neuroinflamació i la neurotoxicitat s'estarien potenciant recíprocament, i tot junt, estaria contribuint a la mort progressiva de les MNs vulnerables, i col·lateralment, de les MNs menys sensibles a l'ELA.



REFERÈNCIES

- Adalbert, R., Nogradi, A., Babetto, E., Janeckova, L., Walker, S. A., Kerschensteiner, M., Misgeld, T., & Coleman, M. P. (2009). Severely dystrophic axons at amyloid plaques remain continuous and connected to viable cell bodies. *Brain*, 132(2), 402–416. <https://doi.org/10.1093/brain/awn312>
- Al-Saif, A., Al-Mohanna, F., & Bohlega, S. (2011). A mutation in sigma-1 receptor causes juvenile amyotrophic lateral sclerosis. *Annals of Neurology*, 70(6), 913–919. <https://doi.org/10.1002/ana.22534>
- Aldskogius, H. (2011). Mechanisms and consequences of microglial responses to peripheral axotomy. *Frontiers in Bioscience*, 3, 857–868.
- Alfieri, J. A., Silva, P. R., & Igaz, L. M. (2016). Early Cognitive/Social Deficits and Late Motor Phenotype in Conditional Wild-Type TDP-43 Transgenic Mice. *Frontiers in Aging Neuroscience*, 8(DEC), 1–14. <https://doi.org/10.3389/fnagi.2016.00310>
- Alvarez, F. J., Titus-Mitchell, H. E., Bullinger, K. L., Kraszpulski, M., Nardelli, P., & Cope, T. C. (2011). Permanent central synaptic disconnection of proprioceptors after nerve injury and regeneration. I. Loss of VGLUT1/IA synapses on motoneurons. *Journal of Neurophysiology*, 106(5), 2450–2470. <https://doi.org/10.1152/jn.01095.2010>
- Appel, S. H., Zhao, W., Beers, D. R., & Henkel, J. S. (2011). The microglial-motoneuron dialogue in ALS. *Acta Myologica*, 30(JUNE), 4–8.
- Arai, T., Hasegawa, M., Akiyama, H., Ikeda, K., Nonaka, T., Mori, H., Mann, D., Tsuchiya, K., Yoshida, M., Hashizume, Y., & Oda, T. (2006). TDP-43 is a component of ubiquitin-positive tau-negative inclusions in frontotemporal lobar degeneration and amyotrophic lateral sclerosis. *Biochemical and Biophysical Research Communications*, 351(3), 602–611. <https://doi.org/10.1016/j.bbrc.2006.10.093>
- Atkin, J. D., Farg, M. A., Walker, A. K., McLean, C., Tomas, D., & Horne, M. K. (2008). Endoplasmic reticulum stress and induction of the unfolded protein response in human sporadic amyotrophic lateral sclerosis. *Neurobiology of Disease*, 30(3), 400–407. <https://doi.org/10.1016/j.nbd.2008.02.009>
- Bączyk, M., Alami, N. O., Delestrée, N., Martinot, C., Tang, L., Commisso, B., Bayer, D., Doisne, N., Frankel, W., Manuel, M., Roselli, F., & Zytnicki, D. (2020). Synaptic restoration by cAMP/PKA drives activity-dependent neuroprotection to motoneurons in ALS. *Journal of Experimental Medicine*, 217(8). <https://doi.org/10.1084/jem.20191734>
- Badimon, A., Strasburger, H. J., Ayata, P., Chen, X., Nair, A., Ikegami, A., Hwang, P., Chan, A. T., Graves, S. M., Uweru, J. O., Ledderose, C., Kutlu, M. G., Wheeler, M. A., Kahan, A., Ishikawa, M., Wang, Y.-C., Loh, Y.-H. E., Jiang, J. X., Surmeier, D. J., ... Schaefer, A. (2020). Negative feedback control of neuronal activity by microglia. *Nature*, 586(7829), 417–423. <https://doi.org/10.1038/s41586-020-2777-8>

- Barber, S. C., Mead, R. J., & Shaw, P. J. (2006). Oxidative stress in ALS: A mechanism of neurodegeneration and a therapeutic target. *Biochimica et Biophysica Acta (BBA) - Molecular Basis of Disease*, 1762(11–12), 1051–1067. <https://doi.org/10.1016/j.bbadi.2006.03.008>
- Bastow, E. L., Peswani, A. R., Tarrant, D. S. J., Pentland, D. R., Chen, X., Morgan, A., Staniforth, G. L., Tullet, J. M., Rowe, M. L., Howard, M. J., Tuite, M. F., & Gourlay, C. W. (2016). New links between SOD1 and metabolic dysfunction from a yeast model of Amyotrophic Lateral Sclerosis (ALS). *Journal of Cell Science*, 129(21), 4118–4129. <https://doi.org/10.1242/jcs.190298>
- Beers, D. R., & Appel, S. H. (2019). Immune dysregulation in amyotrophic lateral sclerosis: mechanisms and emerging therapies. *The Lancet Neurology*, 18(2), 211–220. [https://doi.org/10.1016/S1474-4422\(18\)30394-6](https://doi.org/10.1016/S1474-4422(18)30394-6)
- Beers, D. R., Henkel, J. S., Xiao, Q., Zhao, W., Wang, J., Yen, A. A., Siklos, L., McKercher, S. R., & Appel, S. H. (2006). Wild-type microglia extend survival in PU.1 knockout mice with familial amyotrophic lateral sclerosis. *Proceedings of the National Academy of Sciences*, 103(43), 16021–16026. <https://doi.org/10.1073/pnas.0607423103>
- Beers, D. R., Zhao, W., Liao, B., Kano, O., Wang, J., Huang, A., Appel, S. H., & Henkel, J. S. (2011). Neuroinflammation modulates distinct regional and temporal clinical responses in ALS mice. *Brain, Behavior, and Immunity*, 25(5), 1025–1035. <https://doi.org/10.1016/j.bbi.2010.12.008>
- Bellingham, S. A., Guo, B. B., Coleman, B. M., & Hill, A. F. (2012). Exosomes: Vehicles for the Transfer of Toxic Proteins Associated with Neurodegenerative Diseases? *Frontiers in Physiology*, 3(May), 1–12. <https://doi.org/10.3389/fphys.2012.00124>
- Bendotti, C., Calvaresi, N., Chiveri, L., Prelle, A., Moggio, M., Braga, M., Silani, V., & De Biasi, S. (2001). Early vacuolization and mitochondrial damage in motor neurons of FALS mice are not associated with apoptosis or with changes in cytochrome oxidase histochemical reactivity. *Journal of the Neurological Sciences*, 191(1–2), 25–33. [https://doi.org/10.1016/S0022-510X\(01\)00627-X](https://doi.org/10.1016/S0022-510X(01)00627-X)
- Benedetti, L., Ghilardi, A., Rottoli, E., De Maglie, M., Prosperi, L., Perego, C., Baruscotti, M., Bucchi, A., Del Giacco, L., & Francolini, M. (2016). INaP selective inhibition reverts precocious inter- and motoneurons hyperexcitability in the Sod1-G93R zebrafish ALS model. *Scientific Reports*, 6(1), 24515. <https://doi.org/10.1038/srep24515>
- Berg, A., Zelano, J., Stephan, A., Thams, S., Barres, B. A., Pekny, M., Pekna, M., & Cullheim, S. (2012). Reduced removal of synaptic terminals from axotomized spinal motoneurons in the absence of complement C3. *Experimental Neurology*, 237(1), 8–17. <https://doi.org/10.1016/j.expneurol.2012.06.008>
- Bernard-Marissal, N., Médard, J.-J., Azzedine, H., & Chrast, R. (2015). Dysfunction in endoplasmic reticulum-mitochondria crosstalk underlies SIGMAR1 loss of function mediated motor neuron degeneration. *Brain*, 138(4), 875–890. <https://doi.org/10.1093/brain/awv008>

- Bernstein, J. J., & Bernstein, M. E. (1976). Ventral horn synaptology in the rat. *Journal of Neurocytology*, 5(1), 109–123. <https://doi.org/10.1007/BF01176185>
- Beynon, S. B., & Walker, F. R. (2012). Microglial activation in the injured and healthy brain: What are we really talking about? Practical and theoretical issues associated with the measurement of changes in microglial morphology. *Neuroscience*, 225, 162–171. <https://doi.org/10.1016/j.neuroscience.2012.07.029>
- Birchmeier, C., & Nave, K.-A. (2008). Neuregulin-1, a key axonal signal that drives Schwann cell growth and differentiation. *Glia*, 56(14), 1491–1497. <https://doi.org/10.1002/glia.20753>
- Blinzinger, K., & Kreutzberg, G. (1968). Displacement of synaptic terminals from regenerating motoneurons by microglial cells. *Zeitschrift Für Zellforschung Und Mikroskopische Anatomie*, 85(2), 145–157. <https://doi.org/10.1007/BF00325030>
- Block, M. L., Zecca, L., & Hong, J.-S. (2007). Microglia-mediated neurotoxicity: uncovering the molecular mechanisms. *Nature Reviews Neuroscience*, 8(1), 57–69. <https://doi.org/10.1038/nrn2038>
- Bodian, D. (1970). An electron microscopic characterization of classes of synaptic vesicles by means of controlled aldehyde fixation. *Journal of Cell Biology*, 44(1), 115–124. <https://doi.org/10.1083/jcb.44.1.115>
- Bogdanov, M., Brown, R. H., Matson, W., Smart, R., Hayden, D., O'Donnell, H., Flint Beal, M., & Cudkowicz, M. (2000). Increased oxidative damage to DNA in ALS patients. *Free Radical Biology and Medicine*, 29(7), 652–658. [https://doi.org/10.1016/S0891-5849\(00\)00349-X](https://doi.org/10.1016/S0891-5849(00)00349-X)
- Boillée, S., Vande Velde, C., & Cleveland, D. W. (2006). ALS: A Disease of Motor Neurons and Their Nonneuronal Neighbors. *Neuron*, 52(1), 39–59. <https://doi.org/10.1016/j.neuron.2006.09.018>
- Bosco, D. A., Morfini, G., Karabacak, N. M., Song, Y., Gros-Louis, F., Pasinelli, P., Goolsby, H., Fontaine, B. A., Lemay, N., McKenna-Yasek, D., Frosch, M. P., Agar, J. N., Julien, J., Brady, S. T., & Brown, R. H. (2010). Wild-type and mutant SOD1 share an aberrant conformation and a common pathogenic pathway in ALS. *Nature Neuroscience*, 13(11), 1396–1403. <https://doi.org/10.1038/nn.2660>
- Braakman, I., & Bulleid, N. J. (2011). Protein Folding and Modification in the Mammalian Endoplasmic Reticulum. *Annual Review of Biochemistry*, 80(1), 71–99. <https://doi.org/10.1146/annurev-biochem-062209-093836>
- Brännström, T., & Kellerth, J.-O. (1998). Changes in synaptology of adult cat spinal α-motoneurons after axotomy. *Experimental Brain Research*, 118(1), 1–13. <https://doi.org/10.1007/s002210050249>

- Brettschneider, J., Toledo, J. B., Van Deerlin, V. M., Elman, L., McCluskey, L., Lee, V. M. Y., & Trojanowski, J. Q. (2012). Microglial Activation Correlates with Disease Progression and Upper Motor Neuron Clinical Symptoms in Amyotrophic Lateral Sclerosis. *PLoS ONE*, 7(6), e39216. <https://doi.org/10.1371/journal.pone.0039216>
- Breuer, A. C., Lynn, M. P., Atkinson, M. B., Chou, S. M., Wilbourn, A. J., Marks, K. E., Culver, J. E., & Fleegler, E. J. (1987). Fast axonal transport in amyotrophic lateral sclerosis: An intra-axonal organelle traffic analysis. *Neurology*, 37(5), 738–738. <https://doi.org/10.1212/WNL.37.5.738>
- Brites, D., & Vaz, A. R. (2014). Microglia centered pathogenesis in ALS: insights in cell interconnectivity. *Frontiers in Cellular Neuroscience*, 8(MAY), 1–24. <https://doi.org/10.3389/fncel.2014.00117>
- Brooks, B. R. (1994). El escorial World Federation of Neurology criteria for the diagnosis of amyotrophic lateral sclerosis. *Journal of the Neurological Sciences*, 124(Suppl.), 96–107. [https://doi.org/10.1016/0022-510X\(94\)90191-0](https://doi.org/10.1016/0022-510X(94)90191-0)
- Brotherton, T. E., Li, Y., Cooper, D., Gearing, M., Julien, J.-P., Rothstein, J. D., Boylan, K., & Glass, J. D. (2012). Localization of a toxic form of superoxide dismutase 1 protein to pathologically affected tissues in familial ALS. *Proceedings of the National Academy of Sciences*, 109(14), 5505–5510. <https://doi.org/10.1073/pnas.1115009109>
- Buonanno, A., & Fischbach, G. D. (2001). Neuregulin and ErbB receptor signaling pathways in the nervous system. *Current Opinion in Neurobiology*, 11(3), 287–296. [https://doi.org/10.1016/S0959-4388\(00\)00210-5](https://doi.org/10.1016/S0959-4388(00)00210-5)
- Burkholder, T., Foltz, C., Karlsson, E., Linton, C. G., & Smith, J. M. (2012). Health Evaluation of Experimental Laboratory Mice. *Current Protocols in Mouse Biology*, 2(2), 145–165. <https://doi.org/10.1002/9780470942390.mo110217>
- Cabon, L., Martinez-Torres, A.-C., & Susin, S. A. (2013). La mort cellulaire programmée ne manque pas de vocabulaire. *Médecine/Sciences*, 29(12), 1117–1124. <https://doi.org/10.1051/medsci/20132912015>
- Calderó, J., Ciutat, D., Lladó, J., Castán, E., Oppenheim, R. W., & Esquerda, J. E. (1997). Effects of excitatory amino acids on neuromuscular development in the chick embryo. *The Journal of Comparative Neurology*, 387(1), 73–95. [https://doi.org/10.1002/\(SICI\)1096-9861\(19971013\)387:1<73::AID-CNE7>3.3.CO;2-G](https://doi.org/10.1002/(SICI)1096-9861(19971013)387:1<73::AID-CNE7>3.3.CO;2-G)
- Caleo, M., Spinelli, M., Colosimo, F., Mata, I., Rossetto, O., Lackovic, Z., & Restani, L. (2018). Transsynaptic Action of Botulinum Neurotoxin Type A at Central Cholinergic Boutons. *The Journal of Neuroscience*, 38(48), 10329–10337. <https://doi.org/10.1523/JNEUROSCI.0294-18.2018>
- Calvo, M., & Bennett, D. L. H. (2012). The mechanisms of microgliosis and pain following peripheral nerve injury. *Experimental Neurology*, 234(2), 271–282. <https://doi.org/10.1016/j.expneurol.2011.08.018>

- Calvo, M., Zhu, N., Grist, J., Ma, Z., Loeb, J. A., & Bennett, D. L. H. (2011). Following nerve injury neuregulin-1 drives microglial proliferation and neuropathic pain via the MEK/ERK pathway. *Glia*, 59(4), 554–568. <https://doi.org/10.1002/glia.21124>
- Calvo, M., Zhu, N., Tsantoulas, C., Ma, Z., Grist, J., Loeb, J. A., & Bennett, D. L. H. (2010). Neuregulin-ErbB Signaling Promotes Microglial Proliferation and Chemotaxis Contributing to Microgliosis and Pain after Peripheral Nerve Injury. *Journal of Neuroscience*, 30(15), 5437–5450. <https://doi.org/10.1523/JNEUROSCI.5169-09.2010>
- Cappella, M., Ciotti, C., Cohen-Tannoudji, M., & Bifari, M. G. (2019). Gene Therapy for ALS — A Perspective. *International Journal of Molecular Sciences*, 20.
- Chan, D. C. (2012). Fusion and Fission: Interlinked Processes Critical for Mitochondrial Health. *Annual Review of Genetics*, 46(1), 265–287. <https://doi.org/10.1146/annurev-genet-110410-132529>
- Chang, J.-C., Hazelett, D. J., Stewart, J. A., & Morton, D. B. (2014). Motor neuron expression of the voltage-gated calcium channel cacophony restores locomotion defects in a Drosophila, TDP-43 loss of function model of ALS. *Brain Research*, 1584(1), 39–51. <https://doi.org/10.1016/j.brainres.2013.11.019>
- Chang, Y., Kong, Q., Shan, X., Tian, G., Ilieva, H., Cleveland, D. W., Rothstein, J. D., Borchelt, D. R., Wong, P. C., & Lin, C. G. (2008). Messenger RNA Oxidation Occurs Early in Disease Pathogenesis and Promotes Motor Neuron Degeneration in ALS. *PLoS ONE*, 3(8), e2849. <https://doi.org/10.1371/journal.pone.0002849>
- Chen, A.-Q., Fang, Z., Chen, X.-L., Yang, S., Zhou, Y.-F., Mao, L., Xia, Y.-P., Jin, H.-J., Li, Y.-N., You, M.-F., Wang, X.-X., Lei, H., He, Q.-W., & Hu, B. (2019). Microglia-derived TNF- α mediates endothelial necroptosis aggravating blood brain-barrier disruption after ischemic stroke. *Cell Death & Disease*, 10(7), 487. <https://doi.org/10.1038/s41419-019-1716-9>
- Chen, S., Zhang, X., Song, L., & Le, W. (2012). Autophagy Dysregulation in Amyotrophic Lateral Sclerosis. *Brain Pathology*, 22(1), 110–116. <https://doi.org/10.1111/j.1750-3639.2011.00546.x>
- Cheroni, C., Marino, M., Tortarolo, M., Veglianese, P., De Biasi, S., Fontana, E., Zuccarello, L. V., Maynard, C. J., Dantuma, N. P., & Bendotti, C. (2009). Functional alterations of the ubiquitin-proteasome system in motor neurons of a mouse model of familial amyotrophic lateral sclerosis. *Human Molecular Genetics*, 18(1), 82–96. <https://doi.org/10.1093/hmg/ddn319>
- Chéry, N., Yu, X. H., & De Koninck, Y. (2000). Visualization of lamina I of the dorsal horn in live adult rat spinal cord slices. *Journal of Neuroscience Methods*, 96(2), 133–142. [https://doi.org/10.1016/S0165-0270\(99\)00195-8](https://doi.org/10.1016/S0165-0270(99)00195-8)
- Chi, I. M., Chen, A., Zheng, Y., Kosaras, B., Tsiftsoglou, S. A., Vartanian, T. K., Brown, R. H., & Carroll, M. C. (2008). T lymphocytes potentiate endogenous neuroprotective inflammation in a mouse model of ALS. *Proceedings of the National Academy of Sciences*, 105(46), 17913–17918. <https://doi.org/10.1073/pnas.0804610105>

- Cho, Y., Challa, S., Moquin, D., Genga, R., Ray, T. D., Guildford, M., & Chan, F. K.-M. (2009). Phosphorylation-Driven Assembly of the RIP1-RIP3 Complex Regulates Programmed Necrosis and Virus-Induced Inflammation. *Cell*, 137(6), 1112–1123. <https://doi.org/10.1016/j.cell.2009.05.037>
- Christofferson, D. E., Li, Y., & Yuan, J. (2014). Control of Life-or-Death Decisions by RIP1 Kinase. *Annual Review of Physiology*, 76(1), 129–150. <https://doi.org/10.1146/annurev-physiol-021113-170259>
- Ciechanover, A., & Brundin, P. (2003). The ubiquitin proteasome system in neurodegenerative diseases: sometimes the chicken, sometimes the egg. *Neuron*, 40, 427–446.
- Ciechanover, A., & Kwon, Y. T. a. (2015). Degradation of misfolded proteins in neurodegenerative diseases: therapeutic targets and strategies. *Experimental & Molecular Medicine*, 47(3), e147–e147. <https://doi.org/10.1038/emm.2014.117>
- Clarke, B. E., & Patani, R. (2020). The microglial component of amyotrophic lateral sclerosis. *Brain*, 143(12), 3526–3539. <https://doi.org/10.1093/brain/awaa309>
- Clarke, P. G., & Oppenheim, R. W. (1995). Neuron death in vertebrate development: in vitro methods. *Methods in Cell Biology*, 46, 277–321.
- Clement, A. M., Nguyen, M. D., Roberts, E. A., Garcia, M. L., Boillée, S., Rule, M., McMahon, A. P., Doucette, W., Siwek, D., Ferrante, R. J., Brown Jr., R. H., Julien, J.-P., Goldstein, L. S. B., & Cleveland, D. W. (2003). Wild-Type Nonneuronal Cells Extend Survival of SOD1 Mutant Motor Neurons in ALS Mice. *Science*, 302(5642), 113–117. <https://doi.org/10.1126/science.1086071>
- Conradi, S., & Skoglund, S. (1969). Observations on the ultrastructure and distribution of neuronal and glial elements on the motoneuron surface in the lumbosacral spinal cord of the cat during postnatal development. *Acta Physiologica Scandinavica. Supplementum*, 333, 5–52. <http://www.ncbi.nlm.nih.gov/pubmed/5386538>
- Cooper-Knock, J., Kirby, J., Ferraiuolo, L., Heath, P. R., Rattray, M., & Shaw, P. J. (2012). Gene expression profiling in human neurodegenerative disease. *Nature Reviews Neurology*, 8(9), 518–530. <https://doi.org/10.1038/nrneurol.2012.156>
- Corcia, P., Tauber, C., Vercoullie, J., Arlicot, N., Prunier, C., Praline, J., Nicolas, G., Venel, Y., Hommet, C., Baulieu, J.-L., Cottier, J.-P., Roussel, C., Kassiou, M., Guilloteau, D., & Ribeiro, M.-J. (2012). Molecular Imaging of Microglial Activation in Amyotrophic Lateral Sclerosis. *PLoS ONE*, 7(12), e52941. <https://doi.org/10.1371/journal.pone.0052941>
- Cornaglia, M., Krishnamani, G., Mouchiroud, L., Sorrentino, V., Lehnert, T., Auwerx, J., & Gijs, M. A. M. (2016). Automated longitudinal monitoring of in vivo protein aggregation in neurodegenerative disease C. elegans models. *Molecular Neurodegeneration*, 11(1), 17. <https://doi.org/10.1186/s13024-016-0083-6>

- Crippa, V., Sau, D., Rusmini, P., Boncoraglio, A., Onesto, E., Bolzoni, E., Galbiati, M., Fontana, E., Marino, M., Carra, S., Bendotti, C., De Biasi, S., & Poletti, A. (2010). The small heat shock protein B8 (HspB8) promotes autophagic removal of misfolded proteins involved in amyotrophic lateral sclerosis (ALS). *Human Molecular Genetics*, 19(17), 3440–3456. <https://doi.org/10.1093/hmg/ddq257>
- Cui, H., Kong, Y., & Zhang, H. (2012). Oxidative Stress, Mitochondrial Dysfunction, and Aging. *Journal of Signal Transduction*, 2012, 1–13. <https://doi.org/10.1155/2012/646354>
- Cullheim, S., & Thams, S. (2007). The microglial networks of the brain and their role in neuronal network plasticity after lesion. *Brain Research Reviews*, 55(1), 89–96. <https://doi.org/10.1016/j.brainresrev.2007.03.012>
- Cusack, C. L., Swahari, V., Hampton Henley, W., Michael Ramsey, J., & Deshmukh, M. (2013). Distinct pathways mediate axon degeneration during apoptosis and axon-specific pruning. *Nature Communications*, 4(1), 1876. <https://doi.org/10.1038/ncomms2910>
- D'Acunzo, P., Pérez-González, R., Kim, Y., Hargash, T., Miller, C., Alldred, M. J., Erdjument-Bromage, H., Penikalapati, S. C., Pawlik, M., Saito, M., Saito, M., Ginsberg, S. D., Neubert, T. A., Goulbourne, C. N., & Levy, E. (2021). Mitovesicles are a novel population of extracellular vesicles of mitochondrial origin altered in Down syndrome. *Science Advances*, 7(7), eabe5085. <https://doi.org/10.1126/sciadv.abe5085>
- D'Erchia, A. M., Gallo, A., Manzari, C., Raho, S., Horner, D. S., Chiara, M., Valletti, A., Aiello, I., Mastropasqua, F., Ciaccia, L., Locatelli, F., Pisani, F., Nicchia, G. P., Svelto, M., Pesole, G., & Picardi, E. (2017). Massive transcriptome sequencing of human spinal cord tissues provides new insights into motor neuron degeneration in ALS. *Scientific Reports*, 7(1), 10046. <https://doi.org/10.1038/s41598-017-10488-7>
- Da Costa, M. M. J., Allen, C. E., Higginbottom, A., Ramesh, T., Shaw, P. J., & McDermott, C. J. (2013). A new zebrafish model produced by TILLING of SOD1-related amyotrophic lateral sclerosis replicates key features of the disease and represents a tool for in vivo therapeutic screening. *Disease Models & Mechanisms*, 7(1), 73–81. <https://doi.org/10.1242/dmm.012013>
- Dal Canto, M. C., & Gurney, M. E. (1994). Development of central nervous system pathology in a murine transgenic model of human amyotrophic lateral sclerosis. *American Journal of Pathology*, 145(6), 1271–1279.
- Damiano, M., Starkov, A. A., Petri, S., Kipiani, K., Kiaei, M., Mattiazzi, M., Flint Beal, M., & Manfredi, G. (2006). Neural mitochondrial Ca²⁺ capacity impairment precedes the onset of motor symptoms in G93A Cu/Zn-superoxide dismutase mutant mice. *Journal of Neurochemistry*, 96(5), 1349–1361. <https://doi.org/10.1111/j.1471-4159.2006.03619.x>

- Dayton, R. D., Gitcho, M. A., Orchard, E. A., Wilson, J. D., Wang, D. B., Cain, C. D., Johnson, J. A., Zhang, Y.-J., Petrucelli, L., Mathis, J. M., & Klein, R. L. (2013). Selective Forelimb Impairment in Rats Expressing a Pathological TDP-43 25 kDa C-terminal Fragment to Mimic Amyotrophic Lateral Sclerosis. *Molecular Therapy*, 21(7), 1324–1334. <https://doi.org/10.1038/mt.2013.88>
- de Sevilla, D. F., Nunez, A., Borde, M., Malinow, R., & Buno, W. (2008). Cholinergic-Mediated IP3-Receptor Activation Induces Long-Lasting Synaptic Enhancement in CA1 Pyramidal Neurons. *Journal of Neuroscience*, 28(6), 1469–1478. <https://doi.org/10.1523/JNEUROSCI.2723-07.2008>
- De Vos, K. J., Chapman, A. L., Tenant, M. E., Manser, C., Tudor, E. L., Lau, K.-F., Brownlees, J., Ackerley, S., Shaw, P. J., McLoughlin, D. M., Shaw, C. E., Leigh, P. N., Miller, C. C. J., & Grierson, A. J. (2007). Familial amyotrophic lateral sclerosis-linked SOD1 mutants perturb fast axonal transport to reduce axonal mitochondria content. *Human Molecular Genetics*, 16(22), 2720–2728. <https://doi.org/10.1093/hmg/ddm226>
- Deardorff, A. S., Romer, S. H., Deng, Z., Bullinger, K. L., Nardelli, P., Cope, T. C., & Fyffe, R. E. W. (2013). Expression of postsynaptic Ca²⁺-activated K⁺ (SK) channels at C-bouton synapses in mammalian lumbar α-motoneurons. *The Journal of Physiology*, 591(4), 875–897. <https://doi.org/10.1113/jphysiol.2012.240879>
- Deardorff, A. S., Romer, S. H., Sonner, P. M., & Fyffe, R. E. W. (2014). Swimming against the tide: Investigations of the C-bouton synapse. *Frontiers in Neural Circuits*, 8(September), 1–17. <https://doi.org/10.3389/fncir.2014.00106>
- DeJesus-Hernandez, M., Mackenzie, I. R., Boeve, B. F., Boxer, A. L., Baker, M., Rutherford, N. J., Nicholson, A. M., Finch, N. A., Flynn, H., Adamson, J., Kouri, N., Wojtas, A., Sengdy, P., Hsiung, G.-Y. R., Karydas, A., Seeley, W. W., Josephs, K. A., Coppola, G., Geschwind, D. H., ... Rademakers, R. (2011). Expanded GGGGCC Hexanucleotide Repeat in Noncoding Region of C9ORF72 Causes Chromosome 9p-Linked FTD and ALS. *Neuron*, 72(2), 245–256. <https://doi.org/10.1016/j.neuron.2011.09.011>
- Delestrée, N., Manuel, M., Iglesias, C., Elbasiouny, S. M., Heckman, C. J., & Zytnicki, D. (2014). Adult spinal motoneurones are not hyperexcitable in a mouse model of inherited amyotrophic lateral sclerosis. *The Journal of Physiology*, 592(7), 1687–1703. <https://doi.org/10.1113/jphysiol.2013.265843>
- Dermentzaki, G., Politis, K. A., Lu, L., Mishra, V., Pérez-Torres, E. J., Sosunov, A. A., McKhann, G. M., Lotti, F., Shneider, N. A., & Przedborski, S. (2019). Deletion of Ripk3 Prevents Motor Neuron Death In Vitro but not In Vivo. *Eneuro*, 6(1), ENEURO.0308-18.2018. <https://doi.org/10.1523/ENEURO.0308-18.2018>
- Destombes, J., Horcholle-Bossavit, G., & Thiesson, D. (1992). Distribution of glycinergic terminals on lumbar motoneurons of the adult cat: an ultrastructural study. *Brain Research*, 599(2), 353–360. [https://doi.org/10.1016/0006-8993\(92\)90412-3](https://doi.org/10.1016/0006-8993(92)90412-3)
- Deutsch, E., Weigel, A. V., Akin, E. J., Fox, P., Hansen, G., Haberkorn, C. J., Loftus, R., Krapf, D., & Tamkun, M. M. (2012). Kv2.1 cell surface clusters are insertion platforms for ion channel

delivery to the plasma membrane. *Molecular Biology of the Cell*, 23(15), 2917–2929. <https://doi.org/10.1091/mbc.e12-01-0047>

Di Giorgio, F. P., Boulting, G. L., Bobrowicz, S., & Eggan, K. C. (2008). Human Embryonic Stem Cell-Derived Motor Neurons Are Sensitive to the Toxic Effect of Glial Cells Carrying an ALS-Causing Mutation. *Cell Stem Cell*, 3(6), 637–648. <https://doi.org/10.1016/j.stem.2008.09.017>

Doble, A. (1996). The pharmacology and mechanism of action of riluzole. *Neurology*, 47(Issue 6, Supplement 4), 233S-241S. https://doi.org/10.1212/WNL.47.6_Suppl_4.233S

Dols-Icardo, O., Montal, V., Sirisi, S., López-Pernas, G., Cervera-Carles, L., Querol-Vilaseca, M., Muñoz, L., Belbin, O., Alcolea, D., Molina-Porcel, L., Pegueroles, J., Turón-Sans, J., Blesa, R., Lleó, A., Fortea, J., Rojas-García, R., & Clarimón, J. (2020). Motor cortex transcriptome reveals microglial key events in amyotrophic lateral sclerosis. *Neurology: Neuroimmunology Neuroinflammation*, 7(5), e829. <https://doi.org/10.1212/NXI.0000000000000829>

Dominguez, S., Varfolomeev, E., Brendza, R., Stark, K., Tea, J., Imperio, J., Ngu, H., Earr, T., Foreman, O., Webster, J. D., Easton, A., Vucic, D., & Bingol, B. (2021). Genetic inactivation of RIP1 kinase does not ameliorate disease in a mouse model of ALS. *Cell Death & Differentiation*, 28(3), 915–931. <https://doi.org/10.1038/s41418-020-00625-7>

Dopfer, E. P., Minguet, S., & Schamel, W. W. A. (2011). A New Vampire Saga: The Molecular Mechanism of T Cell Trogocytosis. *Immunity*, 35(2), 151–153. <https://doi.org/10.1016/j.immuni.2011.08.004>

Duchen, L. W., & Tonge, D. A. (1973). The effects of tetanus toxin on neuromuscular transmission and on the morphology of motor end-plates in slow and fast skeletal muscle of the mouse. *The Journal of Physiology*, 228(1), 157–172. <https://doi.org/10.1113/jphysiol.1973.sp010078>

E. Burke; D. Levine; P. Tsairis; Zajac, F. E. (1973). PHYSIOLOGICAL TYPES AND HISTOCHEMICAL PROFILES IN MOTOR UNITS OF THE CAT GASTROCNEMIUS. *J Physiol*, 234, 723–748.

Elmore, M. R. P., Najafi, A. R., Koike, M. A., Dagher, N. N., Spangenberg, E. E., Rice, R. A., Kitazawa, M., Matusow, B., Nguyen, H., West, B. L., & Green, K. N. (2014). Colony-Stimulating Factor 1 Receptor Signaling Is Necessary for Microglia Viability, Unmasking a Microglia Progenitor Cell in the Adult Brain. *Neuron*, 82(2), 380–397. <https://doi.org/10.1016/j.neuron.2014.02.040>

Engelhardt, J. I., & Appel, S. H. (1990). IgG Reactivity in the Spinal Cord and Motor Cortex in Amyotrophic Lateral Sclerosis. *Archives of Neurology*, 47(11), 1210–1216. <https://doi.org/10.1001/archneur.1990.00530110068019>

Esquerda, J. E. (2006). Esclerosis Lateral Amiotrófica. *Mente y Cerebro*, 17, 83–92.

Falls, D. (2003). Neuregulins: functions, forms, and signaling strategies. *Experimental Cell Research*, 284(1), 14–30. [https://doi.org/10.1016/S0014-4827\(02\)00102-7](https://doi.org/10.1016/S0014-4827(02)00102-7)

- Falls, D., Rosen, K. M., Corfas, G., Lane, W. S., & Fischbach, G. D. (1993). ARIA, a protein that stimulates acetylcholine receptor synthesis, is a member of the neu ligand family. *Cell*, 72(5), 801–815. [https://doi.org/10.1016/0092-8674\(93\)90407-H](https://doi.org/10.1016/0092-8674(93)90407-H)
- Fawcett, J. W., Oohashi, T., & Pizzorusso, T. (2019). The roles of perineuronal nets and the perinodal extracellular matrix in neuronal function. *Nature Reviews Neuroscience*, 20(8), 451–465. <https://doi.org/10.1038/s41583-019-0196-3>
- Ferraiuolo, L., Heath, P. R., Holden, H., Kasher, P., Kirby, J., & Shaw, P. J. (2007). Microarray Analysis of the Cellular Pathways Involved in the Adaptation to and Progression of Motor Neuron Injury in the SOD1 G93A Mouse Model of Familial ALS. *Journal of Neuroscience*, 27(34), 9201–9219. <https://doi.org/10.1523/JNEUROSCI.1470-07.2007>
- Ferraiuolo, L., Kirby, J., Grierson, A. J., Sendtner, M., & Shaw, P. J. (2011). Molecular pathways of motor neuron injury in amyotrophic lateral sclerosis. *Nature Reviews Neurology*, 7(11), 616–630. <https://doi.org/10.1038/nrneurol.2011.152>
- Ferraiuolo, L., Meyer, K., Sherwood, T. W., Vick, J., Likhite, S., Frakes, A., Miranda, C. J., Braun, L., Heath, P. R., Pineda, R., Beattie, C. E., Shaw, P. J., Askwith, C. C., McTigue, D., & Kaspar, B. K. (2016). Oligodendrocytes contribute to motor neuron death in ALS via SOD1-dependent mechanism. *Proceedings of the National Academy of Sciences of the United States of America*, 113(42), E6496–E6505. <https://doi.org/10.1073/pnas.1607496113>
- Ferrara, D., Pasetto, L., Bonetto, V., & Basso, M. (2018). Role of Extracellular Vesicles in Amyotrophic Lateral Sclerosis. *Frontiers in Neuroscience*, 12(AUG), 1–9. <https://doi.org/10.3389/fnins.2018.00574>
- Fink, S. L., & Cookson, B. T. (2005). Apoptosis, Pyroptosis, and Necrosis: Mechanistic Description of Dead and Dying Eukaryotic Cells. *Infection and Immunity*, 73(4), 1907–1916. <https://doi.org/10.1128/IAI.73.4.1907-1916.2005>
- Fischer, L. R., Culver, D. G., Tennant, P., Davis, A. A., Wang, M., Castellano-Sanchez, A., Khan, J., Polak, M. A., & Glass, J. D. (2004). Amyotrophic lateral sclerosis is a distal axonopathy: evidence in mice and man. *Experimental Neurology*, 185(2), 232–240. <https://doi.org/10.1016/j.expneurol.2003.10.004>
- Fogarty, M. (2019). Amyotrophic lateral sclerosis as a synaptopathy. *Neural Regeneration Research*, 14(2), 189. <https://doi.org/10.4103/1673-5374.244782>
- Fontana, F., Raimondi, M., Marzagalli, M., Di Domizio, A., & Limonta, P. (2020). The emerging role of paraptosis in tumor cell biology: Perspectives for cancer prevention and therapy with natural compounds. *Biochimica et Biophysica Acta (BBA) - Reviews on Cancer*, 1873(2), 188338. <https://doi.org/10.1016/j.bbcan.2020.188338>
- Foran, E., & Trott, D. (2009). Glutamate Transporters and the Excitotoxic Path to Motor Neuron Degeneration in Amyotrophic Lateral Sclerosis. *Antioxidants & Redox Signaling*, 11(7), 1587–1602. <https://doi.org/10.1089/ars.2009.2444>

Fox, P. D., Loftus, R. J., & Tamkun, M. M. (2013). Regulation of Kv2.1 K⁺ Conductance by Cell Surface Channel Density. *Journal of Neuroscience*, 33(3), 1259–1270. <https://doi.org/10.1523/JNEUROSCI.3008-12.2013>

Frank, E. (2009). A New Class of Spinal Interneurons: The Origin and Function of C Boutons Is Solved. *Neuron*, 64(5), 593–595. <https://doi.org/10.1016/j.neuron.2009.11.030>

Gallart-Palau, X., Tarabal, O., Casanovas, A., Sábado, J., Correa, F. J., Hereu, M., Piedrafita, L., Calderó, J., & Esquerda, J. E. (2014). Neuregulin-1 is concentrated in the postsynaptic subsurface cistern of C-bouton inputs to α-motoneurons and altered during motoneuron diseases. *The FASEB Journal*, 28(8), 3618–3632. <https://doi.org/10.1096/fj.13-248583>

Galvan, M. D., Greenlee-Wacker, M. C., & Bohlson, S. S. (2012). C1q and phagocytosis: the perfect complement to a good meal. *Journal of Leukocyte Biology*, 92(3), 489–497. <https://doi.org/10.1189/jlb.0212099>

Gamez, J., Corbera-Bellalta, M., Nogales, G., Raguer, N., García-Arumí, E., Badia-Canto, M., Lladó-Carbó, E., & Álvarez-Sabín, J. (2006). Mutational analysis of the Cu/Zn superoxide dismutase gene in a Catalan ALS population: Should all sporadic ALS cases also be screened for SOD1? *Journal of the Neurological Sciences*, 247(1), 21–28. <https://doi.org/10.1016/j.jns.2006.03.006>

Geloso, M. C., Corvino, V., Marchese, E., Serrano, A., Michetti, F., & D'Ambrosi, N. (2017). The Dual Role of Microglia in ALS: Mechanisms and Therapeutic Approaches. *Frontiers in Aging Neuroscience*, 9(JUL). <https://doi.org/10.3389/fnagi.2017.00242>

Geracitano, R., Paolucci, E., Prisco, S., Guatteo, E., Zona, C., Longone, P., Ammassari-Teule, M., Bernardi, G., Berretta, N., & Mercuri, N. . (2003). Altered long-term corticostriatal synaptic plasticity in transgenic mice overexpressing human CU/ZN superoxide dismutase (GLY93→ALA) mutation. *Neuroscience*, 118(2), 399–408. [https://doi.org/10.1016/S0306-4522\(02\)00809-6](https://doi.org/10.1016/S0306-4522(02)00809-6)

Giordano, F., Saheki, Y., Idevall-Hagren, O., Colombo, S. F., Pirruccello, M., Milosevic, I., Gracheva, E. O., Bagriantsev, S. N., Borgese, N., & De Camilli, P. (2013). PI(4,5)P2-Dependent and Ca²⁺-Regulated ER-PM Interactions Mediated by the Extended Synaptotagmins. *Cell*, 153(7), 1494–1509. <https://doi.org/10.1016/j.cell.2013.05.026>

Gois, A. M., Mendonça, D. M. F., Freire, M. A. M., & Santos, J. R. (2020). IN VITRO AND IN VIVO MODELS OF AMYOTROPHIC LATERAL SCLEROSIS: AN UPDATED OVERVIEW. *Brain Research Bulletin*, 159(November 2019), 32–43. <https://doi.org/10.1016/j.brainresbull.2020.03.012>

Gong, Y.-N., Guy, C., Olauson, H., Becker, J. U., Yang, M., Fitzgerald, P., Linkermann, A., & Green, D. R. (2017). ESCRT-III Acts Downstream of MLKL to Regulate Necroptotic Cell Death and Its Consequences. *Cell*, 169(2), 286-300.e16. <https://doi.org/10.1016/j.cell.2017.03.020>

Gowing, G., Philips, T., Van Wijmeersch, B., Audet, J.-N., Dewil, M., Van Den Bosch, L., Billiau, A. D., Robberecht, W., & Julien, J.-P. (2008). Ablation of Proliferating Microglia Does Not Affect Motor

- Neuron Degeneration in Amyotrophic Lateral Sclerosis Caused by Mutant Superoxide Dismutase. *Journal of Neuroscience*, 28(41), 10234–10244. <https://doi.org/10.1523/JNEUROSCI.3494-08.2008>
- Grad, L. I., Pokrishevsky, E., Silverman, J. M., & Cashman, N. R. (2014). Exosome-dependent and independent mechanisms are involved in prion-like transmission of propagated Cu/Zn superoxide dismutase misfolding. *Prion*, 8(5), 331–335. <https://doi.org/10.4161/19336896.2014.983398>
- Gravel, M., Béland, L.-C., Soucy, G., Abdelhamid, E., Rahimian, R., Gravel, C., & Kriz, J. (2016). IL-10 Controls Early Microglial Phenotypes and Disease Onset in ALS Caused by Misfolded Superoxide Dismutase 1. *The Journal of Neuroscience*, 36(3), 1031–1048. <https://doi.org/10.1523/JNEUROSCI.0854-15.2016>
- Griffin, J. W., & Watson, D. F. (1988). Axonal transport in neurological disease. *Annals of Neurology*, 23(1), 3–13. <https://doi.org/10.1002/ana.410230103>
- Günther, R., Suhr, M., Koch, J. C., Bähr, M., Lingor, P., & Tönges, L. (2012). Clinical Testing and Spinal Cord Removal in a Mouse Model for Amyotrophic Lateral Sclerosis (ALS). *Journal of Visualized Experiments*, 61, 4–7. <https://doi.org/10.3791/3936>
- Gupta, P. K., Prabhakar, S., Sharma, S., & Anand, A. (2011). Vascular endothelial growth factor-A (VEGF-A) and chemokine ligand-2 (CCL2) in amyotrophic lateral sclerosis (ALS) patients. *Journal of Neuroinflammation*, 8(1), 47. <https://doi.org/10.1186/1742-2094-8-47>
- Gurney, M. E., Pu, H., Arlene Y, C., Canto, M. C. D., Polchow, C. Y., Alexander, D. D., Caliendo, J., Hentati, A., Kwon, Y. W., Deng, H.-X., Chen, W., Zhai, P., Sufit, R. L., & Siddique, T. (1994). Motor neuron degeneration in mice that express a human Cu , Z. *Science*, 264, 1772–1775.
- Haidet-Phillips, A. M., Hester, M. E., Miranda, C. J., Meyer, K., Braun, L., Frakes, A., Song, S., Likhite, S., Murtha, M. J., Foust, K. D., Rao, M., Eagle, A., Kammesheidt, A., Christensen, A., Mendell, J. R., Burghes, A. H. M., & Kaspar, B. K. (2011). Astrocytes from familial and sporadic ALS patients are toxic to motor neurons. *Nature Biotechnology*, 29(9), 824–828. <https://doi.org/10.1038/nbt.1957>
- Haimann, C., Torri-Tarelli, F., Fesce, R., & Ceccarelli, B. (1985). Measurement of quantal secretion induced by ouabain and its correlation with depletion of synaptic vesicles. *The Journal of Cell Biology*, 101(5), 1953–1965. <https://doi.org/10.1083/jcb.101.5.1953>
- Hall, E. D., Oostveen, J. A., & Gurney, M. E. (1998). Relationship of microglial and astrocytic activation to disease onset and progression in a transgenic model of familial ALS. *Glia*, 23(3), 249–256. [https://doi.org/10.1002/\(sici\)1098-1133\(1998\)23:3<249::aid-glia1002>3.0.co;2-1](https://doi.org/10.1002/(sici)1098-1133(1998)23:3<249::aid-glia1002>3.0.co;2-1)
- Hayakawa, K., Esposito, E., Wang, X., Terasaki, Y., Liu, Y., Xing, C., Ji, X., & Lo, E. H. (2016). Transfer of mitochondria from astrocytes to neurons after stroke. *Nature*, 535(7613), 551–555.

<https://doi.org/10.1038/nature18928>

Hayashi, T., & Su, T.-P. (2007). Sigma-1 Receptor Chaperones at the ER- Mitochondrion Interface Regulate Ca²⁺ Signaling and Cell Survival. *Cell*, 131(3), 596–610. <https://doi.org/10.1016/j.cell.2007.08.036>

Hayashi, Y., Homma, K., & Ichijo, H. (2016). SOD1 in neurotoxicity and its controversial roles in SOD1 mutation-negative ALS. *Advances in Biological Regulation*, 60, 95–104. <https://doi.org/10.1016/j.jbior.2015.10.006>

He, S., Wang, L., Miao, L., Wang, T., Du, F., Zhao, L., & Wang, X. (2009). Receptor Interacting Protein Kinase-3 Determines Cellular Necrotic Response to TNF-α. *Cell*, 137(6), 1100–1111. <https://doi.org/10.1016/j.cell.2009.05.021>

Hellström, J., Oliveira, A. L. R., Meister, B., & Cullheim, S. (2003). Large cholinergic nerve terminals on subsets of motoneurons and their relation to muscarinic receptor type 2. *Journal of Comparative Neurology*, 460(4), 476–486. <https://doi.org/10.1002/cne.10648>

Hemler, M. E. (2005). Tetraspanin functions and associated microdomains. *Nature Reviews Molecular Cell Biology*, 6(10), 801–811. <https://doi.org/10.1038/nrm1736>

Henkel, J. S., Beers, D. R., Siklós, L., & Appel, S. H. (2006). The chemokine MCP-1 and the dendritic and myeloid cells it attracts are increased in the mSOD1 mouse model of ALS. *Molecular and Cellular Neuroscience*, 31(3), 427–437. <https://doi.org/10.1016/j.mcn.2005.10.016>

Henkel, J. S., Engelhardt, J. I., Siklós, L., Simpson, E. P., Kim, S. H., Pan, T., Goodman, J. C., Siddique, T., Beers, D. R., & Appel, S. H. (2004). Presence of dendritic cells, MCP-1, and activated microglia/macrophages in amyotrophic lateral sclerosis spinal cord tissue. *Annals of Neurology*, 55(2), 221–235. <https://doi.org/10.1002/ana.10805>

Hensley, K., Abdel-Moaty, H., Hunter, J., Mhatre, M., Mou, S., Nguyen, K., Potapova, T., Pye, Q. N., Qi, M., Rice, H., Stewart, C., Stroukoff, K., & West, M. (2006). Primary glia expressing the G93A-SOD1 mutation present a neuroinflammatory phenotype and provide a cellular system for studies of glial inflammation. *Journal of Neuroinflammation*, 3(1), 2. <https://doi.org/10.1186/1742-2094-3-2>

Hierro-Bujalance, C., Bacskai, B. J., & Garcia-Alloza, M. (2018). In Vivo Imaging of Microglia With Multiphoton Microscopy. *Frontiers in Aging Neuroscience*, 10(JUL), 1–14. <https://doi.org/10.3389/fnagi.2018.00218>

Higgins, C. M. J., Jung, C., & Xu, Z. (2003). ALS-associated mutant SOD1G93A causes mitochondrial vacuolation by expansion of the intermembrane space by involvement of SOD1 aggregation and peroxisomes. *BMC Neuroscience*, 4. <https://doi.org/10.1186/1471-2202-4-16>.

Hirano, A., Nakano, I., Kurland, L. T., Mulder, D. W., Holley, P. W., & Saccomanno, G. (1984). Fine Structural Study of Neurofibrillary Changes in a Family with Amyotrophic Lateral Sclerosis.

- Journal of Neuropathology and Experimental Neurology*, 43(5), 471–480.
<https://doi.org/10.1097/00005072-198409000-00002>
- Hirasawa, T., Ohsawa, K., Imai, Y., Ondo, Y., Akazawa, C., Uchino, S., & Kohsaka, S. (2005). Visualization of microglia in living tissues using Iba1-EGFP transgenic mice. *Journal of Neuroscience Research*, 81(3), 357–362. <https://doi.org/10.1002/jnr.20480>
- Hong, S., Beja-Glasser, V. F., Nfonoyim, B. M., Frouin, A., Li, S., Ramakrishnan, S., Merry, K. M., Shi, Q., Rosenthal, A., Barres, B. A., Lemere, C. A., Selkoe, D. J., & Stevens, B. (2016). Complement and microglia mediate early synapse loss in Alzheimer mouse models. *Science*, 352(6286), 712–716. <https://doi.org/10.1126/science.aad8373>
- Howland, D. S., Liu, J., She, Y., Goad, B., Maragakis, N. J., Kim, B., Erickson, J., Kulik, J., DeVito, L., Psaltis, G., DeGennaro, L. J., Cleveland, D. W., & Rothstein, J. D. (2002). Focal loss of the glutamate transporter EAAT2 in a transgenic rat model of SOD1 mutant-mediated amyotrophic lateral sclerosis (ALS). *Proceedings of the National Academy of Sciences*, 99(3), 1604–1609. <https://doi.org/10.1073/pnas.032539299>
- Huang, C., Tong, J., Bi, F., Zhou, H., & Xia, X.-G. (2012). Mutant TDP-43 in motor neurons promotes the onset and progression of ALS in rats. *Journal of Clinical Investigation*, 122(1), 107–118. <https://doi.org/10.1172/JCI59130>
- Hulisz, D. (2018). Amyotrophic lateral sclerosis: disease state overview. *The American Journal of Managed Care*, 24(15), S320–S326.
- Ilieva, H., Polymenidou, M., & Cleveland, D. W. (2009). Non-cell autonomous toxicity in neurodegenerative disorders: ALS and beyond. *Journal of Cell Biology*, 187(6), 761–772. <https://doi.org/10.1083/jcb.200908164>
- Israelson, A., Arbel, N., Da Cruz, S., Ilieva, H., Yamanaka, K., Shoshan-Barmatz, V., & Cleveland, D. W. (2010). Misfolded Mutant SOD1 Directly Inhibits VDAC1 Conductance in a Mouse Model of Inherited ALS. *Neuron*, 67(4), 575–587. <https://doi.org/10.1016/j.neuron.2010.07.019>
- Ito, Y., Ofengeim, D., Najafov, A., Das, S., Saberi, S., Li, Y., Hitomi, J., Zhu, H., Chen, H., Mayo, L., Geng, J., Amin, P., DeWitt, J. P., Mookhtiar, A. K., Florez, M., Ouchida, A. T., Fan, J., Pasparakis, M., Kelliher, M. A., ... Yuan, J. (2016). RIPK1 mediates axonal degeneration by promoting inflammation and necroptosis in ALS. *Science*, 353(6299), 603–608. <https://doi.org/10.1126/science.aaf6803>
- Jaarsma, D., Rognoni, F., van Duijn, W., Verspaget, H. W., Haasdijk, E. D., & Holstege, J. C. (2001). CuZn superoxide dismutase (SOD1) accumulates in vacuolated mitochondria in transgenic mice expressing amyotrophic lateral sclerosis-linked SOD1 mutations. *Acta Neuropathologica*, 102(4), 293–305. <https://doi.org/10.1007/s004010100399>
- Jha, M. K., Jo, M., Kim, J.-H., & Suk, K. (2019). Microglia-Astrocyte Crosstalk: An Intimate Molecular Conversation. *The Neuroscientist*, 25(3), 227–240. <https://doi.org/10.1177/1073858418783959>

- Jha, M. K., Lee, W.-H., & Suk, K. (2016). Functional polarization of neuroglia: Implications in neuroinflammation and neurological disorders. *Biochemical Pharmacology*, 103, 1–16. <https://doi.org/10.1016/j.bcp.2015.11.003>
- Jia, D.-P., Wang, S., Zhang, B.-C., & Fang, F. (2015). Paraptosis triggers mitochondrial pathway-mediated apoptosis in Alzheimer's disease. *Experimental and Therapeutic Medicine*, 10(2), 804–808. <https://doi.org/10.3892/etm.2015.2531>
- Jiao, J., Wang, Y., Ren, P., Sun, S., & Wu, M. (2020). Necrosulfonamide Ameliorates Neurological Impairment in Spinal Cord Injury by Improving Antioxidative Capacity. *Frontiers in Pharmacology*, 10(January), 1–13. <https://doi.org/10.3389/fphar.2019.01538>
- Johnston, J. A., Dalton, M. J., Gurney, M. E., & Kopito, R. R. (2000). Formation of high molecular weight complexes of mutant Cu,Zn-superoxide dismutase in a mouse model for familial amyotrophic lateral sclerosis. *Proceedings of the National Academy of Sciences*, 97(23), 12571–12576. <https://doi.org/10.1073/pnas.220417997>
- Jon, Lieff. 12.03.2012. Brain Electricity and the Mind. Human Brain. <https://jonlieffmd.com/blog/brain-electricity-and-the-mind>
- Joshi, A. U., Minhas, P. S., Liddelow, S. A., Haileselassie, B., Andreasson, K. I., Dorn, G. W., & Mochly-Rosen, D. (2019). Fragmented mitochondria released from microglia trigger A1 astrocytic response and propagate inflammatory neurodegeneration. *Nature Neuroscience*, 22(10), 1635–1648. <https://doi.org/10.1038/s41593-019-0486-0>
- Julien, J.-P. (1997). Neurofilaments and motor neuron disease. *Trends in Cell Biology*, 7(6), 243–249. [https://doi.org/10.1016/S0962-8924\(97\)01049-0](https://doi.org/10.1016/S0962-8924(97)01049-0)
- Kabashi, E., Bercier, V., Lissouba, A., Liao, M., Brustein, E., Rouleau, G. A., & Drapeau, P. (2011). FUS and TARDBP but Not SOD1 Interact in Genetic Models of Amyotrophic Lateral Sclerosis. *PLoS Genetics*, 7(8), e1002214. <https://doi.org/10.1371/journal.pgen.1002214>
- Kang, S. H., Li, Y., Fukaya, M., Lorenzini, I., Cleveland, D. W., Ostrow, L. W., Rothstein, J. D., & Bergles, D. E. (2013). Degeneration and impaired regeneration of gray matter oligodendrocytes in amyotrophic lateral sclerosis. *Nature Neuroscience*, 16(5), 571–579. <https://doi.org/10.1038/nn.3357>
- Kanning, K. C., Kaplan, A., & Henderson, C. E. (2010). Motor Neuron Diversity in Development and Disease. *Annual Review of Neuroscience*, 33(1), 409–440. <https://doi.org/10.1146/annurev.neuro.051508.135722>
- Kao, W.-T., Wang, Y., Kleinman, J. E., Lipska, B. K., Hyde, T. M., Weinberger, D. R., & Law, A. J. (2010). Common genetic variation in Neuregulin 3 (NRG3) influences risk for schizophrenia and impacts NRG3 expression in human brain. *Proceedings of the National Academy of Sciences*, 107(35), 15619–15624. <https://doi.org/10.1073/pnas.1005410107>
- Karl, T. (2013). Neuregulin 1: a prime candidate for research into gene-environment interactions in

- schizophrenia? Insights from genetic rodent models. *Frontiers in Behavioral Neuroscience*, 7(JUL), 1–8. <https://doi.org/10.3389/fnbeh.2013.00106>
- Kaufman, R. J. (2002). Orchestrating the unfolded protein response in health and disease. *Journal of Clinical Investigation*, 110(10), 1389–1398. <https://doi.org/10.1172/JCI0216886>
- Kawahara, Y., Ito, K., Sun, H., Aizawa, H., Kanazawa, I., & Kwak, S. (2004). RNA editing and death of motor neurons. *Nature*, 427(6977), 801–801. <https://doi.org/10.1038/427801a>
- Kawamata, T., Akiyama, H., Yamada, T., & McGeer, P. L. (1992). Immunologic reactions in amyotrophic lateral sclerosis brain and spinal cord tissue. *American Journal of Pathology*, 140(3), 691–707.
- Kerber, G., Streif, R., Schwaiger, F.-W., Kreutzberg, G. W., & Hager, G. (2003). Neuregulin-1 Isoforms Are Differentially Expressed in the Intact and Regenerating Adult Rat Nervous System. *Journal of Molecular Neuroscience*, 21(2), 149–166. <https://doi.org/10.1385/JMN:21:2:149>
- Kettenmann, H., Kirchhoff, F., & Verkhratsky, A. (2013). Microglia: New Roles for the Synaptic Stripper. *Neuron*, 77(1), 10–18. <https://doi.org/10.1016/j.neuron.2012.12.023>
- Kiernan, M. C., Vucic, S., Cheah, B. C., Turner, M. R., Eisen, A., Hardiman, O., Burrell, J. R., & Zoing, M. C. (2011). Amyotrophic lateral sclerosis. *The Lancet*, 377(9769), 942–955. [https://doi.org/10.1016/S0140-6736\(10\)61156-7](https://doi.org/10.1016/S0140-6736(10)61156-7)
- Kigerl, K. A., Gensel, J. C., Ankeny, D. P., Alexander, J. K., Donnelly, D. J., & Popovich, P. G. (2009). Identification of Two Distinct Macrophage Subsets with Divergent Effects Causing either Neurotoxicity or Regeneration in the Injured Mouse Spinal Cord. *Journal of Neuroscience*, 29(43), 13435–13444. <https://doi.org/10.1523/JNEUROSCI.3257-09.2009>
- Kim, E., Lee, D. M., Seo, M. J., Lee, H. J., & Choi, K. S. (2021). Intracellular Ca²⁺ Imbalance Critically Contributes to Paraptosis. *Frontiers in Cell and Developmental Biology*, 8(January). <https://doi.org/10.3389/fcell.2020.607844>
- Kim, G., Gautier, O., Tassoni-Tsuchida, E., Ma, X. R., & Gitler, A. D. (2020). ALS Genetics: Gains, Losses, and Implications for Future Therapies. *Neuron*, 108(5), 822–842. <https://doi.org/10.1016/j.neuron.2020.08.022>
- Kim, Y. S., Choi, D. H., Block, M. L., Lorenzl, S., Yang, L., Kim, Y. J., Sugama, S., Cho, B. P., Hwang, O., Browne, S. E., Kim, S. Y., Hong, J., Flint Beal, M., & Joh, T. H. (2007). A pivotal role of matrix metalloproteinase-3 activity in dopaminergic neuronal degeneration via microglial activation. *The FASEB Journal*, 21(1), 179–187. <https://doi.org/10.1096/fj.06-5865com>
- Kirby, J., Halligan, E., Baptista, M. J., Allen, S., Heath, P. R., Holden, H., Barber, S. C., Loynes, C. A., Wood-Allum, C. A., Lunec, J., & Shaw, P. J. (2005). Mutant SOD1 alters the motor neuronal transcriptome: implications for familial ALS. *Brain*, 128(7), 1686–1706. <https://doi.org/10.1093/brain/awh503>
- Kong, J., & Xu, Z. (1998). Massive Mitochondrial Degeneration in Motor Neurons Triggers the Onset

- of Amyotrophic Lateral Sclerosis in Mice Expressing a Mutant SOD1. *The Journal of Neuroscience*, 18(9), 3241–3250. <https://doi.org/10.1523/JNEUROSCI.18-09-03241.1998>
- Könnecke, H., & Bechmann, I. (2013). The Role of Microglia and Matrix Metalloproteinases Involvement in Neuroinflammation and Gliomas. *Clinical and Developmental Immunology*, 2013, 1–15. <https://doi.org/10.1155/2013/914104>
- Korkut, C., Ataman, B., Ramachandran, P., Ashley, J., Barria, R., Gherbesi, N., & Budnik, V. (2009). Trans-Synaptic Transmission of Vesicular Wnt Signals through Evi/Wntless. *Cell*, 139(2), 393–404. <https://doi.org/10.1016/j.cell.2009.07.051>
- Kowal, J., Arras, G., Colombo, M., Jouve, M., Morath, J. P., Primdal-Bengtson, B., Dingli, F., Loew, D., Tkach, M., & Théry, C. (2016). Proteomic comparison defines novel markers to characterize heterogeneous populations of extracellular vesicle subtypes. *Proceedings of the National Academy of Sciences*, 113(8), E968–E977. <https://doi.org/10.1073/pnas.1521230113>
- Kucharz, K., Krogh, M., Ng, A. N., & Toresson, H. (2009). NMDA Receptor Stimulation Induces Reversible Fission of the Neuronal Endoplasmic Reticulum. *PLoS ONE*, 4(4), e5250. <https://doi.org/10.1371/journal.pone.0005250>
- Kucharz, K., Wieloch, T., & Toresson, H. (2011). Potassium-induced structural changes of the endoplasmic reticulum in pyramidal neurons in murine organotypic hippocampal slices. *Journal of Neuroscience Research*, 89(8), 1150–1159. <https://doi.org/10.1002/jnr.22646>
- Kwiatkowski, T. J., Bosco, D. A., LeClerc, A. L., Tamrazian, E., Vanderburg, C. R., Russ, C., Davis, A., Gilchrist, J., Kasarskis, E. J., Munsat, T., Valdmanis, P., Rouleau, G. A., Hosler, B. A., Cortelli, P., de Jong, P. J., Yoshinaga, Y., Haines, J. L., Pericak-Vance, M. A., Yan, J., ... Brown, R. H. (2009). Mutations in the FUS/TLS Gene on Chromosome 16 Cause Familial Amyotrophic Lateral Sclerosis. *Science*, 323(5918), 1205–1208. <https://doi.org/10.1126/science.1166066>
- Lagier-Tourenne, C., & Cleveland, D. W. (2009). Rethinking ALS: The FUS about TDP-43. *Cell*, 136(6), 1001–1004. <https://doi.org/10.1016/j.cell.2009.03.006>
- Lee, D., Kim, I. Y., Saha, S., & Choi, K. S. (2016). Paraptosis in the anti-cancer arsenal of natural products. *Pharmacology & Therapeutics*, 162, 120–133. <https://doi.org/10.1016/j.pharmthera.2016.01.003>
- Lee, Y., Morrison, B. M., Li, Y., Lengacher, S., Farah, M. H., Hoffman, P. N., Liu, Y., Tsingalia, A., Jin, L., Zhang, P.-W., Pellerin, L., Magistretti, P. J., & Rothstein, J. D. (2012). Oligodendroglia metabolically support axons and contribute to neurodegeneration. *Nature*, 487(7408), 443–448. <https://doi.org/10.1038/nature11314>
- Lee, Y. II, Li, Y., Mikesh, M., Smith, I., Nave, K.-A., Schwab, M. H., & Thompson, W. J. (2016). Neuregulin1 displayed on motor axons regulates terminal Schwann cell-mediated synapse

- elimination at developing neuromuscular junctions. *Proceedings of the National Academy of Sciences*, 113(4), E479–E487. <https://doi.org/10.1073/pnas.1519156113>
- Leibinger, M., Andreadaki, A., Gobrecht, P., Levin, E., Diekmann, H., & Fischer, D. (2016). Boosting Central Nervous System Axon Regeneration by Circumventing Limitations of Natural Cytokine Signaling. *Molecular Therapy*, 24(10), 1712–1725. <https://doi.org/10.1038/mt.2016.102>
- Lepore, A. C., Rauck, B., Dejea, C., Pardo, A. C., Rao, M. S., Rothstein, J. D., & Maragakis, N. J. (2008). Focal transplantation-based astrocyte replacement is neuroprotective in a model of motor neuron disease. *Nature Neuroscience*, 11(11), 1294–1301. <https://doi.org/10.1038/nn.2210>
- Li, J., Huang, K., & Le, W. (2013). Establishing a novel *C. elegans* model to investigate the role of autophagy in amyotrophic lateral sclerosis. *Acta Pharmacologica Sinica*, 34(5), 644–650. <https://doi.org/10.1038/aps.2012.190>
- Li, J., Li, T., Zhang, X., Tang, Y., Yang, J., & Le, W. (2014). Human superoxide dismutase 1 overexpression in motor neurons of *Caenorhabditis elegans* causes axon guidance defect and neurodegeneration. *Neurobiology of Aging*, 35(4), 837–846. <https://doi.org/10.1016/j.neurobiolaging.2013.09.003>
- Li, Q., & Barres, B. A. (2018). Microglia and macrophages in brain homeostasis and disease. *Nature Reviews Immunology*, 18(4), 225–242. <https://doi.org/10.1038/nri.2017.125>
- Liao, B., Zhao, W., Beers, D. R., Henkel, J. S., & Appel, S. H. (2012). Transformation from a neuroprotective to a neurotoxic microglial phenotype in a mouse model of ALS. *Experimental Neurology*, 237(1), 147–152. <https://doi.org/10.1016/j.expneurol.2012.06.011>
- Liddelow, S. A., Guttenplan, K. A., Clarke, L. E., Bennett, F. C., Bohlen, C. J., Schirmer, L., Bennett, M. L., Münch, A. E., Chung, W. S., Peterson, T. C., Wilton, D. K., Frouin, A., Napier, B. A., Panicker, N., Kumar, M., Buckwalter, M. S., Rowitch, D. H., Dawson, V. L., Dawson, T. M., ... Barres, B. A. (2017). Neurotoxic reactive astrocytes are induced by activated microglia. *Nature*, 541(7638), 481–487. <https://doi.org/10.1038/nature21029>
- Liddelow, S., & Barres, B. (2015). SnapShot: Astrocytes in Health and Disease. *Cell*, 162(5), 1170–1170.e1. <https://doi.org/10.1016/j.cell.2015.08.029>
- Liu, J., Lillo, C., Jonsson, P. A., Velde, C. Vande, Ward, C. M., Miller, T. M., Subramaniam, J. R., Rothstein, J. D., Marklund, S., Andersen, P. M., Bränström, T., Gredal, O., Wong, P. C., Williams, D. S., & Cleveland, D. W. (2004). Toxicity of Familial ALS-Linked SOD1 Mutants from Selective Recruitment to Spinal Mitochondria. *Neuron*, 43(1), 5–17. <https://doi.org/10.1016/j.neuron.2004.06.016>
- Liu, M., Solomon, W., Cespedes, J. C., Wilson, N. O., Ford, B., & Stiles, J. K. (2018). Neuregulin-1 attenuates experimental cerebral malaria (ECM) pathogenesis by regulating ErbB4/AKT/STAT3 signaling. *Journal of Neuroinflammation*, 15(1), 104. <https://doi.org/10.1186/s12974-018-1147-z>

- Liu, Y., Pattamatta, A., Zu, T., Reid, T., Bardhi, O., Borchelt, D. R., Yachnis, A. T., & Ranum, L. P. W. (2016). C9orf72 BAC Mouse Model with Motor Deficits and Neurodegenerative Features of ALS/FTD. *Neuron*, 90(3), 521–534. <https://doi.org/10.1016/j.neuron.2016.04.005>
- Ludolph, A. C., & Jesse, S. (2009). Evidence-based drug treatment in amyotrophic lateral sclerosis and upcoming clinical trials. *Therapeutic Advances in Neurological Disorders*, 2(5), 319–326. <https://doi.org/10.1177/1756285609336399>
- Lushchak, V. I. (2014). Free radicals, reactive oxygen species, oxidative stress and its classification. *Chemico-Biological Interactions*, 224(October), 164–175. <https://doi.org/10.1016/j.cbi.2014.10.016>
- Luty, A. A., Kwok, J. B. J., Dobson-Stone, C., Loy, C. T., Coupland, K. G., Karlström, H., Sobow, T., Tchorzewska, J., Maruszak, A., Barcikowska, M., Panegyres, P. K., Zekanowski, C., Brooks, W. S., Williams, K. L., Blair, I. P., Mather, K. A., Sachdev, P. S., Halliday, G. M., & Schofield, P. R. (2010). Sigma nonopiod intracellular receptor 1 mutations cause frontotemporal lobar degeneration-motor neuron disease. *Annals of Neurology*, 68(5), 639–649. <https://doi.org/10.1002/ana.22274>
- Mackenzie, I. R. A., Bigio, E. H., Ince, P. G., Geser, F., Neumann, M., Cairns, N. J., Kwong, L. K., Forman, M. S., Ravits, J., Stewart, H., Eisen, A., McClusky, L., Kretzschmar, H. A., Monoranu, C. M., Highley, J. R., Kirby, J., Siddique, T., Shaw, P. J., Lee, V. M. Y., & Trojanowski, J. Q. (2007). Pathological TDP-43 distinguishes sporadic amyotrophic lateral sclerosis from amyotrophic lateral sclerosis withSOD1 mutations. *Annals of Neurology*, 61(5), 427–434. <https://doi.org/10.1002/ana.21147>
- Mancuso, R., & Navarro, X. (2015). Amyotrophic lateral sclerosis: Current perspectives from basic research to the clinic. *Progress in Neurobiology*, 133, 1–26. <https://doi.org/10.1016/j.pneurobio.2015.07.004>
- Mancuso, R., Oliván, S., Mancera, P., Pastén-Zamorano, A., Manzano, R., Casas, C., Osta, R., & Navarro, X. (2012). Effect of genetic background on onset and disease progression in the SOD1-G93A model of amyotrophic lateral sclerosis. *Amyotrophic Lateral Sclerosis*, 13(3), 302–310. <https://doi.org/10.3109/17482968.2012.662688>
- Maniatis, S., Äijö, T., Vickovic, S., Braine, C., Kang, K., Mollbrink, A., Fagegaltier, D., Andrusiová, Ž., Saarenpää, S., Saiz-Castro, G., Cuevas, M., Watters, A., Lundeberg, J., Bonneau, R., & Phatnani, H. (2019). Spatiotemporal dynamics of molecular pathology in amyotrophic lateral sclerosis. *Science*, 364(6435), 89–93. <https://doi.org/10.1126/science.aav9776>
- Mantovani, S., Garbelli, S., Pasini, A., Alimonti, D., Perotti, C., Melazzini, M., Bendotti, C., & Mora, G. (2009). Immune system alterations in sporadic amyotrophic lateral sclerosis patients suggest an ongoing neuroinflammatory process. *Journal of Neuroimmunology*, 210(1–2), 73–79. <https://doi.org/10.1016/j.jneuroim.2009.02.012>
- Marchetto, M. C. N., Muotri, A. R., Mu, Y., Smith, A. M., Cezar, G. G., & Gage, F. H. (2008). Non-Cell-Autonomous Effect of Human SOD1G37R Astrocytes on Motor Neurons Derived from Human

- Embryonic Stem Cells. *Cell Stem Cell*, 3(6), 649–657. <https://doi.org/10.1016/j.stem.2008.10.001>
- Martínez-Silva, M. de L., Imhoff-Manuel, R. D., Sharma, A., Heckman, C. J. C., Shneider, N. A., Roselli, F., Zytnicki, D., & Manuel, M. (2018). Hypoexcitability precedes denervation in the large fast-contracting motor units in two unrelated mouse models of ALS. *eLife*, 7(2007), 1–26. <https://doi.org/10.7554/eLife.30955>
- Martins, D., & English, A. M. (2014). SOD1 oxidation and formation of soluble aggregates in yeast: Relevance to sporadic ALS development. *Redox Biology*, 2(1), 632–639. <https://doi.org/10.1016/j.redox.2014.03.005>
- Mattiazzi, M., D'Aurelio, M., Gajewski, C. D., Martushova, K., Kiaei, M., Beal, M. F., & Manfredi, G. (2002). Mutated Human SOD1 Causes Dysfunction of Oxidative Phosphorylation in Mitochondria of Transgenic Mice. *Journal of Biological Chemistry*, 277(33), 29626–29633. <https://doi.org/10.1074/jbc.M203065200>
- Mattson, M. P., Keller, J. N., & Begley, J. G. (1998). Evidence for synaptic apoptosis. *Experimental Neurology*, 153(1), 35–48. <https://doi.org/10.1006/exnr.1998.6863>
- Mavlyutov, T. A., Epstein, M. L., Andersen, K. A., Ziskind-Conhaim, L., & Ruoho, A. E. (2010). The sigma-1 receptor is enriched in postsynaptic sites of C-terminals in mouse motoneurons. An anatomical and behavioral study. *Neuroscience*, 167(2), 247–255. <https://doi.org/10.1016/j.neuroscience.2010.02.022>
- Mavlyutov, T. A., Epstein, M. L., Liu, P., Verbny, Y. I., Ziskind-Conhaim, L., & Ruoho, A. E. (2012). Development of the sigma-1 receptor in C-terminals of motoneurons and colocalization with the N,N'-dimethyltryptamine forming enzyme, indole-N-methyl transferase. *Neuroscience*, 206, 60–68. <https://doi.org/10.1016/j.neuroscience.2011.12.040>
- Mei, L., & Nave, K.-A. (2014). Neuregulin-ERBB Signaling in the Nervous System and Neuropsychiatric Diseases. *Neuron*, 83(1), 27–49. <https://doi.org/10.1016/j.neuron.2014.06.007>
- Michailov, G. V., Sereda, M. W., Brinkmann, B. G., Fischer, T. H., Haug, B., Birchmeier, C., Role, L., Lai, C., Schwab, M. H., & Nave, K. A. (2004). Axonal Neuregulin-1 Regulates Myelin Sheath Thickness. *Science*, 304(5671), 700–703. <https://doi.org/10.1126/science.1095862>
- Miles, G. B., Hartley, R., Todd, A. J., & Brownstone, R. M. (2007). Spinal cholinergic interneurons regulate the excitability of motoneurons during locomotion. *Proceedings of the National Academy of Sciences*, 104(7), 2448–2453. <https://doi.org/10.1073/pnas.0611134104>
- Miller, K. E., & Sheetz, M. P. (2004). Axonal mitochondrial transport and potential are correlated. *Journal of Cell Science*, 117(13), 2791–2804. <https://doi.org/10.1242/jcs.01130>

- Miller, R. A., & Nadon, N. L. (2000). Principles of Animal Use for Gerontological Research. *The Journals of Gerontology Series A: Biological Sciences and Medical Sciences*, 55(3), B117–B123. <https://doi.org/10.1093/gerona/55.3.B117>
- Mitsumoto, H., Santella, R. M., Liu, X., Bogdanov, M., Zipprich, J., Wu, H.-C., Mahata, J., Kilty, M., Bednarz, K., Bell, D., Gordon, P. H., Hornig, M., Mehrazin, M., Naini, A., Flint Beal, M., & Factor-Litvak, P. (2008). Oxidative stress biomarkers in sporadic ALS. *Amyotrophic Lateral Sclerosis*, 9(3), 177–183. <https://doi.org/10.1080/17482960801933942>
- Mizushima, N., & Komatsu, M. (2011). Autophagy: Renovation of Cells and Tissues. *Cell*, 147(4), 728–741. <https://doi.org/10.1016/j.cell.2011.10.026>
- Moloney, E. B., de Winter, F., & Verhaagen, J. (2014). ALS as a distal axonopathy: molecular mechanisms affecting neuromuscular junction stability in the presymptomatic stages of the disease. *Frontiers in Neuroscience*, 8(August), 1–18. <https://doi.org/10.3389/fnins.2014.00252>
- Moran, L. B., & Graeber, M. B. (2004). The facial nerve axotomy model. *Brain Research Reviews*, 44(2–3), 154–178. <https://doi.org/10.1016/j.brainresrev.2003.11.004>
- Morgan, S., & Orrell, R. W. (2016). Pathogenesis of amyotrophic lateral sclerosis. *British Medical Bulletin*, 119(1), 87–98. <https://doi.org/10.1093/bmb/ldw026>
- Muennich, E. A. L., & Fyffe, R. E. W. (2004). Focal aggregation of voltage-gated, Kv2.1 subunit-containing, potassium channels at synaptic sites in rat spinal motoneurones. *The Journal of Physiology*, 554(3), 673–685. <https://doi.org/10.1113/jphysiol.2003.056192>
- Murphy, S. M., Pilowsky, P. M., & Llewellyn-Smith, I. J. (1996). Vesicle shape and amino acids in synaptic inputs to phrenic motoneurons: Do all inputs contain either glutamate or GABA? *The Journal of Comparative Neurology*, 373(2), 200–219. [https://doi.org/10.1002/\(SICI\)1096-9861\(19960916\)373:2<200::AID-CNE4>3.0.CO;2-7](https://doi.org/10.1002/(SICI)1096-9861(19960916)373:2<200::AID-CNE4>3.0.CO;2-7)
- Nagai, M., Aoki, M., Miyoshi, I., Kato, M., Pasinelli, P., Kasai, N., Brown, J., & Itoyama, Y. (2001). Rats expressing human cytosolic copper-zinc superoxide dismutase transgenes with amyotrophic lateral sclerosis: Associated mutations develop motor neuron disease. *Journal of Neuroscience*, 21(23), 9246–9254. <https://doi.org/10.1523/jneurosci.21-23-09246.2001>
- Nagai, Makiko, Re, D. B., Nagata, T., Chalazonitis, A., Jessell, T. M., Wichterle, H., & Przedborski, S. (2007). Astrocytes expressing ALS-linked mutated SOD1 release factors selectively toxic to motor neurons. *Nature Neuroscience*, 10(5), 615–622. <https://doi.org/10.1038/nn1876>
- Neumann, M., Sampathu, D. M., Kwong, L. K., Truax, A. C., Micsenyi, M. C., Chou, T. T., Bruce, J., Schuck, T., Grossman, M., Clark, C. M., McCluskey, L. F., Miller, B. L., Masliah, E., Mackenzie, I. R., Feldman, H., Feiden, W., Kretschmar, H. A., Trojanowski, J. Q., & Lee, V. M.-Y. (2006). Ubiquitinated TDP-43 in Frontotemporal Lobar Degeneration and Amyotrophic Lateral Sclerosis.

- Science*, 314(5796), 130–133. <https://doi.org/10.1126/science.1134108>
- Nimmerjahn, A., Kirchhoff, F., & Helmchen, F. (2005). Resting microglial cells are highly dynamic surveillants of brain parenchyma in vivo. *Science*, 308, 1314–1318. <https://doi.org/10.1126/science.1134108>
- Nishihira, Y., Tan, C.-F., Onodera, O., Toyoshima, Y., Yamada, M., Morita, T., Nishizawa, M., Kakita, A., & Takahashi, H. (2008). Sporadic amyotrophic lateral sclerosis: two pathological patterns shown by analysis of distribution of TDP-43-immunoreactive neuronal and glial cytoplasmic inclusions. *Acta Neuropathologica*, 116(2), 169–182. <https://doi.org/10.1007/s00401-008-0385-z>
- Novikov, L., Novikova, L., Holmberg, P., & Kellerth, J.-O. (2000). Exogenous brain-derived neurotrophic factor regulates the synaptic composition of axonally lesioned and normal adult rat motoneurons. *Neuroscience*, 100(1), 171–181. [https://doi.org/10.1016/S0306-4522\(00\)00256-6](https://doi.org/10.1016/S0306-4522(00)00256-6)
- Oeda, T., Shimohama, S., Kitagawa, N., Kohno, R., Imura, T., Shibasaki, H., & Ishii, N. (2001). Oxidative stress causes abnormal accumulation of familial amyotrophic lateral sclerosis-related mutant SOD1 in transgenic *Caenorhabditis elegans*. *Human Molecular Genetics*, 10(19), 2013–2023. <https://doi.org/10.1093/hmg/10.19.2013>
- Ofengheim, D., Mazzitelli, S., Ito, Y., DeWitt, J. P., Mifflin, L., Zou, C., Das, S., Adiconis, X., Chen, H., Zhu, H., Kelliher, M. A., Levin, J. Z., & Yuan, J. (2017). RIPK1 mediates a disease-associated microglial response in Alzheimer's disease. *Proceedings of the National Academy of Sciences*, 114(41), E8788–E8797. <https://doi.org/10.1073/pnas.1714175114>
- Okamoto, K., Hirai, S., Amari, M., Watanabe, M., & Sakurai, A. (1993). Bunina bodies in amyotrophic lateral sclerosis immunostained with rabbit anti-cystatin C serum. *Neuroscience Letters*, 162(1–2), 125–128. [https://doi.org/10.1016/0304-3940\(93\)90576-7](https://doi.org/10.1016/0304-3940(93)90576-7)
- Olney, J. W. (1989). Glutamate, a Neurotoxic Transmitter. *Journal of Child Neurology*, 4(3), 218–226. <https://doi.org/10.1177/088307388900400315>
- Örnung, G., Shupliakov, O., Lindå, H., Ottersen, O. P., Storm-Mathisen, J., Ulfhake, B., & Cullheim, S. (1996). Qualitative and quantitative analysis of glycine- and GABA-immunoreactive nerve terminals on motoneuron cell bodies in the cat spinal cord: A postembedding electron microscopic study. *The Journal of Comparative Neurology*, 365(3), 413–426. [https://doi.org/10.1002/\(SICI\)1096-9861\(19960212\)365:3<413::AID-CNE6>3.3.CO;2-N](https://doi.org/10.1002/(SICI)1096-9861(19960212)365:3<413::AID-CNE6>3.3.CO;2-N)
- Paolicelli, R. C., Bolasco, G., Pagani, F., Maggi, L., Scianni, M., Panzanelli, P., Giustetto, M., Ferreira, T. A., Guiducci, E., Dumas, L., Ragozzino, D., & Gross, C. T. (2011). Synaptic Pruning by Microglia Is Necessary for Normal Brain Development. *Science*, 333(6048), 1456–1458. <https://doi.org/10.1126/science.1202529>
- Papadeas, S. T., Kraig, S. E., O'Banion, C., Lepore, A. C., & Maragakis, N. J. (2011). Astrocytes carrying the superoxide dismutase 1 (SOD1G93A) mutation induce wild-type motor neuron degeneration in vivo. *Proceedings of the National Academy of Sciences*, 108(43), 17803–17808. <https://doi.org/10.1073/pnas.1108030108>

<https://doi.org/10.1073/pnas.1103141108>

Parone, P. A., Da Cruz, S., Han, J. S., McAlonis-Downes, M., Vetto, A. P., Lee, S. K., Tseng, E., & Cleveland, D. W. (2013). Enhancing Mitochondrial Calcium Buffering Capacity Reduces Aggregation of Misfolded SOD1 and Motor Neuron Cell Death without Extending Survival in Mouse Models of Inherited Amyotrophic Lateral Sclerosis. *Journal of Neuroscience*, 33(11), 4657–4671. <https://doi.org/10.1523/JNEUROSCI.1119-12.2013>

Pasparakis, M., & Vandenberghe, P. (2015). Necroptosis and its role in inflammation. *Nature*, 517(7534), 311–320. <https://doi.org/10.1038/nature14191>

Patritti-Cram, J., Coover, R. A., Jankowski, M. P., & Ratner, N. (2021). Purinergic signaling in peripheral nervous system glial cells. *Glia*, 69(8), 1837–1851. <https://doi.org/10.1002/glia.23969>

Peher, M., O'Riordan, K. J., Burns-Cusato, M., Andrzejewski, M. E., del Alcazar, C. G., Burger, C., Scrable, H., & Puglisi, L. (2010). Altered longevity-assurance activity of p53:p44 in the mouse causes memory loss, neurodegeneration and premature death. *Aging Cell*, 9(2), 174–190. <https://doi.org/10.1111/j.1474-9726.2010.00547.x>

Pena, E., Berciano, M. T., Fernandez, R., Ojeda, J. L., & Lafarga, M. (2001). Neuronal body size correlates with the number of nucleoli and Cajal bodies, and with the organization of the splicing machinery in rat trigeminal ganglion neurons. *The Journal of Comparative Neurology*, 430(2), 250–263. [https://doi.org/10.1002/1096-9861\(20010205\)430:2<250::AID-CNE1029>3.0.CO;2-L](https://doi.org/10.1002/1096-9861(20010205)430:2<250::AID-CNE1029>3.0.CO;2-L)

Pentassuglia, L., & Sawyer, D. B. (2009). The role of Neuregulin-1 β /ErbB signaling in the heart. *Experimental Cell Research*, 315(4), 627–637. <https://doi.org/10.1016/j.yexcr.2008.08.015>

Perry, T. L., Krieger, C., Hansen, S., & Eisen, A. (1990). Amyotrophic lateral sclerosis: Amino acid levels in plasma and cerebrospinal fluid. *Annals of Neurology*, 28(1), 12–17. <https://doi.org/10.1002/ana.410280105>

Perry, V. H., & O'Connor, V. (2010). The Role of Microglia in Synaptic Stripping and Synaptic Degeneration: A Revised Perspective. *ASN Neuro*, 2(5), AN20100024. <https://doi.org/10.1042/AN20100024>

Phatnani, H. P., Guarnieri, P., Friedman, B. A., Carrasco, M. A., Muratet, M., O'Keeffe, S., Nwakweze, C., Pauli-Behn, F., Newberry, K. M., Meadows, S. K., Tapia, J. C., Myers, R. M., & Maniatis, T. (2013). Intricate interplay between astrocytes and motor neurons in ALS. *Proceedings of the National Academy of Sciences*, 110(8), E756–E765. <https://doi.org/10.1073/pnas.1222361110>

Philips, T., Bento-Abreu, A., Nonneman, A., Haeck, W., Staats, K., Geelen, V., Hersmus, N., Küsters, B., Van Den Bosch, L., Van Damme, P., Richardson, W. D., & Robberecht, W. (2013). Oligodendrocyte dysfunction in the pathogenesis of amyotrophic lateral sclerosis. *Brain*, 136(2),

- 471–482. <https://doi.org/10.1093/brain/aws339>
- Philips, T., & Rothstein, J. D. (2014). Glial cells in amyotrophic lateral sclerosis. *Experimental Neurology*, 262(Part B), 111–120. <https://doi.org/10.1016/j.expneurol.2014.05.015>
- Philips, Thomas, & Rothstein, J. D. (2015). Rodent Models of Amyotrophic Lateral Sclerosis. *Current Protocols in Pharmacology*, 69(1), 5.67.1-5.67.21. <https://doi.org/10.1002/0471141755.ph0567s69>
- Philips, Thomas, & Rothstein, J. D. (2017). Oligodendroglia: metabolic supporters of neurons. *Journal of Clinical Investigation*, 127(9), 3271–3280. <https://doi.org/10.1172/JCI90610>
- Piao, Y.-S., Wakabayashi, K., Kakita, A., Yamada, M., Hayashi, S., Morita, T., Ikuta, F., Oyanagi, K., & Takahashi, H. (2006). Neuropathology with Clinical Correlations of Sporadic Amyotrophic Lateral Sclerosis: 102 Autopsy Cases Examined Between 1962 and 2000. *Brain Pathology*, 13(1), 10–22. <https://doi.org/10.1111/j.1750-3639.2003.tb00002.x>
- Picca, A., Beli, R., Calvani, R., Coelho-Júnior, H. J., Landi, F., Bernabei, R., Bucci, C., Guerra, F., & Marzetti, E. (2020). Older Adults with Physical Frailty and Sarcopenia Show Increased Levels of Circulating Small Extracellular Vesicles with a Specific Mitochondrial Signature. *Cells*, 9(4), 973. <https://doi.org/10.3390/cells9040973>
- Powers, S., Kwok, S., Lovejoy, E., Lavin, T., & Sher, R. (2017). Embryonic Exposure to the Environmental Neurotoxin BMAA Negatively Impacts Early Neuronal Development and Progression of Neurodegeneration in the Sod1-G93R Zebrafish Model of Amyotrophic Lateral Sclerosis. *Toxicological Sciences*, 157(1), kfx020. <https://doi.org/10.1093/toxsci/kfx020>
- Pramatarova, A., Laganière, J., Roussel, J., Brisebois, K., & Rouleau, G. A. (2001). Neuron-Specific Expression of Mutant Superoxide Dismutase 1 in Transgenic Mice Does Not Lead to Motor Impairment. *The Journal of Neuroscience*, 21(10), 3369–3374. <https://doi.org/10.1523/JNEUROSCI.21-10-03369.2001>
- Puentes, F., Malaspina, A., van Noort, J. M., & Amor, S. (2016). Non-neuronal Cells in ALS: Role of Glial, Immune cells and Blood-CNS Barriers. *Brain Pathology*, 26(2), 248–257. <https://doi.org/10.1111/bpa.12352>
- Pullen, A. H., & Athanasiou, D. (2009). Increase in presynaptic territory of C-terminals on lumbar motoneurons of G93A SOD1 mice during disease progression. *European Journal of Neuroscience*, 29(3), 551–561. <https://doi.org/10.1111/j.1460-9568.2008.06602.x>
- Ramesh, T., Lyon, A. N., Pineda, R. H., Wang, C., Janssen, P. M. L., Canan, B. D., Burghes, A. H. M., & Beattie, C. E. (2010). A genetic model of amyotrophic lateral sclerosis in zebrafish displays phenotypic hallmarks of motoneuron disease. *Disease Models & Mechanisms*, 3(9–10), 652–662. <https://doi.org/10.1242/dmm.005538>
- Ransohoff, R. M. (2016). A polarizing question: do M1 and M2 microglia exist? *Nature Neuroscience*,

- 19(8), 987–991. <https://doi.org/10.1038/nn.4338>
- Re, D. B., Le Verche, V., Yu, C., Amoroso, M. W., Politi, K. A., Phani, S., Ikiz, B., Hoffmann, L., Koolen, M., Nagata, T., Papadimitriou, D., Nagy, P., Mitsumoto, H., Kariya, S., Wichterle, H., Henderson, C. E., & Przedborski, S. (2014). Necroptosis Drives Motor Neuron Death in Models of Both Sporadic and Familial ALS. *Neuron*, 81(5), 1001–1008. <https://doi.org/10.1016/j.neuron.2014.01.011>
- Reaume, A. G., Elliott, J. L., Hoffman, E. K., Kowall, N. W., Ferrante, R. J., Siwek, D. R., Wilcox, H. M., Flood, D. G., Beal, M. F., Brown, R. H., Scott, R. W., & Snider, W. D. (1996). Motor neurons in Cu/Zn superoxide dismutase-deficient mice develop normally but exhibit enhanced cell death after axonal injury. *Nature Genetics*, 13(1), 43–47. <https://doi.org/10.1038/ng0596-43>
- Rekling, J. C., Funk, G. D., Bayliss, D. A., Dong, X., & Feldman, J. L. (2000). *Synaptic Control of Motoneuronal Excitability*. 80(2), 767–852.
- Renton, A. E., Majounie, E., Waite, A., Simón-Sánchez, J., Rollinson, S., Gibbs, J. R., Schymick, J. C., Laaksovirta, H., van Swieten, J. C., Myllykangas, L., Kalimo, H., Paetau, A., Abramzon, Y., Remes, A. M., Kaganovich, A., Scholz, S. W., Duckworth, J., Ding, J., Harmer, D. W., ... Traynor, B. J. (2011). A Hexanucleotide Repeat Expansion in C9ORF72 Is the Cause of Chromosome 9p21-Linked ALS-FTD. *Neuron*, 72(2), 257–268. <https://doi.org/10.1016/j.neuron.2011.09.010>
- Rexed, B. (1957). *The citoarchitectonic organization of the spinal cord in the cat*. 108(2).
- Ripps, M. E., Huntley, G. W., Hof, Pa. R., Morrison, J. H., & Gordon, J. W. (1995). Transgenic mice expressing an altered murine superoxide dismutase gene provide an animal model of amyotrophic lateral sclerosis. *Proc. Natl. Acad. Scie.*, 92, 689–693.
- Robberecht, W., & Philips, T. (2013). The changing scene of amyotrophic lateral sclerosis. *Nature Reviews Neuroscience*, 14(4), 248–264. <https://doi.org/10.1038/nrn3430>
- Ronnevi, L. O. (1979). Spontaneous phagocytosis of C-type synaptic terminals by spinal alpha-motoneurons in newborn kittens. An electron microscopic study. *Brain Research*, 162(2), 189–199. [https://doi.org/10.1016/0006-8993\(79\)90283-x](https://doi.org/10.1016/0006-8993(79)90283-x)
- Roselli, F., & Caroni, P. (2015). From Intrinsic Firing Properties to Selective Neuronal Vulnerability in Neurodegenerative Diseases. *Neuron*, 85(5), 901–910. <https://doi.org/10.1016/j.neuron.2014.12.063>
- Rosen, D. R., Siddique, T., Patterson, D., Figlewicz, D. A., Sapp, P., Hentati, A., Donaldson, D., Goto, J., O'Regan, J. P., Deng, H. X., Rahmani, Z., Krizus, A., McKenna-Yasek, D., Cayabyab, A., Gaston, S. M., Berger, R., Tanzi, R. E., Halperin, J. J., Herzfeldt, B., ... Brown, R. H. (1993). Mutations in Cu/Zn superoxide dismutase gene are associated with familial amyotrophic lateral sclerosis. *Nature*, 362(6415), 59–62.

- Ross, M., & Pawlina, W. (2015). *Histología texto y atlas* (7a Edición).
- Rothstein, J. D., Jin, L., Dykes-Hoberg, M., & Kuncl, R. W. (1993). Chronic inhibition of glutamate uptake produces a model of slow neurotoxicity. *Proceedings of the National Academy of Sciences*, 90(14), 6591–6595. <https://doi.org/10.1073/pnas.90.14.6591>
- Rothstein, Jeffrey D. (2017). Edaravone: A new drug approved for ALS. *Cell*, 171(4), 725. <https://doi.org/10.1016/j.cell.2017.10.011>
- Rothstein, Jeffrey D., Martin, L. J., & Kuncl, R. W. (1992). Decreased glutamate transport by the brain and spinal cord in amyotrophic lateral sclerosis. *The New England Journal of Medicine*, 326(22), 1464–1468.
- Rowland, L., & Shneider, N. (2001). Amyotrophic Lateral Sclerosis. *The New England Journal of Medicine*, 344(22), 1688–1700.
- Roy, J., Minotti, S., Dong, L., Figlewicz, D. A., & Durham, H. D. (1998). Glutamate Potentiates the Toxicity of Mutant Cu/Zn-Superoxide Dismutase in Motor Neurons by Postsynaptic Calcium-Dependent Mechanisms. *The Journal of Neuroscience*, 18(23), 9673–9684. <https://doi.org/10.1523/JNEUROSCI.18-23-09673.1998>
- Rubio, M. E., & Wenthold, R. J. (1999). Differential Distribution of Intracellular Glutamate Receptors in Dendrites. *The Journal of Neuroscience*, 19(13), 5549–5562. <https://doi.org/10.1523/JNEUROSCI.19-13-05549.1999>
- Ruegsegger, C., & Saxena, S. (2016). Proteostasis impairment in ALS. *Brain Research*, 1648, 571–579. <https://doi.org/10.1016/j.brainres.2016.03.032>
- Sábado, J., Casanovas, A., Hernández, S., Piedrafita, L., Hereu, M., & Esquerda, J. E. (2013). Immunodetection of Disease-Associated Conformers of Mutant Cu/Zn Superoxide Dismutase 1 Selectively Expressed in Degenerating Neurons in Amyotrophic Lateral Sclerosis. *Journal of Neuropathology & Experimental Neurology*, 72(7), 646–661. <https://doi.org/10.1097/NEN.0b013e318297fd10>
- Saccon, R. A., Bunton-Stasyshyn, R. K. A., Fisher, E. M. C., & Fratta, P. (2013). Is SOD1 loss of function involved in amyotrophic lateral sclerosis? *Brain*, 136(8), 2342–2358. <https://doi.org/10.1093/brain/awt097>
- Sanagi, T., Yuasa, S., Nakamura, Y., Suzuki, E., Aoki, M., Warita, H., Itoyama, Y., Uchino, S., Kohsaka, S., & Ohsawa, K. (2010). Appearance of phagocytic microglia adjacent to motoneurons in spinal cord tissue from a presymptomatic transgenic rat model of amyotrophic lateral sclerosis. *Journal of Neuroscience Research*, 88(12), 2736–2746. <https://doi.org/10.1002/jnr.22424>
- Sasaki, S., & Iwata, M. (2007). Mitochondrial Alterations in the Spinal Cord of Patients With Sporadic Amyotrophic Lateral Sclerosis. *Journal of Neuropathology and Experimental Neurology*, 66(1),

- 10–16. <https://doi.org/10.1097/nen.0b013e31802c396b>
- Savastano, L. E., Laurito, S. R., Fitt, M. R., Rasmussen, J. A., Gonzalez Polo, V., & Patterson, S. I. (2014). Sciatic nerve injury: A simple and subtle model for investigating many aspects of nervous system damage and recovery. *Journal of Neuroscience Methods*, 227, 166–180. <https://doi.org/10.1016/j.jneumeth.2014.01.020>
- Saxena, S., Cabuy, E., & Caroni, P. (2009). A role for motoneuron subtype-selective ER stress in disease manifestations of FALS mice. *Nature Neuroscience*, 12(5), 627–636. <https://doi.org/10.1038/nn.2297>
- Saxena, S., Roselli, F., Singh, K., Leptien, K., Julien, J.-P., Gros-Louis, F., & Caroni, P. (2013). Neuroprotection through Excitability and mTOR Required in ALS Motoneurons to Delay Disease and Extend Survival. *Neuron*, 80(1), 80–96. <https://doi.org/10.1016/j.neuron.2013.07.027>
- Schaefer, A. M., Sanes, J. R., & Lichtman, J. W. (2005). A compensatory subpopulation of motor neurons in a mouse model of amyotrophic lateral sclerosis. *The Journal of Comparative Neurology*, 490(3), 209–219. <https://doi.org/10.1002/cne.20620>
- Schafer, D. P., Lehrman, E. K., Kautzman, A. G., Koyama, R., Mardinly, A. R., Yamasaki, R., Ransohoff, R. M., Greenberg, M. E., Barres, B. A., & Stevens, B. (2012). Microglia Sculpt Postnatal Neural Circuits in an Activity and Complement-Dependent Manner. *Neuron*, 74(4), 691–705. <https://doi.org/10.1016/j.neuron.2012.03.026>
- Schiffer, D., Cordera, S., Cavalla, P., & Migheli, A. (1996). Reactive astrogliosis of the spinal cord in amyotrophic lateral sclerosis. *Journal of the Neurological Sciences*, 139(SUPPL.), 27–33. [https://doi.org/10.1016/0022-510X\(96\)00073-1](https://doi.org/10.1016/0022-510X(96)00073-1)
- Schutz, B. (2005). Imbalanced excitatory to inhibitory synaptic input precedes motor neuron degeneration in an animal model of amyotrophic lateral sclerosis. *Neurobiology of Disease*, 20(1), 131–140. <https://doi.org/10.1016/j.nbd.2005.02.006>
- Serio, A., & Patani, R. (2018). Concise Review: The Cellular Conspiracy of Amyotrophic Lateral Sclerosis. *STEM CELLS*, 36(3), 293–303. <https://doi.org/10.1002/stem.2758>
- Shaw, I. C., Fitzmaurice, P. S., Mitchell, J. D., & Lynch, P. G. (1995). Studies on Cellular Free Radical Protection Mechanisms in the Anterior Horn from Patients with Amyotrophic Lateral Sclerosis. *Neurodegeneration*, 4(4), 391–396. <https://doi.org/10.1006/neur.1995.0047>
- Shi, Z., Yuan, S., Shi, L., Li, J., Ning, G., Kong, X., & Feng, S. (2021). Programmed cell death in spinal cord injury pathogenesis and therapy. *Cell Proliferation*, 54(3), 1–9. <https://doi.org/10.1111/cpr.12992>
- Silverman, J. M., Christy, D., Shyu, C. C., Moon, K.-M., Fernando, S., Gidden, Z., Cowan, C. M., Ban, Y., Stacey, R. G., Grad, L. I., McAlary, L., Mackenzie, I. R., Foster, L. J., & Cashman, N. R. (2019). CNS-derived extracellular vesicles from superoxide dismutase 1 (SOD1)G93A ALS mice originate from

- astrocytes and neurons and carry misfolded SOD1. *Journal of Biological Chemistry*, 294(10), 3744–3759. <https://doi.org/10.1074/jbc.RA118.004825>
- Simons, M., & Nave, K.-A. (2016). Oligodendrocytes: Myelination and Axonal Support. *Cold Spring Harbor Perspectives in Biology*, 8(1), a020479. <https://doi.org/10.1101/cshperspect.a020479>
- Simpson, E. P., Henry, Y. K., Henkel, J. S., Smith, R. G., & Appel, S. H. (2004). Increased lipid peroxidation in sera of ALS patients: A potential biomarker of disease burden. *Neurology*, 62(10), 1758–1765. <https://doi.org/10.1212/WNL.62.10.1758>
- Sipe, G. O., Lowery, R. L., Tremblay, M.-È., Kelly, E. A., Lamantia, C. E., & Majewska, A. K. (2016). Microglial P2Y12 is necessary for synaptic plasticity in mouse visual cortex. *Nature Communications*, 7(1), 10905. <https://doi.org/10.1038/ncomms10905>
- Šišková, Z., Page, A., O'Connor, V., & Perry, V. H. (2009). Degenerating Synaptic Boutons in Prion Disease. *The American Journal of Pathology*, 175(4), 1610–1621. <https://doi.org/10.2353/ajpath.2009.090372>
- Smith, E. F., Shaw, P. J., & De Vos, K. J. (2017). The role of mitochondria in amyotrophic lateral sclerosis. *Neuroscience Letters*, 710, 132933. <https://doi.org/10.1016/j.neulet.2017.06.052>
- Smith, R. G., Henry, Y. K., Mattson, M. P., & Appel, S. H. (1998). Presence of 4-hydroxynonenal in cerebrospinal fluid of patients with sporadic amyotrophic lateral sclerosis. *Annals of Neurology*, 44(4), 696–699. <https://doi.org/10.1002/ana.410440419>
- Solsona, C., Esquerda, J. E., & Marsal, J. (1981). Effects of ouabain and electrical stimulation on the fine structure of nerve endings in the electric organ of *Torpedo marmorata*. *Cell and Tissue Research*, 220(4), 857–871. <https://doi.org/10.1007/BF00210467>
- Song, F., Chiang, P., Wang, J., Ravits, J., & Loeb, J. A. (2012). Aberrant Neuregulin 1 Signaling in Amyotrophic Lateral Sclerosis. *Journal of Neuropathology & Experimental Neurology*, 71(2), 104–115. <https://doi.org/10.1097/NEN.0b013e3182423c43>
- Spejo, A. B., & Oliveira, A. L. R. (2015). Synaptic rearrangement following axonal injury: Old and new players. *Neuropharmacology*, 96(Pt A), 113–123. <https://doi.org/10.1016/j.neuropharm.2014.11.002>
- Sperandio, S., de Belle, I., & Bredesen, D. E. (2000). An alternative, nonapoptotic form of programmed cell death. *Proceedings of the National Academy of Sciences*, 97(26), 14376–14381. <https://doi.org/10.1073/pnas.97.26.14376>
- Sreedharan, J., Blair, I. P., Tripathi, V. B., Hu, X., Vance, C., Rogelj, B., Ackerley, S., Durnall, J. C., Williams, K. L., Buratti, E., Baralle, F., de Belleroche, J., Mitchell, J. D., Leigh, P. N., Al-Chalabi, A., Miller, C. C., Nicholson, G., & Shaw, C. E. (2008). TDP-43 Mutations in Familial and Sporadic Amyotrophic Lateral Sclerosis. *Science*, 319(5870), 1668–1672. <https://doi.org/10.1126/science.1154584>

- Stassart, R. M., Fledrich, R., Velanac, V., Brinkmann, B. G., Schwab, M. H., Meijer, D., Sereda, M. W., & Nave, K.-A. (2013). A role for Schwann cell-derived neuregulin-1 in remyelination. *Nature Neuroscience*, 16(1), 48–54. <https://doi.org/10.1038/nn.3281>
- Stephan, A. H., Barres, B. A., & Stevens, B. (2012). The Complement System: An Unexpected Role in Synaptic Pruning During Development and Disease. *Annual Review of Neuroscience*, 35(1), 369–389. <https://doi.org/10.1146/annurev-neuro-061010-113810>
- Stevens, B., Allen, N. J., Vazquez, L. E., Howell, G. R., Christopherson, K. S., Nouri, N., Micheva, K. D., Mehalow, A. K., Huberman, A. D., Stafford, B., Sher, A., Litke, A. M., Lambris, J. D., Smith, S. J., John, S. W. M., & Barres, B. A. (2007). The Classical Complement Cascade Mediates CNS Synapse Elimination. *Cell*, 131(6), 1164–1178. <https://doi.org/10.1016/j.cell.2007.10.036>
- Stifani, N. (2014). Motor neurons and the generation of spinal motor neuron diversity. *Frontiers in Cellular Neuroscience*, 8(OCT), 1–22. <https://doi.org/10.3389/fncel.2014.00293>
- Su, X. W., Broach, J. R., Connor, J. R., Gerhard, G. S., & Simmons, Z. (2014). Genetic heterogeneity of amyotrophic lateral sclerosis: Implications for clinical practice and research. *Muscle & Nerve*, 49(6), 786–803. <https://doi.org/10.1002/mus.24198>
- Sumner, B. E. (1975). A quantitative analysis of the response of presynaptic boutons to postsynaptic motor neuron axotomy. *Experimental Neurology*, 46(3), 605–615. [https://doi.org/10.1016/0014-4886\(75\)90129-6](https://doi.org/10.1016/0014-4886(75)90129-6)
- Sumner, B. E., & Sutherland, F. I. (1973). Quantitative electron microscopy on the injured hypoglossal nucleus in the rat. *Journal of Neurocytology*, 2(3), 315–328. <https://doi.org/10.1007/BF01104033>
- Sun, L., Wang, H., Wang, Z., He, S., Chen, S., Liao, D., Wang, L., Yan, J., Liu, W., Lei, X., & Wang, X. (2012). Mixed Lineage Kinase Domain-like Protein Mediates Necrosis Signaling Downstream of RIP3 Kinase. *Cell*, 148(1–2), 213–227. <https://doi.org/10.1016/j.cell.2011.11.031>
- Takahashi, Y., Fukuda, Y., Yoshimura, J., Toyoda, A., Kurppa, K., Moritoyo, H., Belzil, V. V., Dion, P. A., Higasa, K., Doi, K., Ishiura, H., Mitsui, J., Date, H., Ahsan, B., Matsukawa, T., Ichikawa, Y., Moritoyo, T., Ikoma, M., Hashimoto, T., ... Tsuji, S. (2013). ERBB4 Mutations that Disrupt the Neuregulin-ErbB4 Pathway Cause Amyotrophic Lateral Sclerosis Type 19. *The American Journal of Human Genetics*, 93(5), 900–905. <https://doi.org/10.1016/j.ajhg.2013.09.008>
- Tang, A.-H., Chen, H., Li, T. P., Metzbower, S. R., MacGillavry, H. D., & Blanpied, T. A. (2016). A trans-synaptic nanocolumn aligns neurotransmitter release to receptors. *Nature*, 536(7615), 210–214. <https://doi.org/10.1038/nature19058>
- Tang, Y., & Le, W. (2016). Differential Roles of M1 and M2 Microglia in Neurodegenerative Diseases. *Molecular Neurobiology*, 53(2), 1181–1194. <https://doi.org/10.1007/s12035-014-9070-5>
- Tateishi, T., Yamasaki, R., Tanaka, M., Matsushita, T., Kikuchi, H., Isobe, N., Ohyagi, Y., & Kira, J.

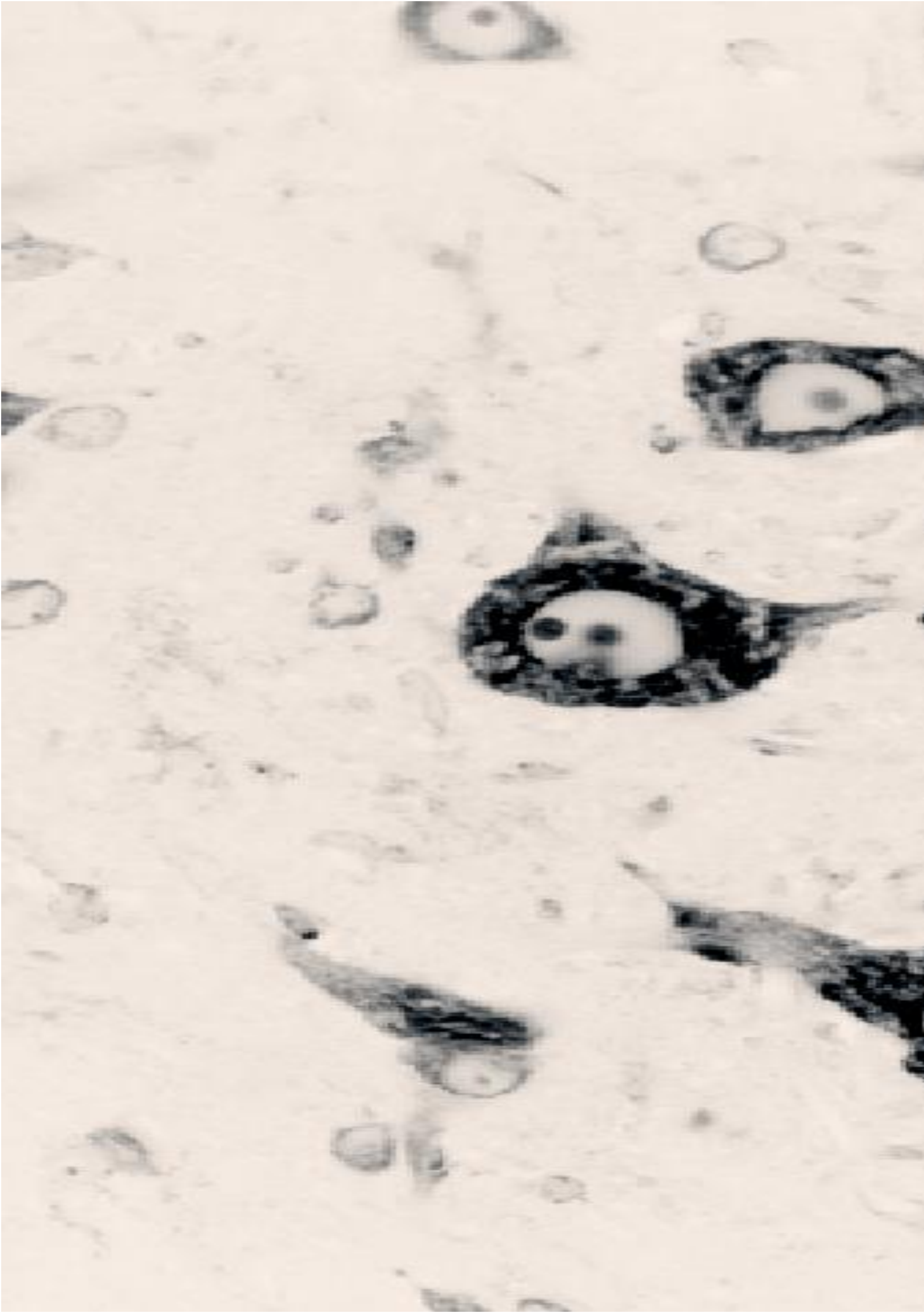
- (2010). CSF chemokine alterations related to the clinical course of amyotrophic lateral sclerosis. *Journal of Neuroimmunology*, 222(1–2), 76–81. <https://doi.org/10.1016/j.jneuroim.2010.03.004>
- Taylor, J. P., Brown, R. H., & Cleveland, D. W. (2016). Decoding ALS: from genes to mechanism. *Nature*, 539(7628), 197–206. <https://doi.org/10.1038/nature20413>
- Tong, J., Huang, C., Bi, F., Wu, Q., Huang, B., Liu, X., Li, F., Zhou, H., & Xia, X.-G. (2013). Expression of ALS-linked TDP-43 mutant in astrocytes causes non-cell-autonomous motor neuron death in rats. *The EMBO Journal*, 32(13), 1917–1926. <https://doi.org/10.1038/emboj.2013.122>
- Traiffort, E., Morisset-Lopez, S., Moussaed, M., & Zahaf, A. (2021). Defective Oligodendroglial Lineage and Demyelination in Amyotrophic Lateral Sclerosis. *International Journal of Molecular Sciences*, 22(7), 3426. <https://doi.org/10.3390/ijms22073426>
- Tremblay, M.-È., Lowery, R. L., & Majewska, A. K. (2010). Microglial Interactions with Synapses Are Modulated by Visual Experience. *PLoS Biology*, 8(11), e1000527. <https://doi.org/10.1371/journal.pbio.1000527>
- Trinidad, J. C., Fischbach, G. D., & Cohen, J. B. (2000). The Agrin/MuSK Signaling Pathway Is Spatially Segregated from the Neuregulin/ErbB Receptor Signaling Pathway at the Neuromuscular Junction. *The Journal of Neuroscience*, 20(23), 8762–8770. <https://doi.org/10.1523/JNEUROSCI.20-23-08762.2000>
- Turner, B., & Talbot, K. (2008). Transgenics, toxicity and therapeutics in rodent models of mutant SOD1-mediated familial ALS. *Progress in Neurobiology*, 85(1), 94–134. <https://doi.org/10.1016/j.pneurobio.2008.01.001>
- Turner, M., Cagnin, A., Turkheimer, F., Miller, C. C., Shaw, C., Brooks, D., Leigh, P., & Banati, R. (2004). Evidence of widespread cerebral microglial activation in amyotrophic lateral sclerosis: an [11C](R)-PK11195 positron emission tomography study. *Neurobiology of Disease*, 15(3), 601–609. <https://doi.org/10.1016/j.nbd.2003.12.012>
- Uchida, A., Sasaguri, H., Kimura, N., Tajiri, M., Ohkubo, T., Ono, F., Sakaue, F., Kanai, K., Hirai, T., Sano, T., Shibuya, K., Kobayashi, M., Yamamoto, M., Yokota, S., Kubodera, T., Tomori, M., Sakaki, K., Enomoto, M., Hirai, Y., ... Yokota, T. (2012). Non-human primate model of amyotrophic lateral sclerosis with cytoplasmic mislocalization of TDP-43. *Brain*, 135(3), 833–846. <https://doi.org/10.1093/brain/awr348>
- Urushitani, M., Ezzi, S. A., & Julien, J.-P. (2007). Therapeutic effects of immunization with mutant superoxide dismutase in mice models of amyotrophic lateral sclerosis. *Proceedings of the National Academy of Sciences*, 104(7), 2495–2500. <https://doi.org/10.1073/pnas.0606201104>
- Urushitani, M., Sik, A., Sakurai, T., Nukina, N., Takahashi, R., & Julien, J.-P. (2006). Chromogranin-mediated secretion of mutant superoxide dismutase proteins linked to amyotrophic lateral sclerosis. *Nature Neuroscience*, 9(1), 108–118. <https://doi.org/10.1038/nn1603>
- Vaccaro, A., Patten, S. A., Aggad, D., Julien, C., Maios, C., Kabashi, E., Drapeau, P., & Parker, J. A.

- (2013). Pharmacological reduction of ER stress protects against TDP-43 neuronal toxicity in vivo. *Neurobiology of Disease*, 55, 64–75. <https://doi.org/10.1016/j.nbd.2013.03.015>
- Vainchtein, I. D., Chin, G., Cho, F. S., Kelley, K. W., Miller, J. G., Chien, E. C., Liddelow, S. A., Nguyen, P. T., Nakao-Inoue, H., Dorman, L. C., Akil, O., Joshita, S., Barres, B. A., Paz, J. T., Molofsky, A. B., & Molofsky, A. V. (2018). Astrocyte-derived interleukin-33 promotes microglial synapse engulfment and neural circuit development. *Science*, 359(6381), 1269–1273. <https://doi.org/10.1126/science.aal3589>
- Valori, C. F., Brambilla, L., Martorana, F., & Rossi, D. (2014). The multifaceted role of glial cells in amyotrophic lateral sclerosis. *Cellular and Molecular Life Sciences*, 71(2), 287–297. <https://doi.org/10.1007/s00018-013-1429-7>
- Van Den Bosch, L., Van Damme, P., Bogaert, E., & Robberecht, W. (2006). The role of excitotoxicity in the pathogenesis of amyotrophic lateral sclerosis. *Biochimica et Biophysica Acta (BBA) - Molecular Basis of Disease*, 1762(11–12), 1068–1082. <https://doi.org/10.1016/j.bbadi.2006.05.002>
- Vance, C., Rogelj, B., Hortobagyi, T., De Vos, K. J., Nishimura, A. L., Sreedharan, J., Hu, X., Smith, B., Ruddy, D., Wright, P., Ganeshalingam, J., Williams, K. L., Tripathi, V., Al-Saraj, S., Al-Chalabi, A., Leigh, P. N., Blair, I. P., Nicholson, G., de Belleroche, J., ... Shaw, C. E. (2009). Mutations in FUS, an RNA Processing Protein, Cause Familial Amyotrophic Lateral Sclerosis Type 6. *Science*, 323(5918), 1208–1211. <https://doi.org/10.1126/science.1165942>
- Vande Velde, C., Miller, T. M., Cashman, N. R., & Cleveland, D. W. (2008). Selective association of misfolded ALS-linked mutant SOD1 with the cytoplasmic face of mitochondria. *Proceedings of the National Academy of Sciences*, 105(10), 4022–4027. <https://doi.org/10.1073/pnas.0712209105>
- Vandenabeele, P., Riquet, F., & Cappe, B. (2017). Necroptosis: (Last) Message in a Bubble. *Immunity*, 47(1), 1–3. <https://doi.org/10.1016/j.immuni.2017.07.002>
- Velanac, V., Unterbarnscheidt, T., Hinrichs, W., Gummert, M. N., Fischer, T. M., Rossner, M. J., Trimarco, A., Brivio, V., Taveggia, C., Willem, M., Haass, C., Möbius, W., Nave, K., & Schwab, M. H. (2012). Bace1 processing of NRG1 type III produces a myelin-inducing signal but is not essential for the stimulation of myelination. *Glia*, 60(2), 203–217. <https://doi.org/10.1002/glia.21255>
- Vinsant, S., Mansfield, C., Jimenez-Moreno, R., Moore, V. D. G., Yoshikawa, M., Hampton, T. G., Prevette, D., Caress, J., Oppenheim, R. W., & Milligan, C. (2013). Characterization of early pathogenesis in the SOD1 G93A mouse model of ALS: part II, results and discussion. *Brain and Behavior*, 3(4), 431–457. <https://doi.org/10.1002/brb3.142>
- Vukojicic, A., Delestrée, N., Fletcher, E. V., Pagiazitis, J. G., Sankaranarayanan, S., Yednock, T. A., Barres, B. A., & Mentis, G. Z. (2019). The Classical Complement Pathway Mediates Microglia-Dependent Remodeling of Spinal Motor Circuits during Development and in SMA. *Cell Reports*, 29(10), 3087–3100.e7. <https://doi.org/10.1016/j.celrep.2019.11.013>

- Vullhorst, D., Mitchell, R. M., Keating, C., Roychowdhury, S., Karavanova, I., Tao-Cheng, J.-H., & Buonanno, A. (2015). A negative feedback loop controls NMDA receptor function in cortical interneurons via neuregulin 2/ErbB4 signalling. *Nature Communications*, 6(1), 7222. <https://doi.org/10.1038/ncomms8222>
- Walker, A. K., & Atkin, J. D. (2011). Stress signaling from the endoplasmic reticulum: A central player in the pathogenesis of amyotrophic lateral sclerosis. *IUBMB Life*, 63(9), n/a-n/a. <https://doi.org/10.1002/iub.520>
- Wang, H., Sun, L., Su, L., Rizo, J., Liu, L., Wang, L.-F., Wang, F.-S., & Wang, X. (2014). Mixed Lineage Kinase Domain-like Protein MLKL Causes Necrotic Membrane Disruption upon Phosphorylation by RIP3. *Molecular Cell*, 54(1), 133–146. <https://doi.org/10.1016/j.molcel.2014.03.003>
- Wang, P., Wander, C. M., Yuan, C.-X., Bereman, M. S., & Cohen, T. J. (2017). Acetylation-induced TDP-43 pathology is suppressed by an HSF1-dependent chaperone program. *Nature Communications*, 8(1), 82. <https://doi.org/10.1038/s41467-017-00088-4>
- Wang, T., Perera, N. D., Chiam, M. D. F., Cuic, B., Wanniarachchilage, N., Tomas, D., Samson, A. L., Cawthorne, W., Valor, E. N., Murphy, J. M., & Turner, B. J. (2020). Necroptosis is dispensable for motor neuron degeneration in a mouse model of ALS. *Cell Death & Differentiation*, 27(5), 1728–1739. <https://doi.org/10.1038/s41418-019-0457-8>
- Watanabe, M., Dykes-Hoberg, M., Cizewski Culotta, V., Price, D. L., Wong, P. C., & Rothstein, J. D. (2001). Histological Evidence of Protein Aggregation in Mutant SOD1 Transgenic Mice and in Amyotrophic Lateral Sclerosis Neural Tissues. *Neurobiology of Disease*, 8(6), 933–941. <https://doi.org/10.1006/nbdi.2001.0443>
- Watanabe, S., Ilieva, H., Tamada, H., Nomura, H., Komine, O., Endo, F., Jin, S., Mancias, P., Kiyama, H., & Yamanaka, K. (2016). Mitochondria-associated membrane collapse is a common pathomechanism in SIGMAR 1 - and SOD 1 -linked ALS. *EMBO Molecular Medicine*, 8(12), 1421–1437. <https://doi.org/10.15252/emmm.201606403>
- Watson, C., Paxinos, G., Kayalioglu, G., & Heise, C. (2009). In C. Watson, G. Paxinos, & K. G (Eds.), *The spinal cord* (1st ed.). Amsterdam: Elsevier
- Watson, M. R., Lagow, R. D., Xu, K., Zhang, B., & Bonini, N. M. (2008). A Drosophila Model for Amyotrophic Lateral Sclerosis Reveals Motor Neuron Damage by Human SOD1. *Journal of Biological Chemistry*, 283(36), 24972–24981. <https://doi.org/10.1074/jbc.M804817200>
- Webster, C. P., Smith, E. F., Shaw, P. J., & De Vos, K. J. (2017). Protein Homeostasis in Amyotrophic Lateral Sclerosis: Therapeutic Opportunities? *Frontiers in Molecular Neuroscience*, 10(May), 1–22. <https://doi.org/10.3389/fnmol.2017.00123>

- Wei, T., Kang, Q., Ma, B., Gao, S., Li, X., & Liu, Y. (2015). Activation of autophagy and paraptosis in retinal ganglion cells after retinal ischemia and reperfusion injury in rats. *Experimental and Therapeutic Medicine*, 9(2), 476–482. <https://doi.org/10.3892/etm.2014.2084>
- Weinhard, L., di Bartolomei, G., Bolasco, G., Machado, P., Schieber, N. L., Neniskyte, U., Exiga, M., Vadisiute, A., Raggioli, A., Schertel, A., Schwab, Y., & Gross, C. T. (2018). Microglia remodel synapses by presynaptic trogocytosis and spine head filopodia induction. *Nature Communications*, 9(1), 1228. <https://doi.org/10.1038/s41467-018-03566-5>
- Wiedemann, F. R., Manfredi, G., Mawrin, C., Beal, M. F., & Schon, E. A. (2002). Mitochondrial DNA and respiratory chain function in spinal cords of ALS patients. *Journal of Neurochemistry*, 80(4), 616–625. <https://doi.org/10.1046/j.0022-3042.2001.00731.x>
- Willem, M. (2016). Proteolytic processing of Neuregulin-1. *Brain Research Bulletin*, 126, 178–182. <https://doi.org/10.1016/j.brainresbull.2016.07.003>
- Williams, T. L., Day, N. C., Ince, P. G., Kamboj, R. K., & Shaw, P. J. (1997). Calcium-permeable a-amino-3-hydroxy-5-methyl-4-isoxazole propionic acid receptors: A molecular determinant of selective vulnerability in amyotrophic lateral sclerosis. *Annals of Neurology*, 42(2), 200–207. <https://doi.org/10.1002/ana.410420211>
- Witts, E. C., Zagoraiou, L., & Miles, G. B. (2014). Anatomy and function of cholinergic C bouton inputs to motor neurons. *Journal of Anatomy*, 224(1), 52–60. <https://doi.org/10.1111/joa.12063>
- Wolpowitz, D., Mason, T. B. A., Dietrich, P., Mendelsohn, M., Talmage, D. A., & Role, L. W. (2000). Cysteine-Rich Domain Isoforms of the Neuregulin-1 Gene Are Required for Maintenance of Peripheral Synapses. *Neuron*, 25(1), 79–91. [https://doi.org/10.1016/S0896-6273\(00\)80873-9](https://doi.org/10.1016/S0896-6273(00)80873-9)
- Wong, P. C., Pardo, C. A., Borchelt, D. R., Lee, M. K., Copeland, N. G., Jenkins, N. A., Sisodia, S. S., Cleveland, D. W., & Price, D. L. (1995). An adverse property of a familial ALS-linked SOD1 mutation causes motor neuron disease characterized by vacuolar degeneration of mitochondria. *Neuron*, 14(6), 1105–1116. [https://doi.org/10.1016/0896-6273\(95\)90259-7](https://doi.org/10.1016/0896-6273(95)90259-7)
- Yamanaka, K., Boilée, S., Roberts, E. A., Garcia, M. L., McAlonis-Downes, M., Mikse, O. R., Cleveland, D. W., & Goldstein, L. S. B. (2008). Mutant SOD1 in cell types other than motor neurons and oligodendrocytes accelerates onset of disease in ALS mice. *Proceedings of the National Academy of Sciences*, 105(21), 7594–7599. <https://doi.org/10.1073/pnas.0802556105>
- Yarden, Y., & Sliwkowski, M. X. (2001). Untangling the ErbB network. *Nature Reviews Molecular Cell Biology*, 2(February), 127–137. www.nature.com/reviews/molcellbio
- Yoon, S., Kovalenko, A., Bogdanov, K., & Wallach, D. (2017). MLKL, the Protein that Mediates Necroptosis, Also Regulates Endosomal Trafficking and Extracellular Vesicle Generation. *Immunity*, 47(1), 51-65.e7. <https://doi.org/10.1016/j.jimmuni.2017.06.001>
- Zagoraiou, L., Akay, T., Martin, J. F., Brownstone, R. M., Jessell, T. M., & Miles, G. B. (2009). A Cluster

- of Cholinergic Premotor Interneurons Modulates Mouse Locomotor Activity. *Neuron*, 64(5), 645–662. <https://doi.org/10.1016/j.neuron.2009.10.017>
- Zang, D. W., Lopes, E. C., & Cheema, S. S. (2005). Loss of synaptophysin-positive boutons on lumbar motor neurons innervating the medial gastrocnemius muscle of the SOD1G93A G1H transgenic mouse model of ALS. *Journal of Neuroscience Research*, 79(5), 694–699. <https://doi.org/10.1002/jnr.20379>
- Zhang, B., Tu, P., Abtahian, F., Trojanowski, J. Q., & Lee, V. M. Y. (1997). Neurofilaments and Orthograde Transport Are Reduced in Ventral Root Axons of Transgenic Mice that Express Human SOD1 with a G93A Mutation. *Journal of Cell Biology*, 139(5), 1307–1315. <https://doi.org/10.1083/jcb.139.5.1307>
- Zhang, H., Tan, C.-F., Mori, F., Tanji, K., Kakita, A., Takahashi, H., & Wakabayashi, K. (2008). TDP-43-immunoreactive neuronal and glial inclusions in the neostriatum in amyotrophic lateral sclerosis with and without dementia. *Acta Neuropathologica*, 115(1), 115–122. <https://doi.org/10.1007/s00401-007-0285-7>
- Zhao, P., Ignacio, S., Beattie, E. C., & Abood, M. E. (2008). Altered presymptomatic AMPA and cannabinoid receptor trafficking in motor neurons of ALS model mice: implications for excitotoxicity. *European Journal of Neuroscience*, 27(3), 572–579. <https://doi.org/10.1111/j.1460-9568.2008.06041.x>
- Zhao, W., Beers, D. R., Henkel, J. S., Zhang, W., Urushitani, M., Julien, J.-P., & Appel, S. H. (2010). Extracellular mutant SOD1 induces microglial-mediated motoneuron injury. *Glia*, 58(2), 231–243. <https://doi.org/10.1002/glia.20919>
- Zhou, B., Zuo, Y., & Jiang, R. (2019). Astrocyte morphology: Diversity, plasticity, and role in neurological diseases. *CNS Neuroscience & Therapeutics*, 25(6), 665–673. <https://doi.org/10.1111/cns.13123>
- Zou, Z.-Y., Zhou, Z.-R., Che, C.-H., Liu, C.-Y., He, R.-L., & Huang, H.-P. (2017). Genetic epidemiology of amyotrophic lateral sclerosis: a systematic review and meta-analysis. *Journal of Neurology, Neurosurgery & Psychiatry*, 88(7), 540–549. <https://doi.org/10.1136/jnnp-2016-315018>



ADDENDA

Addicionalment, durant el període predoctoral, l'autora també ha contribuit a la següent



ORIGINAL RESEARCH
published: 24 January 2020
doi: 10.3389/fncel.2019.00582



The Y172 Monoclonal Antibody Against p-c-Jun (Ser63) Is a Marker of the Postsynaptic Compartment of C-Type Cholinergic Afferent Synapses on Motoneurons

Alaó Gatius¹, Olga Tarabal¹, Paula Cayuela¹, Anna Casanovas¹, Lídia Piedrafita¹, Sara Salvany¹, Sara Hernández¹, Rosa M. Soler², Josep E. Esquerda¹ and Jordi Calderó^{1*}

¹Unitat de Neurobiología Cel·lular, Departament de Medicina Experimental, Facultat de Medicina, Universitat de Lleida and Institut de Recerca Biomèdica de Lleida (IRBLleida), Lleida, Spain, ²Unitat de Senyalització Neuronal, Departament de Medicina Experimental, Facultat de Medicina, Universitat de Lleida and Institut de Recerca Biomèdica de Lleida (IRBLleida), Lleida, Spain

OPEN ACCESS

Edited by:

Thomas Fath,
Macquarie University, Australia

Reviewed by:

Xavier Navarro,
Autonomous University of Barcelona,
Spain

Paul Albert Fuchs,
Johns Hopkins University,
United States

*Correspondence:

Jordi Calderó
jordi.caldero@mex.udl.cat

Received: 20 September 2019

Accepted: 20 December 2019

Published: 24 January 2020

Citation:

Gatius A, Tarabal O, Cayuela P, Casanovas A, Piedrafita L, Salvany S, Hernández S, Soler RM, Esquerda JE and Calderó J (2020) The Y172 Monoclonal Antibody Against p-c-Jun (Ser63) Is a Marker of the Postsynaptic Compartment of C-Type Cholinergic Afferent Synapses on Motoneurons. *Front. Cell. Neurosci.* 13:582. doi: 10.3389/fncel.2019.00582

C-bouton-type cholinergic afferents exert an important function in controlling motoneuron (MN) excitability. During the immunocytochemical analysis of the role of c-Jun in MNs with a monoclonal (clone Y172) antibody against phospho (p)-c-Jun (serine [Ser]63), unexpected labeling was identified in the cell body cytoplasm. As predicted for c-Jun in adult spinal cord, very few, if any MNs exhibited nuclear immunoreactivity with the Y172 antibody; conversely, virtually all MNs displayed strong Y172 immunostaining in cytoplasmic structures scattered throughout the soma and proximal dendrites. The majority of these cytoplasmic Y172-positive profiles was closely associated with VACHT-positive C-boutons, but not with other types of nerve afferents contacting MNs. Ultrastructural analysis revealed that cytoplasmic Y172 immunostaining was selectively located at the subsurface cistern (SSC) of C-boutons and also in the inner areas of the endoplasmic reticulum (ER). We also described changes in cytoplasmic Y172 immunoreactivity in injured and degenerating MNs. Moreover, we noticed that MNs from NRG1 type III-overexpressing transgenic mice, which show abnormally expanded SSCs, exhibited an increase in the density and size of peripherally located Y172-positive profiles. A similar immunocytochemical pattern to that of the Y172 antibody in MNs was found with a polyclonal antibody against p-c-Jun (Ser63) but not with another polyclonal antibody that recognizes c-Jun phosphorylated at a different site. No differential band patterns were found by western blotting with any of the antibodies against c-Jun or p-c-Jun used in our study. In cultured MNs, Y172-positive oval profiles were distributed in the cell body and proximal dendrites. The *in vitro* lentiviral-based knockdown of c-Jun resulted in a dramatic decrease in nuclear Y172 immunostaining in MNs without

publicació:

any reduction in the density of cytoplasmic Y172-positive profiles, suggesting that the synaptic antigen recognized by the antibody corresponds to a C-bouton-specific protein other than p-c-Jun. Our results lay the foundation for further studies aimed at identifying this protein and determining its role in this particular type of synapse.

Keywords: motoneuron, C-bouton, phospho-c-Jun, Y172 antibody, endoplasmic reticulum-plasma membrane contacts

CONTRIBUCIONS A CONGRESSOS

Comunicacions orals

X Simposi de Neurobiologia, 6 i 7 d'octubre de 2016; Dublin, Irlanda; Presentació oral de la comunicació “Neuregulin 1-ErbB module in c-bouton synapses on somatic motor neurons: molecular compartmentation, changes during ALS and response to peripheral nerve injury” Salvany S.; Casanovas A.; Lahoz V.; Tarabal O.; Piedrafita L.; Sabater R.; Hernández S.; Calderó J.; Esquerda J.E.

I Congreso Interdisciplinar Estudiantes Neurología y Neurociencia (CIEN2), 10 i 11 de març de 2017; Lleida, Espanya; Presentació oral de la comunicació “*Molecular architecture in motoneuron c-bouton synapses and its changes during als and in peripheral nerve injury*” Salvany S, Lahoz V, Casanovas A, Tarabal O, Piedrafita L, Sabater R, Hernández S, Calderó J, Esquerda JE

II Congreso Interdisciplinar Estudiantes Neurología y Neurociencia (CIEN2), 8 i 9 de març de 2019; Lleida, Espanya; Presentació oral de la comunicació “*Neuregulin 1 regulation and its organizing functions in C-type cholinergic afferents on normal and altered a-motor neurons*” Sara Salvany, Anna Casanovas, Olga Tarabal, Sara Hernández, Lidia Piedrafita, María Clara Soto-Bernardini, Manuel Santafé, Jordi Calderó, Markus H. Schwab, Josep E. Esquerda

Pòsters

27th International Symposium on ALS/MND, 7-9 de desembre de 2016; Dublin, Irlanda; Presentació del pòster “Neuregulin-1-erbb signaling module is associated with afferent c-type cholinergic terminals on als vulnerable motoneurons and involved in motoneuron diseases” A Casanovas; S Salvany; R Sabater; O Tarabal; V Lahoz; L Piedrafita; S Hernández; J Calderó; J Esquerda

I Congreso Interdisciplinar Estudiantes Neurología y Neurociencia (CIEN2), 10 i 11 de març de 2017; Lleida, Espanya; Presentació del pòster “*Neuregulin 1-ErbB module is associated with c-bouton synapses on als motoneurons and suffer plastic changes during peripheral nerve injury*” S Salvany; V Lahoz; Casanovas A., Piedrafita L., Hernández S., Tarabal O., Calderó J., Esquerda J. E.

29th International Symposium on ALS/MND, 7 – 9 desembre 2018; Glasgow, Escòcia; Presentació del pòster “*Neuregulin 1 regulation and its organizing functions in C-type cholinergic afferents on normal and altered α-motor neurons*” Sara Salvany; Anna Casanovas; Olga Tarabal; Sara Hernández; Lídia Piedrafita; María Clara Soto-Bernardini; Manuel Santafé; Jordi Calderó; Markus H. Schwab; Josep E. Esquerda

II Congreso Interdisciplinar Estudiantes Neurología y Neurociencia (CIEN2), 8 i 9 de març de 2019; Lleida, Espanya; Presentació del pòster “*Neuregulin 1-ErbB module is associated with c-bouton synapses on als motoneurons and suffer plastic changes during peripheral nerve injury*” Sara Salvany, Anna Casanovas, Olga Tarabal, Sara Hernández, Lidia Piedrafita, María Clara Soto-Bernardini, Manuel Santafé, Jordi Calderó, Markus H. Schwab, Josep E. Esquerda

Motor Neuron Diseases; understanding the pathogenetic mechanisms to develop therapies; 6 – 7 Novembre de 2020; Online; Presentació del pòster “*Identification of distinct pathological motor neuron phenotypes according with the expression of misfolded SOD1 and microgliosis during the progression of disease in the SOD1G93A ALS mice*” Salvany S., Casanovas A., Gatius A., Gras S., Blasco A., Piedrafita L., Tarabal O., Hernández S., Calderó J., Esquerda J.E.

31st International Symposium on ALS/MND, 9 – 11 desembre 2020; Online; Presentació del pòster “*The correlative presence of misfolded SOD1, mitochondrial vacuolization and microgliosis defines distinct phenotypes of motor neuron damage during the progression of disease in the SOD1G93A ALS mice*” Sara Salvany, Anna Casanovas, Alaó Gatius, Sílvia Gras, Alba Blasco, Lídia Piedrafita, Olga Tarabal, Sara Hernández, Jordi Calderó, Josep E. Esquerda

ENCALS, 12 - 14 maig 2021; Online; Presentació del pòster “Identification of distinct pathological motor neuron phenotypes according with the expression of misfolded SOD1 and microgliosis during the progression of disease in the SOD1G93A ALS mice” S. Salvany, A. Casanovas, S. Gras, A. Gatius, A. Blasco, L. Piedrafita, O. Tarabal, S. Hernández, J. Calderó, J.E. Esquerda

16th International Congress on Neuromuscular Diseases (ICNMD), 21, 22 – 28, 29 maig 2021; Online; Presentació del pòster “Overexpression of NRG1-type III does not ameliorate ALS clinical outcome in SOD1G93A mouse model” S. Hernández, A. Casanovas, S. Salvany, L. Piedrafita, A. Blasco, A. Gatius, S. Gras, O. Tarabal, J. Calderó, J.E. Esquerda

16th International Congress on Neuromuscular Diseases (ICNMD), 21, 22 – 28, 29 maig 2021; Online; Presentació del pòster “Neuregulin 1 isoforms regulate the pre- and postsynaptic organization of C-type synapses on motor neurons” S. Salvany, A. Casanovas, S. Gras, A. Gatius, A. Blasco, L. Piedrafita, O. Tarabal, S. Hernández, J. Calderó, J.E. Esquerda

XV European Meeting on Glial Cells in Health and Disease, 5-9 juliol 2021; Online; Presentació del pòster “Necroptosis and microglial phagocytosis of extracellular vesicles as an early mechanisms involved in the disruption of afferent synaptic terminals on spinal cord motor neurons after acute peripheral nerve injury” S. Salvany, A. Casanovas, L. Piedrafita, S. Gras, A. Blasco, A. Gatius, O. Tarabal, S. Hernández, J. Calderó, J.E. Esquerda

